seit 1558

Friedrich-Schiller-Universität Jena

Chemisch-Geowissenschaftliche Fakultät

Cationic polymers made from poly(2-oxazoline)s for biomedical applications

Dissertation
(kumulativ)

Zur Erlangung des akademischen Grades
doctor rerum naturalium (Dr. rer. nat.)

vorgelegt dem Rat der Chemisch-Geowissenschaftlichen
Fakultät der Friedrich-Schiller-Universität Jena

von Diplom-Chemiker Christoph Englert
geboren am 20.09.1987 in Weimar

Gutachter:

1. Prof. Dr. Ulrich S. Schubert, Friedrich-Schiller-Universität Jena

2. Prof. Dr. Thomas Heinze, Friedrich-Schiller-Universität Jena

3. Prof. Dr. Stefan Spange, Technische Universität Chemnitz

Tag der öffentlichen Verteidigung: 20.12.2017

To Kathrin, Christiane and Ralf

for their love, caring and unconditional support.

TABLE OF CONTENTS

DOCUMENTATION OF AUTHORSHIP

This section contains a list of the individual authors' contributions to the publications reprinted in this thesis.

P1	C. Englert,[1] J. C. Brendel,[2] T. C. Majdanski,[3] T. Yildirim,[4] S. Schubert,[5] M. Gottschaldt,[6] N. Windhab,[7] U. S. Schubert,[8] "Pharmapolymers for the 21st century: Synthetic polymers in drug delivery applications", *Adv. Healthcare Mater.*, submitted (2017/06/06).							
Author	**1**	**2**	**3**	**4**	**5**	**6**	**7**	**8**
Development of concept	×	×	×	×	×	×	×	×
Preparation of the manuscript	×		×	×	×	×		
Correction of the manuscript	×	×	×	×	×	×		×
Supervision of C. Englert								×
Proposed publication equivalent	0.5							

P2	C. Englert,[1] M. Hartlieb,[2] P. Bellstedt,[3] K. Kempe,[4] C. Yang,[5] S. K. Chu,[6] X. Ke,[7] J. M. García,[8] R. J. Ono,[9] M. Fevre,[10] R. J. Wojtecki,[11] U. S. Schubert,[12] Y. Y. Yang,[13] J. L. Hedrick,[14] "Enhancing the biocompatibility and biodegradability of linear poly(ethylene imine) through controlled oxidation", *Macromolecules* **2015**, *48*, 7420-7427.												
Author	**1**	**2**	**3**	**4**	**5**	**6**	**7**	**8**	**9**	**10**	**11**	**12**	**13**	**14**
Development of concept	×	×		×				×	×	×			×	×
Polymer and material synthesis	×													
Polymer and material characterization	×		×								×			
Biological investigations					×	×	×							
Preparation of the manuscript	×													
Correction of the manuscript		×		×				×	×	×	×	×	×	×
Supervision of C. Englert												×	×	×
Proposed publication equivalent	1.0													

P3	C. Englert,[1] M. Fevre,[2] R. J. Wojtecki,[3] W. Cheng,[4] Q. Xu,[5] C. Yang,[6] X. Ke,[7] M. Hartlieb,[8] K. Kempe,[9] J. M. García,[10] R. J. Ono,[11] U. S. Schubert,[12] Y. Y. Yang,[13] J. L. Hedrick,[14] "Facile carbohydrate-mimetic modifications of poly(ethylene imine) carriers for gene delivery applications", *Polym. Chem.* **2016**, *7*, 5862-5872.

Author	**1**	**2**	**3**	**4**	**5**	**6**	**7**	**8**	**9**	**10**	**11**	**12**	**13**	**14**
Development of concept	×	×						×		×	×			×
Polymer and material synthesis	×	×												
Polymer and material characterization	×	×	×											
Biological investigations				×	×	×	×							
Preparation of the manuscript	×	×												
Correction of the manuscript			×					×	×	×		×	×	×
Supervision of C. Englert												×	×	×
Proposed publication equivalent	1.0													

P4	C. Englert,[1] A. M. Schwenke,[2] S. Hoeppener,[3] C. Weber,[4] U. S. Schubert,[5] "Microwave-assisted polymer modifications", *Adv. Polym. Sci.* **2015**, *274*, 209-240.

Author	**1**	**2**	**3**	**4**	**5**
Development of concept	×	×		×	
Preparation of the manuscript	×	×		×	
Correction of the manuscript			×	×	×
Supervision of C. Englert					×
Proposed publication equivalent	0.5				

P5	T. Bus,[1,‡] C. Englert,[2,‡] M. Reifarth,[3] P. Borchers,[4] M. Hartlieb,[5] A. Vollrath,[6] S. Hoeppener,[7] A. Traeger,[8] U. S. Schubert,[9] "3rd Generation poly(ethylene imine)s for gene delivery", *J. Mater. Chem. B* **2017**, *5*, 1258-1274. ‡ Authors contributed equally.

Author	**1**	**2**	**3**	**4**	**5**	**6**	**7**	**8**	**9**
Development of concept	×	×			×	×		×	
Polymer and material synthesis		×		×					
Polymer and material characterization		×		×					
Biological investigations	×								
Microscopy studies	×		×						
Preparation of the manuscript	×	×							
Correction of the manuscript			×		×		×	×	×
Supervision P. Borchers		×							
Supervision of C. Englert									×
Proposed publication equivalent		0.5							

P6	C. Englert,[1,‡] A-K. Trützschler,[2,‡] M. Raasch,[3] T. Bus,[4] P. Borchers,[5] A. S. Mosig,[6] A. Traeger,[7] U. S. Schubert,[8] "Crossing the blood-brain barrier: Glutathione-conjugated poly(ethylene imine) for gene delivery", *J. Control. Release* **2016**, *241*, 1-14. ‡ Authors contributed equally.							
Author	**1**	**2**	**3**	**4**	**5**	**6**	**7**	**8**
Development of concept	×	×	×	×		×	×	
Polymer synthesis	×				×			
Polymer characterization	×	×						
Biological investigations				×				
Microchip tests			×					
Preparation of the manuscript	×	×						
Correction of the manuscript			×	×		×	×	×
Supervision of P. Borchers	×							
Supervision of C. Englert								×
Proposed publication equivalent	0.5							

P7	C. Englert,[1, ‡] M. Pröhl,[2, ‡] J. A. Czaplewska,[3] C. Fritzsche,[4] E. Preußger,[5] U. S. Schubert,[6] A. Traeger,[7] M. Gottschaldt,[8] "D-Fructose-decorated poly(ethylene imine) for human breast cancer cell targeting", *Macromol. Biosci.* **2017**, *17*, 1600502. ‡ Authors contributed equally.							
Author	**1**	**2**	**3**	**4**	**5**	**6**	**7**	**8**
Development of concept	×	×						×
Sugar synthesis		×	×					
Sugar characterization		×						
Polymer synthesis	×							
Polymer characterization	×							
Biological investigations				×	×		×	
Preparation of the manuscript	×	×						
Correction of the manuscript			×			×	×	×
Supervision of C. Englert						×		
Proposed publication equivalent	0.5							

P8	M. Hartlieb,[1] D. Pretzel,[2] C. Englert,[3] M. Hentschel,[4] K. Kempe,[5] M. Gottschaldt,[6] U. S. Schubert,[7] "Matrix supported poly(2-oxazoline)-based hydrogels for DNA catch and release", *Biomacromolecules* **2014**, *15*, 1970-1978.						
Author	**1**	**2**	**3**	**4**	**5**	**6**	**7**
Development of concept	×	×				×	
Polymer and material synthesis	×						
Polymer and material characterization	×						
DNA binding and release studies	×	×	×				
PCR studies				×			
Preparation of the manuscript	×	×					
Correction of the manuscript			×	×	×	×	×
Supervision of C. Englert							×
Proposed publication equivalent			0.25				

P9	M. N. Leiske,[1,‡] M. Hartlieb,[2,‡] C. Paulenz,[3] D. Pretzel,[4] M. Hentschel,[5] C. Englert,[6] M. Gottschaldt,[7] U. S. Schubert,[8] "Lab in a tube: Purification, amplification and detection of DNA using poly(2-oxazoline) multilayers", *Adv. Funct. Mater.* **2015**, *25*, 2458-2466. ‡ Authors contributed equally.							
Author	**1**	**2**	**3**	**4**	**5**	**6**	**7**	**8**
Development of concept	×	×		×		×	×	
Polymer and material synthesis	×							
Polymer and material characterization	×	×		×				
DNA binding and release studies	×			×				
PCR experiments	×		×		×			
Preparation of the manuscript		×						
Correction of the manuscript	×		×	×	×		×	×
Supervision of C. Englert								×
Proposed publication equivalent						0.25		

P10	M. Hartlieb,[1] D. Pretzel,[2] M. Wagner,[3] S. Höppener,[4] P. Bellstedt,[5] M. Görlach,[6] C. Englert,[7] K. Kempe,[8] U. S. Schubert,[9] "Core cross-linked nanogels based on the self-assembly of double hydrophilic poly(2-oxazoline) block copolymers", *J. Mater. Chem. B*, **2015**, *3*, 1748-1759.								
Author	**1**	**2**	**3**	**4**	**5**	**6**	**7**	**8**	**9**
Development of concept	×	×						×	
Polymer and material synthesis	×		×	×	×	×	×		
Polymer and material characterization	×								
Biological investigations		×							
Preparation of the manuscript	×	×							
Correction of the manuscript			×	×	×	×	×	×	×
Supervision of C. Englert									×
Proposed publication equivalent							0.25		

Erklärung zu den Eigenanteilen des Promovenden sowie der weiteren Doktoranden/Doktorandinnen als Koautoren an Publikationen und Zweitpublikationsrechten bei einer kumulativen Dissertation

Für alle in dieser kumulativen Dissertation verwendeten Manuskripte liegen die notwendigen Genehmigungen der Verlage („Reprint permissions“) für die Zweitpublikation vor.

Die Co-Autoren der in dieser kumulativen Dissertation verwendeten Manuskripte sind sowohl über die Nutzung als auch über die oben angegebenen Eigenanteile informiert und stimmen dem zu.

Die Anteile der Co-Autoren an den Publikationen sind in den vorausgehenden Tabellen aufgeführt.

Christoph Englert ____.____._____ Jena _____

Ich bin mit der Abfassung der Dissertation als publikationsbasiert, d.h. kumulativ, einverstanden und bestätige die vorstehenden Angaben. Eine entsprechend begründete Befürwortung mit Angabe des wissenschaftlichen Anteils des Doktoranden an den verwendeten Publikationen werde ich parallel an den Rat der Fakultät der Chemisch-Geowissenschaftlichen Fakultät richten.

Ulrich S. Schubert ____.____._____ Jena _____

1 INTRODUCTION

Besides its use as primary coagulants in water treatment[1] or as antibacterial agents,[2] cationic polymers hold great promise in treating human diseases in the 21st century. They have proven to be versatile tools in the field of biomedical applications, in particular for gene delivery systems or point-of-care diagnostics.[3] Some of these so-called "pharmapolymers" already entered the market or are currently in different stages of clinical studies, which are discussed in Chapter 2.

Without doubt, gene delivery represents the most prominent application field of polycations. Although viral vectors have superior transduction capabilities, their clinical applications are limited due to their immunogenic and oncogenic potentials.[4-5] To circumvent this problem, numerous non-viral gene delivery systems have been investigated, which include cationic molecules like lipids,[6] peptides[7] and polymers.[8] Among those, synthetic polymers have been established as promising alternatives since they offer several advantages, such as easy large scale production, simple storage conditions, non-significant batch-to-batch variations and numerous possibilities for chemical modifications to achieve the desired properties.[9-10]

While electrostatically interacting with the negatively charged phosphate groups of the genetic material, the cationic polymers form so-called polyplexes (see Figure 1.1A).[11] The condensation of oligonucleotides is often described in the literature by the nitrogen/phosphate ratio (N/P ratio) of the respective polyplexes (polymer/nucleic acid). Besides the condensation of oligonucleotides, the complexation results in the shielding of negative charges and the "protection" of nucleic acids from enzymatic degradation under *in vitro* and *in vivo* conditions. This is essential for a successful gene delivery mechanism.[12] The formed complexes are able to enter the cell by different endocytotic uptake mechanisms summarized by Durzynska *et al.* (Figure 1.1B).[13] Once entered into endosomes, protons accumulate on the cationic functional sites of the polymer initiated by the proton pump vacuolar-type H^+-ATPase (V-ATPase). The influx of chloride anions, which comes along with the proton accumulation, results in an increase of the ion concentration and, simultaneously, in an osmotic swelling of the endosome. Furthermore, the internal charge repulsion leads to the expansion of the polymeric network ("proton-sponge effect").[14] Finally, the endosome membrane ruptures and the cargo is released into the cytosol. It has been reported that this local rupture, forced by the protonation of amines,[15]

is essential for the polyplex release, rendering the pH responsive release an important criterion for the design of gene delivery systems.[16]

Although immense effort has been put into the investigation of the uptake mechanism through the nucleus membrane, the uptake of oligonucleotides is still widely unknown and represents the major limitation for the efficient gene transfer with non-viral systems.

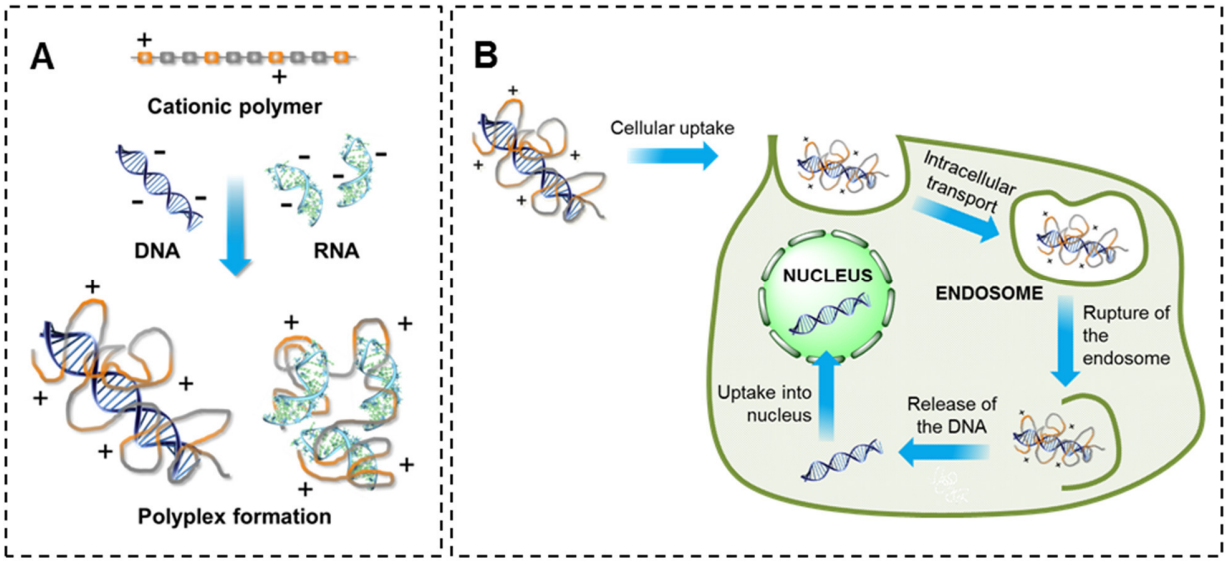

Figure 1.1. A) Polyplex formation of cationic polymers with genetic material (*e.g.* DNA, RNA). B) Gene delivery mechanism of DNA.

The described process requires polymer systems with precisely designed properties which range from the condensation and protection of the genetic material to specific delivery, uptake and expression of the desired genes. Among the investigated systems, poly(ethylene imine) (PEI) is one of the most successfully and widely studied vectors and has been used as the gold standard for gene transfection (1st generation).[8, 17] Linear (LPEI) and branched (BPEI) architectures exist and possess one of the highest cationic charge density potentials of all organic macromolecules.[18] Every third atom is an amine, of which every sixth nitrogen is protonated under physiological conditions[19] which turns PEI into a useful tool to form toroidal complexes that are readily endocytosed by cells.[20-21] Thereby, transfection efficiencies similar to viral vectors can be achieved.[22] Obtained by the ring-opening polymerization (ROP) of unsubstituted aziridines,

BPEI features a branched structure including primary, secondary and tertiary amine groups (Figure 1.2A).[23] However, the lack of control during the synthesis limits the investigation of structure-property relationships.[24] For this reason, along with the high cytotoxicity of branched structures,[18] the linear form, which possesses solely secondary amine functionalities, is often desired. One opportunity to synthesize LPEI is the ROP of *N*-substituted aziridines and subsequent deprotection (Figure 1.2B).[25-27]

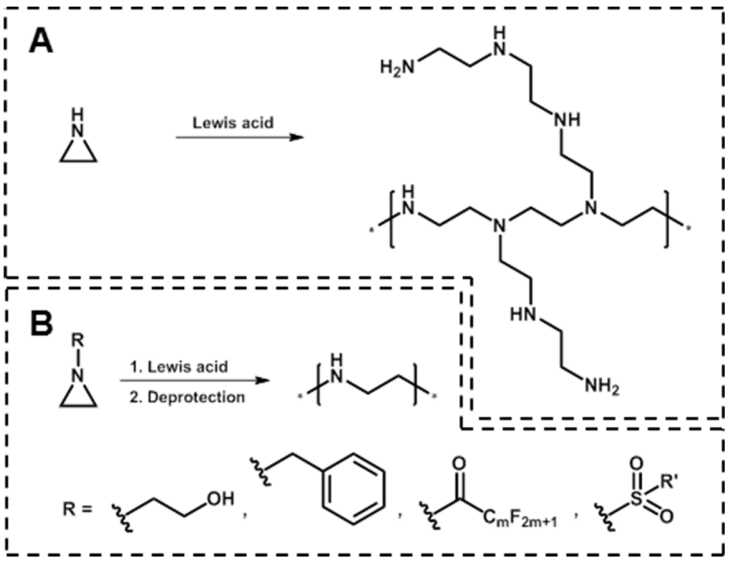

Figure 1.2. Schematic representation of the synthesis of A) branched PEI by ring-opening polymerization of aziridines and B) linear PEI by ring-opening polymerization of *N*-functionalized aziridines.

However, the most common synthesis method uses poly(2-oxazoline)s (POx) as starting materials, which show a stealth effect similar to poly(ethylene glycol) (PEG).[28] The living character of the cationic ring-opening polymerization (CROP) of 2-oxazolines, which was described in 1966 by four different research groups,[29-32] allowed the design of well-defined POx and, later on, LPEI, with narrow dispersities and the access to highly functional systems. The CROP is performed under inert conditions and can be mainly subdivided into three steps. The first step is the initiation of the 2-substituted oxazoline with an electrophile, *e.g.* methyl tosylate or methyl triflate (Scheme 1.1A). The formed oxazolinium species exhibits a weakened C-O-bond which allows the nucleophilic attack of the nitrogen of another monomer. This results in a ring-opening followed by the formation of a carbonyl group. This propagation step can be

repeated until the desired chain length is achieved. The addition of a nucleophile, *e.g.* water, terminates the polymerization.

LPEI is obtained by the acidic[33-34] or basic[35-36] hydrolysis of poly(2-alkyl-2-oxazoline)s, whereas methyl or ethyl side chains have been established as fast and simple moieties for a controlled hydrolysis (Scheme 1.1B, m = n). The reaction time for acidic hydrolysis ranges from a few hours to several days (depending on the POx side chain), while the basic hydrolysis is even slower using a conventional heating procedure. In recent years, microwave-assisted synthesis approaches resulted in a renaissance of POx. Besides the tremendous acceleration of the polymerization from days/hours to minutes,[37] the acceleration of the hydrolysis of POx could be established.[38-39]

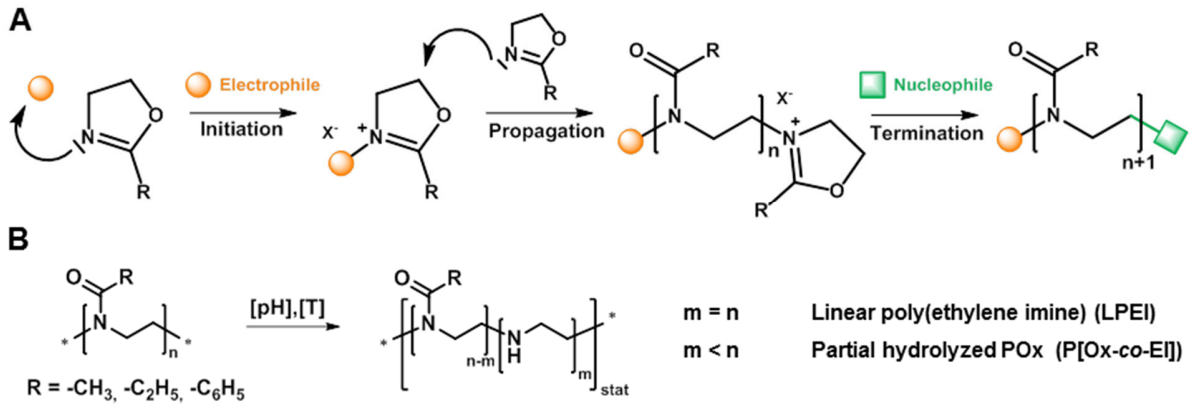

Scheme 1.1. Schematic representation of the A) mechanism for the cationic ring-opening polymerization (CROP) of poly(2-oxazoline)s and B) (partial) hydrolysis of poly(2-oxazoline)s.

Besides enabling for the full hydrolysis of POx, the microwave irradiation supports the tailored partial hydrolysis to yield poly(2-alkyl-2-oxazoline-*stat*-ethylene imine)s (P[Ox-*stat*-EI]) with defined monomer ratios (Scheme 1.1B, m < n).[38, 40] The partial hydrolysis of POx represents a unique opportunity to overcome the major drawbacks that come along with the net positive charge of PEI/polyplexes, comprising poor water solubility (at room temperature), severe cytotoxicity, aggregation and undesired non-specific interactions with cellular and non-cellular components, particularly *in vivo*.[41] A further powerful strategy is the post-hydrolysis chemical modification, comprising the transformation of the amine group of PEI *via* alkylation,

ring-opening of epoxides and carbonates, conjugate addition and acylation, among others.[24] Starting from commercially available LPEI, the design of biodegradable and more biocompatible LPEI – currently an ongoing challenge – *via* simple one-pot modification is described in Chapter 3.

An additional challenge to impart functionality for specific applications is to attach functional groups *via* *N*-acylation to the LPEI backbone. The resulting polymers are obtained by a post-polymerization modification and exhibit POx-like structures (pseudo-POx).[42] The installation of alkene functionalities enables the subsequent application of the thiol-ene photo-addition to attach specific functional groups. Chapter 4 describes the introduction of functional groups to the LPEI backbone, comprising primary amine groups for gene delivery applications and D-fructose moieties with selectivity for the GLUT5 transporter system in human breast cancer cells. Furthermore, the conjugation of glutathione moieties to the cationic backbone allows the transport of genetic material and, simultaneously, the passage through an hCMEC/D3 endothelial cell layer mimicking the highly selective blood-brain barrier within a microfluidically perfused biochip. The general structures of different generations of LPEI (1st, 2nd and 3rd generation) which are mentioned in the following chapters, are depicted in Figure 1.3.

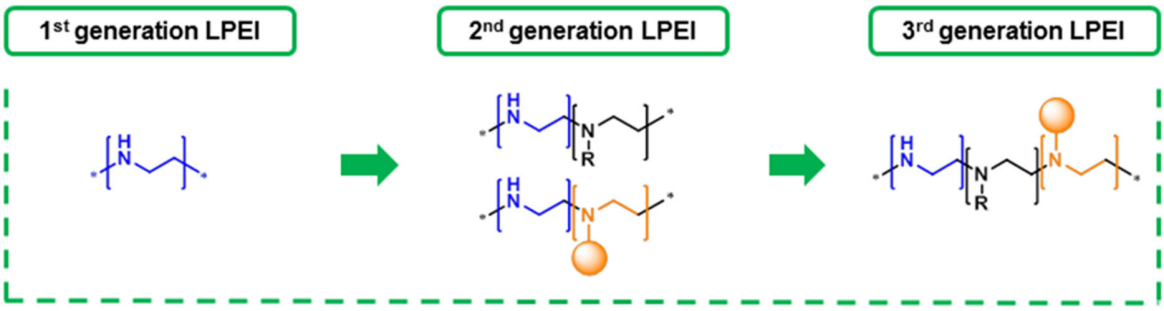

Figure 1.3. Schematic overview of different generations of linear poly(ethylene imine) (LPEI). Compared to the original LPEI (1st generation), the 2nd generation LPEI contains functional monomer units (black or blue) besides the ethylene imine units (blue). The 3rd generation LPEI describes the presence of multiple functional units comprising cationic functionalities (blue), cell viability increasing functional groups (black) as well as a third group of functionalities (orange, *e.g.* primary amine functionalities or targeting molecules).

While poly(2-oxazoline)s show no binding affinity to genetic material since they contain exclusively nitrogen in forms of amide functionalities, the use of suitable amine group containing 2-oxazoline monomers results in copolymers with excellent deoxyribonucleic acid (DNA) binding affinities which are described in Chapter 5. Notably, the absence of chain transfers and termination reactions using CROP under optimal conditions results in a high end-group fidelity that can be used to synthesize block copolymers by sequential addition of different monomers.

The overall aim of this thesis is the development of a versatile platform for the preparation of cationic polymers for biomedical applications, in particular gene delivery, based on POx. The convenient modification of these starting materials enables a straightforward tuning of the properties of the final cationic polymers and, thus, the application in various research fields. In future, this knowledge can be further applied for the straightforward preparation of various functional cationic systems. Even more complex systems seem to be accessible with the presented, convenient modification techniques.

2 POLY(2-OXAZOLINE) DERIVED PHARMAPOLYMERS OF THE 21ST CENTURY

Parts of this chapter will be published in: **P1**) C. Englert, J. C. Brendel, T. C. Majdanski, T. Yildirim, S. Schubert, M. Gottschaldt, N. Windhab, U. S. Schubert, *Adv. Healthcare Mater.*, submitted (2017/06/06).

The administration of genes is one of the main tasks within the area of pharmaceutical applications of cationic polymers. Since the early 1960s, controlled gene delivery has gained increasing interest and developed from macroscopic devices and implants to microscopic and nanoscopic systems.[43] The term "cationic pharmapolymers" covers synthetic cationic polymers based on an artificially produced polymeric backbone which are used for the administration of genes. They represent a useful alternative to liposomes, metal-organic frameworks (MOFs) and natural polymers (such as dextran, chitosan, hyaluronic acid) among others to fulfill the criteria of drug storage and delivery. On average, one out of 5,000 compounds that entered pre-clinical studies becomes an approved product after 10 years from the idea to the market entry.[44]

Cationic polymers that received market approval or are at least under clinical investigations are based on the polymer class of poly(ethylene imine) (PEI) and mainly occur in forms of nanoparticulate drug carriers. Different PEI formulations and modifications which allow overcoming the toxicity issues of pure PEI reveal promising results in clinical phases (Table 2.1). The hydrolysis of tailored poly(2-ethyl-2-oxazoline)s (PEtOx) results in linear PEI (LPEI) which is sold in a formulation under the trade name jetPEI®. One representative example is the polyplex SNS01-T, which is dissolved in a special buffer system and possesses a molar mass (M_n) around 22,000 g mol^{-1}. It contains a B-cell specific expression plasmid deoxyribonucleic acid (pDNA) as well as a small interfering ribonucleic acid (siRNA). The latter suppresses the hypusinated eukaryotic translation initiation factor 5A (eIF5A) which was found to sensitize myeloma cells to apoptosis (clinical phase II).[45] Another transfection agent based on jetPEI® is CYL-02, which is currently in clinical phase II for pDNA delivery. CYL-02 is intratumorally administered using endoscopic ultrasound in patients with pancreatic cancer and sensitizes cancer cells to chemotherapy.[46] Another system that uses the jetPEI® technology is the polyplex formation with pDNA, BC-819. The complex is intravenously administered and targets cancer cells that usually express the H19 gene (activation of diphtheria toxin A leads to cell death), whereas healthy cells

are not affected. In this way, BC-819 works as a "search and destroy" unit. For 2016, BioCancell announced the start of pivotal bladder cancer trials (phase III).[47] In addition, the company is working on a dual-DTA (diphtheria toxin A) expression system named BC-821 driven by the two core promoters H19 and the promoter segment IGF2-P4.[48] The system has the benefit of providing enhanced cell-killing potential as well as the increasing chance that at least one of the promoters will be active in any tumor.

The significant cytotoxicity of PEI is a tremendous challenge in the process of becoming an FDA approved product. The chemical modification of PEI represents a suitable tool to increase its biocompatibility. One pDNA/PEI-based formulation using this approach already entered clinical phase II.[49] In contrast to the former described formulations, EGEN-001 is based on low molar mass branched PEI (BPEI) which is covalently linked with poly(ethylene glycol) methyl ether and cholesterol.[50] EGEN-001 is directly injected into cancerous tissue where the local concentration of interleukin 12 (IL-12) is increased in the tumor microenvironment. IL-12 is one of the most active immunocytokines leading to a robust local and systemic immune response to cancer.[51] In 2014, Celsion Corp. acquired the EGEN Inc. including the product candidate EGEN-001, which was renamed as "GEN-1". Currently, the TheraSilence™ technology platform is used to advance EGEN-RNA-002, which is in preclinical development for the treatment of lung disease by the delivery of a RNA sequence.[52] Another representative based on modified PEI is DermaVir® (phase II). It is a topical application that contains a pDNA expressing all HIV proteins except integrase to induce T-cell mediated immune responses with broad specifity. The pDNA is formulated with a mannosylated jetPEI® in a glucose solution to target antigen-presenting cells (Langerhans cells - precursors of dendritic cells) and to protect the DNA from intracellular degradation.[53] DermaVir-transduced cells migrate from the skin to the draining lymph node and interdigitate as DermaVir-expressing, antigen-presenting dendritic cells.

Besides nanocarrier formulations, PEI has found its way to clinical studies even in a hydrogel-based device. The product, which is marketed under the trade name Aquatrix II™ by Hydromer Inc., consists of two separate aqueous solutions comprising poly(vinyl pyrrolidone) (PVP) and either chitosan or PEI.[54] Pharmaceutical ingredients can be loaded into the drug delivery matrices by the addition to the aqueous solution prior to the network formation.

Poly(2-oxazoline)s (POx) represent another polymer class that possesses significant potential for drug delivery applications and can be used as the precursor for the synthesis of cationic polymers (*e.g.* LPEI). POx are a rather new emerging class of synthetic polymers which has not been under clinical investigation so far. In October 2015, Serina Therapeutics started to recruit participants for a clinical phase I study of their POx-drug conjugate SER-214 (Table 2.1).[55] SER-214 is a PEtOx polymer conjugate of the FDA (Food and Drug Administration)-approved dopamine antagonist rotigotine, which displayed an impressive efficacy *in vivo*.[56] Its continuous dopaminergic stimulation profile represents a powerful tool in the treatment of Parkinson's disease. Beyond, Serina Therapeutics' POx polymer technology represents a unique injectable platform technology with distinct advantages in drug delivery applications. Latest investigations point through an enhanced interest in future POx-based materials. It could be shown that the cellular uptake is influenced by the choice of the oxazoline monomer and architecture.[57-58] Furthermore, *in vivo* studies revealed a low immune response as well as an increased circulation of POxylated proteins.[59] Luxenhofer *et al.* have recently summarized POx drug- and protein-conjugates and their preclinical results.[60]

The coupling of small molecule drugs, such as Ara-C or antibiotic ciprofloxacin, to POx resulted in similar behavior as comparable poly(ethylene glycol) (PEG) conjugates. The latter represent probably the most well-known examples for polymer conjugates. In contrast, the properties and the functionality of POx can be altered with a relative ease and render this polymer class a highly versatile alternative.

Table 2.1. Poly(2-oxazoline) derived pharmapolymers on the market or in clinical trials.

Name	Form	Polymer system	Drug	Indication/Use	Status
SNS01-T	Polyplex	LPEI (jetPEI®)	pDNA, siRNA	Multiple myeloma	Phase II (NCT01435720)
CYL-02	Polyplex	LPEI (jetPEI®)	pDNA	Pancreatic adenocarcinoma	Phase II (NCT02806687)
BC-819/PEI (DTA-H19)	Polyplex	BPEI	pDNA	Bladder cancer, ovarian cancer, pancreatic adenocarcinoma	Phase II (NCT00595088)
EGEN-001 (GEN-1)	Polyplex	Cholesterol and PEG-modified PEI	pDNA	Ovarian, tubal, colorectal peritoneal cancer	Phase II (NCT01118052)
DermaVir® (LC002)	Polyplex	Mannosylated LPEI (jetPEI®)	DNA	HIV vaccine	Phase II (NCT00711230)

Aquatrix II™	Hydrogel	PVP-Chitosan, PVP-PEI	*Broad range of cosmetic and drug ingredients*	Drug delivery matrices (*i.e.* transdermal)	Market
SER-214	Polymer-drug conjugate	POx	Rotigotine	Parkinson's Disease	Phase I (NCT02579473)

3 LINEAR POLY(ETHYLENE IMINE)S – MODIFICATION & APPLICATION

Parts of this chapter have been published in: **P2**) C. Englert, M. Hartlieb, P. Bellstedt, K. Kempe, C. Yang, S. K. Chu, X. Ke, J. M. García, R. J. Ono, M. Fevre, R. J. Wojtecki, U. S. Schubert, Y. Y. Yang, J. L. Hedrick, *Macromolecules* **2015**, *48*, 7420-7427; **P3**) C. Englert, M. Fevre, R. J. Wojtecki, W. Cheng, Q. Xu, C. Yang, X. Ke, M. Hartlieb, K. Kempe, J. M. García, R. J. Ono, U. S. Schubert, Y. Y. Yang, J. L. Hedrick, *Polym. Chem.* **2016**, *7*, 5862-5872.

3.1 Simple one-pot modifications of commercial linear poly(ethylene imine)

Commercially available linear poly(ethylene imine) (LPEI), which can be purchased *e.g.* from Polysciences, is commonly obtained by acidic hydrolysis of methyl-initiated poly(2-ethyl-2-oxazoline) (PEtOx). The main differences to self-made LPEI are the high dispersity, which results from the commercial precursor PEtOx, and the contents of uncleaved *N*-acyl groups (up to 10%).[24] However, commercial LPEI (in particular with M_w = 25,000 g mol^{-1}) represents still the status quo new transfection agents have to compete with.

One opportunity to simply modify commercial LPEI (**1**) in a one-pot reaction was previously described by MacDonald and co-workers.[61] The authors reported the oxidation of the secondary amine groups of branched PEI (BPEI) by hydrogen peroxide *via* the following intermediate species: Hydroxylamine (Scheme 3.1b),[62] nitrone (c),[63] and oxaziridine (d).[64] The ring-opening of the oxaziridine leads to a Beckmann-type rearrangement product and, subsequently, to the formation of a stable amide group (e). In this way, the structure of BPEI can be converted into a poly(glycine)-like structure with potential biocompatibility and biodegradability. The previous report mentioned the possible partial chain degradation (visible by the occurrence of carboxylic acid and aldehyde) which may occur from the oxidation (and subsequent hydrolysis) of the primary amines. For this reason, the oxidation of linear PEI was investigated since the polymer possesses no primary amine functionalities and can be characterized more easily.

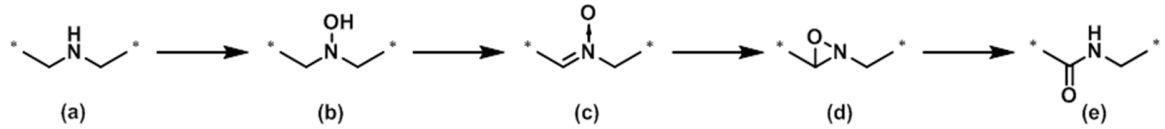

Scheme 3.1. Schematic representation of the oxidation mechanism of a secondary amine (a) *via* hydroxylamine (b), nitrone (c), and oxaziridine (d) intermediates to form the final amide group (e), as proposed by MacDonald *et al.*.[61]

Initial experiments focused on the identification of the optimal reagents and conditions to control the oxidation process. The influence of several parameters like time, temperature and concentration was investigated as well as the nature of the oxidizing agents. Surprisingly, common oxidizing agents such as oxone, *m*-chloroperoxybenzoic acid (mCPBA), or the White catalyst (palladium coordination complex) were outperformed by hydrogen peroxide when surveying the degree of oxidation (DO), which was calculated by proton NMR spectroscopy (for details see Chapter 3.2). Its simplicity together with the efficient purification process of the oxidized material (*i.e.* by precipitation in diethyl ether, centrifugal concentration with a molar cut-off of 3,000 g mol^{-1} followed by freeze-drying) makes this procedure straightforward. The oxidation of **1** is performed in methanol and turns it into a partially oxidized poly(ethylene imine-*stat*-glycine) (P(EI-*stat*-Gly)) consisting of unaffected ethylene imine and newly formed glycine units (Scheme 3.2A). Copolymers with different degrees of oxidation (20 to 85%, **2** to **5**) were synthesized and their structures are summarized in Table 3.1A.

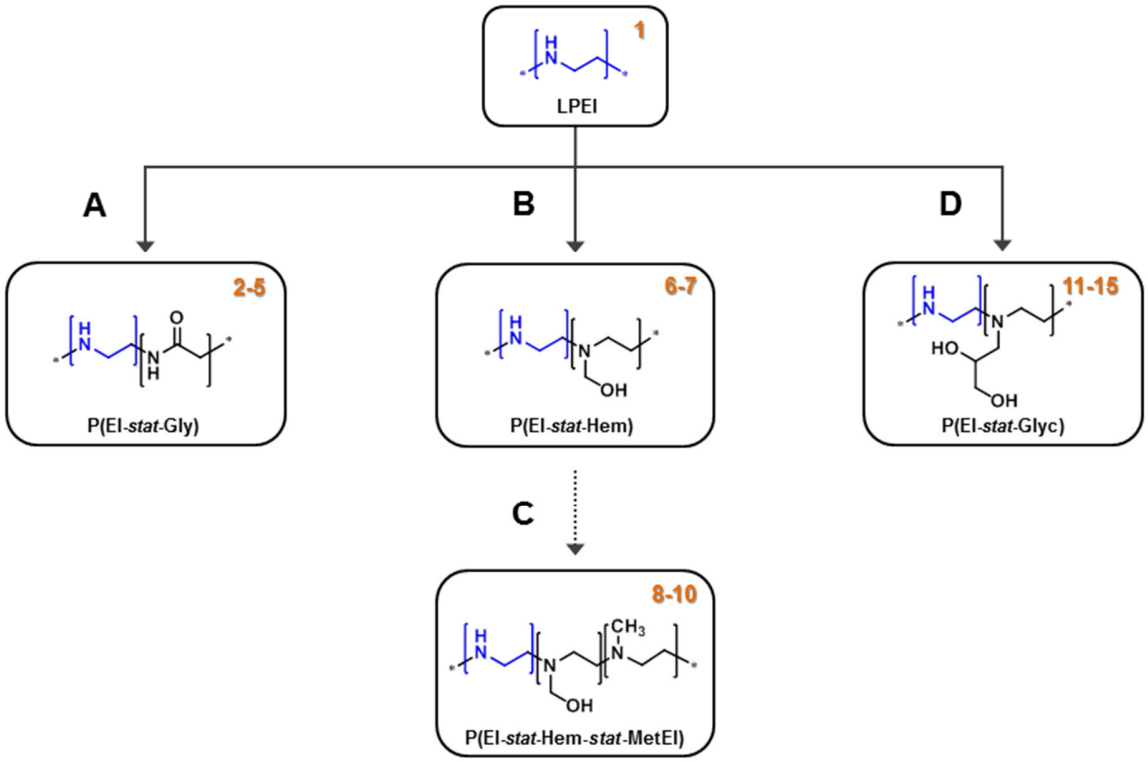

Scheme 3.2. Schematic representation of simple one-pot modifications of commercial linear poly(ethylene imine) (LPEI). A): H_2O_2, MeOH, r.t.. B): < 0.5 equiv. paraformaldehyde (pF), H_2O, 90 °C, 15 h. C): > 0.5 equiv. pF, H_2O, 90 °C, 15 h. D): Glycidol, MeOH, r.t., 20 h.

A second approach for a facile one-pot reaction is the carbohydrate-like modification of **1**. Previously, considerable efforts have been made to install carbohydrate-containing moieties on PEI due to their non-toxicity as well as their potential to target cells exhibiting carbohydrate-receptors. Amongst others, galactose,[65] mannose[66] and oligo-maltose[67] have been grafted successfully onto PEI. However, in most cases multiple step syntheses or harsh experimental conditions were required with often poor control over the composition. A facile and more economical modification strategy represents the installation of hydroxyl moieties in close proximity to the PEI backbone, in an effort to mimic the vicinal diols of sugars. Towards this goal, **1** was modified by a single-step reaction with hemiaminal moieties using paraformaldehyde (Scheme 3.2B and C) and by ring-opening of glycidol (Scheme 3.2D), *i.e.* reagents which are commercially available. The functionalization with different equivalents of paraformaldehyde (pF) per amine functionality (0.15 to 1.2 equiv.) was performed for 15 h at 90 °C in water and

resulted in copolymers with varying compositions (Table 3.1B). While the reaction of **1** with < 0.5 equiv. pF led to polymeric systems consisting of ethylene imine and hemiaminal units (**6**, **7**), *N*-methylation of the PEI backbone occurred for higher pF contents (> 0.5 equiv.) (**8** to **10**).

Table 3.1. Parameters for A) **1** and oxidized samples **2** to **5** and B) functionalized LPEI's **6** to **15**.

A

#	Abbr.	Composition [%]		M_n [g mol^{-1}]	
		a	b[a]	NMR[b]	SEC[c,d]
1	$LPEI_a$	~95		6500	1100
2	$P(EI_a\text{-}stat\text{-}Gly_b)$	80	20	6900	1500
3		60	40	7300	1400
4		33	67	7900	1700
5		15	85	8200	1600

B

#	Abbr.	Equivalents of funct. Agent
6	P(EI-*stat*-Hem)	0.15
7		0.30
8	P(EI-*stat*-Hem-*stat*-MetEI)	0.50
9		0.75
10		1.20
11	P(EI-*stat*-Glyc)	0.15
12		0.30
13		0.50
14		0.75
15		1.20

[a] "b" indicates the degree of oxidation (DO).

[b] Determined by ^{1}H NMR (calculated from LPEI 6,500 g mol^{-1},[68] ratio of PEI and Gly).

[c] Determined by SEC (eluent: DMAc + 0.21% LiCl, calibration against polystyrene standard).

[d] All samples are hardly soluble in the SEC eluent DMAc. Unfortunately, there is no calibration standard available for cationic polymers like LPEI and derivatives.

3.2 Characterization of modified linear poly(ethylene imine)s

In general, the characterization of cationic polymers, in particular LPEI and its derivatives, represents a tremendous challenge due to numerous interactions with column materials. In the cases presented above, the main challenge was to demonstrate the absence of polymeric degradation products. In the following different characterization methods are discussed which allowed to elucidate the molecular structures of the copolymers synthesized.

Proton nuclear magnetic resonance spectroscopy (^{1}H NMR). One of the simplest, fastest and often applied characterization techniques in polymer chemistry is the ^{1}H NMR. In particular, it can be used for the calculation of the polymer composition by comparing the integrals of the signals of different monomer units. For example, the DO of the oxidized P(EI-*stat*-Gly)s was

calculated from the integration of the ^{1}H NMR signals of the copolymer backbones *via* equation 1, where B is the integral of the Gly, A the integral of the ethylene imine, and D the integral of the remaining EtOx units at 1 ppm after incomplete hydrolysis (provided that A << F).

$$DO = \frac{2\left(B-\frac{4}{3}D\right)}{2\left(B-\frac{4}{3}D\right)+A} \quad (1)$$

A comparison of the ^{1}H NMR spectra of the precursor **1** and **2** to **5** is depicted in Figure 3.1A. A higher H_2O_2 concentration resulted in an increasing integral of signal C (7.9 ppm) which represents the formed amide group. Its appearance is rather surprising and cannot be used for quantification of the DO due to proton exchange processes in D_2O. A further evidence for a successful oxidation is the downfield shift of the signal A (EI) to the signal B (Gly). Previous kinetic investigations allowed the adjustment of defined DOs (**2**: 20, **3**: 40, **4**: 67, **5**: 85%) *via* temperature and time controlled reaction. The development of the DO over the time is presented in Figure 3.1B for different temperatures ranging from –20, 0, and 8 to 18 °C.

The molar masses for **1** in Table 3.1A, and, therefore, for the oxidized copolymers **2** to **5**, are based on literature reported values. Indeed, commercial LPEI (Polysciences, M_w = 25,000 g mol^{-1}) has been investigated by several research groups and revealed molar masses (M_n) below 10,000 g mol^{-1}.[68]

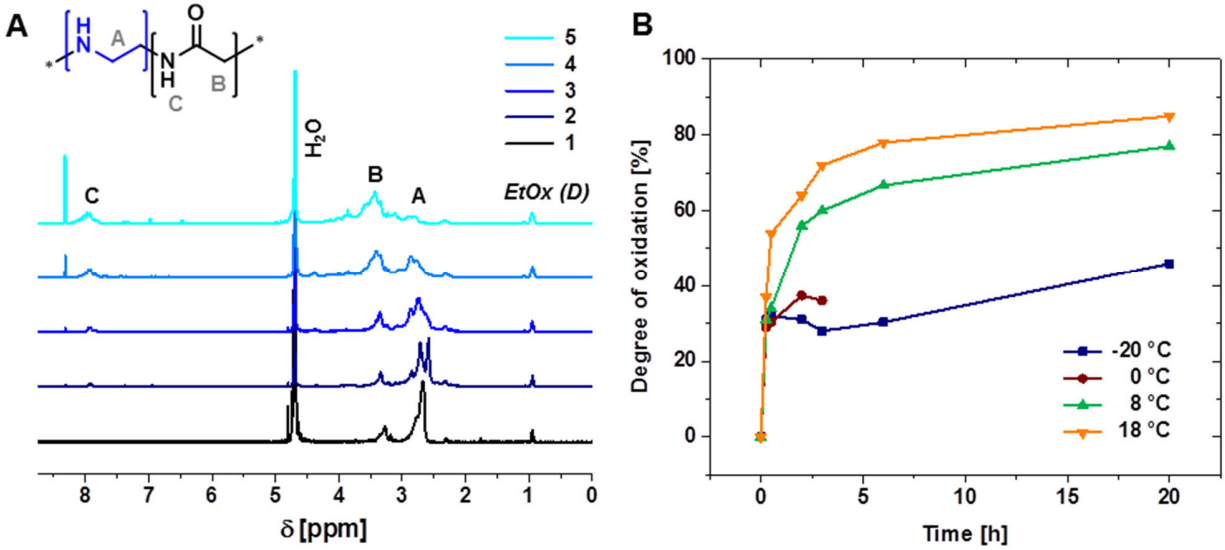

Figure 3.1. A) ^{1}H NMR spectra of **1** and oxidized samples **2** to **5** (D_2O, 400 MHz). B) Kinetic studies of the oxidation of **1** at different temperatures with a 4-fold excess of H_2O_2. Degrees of oxidation were calculated from ^{1}H NMR spectra (D_2O, 400 MHz).

In the case of the carbohydrate-mimicking modifications, various concentrations of pF and glycidol, respectively, were used to synthesize copolymers with different compositions. Using pF, the copolymers **6** to **10** were obtained (Figure 3.2A). An increasing signal C occurred with higher concentration of pF, which is attributed to hemiaminal species. With 0.5 equivalents of pF or higher (**8** to **10**), methylation of the backbone was observed.[69] The methyl group could be identified by DEPT 135/90 NMR experiments (distorsionless enhancement by polarisation transfer) and is the result of an Eschweiler-Clarke-type rearrangement, whereas the iminium intermediate (in the form of a secondary amine) is reduced to the corresponding tertiary amine.[33, 70] This side reaction limits the amount of hemiaminal moieties that can be attached. Using glycidol to modify **1** through a straightforward ring-opening reaction under mild and catalyst free conditions[71] yielded copolymers **11** to **15**. ^{1}H NMR spectroscopy was used once again to track the impact of the increasing epoxide concentration (Figure 3.2B).

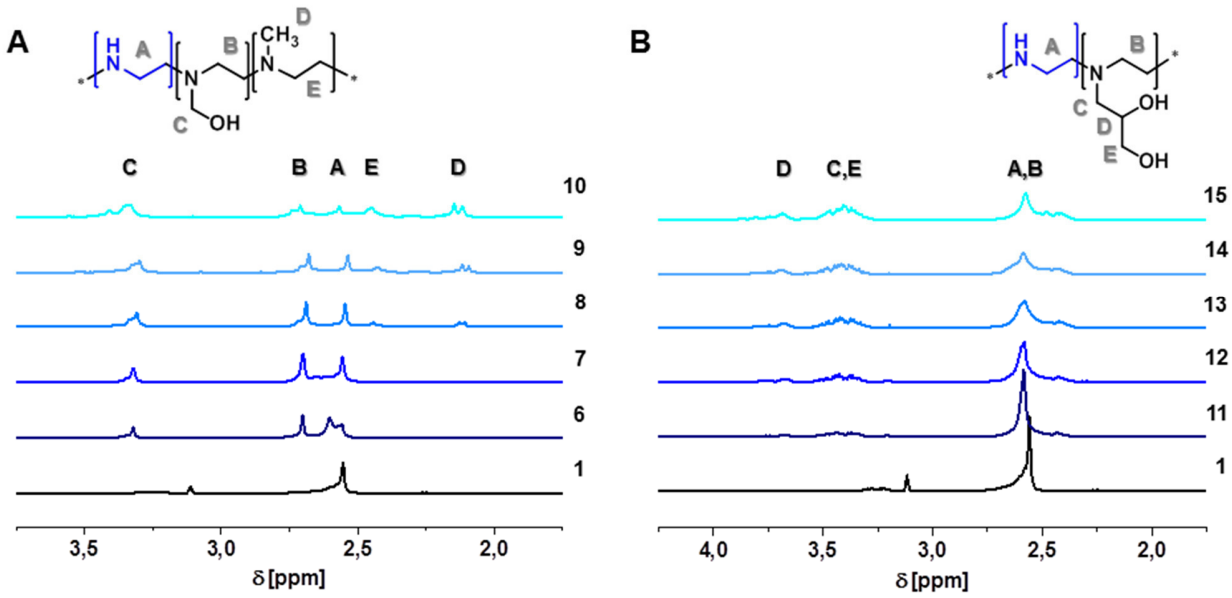

Figure 3.2. ^{1}H NMR spectra of **1** modified with varying contents of A) paraformaldehyde resulting in **6** to **10**, respectively (D_2O, 400 MHz) and, B) glycidol resulting in **11** to **15** (D_2O, 400 MHz).

Diffusion-ordered NMR spectroscopy (DOSY NMR). DOSY NMR represents a helpful technique to confirm the presence of a single (polymeric) species, as indicated by a defined diffusion coefficient and, furthermore, the absence of degradation processes leading to lower molar mass species. Using literature values, the molar mass of LPEI could be determined by DOSY NMR as 4,200 g mol^{-1} by the help of the Mark-Houwink equation.[72] A DOSY NMR spectrum for the oxidized sample **4** is presented in Chapter 3.3, Figure 3.5B.

Size exclusion chromatography (SEC). The poor solubility in common solvents and the known interactions of the cationic polymers with the column material hinder a successful determination of molar masses of the polymeric samples by SEC, a commonly used method for the characterization of polymers. However, **1** to **5** could be dissolved in *N*,*N*-dimethylacetamide (DMAc) at low concentrations and the SEC traces indicate a successful modification without degradation (Figure 3.3A). A missing calibration for cationic polymers complicates a determination of accurate molar masses (see Table 3.1A). Due to the molar masses (M_n) < 10,000 g mol^{-1}, asymmetric field flow fractionation (AF4) coupled to a MALLS (multi-angle laser light scattering) detector cannot be used for a successful determination of the molar masses.

Fourier transform infrared spectroscopy (FTIR). FTIR represents a straightforward and efficient method to investigate the vibrations of different bonds. The IR spectra of polymers **1** to **5** are shown in Figure 3.3B and can be interpreted with regard to literature reports about polyglycine.[73-75] The main vibration at 1660 cm^{-1} results from the carbonyl stretching vibration of the newly formed glycine unit.[76] Potential degradation products, *e.g.* carboxylic acid derivatives, are expected to occur at wavenumbers over 1700 cm^{-1},[77] however, they were not observed. Increasing DOs lead from nearly no carbonyl vibrations (for **1**) to intense carbonyl bands (**2** to **5**). The vibration at 1600 cm^{-1} is likewise attributed to the amide mode. The CH_2 bending and wagging modes of the formed glycine result in vibrations between 1440 and 1340 cm^{-1}.

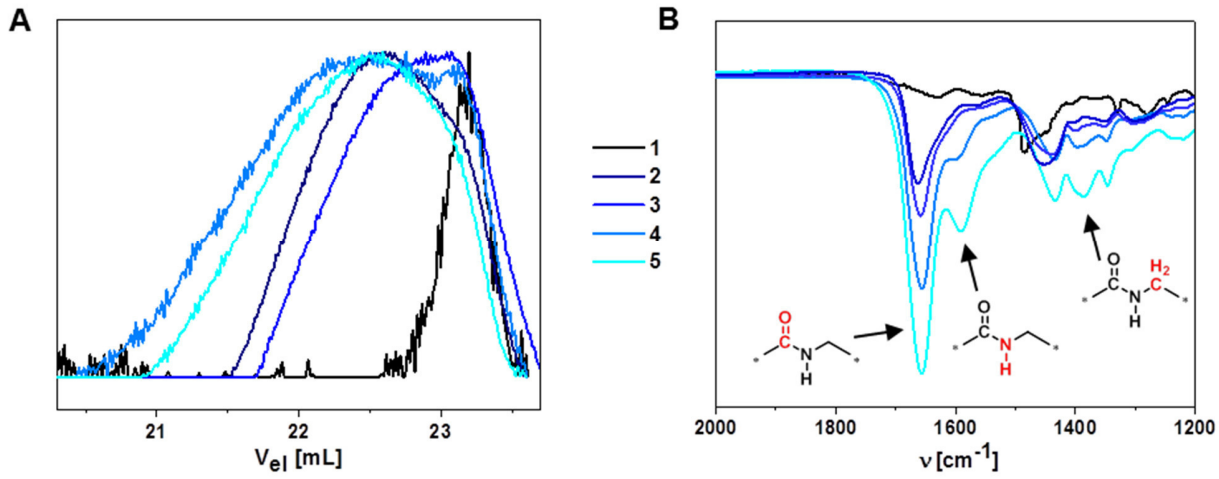

Figure 3.3. A) Size exclusion chromatography traces of **1** to **5** (*N*,*N*-dimethylacetamide, 0.21% LiCl). B) IR spectra of **1** and oxidized samples **2** to **5** in the wavenumber range from 1200 to 2000 cm^{-1}.

3.3 Biocompatibility and -degradability

As previously mentioned, one important parameter of a polymer candidate for biomedical applications is its biocompatibility, which describes the ability to be in contact with a living system without producing an adverse effect.[78] For this purpose, *in vitro* studies were performed on chosen modified PEIs (**2** to **12**) to evaluate their cell viability in the model mammalian cell line human embryonic kidney 293 (HEK 293). The copolymers were compared to commercial LPEI which induces a toxic effect (cell viability < 80%) already at very low concentrations

(< 6.25 µg mL^{-1}). The oxidized LPEIs (**2** to **5**) show cell viability up to a concentration of 25 µg mL^{-1} (Figure 3.4A). Apparently, the degree of oxidation (DO) strongly influences the cell viability. While cell viability values drop below 60% after incubation with **2** at 50 µg mL^{-1} for 48 h, an oxidation degree of 85% (**5**) still does not induce harmful effects even at higher concentrations (200 µg mL^{-1}). Unfortunately, the modification of LPEI with pF (**6** to **10**) and glycidol (**11**, **12**), respectively, did not allow for a significant improvement of the biocompatibility for lower degrees of functionalization (Figure 3.4B). But the use of more than 0.5 equiv. pF (*vs.* -NH) induced *N*-methylation of the backbone, which increased the cell viability by lowering the net positive charge of **1**.[79] A crucial fact for the similar toxicity of pF-modified copolymers **6** to **9** compared to **1** is the instability of hemiaminal moieties at acidic pH values, releasing formaldehyde under endosomal conditions. As expected, the increase of the glycidol content resulted in decreasing cytotoxicities.

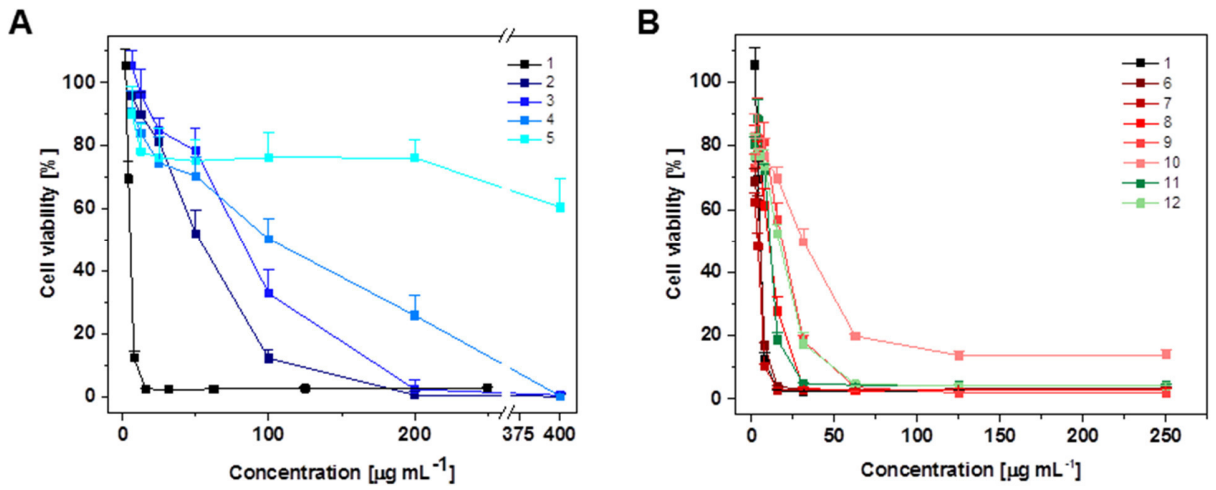

Figure 3.4. Cytotoxicity of A) **1**, oxidized samples **2** to **5** and B) functionalized samples **6** to **10** and **11**, **12** by MTT assay on HEK 293 cells.

Another important parameter for biomedical applications is the interaction of polymers with serum proteins. Therefore, DLS measurements were performed after treatment with fetal bovine serum (FBS) (Figure 3.5A). The starting LPEI (**1**) could not be investigated since its addition to serum immediately resulted in a precipitation of protein components. The Z-average values of the investigated copolymers **2** to **5** were indistinguishable from pure FBS (untreated control sample)

and, therefore, indicated no further aggregation as well as polymer stability in the presence of serum proteins over 48 h. This behavior only demonstrates the absence of serum coagulation, while an interaction of protein and polymer is still possible.

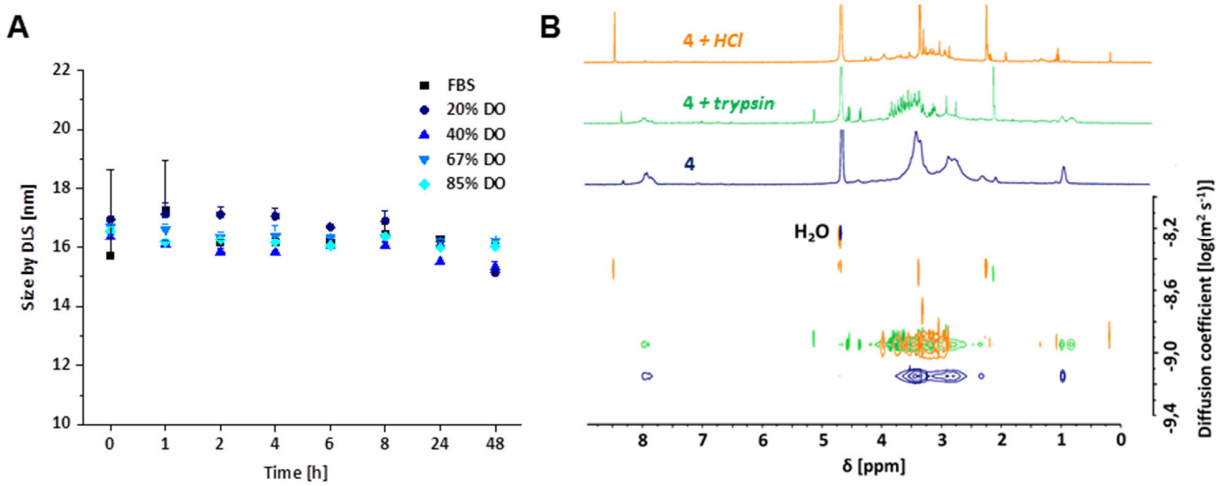

Figure 3.5. A) Serum stability by time-dependent DLS measurements of FBS in the presence of oxidized samples **2** to **5**. B) DOSY NMR of oxidized sample **4** before (blue) and after treatment with 6 mol L^{-1} aqueous hydrogen chloride (orange) and peptidase (trypsin) (green). The solvent signal was used for calibration (D_2O, 400 MHz, 25 °C).

Besides the described cytotoxicity of LPEI, the non-biodegradability represents another challenge that must be overcome. Different literature reports have claimed biodegradable PEI derivatives *via* end-group modification of PEI[80-82] or side chain functionalization with degradable linkers.[83] However, none of these reports describe the full degradation of the polymer backbone. The incorporation of a defined number of amide groups in the backbone of LPEI *via* oxidation would enable biodegradation. To investigate the decomposition behavior, copolymer **4** with a DO of 67% was chosen as a model system and subjected to acidic (6 M hydrochloric acid) and enzymatic (trypsin) conditions. Diffusion-ordered NMR spectroscopy (DOSY NMR) was utilized to confirm successful degradation (Figure 3.5B). While the unmodified polymer **1** revealed no changes under these conditions, the copolymer **4** exhibited increased diffusion coefficients as well as a fractionation of the signals. Furthermore, the ^{1}H NMR spectra revealed sharp and undefined signals. Further evidence is given by the reduction of the peak intensity of the amide bond at 7.9 ppm, which completely disappears upon treatment with hydrochloric acid.

At the same time, the intensity of the sharp signal at 8.45 ppm increases, which is probably attributed to degradation products.

In summary, the specific improvement of the (bio)-properties, such as biodegradation and biocompatibility, was demonstrated and helps to overcome the main drawbacks of commercial LPEI.

4 PSEUDO-POLY(2-OXAZOLINE)S – SYNTHESIS & APPLICATION

Parts of this chapter have been published in: **P4**) C. Englert, A. M. Schwenke, S. Hoeppener, C. Weber, U. S. Schubert, *Adv. Polym. Sci.* **2015**, *274*, 209-240; **P5**) T. Bus, C. Englert, M. Reifarth, P. Borchers, M. Hartlieb, A. Vollrath, S. Hoeppener, A. Traeger, U. S. Schubert, *J. Mater. Chem. B* **2017**, *5*, 1258-1274; **P6**) C. Englert, A.-K. Trützschler, M. Raasch, T. Bus, P. Borchers, A. S. Mosig, A. Traeger, U. S. Schubert, *J. Control. Release* **2016**, *241*, 1-14; **P7**) C. Englert, M. Pröhl, J. A. Czaplewska, C. Fritzsche, U. S. Schubert, A. Traeger, M. Gottschaldt, *Macromol. Biosci.* **2017**, *17*, 1600502.

4.1 Post-polymerization modification of linear poly(ethylene imine)

One opportunity to install different functionalities on a linear poly(ethylene imine) (LPEI) backbone is the hydrolysis of functional poly(2-oxazoline)s (POx), where parts of the functional groups are cleaved off and form ethylene imine units. Since most of the POx functional groups, *e.g.* alkene functionalities, do not withstand the acidic or basic hydrolysis, the post-polymerization modification of LPEI *via N*-acylation represents a meaningful alternative. As a result, poly(2-oxazoline)-like structures (pseudo-POx) are obtained. To enable reproducible modification steps including detailed characterization and evaluation, the precursor LPEI was synthesized in our lab in a well-controlled manner using a microwave synthesizer.

Microwave-assisted synthesis approaches have been reported frequently over the last years. Amongst others, they can be used for the synthesis of well-defined high molar mass poly(2-alkyl-2-oxazoline) (PAlkOx) under inert conditions and their subsequent hydrolysis. In particular, the hydrolysis has been the focus of numerous literature reports. Besides an acceleration of the reaction, the degree of hydrolysis can be easily controlled using different reaction conditions. Using 2-methyl- (MeOx) or 2-ethyl-2-oxazoline (EtOx), the microwave irradiation allows the synthesis of LPEI with EI contents up to 99% and chain lengths of 200 (Table 4.1).[39] An increase of the reaction temperature (up to 180 °C) while using comparatively low acid concentrations has proven to significantly accelerate the full hydrolysis.[40] Furthermore, the use of an ethanol-water mixture enables the differentiation of the hydrophilic poly(2-methyl-2-oxazoline) (PMeOx) and poly(2-ethyl-2-oxazoline) (PEtOx).[84] The tailored hydrolysis of statistical or block copolymers, consisting of different 2-alkyl-2-oxazoline monomer units, allows the synthesis of copolymers

with defined compositions. While the hydrophilic oxazoline units show an enhanced hydrolysis rate, the cleavage of the hydrophobic part is almost inhibited. The different properties of the monomers can be used to synthesize block copolymers, such as poly(2-phenyl-2-oxazoline-*block*-ethylene imine) which exhibits thermoresponsive micellization behavior.[85]

Table 4.1. Overview of microwave-assisted hydrolysis of poly(2-oxazoline)s.

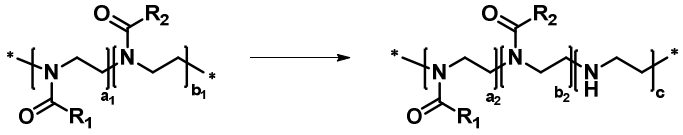

Precursor architecture	R_1	R_2	$(a_1 + b_1)$ [units]	c [%]*	a_2 [%]	b_2 [%]	Hydrolysis conditions	Ref.
Homopolymer	CH_3	-	5-200	99	1	-	HCl (16 wt%), 100 °C	38
	C_2H_5							
Homopolymer	C_2H_5	-	10-200	99	1	-	HCl (16 wt%), 130 °C	39
Homopolymer	C_2H_5	-	30, 500	95	5	-	HCl (3 wt%), 180 °C	40
Homopolymer	C_2H_5	-	100	95	5	-	HCl (16 wt%), 160 °C	86
	n-C_9H_{19}			87	13	-		
Homopolymer	CH_3	-	100	95	5	-	HCl (12 wt%), 100 °C, EtOH:H_2O 4:1	84
	C_2H_5			22	68	-		
	C_6H_5			13	87	-		
Block copolymer	CH_3	C_2H_5	$a_1 = 50$ $b_1 = 50$	48	37	15		
		C_6H_5	$a_1 = 60$ $b_1 = 15$	78	18	4		
Statistical copolymer	CH_3	C_6H_5	$a_1 = 60$ $b_1 = 40$	98	2	0	HCl (16 wt%), 100 °C	85
				59	21	20	NaOH	
Block copolymer				84	16	0	HCl (16 wt%), 100 °C	
				42	36	23	NaOH	

* The maximum degree of hydrolysis can be determined only within the limits of the ^{1}H NMR accuracy.

In order to fulfill the requirements for genetic interactions, well-defined high molar mass PEtOx (**16**) was synthesized with a degree of polymerization of 575 (Đ = 1.3), as starting material.[28] Subsequently, the homopolymer was hydrolyzed in 6 M hydrochloric acid at 100 °C under microwave irradiation (Scheme 4.1A).[38] Kinetic studies were performed in order to obtain cationic polymers with desired contents of EI. The partial hydrolysis resulted in

poly(2-ethyl-2-oxazoline-*stat*-ethylene imine) with an EI content of 46% (**17**), while the full hydrolysis provided LPEI with > 95% EI content (**24**).

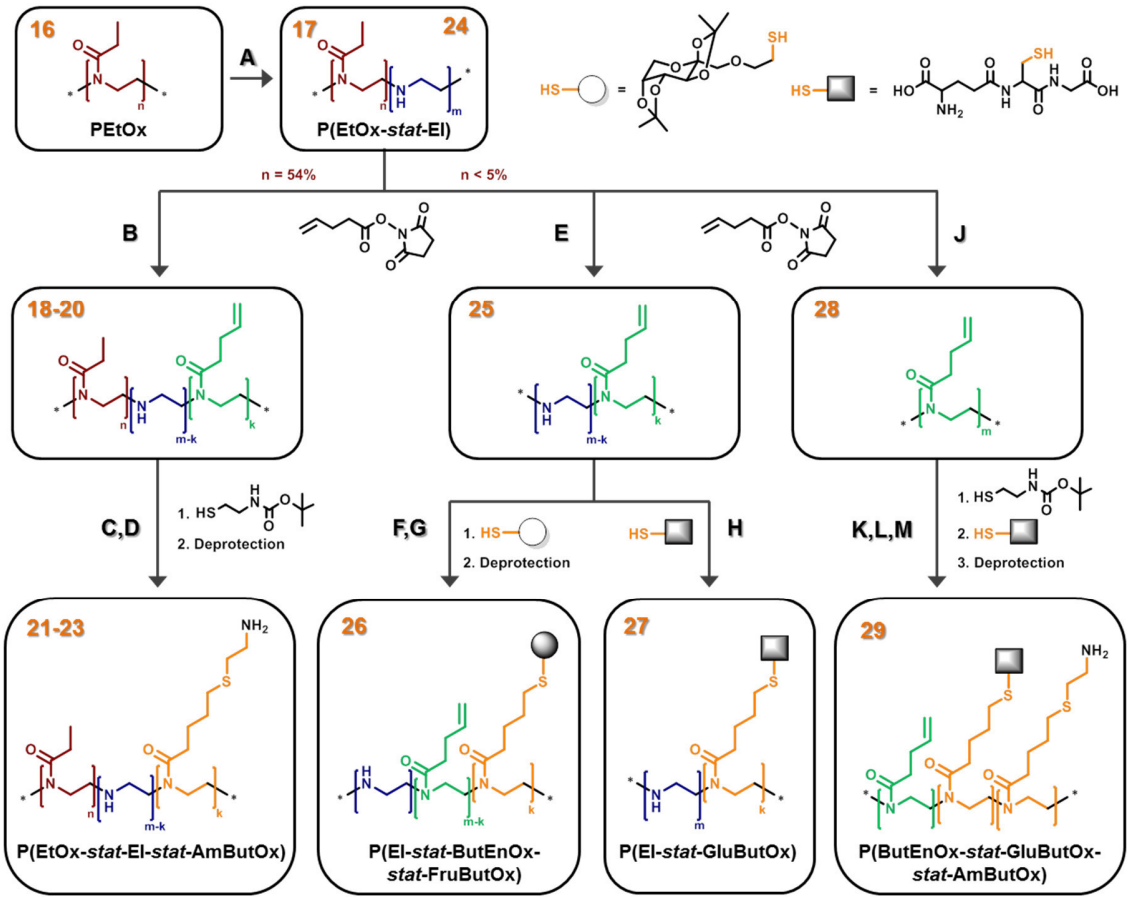

Scheme 4.1. Schematic representation of the synthesis of different pseudo-poly(2-oxazoline)s (**16** to **29**). A) 6 M HCl, µW, 100 °C, 100 min. B), E) and J) *N*-succinimidyl-4-pentenate, 4-*N*,*N*-dimethylamino-pyridine, pyridine, 80 °C, 20 h. C) and K): 2-(Boc-amino)ethanethiol, 2,2-dimethoxy-2-phenylacetophenone, MeOH, 365 nm, r.t., 20 h. D) and M): Trifluoro acetic acid, CH_2Cl_2, 20 h, r.t.. F): 2,2-Dimethoxy-2-phenylacetophenone, MeOH, 365 nm, r.t., 18 h. G): 2 M HCl, THF/H_2O, 40 °C, 12 h (grey circle = deprotected D-fructose). H) and L): Irgacure® 2959, milli-Q H_2O, 365 nm, r.t., 17 h.

Using *N*-succinimidyl-4-pentenate, a post-polymerization modification was performed to install 2-butenyl-2-oxazoline (ButEnOx) units on the PEI backbone (Scheme 4.1B, E, J).[42] Different polymer compositions were obtained by using P(EtOx-*stat*-EI) (**17**) or LPEI (**24**) as starting material for the modification. In all cases, the presence of alkene functionalities enables

their application in thiol-ene photo-addition reactions and the simple attachment of various target molecules. Three different copolymers of P(EtOx-*stat*-EI-*stat*-ButEnOx) (**18** to **20**) with varying contents of secondary amines and ButEnOx (1:3, 1:2, 1:1) were obtained from **17**, while the EtOx content remained constant (54%). An overview of the different polymer compositions is given in Table 4.2. The installation of primary amine functionalities was performed likewise by thiol-ene click reaction. For this purpose, 2-(boc-amino)ethanethiol was used to modify **18** to **20** (Scheme 4.1C, D), resulting in P(EtOx-*stat*-EI-*stat*-AmButOx) after deprotection (**21** to **23**). The post-polymerization modification of **24** allowed the synthesis of P(EI-*stat*-ButEnOx) containing an EI content of 73% (**25**) as well as the homopolymer P(ButEnOx) (**28**). The copolymer **25** was functionalized with a protected thio-fructose (Scheme 4.1F), which was obtained by a five-step synthesis (not shown). However, full conversion of the alkene functionalities could not be achieved even after stepwise photo-addition. One reason might be the steric hindrance of the bulky side chains (*iso*propylidene protecting groups). Deprotection resulted in P(EI-*stat*-ButEnOx-*stat*-FruButOx) (**26**) with 16% D-fructose content (Scheme 4.1G). By using the same copolymer **25** as a precursor, L-glutathione (GSH) moieties were attached *via* the previously described thiol-ene photo-addition (Scheme 4.1H). Surprisingly, in this case the final polymer P(EI-*stat*-GluButOx) (**27**) contained no unmodified ButEnOx (as observed for **26**). Limited solubility properties of GSH require the photoinitiator Irgacure® 2959 to be used to run the click reaction in water. In another approach, polymer **28** was modified in a first step with primary amine moieties (2-(boc-amino)ethanethiol) (Scheme 4.1K), followed by the introduction of GSH using the previously described synthesis of **27** (Scheme 4.1L). The deprotection (Scheme 4.1M) resulted in the final polymer P(ButEnOx-*stat*-AmButOx-*stat*-GluButOx) (**29**). All modified PEI based products were water soluble.

Table 4.2. Parameters for pseudo-poly(2-oxazoline)s and their precursors (**16** to **29**) with a DP of 575.

		Composition [%]						NMR[a]	AF4		SEC	
#	Name	a	b	c	d	e	f	M_n [g mol^{-1}]	M_n [g mol^{-1}]	Đ	M_n [g mol^{-1}]	Đ
16	$PEtOx_a$	100						57,000	57,000	1.2	69,000[b]	1.3
17	$P(EtOx_a$-*stat*-$EI_b)$	54	46					42,100	31,300	1.3	48,000[b]	1.3
18		54	12	34				58,100	25,500	1.4	36,000[b]	2.1
19	$P(EtOx_a$-*stat*-EI_b-*stat*-$ButEnOx_c)$	54	17	29				55,800	30,900	1.3	34,500[b]	1.6
20		54	23	23				53,000	30,400	1.3	36,000[b]	1.6
21		54	12		34			73,200	35,300	1.7	30,500[b]	1.6
22	$P(EtOx_a$-*stat*-EI_b-*stat*-$AmButOx_d)$	54	17		29			68,600	43,700	1.7	39,000[b]	1.6
23		54	23		23			63,100	30,500	1.6	31,500[b]	1.5
24	$LPEI_b$	<5	>95					24,800	9,900	1.4	n.d.	n.d.
25	$P(EI_b$-*stat*-$ButEnOx_c)$	<5	73	27				37,500	n.d.	n.d.	31,400[c]	1.2
26	$P(EI_b$-*stat*-$ButEnOx_c$-*stat*-$FruButOx_e)$	<5	73	11		16		59,600	n.d.	n.d.	9,800[b]	1.2
27	$P(EI_b$-*stat*-$GluButOx_f)$	<5	73				27	85,200	21,000	2.0	n.d.	n.d.
28	$P(ButEnOx_c)$	<5		>95				71,900	n.d.	n.d.	44,000[c]	1.5
29	$P(ButEnOx_c$-*stat*-$AmButOx_d$ -*stat*-$GluButOx_f)$	<5		10	82		8	122,300	63,300	1.8	n.d.	n.d.

[a] Determined by ^{1}H NMR (calculated from PEtOx: 57,000 g mol^{-1} (ratio of tosylate and CH_2-CH_3 signal))

[b] SEC: DMAC, 0.21% LiCl, against PS; [c] SEC: $CHCl_3$/*i*PrOH/NEt_3 94:2:4, against PS

n.d. – not determined, due to insolubility in SEC eluent or undesired interactions with the column/membrane

4.2 Characterization of pseudo-poly(2-oxazoline)s

As already mentioned, the characterization of cationic polymers represents a significant challenge. However, the installation of hydrophilic moieties on the pseudo-POx backbone allows a more comprehensive characterization as for modified commercial LPEI (Chapter 3.2).

Size exclusion chromatography (SEC) and asymmetric field flow fractionation (AF4). SEC represents a suitable method to determine the molar masses of polymeric species. Another well-established method for the detailed characterization is AF4 (RC membrane with molar mass cut-off 10,000 g mol^{-1}). Both methods were used to investigate the synthesized copolymers and the respective precursors. In some cases, the different solubilities of both species limited the choice of the characterization method. The SEC traces for the synthesis of the copolymer **22** and the corresponding precursors **16**, **17** and **19** are shown in Figure 4.1. In general, the molar masses determined by SEC (ranging from 9,800 to 69,000 g mol^{-1}) are lower than the calculated values by ^{1}H NMR (24,800 to 122,300 g mol^{-1}) (see Table 4.2). One explanation is the presence of cationic amine units (primary and secondary) as well as alkene functionalities, which leads to undesired column and membrane interactions, and, therefore, to a change in the elution behavior. Additionally, suitable SEC calibration standards for cationic systems are not available.

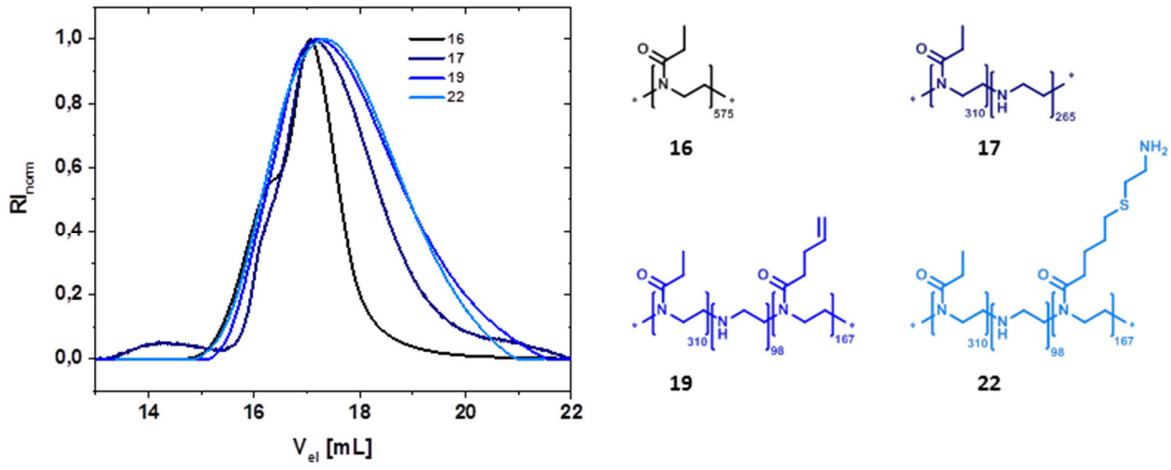

Figure 4.1. Size exclusion chromatography traces of the starting homopolymer **16** and the corresponding copolymers **17**, **19** and **22** (*N*,*N*-dimethylacetamide, 0.21% LiCl, calibration: polystyrene).

Proton nuclear magnetic resonance spectroscopy (^{1}H NMR). A useful characterization method to determine the polymer composition is ^{1}H NMR spectroscopy. The installation of primary amine functionalities starts with the partial hydrolysis of PEtOx (**16**), confirmed by the presence of EtOx as well as EI units (copolymer **17**, Figure 4.2A). Since the signals of the EtOx side chain (A, B) and the backbone (C) remain constant during the modification steps, they can be used as

reference. The successful modification with *N*-succinimidyl-4-pentenate is shown by the proton signals of the double bond that appear at 5.9 ppm (-*H*C=CH_2, signal H) and 5.1 ppm (-HC=C*H*$_2$, signal I) for the copolymer **20**. The signals H, D (EI backbone) and A (methyl protons of the EtOx side chain) are used to calculate the composition of the formed copolymers. Within the next step – the photo-addition of 2-(boc-amino)ethanethiol – the double bond signals disappear and the protected copolymer ***boc*23** is obtained. Besides the signals of the newly formed CH_2 groups at 2.40 (signal I′) and 1.70 ppm (signal H′), a singlet of the *tert*-butyloxycarbonyl (*boc*) protecting group is obtained at 1.50 ppm (signal L). After treatment with trifluoroacetic acid and precipitation in diethyl ether, the successful deprotection of ***boc*23** is confirmed by the disappearance of the protecting group to yield the final copolymer P(EtOx-*stat*-EI-*stat*-AmButOx) (**23**).

The successful installation of alkene moieties on LPEI (**24**) yielded the copolymer **25** (27% degree of functionalization, Figure 4.2B). Its composition was calculated from the integrals of the signals of the double bond (signal H) and the signals of the EI backbone (signal D). Since the EI units are not used for further modifications, their content remains constant (73%) during the following reactions. The successful attachment of 1-*O*-(2-mercapto-ethyl)-2,3:4,5-di-*O*-*iso*propylidene-β-D-fructopyranoside (for a schematic representation of the structure see Scheme 4.1) is shown by the appearance of D-fructose related signals between 4.6 and 3.4 ppm and the decrease of the signals of the double bond after thiol-ene photo-addition (***iso*26**, Figure 4.2B). After treatment with hydrochloric acid, neutralization, and dialysis against water (cut-off: 3,500 g mol^{-1}) the signals of the *iso*propylidene protecting groups between 1.5 and 1.1 ppm (signal L) disappeared, indicating the successful deprotection and formation of the final copolymer P(EI-*stat*-ButEnOx-*stat*-FruButOx) (**26**). The cleavage of the protecting group resulted in the formation of a hemiketal structure and, therefore, in an equilibrium of pyranoses, furanoses and an open-chain form which turns the interpretation of the spectra into a challenging task. However, two-dimensional NMR spectroscopy, in particular heteronuclear single quantum coherence NMR (HSQC NMR), can be utilized to assign the signals according to the literature.[87]

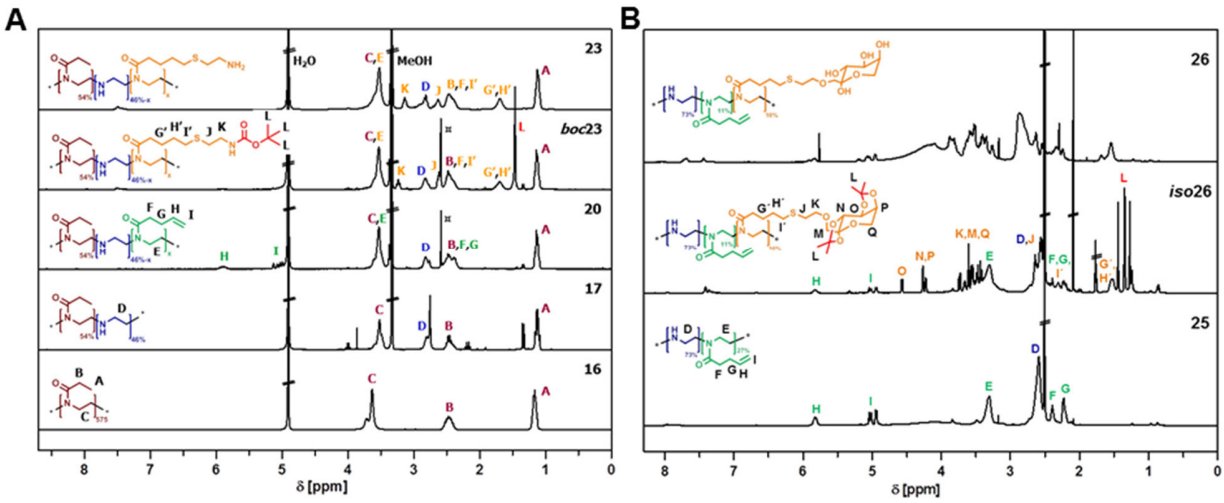

Figure 4.2. Comparison of the ^{1}H NMR spectra of A) the starting homopolymer **16** (PEtOx), the precursors **17**, **20** and ***boc*23** and the final product **23** (¤ side product *N*-hydroxysuccinimide) (300 MHz, MeOD) and B) the precursor copolymer **25**, the protected D-fructose copolymer ***iso*26** and the final product **26** (600 MHz, DMSO-d_6).

In contrast to the sugar-functionalization, the attachment of L-glutathione (GSH) to the copolymer **25** resulted in the disappearance of the alkene functionalities and confirmed the quantitative functionalization (**27**). Besides the additional protons observed after the thiol-ene photo-addition (signal H´ and I´), the signals of GSH can be assigned to the respective protons (Figure 4.3A). The specific signal for the CH group of the cysteine unit appears at 4.54 ppm (signal H). A second approach was the attachment of side chains bearing primary amine groups and GSH moieties to PButEnOx (**28**). The synthesis of the homopolymer (functionalization > 95%) was confirmed by the disappearance of the signals assigned to the EI backbone (between 3.70 and 3.20 ppm) (Figure 4.3B). The successful preparation of the copolymer **29** after stepwise thiol-ene click reaction of GSH and 2-(boc-amino)ethanethiol is shown by the CH_2 signals nearby the amine group at 2.8 ppm, the signal of the boc-protecting group which disappears after deprotection (1.4 ppm) and the specific GSH protons.

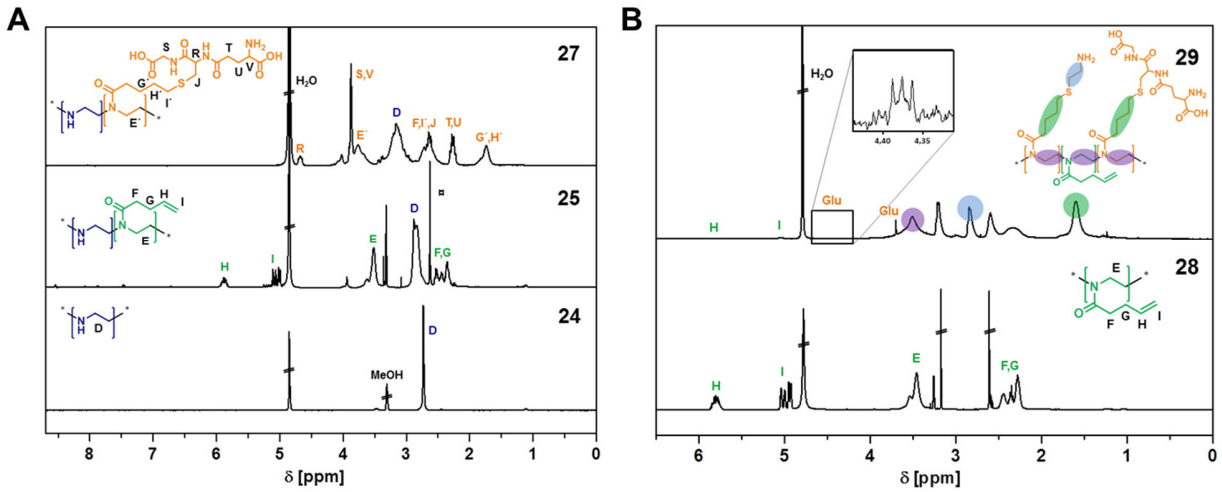

Figure 4.3. Comparison of the ^{1}H NMR spectra of A) the starting homopolymer **24** (LPEI), the precursor **25** and the final product **27** (¤ side product *N*-hydroxysuccinimide) (400 MHz, MeOD/D_2O) and B) the precursor copolymer **28** and the final product **29** (400 MHz, MeOD/D_2O).

Diffusion-ordered NMR spectroscopy (DOSY NMR). To confirm the successful photo-addition of the targeting molecules (D-fructose and L-glutathione, respectively) to the polymer sidechain as well as the formation of a single (polymeric) species, DOSY NMR was utilized. The attachment of D-fructose to the copolymer **25** resulted in a single diffusion coefficient for copolymer **26** which proves the absence of degradation (Figure 4.4A). In combination with a shift to a higher coefficient, indicating a decrease of the hydrodynamic radius of the polymer in solution, a successful installation of the sugar units was confirmed. The deprotection of the single D-fructose molecule resulted in decomposition and, therefore, hindered the determination of the diffusion coefficient.

In contrast, the GSH decorated polymer **27** exhibited a lower diffusion coefficient compared to copolymer **25** (Figure 4.4B). The single GSH molecule has an increased mobility compared to the polymeric species and, therefore, displayed a significantly higher diffusion coefficient.

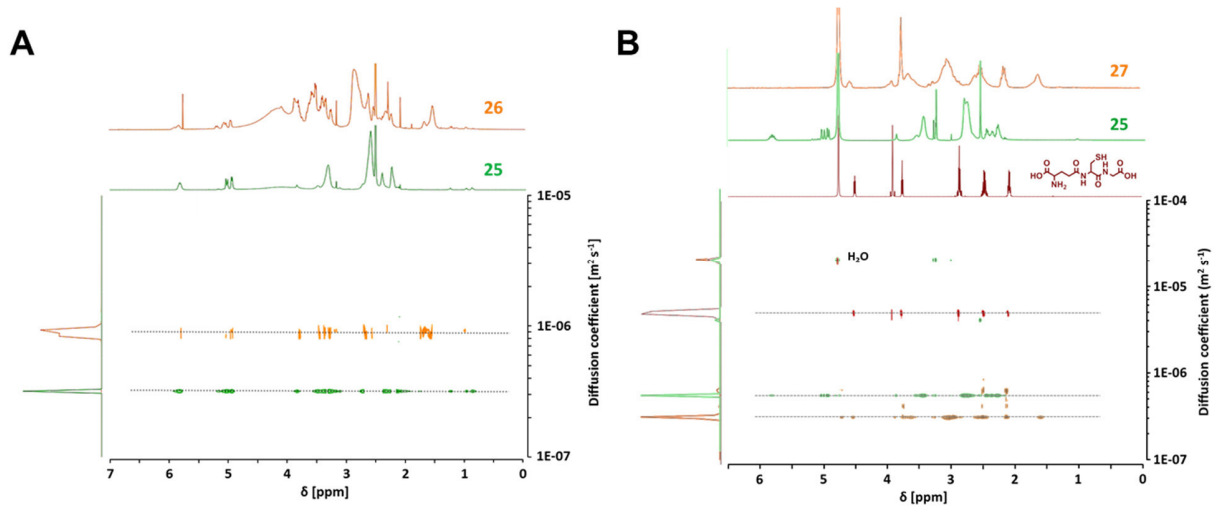

Figure 4.4. Diffusion ordered NMR spectra of A) the precursor **25** (green) and the final product **26** (orange) (600 MHz, DMSO-d_6, 25 °C) and B) L-glutathione (red), the precursor **25** (green) and the final product **27** (400 MHz, D_2O, 25 °C).

4.3 Application as DNA interactive materials

Bio- and hemocompatibility. As mentioned before, biocompatibility represents a critical parameter for PEI-based copolymers as potential non-viral vectors in biomedical applications. Their cationic charge density, molar mass as well as degree of branching represent key parameters for the interaction with the cellular membranes and, consequently, the initiation of apoptosis.[88-89] The impact of tailored functionalization of LPEI was investigated in the non-cancerous fibroblast cell-line L929, routinely used for toxicity screenings. One option to reduce the cytotoxicity of LPEI is the introduction of EtOx units as shown for **17** (oxazoline content of 54%), the precursor for the polymers **21** to **23**. While LPEI (**24**) led to poor cell viability at low concentrations (IC_{50} ~ 4.0 µg mL^{-1}) in agreement with literature reports,[90] **21** to **23** revealed no cytotoxicity after 24 h using polymer concentrations up to 0.5 mg mL^{-1} (IC_{50} > 0.5 mg mL^{-1}) (shown for **23** in Figure 4.5A). This improvement is attributed to the introduced EtOx units and is consistent with literature reports.[91] The D-fructose conjugated polymer **26** shows an improved biocompatibility as well. No significant reduction of the cell viability in mouse fibroblast L929 cells was observed after 24 h treatment with **26** (16% fructose)

for all tested concentrations (IC_{50} > 0.5 mg mL^{-1}). The impact of the sugar moieties on the cell viability as well as the benefit of low sugar contents attached to the polymer backbone have been reported.[65-67] The installation of 27% L-glutathione resulted in a strong reduction of the cytotoxicity. The copolymer **27** revealed no cytotoxic effects (relative viability ≥ 85%) using polymer concentrations up to 150 µg mL^{-1} and an IC_{50} value of ~ 270 µg mL^{-1}. The replacement of the ethylene imine units by flexible primary amine containing side chains as in the case of the copolymer **29** led to an increased cytotoxicity (IC_{50} value of ~ 44 µg mL^{-1}) as compared to **27**.

Blood compatibility represents another important parameter for biomedical applications, in particular for *in vivo* studies. It was investigated by assessment of the hemolytic activity and the aggregation of erythrocytes. All investigated copolymers did not show any hemolytic activity in a concentration range from 10 to 50 µg mL^{-1} (Figure 4.5B). A slight hemolysis (2.4% hemoglobin release) was observed at higher concentrations for **26** (100 µg mL^{-1}). In contrast, **24** (LPEI) revealed an increased interaction with the cellular membranes of the blood cells resulting in hemoglobin releases above 2% (50 to 100 µg mL^{-1}). Moreover, it resulted in a strong agglomeration of erythrocytes. In the presence of certain polymers, irreversible erythrocyte aggregation can occur due to the membrane interactions forming bridges between the polymers and the erythrocytes, which results in an increase of the blood viscosity and can be dangerous for vital organs.[92] The latter was not observed with EtOx containing copolymers **21** to **23**, D-fructose conjugated **26** as well as GSH conjugated **27** (data not shown). In contrast, GSH conjugated **29** revealed distinct interactions with cellular membranes of erythrocytes leading to aggregation. Obviously, the type of amines within the polymer side chain is a crucial factor for the interaction with cells, in particular with the plasma membrane, and is therefore linked to the biocompatibility properties. In the literature, primary amines are reported to display an increased affinity to cellular membranes compared to secondary amines, indicated by a higher toxicity.[93]

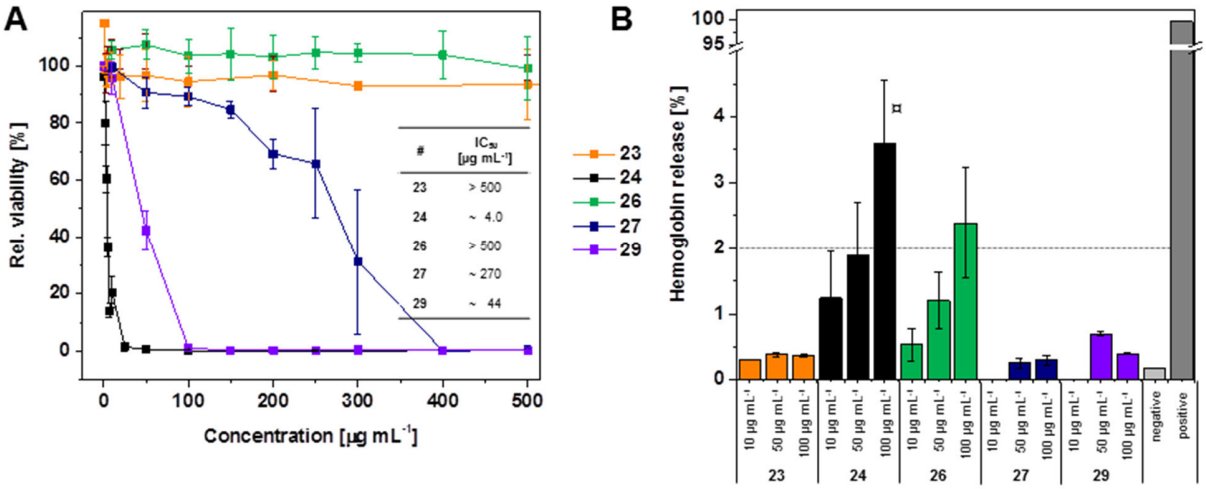

Figure 4.5. Bio- and hemocompatibility. A) Relative viability of L929 cells after 24 h incubation with the respective polymers **23** (primary amine), **24** (LPEI), **26** (D-fructose), **27** (GSH) and **29** (GSH & primary amine) at indicated concentrations as well as IC_{50} values. B) Hemolysis assay of erythrocytes after incubation with respective polymers at indicated concentrations. Triton X-100 was used as positive and PBS as negative control. A value < 2% hemolysis is classified as non-hemolytic, 2 to 5% as slightly hemolytic and values > 5% as hemolytic. Values represent the mean ± S.D. (n = 3). ¤ Hemoglobin release of **24** describes the mean of the different functionalization approaches (as well as the S.D.).

Characterization of the polyplexes. The efficient delivery of nucleic acids (*e.g.* plasmid DNA) into cells depends on several parameters. They comprise the compact condensation of genetic material, the masking of negative charges, the prevention of degradation, the cell uptake and the efficient dissociation from the polymer after transfer into the cellular cytoplasm or nucleus. To investigate the polyplex formation, in particular the binding affinity of the copolymers with plasmid DNA (pDNA), ethidium bromide quenching assays (EBA) were performed. Therefore, polyplexes of the copolymers **21** to **23**, **26**, **27** and **29** were formed at different nitrogen (polymer) to phosphate (pDNA) ratios (N/P). Due to the electrostatic and hydrophobic interactions between the polymer and the nucleic acid, ethidium bromide is excluded from its binding sites within the oligonucleotides resulting in a reduction of fluorescence intensity that correlates with the affinity for complexation.[94-95] The copolymers **21** to **23** revealed decreasing fluorescence below 40% relative fluorescence units (RFU, exemplified for **23** in Figure 4.6A).

A plateau indicates a stable polyplex formation at N/P ratios from 5 to 40 comparable to the gold standard LPEI (**24**, ~ 25% RFU). Since the precursors **16** and **17** did not form appropriate complexes, it can be assumed that the presence of EtOx units hinders a strong binding of pDNA to the secondary amines of the PEI backbone. Obviously, the more flexible side chains of **21** to **23** (containing primary amine functionalities) compensate the reduced complexation affinity. Notably, the combination of EI and AmButOx seems to be beneficial, since a comparable copolymer P(MeOx-*stat*-AmButOx) without EI units revealed a reduced pDNA complexation behavior in a previous study.[93] The sugar-conjugated copolymer **26** did not reach a fluorescence intensity plateau within the displayed N/P ratios (57% RFU at N/P 40). The smaller content of amine functionalities combined with bulky side chains hinders the tight attachment to the pDNA. However, **26** was able to form polyplexes with pDNA, as this RFU was also reported for other transfection polymers.[93] The GSH-conjugated copolymers **27** and **29** revealed a stable polyplex formation at N/P ratios from 20 to 40 reaching 45% and 30% RFU, respectively. The copolymer **29** revealed strong polyplex formation even comparable to LPEI (**24**). One reason could be the presence of primary amines attached through flexible side chains, which are easily accessible for the pDNA and known to promote its complexation.[10]

Besides the strong binding of pDNA, a fast and efficient release from the copolymers is necessary for the efficient delivery of nucleic acids. For this purpose, the heparin dissociation assay was used to analyze the stability and the dissociation properties of the formed polyplexes.[96-97] Heparin is a sulfated glycosaminoglycan with multiple negative charges in the polymer chain. It competes with the pDNA of the polyplex and forces the release of the nucleic acid. Increasing amounts of heparin displace the genetic material of the polyplex. The released pDNA is able to rebind free ethidium bromide (from the polyplex formation) causing an increase of the fluorescence intensity (Figure 4.6B). For all investigated polyplexes, the pDNA was released very fast at low heparin concentrations (10 U mL^{-1}) to nearly 100% RFU. One exception are the copolymers **21** to **23**, achieving only 80% dissociation. The use of an alternative competitor, in particular poly(methacrylic acid) (DP = 200), resulted in a full dissociation of the polyplex. In contrast, LPEI (**24**) required increased amounts of the anionic competitor heparin (40 U mL^{-1}) for almost full dissociation, which underlines the stability of **24**/pDNA polyplexes.

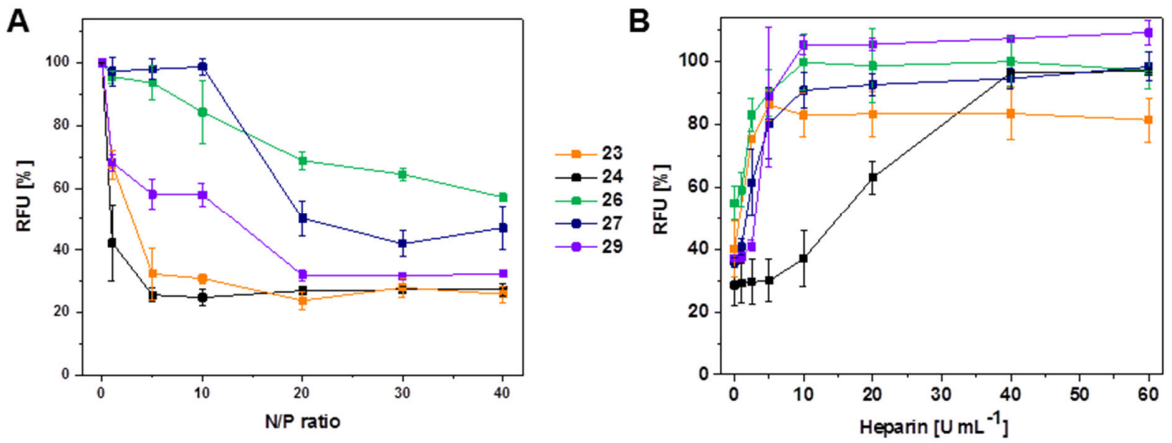

Figure 4.6. Polyplex formation and stability with pDNA using the polymers **23**, **24**, **26**, **27** and **29**. A) Complexation affinity (ethidium bromide quenching assay) of respective polymers at indicated N/P ratios. B) Dissociation assay of polyplexes formed at N/P 20 (**26**), 30 (**23**), 40 (**27**,**29**) using heparin (0 to 60 U mL^{-1}). Values represent the mean ± S.D. (n = 3).

Another task on the way to an efficient delivery is the determination of the sizes and zeta potentials of the polyplexes. The internalization of polyplexes into cells *via* the endocytic pathway requires defined sizes and charges of the complexes. In the literature, sizes of polymeric nanocarriers up to 200 nm are recommended.[58, 98] The here formed polyplexes reveal favorable sizes between 100 and 200 nm with the exception of **27** (Table 4.3). As expected for cationic polymers, the calculated zeta potentials are between 18 and 33 mV evidencing their cationic nature. An explanation for the negative zeta potential of the GSH conjugated copolymer **27** (–7 mV) could be the presence of GSH carboxylic acid moieties at the outside of the polyplex. In contrast, the inversion of charge is not obtained for copolymer **29** (33 mV) where the lower content of GSH and the side chains with more flexible primary amines reduce the effect of the anionic GSH functionalities.

Table 4.3. Size and surface charge (zeta potential) measured in 20 mM 4-(2-hydroxyethyl)piperazine-1-ethanesulfonic acid (HEPES) and 5% (w/v) glucose, pH value 7.2 of pDNA complexes of **21** to **24**, **26**, **27** and **29** at defined N/P ratios measured by dynamic light scattering.

#	z-Average [d/nm]	PDI	Zeta potential [mV]	N/P ratio
21	158 ± 1	0.23	27 ± 0.3	30
22	143 ± 1	0.21	23 ± 0.1	
23	154 ± 1	0.23	23 ± 0.1	
24	132 ± 28	0.24	28 ± 2.7	20
26	165 ± 1	0.26	18 ± 0.4	
27	282 ± 5	0.38	–7 ± 0.1	
29	117 ± 1	0.31	33 ± 1.5	

The investigated polyplexes were used in the following investigations to fulfill particular requirements, including the proof of high transfection efficiency and careful examination of the uptake mechanism, the successful targeting of human breast cancer cells and the passage through the blood-brain barrier. In all cases, polymer concentrations $< 10\ \mu g\ mL^{-1}$ are used for the preparation of the polyplexes, which are in an acceptable range below the cytotoxicity-inducing concentrations (*cf.* Figure 4.5A).

Gene delivery agents. Gene therapy describes the treatment of human diseases by the transport of genetic material to specific cells of the patient. Recent developments enabled the identification of numerous disease-causing genes. The use of cationic polymers as gene delivery agents offers the opportunity to circumvent biological barriers. The combination of primary and secondary amines as well as non-charged EtOx units should turn the copolymers **21** to **23** into promising candidates as non-viral gene delivery agents (3^{rd} generation PEIs). They were investigated for their transfection efficiency (TE) using human embryonic kidney (HEK) cells and pDNA encoding the enhanced green fluorescence protein gene (*egfp*). Flow cytometry was utilized to determine the TE and to analyze all viable cells (propidium iodide staining) which successfully express EGFP. A well-known side effect is the unwanted interaction of cationic polymers with serum proteins. Serum proteins attach to the surface of the polyplexes (shielding) and, therefore, inhibit the cellular uptake process.[99-100] As a consequence, the cells were transfected in serum-reduced media (OptiMEM) and serum-containing media (RPMI1640 supplemented with 10% FBS).

The latter offers test conditions more comparable to an *in vivo* situation and represents an established method to test the performance of polymers. High TEs over 60% were observed under serum-reduced conditions for polyplexes of **22** and **23** at N/P ratios 30 to 50 (Figure 4.7). Comparable values were obtained for **24** (LPEI) at N/P 20. Interestingly, the *egfp* transfection level of **21** to **23** at N/P 50 in serum-containing media did not change significantly compared to transfection in OptiMEM. In contrast, the TE for **24** decreased continuously for increasing N/P ratios (N/P > 20) due to its cytotoxicity and the influence of serum proteins. The combination of high cell viability (no cyto- and hemotoxicity) and impressive transfection performance even in serum containing media underlines the immense potential of **22** and **23** as preferable gene delivery vectors. In particular **23** withstands a comparison to LPEI (**24**), the literature known 'gold standard for transfection'.

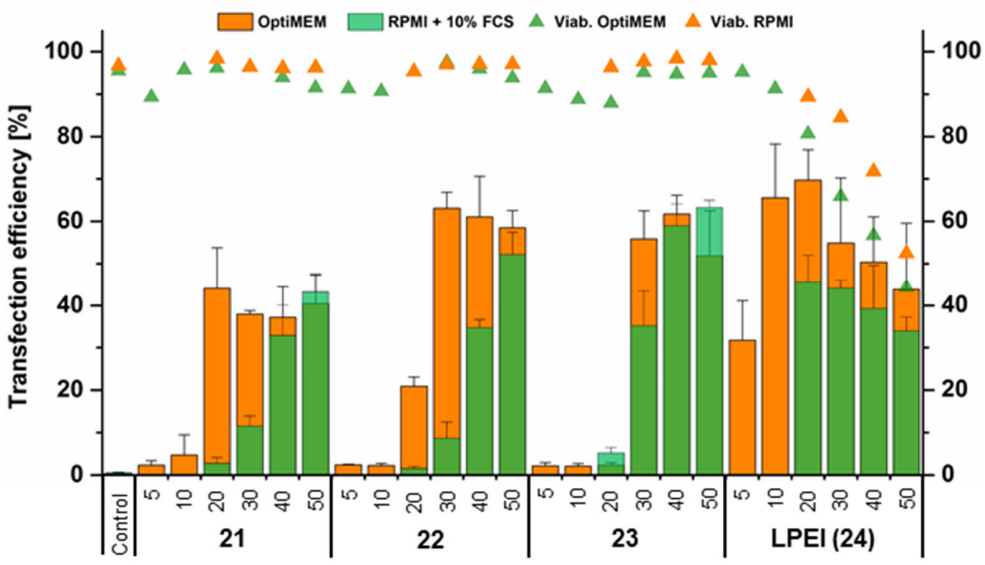

Figure 4.7. Transfection efficiency of LPEI (**24**) and copolymers **21** to **23** for adherent HEK cells in serum reduced (OptiMEM, orange) and serum containing media (RPMI + 10% FBS, green) at different N/P ratios after 24 h. Values represent the mean ± S.D. (n = 3).

To understand the outstanding transfection performance of the prepared copolymers, the uptake mechanism was investigated. For this purpose, polyplexes formed with YOYO-1 labeled pDNA were used for an uptake kinetic in order to detect the internalization within cells by flow cytometry. The polymers **21** to **23** and LPEI (**24**) revealed a fast and time-dependent cellular

uptake. In detail, almost 90% of measured cells internalized the polyplexes after 4 h. Nevertheless, the quantities (mean fluorescence intensities, MFI) differ significantly. Higher internalized polyplex concentrations were detected using the copolymers **21** to **23** compared to **24**. Most probably, the enhanced complexation with pDNA as well as the excellent cellular uptake is based on the presence of primary amine functionalities while the oxazoline content possesses reduced membrane interactions. By performing a temperature-dependent uptake study (4 °C and 37 °C) of YOYO-1 stained polyplexes as well as using a proton pump inhibitor (bafilomycin), the involvement of the endosomal uptake and release as critical steps during the transfection mechanism could be confirmed. Deeper insights into the uptake mechanism were obtained with microscopic studies including confocal microscopy (data not shown), structured illumination microscopy (SIM) and high-angular annular dark-field scanning transmission electron microscopy (HAADF-STEM) (shown for copolymer **23** in Figure 4.8). Fluorescence imaging of cells, in particular SIM images, revealed a co-localization of pDNA-bound **23** polyplexes (blue, Cy5-labeled) within the lysosomes/late endosomes (red, RFP labeling). The detection of the YOYO-signal within the cytoplasm that was not co-localized with lysosomal structures indicates a successful dissociation of the polyplexes. Taking the low concentration of heparin into account, which is required to destabilize the polyplex (see Figure 4.6B), an efficient release of pDNA into the cytoplasm can be assumed. The polyplexes of **23** are mainly localized within the endosome in close vicinity to the endosomal membrane (Figure 4.8A-C). An explanation could be the strong interaction between the polyplex and the cytoplasmic membrane at the time of the cellular uptake or a strong interaction with the endosomal membrane caused by the acidification. In order to study the interaction of the polymers with the endosomal membrane in more detail, STEM on embedded sections was performed. EM images revealed an uptake of single **23** polyplexes into vesicles with sizes of 200 to 500 nm ($n > 10$ vesicles of different sections were analyzed) and confirmed the close vicinity between the polyplex and the endosomal membrane. An uptake event induced by cilia (hair-like structure on the cell body) was observed (Figure 4.8D-F), supporting an energy-dependent uptake, such as by macropinocytosis. Compared to the uptake under non-inhibited conditions, the use of the inhibitor 5-(*N*-ethyl-*N*-*iso*propyl)amiloride resulted in only 30% of cells that internalized **23** polyplexes after 4 h and no detection of polyplexes within the cytoplasm.

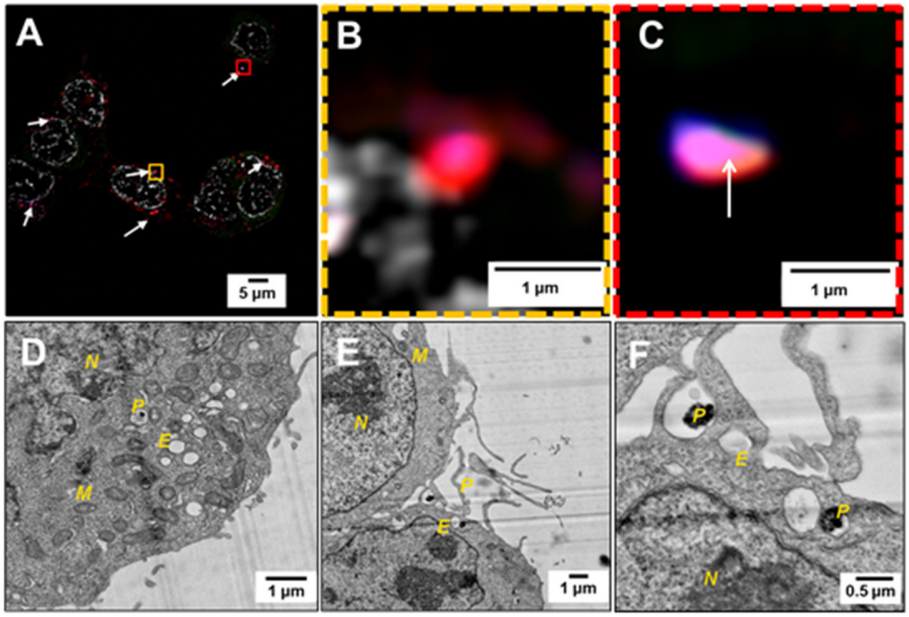

Figure 4.8. High resolution imaging. A) Structured illumination image of **23** based polyplexes taken up by HEK cells (deconvolved data). White arrows indicate co-localization of **23**-pDNA polyplexes within lysosomes. B-C) Magnified view of the yellow and red, dash-lined frame in A: **23-Cy5** polyplex within the endosome. 63 × Oil Obj. 1.4 NA. Grey: Hoechst. Red: Lysosomal membrane (RFP). Green: Plasmid DNA labeling (YOYO-1). Blue: Polymer labeling (Cy-5). D-F) HAADF-STEM image of **23** based polyplexes taken up by HEK cells. The following letters corresponds to cell organelles: N = cell nucleus, M = mitochondria, E = endosomal compartment, P = polyplex.

The outstanding properties of **21** to **23** are based on the tailored combination of oxazoline units and different amine functionalities. The presence of EtOx subunits shields the formed polyplexes from aggregation caused by protein interactions prior to uptake. This could explain the efficient cellular uptake and the high transfection efficiency of the respective copolymers. Besides the installation of primary amine functionalities, the alkene functionalities of the pseudo-POx can be used for the attachment of specific targeting molecules.

Human breast cancer cell targeting. Human breast cancer is one of the main leading death causes for woman nowadays. The expression of GLUT5 in these cells has been controversially discussed in the literature. While Gowrishankar *et al.* argued against the overexpression in all breast cancer tissues,[101] Nualart and co-workers claimed that GLUT5 is overexpressed in 85% out of 33 tested breast cancer cell lines,[102] also confirmed for estrogen-receptor positive MCF-7 and

triple-negative MDA-MB-231.[103] Therefore, high molar mass LPEI (**24**) was modified with D-fructose moieties (**26**) in order to combine the selectivity of the sugar unit for the GLUT5 transporter[104] with the delivery potential of LPEI for genetic material. The cell-type dependent cytotoxicities and specific cellular uptake (MDA-MB-231 breast cancer *vs.* non-cancer L929 cell line/primary human cell line HUVEC) of the designed copolymer **26** and the precursor LPEI (**24**) were investigated. Using the alamarBlue assay, the precursor **24** reveals a concentration dependent cytotoxicity for all cell lines (Figure 4.9A). As already described before, the D-fructose-conjugated copolymer **26** shows no significant reduction of the cell viability in mouse fibroblast L929 cells. Furthermore, no cytotoxicity was observed in the primary human endothelial HUVEC cells after 24 h treatment for all tested polymer concentrations (IC_{50} > 500 µg mL^{-1}). Interestingly, its cytotoxicity against breast cancer cell line MDA-MB-231 is concentration-dependent (IC_{50} ~ 35 µg mL^{-1}). Obviously, the fructose-modification results in a highly enhanced biocompatibility for the non-cancer cell line L929 as well as the primary human cell line HUVEC on one hand and in the selective toxicity for the breast cancer cell line MDA-MB-231 on the other hand.

The cellular uptake of the polyplexes of **24** (LPEI), the respective precursor **25** (without D-fructose) and the final **26** into L929, HUVEC and MDA-MB-231 cells is depicted in Figure 4.9B. The uptake was measured after 1 h (a time point at which no cytotoxicity was observed) at different polymer concentrations by flow cytometry. Polyplexes based on polymer **24** revealed a strong uptake in all tested cell types indicating no cell specifity. In contrast, polyplexes of **25** can be detected in MDA-MB-231 and HUVEC cells at N/P 20. Higher N/P values resulted in pDNA uptake in all three cell lines. The polyplexes of **26** show an enhanced uptake in MDA-MB-231 cells at N/P 50 even outperforming **24** and, even more important, the precursor **25** (no D-fructose). Indeed, the uptake of **26** into L929 is more than doubled for the MDA-MB-231 cells. These results indicate a positive influence of D-fructose towards cell specific gene delivery into breast cancer cells. Non-cancer cell lines L929 and HUVEC efficiently take up polyplexes of **24** and **25**, but with a reduced efficiency as compared to **26**. Overall, specific delivery of pDNA into MDA-MB-231 cells can be obtained with D-fructose targeted polyplexes.

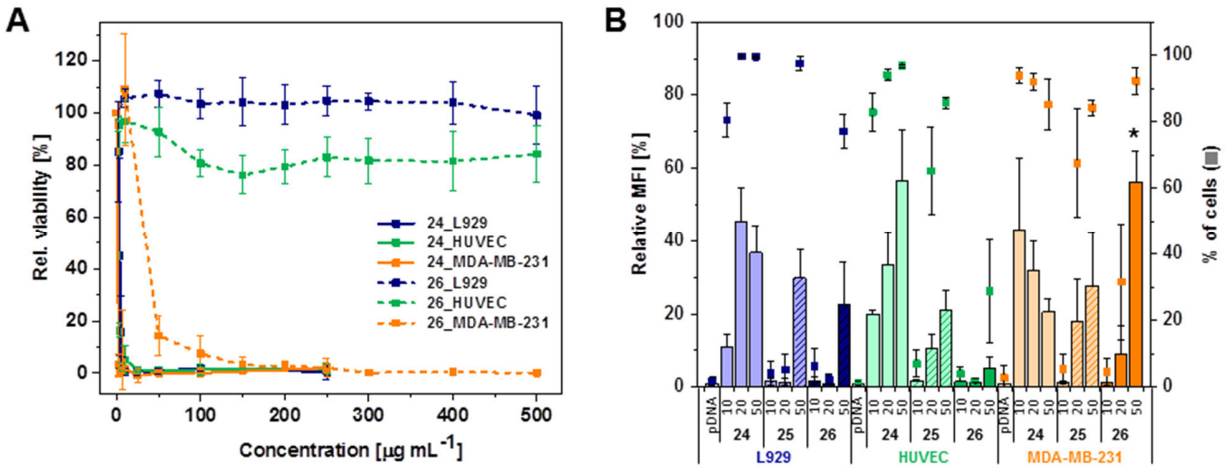

Figure 4.9. A) Cell-type dependent cytotoxicity assay of starting polymer **24** and the final polymer **26** using alarmaBlue. Non-treated cells served as 100% relative viability. Cells were treated 24 h with the indicated concentrations of the polymers. B) Uptake study. Polyplexes formed with YOYO-1 labeled pDNA were incubated with L929, HUVEC, and MDA-MB-231 cells in OptiMEM for indicated time points using the copolymers **24**, **25** and the fructose conjugated polymer **26** at indicated N/P ratios. The amount of cells (%), which have taken up pDNA relative, as well as the mean fluorescence intensity (MFI) of all viable cells compared to pDNA control without polymers were depicted. Values represent the mean ± S.D. ($n \geq 3$); * represents statistical significant difference in MFI to **26** N/P 50 of L929 and HUVEC; ANOVA, p-value < 0.01.

Crossing the blood-brain barrier. Targeted gene delivery to the central nervous system is another challenge in pharmaceutical formulations since its access is strictly limited through the highly selective blood-brain barrier (BBB).[105] The tripeptide L-glutathione (GSH), a well-known antioxidant, has been studied as a potential candidate to facilitate the receptor-mediated transcytosis of nanocarriers.[106-108] In this context, high molar mass LPEI (**24**) was functionalized with GSH moieties to enable the transport of genetic material and, simultaneously, the passage through the BBB. The copolymers **27** and **29**, containing 73% of secondary (**27**) or 82% of primary amine groups (**29**), respectively, were investigated for their ability to cross an hCMEC/D3 endothelial cell layer mimicking the BBB within a microfluidically perfused biochip (see Figure 4.10A). The cells were cultured on a suspended membrane within a MOTiF biochip that was shown to enable an improved culture of endothelial cells under physiological perfusion conditions.[109] The membrane served as a cell substrate that is perfused from the apical side of the cell layer.

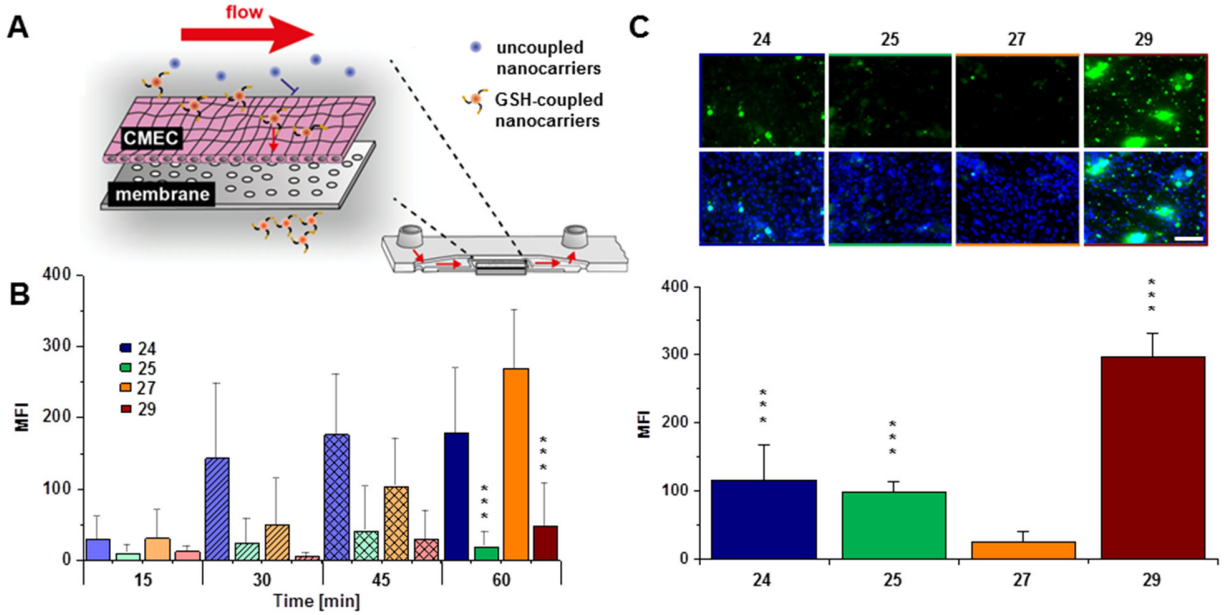

Figure 4.10. Performance of LPEI (**24**), the precursor **25** and the GSH-conjugated polyplexes **27** and **29** in a microfluidically supported biochip assay mimicking permeability of the BBB. A) Chip geometry. Schematic illustration of hCMEC/D3 cultured on top of a porous membrane within the chip. GSH-coupled nanocarriers are perfused on the apical side and passage through the cell layer was investigated basolateral. B) Passage of the respective polyplexes through BBB-like hCMEC/D3 cell layer over time. C) Top: Microscopic images display polyplex uptake (green) with the hCMEC/D3 cells (nuclei stained with DAPI (blue)) under a physiologic shear stress of 4 dyn cm^{-2}. Bottom: Quantificational analysis of polyplexes at the cellular barrier. * significances *vs.* **27**; *** $p < 0{,}001$; n = 3; scale bar 100 nm.

The biochip model enables the exact determination of the total amount of polyplexes that crossed the endothelial barrier as well as the quantification of nanoparticles taken up by the endothelial layer. The pure YOYO-1 labeled pDNA (without nanocarrier) was used to prove the imperviousness of the model system since no pDNA passed through the membrane. This underlined the need for a nanocarrier. The precursor **25** was used for comparative purposes to demonstrate the need of glutathione moieties for a successful passage. To elucidate the trans-endothelial transport of the different polyplexes, their enrichment in the lower chamber underneath the endothelial barrier of the biochip was measured (Figure 4.10B). The polyplex of LPEI (**24**) exhibited a surprising increase of translocation through the endothelial layer after 30 min perfusion, remaining at this level for up to 60 min of perfusion. Although the final

concentration of the investigated polyplex **24** (0.5 μg mL^{-1}) was still in an acceptable range below the cytotoxicity-inducing concentration, a possible explanation for the translocation are the flow conditions. They lead to an increased total amount of polyplexes presented to the cells within the incubation time compared to the static culture conditions. An induced leakage of the hCMEC/D3 cell layer could be an explanation to the unexpected polyplex passage. For the polyplex of polymer **27**, a continuously increasing transport through the layer was observed reaching a maximum at 60 min. In contrast, the precursor polyplex **25** without GSH modification showed only minimal passaging which supports the assumption of GSH-facilitated transcytosis. Surprisingly, the GSH-modified polyplex **29** revealed minimal passaging likewise. Uptake studies revealed a fast polyplex uptake of **29** in HEK cells which can be explained by the strong interaction of **29** with the cellular membrane induced by the primary amine functionalities. Microscopic studies confirmed these interactions by showing the highest uptake into the endothelial cell layer (Figure 4.10C, top) which prevents the passage to the lower chamber. Polymer **29** is supposed to adhere to cells in *in vivo* studies and might be partly internalized by endothelial blood vessel cells, followed by cargo release instead of passing the cell layer. In contrast, **24** and **25** revealed a lower enrichment, while **27** exhibited the weakest enrichment within the layer. An image analysis of the polyplexes at the cellular barrier is depicted in Figure 4.10C (bottom). The amounts of uptaken polyplexes into the cell layer is in accordance with the amounts of passed polyplexes through the hCMEC/D3 cell layer. The GSH-conjugated copolymer **27** showed no interaction neither with HEK cells in uptake studies nor endothelial cells, but was able to pass the BBB. This renders this polymer a promising candidate as a BBB nanocarrier and demonstrates the strong influence of the polymeric design/composition for a BBB carrier balancing the GSH content, DNA binding potential and cellular interactions.

In conclusion, the ease of modification of secondary amine groups enables the introduction of double bonds and, furthermore, the installation of different functional molecules *via* thiol-ene photo-addition. Thus, modified POx could be used for enhanced gene delivery, human breast cancer cell targeting and the passage of a blood-brain barrier model with respect to the targeted delivery of genetic material.

5 POLY(2-OXAZOLINE)S – SYNTHESIS & APPLICATION

Parts of this chapter have been published in: **P8**) M. Hartlieb, D. Pretzel, C. Englert, M. Hentschel, K. Kempe, M. Gottschaldt, U. S. Schubert, *Biomacromolecules* **2014**, *15*, 1970-1978; **P9**) M. N. Leiske, M. Hartlieb, C. Paulenz, D. Pretzel, M. Hentschel, C. Englert, M. Gottschaldt, U. S. Schubert, *Adv. Funct. Mater.* **2015**, *25*, 2458-2466; **P10**) M. Hartlieb, D. Pretzel, M. Wagner, S. Höppener, P. Bellstedt, M. Görlach, C. Englert, K. Kempe, U. S. Schubert, *J. Mater. Chem. B*, **2015**, *3*, 1748-1759.

5.1 Diversity of poly(2-oxazoline)s

Besides the established hydrolysis of poly(2-alkyl-2-oxazoline)s (PAlkOx) to create amine functionalities in the polymer backbone, cationic moieties can be installed in the side chain *via* post-polymerization modification (described in Chapter 4.1). Another alternative approach is the use of amine groups bearing 2-oxazoline monomers in a living cationic ring-opening polymerization (CROP) (see Scheme 1.1A) to synthesize DNA interactive materials. Since the nucleophilic nitrogen would terminate the living cationic chain-end of the polymer,[110] the amine group in the oxazoline side-chain has to be protected to obtain polymerizable monomers. Cesana *et al.* were the first who described the synthesis of such cationic POx.[111]

The monomer 2-(4-((*tert*-butoxycarbonyl)amino)butyl)-2-oxazoline (BocOx) (the schematic representation of the chemical structure can be found in Scheme 5.1) was synthesized, following a protocol described in the literature.[112] Despite the *tert*-butoxycarbonyl (*boc*)-protecting group, the formed amide of the BocOx can still react with small electrophilic compounds such as methyl cation, which is typically used as initiating species. As a consequence, its polymerization has to be performed in a two-step initiation process. First, an 2-ethyl-2-oxazoline (EtOx) oligomer is produced mixing methyl tosylate and three equivalents of EtOx at 140 °C. The formed active species, the oxazolinium group (see Scheme 1.1A), reveals a significantly larger steric hindrance as compared to the methyl cation. Subsequently, BocOx can be added and polymerized.

In order to introduce versatile solubility (particularly in water) and biocompatibility, BocOx was copolymerized with EtOx. Kinetic investigations resulted in similar slopes of the pseudo first order kinetic plots which demonstrated similar reactivities of both monomers.[112] The addition of both monomers in a defined ratio to the active EtOx oligomer, and subsequent microwave-

assisted polymerization[37] and deprotection with trifluoro acetic acid (TFA) resulted in statistical copolymers P(EtOx-*stat*-AmOx) (**30** to **35**, Scheme 5.1). The synthesis of block copolymers, which are the basis for micellar structures, was performed by starting with the polymerization of EtOx followed by the chain extension of the living polymer with BocOx, the *boc*-protected precursor of the cationic AmOx segment. Deprotection after termination of the polymerization gave the block copolymers P(EtOx-*b*-AmOx) (**36** to **40**, Scheme 5.1).

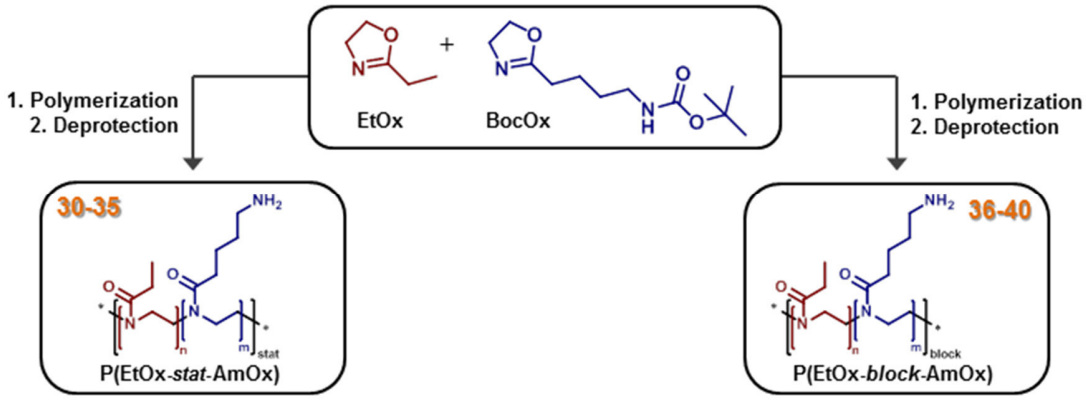

Scheme 5.1. Schematic representation of the copolymerization of EtOx and BocOx and subsequent deprotection to yield statistical (**30** to **35**) as well as block copolymers (**36** to **40**). Polymerization conditions: µW, 140 °C, acetonitrile. Deprotection conditions: Trifluoro acetic acid, CH_2Cl_2, 60 °C, Amberlyst A21.

Copolymers of different contents were prepared by changing monomer-to-initiator ratios ([M]/[I]) and polymerization times (Table 5.1). While the overall degree of polymerization (DP) for the statistical copolymers **30** to **35** was kept constant at around 50 repeating unis, the amine content was varied from 10 to 33%. For the block copolymers **36** to **40**, the total DP was kept around 100 with varying amine contents (5 to 29%). The length of the polymers was determined from ^{1}H NMR investigations directly after polymerization by comparing the tosylate initiator signal to the integral of the total polymer backbone. The experimental ratios of the monomers within the final polymer were calculated from the ^{1}H NMR spectra of the purified samples. Size exclusion chromatography (SEC) of the copolymers revealed M_n values around 5,000 g mol^{-1} for the copolymers **30** to **35** and values around 10,000 g mol^{-1} for **36** to **40**, while the dispersity (Đ) values ranged from 1.13 to 1.34. However, a precise determination of both

values is challenging due to a lack of cationic SEC standards, as well as potential column interactions.

Table 5.1. Parameters for statistical (**30** to **35**) and block poly(2-oxazoline) copolymers (**36** to **40**).

			Composition [%]		NMR[a]	SEC[b]	
#	Name	DP	a	b	M_n [g mol^{-1}]	M_n [g mol^{-1}]	Đ
30	P(EtOx$_a$-*stat*-AmOx$_b$)	48	90	10	5,000	8,100	1.26
31		46	85	15	4,900	8,200	1,24
32		41	78	22	4,400	8,700	1,25
33		53	73	27	5,900	9,500	1,23
34		48	67	33	5,400	9,400	1,24
35		46	80	20	4,900	9,300	1.13
36	P(EtOx$_a$-*b*-AmOx$_b$)	118	95	5	12,000	14,500	1.34
37		102	90	10	10,600	16,800	1.23
38		90	82	18	9,700	16,100	1.22
39		105	78	22	11,400	18,100	1.23
40		90	71	29	10,100	15,600	1.30

[a] Determined by ^{1}H NMR (calculated from the ratio tosylate/backbone signals directly after polymerization (crude)
[b] SEC: DMAC, 0.21% LiCl, against polystyrene

5.2 Application as DNA interactive materials

The isolation and purification of nucleic acids from highly complex samples, such as blood and feces,[99] is of paramount importance for DNA-based detection methods in modern clinical diagnostics,[100] genetic analysis,[104] and pathogen detection.[101] To date, a wide range of DNA purification and extraction techniques have been investigated but an universal purification method is still missing.[102] Solid phase extraction (SPE) represents a well-established and easily adaptable purification method firstly described by McCormick.[113] Although it allows the effective separation of nucleic acids from proteins without generating toxic by-products, there are still remaining issues that have to be overcome, such as the intensive washing procedures, the limited loading capacity of the silica matrix, as well as the limitation of the extraction efficiency.[114]

A highly promising approach is the reversible binding of genetic materials within a three-dimensional hydrogel matrix. Although insoluble due to cross-linking, hydrogels are able to incorporate water up to a multitude of their own mass, which allows the diffusion of guest molecules. Besides a large surface area for binding targeted molecules, these networks can be tailored in pore size and chemical functionality. For instance, the incorporation of cationic functionalities into the network enables the electrostatic interaction with negatively charged DNA. Changes of the pH value, temperature or ionic strength are commonly used methods to support the elution of the genetic material from the hydrogel.

Matrix supported poly(2-oxazoline)-based hydrogels. The statistical copolymers **30** to **34** were used to generate hydrogels and matrix supported hydrogels by cross-linking some of the primary amine groups with epichlorohydrin (ECH). The preparation of supported structures was performed by soaking polyethylene (PE) or polypropylene (PP) filer materials in a copolymer/ECH solution. Heating resulted in cross-linking and, therefore, the formation of a bead-like structure of the gel phase. This could be attributed to a lower critical solution temperature (LCST) behavior of the copolymers, and, therefore, phase separation, prior to gelation. The swelling behavior, the ratio of hydrogel per composite, as well as the ability to absorb and release DNA were tested. Cy5 (Abs. 649 nm, Em. 670 nm) labeled DNA can be detected and quantified by microscopic and spectroscopic techniques tracking the fluorescence of the attached dye. Using fluorescence microscopy, the uptake and stimulated release of the genetic material from PP-based composites by heparin could be investigated and is shown for copolymer **33** in Figure 5.1. The first row displays the autofluorescence of the swollen hydrogel (buffer solution) which is bound to the substrate. A bright fluorescence of the composite is visible after the addition of DNA followed by a washing step (A). The treatment with a 6 mg mL^{-1} heparin solution (a polyanion which is able to replace the DNA) resulted in a partial release of the bound DNA (B). In contrast, the pure PP-matrix showed no change at analogue treatment.

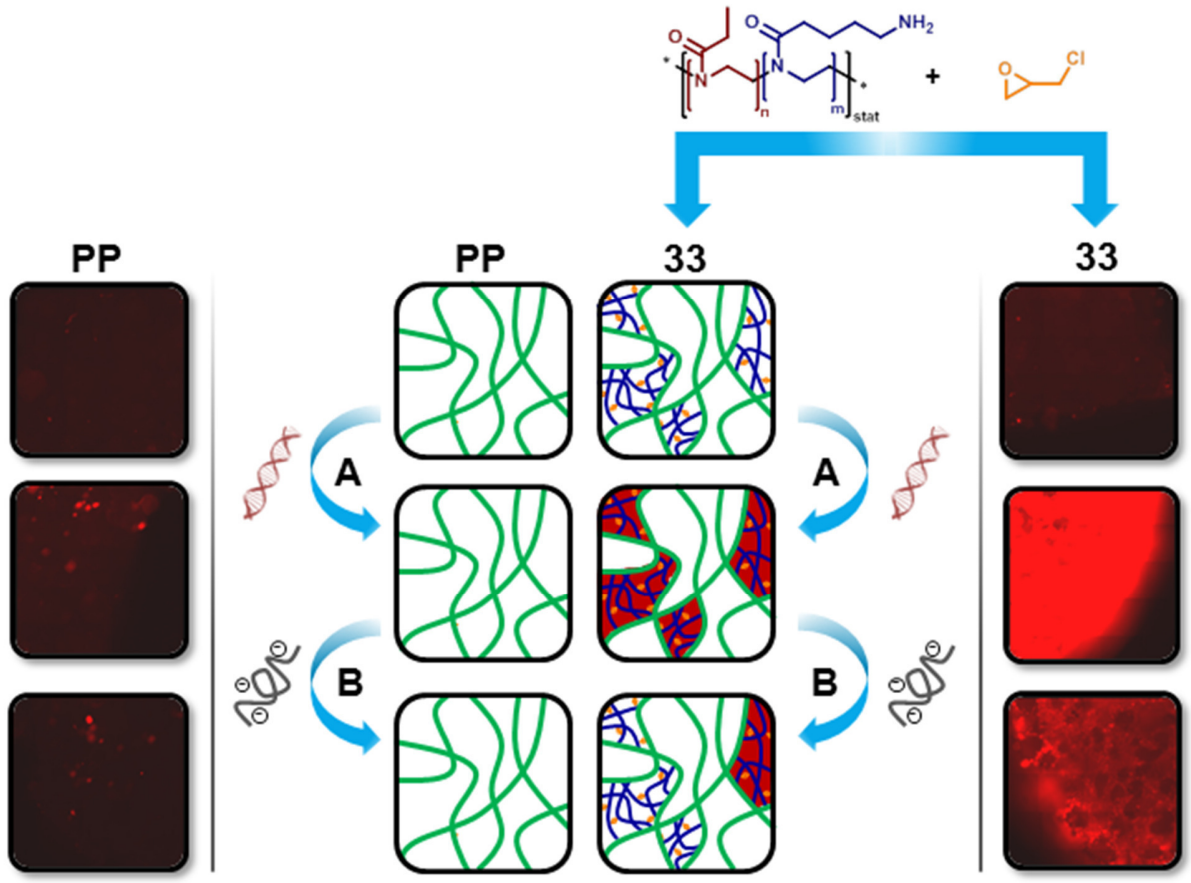

Figure 5.1. Schematic representation of the DNA uptake and release (by heparin) of PP-based cross-linked composite **33** (PP: Green, Polymer: Blue, Cross-linker: Orange) and pure PP-matrix. Cy5-labeled DNA (red) was used to measure fluorescence microscopy of the treated samples.

Although the release of DNA using heparin represents an efficient method, it suffers from drawbacks like the inhibition of the polymerase chain reaction (PCR) at higher heparin concentrations. As a consequence, different stimuli like pH value or temperature were investigated, as well as decreasing heparin concentrations (see Figure 5.2A). The first two did not lead to a sufficient release. As expected, the increase of the heparin concentration resulted in an enhanced DNA release. The detection of the low amounts of DNA in biological samples requires multiplication using a PCR of the genetic material. Therefore, the naturally thermostable enzyme polymerase is used to amplify a few copies of a specific sequence of the genetic material.[115-116]

PCR studies revealed that the recovered DNA, which was released at heparin concentrations up to 1 mg mL^{-1}, could be amplified (Figure 5.2B). In these cases, the heparin concentration seems to be low enough that the majority of the heparin is entrapped within the network and does not disturb the subsequent PCR.

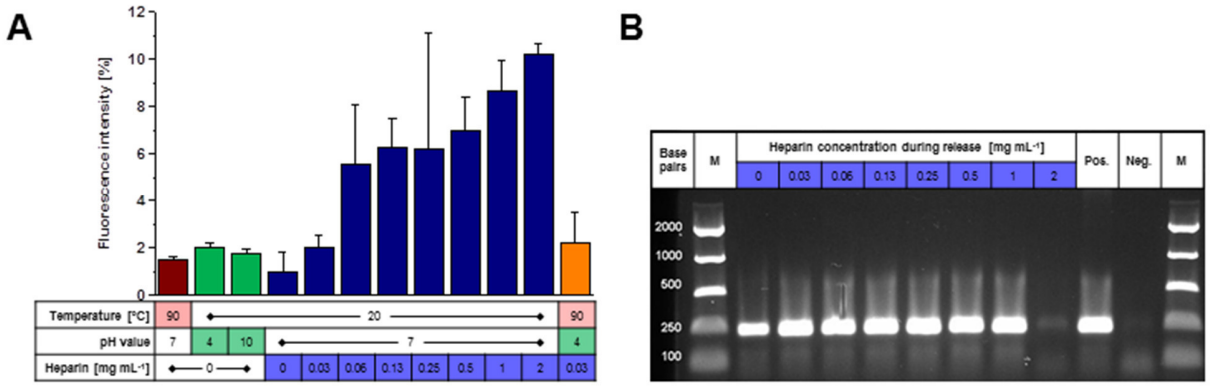

Figure 5.2. DNA uptake and release of PP-matrix supported hydrogels. A) Quantification of DNA release depending on temperature, pH value and heparin concentration, and B) gel electrophoresis of PCR products from release eluates at varying heparin concentrations.

Poly(2-oxazoline)-based multilayers. To combine the advantages of a hydrogel matrix with diffusion independent, surface mediated processes, cationic polymer layers were covalently attached to a surface (glass and PP) by a so-called layer-by-layer (LbL) technique.[117] Although the covalent immobilization of POx on glass substrates has been described in the context of anti-fouling coatings,[118] its bioanalytical potential has not been reported so far. The functionalization of the glass surface comprises the cleaning and activation by plasma and the attachment of an epoxide group bearing siloxane monolayer (3-glycidyloxypropyl trimethoxysilane, GOPTMS) (Scheme 5.2). Subsequently, a monolayer of the amine containing block copolymer **35** was attached *via* the ring-opening reaction of the epoxide.[119] To obtain multilayers, the remaining amine groups were partially functionalized with ECH, the epoxide rings regenerated (alkaline conditions) and reacted with a second layer of **35** as described before. This cycle can be repeated several times to install a defined number of POx coatings on the surface with specific film thicknesses.

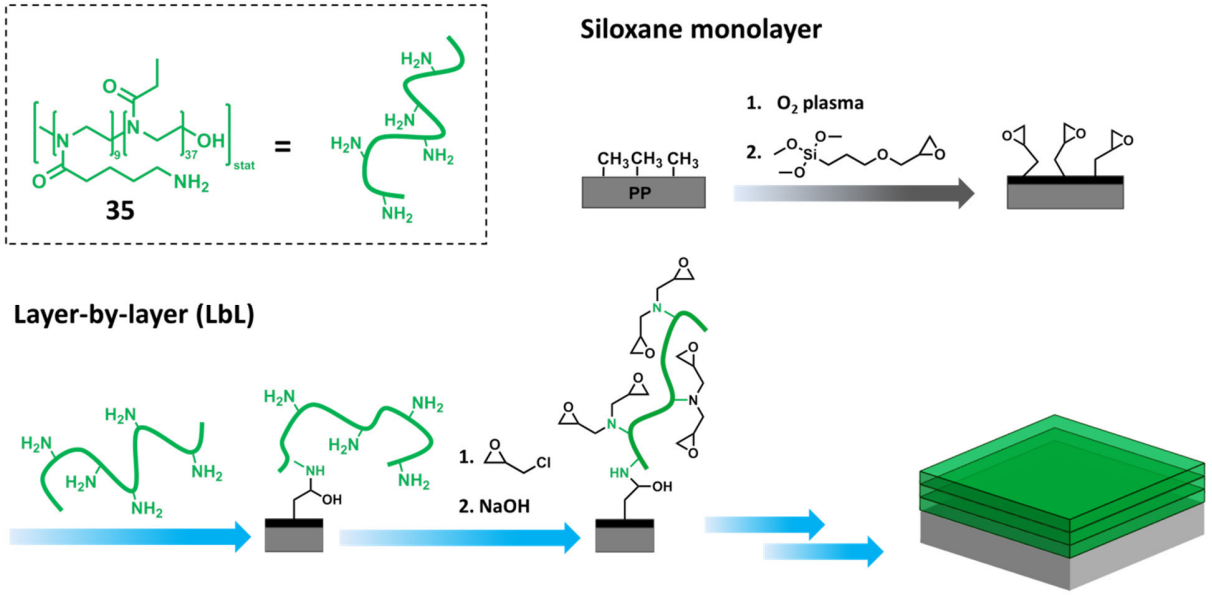

Scheme 5.2. Schematic representation of the deposition of **35** on substrates by layer-by-layer immobilization.

The successful layer deposition was shown by contact angle (CA), thermogravimetric analysis (TGA) and reflectometric interference spectroscopy (RIFS)[120] measurements. Finally, the LbL deposition was successfully proven for the stepwise attachment of three polymer layers by using fluorescently labeled **35** (Fluorescein-NHS-ester). All coatings steps could be tracked by confocal laser scanning microscopy (CLSM) measurements. To investigate the ability of POx multilayers on a PP chip to absorb genetic material in a reversible manner, Cy5-labeled DNA strands were used. Each reaction step was followed by a purification treatment with DMF as well as water. The CLSM measurements did not show an efficient uptake behavior within the first 5 min for one POx multilayer which can be attributed to a low degree of swelling (Figure 5.3A). In contrast, PP chips with two layers revealed an increase of the fluorescence up to 5 min incubation time while three layers resulted in a constant increase in emission up to 2 h. It can be assumed that the DNA absorption behavior depends on the number of polymer layers. To investigate the ability of a controllable DNA release, which is necessary for a subsequent polymerase, PP chips were loaded with DNA for 1 hour and subjected to a temperature dependent washing process (Figure 5.3B). Temperatures of 65 °C or higher resulted in a release of 40% of the initially bound DNA which is in accordance to the conditions of PCR experiments (57 to 95 °C). Since there is no significant

difference for two and three POx layers, the PCR experiments were conducted using POx double layers.

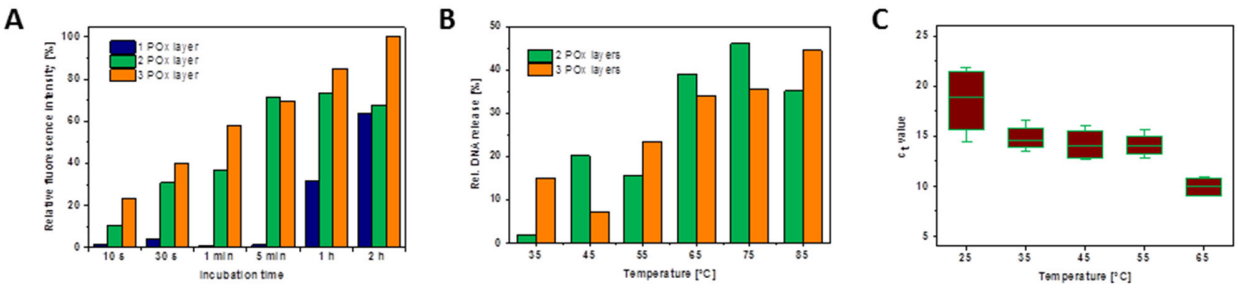

Figure 5.3. A,B) Adsorption and release of Cy5 labeled DNA by POx (**35**) multilayers. A) Time dependent uptake of labeled genetic material determined by mean fluorescence of POx multilayers after treatment. B) Temperature dependent release of POx multilayers loaded with DNA for 1 h displayed as percentage of the initially bound DNA amount. C) Box-plot of qPCR experiments, performed in POx coated (**35**) reaction vessels. The tubes were loaded with genetic material from cell lysates at different temperatures and the c_t value of the amplification was recorded.

In order to create a model system similar to industrial requirements, PCR-tubes (RoboStrip PP white 8-well strips low profile) were coated using unlabeled POx **35**. After successful binding of DNA (from Escherichia coli BL21), a specific primer (for LacZ-Gene) and a PCR master mix was added to the tube and subjected to qPCR. The working principle of the "lab in a tube" approach is depicted in Figure 5.4. The surface binding of DNA revealed positive results for the specific *E. coli*-target LacZ-gene and the PCR product showed the same melting point as the positive control. In order to develop a simple and low-cost system, DNA binding has to be performed directly from a cell lysate tolerating other (charged) cellular components instead of using purified genetic material. To this end, *E. coli* suspension was heated to 95 °C to lyse the cells. A defined amount of cell lysate was filled in different tubes coated with **35** and incubated for 1 h. The samples were incubated at different temperatures ranging from 25 to 65 °C (Figure 5.3C). For all temperatures, E. coli DNA could be detected with the desired melting point around 87.3 °C. Increasing temperature results in a decrease of the c_t value of the qPCR, and therefore, a faster amplification process.

The "lab in a tube" model displays a promising tool for bioanalytics since it enables the collection of DNA samples from biological materials, and allows the purification, amplification and detection within one coated PCR tube.

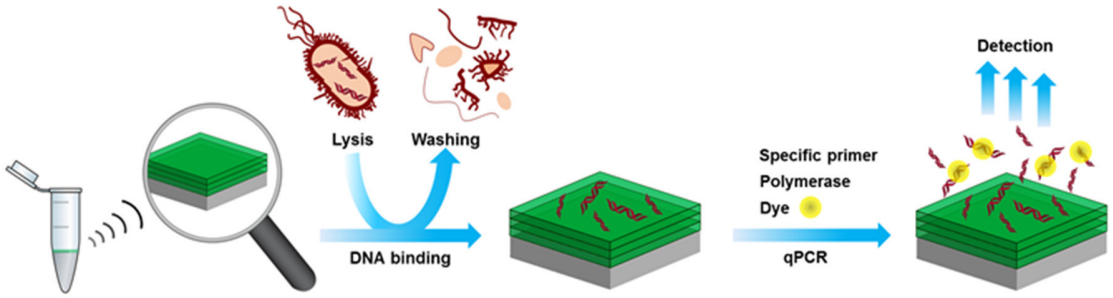

Figure 5.4. Working principle of the "lab in a tube" approach. Cells are lysed by heat treatment and genetic material is adsorbed in POx surface coatings. After addition of a specific primer and a PCR master mix, amplification and detection is accomplished in a qPCR process.

Core cross-linked nanogels. Another challenge is the use of amine containing copolymers for the encapsulation of drugs. A widely studied dosage form for the administration of hydrophobic compounds is the polymeric micelle[121] which is formed *via* the aqueous self-assembly of block copolymers consisting of hydrophobic and hydrophilic segments.[122] As reported recently, the cross-linking of such systems prevents a disassembly and a component exchange even below the critical micelle concentration (CMC).[123] Nanogels combine the beneficial properties of hydrogels (tissue-like structure, stimuli responsiveness) and nano-assemblies (solubility properties, such as nanoparticles or micelles) in the nanometer size range. To obtain nanogels, different approaches have been established. Besides the inverse emulsion[124] and the polymerization induced phase separation,[125] an elegant way is the cross-linking of self-assembled structures. Up to date, only a limited number of reports described the synthesis and the potential of covalently cross-linked POx micelles, comprising the stabilization *via* epoxide-amine cross-linking,[126] light-mediated cross-linking,[127-128] thiol-yne chemistry,[129-130] electron beam irradiation[131] as well as the use of a disulfide bond linker (reversible system).[132]

The copolymers **36** to **40**, consisting of the neutral hydrophilic EtOx and the cationic AmOx block, were self-assembled in organic solvents (Figure 5.5). Since both blocks are readily water soluble, these structures have to be cross-linked to transfer them into aqueous solution. Therefore, glutaraldehyde was used to synthesize core-crosslinked nanogels. As reported in the literature, a full conversion of the amine groups is not possible[133] and residual aldehydes have to be quenched by low molar mass amines. Besides a stabilization of the self-assembled structure, this strategy can be used to simultaneously incorporate drug molecules or fluorescence labels. The nanogel structures of **36** to **40** were quenched with diethylamine (DEA) and loaded with 6-amino fluorescein (6AF), respectively, and could be transferred to aqueous medium. In addition, the reversibility of this system allows a later disassembly of the network.[134]

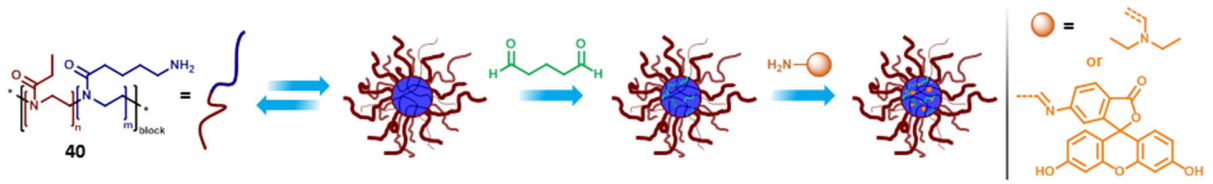

Figure 5.5. Schematic representation of the self-assembly of **40** followed by cross-linking and quenching (diethylamine) or loading (6-amino fluorescein, 6AF).

The self-assembly and subsequent loading of cross-linked copolymer **40** in chloroform (**41**) and *iso*propanol (**42**), respectively, was followed by DLS measurements and AF4 experiments (Table 5.2). Distributions in water are in the same size range as in organic solvents while the PDI values of the quenched systems increased slightly, evidencing aggregation caused by unconsumed aldehyde groups in the core. However, the values are still in the acceptable range for synthetic nano-sized objects. The presence of free amine groups was confirmed by positive zeta potentials for all samples. Besides the calculation of the molar masses of specific polymers, AF4 can be used to determine the hydrodynamic radius (R_h, only DLS) and the radius of gyration (R_g, multi-angle laser light scattering (MALLS)). The sample **41** revealed a similar R_h value as obtained by DLS measurement. In contrast, for **42**, the obtained value is smaller than the size obtained from DLS measurement. This could be due to the AF4 separation technique, which examines single colloidal structures instead of taking also small fractions of aggregates into

account (DLS investigation). Furthermore, AF4 enables the characterization of the particle shape by the ratio of R_g and R_h ($\rho = R_g/R_h$). For **41**, no R_g value could be determined since the value was too small for detection (MALLS detector limit: ~ 15 nm).[135] The obtained ρ ratio below 0.8 describes a hard sphere and, therefore, a compact structure like a micellar architecture.[136] A larger ratio (~ 1.0), as obtained for **42**, is usually attributed to soft and less dense structures, such as vesicles.[136] The vesicular morphology of **42** is supported by the block architecture of P(EtOx-*b*-AmOx) and the fact, that the radius of the assembly is longer than the fully stretched polymer chain (32 nm length). The proposed structures were visualized *via* cryo transmission electron microscopy (cryoTEM) measurements and facilitate the interpretation of micelles and vesicles in good agreement to the results of DLS and AF4 measurements.

Table 5.2. Characterization for cross-linked nanostructures (DLS: 5 mg mL^{-1}, size indication in radius). Polymer **40** served as precursor for the assemblies. The content of fluorescein was determined by the absorbance at 470 nm.

			DLS in water			AF4			
#	Solvent for self-assembly	Capping agent	Size, R_h [nm]	PDI	ζ [mV]	R_g	R_h	ρ	Content of capping agent [wt%]
41	$CHCl_3$	6AF	15	0.20	+17	-	20	<0.8	29
42	*i*PrOH	6AF	50	0.18	+23	40	40	1.00	29

To investigate the cytotoxicity of the assembled structures **41** and **42**, routine XTT assays were performed using the established L929 cell line. After 24 h of incubation, **41** revealed a lower biocompatibility only for the highest concentration of micelles (5 mg mL^{-1}) while the vesicular structures did not show any cytotoxicity within the investigated concentration range (Figure 5.6A). However, the concentration range of potential applications is far below the border to cytotoxicity in both cases. Another challenge is the time and concentration dependent cellular uptake of **41** and **42**, which is quantified by flow cytometric measurements. Increasing sample concentrations resulted in higher fluorescence intensities indicating a concentration dependent uptake (Figure 5.6B). The vesicular structure **42** revealed a stronger increase of fluorescence, in particular for higher concentrations which could be attributed to an increased cellular accumulation/association compared to micelles **41** (three-fold uptake at 0.5 mg mL^{-1}). The same trend could be observed for the time-dependent uptake over 24 h (Figure 5.6C).

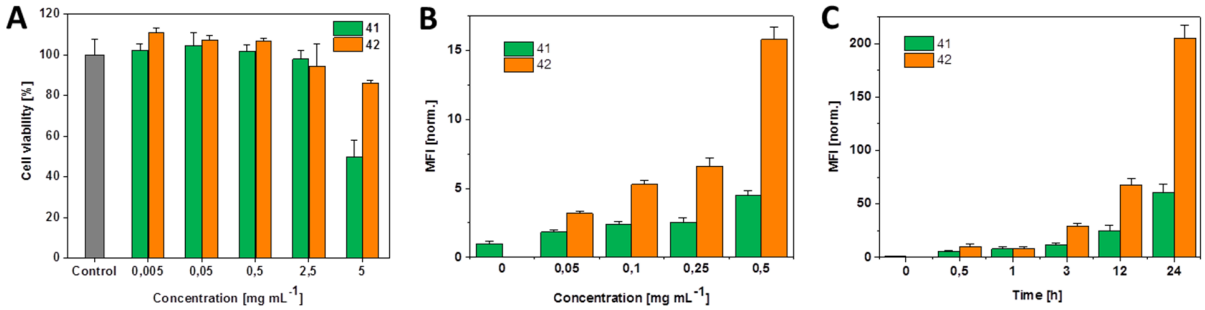

Figure 5.6. A) Cell viability of L929 mouse fibroblasts after incubation with micelles (**42**)/vesicles (**44**) up to 5 mg mL^{-1} for 24 hours. B) Flow cytometry investigation on the concentration and time dependent uptake of 6AF containing micelles/vesicles by L929 mouse fibroblasts at 37 °C. For the concentration dependent uptake, cells were investigated over an incubation time of 24 h using micelle/vesicle concentrations in the range between 0.05 and 0.5 mg mL^{-1}. C) For the time dependent uptake, cells were incubated between 0.5 and 24 h with micelles/vesicles with a concentration of 0.5 mg mL^{-1}.

Confocal laser scanning microscopy (CLSM) was performed to elucidate the cellular internalization and intracellular localization of micelles and vesicles in L929 cells. Figure 5.7 shows a representative distribution of the fluorescent vesicle **42** in the context of cellular structures in detached cells revealing three main observations: 1) Since the 6AF labeled structures (green) are exclusively detectable within the stained cell membrane (orange), CLSM images are in favor of an intracellular localization (Figure 5.7, a_1 to a_3); 2) within the nuclear compartment (blue), no vesicles are observed (Figure 5.7, b_1 to b_3), and 3) co-localization of the vesicles and stained acidic endosomes (red) occurs (Figure 5.7, c_1 to c_3). Since only intact nanostructures can be detected by fluorescence in an intracellular environment, the studies clearly suggest an endosomal location, and, therefore, an internalization by endocytosis can be assumed. In the future, the self-assembling structures should enable the administration of drugs, *e.g.* cytostatic.

In conclusion, the combination of POx and amine bearing side chains results in challenging polymer systems which can be used to design various functional materials.

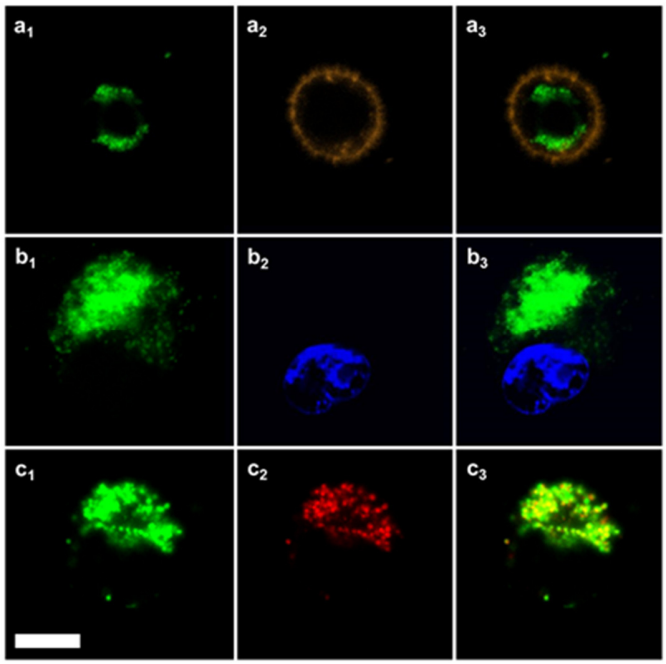

Figure 5.7. Representative CSLM images of detached L929 cells after 24 h incubation at 37 °C with vesicles **42** at 0.1 mg mL^{-1}. Cell membranes (a_2), cell nuclei (b2), or late endosomes/lysosomes (c_2) were specifically stained and correlated with the fluorescence signal of 6AF labeled vesicles (a_1, b_1 and c_1). Superimposition of both channels (a_3, b_3 and c_3) proves an intracellular (a_3) but extra-nuclear (b_3) localization of the vesicles and their apparent co-localization with endosomal structures (c_3). Scale bar: 10 µm.

6 SUMMARY

The treatment of human diseases by the efficient and specific delivery of drugs or genetic material to target cells of the patient is one major task of current and future biomedical research. Besides the well-established delivery systems of lipids, peptides and natural-occurring polymers, synthetic polymers represent promising alternatives with numerous opportunities of modification. Since they enable the circumvention of biological barriers, cationic polymers play a crucial role for biomedical applications, in particular gene delivery. They can electrostatically interact with the negatively charged phosphate groups of nucleic acids (*e.g.* deoxyribonucleic acid) and eventually protect them from enzymatic degradation. The formed polyplexes are able to enter the cell and to release the cargo to the site of action.

Within the last decades, poly(ethylene imine) (PEI) has emerged as the state-of-the-art of gene delivery agents. The linear form (LPEI) is thereby preferred, since it shows reduced cytotoxicity and enhanced synthesis control compared to the branched form. Poly(2-oxazoline)s (POx) represent ideal starting materials for the production of LPEI, since they can be easily converted into cationic polymers bearing primary, secondary and tertiary amine functionalities. The fast and efficient cationic ring-opening polymerization of 2-oxazolines enables the synthesis of well-defined POx and tolerates numerous functionalities as 2-substitutents of the monomers. Furthermore, it allows the introduction of different end-groups which can be exploited for post-polymerization modification processes. The acidic hydrolysis of poly(2-alkyl-2-oxazoline) results in the cleavage of propionic acid and the formation of secondary amine functionalities. The degree of hydrolysis can be well-controlled by using microwave-assisted synthesis approaches. Although the fully hydrolyzed polymer, LPEI, reveals remarkable properties concerning polyplex formation, major drawbacks such as poor water solubility, severe cytotoxicity, and undesired non-specific interactions with cellular and non-cellular components have to be overcome. The present thesis deals with the modification of cationic polymers based on POx to enhance their biological properties and introduce targeting sites, while maintaining the efficiency for biomedical applications (Figure 6.1).

One powerful tool to turn LPEI into a biocompatible polymer is its one-pot modification with hydrophilic moieties. As an alternative to well-established carbohydrates which mostly require

multi-step syntheses, hydroxyl moieties (carbohydrate-mimetics), *i.e.* paraformaldehyde and glycidol, can be installed in a close proximity to the polymer backbone to improve the biocompatibility. A second approach is the oxidation of secondary amine groups in the LPEI backbone using hydrogen peroxide. The conversion of the functional groups into amides turns the polymer into a biocompatible and biodegradable material. The described modification represents a useful technique for future synthesis approaches.

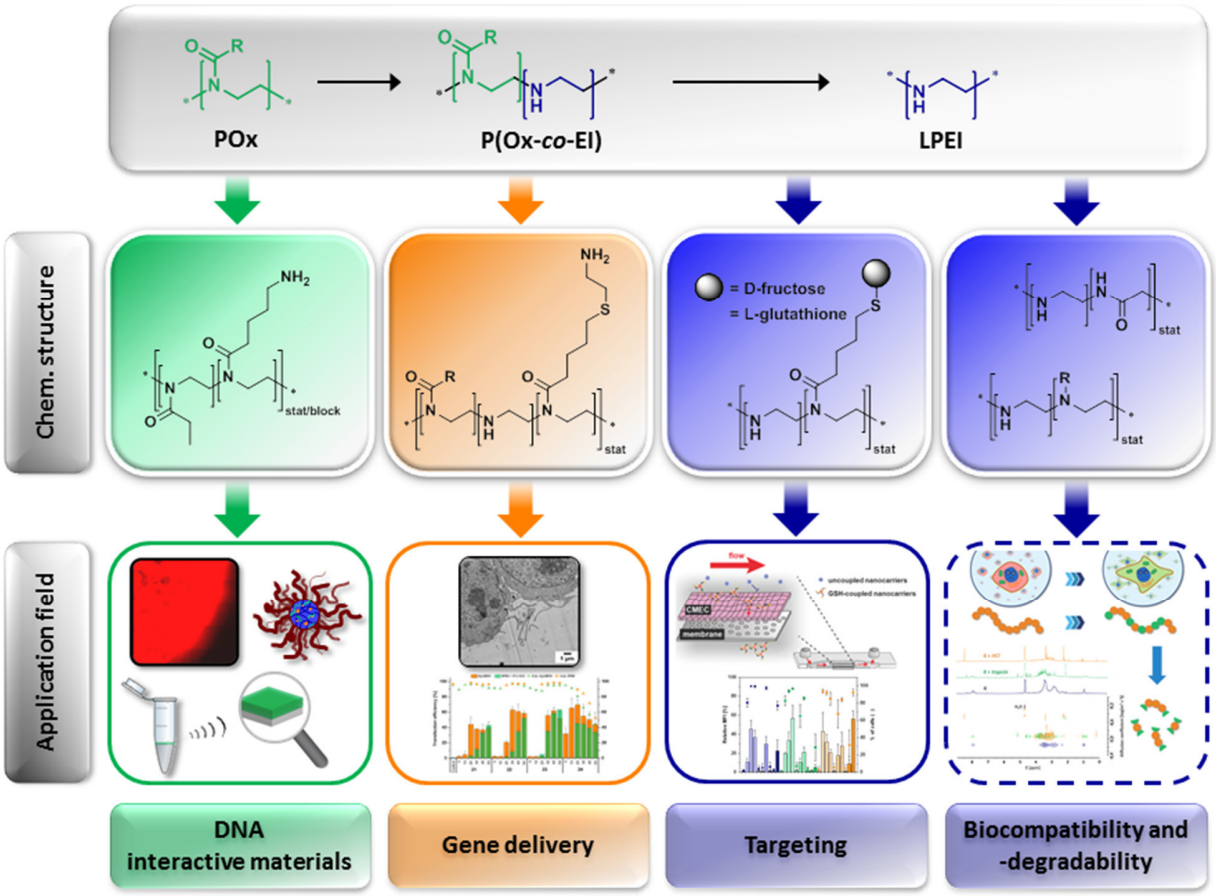

Figure 6.1. Schematic overview of the various cationic polymer structures obtained by the modification of poly(2-oxazoline) and their biomedical application fields.

Besides enhancing the biocompatibility and the transport of genetic material, the specific drug targeting using PEI derivatives represents a major challenge. Since the hydrolysis conditions of POx prevent the simultaneous presence of secondary amine groups and alkene functionalities,

LPEI was modified *via* *N*-acylation (pseudo-POx) followed by the attachment of targeting molecules or functional groups. The attachment of L-glutathione moieties allows the successful crossing of polyplexes through the hCMEC/D3 endothelial cell layer mimicking the blood-brain barrier (BBB), which usually limits the transportation of genetic material, within a microfluidically perfused biochip. The modification with D-fructose enables the specific delivery of genetic material into human breast cancer cells (*i.e.* MDA-MB-231) while revealing cell-type specific cytotoxicities. The combination of partially hydrolyzed PEtOx and the subsequent installation of primary amine groups in the polymer side chain results in non-viral gene delivery agents that even outperform LPEI. Their endosomal release could be identified and investigated in detail by super-resolution and electron microscopy.
Another approach to obtain cationic polymers with strong affinity for nucleic acids is the introduction of amine functionalities to the side chain of 2-oxazoline monomers prior to the polymerization. The obtained statistical and block copolymers can be used for the design of hydrogels, nanogels and surface coatings, which are utilized for either pathogen detection or drug delivery.

In summary, the convenient modification of cationic polymers made from POx results in high functional polymer systems which can serve as platform materials for various biomedical applications. The present work will be the basis for further tailor-made polymer systems and will encourage researchers to continue the investigation of modified cationic polymers. In particular, the combination of drug delivery and cell specific targeting is of tremendous interest for the future treatment of human diseases and has to take the next step from bench to bedside.

7 ZUSAMMENFASSUNG

Die Behandlung von verschiedenen Krankheitsbildern durch den effizienten und zielgerichteten Transport von Wirkstoffen oder genetischem Material zum gewünschten Wirkungsort stellt eine Hauptaufgabe innerhalb der heutigen und der zukünftigen biomedizinischen Forschung dar. Neben den etablierten Transportsystemen wie Lipiden, Peptiden und natürlichen Polymeren haben sich insbesondere synthetische Polymere mit ihren zahlreichen Modifizierungsmöglichkeiten als vielversprechende Alternativen hervorgetan. Eine besondere Bedeutung kommt dabei kationischen Polymeren im Hinblick auf biomedizinische Anwendungen, im Speziellen für den Gentransfer, zu. Die elektrostatische Wechselwirkung ihrer positiven Ladungen mit den negativ geladenen Phosphatgruppen der Nukleinsäuren (z.B. Desoxyribonukleinsäure) führt zur Komplexbildung und gleichzeitig zur Abschirmung des genetischen Materials, welches unter Anderem vor einem enzymatischen Abbau schützt. Die auf diese Weise gebildeten Polyplexe ermöglichen den Transport von Nukleinsäuren in die Zellen und deren Freisetzung am entsprechenden Wirkungsort.

In den letzten Jahrzehnten hat sich Poly(ethylenimin) (PEI) zum „Goldstandard“ für den Gentransfer entwickelt. Dabei wird die lineare (LPEI) gegenüber der verzweigten Form (BPEI) bevorzugt, da sie neben einer reduzierten Zytotoxizität auch eine einfachere Kontrolle der Synthese zulässt. Poly(2-oxazoline) (POx) stellen das ideale Ausgangsmaterial für die Herstellung von LPEI dar, da sie verhältnismäßig einfach in kationische Polymere mit primären, sekundären und tertiären Aminfunktionalitäten umgewandelt werden können. Die schnelle und effiziente kationische Ringöffnungspolymerisation von 2-Oxazolinen ermöglicht die Synthese von gut definierten POx und toleriert gleichzeitig zahlreiche Funktionalitäten in 2-Position der Monomere. Weiterhin erlaubt sie die Einführung von verschiedenen Endgruppen, die zur anschließenden Modifizierung genutzt werden können. Die saure Hydrolyse von Poly(2-alkyl-2-oxazolinen) resultiert in der Abspaltung von Propionsäure und der Ausbildung von sekundären Amingruppen. Der Hydrolysegrad kann dabei durch einen mikrowellenunterstützten Syntheseansatz gut kontrolliert werden. Obwohl das vollständig hydrolysierte Polymer, LPEI, außerordentlich gute Eigenschaften bezüglich einer Polyplexbildung zeigt, existieren zahlreiche Nachteile wie eine schlechte Wasserlöslichkeit, hohe Zytotoxizität sowie unspezifische

Wechselwirkungen mit zellulären und nicht-zellulären Bestandteilen. Die vorliegende Arbeit beschäftigt sich mit der Modifizierung von kationischen Polymeren basierend auf POx mit dem Ziel der Verbesserung ihrer biologischen Eigenschaften und der gezielten Einführung von Funktionalitäten für spezielle biomedizinische Anwendungen (Figure 7.1).

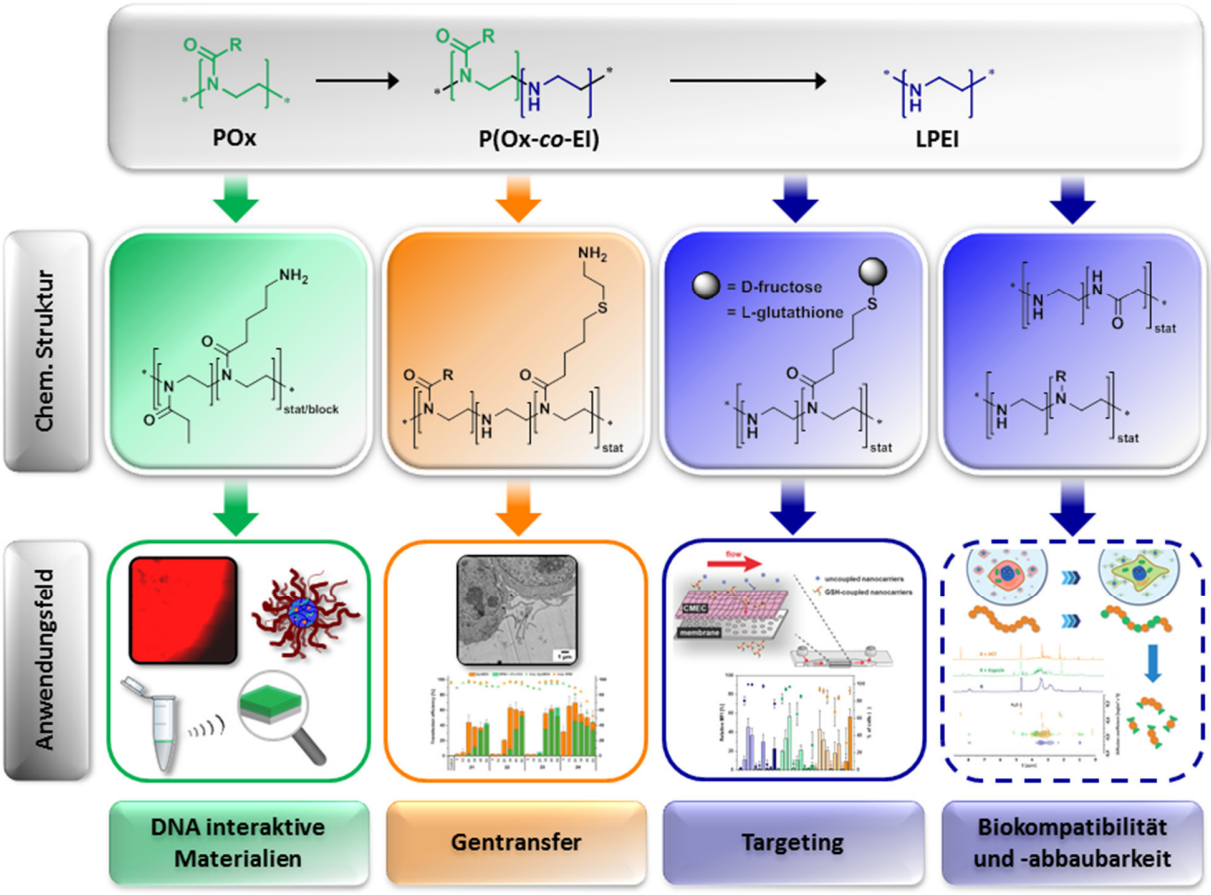

Figure 7.1. Schematische Übersicht über die verschiedenen kationischen Polymere, die durch Modifizierung von Poly(2-oxazolinen) erhalten wurden und ihre biomedizinischen Anwendungsgebiete.

Eine Möglichkeit LPEI in ein biokompatibles Polymer umzuwandeln ist die einstufige Modifizierung mit hydrophilen Resten. Als eine Alternative zu bereits etablierten Kohlenhydraten, welche meistens Mehrstufensynthesen erfordern, können Hydroxylreste, im Speziellen Paraformaldehyd und Glycidol, in unmittelbarer Nähe des Polymer-Rückgrates zur Verbesserung der Biokompatibilität angebracht werden. Ein zweiter Ansatzpunkt ist die

Oxidation von sekundären Amingruppen im LPEI-Rückgrat mittels Wasserstoffperoxid. Die Umwandlung dieser Funkionalitäten in Amidgruppen resultiert in biokompatiblen und gleichzeitig bioabbaubaren Polymeren. Die beschriebene Modifikation stellt eine vielseitig anwendbare Technik für zukünftige Syntheseansätze dar.

Neben den genannten Aspekten der Biokompatibilität und Bioabbaubarkeit stellt die zielgerichtete Anreicherung und Freisetzung eines Wirkstoffes am gewünschten Wirkungsort unter Verwendung von PEI-Derivaten eine weitere Herausforderung dar. Da die Hydrolysebedingungen von POx die gleichzeitige Anwesenheit von sekundären Amin- und Alkenfunktionalitäten verhindern, musste ein alternativer Syntheseweg gefunden werden. Dabei wird LPEI zunächst mittels *N*-Acylierung modifiziert (Pseudo-POx) und anschließend erfolgt die Einführung von Zielmolekülen oder weiteren funktionellen Gruppen. Die Funktionalisierung mit L-Glutathionresten ermöglicht dabei die erfolgreiche Passage von Polyplexen durch die hCMEC/D3 Endothelzellschicht innerhalb eines mikrofluidischen Biochips. Dieser dient als Modell der Blut-Hirn-Schranke, die für gewöhnlich den Transport von genetischem Material verhindert. Die Modifikation von LPEI mit D-Fructose hingegen erlaubt den gezielten Transport von genetischem Material in menschliche Brustkrebszellen (im Speziellen MDA-MB-231) und weist dort zellspezifische Zytotoxizität auf. Weiterhin kann die Kombination aus partiell hydrolysiertem Poly(2-ethyl-2-oxazolin) mit primären Aminfunktionalitäten in der Polymerseitenkette als nicht-viraler Gentransporter verwendet werden. Dieser zeigte verbesserte Eigenschaften gegenüber dem Goldstandard LPEI. Die endosomale Freisetzung konnte mittels hochauflösender Konfokal- und Elektronenmikroskopie untersucht und nachgewiesen werden.

Ein weiterer Ansatzpunkt für kationische Polymere mit ausgeprägter Bindungsaffinität für Nukleinsäuren ist die Einführung von Aminfunktionalitäten in die Seitenkette von 2-Oxazolinmonomereinheiten. Die anschließend synthetisierten Copolymere (Block und statistisch) dienen als Ausgangsmaterial für das Design von Hydrogelen, Nanogelen und Oberflächenbeschichtungen, die sowohl für die Detektion von Krankheitserregern als auch für den gezielten Wirkstofftransport eingesetzt werden können.

Zusammenfassend konnte gezeigt werden, dass die einfache Modifikation von kationischen Polymeren in hochfunktionalisierten Polymersystemen resultieren kann. Diese können als

Plattform für zahlreiche biomedizinische Anwendungen genutzt werden. Die vorliegende Arbeit stellt die Basis für zukünftige maßgeschneiderte Polymersysteme dar und soll Wissenschaftler ermutigen, entsprechende Forschungen weiter voran zu treiben. Insbesondere die Kombination aus Wirkstofftransport und zellspezifischen Zielmolekülen ist von fundamentalem Interesse für die zukünftige Behandlung von humanen Krankheitsbildern und hat den entscheidenden Schritt von der Laborbank zum klinischen Einsatz noch vor sich.

8 REFERENCES

[1] B. A. Bolto, D. R. Dixon, R. J. Eldridge, S. J. King, in *Chemical water and wastewater treatment V*, Springer, **1998**, pp. 173-185.
[2] S. R. Deka, A. K. Sharma, P. Kumar, *Curr. Top. Med. Chem.* **2015**, *15*, 1179-1195.
[3] S. K. Samal, M. Dash, S. Van Vlierberghe, D. L. Kaplan, E. Chiellini, C. van Blitterswijk, L. Moroni, P. Dubruel, *Chem. Soc. Rev.* **2012**, *41*, 7147-7194.
[4] R. Gardlik, R. Palffy, J. Hodosy, J. Lukacs, J. Turna, P. Celec, *Med. Sci. Monit. Basic Res.* **2005**, *11*, RA110-RA121.
[5] W. Walther, U. Stein, *Drugs* **2000**, *60*, 249-271.
[6] C. R. Dass, *Int. J. Pharm.* **2002**, *241*, 1-25.
[7] R. I. Mahato, *J. Drug Targeting* **1999**, *7*, 249-268.
[8] J. L. Merlin, A. N'Doye, T. Bouriez, G. Dolivet, *Drug News Perspect.* **2002**, *15*, 445-451.
[9] U. Lächelt, E. Wagner, *Chem. Rev.* **2015**, *115*, 11043-11078.
[10] A. C. Rinkenauer, S. Schubert, A. Traeger, U. S. Schubert, *J. Mater. Chem. B* **2015**, *3*, 7477-7493.
[11] S. C. De Smedt, J. Demeester, W. E. Hennink, *Pharm. Res.* **2000**, *17*, 113-126.
[12] Y. Zhang, A. Satterlee, L. Huang, *Mol. Ther.* **2012**, *20*, 1298-1304.
[13] J. Durzyńska, Ł. Przysiecka, R. Nawrot, J. Barylski, G. Nowicki, A. Warowicka, O. Musidlak, A. Goździcka-Józefiak, *J. Pharmacol. Exp. Ther.* **2015**, *354*, 32-42.
[14] J.-P. Behr, *Chimia* **1997**, *51*, 34-36.
[15] Z. U. Rehman, D. Hoekstra, I. S. Zuhorn, *ACS Nano* **2013**, *7*, 3767-3777.
[16] S. B. Sieczkarski, G. R. Whittaker, *J. Gen. Virol.* **2002**, *83*, 1535-1545.
[17] M. A. Mintzer, E. E. Simanek, *Chem. Rev.* **2009**, *109*, 259-302.
[18] M. Neu, D. Fischer, T. Kissel, *J. Gene Med.* **2005**, *7*, 992-1009.
[19] O. Boussif, F. Lezoualc'h, M. A. Zanta, M. D. Mergny, D. Scherman, B. Demeneix, J. P. Behr, *Proc. Natl. Acad. Sci. U. S. A.* **1995**, *92*, 7297-7301.
[20] W. T. Godbey, K. K. Wu, A. G. Mikos, *J. Control. Release* **1999**, *60*, 149-160.
[21] W. T. Godbey, M. A. Barry, P. Saggau, K. K. Wu, A. G. Mikos, *J. Biomed. Mater. Res.* **2000**, *51*, 321-328.
[22] B. Abdallah, A. Hassan, C. Benoist, D. Goula, J. P. Behr, B. A. Demeneix, *Hum. Gene Ther.* **1996**, *7*, 1947-1954.
[23] G. D. Jones, A. Langsjoen, S. M. M. C. Neumann, J. Zomlefer, *J. Org. Chem.* **1944**, *9*, 125-147.
[24] M. Jäger, S. Schubert, S. Ochrimenko, D. Fischer, U. S. Schubert, *Chem. Soc. Rev.* **2012**, *41*, 4755-4767.
[25] J. R. Demember, L. D. Taylor, *J. Polym. Sci., Polym. Chem. Ed.* **1979**, *17*, 1089-1101.
[26] E. J. Goethals, P. Bossaer, R. Deveux, *Polym. Bull.* **1981**, *6*, 121-126.
[27] K. F. Weyts, E. J. Goethals, *Polym. Bull.* **1988**, *19*, 13-19.
[28] M. Bauer, C. Lautenschlaeger, K. Kempe, L. Tauhardt, U. S. Schubert, D. Fischer, *Macromol. Biosci.* **2012**, *12*, 986-998.
[29] D. A. Tomalia, D. P. Sheetz, *J. Polym. Sci., Part A: Polym. Chem.* **1966**, *4*, 2253-2265.
[30] T. Kagiya, S. Narisawa, T. Maeda, K. Fukui, *J. Polym. Sci., Part B: Polym. Lett.* **1966**, *4*, 441-445.
[31] T. G. Bassiri, A. Levy, M. Litt, *J. Polym. Sci., Part B: Polym. Lett.* **1967**, *5*, 871-879.

[32] W. Seeliger, E. Aufderhaar, W. Diepers, R. Feinauer, R. Nehring, W. Thier, H. Hellmann, *Angew. Chem.* **1966**, *78*, 913-927.
[33] R. Tanaka, I. Ueoka, Y. Takaki, K. Kataoka, S. Saito, *Macromolecules* **1983**, *16*, 849-853.
[34] J. H. Jeong, S. H. Song, D. W. Lim, H. Lee, T. G. Park, *J. Control. Release* **2001**, *73*, 391-399.
[35] T. Saegusa, H. Ikeda, H. Fujii, *Polym. J.* **1972**, *3*, 35-39.
[36] T. Saegusa, S. Kobayashi, A. Yamada, *Macromolecules* **1975**, *8*, 390-396.
[37] F. Wiesbrock, R. Hoogenboom, C. H. Abeln, U. S. Schubert, *Macromol. Rapid Commun.* **2004**, *25*, 1895-1899.
[38] H. M. L. Lambermont-Thijs, F. S. van der Woerdt, A. Baumgaertel, L. Bonami, F. E. Du Prez, U. S. Schubert, R. Hoogenboom, *Macromolecules* **2010**, *43*, 927-933.
[39] L. Tauhardt, K. Kempe, K. Knop, E. Altuntaş, M. Jäger, S. Schubert, D. Fischer, U. S. Schubert, *Macromol. Chem. Phys.* **2011**, *212*, 1918-1924.
[40] V. R. de la Rosa, E. Bauwens, B. D. Monnery, B. G. De Geest, R. Hoogenboom, *Polym. Chem.* **2014**, *5*, 4957-4964.
[41] P. Chollet, M. C. Favrot, A. Hurbin, J. L. Coll, *J. Gene Med.* **2002**, *4*, 84-91.
[42] C. Englert, L. Tauhardt, M. Hartlieb, K. Kempe, M. Gottschaldt, U. S. Schubert, *Biomacromolecules* **2014**, *15*, 1124-1131.
[43] A. S. Hoffman, *J. Control. Release* **2008**, *132*, 153-163.
[44] K. E. Uhrich, S. M. Cannizzaro, R. S. Langer, K. M. Shakesheff, *Chem. Rev.* **1999**, *99*, 3181-3198.
[45] C. A. Taylor, Z. Liu, T. C. Tang, Q. Zheng, S. Francis, T.-W. Wang, B. Ye, J. A. Lust, R. Dondero, J. E. Thompson, *Mol. Ther.* **2012**, *20*, 1305-1314.
[46] L. Buscail, B. Bournet, F. Vernejoul, G. Cambois, H. Lulka, N. Hanoun, M. Dufresne, A. Meulle, A. Vignolle-Vidoni, L. Ligat, N. Saint-Laurent, F. Pont, S. Dejean, M. Gayral, F. Martins, J. Torrisani, O. Barbey, F. Gross, R. Guimbaud, P. Otal, F. Lopez, G. Tiraby, P. Cordelier, *Mol. Ther.* **2015**, *23*, 779-789.
[47] http://www.biocancell.com/lead-program/bc-819/, last assessed 11th Apr. 2017.
[48] I. J. Matouk, D. Halle, M. Gilon, A. Hochberg, *J. Transl. Med.* **2015**, *13*, 113.
[49] https://clinicaltrials.gov/ct2/show/NCT01118052, last assessed 11th Apr. 2017.
[50] J. G. Fewell, M. Matar, G. Slobodkin, S.-O. Han, J. Rice, B. Hovanes, D. H. Lewis, K. Anwer, *J. Control. Release* **2005**, *109*, 288-298.
[51] R. D. Alvarez, M. W. Sill, S. A. Davidson, C. Y. Muller, D. P. Bender, R. L. DeBernardo, K. Behbakht, W. K. Huh, *Gynecol. Oncol.* **2014**, *133*, 433-438.
[52] http://celsion.com/pipeline/, last assessed 11th Apr. 2017.
[53] F. Lori, J. Trocio, N. Bakare, L. M. Kelly, J. Lisziewicz, *Vaccine* **2005**, *23*, 2030-2034.
[54] http://www.hydromer.com/cosmetics_personal_care.html, last assessed 11th Apr. 2017.
[55] https://clinicaltrials.gov/ct2/show/NCT02579473, last assessed 11th Apr. 2017.
[56] J. K. L. Eskow, D. G. Standaert, T. X. Viegas, M. D. Bentley, Z. Fang, B. Dizman, K. Yoon, R. Weimer, P. Ravenscroft, T. H. Johnston, M. P. Hill, J. M. Brotchie, R. W. Moreadith, *Mov. Disord.* **2013**, *28*, 1675-1682.
[57] J. Tong, R. Luxenhofer, X. Yi, R. Jordan, A. V. Kabanov, *Mol. Pharmaceutics* **2010**, *7*, 984-992.
[58] R. Luxenhofer, G. Sahay, A. Schulz, D. Alakhova, T. K. Bronich, R. Jordan, A. V. Kabanov, *J. Control. Release* **2011**, *153*, 73-82.

[59] T. X. Viegas, M. D. Bentley, J. M. Harris, Z. Fang, K. Yoon, B. Dizman, R. Weimer, A. Mero, G. Pasut, F. M. Veronese, *Bioconjugate Chem.* **2011**, *22*, 976-986.
[60] R. Luxenhofer, Y. Han, A. Schulz, J. Tong, Z. He, A. V. Kabanov, R. Jordan, *Macromol. Rapid Commun.* **2012**, *33*, 1613-1631.
[61] H. C. Haas, N. W. Schuler, R. L. Macdonald, *J. Polym. Sci., Part A-1: Polym. Chem.* **1972**, *10*, 3143-3158.
[62] S. Murahashi, H. Mitsui, T. Shiota, T. Tsuda, S. Watanabe, *J. Org. Chem.* **1990**, *55*, 1736-1744.
[63] H. E. D. L. Mare, G. M. Coppinger, *J. Org. Chem.* **1963**, *28*, 1068-1070.
[64] J. Splitter, M. Calvin, *J. Org. Chem.* **1958**, *23*, 651-651.
[65] K. Kunath, A. von Harpe, D. Fischer, T. Kissel, *J. Control. Release* **2003**, *88*, 159-172.
[66] S. S. Diebold, M. Kursa, E. Wagner, M. Cotten, M. Zenke, *J. Biol. Chem.* **1999**, *274*, 19087-19094.
[67] D. Gutsch, D. Appelhans, S. Höbel, B. Voit, A. Aigner, *Mol. Pharmaceutics* **2013**, *10*, 4666-4675.
[68] K. A. Gibney, I. Sovadinova, A. I. Lopez, M. Urban, Z. Ridgway, G. A. Caputo, K. Kuroda, *Macromol. Biosci.* **2012**, *12*, 1279-1289.
[69] R. Tanaka, M. Koike, T. Tsutsui, T. Tanaka, *J. Polymer Sci., Polym. Lett. Ed.* **1978**, *16*, 13-19.
[70] N. Matubayasi, M. Nakahara, *J. Chem. Phys.* **2005**, *122*, 074509.
[71] S. Wen, F. Zheng, M. Shen, X. Shi, *J. Appl. Polym. Sci.* **2013**, *128*, 3807-3813.
[72] K. F. Weyts, E. J. Goethals, W. M. Bunge, C. J. Bloys van Treslong, *Eur. Polym. J.* **1990**, *26*, 445-447.
[73] K. Fukushima, Y. Ideguchi, T. Miyazawa, *Bull. Chem. Soc. Jpn.* **1963**, *36*, 1301-1307.
[74] S. Suzuki, Y. Iwashita, T. Shimanouchi, M. Tsuboi, *Biopolymers* **1966**, *4*, 337-350.
[75] V. D. Gupta, S. Trevino, H. Boutin, *J. Chem. Phys.* **1968**, *48*, 3008-3015.
[76] K. Taga, M. G. Sowa, J. Wang, H. Etori, T. Yoshida, H. Okabayashi, H. H. Mantsch, *Vib. Spectrosc.* **1997**, *14*, 143-146.
[77] L. Ojamäe, C. Aulin, H. Pedersen, P.-O. Käll, *J. Colloid Interface Sci.* **2006**, *296*, 71-78.
[78] M. Vert, Y. Doi, K.-H. Hellwich, M. Hess, P. Hodge, P. Kubisa, M. Rinaudo, F. Schué, *Pure Appl. Chem.* **2012**, *84*, 377.
[79] M. Breunig, U. Lungwitz, J. Klar, A. Kurtz, T. Blunk, A. Goepferich, *J. Nanosci. Nanotechnol.* **2004**, *4*, 512-520.
[80] Y. Wen, S. Pan, X. Luo, X. Zhang, W. Zhang, M. Feng, *Bioconjugate Chem.* **2009**, *20*, 322-332.
[81] H. Tian, C. Deng, H. Lin, J. Sun, M. Deng, X. Chen, X. Jing, *Biomaterials* **2005**, *26*, 4209-4217.
[82] H. Koo, G.-w. Jin, H. Kang, Y. Lee, K. Nam, C. Zhe Bai, J.-S. Park, *Biomaterials* **2010**, *31*, 988-997.
[83] T. Kim, S. W. Kim, *React. Funct. Polym.* **2011**, *71*, 344-349.
[84] H. P. C. van Kuringen, V. R. de la Rosa, M. W. M. Fijten, J. P. A. Heuts, R. Hoogenboom, *Macromol. Rapid Commun.* **2012**, *33*, 827-832.
[85] H. M. L. Lambermont-Thijs, J. P. A. Heuts, S. Hoeppener, R. Hoogenboom, U. S. Schubert, *Polym. Chem.* **2011**, *2*, 313-322.
[86] A. M. Kelly, V. Kaltenhauser, I. Mühlbacher, K. Rametsteiner, H. Kren, C. Slugovc, F. Stelzer, F. Wiesbrock, *Macromol. Biosci.* **2013**, *13*, 116-125.

[87] C. v. E. Ehe, A. Rinkenauer, C. Weber, D. Szamosvari, M. Gottschaldt, U. S. Schubert, *Macromol. Biosci.* **2016**, *16*, 508-521.
[88] D. Fischer, Y. Li, B. Ahlemeyer, J. Krieglstein, T. Kissel, *Biomaterials* **2003**, *24*, 1121-1131.
[89] S. M. Moghimi, P. Symonds, J. C. Murray, A. C. Hunter, G. Debska, A. Szewczyk, *Mol. Ther.* **2005**, *11*, 990-995.
[90] U. Lungwitz, M. Breunig, T. Blunk, A. Göpferich, *Eur. J. Pharm. Biopharm.* **2005**, *60*, 247-266.
[91] R. Shah, Z. Kronekova, A. Zahoranová, L. Roller, N. Saha, P. Saha, J. Kronek, *J. Mater. Sci.: Mater. Med.* **2015**, *26*, 157.
[92] M. Jawanda, B. F. L. Lai, J. N. Kizhakkedathu, K. Ishihara, R. Narain, *Polym. Chem.* **2013**, *4*, 3140-3146.
[93] A. C. Rinkenauer, L. Tauhardt, F. Wendler, K. Kempe, M. Gottschaldt, A. Traeger, U. S. Schubert, *Macromol. Biosci.* **2015**, *15*, 414-425.
[94] J. B. LePecq, C. Paoletti, *J. Mol. Biol.* **1967**, *27*, 87-106.
[95] A. J. Geall, I. S. Blagbrough, *J. Pharm. Biomed. Anal.* **2000**, *22*, 849-859.
[96] S. Sundaram, S. Viriyayuthakorn, C. M. Roth, *Biomacromolecules* **2005**, *6*, 2961-2968.
[97] A. Kwok, S. L. Hart, *Nanomed. Nanotechnol.* **2011**, *7*, 210-219.
[98] J. Rejman, V. Oberle, I. S. Zuhorn, D. Hoekstra, *Biochem. J.* **2004**, *377*, 159-169.
[99] R. Kircheis, L. Wightman, E. Wagner, *Adv. Drug Delivery Rev.* **2001**, *53*, 341-358.
[100] D. Fischer, T. Bieber, Y. Li, H.-P. Elsässer, T. Kissel, *Pharm. Res.* **1999**, *16*, 1273-1279.
[101] G. Gowrishankar, S. Zitzmann-Kolbe, A. Junutula, R. Reeves, J. Levi, A. Srinivasan, K. Bruus-Jensen, J. Cyr, L. Dinkelborg, S. S. Gambhir, *PLoS One* **2011**, *6*, e26902.
[102] A. Godoy, V. Ulloa, F. Rodríguez, K. Reinicke, A. J. Yañez, M. d. l. A. García, R. A. Medina, M. Carrasco, S. Barberis, T. Castro, F. Martínez, X. Koch, J. C. Vera, M. T. Poblete, C. D. Figueroa, B. Peruzzo, F. Pérez, F. Nualart, *J. Cell. Physiol.* **2006**, *207*, 614-627.
[103] K. K. Chan, J. Y. W. Chan, K. K. W. Chung, K.-P. Fung, *J. Cell. Biochem.* **2004**, *93*, 1134-1142.
[104] K. Miyamoto, S. Tatsumi, A. Morimoto, H. Minami, H. Yamamoto, K. Sone, Y. Taketani, Y. Nakabou, T. Oka, E. Takeda, *Biochem. J.* **1994**, *303*, 877-883.
[105] V. A. Levin, *J. Med. Chem.* **1980**, *23*, 682-684.
[106] R. Kannan, J. F. Kuhlenkamp, E. Jeandidier, H. Trinh, M. Ookhtens, N. Kaplowitz, *J. Clin. Invest.* **1990**, *85*, 2009-2013.
[107] R. Kannan, R. Chakrabarti, D. Tang, K. J. Kim, N. Kaplowitz, *Brain Res.* **2000**, *852*, 374-382.
[108] P. J. Gaillard, C. C. M. Appeldoorn, J. Rip, R. Dorland, S. M. A. van der Pol, G. Kooij, H. E. de Vries, A. Reijerkerk, *J. Control. Release* **2012**, *164*, 364-369.
[109] M. Raasch, K. Rennert, T. Jahn, S. Peters, T. Henkel, O. Huber, I. Schulz, H. Becker, S. Lorkowski, H. Funke, A. Mosig, *Biofabrication* **2015**, *7*, 015013.
[110] J. C. Rueda, H. Komber, J. C. Cedrón, B. Voit, G. Shevtsova, *Macromol. Chem. Phys.* **2003**, *204*, 947-953.
[111] S. Cesana, J. Auernheimer, R. Jordan, H. Kessler, O. Nuyken, *Macromol. Chem. Phys.* **2006**, *207*, 183-192.
[112] M. Hartlieb, D. Pretzel, K. Kempe, C. Fritzsche, R. M. Paulus, M. Gottschaldt, U. S. Schubert, *Soft Matter* **2013**, *9*, 4693-4704.
[113] R. M. McCormick, *Anal. Biochem.* **1989**, *181*, 66-74.

[114] C. W. Price, D. C. Leslie, J. P. Landers, *Lab on a chip* **2009**, *9*, 2484-2494.
[115] R. K. Saiki, D. H. Gelfand, S. Stoffel, S. J. Scharf, R. Higuchi, G. T. Horn, K. B. Mullis, H. A. Erlich, *Science* **1988**, *239*, 487-491.
[116] A. M. Wang, M. V. Doyle, D. F. Mark, *Proc. Natl. Acad. Sci. U. S. A.* **1989**, *86*, 9717-9721.
[117] K. Ariga, J. P. Hill, Q. Ji, *Phys. Chem. Chem. Phys.* **2007**, *9*, 2319-2340.
[118] L. Tauhardt, K. Kempe, M. Gottschaldt, U. S. Schubert, *Chem. Soc. Rev.* **2013**, *42*, 7998-8011.
[119] L. Tauhardt, M. Frant, D. Pretzel, M. Hartlieb, C. Bucher, G. Hildebrand, B. Schroter, C. Weber, K. Kempe, M. Gottschaldt, K. Liefeith, U. S. Schubert, *J. Mater. Chem. B* **2014**, *2*, 4883-4893.
[120] O. Birkert, G. Gauglitz, *Anal. Bioanal. Chem.* **2002**, *372*, 141-147.
[121] H. Wei, R.-X. Zhuo, X.-Z. Zhang, *Prog. Polym. Sci.* **2013**, *38*, 503-535.
[122] W. Xu, P. Ling, T. Zhang, *J. Drug Delivery* **2013**, *2013*, 340315.
[123] M. Talelli, C. J. F. Rijcken, W. E. Hennink, T. Lammers, *Curr. Opin. Solid State Mater. Sci.* **2012**, *16*, 302-309.
[124] S. E. Averick, E. Paredes, A. Irastorza, A. R. Shrivats, A. Srinivasan, D. J. Siegwart, A. J. Magenau, H. Y. Cho, E. Hsu, A. A. Averick, J. Kim, S. Liu, J. O. Hollinger, S. R. Das, K. Matyjaszewski, *Biomacromolecules* **2012**, *13*, 3445-3449.
[125] W. Chen, M. Zheng, F. Meng, R. Cheng, C. Deng, J. Feijen, Z. Zhong, *Biomacromolecules* **2013**, *14*, 1214-1222.
[126] C. Legros, A. L. Wirotius, M. C. De Pauw-Gillet, K. C. Tam, D. Taton, S. Lecommandoux, *Biomacromolecules* **2015**, *16*, 183-191.
[127] H. Huang, R. Hoogenboom, M. A. M. Leenen, P. Guillet, A. M. Jonas, U. S. Schubert, J.-F. Gohy, *J. Am. Chem. Soc.* **2006**, *128*, 3784-3788.
[128] Y. Liu, Y. Wang, Y. Wang, J. Lu, V. Piñón, M. Weck, *J. Am. Chem. Soc.* **2011**, *133*, 14260-14263.
[129] N. t. Brummelhuis, H. Schlaad, *Polym. Chem.* **2011**, *2*, 1180-1184.
[130] N. Engelhardt, A. Ernst, A.-L. Kampmann, R. Weberskirch, *Macromol. Chem. Phys.* **2013**, *214*, 2783-2791.
[131] S. Zschoche, J. C. Rueda, M. Binner, H. Komber, A. Janke, K.-F. Arndt, S. Lehmann, B. Voit, *Macromol. Chem. Phys.* **2012**, *213*, 215-226.
[132] C. Legros, M.-C. De Pauw-Gillet, K. C. Tam, S. Lecommandoux, D. Taton, *Polym. Chem.* **2013**, *4*, 4801-4808.
[133] J. Rodríguez-Hernández, J. Babin, B. Zappone, S. Lecommandoux, *Biomacromolecules* **2005**, *6*, 2213-2220.
[134] C. Legros, M.-C. De Pauw-Gillet, K. C. Tam, S. Lecommandoux, D. Taton, *Eur. Polym. J.* **2015**, *62*, 322-330.
[135] M. Wagner, S. Holzschuh, A. Traeger, A. Fahr, U. S. Schubert, *Anal. Chem.* **2014**, *86*, 5201-5210.
[136] W. Burchard, in *Branched Polymers II* (Ed.: J. Roovers), Springer Berlin Heidelberg, **1999**, pp. 113-194.

LIST OF ABBREVIATIONS

6AF	6-Amino fluorescein
AF4	Asymmetric flow-field flow fractionation
FT-IR	Fourier transform infrared spectroscopy
BBB	Blood-brain barrier
Boc	*tert*-Butyloxycarbonyl
BocOx	2-(4-((*tert*-Butoxycarbonyl)amino)butyl)-2-oxazoline
BPEI	Branched poly(ethylene imine)
ButEnOx	2-(3-Butenyl)-2-oxazoline
CLSM	Confocal laser scanning microscopy
CMC	Critical micelle concentration
CROP	Cationic ring-opening polymerization
Cy5	Cyanine 5
DEPT	Distortionless enhancement by polarization transfer
DLS	Dynamic light scattering
DMAc	*N*,*N*-Dimethylacetamide
DMPA	2,2-Dimethoxy-2-phenylacetophenone
DO	Degree of oxidation
DOSY	Diffusion-ordered spectroscopy
DP	Degree of polymerization
DTA	Diphtheria toxin A
EBA	Ethidium bromide quenching assay
ECH	Epichlorohydrine
E. coli	Escherichia coli
egfp	Enhanced green fluorescence protein
EtOx	2-Ethyl-2-oxazoline
FBS	Fetal bovine serum
GSH	L-Glutathione
HAADF	High-angular annular dark-field
HEK293	Human embryonic kidney 293

IC_{50}	Half maximal inhibitory concentration
LbL	Layer-by-layer
LPEI	Linear poly(ethylene imine)
MALLS	Multi angle laser light scattering
MeOH	Methanol
MFI	Mean fluorescence intensity
M_n	Number average molar mass
NMR	Nuclear magnetic resonance spectroscopy
PAlkOx	Poly(2-alkly-2-oxazoline)
P(ButEnOx)	Poly(2-(3-butenyl)-2-oxazoline)
PCR	Polymerase chain reaction
pDNA	Plasmid deoxyribonucleic acid
PEG	Poly(ethylene glycol)
PEI	Poly(ethylene imine)
PEtOx	Poly(2-ethyl-2-oxazoline)
pF	Paraformaldehyde
PGly	Poly(glycine)
PMeOx	Poly(2-methyl-2-oxazoline)
POx	Poly(2-oxazoline)
PP	Poly(propylene)
PS	Poly(styrene)
qPCR	Quantitative real-time polymerase chain reaction
RC	Regenerated Cellulose
SEC	Size exclusion chromatography
SIM	Structured illumination microscopy
siRNA	Small interfering ribonucleic acid
STEM	Scanning transmission electron microscopy
TE	Transfection efficiency
TFA	Trifluoro acetic acid
µW	Microwave

CURRICULUM VITAE

20.09.1987	Born in Weimar, Germany
1994 - 1998	Public-Elementary School, Weimar
1998 - 2006	Friedrich Schiller Gymnasium Weimar, degree: general qualification for university entrance
2006 - 2007	Civilian service, Thuringian State Archaeological Museum, Weimar
2007 - 2012	Student of Chemistry (Dipl.), Friedrich Schiller University Jena
2011 - 2012	Diploma thesis at the FSU Jena in the group of Prof. Dr. Ulrich S. Schubert, title: "Poly(ethylene imine)-based hydrogels for binding and release of DNA"
Since 01/2013	PhD student at the Laboratory of Macromolecular and Organic Chemistry (IOMC) at the FSU Jena in the group of Prof. Dr. Ulrich S. Schubert, title: "Cationic polymers made from poly(2-oxazoline)s for biomedical applications"
09/2014 – 02/2015	Research scientist at IBM Almaden, San Jose, California in the group of Prof. James Hedrick

Jena, 20.12.2017 Christoph Englert

PUBLICATION LIST

Peer-reviewed publications

[1] **C. Englert**,‡ M. Pröhl,‡ J. A. Czaplewska, C. Fritzsche, E. Preußger, U. S. Schubert, A. Traeger, M. Gottschaldt, "D-Fructose-decorated poly(ethylene imine) for human breast cancer cell targeting", *Macromol. Biosci.* **2017**, *17*, 1600502.

[2] T. Bus,‡ **C. Englert**, ‡ M. Reifarth, P. Borchers, M. Hartlieb, A. Vollrath, S. Hoeppener, A. Traeger, U. S. Schubert, "3rd generation poly(ethylene imine)s for gene delivery", *J. Mater. Chem. B* **2017**, *5*, 1258-1274.

[3] **C. Englert**,‡ A.-K. Trützschler,‡ M. Raasch, T. Bus, P. Borchers, A. S. Mosig, Anja Traeger, U. S. Schubert, "Crossing the blood-brain barrier: Glutathione-conjugated poly(ethylene imine) for gene delivery", *J. Control. Release* **2016**, *241*, 1-14.

[4] **C. Englert**, M. Fevre, R. J. Wojtecki, W. Cheng, Q. Xu, C. Yang, X. Ke, M. Hartlieb, K. Kempe, J. M. García, R. J. Ono, U. S. Schubert, Y. Y. Yang, J. L. Hedrick, "Facile carbohydrate-mimetic modifications of poly(ethylene imine) carriers for gene delivery applications", *Polym. Chem.* **2016**, *7*, 5862–5872.

[5] **C. Englert**, A. M. Schwenke, S. Hoeppener, C. Weber, U. S. Schubert, "Microwave-assisted Polymer Modifications", *Adv. Polym. Sci.* **2015**, *274*, 209-240.

[6] **C. Englert**, M. Hartlieb, P. Bellstedt, K. Kempe, C. Yang, S. K. Chu, X. Ke, J. M. García, R. J. Ono, M. Fevre, R. J. Wojtecki, U. S. Schubert, Y. Y. Yang, J. L. Hedrick, "Enhancing the biocompatibility and biodegradability of linear poly(ethylene imine) through controlled oxidation", *Macromolecules* **2015**, *48*, 7420-7427.

[7] M. Hartlieb, D. Pretzel, M. Wagner, S. Höppener, P. Bellstedt, M. Görlach, **C. Englert**, K. Kempe, U. S. Schubert, "Core cross-linked nanogels based on the self-assembly of double hydrophilic poly(2-oxazoline) block copolymers", *J. Mater. Chem. B*, **2015**, *3*, 1748-1759.

[8] M. N. Leiske,‡ M. Hartlieb,‡ C. Paulenz, D. Pretzel, M. Hentschel, **C. Englert**, M. Gottschaldt, U. S. Schubert, "Lab in a tube: Purification, amplification, and detection of DNA using poly(2-oxazoline) multilayers", *Adv. Funct. Mater.* **2015**, *25*, 2458-2466.

[9] M. Hartlieb, D. Pretzel, **C. Englert**, M. Hentschel, K. Kempe, M. Gottschaldt, U. S. Schubert, "Matrix supported poly(2-oxazoline)-based hydrogels for DNA catch and release", *Biomacromolecules* **2014**, *15*, 1970-1978.

[10] **C. Englert**, L. Tauhardt, M. Hartlieb, K. Kempe, M. Gottschaldt, U. S. Schubert, "Linear poly(ethylene imine)-based hydrogels for effective binding and release of DNA", *Biomacromolecules* **2014**, *15*, 1124-1131.

[11] A. Chojnacka, K. Kempe, H. C. Ven, **C. Englert**, R. Hoogenboom, U. S. Schubert, H.-G. Janssen, P. Schoenmakers, "Molar mass, chemical-composition, and functionality-type distributions of poly(2-oxazoline)s revealed by a variety of separation techniques", *J. Chromatogr. A* **2012**, *1265*, 123-132.

Manuscripts in submission

[12] **C. Englert**, J. C. Brendel, T. C. Majdanski, T. Yildirim, S. Schubert, M. Gottschaldt, N. Windhab, U. S. Schubert, "Pharmapolymers for the 21st century: Synthetic polymers in drug delivery applications", *Adv. Healthcare Mater.*, submitted (2017/06/06).

Patents

[1] M. Gottschaldt, **C. Englert**, M. Pröhl, U. S. Schubert, "Kationische Polymere mit D-Fructose-Substituenten", Ref. No. 102017003004.9, **2017**.

[2] **C. Englert**, L. Tauhardt, M. Gottschaldt, Ulrich S. Schubert, "New poly(ethylene imine)-based copolymers for bonding to and releasing genetic material, in particular DNA/RNA, and method for the production and use of same", WO 2015048940 A1, **2013**.

Oral presentations

[1] U. S. Schubert,§ **C. Englert**, "Novel modifications of poly(ethylene imine)", *ACS National meeting* **2016**, Philadelphia, Pennsylvania.

[2] **C. Englert**,[§] M. Hartlieb, U. S. Schubert, "Functionalized linear poly(ethylene imine)s for effective binding and release of DNA", *European Polymer Congress* **2015**, Dresden, Germany.

[3] U. S. Schubert,[§] L. Tauhardt, M. Hartlieb, **C. Englert**, "Cationic poly(2-oxazoline)s", *ACS National meeting* **2014**, San Francisco, California.

[4] S. Hoeppener,[§] **C. Englert**, M. Hartlieb, D. Pretzel, M. Gottschaldt, U. S. Schubert, "Microwave synthesis of biomedical materials", *MRS Fall Meeting & Exhibit* **2013**, Boston, Massachusetts.

Poster presentations

[1] **C. Englert**,[§] T. Bus, M. Reifarth, M. Hartlieb, A. Traeger, U. S. Schubert, "3rd generation poly(ethylene imine)s for gene delivery", *Polymer conference* **2016**, Warwick, United Kingdom.

[2] A.-K. Trützschler,[§] **C. Englert**, M. Raasch, T. Bus, A. S. Mosig, A. Traeger, U. S. Schubert, "Entering the Brain? Glutathione modified poly(ethylene imine) derivative for brain delivery", *Polymer conference* **2016**, Warwick, United Kingdom.

[3] T. Bus,[§] **C. Englert**, M. Hartlieb, P. Borchers, A. Vollrath, A. Traeger, U. S. Schubert, "Promising polymer library for non-viral gene delivery", *European Polymer Congress* **2015**, Dresden, Germany.

[4] **C. Englert**,[§] L. Tauhardt, D. Pretzel, K. Kempe, M. Gottschaldt, U. S. Schubert, "PEI-based hydrogels for DNA binding", *Euro BioMat* **2013**, Weimar, Germany.

[‡] Equal contribution

[§] Presenter

ACKNOWLEDGEMENT/DANKSAGUNG

At this point, it is time to thank all the people who contributed to this work and who supported me during the last years.

At first, I want to thank my scientific supervisor **Prof. Dr. Ulrich S. Schubert**. Thank you Uli for your continuous support and the opportunity to work in such an interdisciplinary, international and extraordinary well-organized group. You can be really proud of what you developed in Jena. In particular, I want to thank you once more for the possibility to spend six months in the group of **Prof. James Hedrick** at IBM Almaden in the beautiful California.
Dear Jim, I'm more than grateful for the chance to spend six months in your group. The time at IBM was amazing. Even if it was far away from home it was definitely one of the best times in my life! I really enjoyed the nice and familiar working atmosphere and I hope we keep contact.

Furthermore, I would like to thank **Dr. Matthias Hartlieb** for his continuous support during the last years. Matthias, thank you for many helpful discussions, advices and motivating words especially in situations where I wanted to give up. This work would not have been possible without your effort.
I also want to thank the **Deutsche Forschungsgemeinschaft** (DFG) for funding of the collaborative research center ChemBioSys (SFB 1127).

In the following, I would like to gratefully acknowledge all the co-workers outside and within the Schubert group who contributed significantly to the success of this work.

I want to start with the guys from IBM. I'd like to thank all the guys from IBM that made my stay unique and productive: **Dr. Mareva Fevre** (++, M), **Dr. Robert J. Ono** (Stanford football), **Dr. Jeannette M. Garcıá** (The hemiaminal God!) and **Dr. Rudy J. Wojtecki**.
I'd like to thank **Prof. Yi Yan Yang** and co-workers for the nice cooperation with IBN Singapore. Yiyan, it was a pleasure for me to meet you during my first days at IBM and I am sure there will be tons of new ideas for further cooperation projects. In this context, I want to acknowledge all the people from IBN who were involved in the projects, as there are: **Dr. Chuan Yang**, **Dr. Swee Kwang Chu**, **Dr. Xiyu Ke**, **Dr. Wei Cheng** and **Dr. Qingxing Xu**.

I also want to thank our cooperation partners from Analytik Jena AG, in particular **Martin Hentschel** for spending a lot of time together in front of all kinds of UV sources.

I'd like to thank **Dr. Michael Gottschaldt**, **Dr. Kristian Kempe** and **Dr. Christine Weber** for all the helpful discussions, the continuous support and all the projects we did together. A big 'thank you' goes to the bio group, in particular **Dr. Anja Träger** and **Tanja Bus**. Thanks for tons of CLSM images and for giving me (at least any) understanding of biological processes of polymers.☺ In this context, I also want to thank **Dr. Alexander S. Mosig** and **Martin Raasch** for the nice and very efficient collaboration. Furthermore I want to thank **Carolin Fritzsche** and **Elisabeth Preußger** for all the assays and experiments.
I'd like to thank a lot the FSU NMR crew consisting of **Gabriele Sentis** and **Dr. Peter Bellstedt**. Thank you for your abundance of patience and many specific requests again and again.
The Schubert group would not work without all the people operating in the "background", performing service measurements, keeping all the devices running and supplying the group with necessary items. I thank the SEC people (**Grit Festag**, **Nicole Fritz**), the SEM/TEM team (**Dr. Stephanie Höppener**, **Steffi Stumpf**), our IT-specialist **Renzo Paulus** and **Dr. Jürgen Vitz**. Thank you **Sandra Köhn** and **Dr. Uwe Köhn** for ordering and caring about empty cupboards. Uwe, spending time with you means having fun and do not stop laughing. I really enjoyed the time with you and I hope we keep contact.
Such a huge group would not work without people caring about finances and administration. Thank you **Franca Frister** and **Sylvia Braunsdorf** for taking care of these things.

Of course, the life as a chemist would not be worth living without lab mates. Thanks to my former lab mate **Dr. Lutz Tauhardt** (our lab anthem: "Rihanna: We found love") and to my current lab partners **Michael Pröhl**, **Dr. Justyna A. Czaplewska** (teeth buddys for life ☺), **Anne-Kristin Trützschler, Meike N. Leiske**, **Turgay Yildirim**, **Ilknur Yildirim** and **Martin Sahn**. I also want to thank my students **Philipp Borchers** and **Alex Julien**, who contributed to my work and the office #134 for the nice atmosphere. In this context, I also want to thank **Dr. David Pretzel**. Even if there is no scientific stuff (anymore) which is connecting us, you are worth to be mentioned. Thanks for nice talks far away from work.
Since the Review brought me to my personal limits, I want to thank in particular **Dr. Johannes C. Brendel**. Even if you joined late, I am really grateful for your final input which gave me the last 'kick' to finish this "lifework".

Tobias Majdanski. Even if you are a coworker as well, part of my office, lab mate and cooperation partner, you get an own paragraph. We started more than nine years ago studying chemistry, 2012 we finished our diploma thesis at the same day and now we did the next step in our life. I thank you so much for the entire time aside the work: Fenerbace Jenabul, Paradis-Saint Germain, Singstar evenings, Steiger-Partys and tons of fun we had together. I really hope that our friendship lasts a lifetime! In this context, I also want to thank our Mensa-group, which has become an inherent part of my day. **Ali**, **Jörg**, **Steve, William** – thank you for talks far away from work, somewhere between gossip, socca and the middle of nowhere. I also want to acknowledge **Erik**, my childhood friend from Weimar. I will never forget our trip across the Corcovado jungle in Costa Rica between tapirs, crocodiles and giant spiders.
I want to thank my IBM office mates **Gaby**, **Alex** and **Steven** (E/-310, birthday themed farewell party) and my IBM mates **Kay** and **Irem**.

Zum Schluss möchte ich den wichtigsten Menschen in meinem Leben danken, ohne die ich heute nicht hier wäre. Dir, liebe **Melanie**, für all die wunderschöne Zeit, die wir bisher miteinander verbringen konnten. Von unserer Fahrt auf dem Highway #1 die kalifornische Westküste entlang mit offenem Cabrio-Verdeck träume ich noch heute. Ich danke Dir für deine Geduld und Deine Unterstützung in den letzten Jahren, auch wenn es manchmal sicher nicht einfach mit mir war. Wie oft habe ich an meinem Studium gezweifelt und war kurz davor alles hinzuschmeißen. Vielleicht würde ich heute vieles anders machen, aber ohne dieses Studium hätte ich dich niemals kennen gelernt. Und dafür bin ich unendlich dankbar!
Liebe **Kathrin**, ich danke Dir für das tollste Verhältnis, das man als Geschwister nur haben kann. Wie du nach erfolgreicher Ausbildung und Arbeit noch ein Studium durchgezogen hast, entgegen aller Schwierigkeiten, ringt mir höchste Achtung ab. Ich hätte das nicht geschafft!
Der größtmögliche Dank gilt meinen Eltern, **Christiane** und **Ralf**. Ohne Euch wäre nichts von alledem möglich gewesen. Neben Eurer ständigen Unterstützung in jeder Lebenslage habt Ihr mir gezeigt, was es heißt das Leben zu genießen. Wir haben den Ätna bestiegen, sind mit dem Rucksack durch die isländische Vulkanlandschaft gewandert oder in den Grand Canyon hinabgestiegen. Wir haben zahlreiche Orte auf der ganzen Welt gesehen und unsere Reise ist noch nicht zu Ende …

DECLARATION OF AUTHORSHIP/SELBSTSTÄNDIGKEITSERKLÄRUNG

Hiermit erkläre ich, dass ich die vorliegende Arbeit selbständig angefertigt, nicht anderweitig zu Prüfungszwecken vorgelegt und keine anderen als die angegebenen Hilfsmittel verwendet habe. Sämtliche wissentlich verwendete Textstellen, Zitate oder Inhalte anderer Verfasser wurden ausdrücklich als solche gekennzeichnet.

I herbey certify that the work presented here is, to the best of my knowledge and belief, original and the result of my own investigations, except as acknowledged, and has not been submitted, either in part or whole, for a degree at this or any other university.

Jena, den 20.12.2017

_____

Christoph Englert

PUBLICATIONS P1-P10

P1: Reprinted by permission of J. C. Brendel, T. C. Majdanski, T. Yildirim, S. Schubert, M. Gottschaldt, N. Windhab, U. S. Schubert.

P2: Reprinted with permission from *Macromolecules* **2015**, *48*, 7420-7427. Copyright (2015) American Chemical Society.

P3: C. Englert, M. Fevre, R. J. Wojtecki, W. Cheng, Q. Xu, C. Yang, X. Ke, M. Hartlieb, K. Kempe, J. M. García, R. J. Ono, U. S. Schubert, Y. Y. Yang, J. L. Hedrick, *Polym. Chem.*, **2016**, *7*, 5862 - Reproduced by permission of The Royal Society of Chemistry.

P4: Advances in Polymer Science, Microwave-assisted polymer modifications, 274, **2016**, 209-240, C. Englert, A. M. Schwenke, S. Hoeppener, C. Weber , U. S. Schubert, with permission of © Springer International Publishing Switzerland 2016.

P5: T. Bus, C. Englert, M. Reifarth, P. Borchers, M. Hartlieb, A. Vollrath, S. Hoeppener, A. Traeger, U. S. Schubert, *J. Mater. Chem. B,* **2017**, *5*, 1258-1274 - Reproduced by permission of The Royal Society of Chemistry.

P6: Reprinted from J. Controlled Release, 241, C. Englert,‡ A-K. Trützschler,‡ M. Raasch, T. Bus, P. Borchers, A. S. Mosig, A. Traeger, U. S. Schubert, Crossing the blood-brain barrier: Glutathione-conjugated poly(ethylene imine) for gene delivery, 1-14, Copyright (**2016**), with permission from Elsevier.

P7: C. Englert, M. Pröhl, J. A. Czaplewska, C. Fritzsche, E. Preußger, U. S. Schubert, A. Traeger, M. Gottschaldt, *Macromol. Biosci.* **2017**, *17*, 1600502 - Reproduced by permission of John Wiley & Sons Ltd., UK. Copyright © **2017** WILEY-VCH Verlag GmbH & Co. KGaA, Weinheim.

P8: Reprinted with permission from *Biomacromolecules* **2014**, *15*, 1970-1978. Copyright (2014) American Chemical Society.

P9: M. N. Leiske,‡ M. Hartlieb,‡ C. Paulenz, D. Pretzel, M. Hentschel, C. Englert, M. Gottschaldt, U. S. Schubert, *Adv. Funct. Mater.* **2015**, *25*, 2458-2466 - Reproduced by permission of John Wiley & Sons Ltd., UK. Copyright © 2015 Wiley Periodicals, Inc..

P10: M. Hartlieb, D. Pretzel, M. Wagner, S. Höppener, P. Bellstedt, M. Görlach, C. Englert, K. Kempe, U. S. Schubert, J. Mater. Chem. B, **2015**, 3, 1748-1759 - Reproduced by permission of The Royal Society of Chemistry.

‡ Equal contribution

PUBLICATION 1

Pharmapolymers in the 21st century: Synthetic polymers in drug delivery applications

C. Englert, J. C. Brendel, T. C. Majdanski, T. Yildirim, S. Schubert, M. Gottschaldt, N. Windhab, U. S. Schubert

Adv. Healthcare Mater., submitted (2017/06/06)

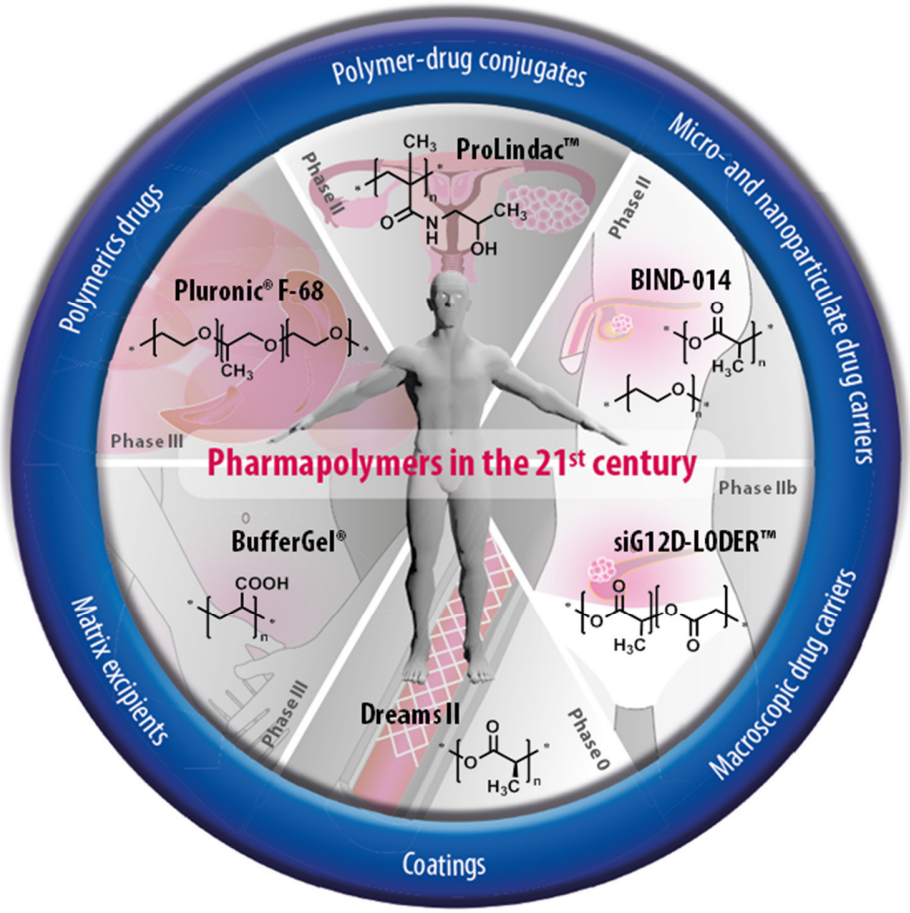

Pharmapolymers in the 21st Century:

Synthetic Polymers in Drug Delivery Applications

Christoph Englert,[a,b] Johannes C. Brendel,[a,b] Tobias C. Majdanski,[a,b] Turgay Yildirim,[a,b] Stephanie Schubert,[b,c] Michael Gottschaldt,[a,b] Norbert Windhab,[d] Ulrich S. Schubert[a,b,]*

[a] Laboratory of Organic and Macromolecular Chemistry (IOMC), Friedrich Schiller University Jena, Humboldtstrasse 10, 07743 Jena, Germany

[b] Jena Center for Soft Matter (JCSM), Friedrich Schiller University Jena, Philosophenweg 7, 07743 Jena, Germany

[c] Department of Pharmaceutical Technology, Friedrich Schiller University Jena, Otto-Schott-Strasse 41, 07747 Jena, Germany

[d] Evonik Nutrition and Care GmbH, Kirschenallee, Darmstadt 64293, Germany

Email: ulrich.schubert@uni-jena.de

Graphical abstract

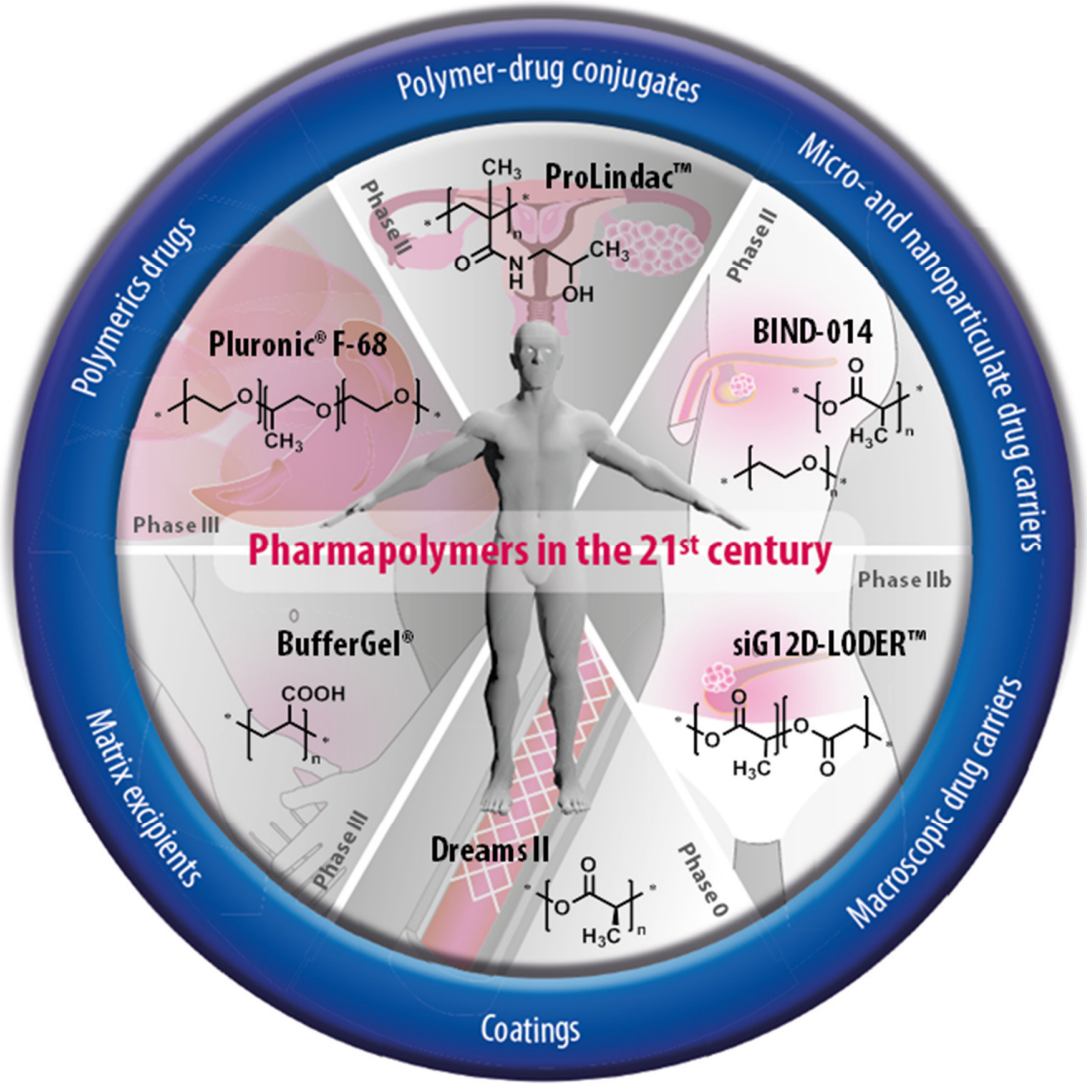

Abstract

The administration of drugs, as a main challenge of pharmaceutical and medicinal applications, has certainly benefited from the application of synthetic polymers. However, despite an enormous effort to develop new materials for drug delivery applications, only few of them have entered the market due to the hurdles of regulation, production, cost efficiency and both industrial's and patients' acceptance. In this review, we summarize all these classes of synthetic polymers, which are on the market as well as the latest developments in clinical trials, and describe their application in polymer-drug conjugates, as excipients, in nano-/microscopic and macroscopic drug carriers, as polymeric coatings, or as polymeric drugs. Our intention is to create a link between the underlying chemical structures, the properties of the polymers, and their area of application, where they are often just known by their trade names or abbreviations. In addition selected types of synthetic polymers are highlighted that feature interesting properties and have the potential to make it to the market in future.

FROM THE CONTENTS

1. Introduction

The administration of drugs is one of the main tasks within the area of pharmaceutical and medicinal applications. Drugs are defined as "articles intended for use in the diagnosis, cure, mitigation, treatment, or prevention of disease" and "articles (other than food) intended to affect the structure or any function of the body of man or other animals" by the Federal Food, Drug, and Cosmetic Act (FD&C Act). Starting in the early 1960s, controlled drug delivery research has broadened and has developed from macroscopic devices and implants (1970s and 1980s) to microscopic (1980s and 1990s) as well as nanoscopic systems.[1] Besides liposomes, nanocrystals, bio-compatible metal-organic frameworks and others, polymeric materials represent a useful option to fulfill the challenges of drug storage and delivery. They can be subdivided into natural, pseudo-synthetic and synthetic macromolecules. The latter offer several advantages compared to natural polymers like an easier synthesis of large quantities, nonsignificant batch-to-batch variations and countless possibilities for modifications to achieve the desired properties. These factors turn polymers into very promising candidates to solve numerous problems in drug administration.

In this review, we introduce the term 'Pharmapolymers', which describes synthetic polymers used during the administration of drugs. They are based on an artificially made polymeric backbone, excluding chemically modified natural polymer species plus dendrimers, which do not reveal a distribution in the number of repeating units per molecule (molar mass distribution). The first part comprises an overview of potential polymer classes, which are discussed concerning their suitability (structure, properties etc.) as potential drug delivery systems. This represents the basis for the following parts of the work. To be considered as drug delivery system, the polymer structure has to fulfill at least parts of the following requirements: Biocompatibility, biodegradability or complete chemical inertness as well as sufficient control over its synthetic structure. In 1999, Uhrich *et al.* already reviewed polymeric systems for controlled drug delivery.[2] Almost two decades later, this work misses completeness and the modern developments of the polymer classes applied nowadays. The second part summarizes all pharmapolymers which are currently or have previously been on the market subdivided according to their form of appearance. In addition, we included materials which are currently undergoing clinical trials. The main routes of drug administration discussed here are oral, topical and by injection (intravenous, intramuscular, subcutaneous). The third section highlights recent progress in research and exemplarily describes a few chosen *in vivo* studies to emphasize future prospects of pharmapolymers in drug delivery applications. On average, only one out of 5,000 compounds that enters pre-clinical studies (and only one out of 10 that enters clinical studies) becomes an approved drug after 10 years from the starting idea to the market approval.[2] The clinical phases necessary for market approval and a short description are listed in Table 1.

The present study is the most comprehensive summary of established synthetic polymers in drug administration so far, comprising far more than 100 polymeric products on the market and 70 under clinical investigations. Our intent is to provide a link between chemical structures as well as properties of the polymers and their area of application, where they are often just known by their trade names or abbreviations. Even so, the authors apologize in advance for all omissions since it is nearly impossible to keep track of the whole wealth of materials applied in drug delivery.

Table 1. Overview of clinical trial phases.

Phase	Primary goal	Secondary goal	Participants	Duration	Special Features
Preclinical	Checking for preliminary safety, efficacy and pharmacokinetic information (*in vitro* & *in vivo*)		-	Several years	
Phase 0	Pharmacokinetics (*i.e.* oral bioavailability and half-life of the drug)		10		Often skipped for phase I, subtherapeutic, doses too low to cause any therapeutic effect
Phase I	Checking for safety	Establish the max. tolerated dose, determine side effects, determine the metabolism and pharmacologic actions of drugs	20 to 100	Several months	Often first time tested in humans, subtherapeutic with ascending doses
Phase II	Checking for efficacy	Determine the common short-term side effects and risks	Several hundred	Up to 2 years	Therapeutic doses, "Proof of concept"
Phase III	Confirm findings in large patient population	Evaluate the overall risk-benefit ratio	300 to 3,000	1 to 4 years	Usually randomized controlled trials, pivotal studies for drug licensing
Phase IV	Testing long-term safety in diverse patient population	Identify additional, unusual side effects	"Real-life patients", several thousands	*Ongoing*	

2. Polymer classes

The Food and Drug Administration (FDA) is a federal agency of the United States Department of Health and Human Services, which is responsible for the monitoring of trading and safety standards in the food and drug industries in the United States. A large number of different polymer types are used in pharmaceutical research and applications nowadays, whether in an early scientific stage or already in FDA approved formulations. To fulfill specific requirements, often different polymer classes have to be combined to create smart solutions for specific problems. The following chapter discusses the most important polymer classes including individual representatives of pharmapolymers. All structures of homopolymer systems mentioned later in the application Chapter 3 or the future prospects Chapter 4 are marked in bold and can be found in Table 2.

2.1 Polyethers

The term polyether generally describes polymers that contain the ether functional group in their main chain. Although there are several FDA approved polyethers, they all reveal one major drawback: They lack biodegradability (referring to the degradation of the polymer backbone, independent of the molar mass of the respective polymer species).

Among them, **poly(ethylene glycol) (PEG)** (also poly(ethylene oxide) (PEO) for M_n >20,000 g mol^{-1}) represents probably the most well-known polyether in pharmaceutical applications. The oldest[3] and most frequently used method to synthesize PEG in laboratory and industrial scale is *via* anionic ring-opening polymerization of ethylene oxide[4] resulting in polymers with a wide range of possible molar masses and very low dispersities.[5] Cationic polymerization is also feasible, with the drawback of broad molar mass distribution due to backbiting reactions.[6] A variety of functionalized PEGs are offered from commercial sources, with different α and/or ω functionalities, *e.g.* methoxy groups, amines, or thiols. Furthermore, side group functionalized PEG derivatives are known in literature, *e.g.* functionalized with furfuryl.[7] PEG has several interesting advantages for pharmaceutical applications. It is water soluble, even at higher molar masses,[8] non-ionic, non-toxic and biocompatible. Furthermore, it was already approved by the FDA for different applications in foods, cosmetics and pharmaceuticals.[9] The success of PEG in the biomedical area started with the covalent decoration of bio(active) molecules,[10] often named PEGylation,[11] which will be described in detail in Chapter 3.1.1. One outstanding property of PEG is the so-called “stealth-effect”, discovered in 1990 for modified liposomes.[12] It describes the ability to protect molecules or nanoscopic objects against unspecific interactions with blood components (*e.g.* opsonization), by attaching specific proteins to the surface.[13] Until now, PEG is still regarded as the gold standard for stealth behavior. Furthermore, renal filtration was found to be decreased by the attachment of PEG which comes along with an increase of the molar masses. These two points lead to significantly elongated *in vivo* blood circulation times of formulations associated with PEG.[13-14] Besides all the advantages of PEG a few drawbacks have to be addressed as well.[15] With increasing molar mass of the polymers, PEG tends to accumulate within certain organs, which has to be avoided.[16] If, however, the applied product contains oligomers below 400 g mol^{-1} or becomes fragmented, toxic species can be produced by oxidation *in vivo*.[17] A second issue concerns the possibility of an immune response due to compliment C activation, which can lead to hypersensitive reactions and, consequently, to an anaphylactic shock.[18] Furthermore – despite the established large scale production – the anionic polymerization technique requires still an high effort, in particular considering the highly toxic and explosive monomer and the purification of the polymer for pharmaceutical applications (formaldehyde and 1,4-dioxane can occur as side products, which need to be excluded from pharmacological grade PEG). Nevertheless, PEG remains the most commonly used polymer in drug administration and can be considered as the standard.

Poly(propylene glycol) (PPG) (also named poly(propylene oxide): PPO) represents another polyether which is applied for drug delivery. The common way to synthesize PPG is anionic ring-opening polymerization with an alcoholate as initiator and a base as catalyst resulting in the atactic product. The change of the catalyst enables the synthesis of the isotactic product. However, like most mono-substituted epoxides, the monomer tends to induce chain transfer reactions during the polymerization limiting the maximum molar mass (M_n) of the resulting polymer to approximately 6,000 g mol^{-1}.[4-5] The water solubility of the polymer is, compared to PEG, reduced considerably, which causes an lower critical solution temperature (LCST) between 15 and 42 °C depending on the molar mass[19] ($LCST_{PEG} \approx 100$ °C),[20] whereas the biocompatibility is even more distinct as for PEG.[21] The polymer appears mostly as a central, non-ionic, hydrophobic, non-toxic segment in PEG-*b*-PPG-*b*-PEG block copolymers named poloxameres, which are also known by their trade names Pluronic®, Synperonic® and Kolliphor® (a subgroup are poloxamines consisting of an ethylene diamine core). The commercial products are available in various compositions. The polymerization of the block copolymer is similar to the PPG homopolymer synthesis. After the homopolymer is formed, ethylene oxide is added to the reaction, which then grows from both sides of the PPG homopolymer. The resulting products often contain admixtures, *e.g* homopolymer, di- and triblock polymers, which can be removed by chromatographic fractionation. Poloxameres are increasing the rate of wound and burn healing, which is the reason why they can be found in skin healing creams and skin substitutes. Furthermore, they form micelles in aqueous solution, making them attractive for drug delivery applications.

Poly(glycerol) (PG) represents an alternative for PEG and PPG in terms of solubility- and biological behavior. PG's are produced by anionic[22] or cationic[23] ring-opening polymerization of glycidol leading to branched polymer architectures. Using anionic ring-opening polymerization, high molar mass polymers comprising a relatively narrow distribution (up to 700,000 g mol^{-1} at dispersities of below 1.4) can be synthesized.[24] The main advantage of PG compared to PEG is the presence of hydroxyl groups at the main chain, which can be utilized to introduce additional functionalities to the polymer backbone.[25] If the alcohol group on the monomer is protected, a linear polymerization with molar masses (M_n) up to 30,000 g mol^{-1} can be accomplished.[26] Both, linear and hyperbranched PGs are fully biocompatible,[27] revealing even better profiles compared to PEG.[28] Similar to PEG, modifications with PG lead to an elongated circulation time.[29] A rather well-known example is poly(glycerol) polyricinoleate (PGPR) as food additive being considered by the FDA as general recognized as safe (GRAS) for human consumption (Code of Federal Regulations: 21 CFR 172.854). Several other poly(glycerol) esters are known for their application as emulsifier in food, cosmetics and pharmaceutical preparations.

2.2 Poly(ethylene imine)s

Poly(ethylene imine)s (PEI) are characterized by the presence of amine group functionalities within the polymer backbone, which determine their chemical and physical behavior. PEI reveals one of the highest cationic-charge-densities of all organic macromolecules.[30] Every third atom is an amine group of which every sixth nitrogen atom is protonated under physiological conditions.[30] This high charge density enables the interaction with the phosphate groups of genetic material leading to the formation of toroidal complexes that are readily endocytosed by cells.[31] This feature makes PEI a highly efficient vector for delivering oligonucleotides *in vitro* and *in vivo*.[32] It occurs in two different forms: Linear and branched PEI.

Branched poly(ethylene imine) (BPEI) can be synthesized by the ring-opening polymerization of unsubstituted aziridine as described in 1944 by Jones *et al.* leading to uncontrolled branching and chains with primary, secondary, and tertiary amine groups.[33] Increasing molar masses result in higher degrees of branching and, to this end, cross-linking becomes more likely. The handling of explosive and toxic aziridine requires safety precautions, which are often not applicable in most chemistry laboratories. The molar masses of commercially available BPEI cover the

complete range up to 750,000 g mol^{-1} (M_w), however, no dispersities are reported. The exact determination of the number average molar mass M_n of PEI is extremely complex and has been in the focus of several literature reports.[31a, 34] The synthesis of **linear poly(ethylene imine) (LPEI)** *via* hydrolysis of poly(2-alkyl-2-oxazoline)s was first described in the 1960s.[35] Therefore, linear 2-methyl or 2-ethyl substituted poly(2-oxazoline)s (POx) are mainly used as precursors. The hydrolysis can be performed under acidic[35b, 36] or basic conditions[35b, 37] and results in products hydrolyzed up to 97%. The molar mass of LPEI and its distribution is limited by the respective POx precursor. However, the living character of the cationic polymerization of POx (see Chapter 2.7) produces well-defined polymers with controlled molar masses and low dispersities, which comply with the biological demands for LPEI (M_n up to 25,000 g mol^{-1}, $Đ < 1.2$).[38] LPEI can be purchased in the range from 400 to 250,000 g mol^{-1} (M_w). The robust polymerization protocols tolerate a variety of comonomers, initiators, and quenchers, including allyl and aryl groups enabling the selective introduction of various functionalities to the LPEI backbone.[39] An alternative is the controlled partial hydrolysis of the amide bonds which has been studied in the last decades.[40] A further approach to LPEIs is the controlled polymerization of *N*-substituted aziridines followed by the deprotection of the amines.[37a] However, this route comes along with unwanted side reactions due to the harsh conditions or incomplete cleavage.[41] None of the products based on PEI have been approved by the FDA so far, which is mainly related to its cytotoxicity.

2.3 Polyesters

Polyester describe a class of polymers containing the ester functional group in their main chain which renders most of these polymers biodegradable.

One of the earliest polymers was **poly(caprolactone) (PCL)** synthesized by the Carothers team in the 1930's. PCL is a non-toxic, biodegradable, semi-crystalline aliphatic polyester, which is approved by the FDA for several applications, *e.g.* drug delivery systems, sutures, long-term implants and adhesion barriers as well as new tissue scaffold host systems. It is hydrophobic, but soluble in several solvents, can be blended with a variety of other materials and degrades very slowly under physiological conditions (from months to years) compared to other polyesters.[42] The main reason for the extended degradation time is the lack of enzymes suitable to hydrolyze the ester in the human body.[43] Furthermore, the hydrolysis time of PCL depends on the physical and chemical properties of the polymer, in particular the crystallinity and the molar mass. However, this degradation profile makes PCL very attractive for long term drug delivery devices or implants.[44] PCL degrades into 6-hydroxyhexanoic acid, which is less acidic than degradation products from other polyesters reducing the effect of autocatalysis occurring with the hydrolysis of polyesters. Besides the degradability, PCL exhibits a high permeability for most drug molecules. Furthermore, functional groups can be introduced for example by copolymerization, which enables an adjustment of several properties, including hydrophilicity, adhesivity and biocompatibility.[45] PCL can be synthesized in several ways, such as by anionic, cationic, coordination or free radical ring-opening polymerization (ROP) processes first described by Carothers for PLA. The most common synthesis routes comprise the ring-opening polymerization using metal catalysts which have to be removed afterwards and the often used polycondensation. A well-known catalyst for ROP is stannous octoate due to its high efficiency and its approval by the FDA as food additive.[46] The reported molar masses (M_n) range from 530 to 630,000 g mol^{-1}.[47] Numerous strategies to improve the degradation and mechanical properties of PCL, such as copolymerization and blending with different polymers, are described in literature.[42a, 44e, 48] The exceptional compatibility of PCL in blends is utilized to improve the material properties by mixing PCL with polysaccharides, PLA, chitosan and many more.[48-49]

Poly(lactic acid) (PLA) and **poly(glycolic acid) (PGA)** are aliphatic polyesters approved by the FDA for a wide range of applications. These materials are well-established in pharmaceutical industry as drug carriers and traditionally

applied as suture material.[50] Major advantages are their biocompatibility, biodegradability and their mechanical strength.[51] The degradation products are further non-toxic and can be cleared or consumed within bioprocesses occurring in the body, which makes them a powerful tool for *in vivo* delivery. Similar to PCL, the material properties such as degradation rate and mechanical strength depend on the structural features of the polymer including crystallinity and chain length.[52] High molar mass species are obtained by ROP[53] using stannous octoate as catalyst.[50b, 51a] Additional metal-free methods including enzymatic techniques are under investigation for the polycondensation of PLA.[52b, 54] PLA represents a stiff and hard polymer revealing versatile properties depending on the tacticity and molar mass. Compared to PGA it comprises an extra methyl group, and, therefore, a stereocenter, which results in three possible products: Poly(L-lactic acid) (PLLA), poly(D-lactic acid) (PDLA) and the mixture of both, poly(D-lactic acid-*co*-L-lactic acid) (PDLLA). PLLA and PDLA are semi-crystalline, while PDLLA is amorphous and, consequently, reveals the fastest degradation rate.[50c, 52b] Nevertheless, the hydrophobic methyl side group increases the steric hindrance and shields the ester bond from hydrolysis by water which results in a decreased degradation time compared to PGA. In consequence, PLA is a promising material for long term applications.[55] PGA has been known since 1954 as potential low cost fiber forming, highly crystalline polymer.[50b] However, the high sensitivity towards hydrolysis and the poor solubility in organic solvents limits its use for pharmaceutical applications.[47, 51b] The respective copolymer poly(lactic-*co*-glycolic acid) (PLGA) is probably the best established and studied polymer for pharmaceutical applications and tissue engineering.

Poly(oxalate)s (PO) represent another subgroup of polyesters, which is prepared by the ester interchange reaction of diols with the diester of the oxalic acid. In 1980, Shalaby *et al.* filed a patent for the preparation of polyalkylene oxalates from different aliphatic diols.[56] Since that time, POs and copoly(oxalate)s have been reported only a few times in literature. They represent a family of biocompatible and biodegradable polymers, which degrade hydrolytically (and comparatively rapid) into non-toxic products that can easily be removed from the body.[57] Oxalate-based polymers allow a facile control over their biodegradability, crystallinity and mechanical strength. Their hydrolytic stability and their mechanical properties are mainly influenced by the composition and hydrophobicity of the incorporated diol. Compared to the commercial biodegradable polymers PCL or PLGA, they exhibit faster degradation kinetics. This turns POs into useful materials for medical grade plastics and devices (*e.g.* syringes and scrub brushes).[58] Garcia and Miller established the oxalate metathesis polymerization using diols from renewable sources and without the need of any solvents. They obtained POs with molar masses (M_n) ranging from 40,000 to 70,000 g mol^{-1}.[58] Despite its biocompatibility and degradability none of the polymers in this class is yet approved by the FDA.

Poly(butylene terephthalate) (PBT) is obtained by the ester interchange reaction of 1,4-butanediol and terephthalic acid and subsequent polycondensation. Its resistance to solvents, heat and mechanical strongness turns PBT into a basic module in many electronic devices and home appliances. Considering biomedical application PBT has not gained much attention, yet.

2.4 Polycarbonates

Polycarbonates (PC) are a group of thermoplastic polymers containing carbonate links in their backbone, firstly discovered in 1898 by Alfred Einhorn.[59] After 50 years without commercialization, Schnell (Bayer AG, Germany) patented the synthesis of linear PCs in 1953.[60] In the same year, Fox (General Electric Company, USA) synthesized independently a branched PC.[61] Since the late 50's, PCs became frequently used in commercial applications. The excellent biocompatibility, non-toxic degradation products and the absence of autocatalytic degradation processes render aliphatic PCs interesting polymeric materials.[62] The polymers are commonly synthesized by polycondensation methods (step growth), as performed by the phosgenation of hydroxyl compounds or the

transesterification of diols with lower dialkyl carbonates.[63] Another approach is the utilization of CO_2 and oxiranes to produce "green" PCs (up to 100,000 g mol^{-1}, Đ < 1.2) *via* an addition polymerization,[64] whereas the low reactivity of CO_2 requires very efficient catalysts.[65] However, these polymerization techniques suffer from drawbacks such as the poor control over molecular parameters and broad molar mass distributions.[66] A suitable preparation method to obtain well-defined PC is the ring-opening polymerization (ROP) of cyclic carbonates (chain growth, "living"), which can be performed by both cationic and anionic polymerization. The ROP allows the control of molar masses (M_n) with low dispersities (30,000 g mol^{-1}, Đ < 1.1[67]) at fast polymerization rates and facilitates the formation of more complex architectures like block polymers[68] and star shaped polymers.[69] Furthermore, in contrast to polycondensation, no by-products are obtained from the polymerization. Compared to aliphatic polyesters (*i.e.* PCL or the copolymer PLGA), polycarbonates are degraded *in vivo* by surface erosion.[70] Their degradation does not cause an acidic environment, which may occur during polyester degradation and might be hazardous for loaded drugs or healthy tissues. PC resins are solely FDA approved for use as articles or components of articles intended for use in producing, manufacturing, packing, processing, preparing, treating, packaging, transporting, or holding food in accordance with defined conditions (21 CFR 177.1580). Nowadays, the design of functional cyclic carbonate monomers has gained increasing interest, comprising hydroxyl,[71] carboxyl,[72] amine,[73] alkene[74]/alkyne,[75] halogen,[76] azido[77] and sugar[78] pendant groups.

2.5 Poly(amino acid)s

Synthetic polypeptides are based on the same peptide bonds present in natural proteins and, therefore, exhibit a good biodegradability and excellent biocompatibility. Nevertheless, they are prepared by purely synthetic reaction processes and therefore included in this review.[79] As almost all types of amino acids can be applied for the polymerization, a large variety of different functionalities such as ionic or stimuli responsive side groups are accessible and complex superstructures including micelles and gels can be formed.[80] In 1906, Hermann Leuchs first reported the synthesis and polymerization of α-amino acid *N*-carboxyanhydrides (NCAs).[81] Since this time, NCAs have gained increasing interest for the synthesis of homo- and copolymers as well as cyclic polypeptides. A large number of reviews can be found dealing with the immense variety of synthetic procedures.[82] Nowadays, the most established way to obtain synthetic polypeptides is the ring-opening polymerization (ROP) of NCAs using amine-based initiators. Remarkable reactions have been developed to synthesize polypeptides and polypeptide-based copolymers with controlled molar masses and dispersities as well as complex architectures. Deming and co-workers reached macromolecules with M_n up to 500,000 g mol^{-1} (Đ < 1.2) by applying different transition-metal-based initiators in a living ROP.[83] Conventional amines as initiators allow the synthesis of polypeptides with 100,000 g mol^{-1} and comparable dispersities.[84] Side reactions can further be suppressed using ammonium chloride functionalized macro-initiators[85] or an organosilicon.[86] The functionalization of polypeptides has gained increasing attention in recent years. The introduction of various functional groups or stimuli-sensitive moieties to the side chains of the polypeptides render them particularly appealing for the design and development of multi-functional active biomaterials. The functionalization is mainly achieved by two approaches: I) The one-step ROP of NCA monomers, already containing the desired functional moieties or II) the post-polymerization modification of polypeptides. Reported modifications comprise click chemistry, in particular alkyne-azide cycloadditions and thiol-ene reactions, controlled free-radical polymerizations, aminolysis and transesterifications, which have extensively been reviewed.[82c, 87] The modularity of using unnatural amino acid derivatives as monomers leads to a versatility of polymer structures with molecular and physical properties far from those of proteins. Trifunctional amino acids, such as glutamic acid, lysine and aspartic acid, are often used to achieve structural viability within the respective polymer, in particular **poly(glutamic acid) (PGluA)**,[88] **poly(lysine)**[89] or **poly(aspartic acid)**.[90] The FDA classifies chosen poly(amino acid)s under the GRAS status for different food applications.

2.6 Poly(peptoid)s

In 1982, Farmer and Ariens introduced the term "peptoid" as a peptidomimetic/pseudopeptide that is able to mimic the biological action of peptides while not resembling them structurally.[91] One decade later, Bartlett and co-workers defined them more specifically as oligomers of *N*-substituted glycine (poly(α-peptoids)).[92] Nowadays, most reports of peptoids, *e.g.* those indexed in PubMed, refer to the mentioned *N*-substituted glycines or respective poly(β-/γ-peptoids). In both cases, side chains are attached to the amide nitrogen and make the polymer resistant to protease degradation.[93] **Poly(peptoid)s (PoP)** are particularly interesting due to their convenient synthesis, chemical diversity and biological relevance. They can be synthesized in a sequence defined (stepwise) or statistical (chain growth) manner.[94] They are routinely obtained in a stepwise procedure, particularly the submonomer solid phase synthesis developed by Zuckermann *et al.*,[95] and have been reviewed continuously.[96] This two-step sequence method does not require the protection of the backbone and a variety of primary amines (most of them commercially available) can be incorporated.[97] Monodisperse PoPs of 100 monomer units (M_n = 8,500 g mol^{-1}) have been synthesized by coupling together two submonomer-synthesized 50-mers.[98] The submonomer method represents a relatively inexpensive route compared to the preparation of the corresponding α-peptides.[99] Microwave heating can be used to accelerate the submonomer synthesis and increases the efficiency of coupling sterically hindered and electrostatically deactivated amines.[100] An alternative approach for their synthesis is the (living) ring-opening polymerization of *N*-substituted *N*-carboxyanhydride (NCA) monomers in solution or from solid substrates.[94b, 96b, 101] This chain growth polymerization yields PoPs with degrees of polymerization >100, but with limited sequence control.[102] Their structural similarity compared to peptides, their resistance against protease, the proteolytic stability, the convenient synthesis and their superior biocompatibility make PoPs an interesting class of materials for a variety of applications, *e.g.* as transfection and therapeutic agents,[103] diagnostic agent[104] and lung surfactant mimetic.[105] Optionally, they can be incorporated into polypeptides at specific sites.[106] Luxenhofer and co-workers could recently show the degradation of PoPs v*ia* oxidative degradation under biologically relevant conditions.[107] This polymer class is not yet approved by the FDA.

2.7 Poly(2-oxazoline)s

Concerning biocompatible, hydrophilic polymers, **poly(2-oxazoline)s (POx)** gained increasing attention.[15] This class of polymers was introduced in 1966 by four independent research groups.[35, 108] The polymers are prepared by a cationic ring-opening polymerization (CROP) of 2-substituted oxazolines resulting in repeating amide functionalities at the interface between polymer backbone and side chain. Since 2004, the microwave assisted synthesis is most commonly used to shorten reaction times from days to minutes.[109] As the CROP is not as sensitive as most anionic polymerization methods, the production of POx in a lab scale is comparably convenient, and a large variety of possible functionalization strategies can be applied.[110] Besides the variation of start- and end-groups, the 2-substitution of the monomer can be modulated within the borders of tolerated functionalities in a CROP. The achievable molar mass strongly depends on the used monomer. POx derivatives bearing short side chains (methyl or ethyl) are reported to be biocompatible[111] and even feature a stealth effect similar to PEG (see Chapter 3.1.2),[112] which turns these polymers into highly favorable materials for biomedical applications.[113] By the incorporation of longer side chains, the solubility behavior can be tailored creating systems being thermoresponsive or water insoluble.[114] Just as PEG, POx is not biodegradable. A degradation of the amide group leads to an abstraction of the side group rather than a decomposition of the backbone and, hence, the formation of linear poly(ethylene imine) (see Chapter 2.2). Since 2016, poly(2-ethyl-2-oxazoline) is approved by the FDA as indirect additive used in food contact substances (21 CFR 175.105).

2.8 Poly(*N*-acrylamide)s

Poly(*N*-acrylamide)s describe a polymer class that bear amide functionalities in the side chain. There is a large variety of monomers commercially available, however, the most commonly applied and studied polymers are doubtlessly poly(*N*-(2-hydroxypropyl)methacrylamide) and poly(*N*-isopropylacrylamide). Furthermore, poly(2-acrylamido-2-methylpropane sulfonate) is utilized.

Poly(*N*-(2-hydroxypropyl)methacrylamide) (PHPMA) is a hydrophilic, chemically and hydrolytically stable, biocompatible polymer, often described simply as "HPMA" in literature. Moreover, it mimics living tissue and features a well-established safety profile in the human body. Its hydroxyl group functionalities allow the convenient conjugation of drugs and targeting molecules. However, PHPMA-based polymers are nonbiodegradable, which limits their use for some pharmaceutical applications.[115] Otherwise, they are hydrophilic and known to be non-toxic in the rat, even at higher doses (30 g kg^{-1}).[116] PHPMA can be synthesized by conventional free radical polymerization of *N*-(2-hydroxypropyl) methacrylamide or by several controlled radical polymerization techniques including atom transfer radical polymerization (ATRP) and reversible addition-fragmentation chain transfer (RAFT) polymerization.[117] Other techniques include the post-polymerization modification of poly(pentafluorophenyl methacrylate) (PPFMA), which contains activated ester side chains, by reacting with 1-amino-2-propanol.[118] Compared to the free radical polymerization, controlled radical polymerization techniques provide access to a vast number of macromolecular architectures including PHPMA copolymers with improved control over the molar mass and dispersity.[119] Despite the extensive research effort spent on PHPMA, none of the materials has yet been approved by the FDA.

Poly(*N*-isopropylacrylamide) (PNIPAAm) is one of the most intensively studied temperature responsive polymers of the past four decades.[120] The PNIPAAm homopolymer exhibits a lower critical solution temperature (LCST) of around 33 °C in aqueous solution, which is close to the body temperature.[121] In addition, the LCST of PNIPAAm can be easily tuned by copolymerizing various functional monomers to alter the polymer backbone.[122] When the temperature is lower than the LCST, PNIPAAm is water soluble due to a complex H-bond network along the PNIPAAm chains. In contrast, at temperatures above the LCST PNIPAAm becomes water insoluble because of the destroyed H-bond network and the release of water molecules.[123] Due to this reversible transition in water, its good biocompatibility and low toxicity, PNIPAAm-based polymers are found in numerous biological and biomedical applications including controlled drug release, tissue engineering, bio-detection, bio-separation, smart microfluidic devices and biochips.[123-124] However, PNIPAAm is not biodegradable which limits its use in some pharmaceutical applications.[125] PNIPAAm can be synthesized by a variety of polymerization techniques including conventional free radical polymerization, ATRP, and RAFT polymerization of *N*-isopropylacrylamide.[120a, 126] Although an enormous progress has been made, to the best of our knowledge, there is no FDA approval of PNIPAAm-based materials, nor are there any materials under clinical investigation for drug delivery.

2.9 Polyphosphoesters

Polyphosphoesters are constructed by repeating phosphoester groups (-POR'-O-R-O-)$_n$ in the main chain. They can be subdivided into polyphosphites, polyphosphonates, polyphosphoramidates and polyphosphates.[127]

Among them, **polyphosphates (PP)** (R' = OR^1) represent the most important class of polymers, due to their structural similarity with nucleic and teichoic acids.[128] Inorganic PPs are salts or esters of polymeric oxoanions built on tetrahedral phosphate (PO_4) units and occur as linear or branched forms, or cyclic ring structures. They are commonly synthesized by dehydration of orthophosphate (PO_4^{3-}) at an elevated temperature. Other methods include an olefin metathesis reaction *via* an acyclic diene and the ring-opening metathesis polymerization.[129]

A variety of synthetic methods has been summarized by Wang *et al.*.[130] PP can be found in all bacterial, fungal, plant or animal life forms. PP was first isolated from yeast by Lieberman[131] in 1888 and has been reviewed frequently since the 80's.[132] The numerous and different biological functions and their biocompatibility have made these materials the subject of several research areas investigating the substitution for adenosine triphosphate (ATP) in kinase reactions,[133] chelation of metals,[134] or their role in the physiological regulation of growth, development, stress, and deprivation.[135] PPs allow for numerous opportunities of modifications due to the pentavalent nature of the phosphorus atoms. Examples for such modifications are the introduction of double[136]/triple bonds,[137] hydroxy[138] and amine groups[139] to the side chain or polymer backbone. Since Yan and co-workers reported the synthesis of highly pure hyperbranched polyphosphates (HBPPs) *via* the self-condensing ring-opening polymerization, this method attracted considerable attention.[140] The convenient modification of the side group of the cyclic phosphate monomers resulted in a variety of structures and functionalities.[128] Well-defined PPs with approximately 30,000 g mol^{-1} (M_n) can be synthesized with dispersities $Đ < 1.1$[141] while also high molar mass PPs are possible (M_n = 150,000 g mol^{-1}).[142] Under physiological conditions, PPs can degrade into non-toxic, low molar mass species through the hydrolysis or enzymatic cleavage of the phosphate bond. The FDA classifies chosen PPs used in food under the GRAS status. They can be found in all types of food including baby food, meat, seafood and cheese according to the stipulated rules (food industry: < 5000 pm,[143] meat: < 0.5% weight of the final product[144]). Polyphosphates have shown to stabilize the protein structure, form a surface layer coagulated protein around meat or to retain the natural moisture of seafood.

2.10 Polysiloxanes

Materials composed of a backbone of alternating silicon and oxygen atoms with two alkyl or aryl moieties attached to the tetravalent silicon (-R_2Si-O-) are generally referred to as silicon polymers.[145] They can be considered as hybrid materials due to the combination of polar inorganic siloxane bonds (-Si-O-) in the backbone and organic alkyl or aryl side chains. Since the invention of the so-called "Direct Synthesis" of methylchlorosilane by Rochow and Müller (also called "Müller-Rochow-Process") in the early 1940s, polysiloxanes have been prepared industrially. This large scale production of silicon polymers is realized by an equilibration polymerization of cyclic and linear oligosiloxanes in the presence of an acid or a base as catalyst.[146] The method enables easy scale-up and cost effective production. However, it does not provide a good control over molar masses of the polymers and their dispersity. Only with the development of an ionic ring-opening polymerization using cyclic oligosiloxanes as monomers, well-defined polysiloxanes with defined molar masses and narrow dispersities became accessible.[147] Compared to the carbon-based polymers, silicon polymers feature superior physical and chemical properties in terms of thermal and oxidative stability, as well as flexibility combined with a low thermal glass transition temperature.[148]

Poly(dimethylsiloxane) (PDMS), for pharmaceutical applications better known as "dimethicone", bears two methyl groups on each silicon atom and represents the most prominent member of the silicone family. It is used in various pharmaceutical applications due to its excellent biocompatibility, low toxicity, optical transparency, gas permeability, high thermal stability, elasticity and low production costs.[149] However, due to the extreme hydrophobicity, PDMS-based materials suffer from low wettability and biofouling problems.[150] In consequence, increasing concerns arise about the safety of PDMS polymers in long term applications in blood contacting environments. To overcome these limitations, the focus of recent silicon related research has been concentrated on modifications to enhance the hydrophilicity and anti-fouling capability.[151] PDMS is not biodegradable in processes occurring *in vivo*; however, it slowly degrades within the environment to yield silica, carbon dioxide and water as non-toxic degradation products.[152] The FDA approved the use of PDMS in foods (except milk), cosmetic and pharmaceutical products (21 CFR 173.340).

2.11 Poly(vinyl ester/alcohol/ether)s

Poly(vinyl esters/alcohols/ethers) are all based on the polymerization of a vinyl group linked to an adjacent oxygen group. Poly(vinyl ester)s comprise polymer species, which are mainly prepared by free radical polymerization of vinyl esters. Technically important is **poly(vinyl acetate) (PVAc)**. More than one decade ago, the preparation of well-defined PVAc by controlled radical polymerization (M_n = 50,000 g mol^{-1}, Đ < 1.4) by "macromolecular design *via* interchange of xanthate"/reversible addition-fragmentation chain-transfer (MADIX/RAFT) polymerization became popular.[153] PVAc reveals a glass transition temperature (T_g) around room temperature. Since it is rather brittle below the T_g, plasticizers are usually added for improved flexibility. The homopolymer is often applied as adhesive in water-based emulsions. To overcome its stiffness, PVAc is often copolymerized with other monomers. Furthermore, PVAc can be partially or fully hydrolyzed to obtain the water-soluble **poly(vinyl alcohol) (PVA)**. It cannot be prepared by polymerization of the respective monomer vinyl alcohol since it is unstable. Depending on the length of the initial PVAc and the degree of hydrolysis under acidic or alkaline conditions, PVA with molar masses (M_n) from 20,000 to 400,000 g mol^{-1} can be obtained with varying solubility, tensile strength and adhesiveness.[154] It has a number of desirable properties like mechanical strength and high elasticity that make it a useful pharmapolymer. The hydroxyl groups are suitable for cross-linking (*e.g.* with ethylene glycol diglycidyl ether[155] or glutaraldehyde[156]) to create hydrogel networks with low or high swelling behavior in water. They have been well-established as drug delivery carriers. The FDA approved PVA for various uses, *e.g.* as indirect food additive in products, which are in contact with food (21 CFR 177.1670), as diluent in color additive mixtures for coloring shell eggs (21 CFR 73.1) and as ophthalmic demulcent (21 CFR 349.12).[154] Several microorganisms are able to degrade PVA as well as PVAc through enzymatic processes. The degradation by human enzymes has not been reported so far. The copolymer poly(ethylene-*co*-vinyl acetate) (PEVA) is often used in drug delivery research to slowly release a compound. Furthermore, it reveals only little or no reaction after implantation.

Since 1930, **poly(vinyl ether)s (PVE)** have been produced on an industrial scale. PVEs are polymers bearing the functional ether group in the side chain. They are made from the respective vinyl ethers *via* chain-growth polymerization. The functional versatility of the starting material allows the incorporation of alkyl or amine moieties. Different synthesis routes and industrial processes are described in literature.[157] Probably the most important PVE is the amphipathic butyl- and amine modified one (PBAVE) that has shown remarkable performances in trial experiments.

2.12 Poly(*N*-vinyl amide)s

Poly(*N*-vinyl amide)s describe a polymer class that comprises amide functionalities in the side chain. Compared to poly(*N*-acryl amide)s, the amide group is linked to the polymer backbone through the nitrogen atom. The most prominent representative is **poly(vinyl pyrrolidone) (PVP)**.

Linear PVP was first synthesized by Reppe in 1939 as one of the numerous products originating from acetylene chemistry. It is a water soluble, non-ionic, biocompatible and stable polymer, which is not metabolized by the organism.[158] In the very beginning during World War II, it was mainly used as plasma expander.[159] Today, it is well established in several products of cosmetic and pharmaceutical industry, *e.g.* as binder in pills. A special feature of PVP, also known as "povidone", is its possibility to form strong hydrogen bonds, which also explains its good solubility properties in water. Furthermore, the hydrogen bond formation enables complexation of polar compounds which increases the water solubility and the bioavailability, as reported for acetaminophen.[160] The complex formation constants as well as solubility properties were furthermore determined for several other substances.[161] It could be shown that PVP, similar to PEG, increases the water solubility and blood circulation time

for liposomes.[162] PVP is approved by the FDA for numerous applications, *e.g.* in food for human consumption (21 CFR 173.55). A reported method to synthesize PVP in laboratory scale is MADIX/RAFT polymerization. In industrial scale, it is synthesized by free radical polymerization in most cases, whereat a broad range of molar masses can be obtained. The commercially available polymers comprise ranges (M_w) from 2,000 to 2,500 × 10^3 g mol^{-1}.[163] In order to achieve high molar masses, a polymerization in aqueous solution is commonly applied using hydrogen peroxide as initiator. Organic solvents generally lead to low molar mass PVP. Using hydrogen peroxide as initiator, the solvent for the polymerization is of high importance for the final product, since it is responsible for the polymer end group. Other possibilities to create different functional endgroups include the usage of suitable transfer agents or specific chain capping agents. Post modifications are also possible but difficult to control, and the products are hard to purify. Another way to alter or to improve the polymer properties of PVP is copolymerization.[160] The synthesis is performed by radical polymerization in an organic solvent similar to the synthesis of the linear homopolymer. A frequently used comonomer is vinyl acetate (polymer: copovidone). The amount of vinyl acetate increases the hygroscopicity of the product, allowing the preparation of less brittle films, which is preferable for the use as soluble binder or film-forming agent.[161] One opportunity to obtain water insoluble PVP is cross-linking, resulting in so-called crospovidone. The ways to synthesize cross-linked PVP are versatile, reaching from the use of cross-linking agents or cross-linking monomers to subsequent cross-linking with peroxides. A well-known way to obtain highly cross-linked products is the so-called "popcorn polymerization". This method uses either an alkali hydroxide, yielding some bifunctional monomers, or a small amount of bifunctional monomers for cross-linking.[161, 164] The mechanism of this polymerization method is not well-determined, since it was primary observed as a side reaction in radical polymerization processes. It could be found that this polymerization starts by a highly reactive nucleus initiating the whole process, similar to the formation of popcorn.[165] Infrared measurements revealed that there is no structural difference between the cross-linked PVP obtained by popcorn polymerization and the linear PVP, but a difference was observed for chemically cross-linked PVP. Therefore the cross-linking of PVP *via* popcorn polymerization is essentially of a physical nature.[161] The cross-linked PVP is widely used in beverage and pharmaceutical industry. The good adsorptive properties are used to remove polyphenols or azo dyes from beverages. A rather well-known example in the pharmaceutical industry is the PVP-iodine complex which is used as disinfectant, also known as betaisodona and with several other trade names. Furthermore, crospovidone shows beneficial disintegration properties, thus it is used as additive in tablets promoting their break up and, therefore, speed up the drug release from solid dosage forms.[161, 166]

2.13 Poly(allylamine)s

Poly(allylamine) (PAAm) is a cationic polymer obtained from the radical or cationic polymerization of allylamine. While the backbone contains no nitrogen, as described for poly(ethylene imine), the polymer side chain contains primary amine groups which can be converted into secondary or tertiary amine functionalities. This turns PAAm into a highly promising gene delivery agent.[167] Poly(allylamine hydrochloride) in combination with an anionic polyelectrolyte (*e.g.* poly(styrene sulfonate)) can be used to form layer-by-layer adsorbed films.[168]

2.14 Poly((meth)acrylate)s

Poly(acrylate)s and poly(methacrylate)s are synthetic polymers of acrylic and methacrylic acids or their esters, respectively.[169] They are prepared on an industrial scale by free radical polymerization applying a variety of different methods, which include bulk, solution, suspension, and emulsion polymerization.[170] Poly(meth)acrylates can also be synthesized by various controlled radical polymerization techniques, which allow

a better control over molar mass, dispersity, polymer composition, and polymer architecture compared to free radical polymerization.[171] Poly(methacrylate)s generally display a higher glass transition temperature (T_g) and a lower decomposition temperature than the corresponding poly(acrylate)s.[172] The properties of poly(meth)acrylates can conveniently be tuned by varying the molecular structure of the ester side chain. These modifications enable access to polymers spanning the whole range from water to oil soluble or from brittle to elastic. The FDA has approved the safety of poly(meth)acrylates in several pharmaceutical applications, *e.g.* as basic components of food contact surfaces (21 CFR 177.1010).

Poly(acrylic acid) (PAA) and **poly(methacrylic acid) (PMAA)**, bearing a carboxylic acid unit on every second carbon atom of the main chain, are water soluble, weak anionic polyelectrolytes.[173] Besides their linear form they can be cross-linked by several cross-linking agents. The backbone of PAA and PMAA are not biodegradable, but they exhibit a low toxicity and excellent biocompatibility.[160] In aqueous solution, PAA and PMAA display a reversible coil-to-globule transition at pH 5. At lower pH values, these polymers undergo a transition to a compact globular conformation. However, if the pH value is increased, the chains expand into a fully solvated coil conformation due to the ionization of the carboxyl groups.[174] This reversible ionization of PAA and PMAA enables the formulation of pH- and ionic strength responsive materials. For instance, PAA-based hydrogels swell rapidly when placed in an aqueous environment due to the ionization of carboxyl groups. This feature makes PAA and its sodium salt (poly(sodium acrylate)) the most prominent materials for super absorbers, which are applied in diapers and membranes for hemodialysis or ultrafiltration.[175] Concerning drug delivery applications, PAA provides sufficient flexibility and excellent bioadhesion properties. Hence, they are frequently used for oral and mucosal contact applications such as tablets, oral suspensions and bioadhesives. An advantage of PAA is the convenient modification of the carboxyl side chains with alcohols or amines to introduce additional functionalities. In consequence, drugs and/or bioactive molecules can easily be attached to the PAA backbone in accordance with the concept of Ringsdorf.[176] **Poly(2-hydroxyethyl methacrylate) (PHEMA)** represents another water soluble, biocompatible poly(methacrylate) modified with hydroxyl functionalities in each repeating unit. These hydroxyl groups enable the material to form strong hydrogen bonds and make it very hydrophilic without need for charged side chains. As a consequence, PHEMA is often used as the main material for contact lenses. Moreover, the hydroxyl functionality of PHEMA can further be modified in post-polymerization reactions to conjugate any bio-active molecule.

Poly(methyl methacrylate) (PMMA) represents probably one of the best-known poly(methacrylate)s containing a methyl ester functionality at the side chain, which makes this material hydrophobic and non-soluble in water. PMMA was first developed in 1928 by Röhm, Chalmers and Bauer. The first commercial product was brought to the market in 1933 by the Rohm and Haas company under the trademark "Plexiglas®".[177] In the following years, PMMA rapidly became the most important plastic glass due to its excellent transparency and ease of production. Concerning pharmaceutical applications, PMMA is characterized by an excellent biocompatibility, convenient processability, low toxicity, minimal inflammatory reactions with tissues, and low production costs.[178] Being nonbiodegradable and fracture resistant, it is an essential material for implant materials, in particular in case of long term applications. PMMA-based materials have further found application in dermal fillers, bone cements, intraocular lenses and membranes in dialyzers for hemodialysis.[179] However, there are some limitations to the use of PMMA, which are related to its brittleness and shrinkage, the generation of voids during processing steps, a lack of adherence to bone tissue, and the heat created by the exothermic reaction during cement polymerization, which can damage bone tissue.[180] To overcome these problems, alternative poly(meth)acrylates are currently under investigation, in particular for use as long term implant materials. One example is **poly(*n*-butyl methacrylate) (PBMA)**, which possesses a butyl ester at the side chain. This material features a lower toxicity, a higher fracture toughness, and a better fatigue life, while reducing the exothermic effects compared to PMMA.[181]

Another important modification of poly(methacrylate) is **poly(2-dimethylaminoethyl methacrylate) (PDMAEMA)**, which contains an ionizable tertiary amine group. In water it may be protonated and becomes a weak cationic polyelectrolyte depending on the pH value. The pK_a value of the polymer depends on the composition as well as the molar mass, whereas values between 7 and 8 have been reported. Additionally, PDMAEMA exhibits LCST behavior in water depending on the molar mass of the polymer and the pH value of the solution.[182] However, the positive charge on the polymer causes these materials to be quite cytotoxic, which, in combination with the lack of biodegradability, limits its use in pharmaceutical applications.[183] Concerning drug delivery systems, the monomer DMAEMA is so far only applied as comonomer in combination with other methacrylates or methacrylic acid to modulate the overall charge and create a defined pattern for dissolution at specific pH values. Apart from changing the ester functionality or its alkyl moiety, physicochemical properties of the poly(meth)acrylates can also be altered by copolymerizing different functional monomers and by varying the monomer composition of the polymers. Incorporating the ionizable segments in the backbone of the polymers, such as amine and/or carboxyl groups, can render a tunable pH-dependent water solubility to the corresponding polymers. Accordingly, they are used for pH-dependent drug release applications due to salt formation.[184] These copolymers are more commonly known as EUDRAGIT® polymers in pharmaceutical industry and described in Chapter 3.

Furthermore, in addition to hydrogen and methyl groups, some other functionalities can be installed on the α-position of the acrylic backbone. For instance, acrylates with a nitrile group are called cyanoacrylates. Various alkyl groups can be added to the ester group, *e.g*. methyl, butyl, or hexyl. Cyanoacrylates polymerize rapidly in the presence of traces of water by an anionic polymerization mechanism to corresponding poly(cyanoacrylate)s. Therefore, they are commonly used as instant adhesives or "superglues".[185] For medical adhesive applications, cyanoacrylates with long alkyl groups are preferred since poly(cyanoacrylate)s with short groups can irradiate the tissues. Poly(cyanoacrylate)s, in particular **poly(isobutyl cyanoacrylate)** and **poly(isohexyl cyanoacrylate)**, have also been used in drug delivery applications. The installation of the heavier element fluorine on the α-position results in α-fluoroacrylates. Poly(α-fluoroacrylate)s can be obtained by the free radical polymerization of the α-fluoroacrylate.[186] Compared to the conventional (meth)acrylates these polymers exhibit better thermal and chemical stabilities. These polymers are mainly used for optical applications, but also found to be useful in cross-linked copolymers as polymer sequestrant.

2.15 Polyacrylonitriles

Polyacrylonitriles (PAN) are synthetic, semicrystalline organic polymers consisting of nitrile units attached to the carbon backbone. First synthesized in 1930 by Fikentscher and Heuck (IG Farben, Ludwigshafen),[187] it took more than 16 years for establishing the large scale production of PAN (brand name Orlon®) by Du Pont®.[188] Commercial PAN with high molar mass is synthesized by free radical polymerization of acrylonitrile. As a result, the control of the molar mass distribution is limited and high dispersities are obtained ($M_n < 10^6$ g mol^{-1}, $Đ > 3$). More controlled processes like the ATRP and the RAFT polymerization enable the control of the molar mass distribution for molar masses (M_n) up to 100,000 g mol^{-1} (ATRP[189]: $Đ < 1.3$; RAFT[190]: 60,000 g mol^{-1}, $Đ = 1.2$ to 1.4). In many cases, various vinyl monomers are copolymerized to modify the structure for final applications.[191] Anionic polymerization has been applied for the polymerization of PAN as well,[192] but this method results in branched structures, which affects the mechanical behavior of the PAN.[193] In general, the active nitrile groups in PAN can be converted to other functional groups like carboxyls (*via* hydrolysis)[194] and amines (*via* reduction),[195] which subsequently facilitate further modifications. Recently, Nataraj *et al.* reviewed the application of PAN-based nanofibers in various fields.[196] Several investigations have demonstrated that the relatively poor biocompatibility of the conventional PAN could be improved by bulk or surface modification.[197] Another simple and low-cost alternative modification is

blending.[198] The FDA approved the use of PAN in the production of semi-rigid and rigid acrylic plastics, which are intended for use in contact with food (21 CFR 177.1010).

2.16 Polyurethanes

Discovered 75 years ago, **polyurethanes (PU)** represent a versatile polymer class based on a modular structure which is generated by the combination of a variety of polyols and isocyanates as building blocks.[199] The urethane groups are formed in the polymer backbone by the polyaddition of respective isocyanates and alcohol groups. The chemical nature of the building blocks, the reaction sequence as well as the ratio of the OH/isocyanate components determines the properties of the polymers. Polyols with molar masses (M_n) larger than 1,000 g mol^{-1} are used to make soft and elastic PUs (*e.g.* PEG-diols) while short chains result in hard, rigid PUs (*e.g.* dipropylene glycol). The latter can be further supported by cross-linkages. The most common used isocyanates are aromatic diisocyanates (*e.g.* toluene and methylene diphenyl diisocyanate) since they reveal higher reactivity compared to aliphatic isocyanates (*e.g.* hexamethylene diisocyanates). Often the reaction of three components, in particular a diisocyanate, a bifunctional polyol and a dihydroxy chain extender, is described to form linear, segmented copolymers consisting of alternating hard and soft segments. The structural diversities and tailorable properties (*e.g.* biodegradability, blood compatibility, hydrophilicity) make these materials extremely versatile for bioapplications and other high-tech products.[200] Doubtless, the most prominent application for PUs are foams of different nature. The FDA approved PU resins for use as basic components of food contact surfaces (21 CFR 177.1680). Other materials, which are closely related to PUs, are polyureas (often summarized as polyurethanes); these are the product of the addition of isocyanates with amines.[201] In general PUs for biomedical applications are mainly found in gels of various sizes.

2.17 Polystyrenes

Polystyrenes (PS) are synthetic aromatic polymers made from the styrene monomers. The first commercially available polymers were manufactured by the company I. G. Farben in 1931.[202] The most prominent applications are the PS foams. Pioneering work on its polymerization was done by Natta (1960) and Ishihara (1986) who reported the synthesis of iso- (phenyl groups on the same side) and syndiotactic polystyrenes (phenyl groups on alternating sides of the backbone). The latter is commonly prepared in a so-called Ziegler-Natta-polymerization.[203] This kind of polymerization uses metallocene catalysts in order to control the orientation of the monomer in the moment of addition.[204] Further synthesis routes comprise radical, anionic as well as cationic polymerization. The syndiotactic PS exhibits a crystallization rate, which is around two orders of magnitude larger than the isotactic form. Several routes for the synthesis of functional materials are described in literature, comprising *in situ* functionalization, post-polymerization modification or the application of pre-functionalized monomers.[205] For instance, the introduction of sulfonic acid groups in the para-position of the benzene ring turns the resulting PS into the water soluble **poly(styrene sulfonic acid)**. Different cross-linking agents have been incorporated into the PS resins, including the most commonly applied divinylbenzene, but also other monomers have been used to adjust different solvation properties (*e.g.* dimethacrylate, tetraethylene glycol).[206] Basically, PS is hard and rather brittle and occurs in the solid or foam state. It is a widely used plastic for packaging where hygiene is important. Above its glass transition temperature (100 °C) it becomes liquid, while cooling down results in rigidity again. Using this temperature behavior, PS can be processed *via* extrusion, molding or vacuum forming.[207] PS is approved by the FDA as food packaging material (21 CFR 177.1640) updated in 2013 by the Plastics Foodservice Packaging Group.[208]

2.18 Polyanhydrides

Polyanhydrides are commonly obtained by the dehydration reaction between diacids by either melt polycondensation or solution polymerization to form the functional group (-O-CO-R-CO-). Different structures, their characterization and biocompatibility have extensively been reviewed.[209] The polymers were prepared with the intention to obtain a material that should degrade within the time range of their application due to the presence of the most reactive functional group available for degradation on the basis of passive hydrolysis.[210] They degrade *in vivo* into non-toxic monomer counterparts, which can be eliminated from the body as metabolites. High molar mass polyanhydrides (M_n up to 30,000 g mol^{-1}) can be synthesized by utilizing heterogenic coordination catalysts.[211] Often used monomers are the naturally occurring sebacic acid (**poly(sebacic acid)**, FDA: 21 CFR 175.105) and the 1,3-bis(4-carboxyphenoxy)-propane (**poly(*bis*-(p-carboxyphenoxy)propane**). While aromatic polyanhydrides can fragment after exposure to water, resulting in a rapid release of water-soluble drugs, copolymers prepared from fatty acids (*e.g.* sebacic acid) show controlled degradation rates from days to years. The copolymer poly(styrene-*co*-maleic anhydride) was approved by the FDA as indirect food additive for use as articles or components of articles that contact food items (21 CFR 177.1820).

Containing the functional groups in the side chain, **poly(maleic anhydride)** represents another form of polyanhydrides made from maleic anhydride in the presence of free radical catalysts and various organic bases, among others.[212] It is mainly used as comonomer, *e.g.*, for the polymerization with styrene (poly(styrene-*co*-maleic anhydride)). A unique feature is the preparation of almost perfectly alternating copolymers which are the first polymers that were used for drug conjugates.

2.19 Polyolefins

Polyolefins describe a class of polymers obtained from a simple alkene (olefin) as monomer. These materials are produced in million ton scales and are the most common plastics used in commodity products. Besides radical processes or the frequently used coordination polymerization, the living alkene polymerization method catalyzed by transition metal complexes is becoming more and more popular to synthesize polyolefins with a precise molar mass control as well as a wide array of polymer architectures.[213] Their properties are mainly determined by their molar mass and degree of crystallinity (from liquid-like to rigid plastics). All practical or commercial relevant polyolefines are poly-α-olefins. The FDA approved **poly(ethylene)** for use as basic component of food contact surfaces (21 CFR 177.1520). It represents the simplest representative and most common plastic, which is made from ethylene in the presence of the Ziegler-Natta catalyst.[214]

Further often used olefins are **poly(isobutylene)** (by cationic polymerization of isobutylene),[215] the non-reactive fluoropolymer **poly(vinylidene fluoride) (PVDF)** (by radical polymerization of vinylidene difluoride)[216] and **poly(hexafluoropropylene) (PHFP)**. *Bis*functional polyolefins like **poly(octa-1,7-diene)** can be used for cross-linking reactions to obtain network architectures.

Table 2. Overview of polymer classes that exhibit pharmaceutical relevance.

POLYMER CLASS	STRUCTURE	R	NAME (ABBREVIATION)	WATER SOLUBILITY	BIODEGR.[a] (Y/N)	APPLICATION (see corresponding chapter)
Polyether	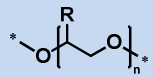	H	Poly(ethylene glycol) (PEG)	Good	N	Polymer-drug conjugates, solid colloidal dispersions, polyplexes, microgels, hydrogels, solid implants and inserts, matrix excipients
		CH_3	Poly(propylene glycol) (PPG)	LCST ~ 50 °C	N	Solid colloidal dispersions, polyplexes, matrix excipients, polymeric drugs
		OH	Poly(glycerol) (PG)	Good	N	Future prospects
		CH_2Cl	Poly(epichlorohydrin) (Poly(chlormethyl)oxiran)	No	N	Polymeric drugs
	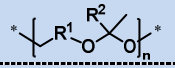		Poly(ketal) (PK)	Dependent on R^2	Y	Future prospects
Poly(ethylene imine)	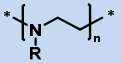	H	Linear poly(ethylene imine) (LPEI)	Good for > 70 °C	N	Polyplexes, hydrogels, future prospects
		CH_2CH_2NHR	Branched poly(ethylene imine) (BPEI)	Good	N	Polyplexes, hydrogels, future prospects
Polyester	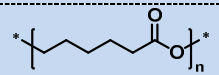		Poly(caprolactone) (PCL)	Degradation	Y	Drug-eluting stents, future prospects
	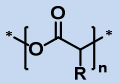	H	Poly(glycolic acid) (PGA)	Degradation	Y	Solid colloidal dispersions, hydrogels, solid implants and inserts, drug-eluting stents, future prospects
		CH_3	Poly(lactic acid) (PLA) (*i.e.* PDLLA, PLLA and PDLA)	Degradation	Y	Solid colloidal dispersions, hydrogels, solid implants and inserts, drug-eluting stents, future prospects
	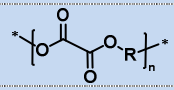		Poly(oxalate) (PO)	Degradation	Y	Future prospects
	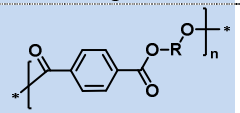	$(CH_2)_4$	Poly(butylene terephthalate) (PBT)	Degradation (> 60 °C)	Y	Microgels
Polycarbonate	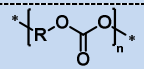			Good	Y	Future prospects
Poly(amino acid)	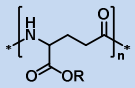	H	Poly(γ-glutamic acid) (PGluA)	Good	Y	Polymer-drug conjugates, future prospects
			Poly(γ-glutamate) (PGlu)	Good	Y	Solid colloidal dispersions, nanogels
	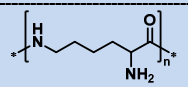		Poly(lysine)	Good	Y	Polyplexes, future prospects

	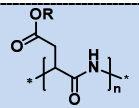		α-Poly(aspartate) (PAs)	Good	Y	Solid colloidal dispersions
Poly(peptoid)	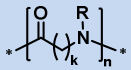		(PoP)	Good	Y	Future prospects
Poly(2-oxazoline)	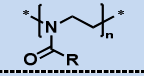		(POx)	Good (only for CH_3, C_2H_5)	N	Polymer-drug conjugates, future prospects
Poly(*N*-acrylamide)	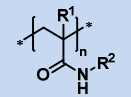	R^1 = H; R^2 = $CH(CH_3)_2$	Poly(*N*-isopropylacrylamide) (PNiPAAm)	Depending on temp.	N	Future prospects
		R^1 = CH_3; R^2 = $CH_2CH(CH_3)(OH)$	Poly(*N*-(2-hydroxypropyl)-methacrylamide) (PHPMA)	Good	N	Polymer-drug conjugates, future prospects
Polyphosphoester	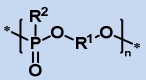	R^2 = OR	Poly(phosphate) (PP)	Good	Y (Depend. on R^2)	Future prospects
Polysiloxane	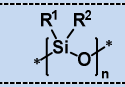	R^1,R^2 = CH_3	Poly(dimethylsiloxane) (PDMS, dimethicone)	No	N	Hydrogels, solid implants and inserts, matrix excipients, future prospects
Poly(vinyl ester/alcohol/ether)	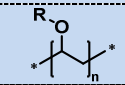	$COCH_3$	Poly(vinyl acetate) (PVAc)	Good	Y	Solid implants and inserts, drug-eluting stents, Future prospects
	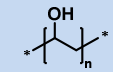		Poly(vinyl alcohol) (PVA)	Good	Y	Microgels, solid implants and inserts, solid oral dosage forms, matrix excipients
	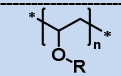		Poly(vinyl ether) (PVE)	No	N	Polymer-drug conjugates
Poly(*N*-vinyl amide)	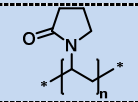		Poly(vinyl pyrrolidone) (PVP)	Good	N	Hydrogels, drug-eluting stents, matrix excipients, future prospects
Poly(allylamine)	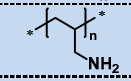		(PAAm)	Good	?	Polymeric drugs, future prospects
Poly(acrylate)	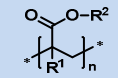	R^1 = H; R^2 = H	Poly(acrylic acid) (PAA)	Good	N	Hydrogels, matrix excipients, future prospects
		R^1 = H; R^2 = CH_3	Poly(methyl acrylate)	No	N	Solid oral dosage forms
		R^1 = H; R^2 = C_2H_5	Poly(ethyl acrylate)	No	N	Solid oral dosage forms
		R^1 = F; R^2 = H	Poly(2-fluoroprop-2-enoate)	Good	N	Polymeric drugs
Poly(methacrylate)	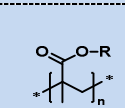	R = H	Poly(methacrylic acid) (PMAA)	Good	N	Microgels, solid oral dosage forms, future prospects
		R = CH_3	Poly(methyl methacrylate) (PMMA)	No	N	Solid implants and inserts, solid oral dosage forms, matrix excipients, future prospects

		R = C_4H_9	Poly(*n*-butyl methacrylate) (PBMA)	No	N	Drug-eluting stents, matrix excipients
		R = $CH_2CH_2N(CH_3)_2$	Poly(dimethylaminoethyl methacrylate) (PDMAEMA)	Good	N	Solid oral dosage forms, matrix excipients, future prospects
		R = $CH_2CH_2N(C_2H_5)_2$	Poly(diethylaminoethyl methacrylate) (PDEAEMA)	Depending on pH value	N	Solid oral dosage forms
		R = $CH_2CH_2N(CH_3)_3^+$	Poly(trimethylammonioethyl methacrylate chloride) (PTMAEMA)	Depending on pH value	N	Solid oral dosage forms
		R = CH_2CH_2OH	Poly(2-hydroxyethyl methacrylate) (PHEMA)	Good (low molar masses)	N	Hydrogels
Poly(cyanoacrylate)	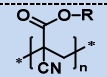	R = $CH_2CH(CH_3)_2$	Poly(isobutyl cyanoacrylate)	No	N	Solid colloidal dispersions
		R = $(CH_2)_3CH(CH_3)_2$	Poly(isohexyl cyanoacrylate)	No	N	Solid colloidal dispersions
Polyacrylonitrile			(PAN)	Good (in aq. inorganic salt solutions)	N	Hydrogels, future prospects
Polyurethane	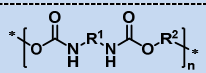		(PU)	No	Y	Hydrogels, solid implants and inserts
Polystyrene	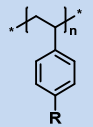	H	(PS)	No	N	Polymer-drug conjugates, drug-eluting stents, polymeric drugs, future prospects
		SO_3H	Poly(styrene sulfonic acid)	Good	N	Polymeric drugs
		$[-CHCH_2]_n$	Poly(divinylbenzene)	No	N	Polymeric drugs
Polyanhydride	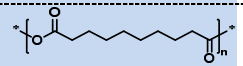		Poly(sebacic acid)	Decomposition	Y	Solid implants and inserts
	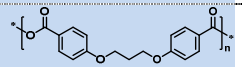		Poly(*bis*-(p-carboxy-phenoxy)propane)	Decomposition	Y	Solid implants and inserts
	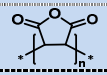		Poly(maleic anhydride)	Decomposition	N	Polymer-drug conjugates, future prospects
Polyolefin		R^1 = H; R^2 = H	Poly(ethylene)	No	N	Solid implants and inserts, drug-eluting stents
		R^1 = CH_3; R^2 = CH_3	Poly(isobutylene)	No	N	Drug-eluting stents
		R^1 = F; R^2 = F	Poly(vinylidene fluoride) (PVDF)	No	N	Drug-eluting stents
	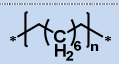		Poly(octa-1,7-diene)	No	N	Polymeric drugs
			Poly(hexafluoropropylene) (PHFP)	No	N	Drug-eluting stents

[a] Biodegradability in this review designates the potential of polymer chain cleavage by enzymes or proteases (Y = yes, N = no).

3. Polymers in pharmaceutical applications

The following chapter describes different forms of applications of pharmapolymers which are already available on the market or currently undergoing clinical trials. The current clinical status and the respective NTC number (clinicaltrials.gov identifier) usually refer to the official webpage https://clinicaltrials.gov/. In some cases, the availability and the approved indication of use for the applied materials vary between countries. The described forms of appearance include polymer-drug conjugates, drug carrier systems in scales ranging from nano- to macroscopic size, polymers as coatings and matrix excipients as well as polymeric drugs.

3.1 Polymer-drug conjugates

The conjugation to polymers is a well-established technique to improve the properties of therapeutically active substances. In the last decades, numerous polymers have been tested for this purpose. The cytostatic agents that have been mainly used for preparing polymer-drug conjugates are doxorubicin (DOX), camptothecin (CPT), paclitaxel (TXL) and platinum complexes (Figure 1), but also other, more specialized drugs are conjugated.

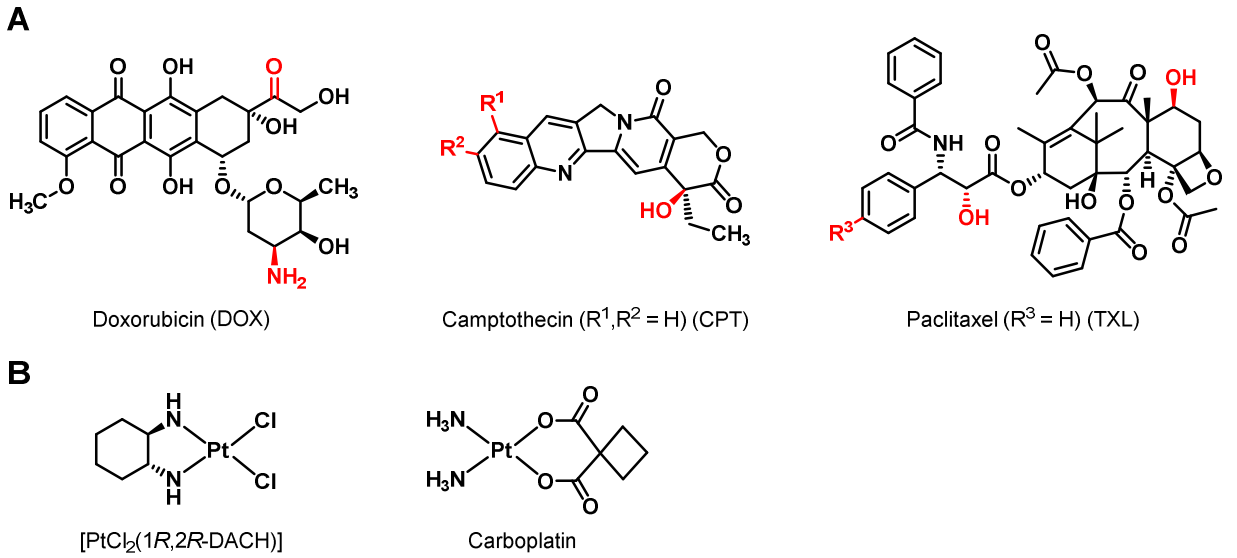

Figure 1. Schematic representation of the structures of the most common cytostatic agents used for preparing polymer-drug conjugates. A) Literature reported conjugation sites (marked in red) and B) selected examples for platinum complexes.

3.1.1 PEG conjugates

One of the first and probably the most well-known example is the attachment of poly(ethylene glycol) (PEG), also called PEGylation. In drug delivery, PEGylation can be subdivided into three categories: The attachment of PEG to proteins, to small drug molecules and to other polymers. The latter is often related to the formation of nanocarriers, which are described in detail in Chapter 3.2. With the attachment of PEG chains, some of the beneficial properties of this polymer are transferred to the pharmacological active compounds, which can improve

the accessibility of drugs in biological systems.[15, 217] Pioneered by Davis and his colleagues, the first PEGylation was successfully demonstrated on a protein.[10a] The initial goal was the protection from destruction during the delivery process. As an unexpected finding, the authors observed that the PEGylation improved the pharmacokinetic and pharmacodynamics of the protein.[218] Similar observations are found for small drug molecules, which often suffer from poor solubility and, therefore, low bioavailability. The attachment of PEG strongly improves their properties by adapting the beneficial properties of the PEG polymer.

PEGylation of proteins. Since the first PEGylation of a protein, a variety of accessible functional groups on protein surfaces has been explored as potential linking sites. In general, the functionalization with PEG introduces several advantageous properties compared to the native protein. PEGylated proteins show an improved pharmacokinetic and pharmacodynamic, which is related to an increased water solubility, an increased stability, shielding from metabolic enzymes, a reduced immunogenicity and retarded renal clearance (due to stealth behavior) leading to an elongated blood circulation time.[11b] Depending on the molar mass of the attached PEG chains, the clearance by the kidneys can also be circumvented.[15, 218-219] The conjugation additionally reduces the immunogenicity of the native protein, increases its stability and prolongs the biological half-life which helps to reduce the frequency of administration. In the last decade, several new conjugation methods have been developed, allowing a more effective and selective attachment of PEG polymers. The PEGylation techniques of proteins can be separated into first and second generation.[220] The first generation is performed using short PEGs (M_n = 5,000 to 12,000 g mol^{-1}) being randomly bound to the protein surface. A disadvantage when using a PEG-diol is the formation of a high content of protein dimers, trimers and even fully cross-linked materials. In consequence, the α-methylated mPEGs are preferred to avoid this problem, although minor contaminations with PEG-diol are still present.[221] As activation agents or linkers between the protein and the PEG chains, cyanuric chloride, tresyl chloride and many more compounds are applied.[11a, 222] The second generation of PEGylation improved the selectivity of the attachment to specific areas of the protein while reducing the influences on the protein structure. Common groups for functionalization are maleimide targeting free thiol groups, NHS activated acids reacting with amines, benzotriazoles, which create a pH-responsive linkage, and aldehydes such as propionaldehyde. Furthermore, second generation PEGs allow an easier purification and removal of remaining PEG-diol, *e.g.* in the case of PEG with activated acids up to 97% of the remaining diol content can be removed by ion-exchange chromatography.[218] PEGylation techniques forming disulfide bridges enable the site specific PEGylation to the few free cysteine residues on the protein surface, which minimizes the loss of biological activity, but preserves the low immunogenicity. A rather new method is described by DeFrees *et al.* called glycopegylation. This method basically uses enzymes for *N*-acetylgalactosamine (GalNAc) glycosylation at specific serine and threonine residues, which subsequently conjugate to salic acid conjugated PEG by enzymatic transfer.[223] These improvements on the conjugation methods allow the synthesis of drug conjugates with well-defined amounts of PEG and selective binding to non-active parts of the protein.[224] A more detailed overview on different protein PEGylation techniques is given by Roberts *et al.*.[11d]

Considering the above mentioned improvements on the synthesis, in particular the excellent selectivity of conjugation and the general benefits like the improved pharmacokinetics, it is not surprising that a number of PEGylated proteins already entered the market and several new materials are in clinical trials. Overall, thirteen different PEGylated proteins are nowadays approved and commercialized (Table 3). The first clinically approved PEGylated protein drug was the enzyme Adagen® (Enzon Pharmaceuticals). After its approval, several other PEGylated protein drugs found their way to commercialization and entered clinical trials within a short period of time. A milestone in the pharmaceutical development was certainly the approval of Macugen®, being the first approved aptamer used as therapeutic agent in humans.[225] The latest protein drug that has been approved by the Food and Drug Administration (FDA, Nov. 2015) is the PEGylated full length Factor VIII (Adynovate®) for use in patients aged 12 years and older suffering from haemophilia A and.[226] Once approved by the FDA or European

Medicines Agency (EMA), established PEGylated proteins are investigated in clinical trials. Due to the large number of clinical studies, only a selection of investigated diseases can be found in Table 3.

Table 3. PEGylated proteins and small drugs on the market approved by the FDA and EMA as well as their use for other diseases.

TRADE NAME	CONJUGATE	INDICATION/USE	MANCUFACTURER	M_n (PEG) (g mol^{-1}) [# of PEGs/drug molecule]	CURRENT CLINICAL TRIALS ON …
			PROTEIN		
Adagen®	PEG-Adenosine Deaminase	SCID[a]	Enzon Pharmaceuticals	5,000 [11 to 17]	Severe combined immunodeficiency disease
Oncaspar®	PEG-Asparaginase	Leukaemia	Enzon Pharmaceuticals	5,000 [69 to 82]	Various cancers (neoplasms, multiple myeloma)
PegIntron®, ViraferonPeg®	PEG-Interferon-α2b	Hepatitis C	Schering-Plough	12,000 [1]	Hepatitis B, various cancers (*e.g.* fallopian tube-, ovarian-, peritoneal cavity cancer, neoplasm, melanoma), HIV Infection
	PEG-Interferon-α2a	Hepatitis C	Hoffman-La Roche	40,000 [1 branched]	Hepatitis B, various cancers (*e.g.* kidney cancer, leukemia), HIV infection
Somavert®	PEG-Human growth hormone mutein antagonist	Acromegaly	Pfizer	5,000 [4 to 6]	Different neoplasms (colorectal, lung, breast, prostatic)
Neulasta®	PEG-G-CSF[b]	Neutropenia	Amgen®	20,000 [1]	Various cancers (*e.g.* breast cancer)
Macugen® (Pegaptanib)	PEG-anti-VEGF aptamer	WARMD	OSI Pharmaceuticals/ Pfizer	40,000 [1 branched]	Wet age related macular degeneration
Mircera®	PEG-Erytropoietin	AACKD	Hoffman-La Roche	30,000 [1]	Various cancers (*e.g.* breast, prostate cancer, lymphoma, neoplasms)
Cimzia®	PEG-anti-TNF Fab[c]	Rheumatoid arthritis & Crohn's disease (RACD)	UCB Cares®	40,000 [1 branched]	RACD
Krystexxa® (Pegloticase)	PEG-Uricase	Chronic gout	Horizon Pharma	10,000 [9 per homo-tetramer (4)]	Chronic kidney disease stage 5
Omontys®	Peginesatide	AACKD	Affymax/Takeda[d]	40,000 [1 branched]	Anaemia associated with chronic kidney disease
Lonquex® (Lipegfilgrastim)	Glycopegylated G-CSF	Neutropenia[e]	TEVA	20,000 [1]	Various cancers (*e.g.* breast, ovarian cancer)
Plegridy®	PEG-interferon beta 1a	Relapsing multiple sclerosis (RMS)	Biogen™	20,000 [1]	RMS
Adynovate®	PEG-Factor VIII (full-length Coagulation Factor VIII) (BAX 855)	Haemophilia A[a]	Shire	20,000 [2]	Different blood diseases (von Willebrand Disease, thrombosis)
			SMALL DRUG		
Moventig® (EU: Movantik®) (Naloxegol)	PEG-Naloxone[b]	Opioid-induced constipation	AstraZeneca	< 1,000 [1]	

[a] Only approved by the FDA, [b] G-CSF: Granulocyte-colony stimulating factor, [c] approved for different disease in U.S. and E.U. (Nektar®), [d] withdrawn by Takeda, [e] Only approved by the EMA.

Selected PEGylated protein drugs in clinical trials. Due to the high number of materials in clinical trials, we only like to highlight a few materials in late stages of clinical testing (phase III) used for different kinds of diseases (Table 4).

Inherent bleeding disorder due to a deficiency or dysfunction of coagulation proteins is called haemophilia (A in case of Factor VIII, B in case of Factor IX). The only treatment of haemophilia patients is the intravenous injection of the deficient coagulation factors, prophylactic or in case of acute trauma. A drawback of native coagulates is their short half-life (FVIII 8: 12 h, FIX 18: 24 h) and the resulting frequent need for administration. In comparison, PEGylated FVIII and FIX show extended half-life and increased blood concentration after injection.[227] Besides the FDA approved PEGylated recombinant Factor VIII several other products are currently undergoing clinical trials including PEGylated Factor IX proteins. These drugs differ mainly in the way of PEG-binding, the chain length of the PEG or the modification of the protein (mutant Factor VIII (K1804C)).[227b, 227c, 228] The aim of these modifications is of course an increased activity.[229] Two conjugates are currently undergoing clinical trials in phase III (N8-GP and N9-GP).[230] The effects of these products are discussed in detail in literature.[227c, 231] Age related macular degeneration (AMD) is a medical condition causing blurred or impeded vision on focused objects, which in case of the more common wet AMD is related to the formation of abnormal blood vessels in the middle part of the retina. Initiated by the approval of the previously mentioned Macugen®, further PEGylated protein aptamers are under investigation, such as Fovista®. In contrast to Macugen®, Fovista® is developed to inhibit the platelet-derived growth factor (PDGF) and, therefore, the formation of abnormal vessel growth. For the treatment of AMD, it is combined with ranibizumab, an anti-Vascular Endothelial Growth Factor (anti-VEGF), and just passed the clinical trials phase II and entered phase III showing significantly improved results compared to native ranibizumab.

Patients with an inactive recombinant phenylalanine ammonia lyase suffer from an enrichment of phenylalanine (Phe) or hyperphenylalaninemia, which is mainly caused by a recessive gene disorder and results in mental retarding, if not recognized and treated timely.[232] A possible treatment is an enzyme substitution therapy. However, injections of pure phenylalanine ammonia-lyase (PAL) have only a short half-life and low activity in gastric secretions. In consequence, research focused on the development of more efficient forms realized by site-directed mutagenesis and PEG modifications. As a result, the concentration of Phe in blood could be decreased significantly and the symptoms are diminished.[233] Another PEGylated protein that reached phase III clinical trials is Peglispro,[234] a PEGylated insulin for the application as long term drug for diabethis mellitus patients. It could be shown that Peglispro has improved pharmakokinetic and pharmakodynamic profiles and, preferentially, hepatic *versus* peripheral action compared to insulin glargine. Nevertheless, end of 2015 the development of the project was discontinued by the supplier Lilly due to late stage observations regarding liver fat changes leading to unresolved questions.[235]

Table 4. PEGylated proteins under active clinical trials in phase III.

NAME	PEGYLATED PROTEIN	INDICATION/USE	MANUFACTURER	M_n (PEG) (g mol^{-1}) [# of PEGs/drug molecule]	IDENTIFIER NUMBER
N8-GP	Glycopegylated recombinant coagulation Factor VIII (K1804C)	Haemophilia A	Novo Nordisk®	40,000 [1]	NCT01489111
N9-GP	PEGylated recombinant Factor IX	Haemophilia B	Novo Nordisk®	40,000 [1]	NCT02141074
Fovista®	PEGylated anti-platelet-derived growth factor	Age related macular degeneration	Ophthotech/ Nektar®	40,000 [1 branched]	*e.g.* NCT01944839
Pegvaliase	PEGylated recombinant PAL enzyme[a]	Phenylketonuria	BioMarin®	20,000 [1]	NCT01819727

[a] PAL: Phenylalanine ammonia lyase.

PEGylation of small molecule drugs. In comparison to proteins, small molecules provide only a limited number of reactive side chains that are suitable for modifications. The lack of functional side groups in linear PEGs makes the coupling capacity of small molecules a critical issue. In order to improve the loading capacity, different architectures were investigated, *e.g.* forked, multi-arm, star-like and dendritic or branched polymers for the conjugation of small molecule drugs.[236] [217b, 237] Despite the immense research effort, it took a comparably long time for PEGylated small molecule drugs to enter the market. Small molecule drugs, such as antitumor agents, often suffer from poor solubility, high toxicity, rapid excretion and untargeted biodistribution. Therefore, conjugation of PEG represents an obvious way to improve their profiles. However, until now PEG-Naloxone (Moventig®) is, to the best of our knowledge, the first and only marketed PEGylated small molecule drug (approved by FDA and EMA) (Table 3). PEG-Naloxone is applied for treatment of opioid-induced constipation and approved for adult patients with chronic non-cancer pain.[217a] Being approved in 2014, Moventig® entered the market comparably late considering that PEGylation of proteins is performed for decades. Li *et al.* summarized 20 to 25 PEGylated small molecules at different stages of development and several research examples which show that PEGylated small molecules principally have improved properties. However, those examples failed in clinical trials due to a reduced activity, an inherent instability or their toxicity.[237b] Nevertheless, with the first approval of a PEGylated small drug we are confident that further examples will follow.

A list of PEGylated small molecule drugs undergoing clinical trials is given in Table 5. NKTR-181 is a PEGylated agonist for the μ-opioid receptor developed by Nektar®. Currently, it undergoes clinical trials in phase III.[238] Modified opoids are the most common medication types to treat chronic pain. In preclinical and clinical trials, the PEG modified drug revealed a slower uptake by the central nervous system (CNS) due to a reduced crossing of the blood-brain barrier (BBB), resulting in fewer CNS related side effects.[239] The aim of NKTR-181 is the treatment of patients with chronic low back pain (SUMMIT-07).[240]
Etirinotecan pegol comprises the prodrug irinotecan which is conjugated to a 20,000 g mol^{-1} four arm PEG by a degradable linker. Irinotecan is widely used as chemotherapeutical agent.[241] After enzymatic hydrolysis of the linker, it metabolizes into SN38, a potent topoisomerase I inhibitor and the active moiety of irinotecan, resulting in a 1000-fold increased activity in comparison to irinotecan itself.[242] The conjugation to PEG using slowly hydrolysable linkers based on esters aims at an application as long-acting agent with continuous and targeted drug release. In consequence, the concentration of SN38 is reduced in the plasma and undesired side effects are diminished.[243] As a result of the beneficial properties observed in phase II, Etirinotecan pegol is now undergoing clinical trials in phase III for advanced breast cancer and brain metastases in the US (Onzeald™).[243] In addition to this trial, further studies in different stages are currently ongoing to test its use for other cancerous diseases. In phase II of clinical trials, toxic side-effects associated with common chemotherapies appeared less frequent or were completely absent.[244] These preliminary results make etirinotecan pegol an attractive and interesting candidate for chemotherapies in the future. Other PEGylated small molecules produced by Nektar® are in earlier stages of clinical trials (I and II), including EZN-2208 for advanced solid tumors/lymphoma, and NKTR-171 for neuropathic pain.[238, 245]

Table 5. PEGylated small molecule drugs undergoing active clinical trials.

NAME	PEGYLATED DRUG	INDICATION/USE	MANUFACTURER	M_n (PEG) (g mol^{-1}) [# of PEGs/drug molecule]	STATUS
NKTR-181	n.a.	Neuropathic pain	Nektar®	< 1,000	Phase III (*e.g.* NCT01619839)
NKTR-102 (US: Onzeald™)	Etirinotecan pegol (SN38)	Several cancer	Nektar®	20,000 [1 four-arm]	Phase III (*e.g.* NCT01492101)

EZN-2208	SN38	Several cancer	Enzon Pharmaceuticals	40,000 [1 four-arm]	Phase II (*e.g.* NCT00520637)
NKTR-171	n.a.	Neuropathic pain	Nektar®	< 1,000	Phase I[246]

n.a.: not applicable.

3.1.2 Non-PEG conjugates

Some limitations of PEGylation have emerged specifically including an increased occurrence of immunogenic reactions and the accumulation in tissues which is a result of the nondegradability.[247] Hypersensitivity has been observed in some cases, which diminishes the benefits of PEGylation in case of some patient populations.[248] Even though PEG is not biodegradable, degradation occurred under certain circumstances (light, heat etc.) with the possibility of a build-up of toxic side products while stored.[15] Nevertheless, PEG is currently still the most tested and best understood polymer available with the longest clinical track record, but research efforts have increased to develop alternative materials addressing these limitations of PEG and adding further functionalities to polymer-drug conjugates. The number of potential alternatives for PEGylation has increased tremendously in the last years.[249] Requirements for potential substitutes for PEG include a high water-solubility, non-toxicity, non-immunogenicity, low accumulation during a therapy and clearance from the body.[250] Besides natural polymers such as heparin, dextran, chitosan, hyaluronic acid and human serum albumin, several synthetic polymers have emerged as suitable conjugate alternatives to PEG. In the following chapter we focus on these synthetic PEG alternatives and summarize all materials which entered clinical trials or the market already (Table 6).

Poly(styrene-*co*-maleic anhydride). The conjugation of poly(styrene-*co*-maleic anhydride) to the antitumor protein neocarzinostatin (SMANCS) was the first clinically approved polymer-drug conjugate (Zinostatin Stimalmer®) and is to this date the only non-PEG polymer-protein therapeutic that made it to the market. Maeda *et al.* reported the synthesis of SMANCS in the late 1970's. The copolymer consisting of styrene and maleic anhydride (SMA) was partially modified (30 to 50%) with butanol which was found to provide considerable hydrophobicity (Figure 2). Once added into aqueous solution, the residual anhydrides open and quickly form the acid. The modified SMA polymer chains were covalently linked to neocarzinostatin (NCS).[251] This characteristic enables dispersion in the phase-contrast agent lipiodol used in lymphangiography and, therefore, local administration through the feeding artery of the primary cancer, in particular liver cancer, of patients.[252] With the aid of X-ray, a precise localization of SMANCS to tumor tissue became realizable. Preclinical studies revealed the highest tumor-blood ratio (> 2.500) of the prodrug location ever reported for targeting approaches.[253] Maeda mentioned for the first time the importance of passive tumor targeting by the "enhanced permeability and retention effect" (EPR effect) describing that molecules of certain sizes (M_n = 30,000 to 50,000 g mol^{-1})[254] tend to accumulate preferentially in tumor tissue not in normal tissue.[255] Recently, lipiodol has been proven to be essential for the anti-tumor activity of SMANCS.[256] The protein conjugate successfully passed the clinical phases with high response rates (36 to 40%).[257] SMANCS received its approval for the market in 1990 (Japan) as part of the treatment of hepatocellular carcinoma and is distributed by Astellas Pharma (formerly Yamanouchi).[258] The highest chance of success is given in a 'patient-individualized treatment' (dose per tumor size/area) and follow-up treatments are only administered if the tumor is not regressing. Despite the efforts made to develop novel polymer carriers, the modified copolymer SMA remains the only commercialized synthetic alternative to PEG. However, a few other types of polymers or their drug conjugates, respectively, have been evaluated in clinical studies and mainly comprise poly(*N*-(2-hydroxypropyl)methacrylamide) (PHPMA) and poly(glutamic acid) (PGluA).

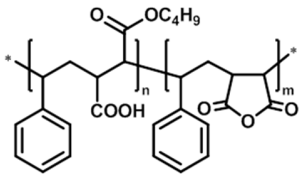

Figure 2. Schematic representation of the chemical structure of poly(styrene-*co*-maleic anhydride/acid/ester).

Poly(*N*-(2-hydroxypropyl)methacrylamide) (PHPMA). Testing conjugates of the PHPMA with anthracyclines, the homopolymers and respective copolymers were found to be chemically inert in biological media and showed no immunogenic response.[259] The first polymer-drug conjugate that entered clinical trials was the PHPMA conjugate PK1 (FCE28068), which included doxorubicin (DOX) covalently bound by a tetrapeptide linker.[116] The peptide (Gly-Phe-Leu-Gly) is stable in the plasma, but can be cleaved off by lysosomal enzymes of tumor cells[260] enabling the controlled release of the DOX within the tumor cell.[261] In addition, the conjugate has shown to concentrate within the solid tumor models of rats.[262] After phase I studies revealed signs of activity and a 5-fold decrease in toxicity compared to the pure anthracycline,[116] phase II trials on application for breast, non-small cell lung and colon cancer were initiated. Positive responses were indicated for breast and for non-small cell lung, while none were observed in case of colorectal cancer. A related compound to PK1, named PK2 (FCE28069), was modified by incorporation of a galactosamine group, which was designed to increase the uptake in liver tumor cells by interaction with the asialoglycoprotein receptor. After the PHPMA-DOX-galactosamine conjugate was investigated in preclinical studies,[263] the phase I trial revealed that the maximum tolerated dose (MTD) was reduced to approximately half the value of PK1, although the molar mass and the loading ratio were similar.[264] An increased uptake due to the hepatic targeting was confirmed by planar imaging and single photon emission computed tomography (SPECT) with ^{123}I-labeled PK2, while the conjugate without galactosamine (PK1) revealed no effect. However, despite showing promising results, both clinical studies (PK1 and PK2) were discontinued for undisclosed reasons.

For decades, platinum complexes have represented a major class of chemotherapeutics, which have been used for the treatment of solid tumors. Although numerous different Pt analogues have been investigated in preclinical and clinical studies, cis-, carbo-, and oxaliplatin are the only metal-based anticancer agents in routine clinical use. Recently, the drug conjugates AP5280 and AP5286 have entered clinical trials. A diamine platinum(II) (AP5280) or a diaminocyclohexane platinum(II) (AP5286) moiety, respectively, are bound to a dicarboxylate ligand that is linked to PHPMA *via* the tetrapeptide spacer Gly-Phe-Leu-Gly.[265] This cathepsin B sensitive linker has already been mentioned for PK1 and PK2. For AP5280, preclinical studies revealed a high antitumor efficiency and increased MTD compared to the established clinical standards cis- and carboplatin.[266] In the case of AP5286, we can only refer to a handful of references that claim phase I trials that are currently ongoing.[236, 267] Abeona Therapeutics (formerly Access Pharmaceuticals) has decided to focus on a third generation polymer which is based on an improved polymer carrier.[115] ProLindac™ (AP5346) represents a 25,000 g mol^{-1} (M_w) polymer delivery vehicle based on PHPMA, to which a diaminocyclohexane (DACH) platinum is conjugated.[268] The pH-sensitive linker causes a more rapid release of the platinum in environments of low pH value, as it is typically found in many tumor sites. ProLindac™ is currently in clinical development phase II in cancer patients with solid tumors. The phase I/II monotherapy study on patients with recurrent ovarian cancer has been completed and demonstrated efficiency and safety.[268-269] This opens the field for further clinical studies of ProLindac™ in combination with other chemotherapeutic agents, *e.g.* TXL.[270] Two other PHPMA conjugates, which entered clinical phase I trials, are bound to TXL or CPT, respectively. In the case of TXL (PNU-166945), the drug is conjugated to the PHPMA backbone *via* the previously mentioned enzymatically degradable tetrapeptide linker. One patient with advanced breast cancer had a partial response. The study had to be discontinued due to severe neurotoxic effects observed in additional rat studies.[271] PNU-166148 is a copolymer consisting of HPMA, very few units of *N*-(2-hydroxypropyl)methacryloyl glycinamide and methacrylamide units, to which CPT is bound through the degradable Gly-6-amino-hexanoyl-Gly spacer (**Figure 3**). The conjugate was developed by Pharmacia and Upjohn to overcome problems in the clinical delivery of CPT, which are related to the limited solubility of the active form (closed lactone ring) or the poor activity of the more soluble open ring form. With conjugation of the closed form of CPT to the copolymer, the solubility was maintained while the drug can be released by the pH-dependent or enzymatic degradation of the linker. There are three different phase I studies described in literature.[272]

The obtained results revealed changes in the pharmacokinetics of CPT with a prolonged half-life for both carrier-bound and released-CPT. However, the studies lacked answers to potential pharmacodynamic benefits, and revealed no sign of significant antitumor activity. The toxicities of the studied conjugates were similar to the pure compound CPT. Therefore, Pharmacia and Upjohn decided to discontinue further clinical development of PNU-166148.

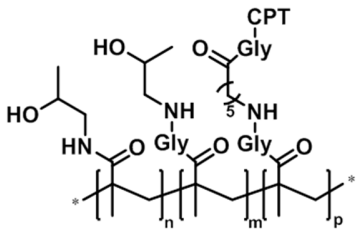

Figure 3. Schematic representation of the chemical structure of the camptothecin(CPT)-conjugate of the copolymer PNU-166148.

All PHPMA conjugates which have been investigated in clinical studies are exclusively applied for cancer treatment. Although PHPMA is well-established as a biocompatible drug carrier and a promising alternative to PEG, protein conjugates of this polymer class are less developed. However, in recent years, the research on PHPMA copolymers for the treatment of non-cancerous diseases has increased tremendously (see Chapter 4). These innovative and promising developments in the rational design, synthesis, and evaluation of novel PHPMA copolymer-drug conjugates have been highlighted elsewhere.[273]

Poly(glutamic acid) (PGluA). PGluA represents a well-established type of polymer which frequently appears in clinical studies. The conjugate with TXL (CT-2103) is one of the few successful polymer-drug conjugates to date which is known under the name Opaxio™ (formerly as Xyotax™, CTI BioPharma). It has already successfully finished phase III trials where it proved its efficacy against ovarian and non-small cell lung cancer in combination with other standard chemotherapeutics.[274] Opaxio™ features an extremely high loading capacity (~37 wt% TXL) compared to other polymer conjugates. Key advantages of the material are the inherent biodegradability of the polymer backbone and the related release of TXL or its derivatives *in vitro* and *in vivo* by enzymatic cleavage in the presence of cathepsin B.[275] In 2006, CTI BioPharma planned a new phase III study of 1,500 women suffering from ovarian cancer with the aim to improve survival rates. Two years later, CTI announced that the European Medicines Agency (EMA) has accepted to review CTI's Marketing Authorization Application for Opaxio™ for first-line treatment of patients with non-small cell lung cancer.[276] We expect that Opaxio™ will be on the market for the treatment of different types of cancer in the near future. In a similar manner, CPT was conjugated to PGluA (CT-2106) and the polymer-drug conjugate has already finished a phase I study (advanced solid malignancy).[277] According to an exclusive record, a phase II study on the treatment of advanced metastatic ovarian cancer was completed, but no results were published so far (NCT00291837).

Poly(2-oxazoline)s (POx). The conjugation of the FDA-approved dopamine agonist, rotigotine (high affinity for the subclass of dopamine receptors in the brain that mediate dopamine signaling), to a poly(2-ethyl-2-oxazoline) (PEtOx) backbone (SER-214) resulted in a stimulant, which displayed an impressive efficacy *in vivo*.[278] The continuous dopaminergic stimulation profile provided by SER-214 represents a powerful tool in the treatment of the Parkinson's disease. In October 2015, Serina Therapeutics started to recruit participants for a clinical phase I study (NCT02579473). Serina Therapeutics is furthermore offering a versatile POx-platform (POZ™) for multiple applications in drug delivery.[279]

Poly(vinyl ether) (PVE). Arrowhead Pharmaceuticals follows a concept of covalent attachment of the genetic material to the polymer backbone with triggered intracellular release. This platform is named Dynamic PolyConjugate (DPC). DPCs are composed of an amphipathic butyl- and amine PVE (PBAVE, **Figure 4**) that has shown the best transfection performance in trial and error experiments.[280] To this backbone, GalNAc as hepatic targeting ligand and PEG are attached as

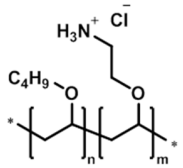

Figure 4. Schematic representation of the chemical structure of the amphipathic butyl- and amine poly(vinyl ether) (PBAVE).

well as a siRNA that is linked *via* a disulfide bond.[281] Once taken up by a cell, PEG and GalNAc are split off and the membrane-disrupting PBAVE is exposed to promote the endosomal escape (Figure 5). The siRNA is then released in the cytosol under the existing reducing conditions. ARC-520, ARC-521 and ARC-AAT are the formulations in clinical trials for the treatment of liver related diseases that are based on the DPC platform.

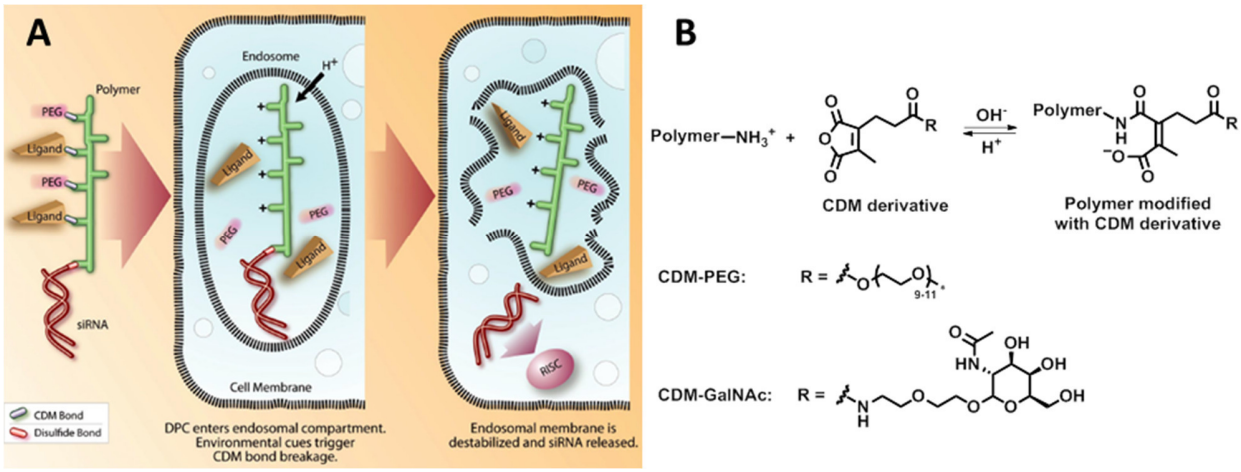

Figure 5. The proposed mechanism of siRNA delivery. A) Schematic representation of the siRNA Dynamic PolyConjugate (DPC), its cellular uptake, disassembly in the low pH environment of the endosome, and release of the siRNA into the cytoplasm of the target cell (CDM = Carboxylated dimethyl maleic acid); B) mechanism of pH-sensitive CDM chemistry and the structures of the CDM derivatives used in this study. Depicted is the reaction of CDM with free tertiary amines on the polymer, which is reversible under acidic conditions. Reprinted from [281] with permission of National Academy of Sciences, Copyright (2017).

Table 6. Synthetic polymer-drug conjugates in clinical trials (PEG-alternatives).

TRADE NAME	POLYMER SYSTEM	DRUG	INDICATION/USE	MANUFACTURER	STATUS
Zinostatin Stimalmer® (SMANCS)	Poly(styrene-*co*-maleic anhydride)	NeoCardioStatin	Hepatocellular carcinoma	Astellas Pharma	Market
PK1, FCE28068	PHPMA	DOX	Lung and breast cancers	Pfizer	Phase II (NCT00003165, Disc.)
PK2, FCE28069	PHPMA	DOX-Galactosamine	Hepatocellular carcinoma	Pfizer	Phase I[264] (Disc.)
AP5280	PHPMA	Carboplatin platinate	Various cancers	Abeona Therapeutics	Phase I/II[282]
AP5286			Various cancers	Abeona Therapeutics	Phase I[236]
ProLindac™, AP5346	PHPMA	DACHplatin	Ovarian, melanoma & colorectal cancers	Abeona Therapeutics	Phase II (NCT00415298)
PNU-166945	PHPMA	TXL	Various cancers (Breast cancer)	Pfizer	Phase I[271] (Disc.)
PNU-166148	PHPMA	CPT (MAG)	Various cancers	Pfizer	Phase I (NCT00004076, Disc.)
OPAXIO™, CT-2103, Paclitaxel poliglumex, (formerly Xyotax™)	PGluA	TXL	Lung, ovarian, colorectal, breast & esophageal cancers	CTI BioPharma	Market

CT-2106	PGluA	CPT	Colorectal, lung & ovarian cancers	CTI BioPharma	Phase II (NCT00291837)
SER-214	POx	Rotigotine	Parkinson's Disease	Serina Therapeutics	Phase I (NCT02579473)
ARC-AAT	PBAVE	siRNA	Liver disease associated with alpha-1 antitrypsin deficiency	Arrowhead Pharmaceuticals	Phase II (NCT02900183)
ARC-520	PBAVE	siRNA	Hepatitis B	Arrowhead Pharmaceuticals	Phase II (*e.g.* NCT02065336, NCT02738008)
ARC-521	PBAVE	siRNA	Hepatitis B	Arrowhead Pharmaceuticals	Phase I (NCT02797522)

DOX: doxorubicin, DACH: diaminocyclohexane, TXL: paclitaxel, MAG: (20-O-(N-methacryloyl-glycyl-aminohexanoyl-glycyl)), CPT: camptothecin.

3.2 Micro- and nanoparticulate drug carriers

Polymeric micro- and nanoparticulate drug carriers for active pharmaceutical ingredients (APIs) have been in the focus of intense research since the mid 90's. In the best case, the API is protected during the delivery and released in a controlled way at the targeted site, which reduces the required frequency of administration, the therapeutic dose, and the possibility of adverse side effects, reducing issues related to patients' compliance.[283] The term 'microparticle' by definition refers to particles with dimensions between 100 nm and 100 µm, while particles are called 'nanoparticles' if their size ranges from 1 to 100 nm.[284] However, several materials are considered as nanoparticles in literature although they slightly exceed the defined limit, but still exhibit similar properties. Therefore, we do not strictly comply with the given definition, but subdivide the materials according to their properties or the route of administration, respectively. Nevertheless, the size of all mentioned nanoparticles does not exceed 500 nm, which is still accepted.[284]

In the context of this review, the terms polymeric micro- and nanoparticles summarize stable solid dispersions (prepared by emulsion polymerization of monomers or direct dispersion of premade polymers), which also include polymeric micelles (including cross-linked micelles) or vesicles (often called polymersomes) as well as modified liposomes, and polymer-based micro- and nanogels, but also polyplexes. The latter are formed by electrostatic interactions between genetic materials (DNA, siRNA, mRNA) and cationically charged hydrophilic polymers in solution. The different sizes of nano- and microparticles obviously influence their properties as for example nanoparticles have a reduced tendency to aggregate in comparison to microparticles. Concerning drug delivery applications, the size influences key parameters like the distribution within the body, the ability to cross biological barriers, or the uptake into cells. Larger microparticles, for example, need to be delivered directly to the site of action, but they also remain at this location and act as a depot releasing their payload over weeks, *e.g.* by slow degradation of the microparticles. On the contrary, nanoparticles distribute in the body and cross barriers, but they are also able to penetrate into leaky vascular tissue usually observed in tumors and inflamed sites.[285] Moreover, they are small enough to enter cells *via* pinocytosis, which is the "cell drinking" of any cell type, while microparticles are only taken up by phagocytosis. As a consequence of these variations in the properties, the question of the right size of the drug delivery vehicle strongly depends on the application and the route of administration. The most common way of administration is certainly the oral uptake. The main challenges for particulate carriers are the protection of the drug during the harsh conditions in the gastrointestinal (GI) tract and the transport through the GI epithelium including a mucus layer as additional barrier.[286] For the direct targeting of the GI barrier layers itself, particles of about 2 µm reveal the best adsorption after oral application.[283] Smaller nanoparticles are found to cross these barriers, but for a more detailed understanding the area of oral

administration of nanosized materials still requires significant basic research.[287] In pulmonary administrations, particles around 5 µm penetrate deeply in the smaller airways of the lung, which is well-suitable for topical treatment.[288] In contrast, 1 to 2 µm particles are able to deposit in the capillary-rich alveoli, where systemic drug delivery is targeted. Nanoparticles can be exhaled if they are not immobilized by aggregation or in suspension as droplets. In the case of an intravitreal, subcutaneous or intramuscular administration, microspheres are preferably in the order of 10 to 250 µm to avoid uptake by macrophages while minimizing inflammatory reactions. For local administration in the brain, the microspheres should not be larger than 100 µm to preserve the structure of the brain. Considering intravenous nanotherapies, particles should preferably have a size below 200 nm to increase the circulation time in the blood stream and avoid filtration by the spleen or clearance by renal excretion.[289] The probably most difficult route of administration is the transport through the skin, which represents a natural barrier against particle penetration if not damaged.[290] Common nano- and microparticles (above 10 nm) are not able to cross the stratum corneum, but may accumulate in the hair follicles (300 to 600 nm sized particles).[291] An overview of these different routes of administration and the suitable size range is given in Figure 6.

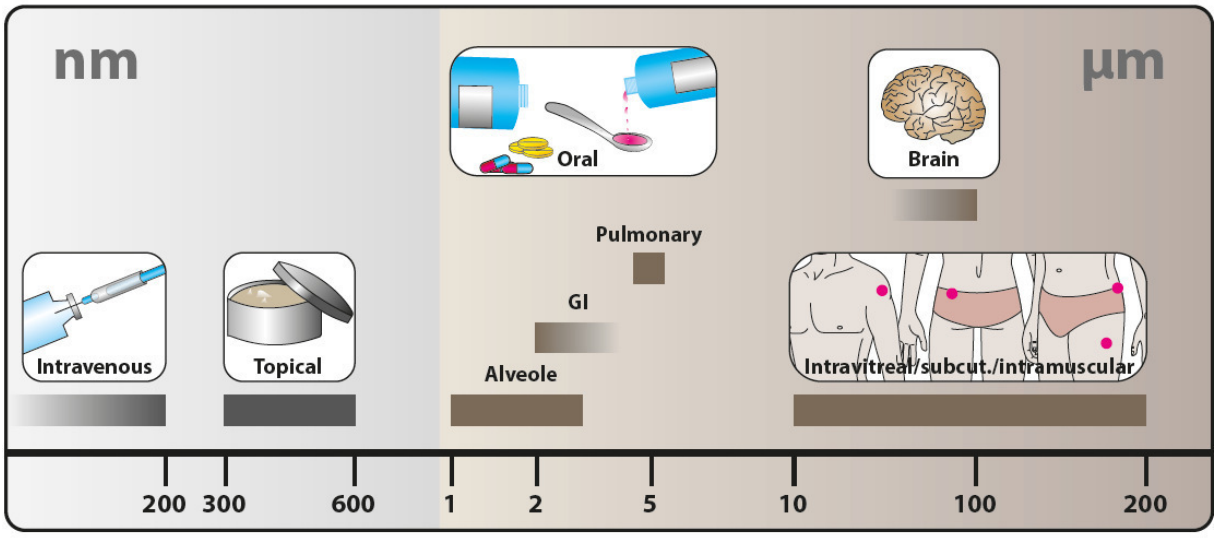

Figure 6. Overview of different routes of administration of micro- and nanoparticulate drug carriers; GI: gastrointestinal tract.

3.2.1 Solid colloidal dispersions

Microparticle dispersions. For the local and continuous delivery of APIs, injections of degradable microparticles certainly are the most commonly chosen route of administration. The particles are usually produced by emulsion techniques, *i.e.* the polymer and the drug are dissolved in a suitable organic solvent and the mixture is suspended in water, while the solvent is evaporated by continuous stirring. Additional surfactants such as PVA might be added to stabilize the resulting particles. Besides the classic procedure more sophisticated double (multiple) emulsion techniques were developed for example to encapsulate water soluble compounds, but also other methods like spray drying or precipitation

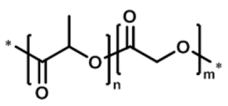

Figure 7. Schematic representation of the chemical structure of poly(lactic-*co*-glycolic acid) (PLGA).

techniques are applied.[292] As polymers poly(lactide acid) and the copolymer poly(lactic-*co*-glycolic acid) (PLGA, Figure 7) are the most accepted and also approved materials for microparticle formation. The tunable biodegradability of the polymer (by varying molar mass, structure (end-group) and composition (lactic acid/glycolide ratio)) and morphology of the particles enables PLA/PLGA to be easily engineered regarding their aimed distribution and release profiles. Marketed products of PLGA microparticles include long-acting dosage forms with *in vivo* life-times ranging from 2 to 80 weeks if administered as a gluteal intramuscular or abdominal subcutaneous depot for peptides, proteins but also small molar mass drugs.[293] Table 7 provides an overview of marketed PLGA microparticle products (no other polymers are used in marketed microparticle formulations) treating various diseases such as cancer and psychological disorders. They are also used in dentistry as local antibiotics and in animal husbandry for deworming.

An innovative route of administration is the *in situ* formation of biodegradable matrices after the liquid carrier (*e.g.* DMSO) has diffused quickly from the polymeric solution towards surrounding tissue. Risperidone ISM® represents a PLGA microparticle releasing risperidone for the treatment of schizophrenia. Clinical phase II trials have been successfully performed (NCT02086786).[294]

Table 7. List of marketed controlled release parenteral microspheres based on PLGA.

TRADE NAME	DRUG	INDICATION/USE	MANUFACTURER[a]
Risperdal Consta®	Risperidone	Schizophrenia	Janssen
Zoladex®	LHRH agonists	Prostate cancer	AstraZeneca
Lupron Depot®, Eligard®, Enantone®/Trenantone®	Leuprolide	Prostate cancer	AbbVie, TOLMAR Pharmaceuticals, Takeda
Decapeptyl®, Trelstar®, Pamorelin®	Triptorelin	Prostate cancer	Ferring Pharmaceuticals, Allergan™, Ipsen Pharma
Profact Depot®, Suprefact Depot®	Buserelin	Prostate cancer, endometriosis	Sanofi
Bydureon®	Exenatide	Diabetis	AstraZeneca
Sandostatin® LAR, Somatuline® LA	Octreotide	Acromegaly, diarrhea	Novartis
Nutropin Depot®	Somatropin	Growth hormone deficiency	Genentech/Alkermes® (disc.)
Vivitrol®	Naltrexone	Opioid- & alcohol dependence	Alkermes®
Arestin®	Minocycline HCl	Peridontal disease	Valeant® (disc.)
Longrange®	Eprinomectine	Parasitic disease	Merial (Sanofi)

[a] Selection thereof.

The versatility and unique properties of PLGA and PLA certainly promote the domination of the market of these materials considering microparticles for drug delivery. As a consequence, it is no surprise that further developments, which are currently in clinical trials, are also based almost exclusively on these polymers. To the best of our knowledge, only two alternatives have at least entered the stage of clinical testing. The first one is a microparticulate formulation consisting of paclitaxel and a biodegradable polyphosphoester (NCT00005046).

The polymer is a copolymer of short PLA oligomers and ethyl phosphate (P(DAPG-EOP)) (Figure 8).[295] The microparticles (Paclimer®) were injected into the peritoneal cavity for treatment of recurrent ovarian cancer.[296] The study (phase I) verified the beneficial properties of the material ensuring a controlled and continuous release over more than eight weeks. However, the presence of polymer filaments after several months indicated a slow degradation and caused a marked inflammatory response. The second one is the microsphere Retin-A Mikro® (Valeant®), which is based on the Microsponge® technology comprising styrene, divinylbenzene and methyl methacrylate and the starting material ethylene glycol dimethacrylate in its polymer backbone.[297] Tretinoin is encapsulated in the polymer in the application form of a skin cream that slowly releases the active medication to treat acne vulgaris.

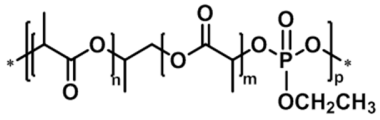

Figure 8. Schematic representation of the chemical structure of the copolymer consisting of short PLA oligomers and ethyl phosphate (P(DAPG-EOP)).

Amphiphilic block copolymer micelles. Polymeric micelles are created by dispersion of a block copolymer consisting of a hydrophobic and a hydrophilic domain. The block-like and amphiphilic structure is essential for polymeric micelles and their self-assembly behavior.[284] In contrast to small molecule surfactants, polymeric micelles often seem to be not dynamic, which means that there is almost no exchange of polymer molecules between the aggregates, and the polymeric micelles are kinetically frozen.[298] However, in most cases these exchange dynamics are simply not investigated as the experiments require long acquisition times (up to several days or weeks) to provide a detectable signal. According to its definition, polymeric micelles are still in an equilibrium with its dissolved polymer chain.[284] Consequently, the formation and stability of the micelles depend on the concentration. However, with increasing size of the hydrophobic block this equilibrium can be shifted towards the formation of micelles, and the critical micelle concentration (CMC) might be below the detection limit.[299] Nevertheless, a common concept to overcome any stability issues related to polymeric micelles is the cross-linking of the micellar core, which ideally can be used to covalently entrap the API.[300] The research and development of polymeric micelles has a very strong focus on cancer therapy. The toxic and undesirable side effects of chemotherapeutic agents are supposed to be diminished by using these nanoparticulate carrier systems.[301] The low lymphatic drainage of tumors and the highly vasculature tumor tissue results in an enhanced penetration and retention (EPR) effect of the micelles, which consequently yields a passive targeting of tumor tissue. Even more efficient is the use of micelles bearing targeting moieties, which allow selective recognition of specific receptors that are overexpressed in cancer cells. Recently published review articles cover the outcomes of clinical research and also show the results of preclinical studies in terms of polymeric nanoparticles in cancer therapy.[301-302] However until now, none of these formulations reached FDA approval for cancer therapy. Only one micellar delivery system is on the South Korean market (Table 8).[303] Genexol® PM is a paclitaxel encapsulating polymeric micelle consisting of a block copolymer of methoxy-PEG and poly(D,L-lactic acid) (Figure 9A).[304]

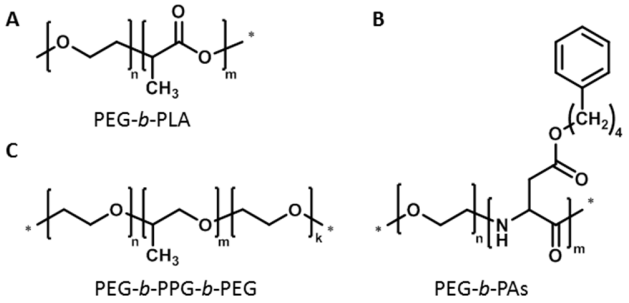

Figure 9. Schematic representation of the chemical structures of the block copolymers of A) methoxy-PEG and poly(D,L-lactic acid) (Genexol® PM); B) PEG and esterified PAs (4-phenyl-1-butanol) (NK105); C) PEG and PPG (also called Pluronic®, SP1049C).

Nevertheless, a considerable number of micellar systems are currently undergoing clinical trials in various stages. In the following, we provide an overview of the various materials, which are clinically tested, and exemplarily describe the applications where these materials are in latest stage of clinical trials. In general, most of these micellar

formulations are also in preclinical/clinical trials for treatment of other cancerous diseases, which shows the potential of polymeric nanoparticles in cancer therapy in future. A good example is the block copolymer PEG-*b*-PLA which is identical to the material used in Genexol® PM. This polymer is further used for the formulation of docetaxel encapsulating PEG-*b*-PLA polymeric micelles with similar sizes (20 to 50 nm) named Nanoxel®-PM, which is in clinical phase I.[305] Other materials also take advantage of the generally accepted use of PEG for the hydrophilic block. In contrast, a variety of different polymers is used for the hydrophobic block. NK105 uses a block copolymer of PEG and partially hydrophobized poly(aspartate) (PAs) (esterification of the carboxylic groups with 4-phenyl-1-butanol, Figure 9B) for the delivery and release of docetaxel.[306] SP1049C is a mixture of non-ionic PEG-*block*-PPG-*block*-PEG copolymers (Pluronic® L61, Pluronic® F127, Figure 9C) that form a micelle to encapsulate doxorubicin.[307] SP1049C has the state as an orphan drug for gastric cancer as approved by the FDA.

With the effort to improve the specifity of nanoparticles, targeted strategies were developed and already entered clinical trials. BIND-014 is the outcome of a combinatorial library of nanoparticles based on PEG-*b*-PLA and PEG-*b*-PLGA that encapsulate docetaxel and bear a prostate-specific membrane antigen (PSMA) on the micelle surface. PSMA is a tumor antigen preferentially expressed on prostate cancer cells and vasculature of non-prostate solid tumors.[308] The PSMA substrate analog inhibitor S,S-2-(3-(5-amino-1-carboxypentyl)-ureido)-pentanedioic acid (ACUPA) is covalently attached to a PEG-*b*-PLA. A mixture of PEG-*b*-PLA and PEG-*b*-PLA-ACUPA is finally used for the micelle formation in a microfluidic supported emulsion/solvent evaporation process. BIND-014 was the best performing candidate in terms of particle size, drug loading, targeting ligand density, PEG/PLA ratio and so on. The same technology (Accurins® technology) was recently used to deliver a selective Aurora B kinase inhibitor, AZD2811, that induces apoptosis in tumor cells.[309] Increased encapsulation efficiency and reduced drug leakage could be achieved by simple ion pairing of AZD2811 and are currently tested in phase 1 studies. Preclinical studies using the same Accurins® portfolio involve BIND-510 (encapsulated drug: Vincristine, PEG-*b*-PLA with PSMA targeting) and others as proposed by BIND Therapeutics.[310] A critical point is that the physical entrapment of drugs can be associated with drug leakage before reaching the side of action.

Therefore, the covalent attachment *via* labile linkers to the polymer backbone can be advantageous. A popular system is a block copolymer of PEG and polyglutamate. The polyaminoacid is able to complex different platinum complexes, which renders the polymer amphiphilic. NC-6004 is delivering *cis*-platin and already entered clinical phase III. The same concept is applied for NC-4016 in phase I, using 1,2-diaminocyclohexane platinum (DACHplatin) to modify PEG-*b*-PGlu block copolymers. Also other anti-cancer drugs were covalently attached to the PGlu block: NK012 is functionalized with SN-38, a camptothecin derivative, and completed clinical phase II for the treatment of breast and lung cancer. A similar system using poly(amino acid) is NK911, with DOX covalently linked to the carboxy groups of the copolymers of PEG and PAs. NK911 revealed less stability and more drug release but also higher accumulation at other cell regions compared to liposomal doxorubicin (Doxil®).[311] Clinical phase I finished in 2004 and did not recruit for phase II until now. There are only few examples of materials in clinical trials that are not aiming at the treatment of cancer. SEL-068 is a PEG-*b*-PLGA-based micelle loaded with peptides for the treatment of nicotine addiction.[312] This nicotine vaccine creates nicotine specific antibodies that bind free nicotine and prevent it from crossing the BBB. The same particle platform (Synthetic Vaccine Particle (SVP™)) is used for the design of SEL-110 in antigen-specific immunotherapy. SEL-110 is loaded with specific protein- or peptide antigens and rapamycin and aims to prevent unwanted anti-drug-antibodies from forming.[313]

Table 8. List of active clinical trials using amphiphilic block copolymer micelles.

TRADE NAME	POLYMER SYSTEM	DRUG	INDICATION/USE	MANUFACTURER	STATUS
Genexol® PM (US: Cynviloq™, IG-001)	PEG-*b*-PLA	Docetaxel	Breast, lung, ovarian cancer	Samyang Biopharm	Market (South Korea)

Nanoxel®-PM (Docetaxel-PNP)	PEG-*b*-PLA	Docetaxel	Solid tumors	Samyang Biopharm	Phase I (NCT02274610)
NK105	PEG-*b*-PAs	Docetaxel	Gastric, breast cancer	NanoCarrier®	Phase III (NCT01644890)
SP1049C	PEG-*b*-PPG-*b*-PEG (Pluronic® L61, F127[a])	DOX	Adenocarcinoma	Supratek Pharm	Phase II[307]
BIND-014 (Accurins® technology)	PEG-*b*-PLGA, PEG-*b*-PLA	Docetaxel	Solid tumors	BIND Therapeutics/ Pfizer	Phase II (*e.g.* NCT01812746, NCT01792479,)
AZD2811 (Accurins® technology)	PEG-*b*-PLA	AZD2811	Solid tumors	AstraZeneca	Phase I (NCT02579226)
NC-6004	PEG-*b*-PGlu	Cisplatin	Solid tumors	NanoCarrier®	Phase III (NCT02043288)
NC-4016	PEG-*b*-PGlu	DACHplatin	Solid tumors	NanoCarrier®	Phase I[314]
NK012	PEG-*b*-PGlu	SN-38	Breast, lung, colorectal cancer	Nippon Kayaku	Phase II (*e.g.* NCT00951613, NCT00951054)
NK911	PEG-*b*-PAs	DOX	Pancreatic, colorectal cancer	n.a.	Phase I[311] (disc.)
SEL-068	PEG-*b*-PLGA	TLR agonist and T cell helper peptide	Nicotine addiction	Selecta Biosciences	Phase I (NCT01478893)
SEL-110	PEG-*b*-PLGA	Rapamycin, peptide antigen	Production of anti-drug antibodies, unwanted immune response	Selecta Biosciences	Phase I (NCT02648269)

DOX: doxorubicin, DACH: diaminocyclohexane; [a] L = liquid, F = flake/solid, the first one or two digits (in a three-digit number) in the code, multiplied by 300, indicates the approximate molar mass of the PPG block and the last digit of this code × 10 provides the percentage PEG content; n.a.: not applicable.

Nanoparticle dispersions. Besides the large number of micellar structures made from amphiphilic block copolymers only few systems have entered clinical studies, which are solid nanoparticle dispersions prepared by nanoprecipitation or emulsion polymerization (Table 9). CRLX101 is a nanoparticle formulation consisting of a statistical copolymer based on β-cyclodextrin and PEG, that is hydrophobized by conjugation of CPT to the cyclodextrin ring *via* an acid labile glycine linker.[315] The current studies are recruiting participants for several clinical studies in cancer therapy, which shows the potential of this formulation as novel nanomedical device. CRLX301 has recently started phase IIa and uses the same polymer platform as CRLX101 but with docetaxel as active agent.[316] While the previously mentioned system is still stabilized by the amphiphilic character of the polymer, DOX-Transdrug is a solid nanoparticle dispersion that is produced by emulsion polymerization of isohexyl cyanoacrylate in the presence of DOX. DOX-Transdrug is used for the treatment of liver cancer by local injection *via* the hepatic artery and has recently entered clinical phase III. This system was also successfully applied to pass the BBB for the therapy of glioblastomas as observed in rats.[317] Another acrylate-based nanocarrier is prepared in a comparable way resulting in mitoxantrone (dihydroxyanthracenedione, DHAD) encapsulating poly(isobutyl cyanoacrylate) nanoparticles (DHAD-PBCA-NP). The formulation shows good efficacy in treating liver cancer and, thus, enhances the survival period.[318] DHAD-PBCA-NP reached clinical phase II but did not continue since 2009.

Table 9. List of active clinical trials using nanoparticle dispersions.

TRADE NAME	POLYMER SYSTEM	DRUG	INDICATION/USE	MANUFACTURER	STATUS
CLRX101 (IT-101)	P(EG-*co*-cyclodextrin)	CPT	Lung cancer, renal cell carcinoma	Cerulean™	Phase II (*e.g.* NCT02010567, NCT02769962)

CRLX301	P(EG-*co*-cyclodextrin)	Docetaxel	Solid tumors	Cerulean™	Phase I/IIa (NCT02380677)
Livatag® (DOX-Transdrug)	Poly(isohexyl cyanoacrylate) coated with Tween 80	DOX	Liver cancer	Onxeo	Phase III (NCT01655693)
DHAD-PBCA-NP	Poly(isobutyl cyanoacrylate)	Mitoxantrone	Liver cancer	n.a.	Phase II[318] (Disc.)

CPT: campthothecin, DOX: doxorubicin; n.a.: not applicable.

Modified liposomes. Liposomes are structurally slightly different species also using polymers in a nanoparticular device. They are composed of phospholipids, which self-assemble into lipid bilayers (able to incorporate lipophilic molecules) surrounding an aqueous core (able to incorporate hydrophilic molecules).[319] For improving the desired properties, the phospholipids can be covalently modified with polymers or targeting functions resulting in surface modified liposomes. For example, PEG is generally used to improve the circulation and drug retention. In addition to the stealth effect, PEG is acting as spacer molecule between lipid structures and targeting functions. Besides Doxil® being the most prominent example of a PEG-containing liposome on the market[320] there are also Lipodox®,[321] Oncodox® PEG[322] and Lipoplatin™[323] showing good performances in cancer treatment with DOX and cisplatin, respectively, as APIs (Table 10). The heat-responsive liposomal formulation ThermoDox® is now recruiting patients for a phase III study of PEGylated liposomal DOX.

Table 10. List of PEG-modified liposomes on the market or in active clinical trials in phase III.

TRADE NAME	DRUG	INDICATION/USE	MANUFACTURER	STATUS
Doxil® (Caelyx®)	DOX	Ovarian cancer, AIDS-related Kaposi's sarcoma, multiple myeloma	Janssen	Market
Lipodox®	DOX	Metastatic carcinoma of the ovary, metastatic breast cancer, AIDS related Kaposi's Sarcoma	Sun Pharma	Market
Oncodox® PEG	DOX	Ovarian cancer, breast cancer, AIDS related Kaposi's Sarcoma	Ciplamed	Market
Lipoplatin™	Cisplatin	Pancreatic cancer, head and neck cancer, mesothelioma, breast cancer, non-cell lung cancer	Regulon	Phase III[324]
ThermoDox®	DOX	Primary liver cancer, breast cancer	Celsion	Phase III (NCT02112656)

DOX: doxorubicin.

3.2.2 Polyplexes

The delivery of small molecules either encapsulated or conjugated to yield apoptosis in cancer cells is only one strategy in cancer therapy. The pharmaceutical industry also holds promise on gene therapy. However, to transport genetic material such as plasmid DNA (pDNA), short interfering RNA (siRNA) and messenger RNA (mRNA) into body cells these structures must be protected against degradation and shielded to avoid clearance. A common way is the complexation of the negatively charged genetic material with cationically charged polymers *via* electrostatic interactions. The result is a so-called polyplex, which ideally should mimic the nature of viruses and result in efficient gene delivery and transfection without showing an immune response. Poly(ethylene imine) (PEI) and its variations are among the most studied materials for this purpose. In contrast to other cationic polymers, linear and branched PEI are capable of mediating endosomal escape, which is essential for transfection.[325] Other prominent examples are poly(L-lysine) or poly(2-(dimethylamino)ethyl methacrylate) (PDMAEMA).[326] In general, it can be said that only pDNA and RNA therapeutics passed preclinical studies so far for clinical trials.[325, 327]

Different PEI formulations and modifications that all resolved general toxicity issues of PEI *in vitro* and *in vivo* reveal encouraging results in clinical phases (Table 11). SNS01-T is a jetPEI® formulation, *i.e.* a linear PEI dissolved in a special buffer system. Although the precise composition is undisclosed, it is expected to have a molar mass (M_n) of about 22,000 g mol^{-1}. The polyplex contains both a B-cell-specific expression pDNA and a siRNA, which suppresses hypusinated eIF5A. A reduction of eIF5A levels was found to sensitize myeloma cells to apoptosis.[328] CYL-02 is also based on jetPEI® as transfection agent and in clinical phase II for pDNA delivery. It strongly inhibits tumor progression and dissemination of pancreatic cancer after intratumoral administration using endoscopic ultrasound.[329] A promising intravenously administered system is a polyplex of the pDNA BC-819 with PEI. BC-819/PEI targets cancer cells that generally express the H19 gene, which activates Diphtheria Toxin A (DTA) and leads to cell death, whereas healthy cells that are also exposed to the pDNA are not affected. In 2016, BC-819 was announced to commence phase III.[330] In addition, BioCancell developed a dual-DTA expression system named BC-821, which is a pDNA that is again transfected with PEI and switches the distinct promoters H19 and IGF2-P4.[331] The dual expression system may have the benefit of enhanced cancer cell toxicity and a higher chance that at least one of the promoters will be active in any tumor. A further pDNA PEI-based formulation in clinical trials is EGEN-001. It contains a cholesterol modified low molar mass branched PEI that is also PEGylated.[332] EGEN-001 is designed for direct injection into cancerous tissue where it increases the local concentration of interleukin 12 (IL-12) in the tumor microenvironment. IL-12 has several functions, amongst them it is known to potentiate antitumoral functions of the host immune system.[333] The delivery of a RNA sequence is also in the focus of Celsion by using the TheraSilence™ technology platform.[334] In general, the intrinsic cytotoxicity of PEI is a serious problem in the transfer to a FDA approved PEI-based product.

The benefit of non-viral siRNA delivery is to selectively silence gene expression *in vivo*. The first targeted (siRNA) nanoparticle formulation in clinical trials is denoted as CALAA-01.[335] The polymer matrix is a cationic cyclodextrin containing polymer prepared by polycondensation of a diamine-functionalized cyclodextrin and dimethyl suberimidate leading to a polyamidine. Adamantyl functionalized PEG with and without human transferrin ligands is complexed with the cyclodextrin moieties for steric stabilization and also for the targeting ability of the polyplexes. CALAA-01 completed phase I in 2012 but did not proceed further. However, this study was the first evidence that systemically administered siRNA induces RNA interferences in humans.[336]

In the early days of gene therapy, the discovery of interferon caused much excitement. Various forms of interferon are produced by virally infected cells and interfere with further viral growth and, thus, show promise in antitumor and antiviral therapy. The synthetic double-stranded RNA (dsRNA), an interferon that consists of a pair of polyinosinic and polycytidylic acids, is condensed with poly(L-lysine) and supplemented with carboxymethylcellulose to form Hiltonol®.[337] Probably the first clinical study using this system was already conducted in 1978.[338] Nowadays, there are many clinical trials of Poly-ICLC for various types of cancer. However, Poly-ICLC is also in clinical trials to test its efficacy as adjuvant (to boost the immune response) in HIV-infected patients. A further polylysine-based polyplex is a PEGylated version that demonstrated an effect for cystic fibrosis patients after administration of the complexed pDNA carrying the cystic fibrosis transmembrane regulator-encoding gene to the nasal mucosa in an early phase I study.[339]

Although cancer is certainly the most prominent disease to be treated by polyplex-based gene delivery, the treatment of other human diseases can also benefit of the approach if applied at the right site or by using targeting functions. The DermaVir patch is a topical application of a pDNA, encoding the entire HIV genome minus the integrase gene that is formulated with mannosylated jet-PEI® in a glucose solution.[340] For this purpose, the stratum corneum needs to be interrupted to deliver the polyplex to the Langerhans cells to be transported to the lymph nodes in order to express the HIV antigens. The DermaVir therapeutic vaccination completed phase II but did not proceed further maybe due to infection risks of the skin. A different pDNA vaccination that already started phase III trials is ASP0113. It is designed to suppress the activation of the cytomegalovirus (CMV) in transplant recipients. It basically consists of two plasmids encoding CMV glycoprotein B and phosphoprotein 65, respectively,

formulated with poloxamer, a triblock PEG-*b*-PPG-*b*-PEG (CRL1005), and a mixture of alkyl-benzyldimethylammonium chlorides (BAK, alkyl chains: C12, C14, C16, C18).[341] The hydrophobic cationic surfactant BAK and the hydrophilic CRL1005 self-assemble with the pDNA into nanoparticles.

Table 11. List of active clinical trials using polyplexes.

TRADE NAME	POLYMER SYSTEM	DRUG	INDICATION/USE	MANUFACTURER	STATUS
SNS01-T	LPEI (jetPEI®)	pDNA, siRNA	Multiple myeloma	Sevion Therapeutics	Phase II (NCT01435720)
CYL-02	LPEI (jetPEI®)	pDNA	Pancreatic adenocarcinoma	InvivoGen	Phase II (NCT02806687)
BC-819/PEI (DTA-H19)	BPEI	DNA	Bladder cancer, ovarian cancer, pancreatic adenocarcinoma	BioCancell	Phase II (NCT00595088)
EGEN-001 (GEN-1)	Cholesterol and PEG-modified PEI	DNA	Ovarian, tubal, colorectal peritoneal cancer	GOG® Foundation	Phase II (NCT01118052)
CALAA-01	Cationic cyclodextrin, adamantane modified PEG	siRNA	Solid tumors	Calando Pharmaceuticals	Phase I (NCT00689065) (disc.)
Hiltonol® (Poly-ICLC)	Polylysine, carboxymethyl cellulose	dsRNA	Brain tumor, non-small cell lung cancer, skin cancer, breast cancer	Oncovir	Phase II (*e.g.* NCT01984892, NCT02423863)
			HIV		Phase I/II (NCT02071095)
DermaVir (LC002)	Mannosylated LPEI (jetPEI®)	DNA	HIV vaccine	Genetic Immunity	Phase II (NCT00711230)
ASP0113 (VCL-CB01, formerly TransVax®)	PEG-*b*-PPG-*b*-PEG, (CRL1005)	DNA	CMV vaccine	Vical	Phase III (NCT01877655)

pDNA: plasmid deoxyribonucleic acid, siRNA: small interfering ribonucleic acid, dsRNA: double-stranded ribonucleic acid, CMV: cytomegalovirus.

3.2.3 Micro-/Nanogels

Microgels. ‚Microgels' (IUPAC name) are defined as hydrogel microparticles (also mentioned as 'microhydrogels' or 'hydrogel microspheres') formed by water soluble polymers which are physically or chemically cross-linked. In physical gels, the cross-linking points of the network are formed by non-covalent or supramolecular interactions, such as hydrogen bonds, ionic or hydrophobic interactions, respectively. On the other side covalent bonds form the links of the network in chemical gels, *i.e.* cross-linking of ready polymers on functional groups or polymerization of multivalent monomers. These three-dimensional networks fill the size gap between dendrimers/polymers (10 to 20 nm) and macroscopic hydrogels (see Chapter 3.3.1) comprising sizes from 100 nm to 100 µm according to the definition of microparticles.[342] Microgel systems possess high capacity for drug loading, are mostly biocompatible, and can be modified for biodegradability, which represent the key points to design an effective drug delivery system. Their structure features some key advantages in comparison to dendritic systems including their superior swelling behavior, the opportunity to introduce responsive modalities, and the presence of suitable gaps for encapsulation of other compounds (without the need of a chemical attachment). Besides their application as drug delivery systems, they have shown promising potential for use in adjacent fields such as diagnostics, antiviral compounds, and embolic therapies.[343] Microgel-based formulations for drug delivery have shown significant enhancements in effectiveness and safety considering certain anti-cancer drugs or other pharmaceutically active compounds, which was confirmed by numerous *in vivo* studies. Despite this progress, only very few microgels have been explored in clinical studies and several safety issues have to be overcome. The challenges in terms of cargo

delivery and their efficient clearance once they have accomplished their mission *in vivo* demand careful engineering of the microgels. This remains challenging due to the complexity of the systems and the unique structural features. To date, there are only three microgel systems based on synthetic polymers that are approved for use as drug delivery system. They are all used in the treatment of hepatocellular carcinoma (Table 12). DC Bead® is an embolic hydrogel microsphere product that is capable of being loaded with anthracycline drugs just before administration in a transarterial chemoembolization (TACE) procedure. TACE is a minimally invasive (non-surgical) procedure performed by an interventional radiologist. In this process, the microgel is not just delivering the drug, but also occludes the arteries supplying the tumor. DC Bead® is composed of a biocompatible PVA hydrogel, which has been modified with the ionic monomer sodium 2-acrylamido-2-methylpropanesulfonate (AMPS, Figure 10). The latter enables the electrostatic loading and delivery of chemotherapeutic drugs. The beads are produced by an inverse emulsion polymerization and are available in sizes from 100 to 900 µm.[344] Injected into the local artery, the formulation occludes the blood flow to the target tissue and delivers a local and sustained dose of the drug directly to the tumor. DC Bead® is approved as anti-tumor formulation with doxorubicin (DEBDOX™)[345] and irinotecan (DEBIRI™).[346] Current research is focusing on an increase of the drug doses of administered drug.[347] In addition, the microbeads can be loaded with idarubicin (IDASPHERE II) by the interaction of the positively charged protonated amine group of idarubicin hydrochloride with the sulphonate of the DC Beads®.[348] They are currently in randomized phase II studies. Special radiopaque beads (RO Beads), which are also based on the DC Bead® platform, have been investigated to not only be pharmacologically active, but allow the imaging of the active site in a rabbit VX2 liver tumor model by X-ray scans. These RO Beads were covalently modified with a triiodobenzyl group to allow a better traceability in comparison to DC beads® which were loaded with a soluble contrast agent.[349] The first commercially available RO bead, LC Bead LUMI™, was cleared by the FDA for the chemoembolization of hypervascular tumors and arteriovenous malformations.[350]

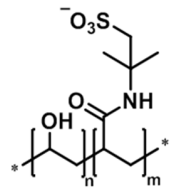

Figure 10. Schematic representation of the chemical structure of P(VA-co-2-acrylamido-2-methylpropane sulfonate).

Other commercialized microgels include the Tandem® microspheres, which are spherical, biocompatible, non-resorbable hydrogel cores based on cross-linked poly(methacrylic acid) (PMAA).[351] They are subdivided into two classes of microspheres, Oncozene® and Embozene®, which are both available in a size range from 40 to 100 µm. The latter features an additional outer layer of CeloNova's proprietary Polyzene®-F, a poly(bis(trifluoroethoxy)phosphazene) (Figure 11), which is introduced to enhance biocompatibility and reduce inflammation. These materials have been optimized for loading with a variety of drugs (Table 12). Current studies focus on the use of DOX (NCT02141906) or idarubicin,[352] loaded in the Oncozene® microspheres. Hepasphere™ represents another hydrogel microsphere, which is approved for clinical use and commercially available (in the range from 30 to 200 µm). In general, DOX is loaded into a polymer network of poly(vinyl alcohol-*co*-acrylic acid).[353] The microsphere binds drugs with the same mechanism as DC Bead®, using carboxylate instead of sulfonate groups. Recent developments in the treatment of hepatocellular carcinoma with Hepasphere™ were summarized by Malagari *et al.*.[354] LifePearl® is a PEG-based embolization hydrogel that can be loaded with chemotherapeutic agents to treat primary hyper vascular tumors or liver metastasis. The microspheres are biocompatible, hydrophilic, and precisely calibrated.[355]

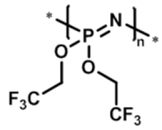

Figure 11. Schematic representation of the chemical structure of poly(bis(trifluoroethoxy)phosphazene) (Polyzene®-F).

A new injectable formulation for the delivery of IFN-α 2b is Locteron®, which is one of the few systems for continuous release of proteins that reached late-stage clinical trials. It is a microparticulate formulation encapsulating a protein which is suspended in an injection vehicle prior to subcutaneous administration.

The technology is based on PolyActive® – a variety of biodegradable poly(ether ester) segmented copolymers based on PEG and PBT. The polymers absorb water up to 65% of their weight resulting in a hydrogel network. Biolex Therapeutics announced that its remaining asset (phase III) for the treatment of hepatitis C virus (HCV) and hepatitis B virus (HBV) is finally commercialized.[356]

Nanogels. When the size of microgels is in submicron range (1 to 100 nm), they are usually specified as nanogels ('nanohydrogels', 'hydrogel nanospheres').[357] Although significant effort has been dedicated into their research,[358] there is only a limited number of nanogel systems under clinical investigations that are based on synthetic polymers. A new gel-based approach with the ability to form a depot (Medusa®) has been developed by Flamel Technologies (today: Avadel Pharmaceuticals). It enables a controlled drug release within an adjustable time ranging from one day up to one week without the often observed initial burst effect or a decreasing activity. The formulation will be administered as a subcutaneous injection. The polymer platform is based on poly(α-glutamate) (hydrophilic), where vitamin E is grafted onto (Figure 12). The resulting amphiphilic polymer spontaneously forms stable nanogels (20 to 50 nm) when dissolved in water due to the hydrophobic domains of vitamin E.[359] Different cargos (*e.g.* peptide, protein, small molecule) can be loaded into the nanogel simply by mixing the two components, and the uptake into the nanogel is solely based on non-covalent, hydrophobic and electrostatic interactions. The formulations with several therapeutic proteins (*e.g.* IL-2, IFN-α 2b and IFN-β 1a) revealed a release period of one week in animal models.[360] Clinical phase I trials were performed on the application of the interferon IFN-α 2b, which was administered to patients with genotype 1 hepatitis C virus (HVC), and the outcomes were compared to the established treatment with the respective PEGylated interferon PegIntron® (Table 3). The study demonstrated a favorable antiviral activity and safety profile using the Medusa® technology.[361] A phase II study followed (over a period of 12 weeks) in order to compare this formulation to PegIntron®, which was combined with ribavirin.[362] Currently, Avadel Pharmaceuticals explores the product Medusa® exenatide, which is called a once-a-week formulation. After successful preclinical studies on the administration to minipigs (June 2014), the company reported the completion of phase 1b trials for type 2 diabetes mellitus.[363]

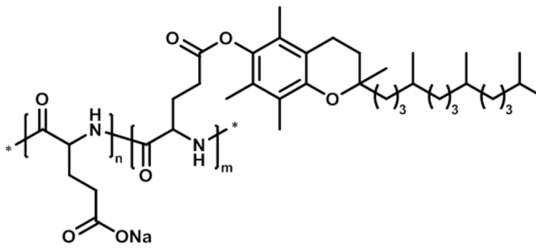

Figure 12. Schematic representation of the chemical structure of vitamin E-grafted poly(α-glutamate) (α-PGlu).

Table 12. Micro- and nanogels based on synthetic polymers on the market or in clinical trials.

TRADE NAME	SUBNAME	POLYMER SYSTEM	DRUG	INDICATION/USE	MANUFACTURER	STATUS
			Microgel			
DC Bead® (US: LC Bead®)	DEBDOX™	P(VA-*co*-AMPS)	DOX	Malignant hypervascular tumor	BTG	Market
	DEBIRI™	P(VA-*co*-AMPS)	Irinotecan	Metastatic colorectal cancer	BTG	Market
	IDASPHERE II	P(VA-*co*-AMPS)	Idarubicin	Liver cancer	Federation Franco-phone de Cancer-ologie Digestive	Phase II (NCT02185768)
Tandem®	Oncozene®	PMAA	DOX, epirubicin, idarubicin, irinotecan	Neurovascular arteriovenous malformations, hypervascular tumors	CeloNova BioSciences	Market
	Embozene®	PMAA + Polyzene®-F				Market

HepaSphere™ (US: QuadraSphere®)		Poly(VA-*co*-AA)	DOX	Hepatocellular carcinoma	Merit Medical®	Market
LifePearl®		PEG	DOX, irinotecan	Hyper vascular tumor, liver metastasis	Terumo	Market
PolyActive®	Locteron® (OctoPlus)	PEG-*b*-PBT (Multiblocks)	IFN-α 2b	Hepatitis C virus	Biolex Therapeutics	Phase III (NCT00863239)
			Nanogel			
Medusa®		α-PGlu grafted with vitamin E	IL-2, IFN-α 2b, IFN-β 1a, exenatide	Various cancers, viral infections	Avadel Pharmaceuticals	Phase I/II[363]

DOX: doxorubicin.

3.3 Macroscopic drug carriers

3.3.1 Hydrogels

Hydrogels. Hydrogels represent macroscopic, hydrophilic polymer networks, which are able to absorb water or aqueous biological fluids in amounts ranging up to multiple times of their own mass. In analogy to microgels, they can be subdivided by their type of cross-linking, *i.e.* chemical or physical cross-linking. Hydrogels are able to imitate natural living tissue more than any other class of synthetic biomaterials due to their high water content, soft consistency and porosity. Undoubtedly, their most advanced application field is their usage as contact lenses, in particular in form of soft lenses. However, the relatively low drug loading capacity and the burst release upon ocular administration is a challenge that has to be overcome. To date, no drug loaded contact lens is on the market.

An advanced alternative to frequent application of eye drops for steroid therapy is the hydrogel punctum plug Dextenza™. The dexamethasone loaded depot for ophthalmic drug delivery is based on branched PEG and represents the first sustained release ophthalmic product that entered phase III trials (**Table 13**).[364] As cross-linker, a molecule with four arms is used bearing complimentary reactive sites on each end which are not further described in literature. Very recently, Ocular Therapeutix™ announced positive results from this clinical trial for the treatment of post-surgical ocular inflammation and pain.[365] It is placed through the punctum (natural opening in the eye lid) into the lacrimal canaliculus and allows a controlled delivery of corticosteroid to the eye (Figure 13). After an application period of four weeks, the hydrogel degrades and liquefies through bulk hydrolysis[366] and naturally exits the nasolacrimal system. Besides the treatment of post-operative inflammation, as well as allergic conjunctivitis (phase III), the system is studied in phase II trials to treat the inflammatory dry eye disease.

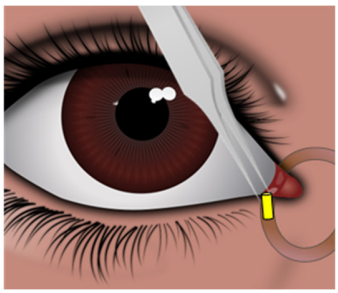

Figure 13. The hydrogel plug Dextenza™ (loaded with dexamethasone to treat inflammatory dry eye disease) is placed through the punctum (natural opening in the eye lid) into the lacrimal canaliculus and allows a controlled delivery of corticosteroid too the eye.

Besides ocular applications, hydrogels represent a promising platform for injection into the human body which facilitates the well-controlled administration of drugs at the desired rate and site. An overview of recent patent applications has been given by Calo and Khutoryanskiy.[367] A successful example for a hydrogel-based (non-ocular) drug delivery system is the vaginal insert Propess® (US: Cervidil®) used to induce cervical ripening, which is on the market since 1995. The network consists of polyurethane (PU) obtained from the cross-linking of PEG-diol and diisocyanates units (Figure 14) and releases the previously loaded drug dinoprostone continuously over a period of 12 h. This release is induced by the swelling of the hydrogel when it is placed in the moist vaginal environment.[368]

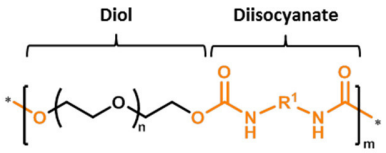

Figure 14. Schematic representation of the chemical structure of polyurethane (orange: urethane unit) obtained by a diol (*i.e.* PEG-diol) and a diisocyanate (R^1 = aliphatic, aromatic moiety).

Based on a similar polymer system, Moraxen® represents a hydrogel that features a slow, controlled release of morphine sulfate over a whole day and is mainly used to relieve pain related to end-stage cancer.[369] It is used for rectal delivery, but it is not considered a classic suppository. The hydrogel is rather a reservoir type device which has to be removed and replaced if needed due to the lack of biodegradability. In 2008, Marillion Pharmaceuticals and Cytokine PharmaSciences announced that they signed a license agreement concerning the delivery system Pilobuc™, which is a buccal insert containing pilocarpine for the treatment of symptoms associated with primary and secondary Sjögren's syndrome, *e.g.* xerostomia.[370] Pilobuc™ is based on a PU hydrogel system, which is an adaption of the marketed products Propess® and Moraxen®.[371] It is placed between the buccal mucosa and gingiva at the back of the mouth.[371] In 2015, the phase II trial for the treatment of xerostomia has been discontinued.[372] A second controlled release system for vaginal delivery is Mysodelle®/Myspess® (US: Misodel®), which is based on a similar cross-linked system, synthesized from PEG, 1,2,6-hexanetriol and dicyclohexylmethane-4,4'-diisocyanate. The drug misoprostol, which is applied for the induction of labor, is released from a reservoir over a period of 24 h. The product is equipped with a withdrawal tape that enables rapid removal when active labor begins.[373] The product Supprelin® LA is a hydrogel system that is used as subcutaneous insert. The system acts as a reservoir and releases histrelin acetate (gonadotropin-releasing hormone agonist) for the treatment of children with central precocious puberty. The drug decreases the luteinizing hormone levels and the serum concentration of sex steroids. The formulation is composed of 2-hydroxyethyl methacrylate (HEMA), 2-hydroxypropyl methacrylate, trimethylolpropane trimethacrylate, benzoin methyl ether, di(4-tert-butylcyclohexyl) peroxydicarbonate (Perkadox-16) and Triton X-100 (non-ionic surfactant).[374] Histrelin acetate is continuously delivered over a period of 12 months until the implant has to be removed as it is nonbiodegradable.[375] Another subcutaneous insert based on a similar polymer reservoir release system of histrelin acetate is Vantas®,[376] which is indicated to treat the symptoms of advanced prostate cancer.

Aquamere® and Aquatrix® II are types of hydrogel-based devices, which are produced by Hydromer®. The trademark Aquamere® comprises several hydrogels based on poly(vinyl pyrrolidone) (PVP) containing PU segments acting as cross-linker.[377] The materials are mainly used for topical applications, but some are applied in oral drug delivery systems. The product line includes four different polymer types (H-, A-, C- and S-series) which contain various comonomers to adjust the properties of the final hydrogel. The H-series products are solutions of PVP and hydrophilic PU that facilitate high viscosity, superb film formation properties and excellent compatibility. Based on the same polymer system as the H-series, the A-series exhibits polymers that are dispersed in ethanol for quick drying. The C-series products of cationic grafted PDMAEMA/PVP copolymers and hydrophilic PU have excellent adhesion and greater substantivity to skin and hair than H-series while maintaining excellent film forming properties. The S-series contains unique silicone-based copolymers of dimethiconylacrylate/PVP and hydrophilic PU, exhibiting a low viscosity and silky feel without oily residue. As a consequence, they are used for applications where sheen or tack reduction is required. The products under the trademark Aquatrix® II are sold as two separate aqueous solutions, forming a hydrogel upon mixing and result in superior cohesive and elastic properties. One part is a solution of PVP in water and the other one contains either chitosan or PEI depending on the specific product.[378] The resulting network can be loaded with active cosmetic and pharmaceutical ingredients by addition to the aqueous solution prior to the gel formation. Another hydrogel system, Hypan® is based on a segmented copolymer structure consisting of hard blocks (PAN sequences, good mechanical properties) and soft blocks (hydrophilic derivatives of acrylic acid obtained by controlled partial hydrolysis of PAN, good water binding capability) whereby more than one block of each kind is present per chain.[379] Hypan® hydrogels are used for the treatment of colon diseases and various cancers. The materials can be processed by extrusion and injection molding, which represent rather unusual methods considering hydrogels. Hypan® is produced and sold by

Hymedix.[380] SQZ Gel™ is a hydrogel system for oral medication composed of chitosan and PEG, which allows a pH-sensitive release of diltiazem hydrochloride to treat hypertension.[369, 381] In the basic environment of the gut, the swollen network shrinks and releases the drug.

Smart Hydrogel™ is a blend of the polymers PAA and PEG-*b*-PPG-*b*-PEG (Pluronic®) that forms a gel when it is warmed to body temperature. Once injected at the desired body surface, it gels and enables a constant dosing of drugs *in situ* for hours.[382] Increasing temperatures result in the aggregation of the hydrophobic ends of adjacent Pluronic®-PAA molecules and, therefore, the formation of micelles. In this conformation, the hydrophilic ends connect with each other to form a network that provides rigidity and structure to the mixture.[383] An intensely investigated thermo-gelling hydrogel is the Oncogel™ system, which is a network loaded with paclitaxel (TXL). It is currently investigated for its application in the treatment of different cancer types.[384] As an example, it has been proven to be effective in the treatment of malignant gliomas in rat models.[385] The physically cross-linked hydrogel by itself is known under the trade name ReGel® and consists of an amphiphilic triblock copolymer (PLGA-*b*-PEG-*b*-PLGA).[386] The system is soluble at low temperatures (< 15 °C), but upon injection into the body, ReGel® forms a gelled depot. The temperature increase towards the critical gelation temperature results in hydrophobic interactions of the PLGA segments and a strong micellar aggregation.[387] As a consequence, the entrapped active compounds are released for systemic/local delivery over several weeks. OncoGel™ has been evaluated in clinical studies on solid tumors[388] and in combination with radiotherapy on esophageal cancer.[389] A recent phase IIb study failed as it showed no impact on the tumor in patients with esophageal cancer. Based on these results, BTG has discontinued its clinical studies and its search for new partners to further develop OncoGel™.[390] Nevertheless, they will continue studies on ReGel® as a drug delivery technology.

Table 13. Hydrogels based on synthetic polymers on the market or in clinical trials.

TRADE NAME	POLYMER SYSTEM	DRUG	INDICATION/USE	MANUFACTURER	STATUS
DEXTENZA™	PEG	Dexamethasone	Post-operative inflammation, allergic conjunctivitis	Ocular Therapeutix™	Phase III[364]
			Inflammatory dry eye disease	Ocular Therapeutix™	Phase II[364]
Propess® (US: Cervidil®)	PU (PEG-diol)	Dinoprostone, 10 mg (prostaglandin E_2/PGE_2)	Induction of labor	Ferring Pharmaceuticals	Market
Moraxen®	PU (PEG-diol)	Morphine sulfate	End-stage cancer pain	BTG, PAION	Market
Pilobuc™	PU (PEG-diol)	Pilocarpine	Sjögren's syndrome (Xerostomia)	Ferring Pharmaceuticals	Phase II[372] (Disc.)
Mysodelle®, Myspess® (US: Misodel®)	PU (PEG-diol)	Misoprostol, 200 µg (prostaglandin E_1/PGE_1)	Induction of labor	Ferring Pharmaceuticals	Market
Supprelin® LA	2-Hydroxyethyl/propyl methacrylate, trimethylolpropane trimethacrylate	Histrelin acetate	Treatment of children with central precocious puberty	Endo®	Market
Vantas®	2-Hydroxyethyl/propyl methacrylate, trimethylolpropane trimethacrylate	Histrelin acetate	Advanced prostate cancer	Endo®	Market

Aquamere®	PVP and PVP-grafted copolymers (cl[a]: PU segments) (H-, A-, C-, S-series)	*Broad range of cosmetic & drug ingredients*	Topical and oral drug delivery	Hydromer®	Market
Aquatrix® II	PVP (cl: Chitosan), PVP (cl: PEI)	*Broad range of cosmetic & drug ingredients*	Drug delivery matrices (*i.e.* transdermal)	Hydromer®	Market
Hypan®	Multiblocks of PAN-b-PAA	[b]	Colon diseases, various cancers	Hymedix	Market
SQZ Gel™	PEG, Chitosan (blend)	Diltiazem	Hypertension	BTG, Macromed	Market
Hycore-V™, Hycore-R™	*Not discclosed*	Metronidazole	Vaginal and rectal infections	BTG , PAION	Market
Smart Hydrogel™	PAA, Pluronic® (blend)	*Broad range of drug ingredients*	Drug delivery matrices	MedLogic Global	Market
OncoGel™	PLGA-*b*-PEG-*b*-PLGA (ReGel®)	TXL	Esophageal cancer	BTG	Phase IIb[390] (disc.)
			Recurrent glioma		Phase I/II (NCT00479765)

TXL: paclitaxel; [a] cl = cross-linker; [b] Hymedix has developed a line of seven products for the chronic wound care market. Which of them are used for drug delivery applications has not been described in publicly available resources.[380]

3.3.2 Solid implants and inserts

Solid drug delivery devices, which are implanted or simply inserted into natural orifices, possess several advantages over parenteral or oral dosage forms. Besides the site specific drug administration and, hence, significantly lower doses of the applied drugs, implantable or insertable devices usually allow a sustained and continuous release of the therapeutic agents. Furthermore, the medication by implantable devices guarantees a better patient compliance and acceptance than frequent injections or the taking of several pills a day. In this chapter, we focus on passive delivery devices that provide continuous release over time periods ranging from weeks to several years without the need for replenishment. These systems are particularly applied for the delivery of highly potent drugs, which work at low doses such as hormones. Numerous commercial systems are available for applications ranging from the prevention of HIV and the treatment of glaucoma to various methods for contraception.

Vaginal inserts. Currently, five different vaginal rings are commercially available (Table 14). For decades, silicone elastomers (PDMS-based) are used for their fabrication due to the low weight, high flexibility and excellent biocompatibility of these materials. Estring® and Femring® are used for hormone replacement therapy, whereas Progering® represents a contraceptive. Fertiring® combines both applications. The only commercialized vaginal ring that is based on poly(ethylene-*co*-vinyl acetate) (PEVA, Figure 15) is NuvaRing® for contraception. Numerous vaginal rings based on PDMS are currently under clinical investigations, which are not only used for contraception but also as prevention for sexually transmitted diseases. Milprosa™ and NES/EE already went through clinical phase III and are close to commercialization. The most advanced microbicide ring, dapivirine (DPV) Ring-004, was designed for HIV prevention and is in phase III trials.[391] Different rings for the controlled and simultaneous delivery of preventives for HIV (maraviroc, levonorgestrel) have recently entered clinical phase I. UPA-CVR, a vaginal ring releasing ulipristal acetate, is already investigated in clinical phase II studies.[392] The trend goes towards multifunctional applicable drug reservoirs. The dual protection vaginal ring of CONRAD is currently in phase I trials. It consists of two segments, which are based on different aliphatic polyether-based PUs from the Tecoflex® family (variable in

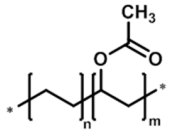

Figure 15. Schematic representation of the chemical structure of poly(ethylene-*co*-vinyl acetate) (PEVA).

hardness and hydrophilicity based on varying contents of PEG and poly(tetramethylene ether glycol) (PTMEG)). The system is optimized to deliver a high flux of tenofovir (HIV/herpes prevention) from one segment and a low flux of levonorgestrel (contraception) from the other.[393] Another polyurethane-based ring entering clinical trials is VR101, which releases glycerin to counteract vaginal dryness. Currently, the Population Council is developing a PEVA ring for simultaneous delivery of medivir-150 (targets HIV), carrageenan (targets human papilloma virus (HPV) and herpes simplex virus-2 (HSV-2)), zinc acetate (targets HIV and HSV-2) and levonorgestrel (targets unintended pregnancy).[394]

Another option for reliable contraception is the insertion of an intrauterine device (IUD, **Figure 16**). The hormonal IUD's are usually made of PDMS (Table 14). The levonorgestrel-releasing system Mirena® was approved by the FDA in 2000, after it had been used in Europe since 1991. A new version of Mirena®, called Skyla® (U.K.: Jaydess®), which is based on the same mechanism of action, was introduced to the US market in 2013. It features a smaller size and a reduced dose of the released hormone levonorgestrel. The latest IUD entering the market (Liletta®) was approved by the FDA in 2015 and exhibits similar characteristics (shape and dose of released levonorgestrel) compared to Mirena®. Intrauterine copper contraceptives (*e.g.* Paragard®) are not described herein, although their monofilament threads and T-frames are usually made of polyethylene (PE).

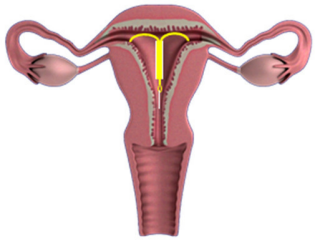

Figure 16. Schematic representation of an intrauterine device (IUD).

Table 14. Vaginal inserts on the market and selected inserts in clinical trials.

TRADE NAME	POLYMER SYSTEM	DRUG	INDICATION/USE	MANUFACTURER	STATUS
			VAGINAL RING		
Estring®	PDMS	17β-Estradiol	Hormone replacement (menopause)	Pfizer	Market
Femring®	PDMS	17β-Estradiol-3-acetate	Hormone replacement (menopause)	Allergan	Market
Progering®	PDMS	Progesterone	Contraception	Population Council, Grünenthal	Market (South America)
Fertiring®	PDMS	Progesterone	Contraception & hormone replacement (menopause)	Population Council, Grünenthal	Market
NuvaRing®	PEVA	Etonogestrel & ethinyl estradiol	Contraception	Merck & Co.	Market
Milprosa™	PDMS	Progesterone	Contraception	Ferring Pharmaceuticals	Phase III[395]
NES/EE	PDMS	Nestorone® (NES) & ethinyl estradiol	Contraception	Population Council	Phase III finished (NCT00455156)
NES/E2	PDMS	Estradiol & nestorone® (NES)	Contraception	Population Council	Phase II (NCT02626208)
DPV-Ring	PDMS	Dapivirine (DPV), (DPV Ring-004)	HIV prevention	IPM	Phase III finished[396]
		DPV/ levonorgestrel			Phase I (NCT02855346)
		DPV/maraviroc			Phase I (NCT01363037)

UPA-CVR	PDMS	Ulipristal acetate	Contraception	HRA Pharma, Population Council	Phase II[392]
Dual protection	PU, PEG & PTMEG (Tecoflex™, Lubrizol Corp.)	Levonorgestrel, tenofovir	Contraception & HIV/herpes prevention	CONRAD	Phase I (NCT02235662)
VR101	PU	Glycerin	Vaginal dryness	J3 Bioscience (formerly ViroPan)	Phase 0 (NCT02029053)
			INTRAUTERINE DEVICE		
Mirena®	PDMS	Levonorgestrel	Contraception	Bayer, Population Council	Market (as Levosert® in GB)
Skyla®	PDMS	Levonorgestrel	Contraception	Bayer	Market (as Jaydess® in GB)
Liletta® (LNG20)	PDMS	Levonorgestrel	Contraception	Allergan, Odyssea Pharma	Market

Subcutaneous implants. An effective contraception can further be accomplished by subcutaneous implants which are implanted at the inside of the upper arm (Figure 17) and continuously release hormones into the blood. After discontinuing the production of Norplant® (silicone capsules containing levonorgestrel),[397] Norplant® II (Jadelle®) was developed, which consists of small rods based on PDMS (Table 15). Once inserted, Norplant® II lasts up to 5 years. Utilizing the same mechanism of action, Sino-Implant II (two thin, flexible silicone rods) represents one of the most effective birth control products with annual pregnancy rates below 1%.[398] The product is considered for four years of use, so far.[399] Another type of subdermal implant is Nexplanon®, which is based on a PEVA copolymer. Nexplanon® reveals two main advantages compared to its predecessor Implanon®, which is replaced gradually: I) The easier insertion that avoids placing the implant too deep under the skin; II) the rod allows localization *via* X-ray since it is radiopaque due to the addition of 15 mg barium sulphate.[400] Despite showing great promise for being another contraceptive alternative, the development of PCL-based Capronor releasing levonorgestrel was abandoned in the 1990s due to skin irritation and stability in storage issues. Furthermore, there were concerns about removal of the device and a long release tail.[401] However, the single, tubular implant was able to achieve up to one year of ovulation suppression. [402] Very recently, the FDA approved another implant based on PEVA, called Probuphine®, which is the first device for the continuous release of buprenorphine. It is used for the maintenance treatment of opioid dependence as part of a complete treatment program including counseling and psychosocial support. Probuphine® consists of four rods that are implanted under the skin on the inside of the upper arm and provides treatment for six months.[403] VC-01™ is a subcutaneous implant currently under clinical investigation (phase I/II) to treat diabetes type I. It is composed of ViaCyte's Encaptra® drug delivery technology (made of undisclosed polymers[404]) and is used to deliver human embryonic stem cells (pancreatic PEC-01™ cells).

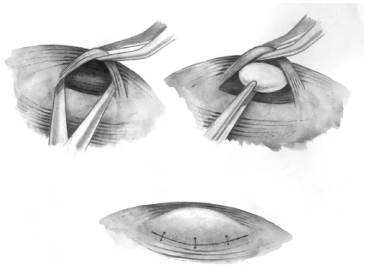

Figure 17. Schematic representation of the implantation of a subcutaneous implant. Reprinted from Acta Cir. Bras. 2009, *24*, 7-12. with permission of Creative Commons Corporation (2009).

Table 15. Subcutaneous implants on the market and in clinical trials.

TRADE NAME	POLYMER SYSTEM	DRUG	INDICATION/USE	MANUFACTURER	STATUS
Jadelle® (Norplant® II)	PDMS	Levonorgestrel	Contraception	Bayer, Population Council	Market (not in US)
Sino-Implant II	PDMS	Levonorgestrel	Contraception	Shanghai Dahua Pharmaceuticals	Market (as Zarin®, Fem-plant®, Trust®, Simplant® etc. registered in 24 countries)
Nexplanon®	PEVA	Etonogestrel	Contraception	Merck & Co.	Market
Capronor	PCL	Levonorgestrel	Contraception	RTI International	Phase II[401] (disc.)
Probuphine®	PEVA	Buprenorphine HCl	Opioid dependence	Titan & Braeburn™ Pharmaceuticals	Market
VC-01™	*undisclosed* (Encaptra®)	PEC-01™ cells[a]	Diabetes type 1	ViaCyte	Phase I/II (NCT02239354)

[a] Embryonic stem cell–derived precursors of insulin-producing beta cells.

Ocular implants and inserts. Implantable or insertable devices are well-established for the local treatment of eye diseases. Ocusert® Pilo was one of the first ocular delivery devices and represents an ocular insert, which is placed in the lower cul-de-sac of the eye to be used for the treatment of glaucoma (Table 16).[405] It contains a core reservoir consisting of pilocarpine and alginic acid and a framework of hydrophobic poly(ethylene-*co*-vinyl acetate) (PEVA) membrane that regulates diffusion of pilocarpine. However, the product has been withdrawn from the market, which is mainly related to the difficulties (in particular for elderly people) replacing the insert.[406] The first intravitreal implant was Vitrasert®. This ganciclovir pellet was used for the treatment of cytomegalovirus retinitis. The antiviral medication is coated by nondegradable layer of impermeable PEVA, which is sandwiched in between two permeable layers of PVA. This design enables a well-controlled rate of release of the drug by the diffusion only through the areas where no impermeable material is present. As a consequence, reimplantation is necessary after 5 to 8 months.[407] Due to market forces, Vitrasert® has not been produced since 2014, and all remaining implants have passed their expiration dates.[408] Retisert® followed as the second generation of reservoir-based implants, which are used for treatment of chronic noninfectious uveitis (Figure 18).[409] This implant for sustained release consists of a silicon laminate and PVA coating, which control the release of fluocinolone acetonide (FA). Further studies have proven the potential of this device in the treatment of edema (caused by diabetes) and central retinal vein occlusions.[410] Another implant for the delivery of FA and the treatment of diabetic macular edema is Iluvien®. This rod-like device is based on polyimide tubes (Figure 19) with a PVA membrane at the caps. Due to its small size, it can remain in the cavity even after the whole drug has been released. A similar, small rod-like device, which is injected into the white of the eye, is Ozurdex®. This system is designed to deliver the corticosteroide dexamethasone also applied for the treatment of macular edema. In contrast to previous devices, the use of degradable PLGA allows the dissolution of the implant and, therefore, eliminates the need of surgically removal. Another biodegradable PLGA-based implant is Surodex®, which is a rod-shaped device inserted into the anterior chamber after a cataract surgery in order to control postoperative inflammation.[407]

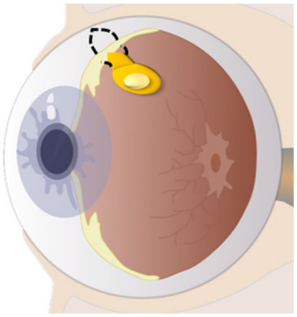

Figure 18. Schematic representation of the reservoir-based Retisert® implant.

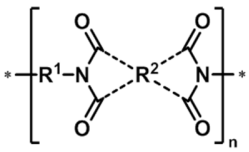

Figure 19. Schematic representation of the chemical structure of polyimides.

Further ophthalmic inserts (*e.g.* I-vation™ or Helios™), which are currently under clinical investigations, have been nicely reviewed elsewhere.[407, 411]

Table 16. Ocular implants and inserts on the market and in clinical trials.

TRADE NAME	POLYMER SYSTEM	DRUG	INDICATION/USE	MANUFACTURER	STATUS
Ocusert® Pilo	PEVA	Pilocarpine	Treatment of glaucoma	Johnson & Johnson, Alza Cooperation	Market (withdrawn)
Vitrasert®	PVA, PEVA (Versa™ platform)	Ganciclovir	Cytomegalovirus retinitis	Auritec Pharmaceuticals	Market (withdrawn)
Retisert®	PVA, PDMS (Versa™ platform)	Fluocinolone acetonide	Chronic non-infectious uveitis	Valeant® (Bausch & Lomb), Auritec Pharmaceuticals	Market
Iluvien®	Polyimide, PVA	Fluocinolone acetonide	Diabetic macular edema	AlimeraSciences	Market
Ozurdex®	PLGA (Novadur®)	Dexamethasone	Diabetic macular edema	Allergan	Market
Surodex®	PLGA, hydroxypropyl methylcellulose	Dexamethasone	Postcataract surgery inflammation	Oculex Pharmaceuticals	Market (China, Singapore, etc.)
I-vation™	PMMA, PEVA	Triamcinolone acetonide	Diabetic macular edema	SurModics	Phase II finished (NCT00692614)
Helios™	PDMS	Bimatoprost	Intraocular pressure (IOP)-lowering	ForSight™ VISION5	Phase II (NCT02537015)
*	PLGA	Brimonidine tartrate	Retinitis pigmentosa	Allergan	Phase II (NCT00661479)
			Age-related macular degeneration	Allergan	Phase II (NCT00658619)

* No trade name listed.

Implants for deeper tissue. While the majority of implantable devices comprises subcutaneous or ocular systems, which do not require major surgery to be applied, replaced or removed, a few devices were developed to be implanted into deeper tissue in the body (Table 17). Based on a biodegradable polymer (a copolymer of *bis*-(*p*-carboxyphenoxy)propane and sebacic acid called Polifeprosan 20) the Gliadel® wafer is approved for the treatment of malignant glioma.[412] It is inserted into cavities resulting after the surgical removal of the tumor in the brain (Figure 20) and will be degraded by the body to release the cytostatic drug carmustine. Another commercialized implant for the application in deeper tissue is Propel® based on the biodegradable polymer PLGA.[413] This steroid-eluting device is implanted after surgery into the nose to assist in the treatment of chronic sinusitis.

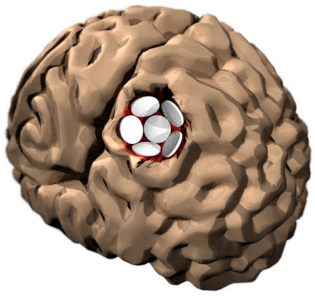

Figure 20. Schematic representation of the inserted Gliadel® wafer (polymer system) in the brain.

The presented implant systems reflect only a selection of currently commercially available systems. Besides, a large pipeline of polymer-based implant delivery technologies has been studied in promising clinical trials. The biodegradable implant siG12D-LODER™ (PLGA-based) is inserted into the tumor and releases a siRNA drug against KRASG12D over four months. In combination with chemotherapy it is used as targeted therapy for locally advanced pancreatic cancer (phase IIb).[414] Restora™ represents a transmucosal PU steroid-eluting device[415] for thirty day treatment of sinusitis (phase II/III).[416] In contrast, LiRIS® is a pretzel-shaped silicone tube that could be inserted into the bladder, releasing lidocaine over two weeks in females with interstitial cystitis (phase II).[417]

Table 17. Implants for deeper tissue on the market and in clinical trials.

TRADE NAME	POLYMER SYSTEM	DRUG	INDICATION/USE	MANUFACTURER	STATUS
Gliadel® Wafer	Polifeprosan 20[a]	Carmustine	Malignant glioma	Arbor Pharmaceuticals	Market
Propel®	PLGA, PEG	Mometasone furoate	Chronic sinusitis	Intersect® ENT	Market
siG12D-LODER™	PLGA (Loder™)	siRNA therapeutic (KRASG12D)	Pancreatic tumor	Silenseed	Phase IIb (NCT01676259)
Restora™	PU	Steroid	Sinusitis	SinuSys™	Phase II/III (NCT02627794)
LiRIS®	PDMS	Lidocaine	Interstitial cystitis/ bladder pain syndrome	Allergan	Phase II (*e.g.* NCT01475253, NCT01824303)

[a] Polifeprosan 20 (poly[bis (p-carboxy-phenoxy)] propane and sebacic acid).

Several companies are working continuously on new technologies (*e.g.* Medidur™, DebioStar™, Duros®, MedLaunch™), which can be used as polymer platform for different drugs. Implanted drug-eluting stents are described in Chapter 3.4.2 as the polymers are used as coatings in that case. Implanted devices built up from hydrogel networks, *e.g.* Supprelin® LA and Vantas®, are described in Chapter 3.3.1.

3.4 Coatings

3.4.1 Solid oral dosage forms

Despite the complexity of the related uptake mechanism, oral administration of pharmaceutical compounds is the preferred route for the drug delivery applications due to the ease of ingestion, the avoidance of painful procedures, its versatility, the high patient compliance, reduced sterility constraints, and flexibility of dosage form design (*e.g.* solids: Powder, granules, capsules).[418] In addition, the oral uptake allows patients to conveniently self-administer drugs without the need of any health care professionals.[419] But the oral delivery of pharmaceuticals remains challenging for several reasons: I) The typical transit time in the gut (from mouth to anus) is about 30 hours, which limits the use of drugs that aim at longer dosing times;[420] II) the physiological parameters and the biological environment of the gastrointestinal (GI) tract can vary quite significantly from one stage to the next. For example, the pH value of the saliva in the mouth is usually in the range of 5.8 and 7.4. Inside the stomach the pH value decreases dramatically to 1 (extremely acidic) and increases back to 7 (neutral) in the bowels; III) the food and beverage intake causes dynamic changes in the concentration of bile salts, lipids, carbohydrates and digestive enzymes throughout the GI tract that can interact with the drug;[421] IV) finally, before reaching the bloodstream, the drug has to overcome some anatomical obstacles including the degradative environment in the lumen and traversing the mucosa and epithelial cells. However, one of the main concerns remains the patient compliance considering the oral uptake of pharmaceuticals, in case the drugs have disagreeable taste and require frequent dosing. As a result of these limitations, various functional coatings based on polymers have been designed to improve the efficacy of the oral route of administration. These polymer coatings are mainly applied to solid dosage forms, *i.e.* tablets, granulates and capsules, with the aim to achieve selective delivery of active ingredients to a particular gastrointestinal (GI) tract, such as the small intestine or the large bowel, or to improve the patient compliance by improving the odor or masking the taste. Since the established systems comprise proven and versatile materials, there doesn't exist an immediate need for new polymer systems.

Polymer coatings for site specific delivery. The release of a drug at a specific site in the GI guarantees an optimized uptake into the blood stream or activity of the delivered active ingredient at the desired side, but avoids complications with other parts of the tract. Several polymer-based coatings have been developed to target various sites of the GI. An enteric polymer coating prevents the release of the drug in the gastric environment and facilitates the release in the small intestine or in the colon. This enables: I) The protection of the stomach from some drugs, which may cause stomach ulcers, such as aspirin, diclofenac and naproxen; II) the protection of special pharmaceutical compounds such as proton pump inhibitors (PPIs) (*e.g.* omeprazole or pantoprazole) against the acidic environment in the stomach, and, III) the targeting of the small intestine or colon.[422] Enteric coatings contain carboxylic acid groups, which remain in an unionized (protonated) form at low pH values and, therefore, are insoluble in the acidic aqueous environment of the stomach.[169] However, as the pH value increases in the small intestine, the carboxylic acids become deprotonated (negatively charged), which results in the dissolution of the polymers in the intestinal fluid.[423] Table 18 summarizes marketed poly(meth)acrylate copolymers, which are used for enteric coatings, including their chemical composition, product form and the pH value at which they become soluble. The critical pH value for dissolution of the polymers mainly depends on the content of the carboxylic acid and esterified groups. The different dissolution properties of enteric coatings enable targeting specific areas of the intestine. For example, EUDRAGIT® L100-55 and EUDRAGIT® L100 dissolve above pH value of 5.5 and 6.0, respectively, and are used for targeting the small intestine, whereas EUDRAGIT® S100 and EUDRAGIT® FS 30D (Figure 21) dissolve above pH value of 7.0 and are used for colon targeting.[424] In addition, the release of the encapsulated drugs can further be controlled by the thickness of the coating material or simply by blending the different enteric polymers in different ratios.[422]

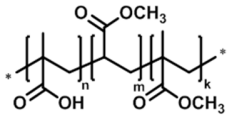

Figure 21. Schematic representation of the chemical structure for the copolymer poly(MAA-*co*-methyl acrylate-*co*-MMA), named EUDRAGIT® FS 30D.

Table 18. Marketed poly(meth)acrylates as enteric coatings.

TRADE NAME	PRODUCT FORM	POLYMER SYSTEM	DISSOLUTION pH	MANUFACTURER
EUDRAGIT® L 100-55	Powder	Poly(MAA-*co*-ethyl acrylate) 1:1	Soluble > pH 5.5	Evonik
EUDRAGIT® L 30D-55	Aqueous dispersion 30%			
Kollicoat® MAE 30 DP	Aqueous dispersion 30%		Soluble > pH 5.5	BASF
Kollicoat® MAE 100 P	Powder			
EUDRAGIT® L 100	Powder	Poly(MAA-*co*-MMA) 1:1	Soluble > pH 6.0	Evonik
EUDRAGIT® L 12.5	Organic solution 12.5%			
EUDRAGIT® S 100	Powder	Poly(MAA-*co*-MMA) 1:2	Soluble > pH 7.0	Evonik
EUDRAGIT® S 12.5	Organic solution 12.5%			
EUDRAGIT® FS 30D	Aqueous dispersion 30%	Poly(MAA-*co*-methyl acrylate-*co*-MMA) 7:3:1	Soluble > pH 7.0	Evonik

Apart from enteric coatings, sustained release coating polymers releasing the drug over time can also be used for modified/controlled release applications. These polymers lack ionizable groups and they are not soluble in the entire GI tract. However, they can swell with exposure to the gastrointestinal fluids and, consequently, release the active ingredients by a diffusion-controlled mechanism. These polymer coatings are mainly used in prolonged-action dosage forms. EUDRAGIT® RL and RS, which contain 10% or 5% quaternary ammonium groups, respectively,

as well as the neutral EUDRAGIT® NE and NM, which are the copolymers of ethyl acrylate and methyl methacrylate, are preferred coating materials for a sustained release. Table 19 includes marketed poly(meth)acrylate based copolymers which are used for sustained release coatings and their chemical composition as well as dissolution properties.

Table 19. Various marketed poly(meth)acrylates for sustained release.

TRADE NAME	PRODUCT FORM	POLYMER SYSTEM	PROPERTIES	ADVANTAGES
EUDRAGIT® RL 30 D	Aqueous dispersion 30%	Poly(ethyl acrylate-*co*-MMA-*co*-TMAEMA) 1:2:0.2	Insoluble, high permeability, pH-independent swelling	Customized release profiles by combination of RL and RS grades in different ratios, suitable for matrix structures
EUDRAGIT® RL PO	Powder			
EUDRAGIT® RL 100	Granules			
EUDRAGIT® RL 12.5	Organic solution 12.5%			
EUDRAGIT® RS 30 D	Aqueous dispersion 30%	Poly(ethyl acrylate-*co*-MMA-*co*-TMAEMA) 1:2:0.1	Insoluble, low permeability, pH-independent swelling	
EUDRAGIT® RS PO	Powder			
EUDRAGIT® RS 100	Granules			
EUDRAGIT® RS 12.5	Organic solution 12.5%			
EUDRAGIT® NE 30 D	Aqueous dispersion 30%	Poly(ethyl acrylate-*co*-MMA-*co*-TMAEMA) 2:1:0	Insoluble, low permeability, pH-independent swelling	No plasticizer required, highly flexible, suitable for matrix structures
EUDRAGIT® NE 40 D	Aqueous dispersion 40%			
EUDRAGIT® NM 30 D	Aqueous dispersion 30%			

TMAEMA = trimethylammonioethyl methacrylate chloride.

Polymer coatings for odor or taste masking. Polymer coatings are also applied to protect the sensitive ingredients from environmental influences such as light and moisture or to mask the unpleasant taste of the formulations.[169, 425] Methacrylates containing tertiary amino groups are commonly applied for masking the taste and moisture protection (Table 20). These pH-responsive polymer coatings take advantage of the differences in pH values between the oral cavity (pH 5.8 to 7.4) and the stomach (pH 1 to 3.5).[426] The polymers are insoluble in water at the neutral pH value of the saliva. Therefore, they suppress the release of the drug, which usually exhibit an unpleasant taste, and the diffusion of water molecules to the core of the system protecting any moisture sensitive ingredients. However, they become protonated and water-soluble at acidic conditions resulting in the release of the content in the stomach or in the small intestine.

Table 20. Marketed pH-responsive poly(meth)acrylates as protective coatings.

TRADE NAME	PRODUCT FORM	POLYMER SYSTEM	DISSOLUTION pH	MANUFACTURER
EUDRAGIT® E 100	Granules	Poly(BMA-*co*-DMAEMA-*co*-MMA) 1:2:1	Soluble < pH 5.0	Evonik
EUDRAGIT® E 12.5	Organic solution 12.5%			
EUDRAGIT® E PO	Powder			
Kollicoat® Smartseal 30D	Aqueous dispersion	Poly(MMA-*co*-DEAEMA[a]) 7:3	Soluble < pH 5.0; Stable in saliva	BASF

[a] DEAEMA= diethylaminoethyl methacrylate.

Apart from these pH-responsive methacrylates, some other water soluble synthetic polymers, including vinyl polymers and hydrophilic copolymers, are also applied for masking unpleasant tastes or protecting against moisture (Table 21). These polymers do not contain any ionic groups, which decreases the risk of chemical interactions with any other ingredient of the formulation.[425]

Table 21. Marketed water soluble synthetic polymers as protective coatings.

TRADE NAME	PRODUCT FORM	POLYMER SYSTEM	MANUFACTURER
Kollidon®	Powder	PVP	BASF
Kollicoat® IR	Powder	PVA-PEG-graft copolymer	BASF
Kollicoat® Protect	Powder	PVA-PEG-graft copolymer (Kollicoat® IR), PVA	BASF
Opadry® AMB	Powder	PVA	Colorcon®

Moreover, the previously mentioned enteric polymers (see Table 18) and coatings for sustained release (see Table 19) can also be used for taste masking and moisture protection if they provide a sufficient suppression of the drug release in the mouth and prevent moisture to pass into the formulation. However, to realize the desired fast drug release after swallowing, relatively thin coatings are applied.[425] Table 22 represents selected examples of commercialized drug formulations which are coated with EUDRAGIT® polymers.

Table 22. Examples for marketed dosage forms coated with EUDRAGIT® polymers.

TRADE NAME	POLYMER SYSTEM	DRUG	INDICATION/USE	MANUFACTURER
Clipper®	EUDRAGIT® L 100-55	Beclometasone dipropionate	Inflammatory bowel disease	Chiesi
Colo-Pleon®	EUDRAGIT® L 100-55	Sulfasalazine	Inflammatory bowel disease	Sanofi-Aventis
Entocort®	EUDRAGIT® L 100-55	Budesonide	Inflammatory bowel disease	Prometheus Lab.
Salofalk®	EUDRAGIT® L 100	Mesalazine	Inflammatory bowel disease	Dr. Falk Pharma
Ipocol®	EUDRAGIT® S 100	Mesalazine	Inflammatory bowel disease	Sandoz
Budenofalk®	EUDRAGIT® S 100 & EUDRAGIT® L 100	Budesonide	Inflammatory bowel disease	Dr. Falk Pharma
Premique®	EUDRAGIT® NE 30 D	Conjug. estrogens & medroxyprogesterone acetate (MPA)	Hormone replacement therapy for estrogen deficiency symptoms in postmenopausal women within an intact uterus	Pfizer
Nutrizym 22	EUDRAGIT® L 30 D	Pancreatin BP	Symptomatic relief of pancreatic exocrine insufficiency such as in fibrocycstic disease of the pancreas & chronic pancreatitis	Merck Serono
Convulex® CR	EUDRAGIT® RL 30 D	Sodium valproate	Epilepsy and bipolar disorder	G. L. Pharma GmbH
Amisulpride film-coated tablets	EUDRAGIT® E 100	Amisulpride	Acute & chronic schizophrenic disorders	Lek Pharmaceuticals D. D., Salutas Pharma GmbH
Adanif® XL	EUDRAGIT® E	Nifedipine	Hypertension, prophylaxis of chronic stable angina pectoris	Focus Pharmaceuticals

3.4.2 Drug-eluting stents

Coronary artery disease (CAD) is a heart disease, which is considered to be one of the leading causes of death worldwide.[427] The lining of the coronary arteries, which guarantee the blood supply to heart muscle, becomes harder and stiffer, and, finally, the artery's diameter is narrowed due to the accumulation of plaque on their inner walls (atherosclerosis). The percutaneous transluminal coronary angioplasty (PTCA) is a well-established method to counteract the symptoms of the CAD. However, this treatment is not sufficient as the risks of early abrupt closure, intimal hyperplasia and late restenosis are considerably high, if it is not accompanied by further therapies.[428] An early approach to overcome these limitations resulted in the development of bare metal stents (BMS).[429] BMS are devices, which are first inserted in the narrowed coronary artery by an inflatable catheter. At the side of action, the BMS gets expanded by the attached balloon and acts as a mechanical scaffold to recover the original dimensions of the vessel (Figure 22).[430] Despite an initial improvement, the implantation of the BMS commonly results in an in-stent restenosis (ISR) due to the migration of vascular smooth cells within the stents.[431] The first attempts to prevent this restenosis by systematic drug delivery systems failed. As a consequence, focus was set on the development of drug-eluting stents (DES). These systems carry an antiproliferative drug, which is incorporated into a polymer coating of the BMS. The drugs are directly released at the injured sites to prevent the ISR by the suppression of the neointimal growth.[432] The first generation of DES comprises the sirolimus-eluting stent (Cypher®) and the paclitaxel-eluting stent (Taxus®), which are made of a stainless steel (SS) scaffold coated with the polymers poly(*n*-butyl methacrylate) (PBMA) and poly(ethylene-*co*-vinyl acetate) (PEVA) or poly(styene-*b*-isobutyelene-*b*-styrene) (PSIBS), respectively. The application of these modified stents resulted in a remarkable reduction of the usually occurring restenosis. However, safety concerns have been raised regarding the possibility of late stent thrombosis in case of a long term use.[433] In recent years, a second generation of DES has been developed with the aim to improve the efficacy and the long term safety of the stents. For this purpose, stent frames with thinner struts were introduced, and novel, more effective drugs were incorporated compared to the first generation DES. Similar to the first generation, these DES still use synthetic, nonbiodegradable polymers such as PBMA, PEVA, PSIBS, poly(hexafluoropropylene) (PHFP), and poly(vinylidene fluoride) (PVDF), sometimes in combination with a phosphorylcholine polymer (PCh) (Figure 23),[434] as coating materials of a metal surface. Table 23 summarizes all DES approved by the FDA that use polymer coatings.[428-429, 431, 435] Keeping in mind that the above mentioned polymers are nonbiodegradable, these coatings remain on the stent even after the drug is fully released, which may induce local hypersensitivity, inflammation and delayed vascular healing resulting in the development of late stent thrombosis.[436]

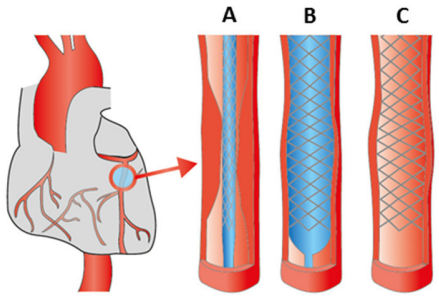

Figure 22. General mechanism of the insertion of a stent. A) Insertion of the stent by an inflatable catheter; B) expansion of the stent by the attached ballon; C) removal of the ballon.

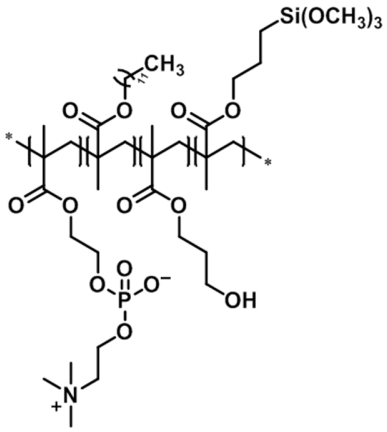

Figure 23. Schematic representation of the chemical structure of an exemplary phosphorylcholine polymer (PCh, PC technology™).

Table 23. Drug-eluting stents (DES) with nonbiodegradable polymers as coating materials on the market or in clinical trials.

TRADE NAME	STENT PLATFORM[a]	POLYMER SYSTEM	DRUG	DRUG RELEASE (DAYS)	MANUFACTURER	APPROVAL
Cypher®	SS	PEVA, PBMA, PCh	Sirolimus	40% (5); 85% (30); 100% (90)	Cordis Corporation	FDA[b]
Taxus®	SS	Poly(styrene-*b*-isobutylene-*b*-styrene)	TXL	<10% (28)	Boston Scientific	FDA
Promus PREMIER™	Pt-Cr	PBMA, poly(vinylidene-*co*-hexafluoropropylene)	Everolimus	71% (28); 100% (120)	Boston Scientific	FDA
Xience V®	Co-Cr	PBMA, poly(vinylidene-*co*-hexafluoropropylene)	Everolimus	80% (28); 100% (120)	Abbot Vascular	FDA
Endeavor®	Co-Cr	PCh	Zotarolimus	75% (2); 95% (15); 100% (28)	Metronic	FDA
Endeavor® Resolute	Co-Cr	Blend of PVP, poly(hexyl methacrylate)-*co*-PVP-*co*-PVAc and PBMA-*co*-PVAc (BioLinx)	Zotarolimus	50% (7); 70% (28); 100% (31)	Metronic	FDA
Firebird2®	Co-Cr	Poly(styrene-butylenes-styrene)	Sirolimus	50% (7); 90% (30)	Essen Technology (Beijing)	Phase IV (NCT01257373)

TXL: paclitaxel; [a] Pt-Cr: platinum chromium, SS: stainless steel, Co-Cr: cobalt chromium; [b] FDA approved stents also have CE approvals.

These issues have promoted the recent development of stents coated with fully biodegradable polymers such as PLGA and PLA. A successful example is the everolimus-eluting stent, which consist of a platinum chromium (Pt-Cr) platform coated with a biodegradable PLGA copolymer. A summary of FDA and CE approved DES based on biodegradable polymers are listed in Table 24.[429, 437]

Table 24. Drug-eluting stents (DES) with biodegradable polymers as coating materials.

TRADE NAME	STENT PLATFORM[a]	POLYMER SYSTEM	DRUG	DRUG RELEASE (DAYS)	MANUFACTURER	STATUS
Synergy™	Pt-Cr	PLGA	Everolimus	50% (60); 100% (90)	Boston Scientific	FDA[b]
Axxess™	Nitinol	PLA	Biolimus A9	45% (30)	Biosensors	CE
BioMatrix Flex™	SS	PLA	Biolimus A9	45% (30)	Biosensors	CE
Nobori®	SS	PLA	Biolimus A9	45% (30)	Terumo	CE
Supralimus®	SS	PLLA-PLGA-PCL-PVP	Sirolimus	100% (48)	SMT	CE
Orsiro	Co-Cr	PLLA + silicon carbide	Sirolimus	50% (30); 80% (90)	Biotronik	CE
BioMime™	Co-Cr	PLLA + PLGA	Sirolimus	100% (30)	Meril	CE
Inspiron®	Co-Cr	PLLA, PDLLGA	Sirolimus	60% (10); 100% (45)	Scitech Medical	Phase IV (NCT01856088)
Firehawk®	Co-Cr	PDLLA	Sirolimus	90% (90)	MicroPort Medical	CE
DESyne® BD	Co-Cr	PLA	Novolimus™	90% (90)	Elixir®	CE
MiStent SES®	Co-Cr	PLGA	Sirolimus	100% (270) (sustained release)	Micell Technologies	CE
Tivoli®	Co-Cr	PLGA	Sirolimus	50% (7); 80% (28)	Essen Technology (Beijing)	Phase III (NCT02448524)

[a] Pt-Cr: platinum chromium, SS: stainless steel, Co-Cr: cobalt chromium; [b] FDA approved stents also have CE approvals.

Although the above mentioned efforts have increased the efficacy and lifetime of stents, it has to be kept in mind that even after the degradation of the polymer coatings the metal scaffold (BMS) remains in the artery, which still might cause restenosis.[438] As a consequence, the development of fully biodegradable stents has gained considerable attention. Several fully degradable DES have been investigated clinically or are still in clinical trials, but so far only the evorolimus-eluting stent Absorb™ is FDA approved and the Novolimus™-eluting DESolve® is CE approved for commercial use in coronary patients (Table 25).[429, 439] In addition to these fully degradable systems, dual drug-eluting stents (DDES) are tested to deliver both anti-proliferative and pro-healing agents reducing the occurrence of stent thrombosis. Although some of the DDES have shown promising results in clinical trials, the Combo stent (OrbusNeich) is the only marketed DDES, which has CE approval. Combo stent uses stainless steel as stent platform and elutes the sirolimus and CD-34 antibody as drugs from a biodegradable polymer matrix that achieves the complete release within 30 days. Unfortunately, the chemical formulation of the used polymer matrix is not specified. Moreover, since the DDES in clinical trials are either polymer free or use no synthetic polymers, readers are referred to literature for more information.[429]

Table 25. Drug-eluting stents (DES) with fully biodegradable scaffolds and coatings.

TRADE NAME	STENT PLATFORM	POLYMER SYSTEM	DRUG	DRUG RELEASE (DAYS)	MANUFACTURER	STATUS
Absorb™	PLLA	PDLLA	Evorolimus	80% (28)	Abbot Vascular	FDA approval
DESolve®	PLLA	PLLA	Novolimus™	100% (180 to 270)	Elixir®	CE approval
Dreams I	Mg[a]	PLGA	TXL	100% (90)	Biotronik	Phase 0 (NCT01168830)
Dreams II	Mg	PLLA	Sirolimus	n.a.	Biotronik	Phase 0 (NCT01960504)
ReZolve2	PTD-PC[b]	n.a.	Sirolimus	Majority of drug (90)	REVA	Clinical study[c] (NCT01845311)

[a] Mg, magnesium; [b] PTD-PC, poly-tyrosine-derived polycarbonate; [c] status not clear; n.a.: not applicable.

3.5 Polymers as matrix excipients

Besides the previously described application forms, several synthetic polymers are added to pharmaceutical dosage forms. By definition they have to be inactive ingredients (all materials other than the API) in final drug products to belong to the so-called excipients.[440] The FDA provides an online database comprising all inactive ingredients approved for certain formulations for their particular route of administration, amount and concentration (also the polymers used for coatings, *e.g.*, several Eudragit® products, can be found here, see Chapter 3.4.1).[441] Excipients have undergone a paradigm shift from being “inert ingredients” to “functional ingredients”. For instance, polymers on one hand act as binders in tablets, capsules and granules, as solubilizing, lyophilizing, wetting or taste masking agents[442] but also as mucoadhesives.[443] They are referred to provide sustained release of drugs, to solubilize and protect them from degradation or to enhance their bioavailability. They ensure mucus permeability of the formulation and enhance the probability for the drug to permeate epithelial barriers (intestinal, nasal, pulmonary).[444] Thus, in fact they are used to modulate the overall efficacy of a drug and are, therefore, major components in so-called modified release (MR) drug delivery systems. Based on the solubility and permeability of an API, a Biopharmaceutical Classification System (BCI) has been introduced grouping the APIs into 4 classes (I to IV).[445] According to FDA, an API is for instance highly soluble when its highest clinical dose strength is soluble in 250 mL of aqueous media over a pH range of 1 to 7.5 at 37.5 °C, and it is considered to be highly permeable if the absorption of an orally administered dose in humans is > 90% when determined using mass balance or in comparison to an intravenous reference dose.[446] Such API is referred to as a class I API and can be more easily

delivered *via e.g.* an oral dosage form. For class II drugs (low solubility and high permeability) different formulation strategies have to be applied to deliver them orally, *e.g.* as polymeric amorphous solid dispersion.[447] Related to this, polymer matrix excipients can be classified as hydrophilic or hydrophobic matrices. The class of hydrophilic matrices is dominated by different celluloses (most often hydroxypropyl methylcellulose, HPMC) and polysorbates (both not subject of this review), but also PVP and PEG as synthetic polymers are used.
Due to the vast number of products on the market containing synthetic polymers as matrix excipients, herein only an impression of the most superficial functions of each polymer class is provided followed by an arbitrary selection of commercially available dosage forms. Often polymers can be included into formulations to fulfill several tasks depending on the formulation technology. Therefore, assignment of a certain polymer or polymer class to a particular function, dosage form or manufacturing process is difficult since it can perform different functions in different dosage forms (Table 26).

Eudragit®. Different poly(methacrylate)s (Eudragits®) are most frequently applied as synthetic hydrophobic matrices.[448] For instance, Eudragit® NE 30 D can serve as a coating material or can be processed into a tablet formulation acting as matrix (with up to 20 wt%), *e.g.* by wet granulation or direct compression of powders. The drug and other excipients are partially impregnated with the polymer. Subsequent compression results in embedment of the drug in a sponge-like network of thin polymer layers. The polymer network controls the penetration of digestive fluid into the tablet as well as the diffusion of the dissolved drug through the pores. In this way, a time controlled release and pH value independent formulation for sustained-release formulation can be realized. Eudragit® E PO (EE) is a cationic copolymer based on dimethylaminoethyl methacrylate, butyl methacrylate, and methyl methacrylate (for exact composition, see Table 20). It is soluble in gastric fluid up to pH 5, thus the drug release can be controlled to occur only in acidic environment. It is frequently used as a coating agent due to its film forming capability, but also finds application as a binder in tablets prepared by direct compression in 10% to 50% concentration. The coating of solid oral dosage forms is highlighted separately in Chapter 3.4.1.

Carbomer. "Carbomers" (Carbopol™) are high molar mass poly(acrylic acid)s (PAA), sometimes cross-linked with small amounts of allyl ethers of polyalcohols. The different numbers in the labels of carbomers (934, 934p, 940, 941) denote their different molecular sizes as well as the use of benzene during the manufacturing process. If benzene is not used during the manufacture, carbomers of type a, b or c are distinguished according to the viscosity of their solutions in water. They are most commonly used in cosmetic industry but also in tablet formulations, in particular for oral mucoadhesive controlled drug delivery systems.[449] Carbomers can absorb large amounts of water, thus increasing in volume up to 1,000 times to form gels and thick solutions that are stable and resistant to spoilage. Usually, carbomers are provided as a dried, white powder. Carbomers are considered to be generally regarded as safe by the FDA, although high concentrations may lead to eye and skin irritation.

Polycarbophil. Poly(acrylic acid) cross-linked with divinyl glycol is named polycarbophil. It is a bulk-forming laxative that increases the amount of water in stools to make them softer and easier to pass. Polycarbophil is used to treat constipation and to help to maintain regular bowel movements. It has been developed as pharmaceutical polymer with superior bioadhesive properties used in the field of controlled drug delivery systems. It could be used as a highly efficient thickener, bioadhesive agent, suspending aid and emulsion stabilizer when dispersed in water or other polar solvents.[450] Polycarbophil can also be used as a controlled release polymer in oral solid dose applications (*e.g.* Striant®). Typical usage levels for achieving controlled release characteristics in tablets manufactured by aqueous granulation are 5 wt% to 10 wt%, depending on the drug properties, co-excipients and processing parameters.

Dimethicone. Poly(dimethylsiloxane) (PDMS) is widely used under the name "dimethicone"' as lubricant and conditioning agent, but is also present in tablet capsules (*e.g.* Keflex®). An orally administered dosage form is the

over-the-counter drug "simethicone" (mixture of 90% to 99% of PDMS with siliciumdioxide, see Chapter 3.6). It is also used as excipient in tablets and capsules (*e.g.* Antara®). The presence of PDMS was found in many registered drugs, including familiar ones such as Augmentin™, Maalox®, and VapoSteam™, just to name a few examples.

Poly(ethylene glycol) (PEG). PEG is frequently used as stealth polymer covalently coupled to drugs (Chapter 3.1) or in micro- and nanoparticulate drug delivery systems (Chapter 3.2),[15] but also as matrix excipients in oral and parenteral dosage forms and more.[451] PEG is mainly added to solubilize poorly water soluble drugs to enhance their bioavailability and to reduce inter-subject variability of plasma concentrations. In particular, clear liquid PEG with low molar masses (M_n) of 300 to 600 g mol^{-1} is frequently used to solubilize poorly water soluble drugs in soft gelatin or HPMC capsules for oral application (*e.g.* Cetirizine capsules) and for almost all parenteral formulations (*e.g.* Robaxin®, Ativan®). PEG with molar masses (M_n) exceeding 4,000 g mol^{-1} is found in hard shell capsules, which is related to the administered drugs and the required stability of the capsules during passage.[452] Another reason is that the solubility of most drugs in PEG drops significantly upon dilution with water (leading to re-precipitation of the drug). Therefore, also surfactants are often added, which reduce the risk of precipitation of the drug from the PEG solution (*e.g.* phosphadidylcholine or polysorbat 80). Other solubility enhancers are further added to increase the solubility of drugs in PEG. These are commonly used ionizing agents; for acidic compounds (*e.g.* ibuprofen or naproxen) bases are added and for basic compounds (*e.g.* thioridazin or ranitidine) acids. Furthermore, hydrophilic polymers (*e.g.* povidone or cellulose derivatives) are added for the same reason. Administration of capsules results in increased rates of absorption and faster achievement of maximum plasma concentration, as shown for instance for the Ibuprofen containing soft gel capsules Spalt-Liqua® compared to a standard tablet formulation.[453] PEG (*i.e.* PEG 1000 and PEG 540) serves as a formulation base for some suppositories to dissolve the active substance in order to allow enhanced bioavailability by facilitating effective and complete release of the active substance in the body. Rather high molar mass PEGs are used to coat suppositories, providing elasticity and lubricity.

Poloxamer. Poloxamers represent another important group in the field of polymer excipients, which are triblock amphiphilic copolymers of the structure PEG-*b*-PPG-*b*-PEG (also known as Pluronic® from BASF). They are used for drug delivery as formulation excipients. They act as surfactants, emulsifying agents, solubilizing agents, dispersing agents, and as *in vivo* absorbance enhancers. They are also used in topical dosage forms, rectal suppositories, for the modification of the surface of hydrophobic drugs,[454] for drug delivery,[455] as micelles and micellar drug formulations for gene delivery,[456] and as components in formulations for transdermal drug delivery.[457] Because of the different customized block-lengths in the copolymers various poloxamers exist. Due to their inertness, a few poloxamers are on the rather tight list of excipients that were officially approved by the European Pharmacopoeia as well as the U.S. Pharmacopoeia even for human parenteral administration acting as dispersing, emulsifying and coemulsifying excipient, as tablet lubricant or wetting agent.

Poly(vinyl pyrrolidone) (PVP). PVP, also known as "povidone", is used in the pharmaceutical industry as a synthetic polymer vehicle for dispersing and suspending drugs. It has multiple uses, including as a binder for tablets and capsules, a film former for ophthalmic solutions, to aid in flavoring liquids and chewable tablets, and as an adhesive for transdermal systems. In oral dosage forms it is also added as a wicking agent to facilitate the entry of water to the inner surface of the core of the tablet by the formation of channels. A wide range of vinyl pyrrolidone homopolymers (povidone k12 to k90) with different molar masses are also available from BASF under the name Kollidon®. The k number refers to the mean molar mass of the PVP. The polymers with higher k-values (*i.e.* k90) are not usually administered by injection since their high molar masses prevent excretion by the kidneys and lead to accumulation in the body. The best-known example of PVP formulations is povidone-iodine, an important disinfectant. "Crospovidones" (polyplasdones, polyvinylpolypyrrolidone) are synthetic, insoluble, cross-linked

homopolymers of *N*-vinyl-2-pyrrolidone. They are insoluble in water, though they still absorb water and swell very rapidly generating a swelling force. As a consequence, they are used as disintegrants and dissolution agents for solid oral dosage forms and are even effective for poorly soluble dosage forms. Such orally disintegrating tablets have emerged as one of the novel solid oral dosage forms with the potential to deliver a wide range of drug candidates.[458] Polyplasdone™ XL crospovidone (Ashland) is a commonly used polyplasdone.

Poly(vinyl alcohol). Poly(vinyl alcohol) (PVA) as a water-soluble synthetic polymer is used to increase viscosity in pharmaceuticals but also as a lubricant and protectant in ophthalmic preparations (known as "artificial tears").[459] PVA is often found in over-the-counter eye redness and eye lubricant drops (Liquifilm Tears). PVA is the lubricant, and works by providing moisture to the eye, which helps to relieve dryness and protects the eye from becoming more irritated sometimes in combination with, for instant, phenylephrine.

Table 26. Selected examples of synthetic polymers as matrix excipients.

TRADE NAME	POLYMER SYSTEM	PREDOMINANT DOSAGE FORMS USED IN …	FUNCTION IN DOSAGE FORMS AS MATRIX EXCIPIENT
Eudragit®	P(MAA-*co*-MMA)	Oral	Film former, tablet binder, tablet diluent
Carbomer/Carbopol™	PAA	Ophthalmic	Mucoadhesive , viscosity enhancer, thickening agent
Polycarbophil	Poly(acrylic acid) cross-linked with divinyl glycol	Oral, vaginal gels	Mucoadhesive
Dimethicone	PDMS	Oral	Antifoaming agent, emollient
Poly(ethylene glycol)	PEG	Oral, parenteral, rectal	Ointment base, plasticizer, solvent, suppository base, tablet and capsule lubricant, mucoadhesive, tablet binder, thickening agent
Poloxamer/Pluronic®	PEG-*b*-PPG-*b*-PEG	Parenteral	Dispersing agent, emulsifying and coemulsifying agent, solubilizing agent, tablet lubricant, wetting agent, non-ionic surfactant
Povidone	PVP	Oral, ophthalmic	Disintegrant, dissolution aid, suspending agent, tablet binder
Crosspovidone	Polyvinylpolypyrrolidone (highly cross-linked povidone)	Oral	Tablet disintegrant
Copolyvidone	P(VP-*co*-VAc)	Oral	Film-former, granulating agent, tablet binder
Poly(vinyl alcohol)	PVA	Ophthalmic	Viscosity enhancer, lubricant & protectant

3.5.1 Oral dosage forms

Oral drug delivery combines several advantages and is, as already described, the most frequently used route for introducing drugs into the body.[460] The drug absorption depends on different factors making this process a complex one. One important issue is the solubility of the API's in the GI fluids to enable oral absorption (see coating of solid oral dosage forms, Chapter 3.4.1). Indeed, more than 50% of potential new drug candidates are expected to be lipophilic and have poor aqueous solubility.[461] In recent years, polymeric excipients have been widely used to overcome low solubility and formulation difficulties. Furthermore, various new solid formulations have been developed using technologies that involve polymer excipients. Selected examples of commercial oral drug formulations containing different synthetic polymers as matrix excipients are summarized in Table 27. Further oral products containing PEGs are nicely summarized by Gullapalli *et al.*.[451a]

Table 27. Selected examples of oral drug formulations on the market containing different synthetic polymers as matrix excipients.

NAME	DRUG[a]	POLYMER SYSTEM	INDICATION/ USE	MANUFACTURER
Diethylpropion	Diethylpropion hydrochloride	Carbomer homopolymer type a	Treatment of obesity (anorexiant)	Lannett
Metformin	Metformin hydrochloride	Carbopol® 974P NF	Blood sugar control in people with type 2 diabetes	Aurobindo Pharma Limited
Alfuzosin	Alfuzosin hydrochloride	Carbomer homopolymer type b	Benign prostatic hyperplasia	Aurobindo Pharma Limited
Macrobid®	Nitrofurantoin	Carbomer 934[b]	Urinary tract infection	Norwich Pharmaceuticals
Striant®	Testosterone	Polycarbophil	Treatment of hypogonadism	Columbia Laboratories
Keflex®	Cephalexin	Dimethicone	Bacterial infection, skin or soft tissue infection, bladder infection, upper respiratory tract infection	Advancis Pharmaceutical
Antara®	Fenofibrate	Simethicone	Lowering high cholesterol & triglyceride levels in the blood	Lupin
Zarontin®	Ethosuximide	PEG 400[c]	Prevention and control of a certain type of seizure	Pfizer
Advil®	Ibuprofen	PEG 600	Pain relief for headaches, migraines & minor arthritis	Pfizer
Lybrel®	Ethinyl estradiol/ levonorgestrel	PEG 400, PEG 1450	Abnormal uterine bleeding, birth control, ovarian cysts, endometriosis, polycystic ovary syndrome	Wyeth
Augmentin™	Amoxicillin/clavulanic acid	PEG 4000, PEG 6000, dimethicone	Antibiotic (beta-lactamase inhibitors) for short term treatment of a wide range of infections caused by bacteria	GlaxoSmithKline
Lipofen®	Fenofibrate	PEG 8000, PEG 20000	Primary hypercholesterolemia, mixed dyslipidemia, severe hypertriglyceridemia	Cipher™
Maalox®	Aluminium & magnesium hydroxide/calcium carbonate	Simethicone	Acid indigestion, heartburn & sour stomach	Novartis
VapoSteam™	Camphor	PDMS, poloxamer 124[d]	Cold symptoms	Vick
Alprazolam	Alprazolam	Poloxamer 188 (Pluronic F 68)	Anxiety, panic disorder, depression, tinnitus, dysautonomia	TEVA
Accretropin™	Somatropin (recombinant human growth hormone (r-hGH))	Poloxamer 188 (Pluronic F 68)	Pediatric growth hormone deficiency, Turner syndrome	Cangene Corporation
Famciclovir	Famciclovir (guanosine analogue antiviral drug)	Poloxamer 407 (Pluronic F 127 NF)	Herpes zoster, herpes simplex	Apotex
Endocet®	Acetaminophen/oxycodone	Povidone	Chronic pain	Endo®
Naproxen	Naproxen	Povidone	Back pain, ankylosing spondylitis, sciatica, bursitis, tendonitis	TEVA
Cetirizine	Cetirizine hydrochloride	Povidone k29/32	Allergic rhinitis, urticaria	Northstar Rx LLC
Tinidazole	Tinidazole	Povidone k12	Bacterial vaginitis, trichomoniasis, giardiasis, amebiasis	Roxane Laboratories
Adenovirus vaccine		Plasdone C (PVP)	Adenovirus type 4 & type 7 vaccination	Barr Labs
Isoptin® SR	Verapamil hydrochloride	PEG, Povidone	Cluster headaches, migraine prevention, arrhythmia, high blood pressure	Ranbaxy Pharmaceuticals
Opana® ER	Oxymorphone	PVA, PEG	Narcotic analgesic	Endo®
BuPROPion	Bupropion hydrochloride	PVA, copovidone, povidone	SSRI induced sexual dysfunction, major depressive disorder, anxiety	Actavis

[a] All mentioned drugs are used in various drug formulations. However, in most cases they do not comprise a polymeric matrix excipient; [b] carbomer codes (*e.g.* 934) are an indication of molar mass and the specific components of the polymer; [c] PEG # (*e.g.* PEG 400) indicates the average molar mass of the specific PEG (*i.e.* 400 g mol^{-1}); [d] the first two digits code the molar mass of the PPG core, and the last digit codes the PEG content.

3.5.2 Parenteral dosage forms

Parenteral dosage forms describe all forms of administration avoiding any part of the gastrointestinal tract. The advantages of parenteral injection through the skin or other external boundary tissue are immediate systemic drug availability and rapid onset of action, as well as a long-term drug delivery by the formation of a depot or reservoir at the injection site. The sustained release of the drugs results from its long-acting property and its residence in the blood stream or the bone. However, the use of excipients for injectable drugs is more limited than for oral administration.[462] The application of novel excipients or the increase of their established concentration requires additional safety studies, which impedes the continuous progress of novel matrix excipients. Therefore, the well-established PEG is still the method of choice for polymeric excipients (Table 28).[451a] In comparison to compounds that are soluble and stable in a PEG vehicle (formulation as solution), insufficient solubility requires the formulation as suspension. Therefore, higher molar mass PEGs are used as suspending agents (viscosifying) to prevent setting of the dispersed material and to maintain homogeneity.

Table 28. Selected examples of parenteral drug formulations on the market containing PEG as matrix excipients.

TRADE NAME	DRUG	POLYMER SYSTEM	INDICATION/ USE	MANUFACTURER
		Solutions		
VePesid®	Etoposide	PEG 300[a]	Antineoplastic	Bristol-Myers Squib
Robaxin®	Methacarbamol	PEG 300	CNS depressant, musculoskeletal relaxant	Wyeth
Busulfex® (Myleran®)	Busulfan	PEG 400	Preparatory regimen prior to allogeneic hematopoietic progenitor stem cell transplantation	Otsuka Pharmaceutical
Ativan®	Lorazepam	PEG 400	Antianxiety, anticonvulsant	Biovail Laboratories
Persantine®	Dipyridamole	PEG 600	Coronary vasodilator	Boehringer Ingelheim (disc.)
		Extended-release suspensions		
Bioclate™	Antihemophilic factor VIII	PEG 3350	Prevention of bleeding episodes in persons with hemophilia A, control the bleeding related to surgery or dentistry in a person with hemophilia	Baxter Healthcare, Genetics Institute
Depo-Provera®	Medroxyprogesterone acetate	PEG 3350	Contraception	Pfizer
Depo-Medrol Lidocaine®	Methylprednisolone acetate, lidocaine	PEG 3350	Osteoarthritis, rheumatoid arthritis, acute & subacute bursitis	Pfizer
Aristocort® Forte	Triamcinolone	PEG 3350	Asthma, atopic dermatitis, drug hypersensitivity reactions	Sandoz
Invega Sustenna®	Paliperidone palmitate	PEG 4000	Schizophrenia	Janssen

[a] PEG # (*e.g.* PEG 300) indicates the average molar mass of the specific PEG (*i.e.* M_n = 300 g mol^{-1}).

3.5.3 Rectal, vaginal and urethral dosage forms

Suppositories. Suppositories are one type of solid dosage forms and can be administered rectal,[463] vaginal,[464] and to a much lesser extent, urethral. Although there are different suppository types, the systemic absorption is limited

to the rectal absorption, while the other two forms are mainly intended for local action. The rectal route is the method of choice if the oral dosage is not possible because of nausea, incapability of swallowing, or if the patient is unconscious. Different advantages and disadvantages of rectal administration have been nicely summarized by Vora and AliChisty.[463] The suppositories should melt or dissolve in the respective fluids in order to release the drug. Depending on the drug and the site of action different "suppository bases" are used, mainly fatty and oleaginous bases as well as water soluble and water miscible bases. Whereas the former ones are mostly derived from cocoa butter (also cottonseed oil, vegetable oils) the latter ones contain reasonable amounts of various PEGs of different molar masses (Table 29).[463] Certain PEG polymers may be used singly as suppository bases, but more commonly, formulas call for compounds of two or more molar masses mixed in various proportions as needed to yield a finished product of satisfactory hardness and dissolution time. Since the water miscible suppositories dissolve in body fluids and need not be formulated to melt at body temperature, they can be formulated with much higher melting points and thus may be safely stored at room temperature.

Table 29. Selected examples of suppositories on the market containing PEG as matrix excipients.

TRADE NAME	DRUG	POLYMER SYSTEM	INDICATION/ USE	MANUFACTURER
		Rectal		
THE MAGIC BULLET™	Bisacodyl	PEG	Relief of occasional constipation	Concepts in Confidence, USA
Acephen™	Acetaminophen	PEG 100 stearate[a]	Reduction of fever, relieve minor aches, pains & headache	G & W Laboratories
Indocin®	Indomethacin	PEG 3350,PEG 8000	Severe rheumatoid arthritis, ankylosing spondylitis, osteoarthritis, gouty arthritis	G & W Laboratories
Numorphan®	Oxymorphone	PEG 1000, PEG 3350	Relief of moderate to severe pain	Endo®
		Vaginal		
AVC	Sulfanilamide	PEG 400, PEG 3350	Treatment of Candida albicans infections	Monarch
Encare®	Nonoxynol-9	PEG	Contraception	Thompson Medical
Endometrin®	Progesterone	PVP	Help to become & stay pregnant	Ferring
		Urethral		
MUSE®	Alprostadil	PEG 1450, PEG 400	Treatment of erectile dysfunction (male)	Meda Pharmaceuticals

[a] PEG # (*e.g.* PEG 100) indicates the average molar mass of the specific PEG (*i.e.* M_n = 100 g mol^{-1}).

Gels. Gels have been established as useful dosage form for vaginal applications of different drugs endowed with moisturizing and lubrication effect, physiological pH restoring effect, as contraceptive, and as labor inducer.[465] They represent semi-solid systems comprising small amounts of solid, dispersed in a large volume of liquid. Gels show several advantages over other vaginal drug delivery systems such as higher bioavailability, safety, versatility, and economical savings.[466] Among the common natural derivatives (cellulose, chitosan etc.), PAA derivatives are mainly used as synthetic polymeric excipients (Table 30). Thanks to the high content in water, gels based on mucoadhesive polymers, without addition of drugs, are proposed for moisturization of the vagina in cases of vaginal dryness. Such Vaginal gels contain polycarbophil that forms the basis of well-consolidated marketed products (*e.g.* Replens®, Miphil®).[467]

Table 30. Selected examples of vaginal gels on the market containing different synthetic polymers as matrix excipients.

TRADE NAME	DRUG	POLYMER SYSTEM	INDICATION/ USE	MANUFACTURER
Zidoval®	Metronidazole	Carbomer 974P[a]	Bacterial vaginosis	Meda Pharmaceuticals
Metrogel®	Metronidazole	Carbomer 934P	Inflammatory papules & pustules of rosacea	Galderma
Replens®		Polycarbophil	Vaginal dryness	Church & Dwight
RepHresh® (Miphil®)		Polycarbophil	Vaginal dryness, bacterial vaginosis	Sanol
Advantage S	Nonoxynol-9	Carbomer 934P, polycarbophil	Contraception	Columbia Laboratories
Crinone®	Progesterone	Carbomer 934P, polycarbophil	Infertile women with progesterone deficiency, secondary amenorrhea	Watson
Conceptrol®	Nonoxynol-9	Povidone	Contraception	Revive

[a] Carbomer codes (*e.g.* 974P) are an indication of molar mass and the specific components of the polymer.

3.5.4 Ophthalmic dosage forms

Typically, gels with high water content but with certain viscosity are applied in ophthalmic drug formulations. To impart a high viscosity and a water content > 90%, in particular carbomers/carbopols™[468] and poloxamers[469] are used (Table 31). The polymers have to prolong the contact time on the ocular surface and to slow down the drug elimination. Eye drops represent an alternative dosage form to achieve therapeutic concentrations of drugs in ocular tissues. Thereby, the topical administration is effective for molecules with poor ocular uptake or poor efficacy-to-safety ratio when given systematically. The poor bioavailability and therapeutic response exhibited by conventional ophthalmic solutions due to pre-corneal elimination of the drug may be overcome by the use of *in situ* gel forming systems. *In situ* gelling systems increase the viscosity by changing the pH value or temperature in the pre-corneal region and lead to an increase of drug bioavailability by slowing drainage. Poloxamers possess thermal gelling properties and are frequently included in ophthalmic formulations to improve the ocular bioavailability of drugs by increasing the viscosity.[470] Future prospects are the delivery of peptides and proteins with the help of stimuli-responsive polymers.[471]

Table 31. Selected examples of ophthalmic drug formulations on the market containing different synthetic polymers as matrix excipients.

TRADE NAME	DRUG	POLYMER SYSTEM	DOSAGE FORM	INDICATION/ USE	MANUFACTURER
Pilopine HS®	Pilocarpine hydrochloride	Carbopol 940	Gel	Control intraocular pressure	Alcon Laboratories
Zirgan®	Ganciclovir	Carbomer	Gel	Acute herpetic keratitis (dendritic ulcers)	Bausch & Lomb
RESTASIS®	Cyclosporine	Carbomer copolymer type A	Emulsion	Chronic dry eye	Allergan
AzaSite®	Azithromycin	Poloxamer 407/ polycarbophil (DuraSite®)	Solution	Bacterial conjunctivitis	Akorn
ALREX®	loteprednol etabonate	Povidone	Suspension	Seasonal allergic conjunctivitis	Bausch & Lomb
Refresh Redness Relief®	Phenylephrine hydrochloride	PVA	Solution	Eye redness & dryness	Allergan

3.6 Polymeric drugs

Polymers that act as pharmaceutically active ingredients are relatively rare. Besides several attempts already in the 1960s, poly(ethylene sulfonate) and poly(maleic anhydride-*co*-divinylether) (DIVEMA) were studied for their effects, *e.g.* as anti-tumor agents, but failed due to toxicity issues. The pharmaceutical industry remarked strong doubts that a polymer can be a therapeutic agent in diseases where small molecules failed.[472] Major concerns were the presumably high dispersity (Đ) and the structural heterogeneity, in particular with regard to regulatory issues. However, in the last years a new market grew up with polymeric drugs that are approved and have defined and well-characterized structural features. The polymer characteristics but also the administration routes strongly influence the therapeutic effect of the polymeric drugs.

Polymeric sequestrants. One field of application is the removal of detrimental species from the gastrointestinal (GI) tract in a selective manner. Such polymeric sequestrants work as therapeutic agents and are able to bind and subsequently eliminate harmful species that were either ingested or produced by the human body itself. These polymers are usually ion exchange resins in the form of hydrogels that are not adsorbed by the GI tract. For the treatment of hyperkalemia (*i.e.* high levels of potassium ions in the serum, which can cause abnormal heart rhythms and other health problems), a sodium polystyrene sulfonate (Kayexalate®) is used as cation-exchange resin since decades (Table 32).[473] However, the high levels on resulting sodium may cause other critical effects.[474] Recently, Valtessa® was approved as a new medication to treat hyperkalemia.[475] This cross-linked polymer based on calcium 2-fluoroprop-2-enoate, divinylbenzene and octa-1,7-diene (also named patiromer) with a calcium-sorbitol counterion is established as a formulation of 100 µm beads.

Patients suffering from chronic or end-stage renal diseases often have elevated serum phosphate concentrations (hyperphosphatemia) that can be treated with sevelamer hydrochloride marketed under the brand name Renagel®, which is a poly(allylamine) cross-linked with epichlorohydrin (Figure 24).[476] Comparing to this, Renvela®, a sevelamer carbonate, shows fewer side effects. Bile acid sequestrants are one strategy in the treatment of elevated cholesterol levels. Cholestyramine (quarternized ammonium groups attached to poly(styrene-co-divinylbenzene)) and colestipol (copolymer of diethylenetriamine and epichlorohydrin) are polymeric therapeutics that bind bile acid, which is necessary for the production of cholesterol in the liver, but both therapeutics lack on low clinical efficiency.[477] Besides diverse other amine containing cross-linked polymers that entered clinical trials, Colestilan (poly(2-methylimidazol-*co*-(chlormethyl)oxiran) and Colesevelam hydrochloride (poly(allylamine) with 1-chloro-2,3-epoxypropane, (6-(allylamino)-hexyl)trimethylammonium chloride and *N*-allyldecylamine) are already on the market and show better performances as bile acid sequestrants for the treatment of hypercholesterolemia.[478] Micronized crospovidone can be used in the treatment of diarrhea based on its ability to form complexes with toxins.[164b]

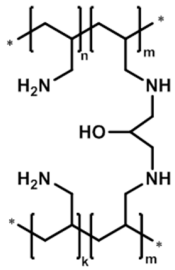

Figure 24. Schematic representation of the chemical structure for sevelamer, a poly(allylamine) cross-linked with epichlorohydrin (hydrochloride: Renagel®, carbonate: Renvela®).

For binding and removing toxins, originating *e.g.* from bacteria, such ion exchange resins are not efficient enough. More specific binding sides are necessary to reach multivalency. Tolevamer®, a high molar mass poly(styrene sulfonic acid), is such a toxin binder that is used to treat diarrhea.[479] However, this alternative to antibiotics failed in final clinical trials. The concept of multivalency is also used in research for the treatment of viruses, but none of them did reach the market yet. For example, specific peptides, that are conjugated to different polymer backbones, are able to protect cells from the anthrax toxin action.[480] A linear poly(acrylamide) bearing the C-glycoside of sialic acid shows antiviral activity against the influenza virus.[481] As preventional medicine for HIV infections, a naphthalene sulfonate polymer (PRO-2000®) was developed but also

failed in clinical phase studies.[482] The development of fat binding hydrogel-like polymers for the treatment of human obesity is also a growing area of research. Such polymers should inhibit fat hydrolysis and absorb unhydrolyzed fat droplets. They are based on *e.g.* poly(acrylamide)s, poly(meth)acrylates and other polymers that contain both cationic and hydrophobic moieties.[483] An even higher efficiency is aimed by additional conjugation of a lipase inhibitor to the polymer backbone (GT 389-255).[484]
Dimethicone (PDMS) and Espumisan® (dimethicone compounded with 4 to 7% silicone dioxide) are used as active pharmaceutical ingredients (API) in medicinal products such as chewable tablets, granulations, tablets, capsules, suspensions and drops.[485] These polymers are used in gastroenterology to relieve flatulence, tension in stomach, bowel colic and gastric ulceration due to their anti-foaming and anti-flatulent properties.[486] Moreover, simethicone can be used prior to upper GI endoscopy to reduce the amount of air bubbles and foam.[487] This increases the visibility during the procedure and provides the possibility of more accurate evaluation of the mucosa and consequently decreases the endoscopy duration.

Synthetic analogues of antigens. There are basically only very few polymeric drugs that are not related to sequestration of small molecules. They act as synthetic analogues of specific disease-associated antigens for systemic therapy. The first developed drug as such is glatiramer acetate (also known and marketed as Copaxone®). Glatiramer acetate is a copolymer of four L-amino acids (alanine, lysine, glutamic acid, and tyrosine in a molar ratio of 4.2 : 3.4 : 1.4 : 1.0) that are randomly copolymerized in a ring-opening polymerization of the corresponding amino acid anhydrides.[488] Glatiramer acetate acts *via* immunomodulation of pathways involved in the pathogenesis of multiple sclerosis. However, the complete mode of action is not yet fully understood. Patients suffering from multiple sclerosis demonstrate a significant decrease in the number of relapses and rate of progression when treated with glatiramer acetate. A recent study also shows a reduction of symptoms in patients with the Rett syndrome.[489] There was also a clinical trial where age-related macular degeneration could successfully be treated with glatiramer acetate.[490] The most recent research goes to other poly(amino acid) combinations that might also show a high potential as drugs for modulating immune responses.[491]

Miscellaneous polymeric drugs. Another polymeric drug is the commonly used highly purified non-ionic surfactant poloxamer 188, a block copolymer consisting of PEG-*b*-PPG-*b*-PEG (Pluronic® F-68). It is used in treating sickle cell disease to reduce inflammation and pain.[492] Clinical trials showed rheologic, cytoprotective, anti-adhesive and antithrombotic effects that help to reduce the overall duration of painful episodes of patients suffering from the sickle cell disease. The trials passed phase III (NCT00004408) but the drug (Flocor®) did not come to the market yet. An innovative approach is the PolyHeal™ technology, using negatively charged microspheres (~ 5 µm). They consist of nonbiodegradable, medical grade polystyrene (PS) in a suspension of serum-free nutrient medium. Cells and macromolecules are able to attach to the surface of the microspheres and to participate in the wound healing process. Further polymer-based wound healing dressings have been nicely summarized by Ghadi *et al.*.[493]

Table 32. Selected examples of polymeric drugs on the market.

TRADE NAME	POLYMER SYSTEM	INDICATION/USE	MANUFACTURER
Kayexalate®	Cross-linked sodium poly(styrene sulfonate)	Hyperkalemia	Sanofi
Valtessa®	Cross-linked calcium 2-fluoroprop-2-enoate, divinylbenzene, octa-1,7-diene (patiromer)	Hyperkalemia	Relypsa
Renagel®	Cross-linked poly(allylamine) (sevelamer hydrochloride)	Hyperphosphatemia	Sanofi (Genzyme)

Renvela®	Cross-linked poly(allylamine) (sevelamer carbonate)	Hyperphosphatemia	Sanofi (Genzyme)
BindRen® (Colestilan)	Cross-linked poly(2-methylimidazol-*co*-(chlormethyl)oxiran)	Hypercholesterolemia	Mitsubishi Tanabe Pharma
Welchol®, Cholestagel® (Colesevelam)	Cross-linked poly(allylamine)	Hypercholesterolemia	Sanofi (Genzyme)
Espumisan®	PDMS (simethicone)	Flatulence	Berlin-Chemie
Copaxone®	Glatiramer acetate	Multiple sclerosis	TEVA
PolyHeal™	PS	Wound healing	TEVA

4. Future prospects and concluding remarks

Besides the previously described systems on the market or in clinical trials, a large variety of polymer-based materials are currently under preclinical investigations, and these materials show immense potential concerning drug delivery applications. In the following chapter, we highlight a few exemplarily chosen systems used for pharmaceutical applications, which in our opinion hold an enormous potential and will certainly be in forthcoming clinical studies.

Polymer-drug conjugates. Although polymer-drug conjugates are under investigation for several decades now, the research interest in this field is still unabated. PEGylation has certainly dominated the area so far, but increasing concerns about its immunogenicity have promoted the development of new polymers and their conjugates. Some of these materials already reached the stage of clinical testing (conjugates of poly(*N*-(2-hydroxypropyl)methacrylamide (PHPMA), poly(2-oxazoline) (POx), see Chapter 3.1.2), and based on their performance more conjugates are currently in preclinical studies. The latest investigations, however, focused on the development of biodegradable polymers such as polyphosphoesters to substitute the nondegradable PEG. In the following some of the most promising systems are described.

Nondegradable polymers for drug conjugates. Among the vinyl based materials prepared by radical polymerizations PHPMA had certainly the highest impact on the area of polymer-drug conjugates. Due to the good compatibility and shielding capacity it is no surprise that more studies are ongoing. Besides the previously described drug conjugations, PHPMA has, *e.g.*, successfully been conjugated to NPC1161 (8-[(4-amino-1-methylbutyl) amino]-5-[3,4-dichlorophenoxy]-6-methoxy-4-methylquinoline), an 8-aminoquinoline analog with anti-leishmanial activity, and already passed successfully preclinical studies (*in vivo*).[494] In combination with *N*-acetylmannosamine (ManN) in the side chains, this polymer conjugate represents a promising candidate for clinical studies with reduced toxicity and increased efficiency of anti-leishmanial drugs for the treatment of visceral leishmaniasis. Mannose-grafted systems allow a selective delivery of anti-leishmanial drugs and a maximization of the potential of the drug to destroy the parasite at the site where it resides by mimicking the invasion process (mannose-dependent receptor-mediated endocytosis).
Further candidates based on vinyl polymers, which are close to be tested in clinical studies, rely on established systems, such as the Dynamic PolyConjugate (DPC) products: ARC-F12 (thrombosis, angioedema, inhibits the production of factor 12), ARC-LPA (cardiovascular diseases, reduces the production of apolipoprotein A), and ARC-HIF2 (clear cell renal cell carcinoma, first candidate to target tissue outside of the liver).[495]

During the last two decades, the class of POx has gained increasing attention for biomedical and drug delivery applications. Besides the already mentioned first POx conjugate (SER-214) under clinical investigations, several studies deal with the conjugation to drugs or proteins. The first report on a protein coupled to POx was published in 1990 by Miyamata *et al.*.[496] Preparing POx with a carboxylic acid as end-group allowed to attach the polymer to amine groups of the protein (lysine groups) using DCC/NHS chemistry. Other publications also show the increasing thermal stability,[497] as well as a decreasing rate of aggregation[498] using POx ligated proteins. The coupling of carboxy functionalized POx using NHS chemistry is the most common reaction for protein conjugation,[499] alongside using pyromelitic anhydride,[500] CuAAc,[501] reductive amination,[499b] native chemical ligation,[502] or the direct reaction of a protein with the living chain end of the polymerization.[503] Luxenhofer *et al.* recently summarized poly(2-oxazoline) drug and protein conjugates in different stages of their preclinical investigations.[113b] An interesting feature of POx is the versatility of the various types of oxazolines allowing to alter the properties and functionalities of the resulting polymers. For example, it was demonstrated that the cellular uptake can be influenced by the choice of the oxazoline monomer and architecture[499a, 503] and *in vivo* investigations showed a low immune response, as well as an increased circulation of POxylated proteins.[504] Besides these protein conjugates, POx was also conjugated to small molecule drugs in order to alter their pharmacokinetics. The anticancer drug Ara-C[498] as well as the antibiotic ciprofloxacin[505] showed similar behavior when conjugated to PEtOx as comparable PEG conjugates. In summary, it seems that in terms of biocompatibility and pharmacokinetic POxylation and PEGylation have very similar effects,[506] however, from a synthetic point of view the properties of POx can be altered with relative ease compared to PEG, just by changing the type of monomer used rendering POx a highly versatile tool.

A further alternative are zwitterionic polymers, that are mainly represented by polycarboxybetaine, polysulfobetaine and poly(methacryloyloxyethyl phosphorylcholine) (Figure 25). They are postulated to partially substitute the current benchmark polymer for protein conjugates, PEG, and to take a key role in the future of protein therapeutics.[507] These polymers are able to maintain the stability of proteins without diminishing their binding affinity, which represents a major improvement over the current PEGylation technique. An interesting example for this class of polymers is the hyperbranched copolymer poly(3-ethyl-3-(hydroxymethyl)oxetane)-*co*-(carboxybetaine) which is used as a biomimetic material in drug delivery carriers.[508] Another promising candidate is poly(carboxybetaine methacrylate) that was modified with the charged drug DOX.[509] The resulting conjugate features a low cytotoxicity, prolonged circulation time and a controlled release of DOX under mild acid conditions. Studies on tumor-bearing mice showed a tumor-inhibition rate of 55% without resulting in any body weight loss which usually accompanies this treatment. As previously mentioned, zwitterionic polymers are very promising materials to maintain the bioactivity of proteins. In this context, Chen and co-workers synthesized a zwitterionic block copolymer poly(methyl acrylic acid-*b*-sulfobetaine methacrylate) to modify a protein drug (uricase).[510] They demonstrated that the stability of the enzyme is improved without causing any destructive effects on its bioactivity by the conjugation of a zwitterionic copolymer with a short poly(methyl acrylic acid) block.

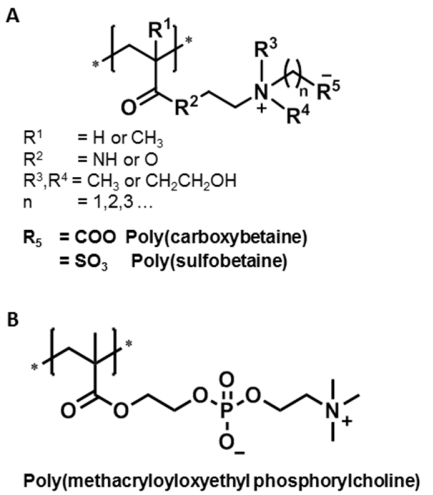

Figure 25. Schematic representation of the chemical structures of zwitterionic polymers: A) Poly(carboxybetaine) (R_5 = COO^-) and poly(sulfobetaine) (R_5 SO_3^-); B) poly(methacryloyloxyethyl phosphorylcholine).

Degradable polymers for drug conjugates. Undoubtedly, the degradability in biological relevant environment or at least the possibility for excretion of the applied polymers is a key aspect for their application in drug delivery. As a consequence, the nondegradable nature of many polymer conjugates using PEG or PHPMA has certainly hindered their progression towards market approval, although many of them have progressed into clinical development. Despite the efficiency of these materials, the safety of their administration is of utmost importance, and therefore it would not be surprising, if biodegradable polymer conjugates will have a much higher probability of clinical success.

Polyphosphoesters (PPE) represent a promising class of polymers which is not only biocompatible, but also degradable under physiological conditions. These alternatives have already been proposed as PEG substitutes in polymeric prodrugs.[130, 132d, 511] The simple and versatile adjustment of the hydrophobicity and polyvalence by attachment of different pendant ester groups of the variation of the backbone in PPEs allows the formation of fully biodegradable polymer-drug or -protein conjugates ("PPEylation"[512]) as well as the encapsulation of different drugs (*e.g.* low-molar-mass drugs, proteins, DNA, and plasmids) depending on the functionalities of the polymers. Recently, Zhang *et al.* presented a novel drug system containing ultra-high levels of drug loading *via* covalent attachment.[513] In this case, PEG-*b*-PPE-based paclitaxel (TXL) drug conjugates were synthesized by organocatalyst-promoted ring-opening polymerization (ROP) followed by click-reaction-based conjugation of PTX to the PPE block of the copolymer. The resulting amphiphilic polymer forms micelles with a loading capacity of 65 wt% of PTX and demonstrated to be effective against several cancer cell lines. In another study, dual pH-sensitive nanoparticles (PPC-Hyd-DOX-DA) have been designed, which are able to reverse their surface charges when exposed to tumor tissue to facilitate cell uptake.[514]

Polymers based on repeating ester units are another potential biodegradable class of polymers which is intensively investigated for polymer-drug conjugate approaches and also possesses a wide range of functionalities and properties.[515] Among them, polycarbonates have recently received much attention for protein/peptide conjugation.[516] Hedrick and co-workers demonstrated the synthesis of functional polycarbonates by ROP starting from the monomer pentafluorophenyl 5-methyl-2-oxo-1,3-dioxane-5-carboxylate (MTC-OC_6F_5, Figure 26). The active pentafluorophenyl esters enable a substitution with suitable nucleophiles such as alcohols and amines and, thus, the functionalization with other active groups.[517] The versatility of this approach was demonstrated by the preparation of numerous functional polycarbonates, which are of particular relevance to polymer-drug conjugates, including polycarbonates with PEG,[516] hydroxyl-containing[518] and zwitterionic side-chains.[519] Recently, Cheng *et al.* reported an *in vivo* efficacy for the first example of a polymeric therapeutic based on polycarbonates for the treatment of systemic methicillin-resistant *Staphylococcus aureus* (MRSA) infection. Other novel functional nanocarriers for biomedical applications have been extensively reviewed by numerous research groups, highlighting these polycarbonate-based degradable alternatives to PEG with minimal toxicity.[518, 520]

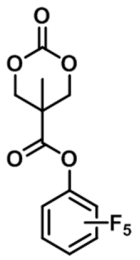

Figure 26. Schematic representation of the chemical structure of pentafluorophenyl 5-methyl-2-oxo-1,3-dioxane-5-carboxylate (MTC-OC_6F_5).

Micro- and nanoparticulate drug carriers. Although polymer-drug conjugates have certainly made a huge impact in the research area of synthetic pharmapolymers, great promises have been expected from particulate drug carrier systems. The versatility and diversity of potential materials used for their preparation allows a flexible design with tailor made properties, which has certainly resulted in the success of various systems in clinical trials or on the market. However, several issues still have to be addressed and the potential of these systems has by far not been fully exploited. The transfer of degradability to nondegradable polymers often represents a missing link between the design of advanced materials and their use in biomedical applications. To fulfill the criteria of degradability

appropriate units have to be integrated into the main chain during the synthesis. Another big issue in the application of particles, in particular microparticles, for drug delivery is the initial burst release.[521] This problem can be overcome by choosing the optimal conditions for the formulation processing or by changing the properties of the drug or the polymer itself to prevent polymer-drug separation. Doubtless, the main challenge is the targeted delivery that is necessary for cancer and some other diseases to perform better than conventional medications. An analysis of over 100 cancer studies has shown that in the average only 0.7% of injected particles reach their targets.[522] And what is more surprising, this number did not change within the last 10 years. Reasons for this are the increased immunogenicity and plasma protein adsorption *in vivo*, which masks the targeting molecules and also results in decreased blood circulation times.[301] Consequently, targeted nanoparticles behave with the same or less efficacy than untargeted particles. Even the often studied EPR effect only yielded poor delivery efficiency and shows the lack of 'proof-of-concept' studies to be translated to patient care.[522] A better understanding of the *in vivo* nanoparticle transport is necessary and can be accomplished by quantitative analysis with subsequent collection of all the information in databases including organization and interpretation of the data also with the help of computational tools. Such open excess databases are already established and supported by several programs (*e.g.* DaNa2.0[523] and Cancer Nanomedicine Repository[524]). Only a translation from research to the patient might stimulate the application of nanotechnology for treating human diseases as promised.

Solid colloidal dispersions. One strategy is the use of copolymers of PLGA and PEG making the particles more hydrophilic and in consequence more suitable for protein delivery.[525] The hydrophilic domains facilitate a slow and controlled release by diffusion. Further improvements on the release profiles and an additional increase in the loading capacity could be achieved by a triblock copolymer system consisting of PLGA, PEG and poly(allyl glycidyl ether); the latter can also be used to conjugate targeting ligands.[526] Several other systems based on these classic release mechanisms of drugs (diffusion through water filled pores, diffusion through the polymer matrix, osmotic pumping, and erosion) encapsulated in polymeric nano- and microparticles are currently still under intensive investigation in *in vitro*, *in vivo* and preclinical studies.[527] However, besides these systems rapid progress has been made in the development of stimuli-responsive nano- and microparticles as smart alternatives within the last years.[528] In this case, the release can be triggered by internal (coming from the cells/tissue itself) or external (coming from outside) stimuli. Such triggers can for example be temperature, light, ultrasound, pH-value, redox environment, or specific biomolecules and enzymes.[528] The development of more efficient targeting structures may further improve the efficiency of nano-/microparticles. For example, particles carrying siRNA and targeting molecules are able to simultaneously attack numerous pathways.[529] The given examples display only a small fraction of the numerous systems in development. The wide field of polymeric materials with countless variations in constitution, conformation, configuration, and molar mass will definitely yield nano- and microparticles that have the potential to show efficacy beyond the current products in clinical stages and on the market. However, a translation from bench to bedside is more cost- and time efficient if the polymeric material is already used in pharmaceutical products.[308] An interesting study shows the beneficial properties of doxorubicin (DOX) loaded PLGA microparticles that could be used in transarterial chemoembolization (TACE) instead of recently developed PLGA based microgels.[530] Such PLGA microparticles allow a re-entry into the tumor feeding arteries after an initial TACE trial combined with higher drug release rates. A further important step is the development of a robust and scalable process for the fabrication of micro-/nanoparticles with reproducible quality and the subsequent GMP (good manufacturing practice) production in kilogram quantities.

An interesting alternative to PLGA is poly(caprolactone) (PCL), which has a slower degradation rate than PLGA (up to one year), a high permeability for the diffusion of small molecules and does not generate an acidic environment after degradation often causing the destabilization of proteins.[531] Up to now, PCL is most commonly used in tissue engineering. Its use as therapeutic molecule delivery system is still limited since PCL carriers reveal in many cases low encapsulation efficiency, burst release and low bioactivity. In contrast, besides its beneficial slow

degradation rate, PCL is a rubbery at room temperature, which allows high permeability for many drugs. In recent years, PCL-materials have been intensively investigated in *in vitro* and *in vivo* biocompatibility and efficiency studies in order to deliver drugs, genetic materials and proteins. They have been nicely reviewed by Venkatraman and co-workers.[532] One example is the encapsulation of chloramphenicol in PCL-Pluronic® composite nanoparticles (CAM-PCL-NP). These systems exhibited significantly enhanced anti-MRSA (*methicillin-resistant Staphylococcus aureus*) activity against ten clinical isolates of MRSA strains. Compared to free-chloramphenicol treatment, the *in vivo* study of CAM-PCL-NPs in MRSA-infected burn-wound mice models revealed quicker efficiency in MRSA clearance and an improved survival rate.[533] Preclinical studies of a further formulation named NC-6300 show promising results in mice and are now under way for clinical studies in Japan.[534] In NC-6300, epirubicin is attached *via* an acide-labile hydrazone bond to PEG-PAs, which can be beneficial due to a better controlled release kinetic. Further attempts are also in the development of targeted drug delivery systems, which was already shown, *e.g.* by attaching several anti-TF antibodies resulting in an enhanced antitumor activity against TF-high expressing human pancreatic cancer cells, a subunit toolbox with insensibly large possible combinatorial combinations of desired bio-functionality and evolutionary optimization techniques.[535]

Polyplexes. Cationic polymers have already been bloomed over years as non-viral vectors in gene therapy. They show tremendous potential in treating different types of cancer and genetic disorders without using conventional drugs. One approach is to develop alternative gene delivery platforms by creating higher ordered macromolecular structures such as multi-component supramolecules or 2D and 3D scaffolds.[536] Another approach is to enhance existing vector platforms (*e.g.* by functionalization). For instant, the successful clinical application of the gold standard poly(ethylene imine) (PEI) for gene delivery depends mainly on three factors: I) The enhancement of the transfection efficiency; II) the reduction of toxicity, and, III) the ability of the vectors to overcome numerous biological barriers after systemic or local administration. Current research is focusing on the design of biodegradable[537] and more biocompatible derivatives[538] by modifying the PEI backbone. Very recently, our group introduced a new generation of linear PEI (3rd generation, Figure 27) bearing multiple functional groups comprising cationic functionalities, cell viability increasing functional groups as well as a third group of functionalities which can be used, *e.g.*, for targeting molecules.[38] One promising opportunity is the conjugation of glutathione moieties to the cationic backbone which enables the transport of genetic materials and, simultaneously, the passage through an hCMEC/D3 endothelial cell layer mimicking the highly selective blood-brain barrier (BBB) within a microfluidically perfused biochip.[539] Cationic methacrylate copolymers are another upcoming polymer platform able to interact with genetic material. Poly(2-dimethylaminoethyl methacrylate) (PDMAEMA) has shown promising gene transfection activity due to its cationic character.[540] Jiang and co-workers synthesized PEGylated PDMAEMA/DNA polyplexes for efficient brain-targeted gene delivery in mice. As mentioned for phosphates, inorganic safe materials will add an important basis for composites with synergistic functions.[541]

Figure 27. Schematic representation of the general chemical structure for the 3rd generation LPEI which describes the presence of multiple functional units comprising cationic functionalities (blue), cell viability increasing functional groups (black) as well as further functionalities (orange, *e.g.* targeting molecules).

Microgels. The importance of degradability has also been recognized for the design of carrier gels and, in particular, micro- and nanosized structures. One quite established example is a PEG microgel, which contains degradable PLGA sequences. Injecting them into the cavity of sheep shoulder joint, the new PEG-hydrogel microspheres were compared to nondegradable microgels with regard to location, degradation and inflammation.[542] The degradable microgel offers several advantages over the nondegradable material considering drug delivery in synovial tissue as it reduces the intensity of inflammatory reactions triggered in synovium. An interesting strategy for the continuous *in vivo* expression of a protein is the direct delivery of an *ex vivo* modified

cell encapsulated in a gel structure to shield it from the immune system. Sonnet *et al.* have developed a PEG-diacrylate (PEGDA) microgel with allogeneic carrier cells transduced with an adenovirus expressing BMP2 for bone regeneration.[543] The PEGylated microsphere system shields the cell and, thus, suppresses the destructive inflammatory processes. Within 3 weeks, a 5 mm long femur defect in a rat model was healed completely through secretion of 100-fold lower levels of protein compared to similar studies using recombinant protein. For the future, this class of injectables opens the macroscopic functional embodiment space staying close to a minimal invasive paradigm replacing larger drug eluting devices.

Nanogels. Besides the already discussed Medusa® technology (Chapter 3.2.3), the only nanogel examples that have been evaluated under clinical trials are based on a polysaccharide structure, *e.g.* cholesterol-bearing pullulan (CHP) network,[544] which are described elsewhere.[545] However, researchers still consider tailored nanogel systems as a very promising platform for drug delivery applications.[546] Recent successful studies prove the efficiency of nanogels by targeting multiple immune cell subsets in the draining lymph nodes.[547] In contrast to other gel materials, these systems are fabricated by the synthesis of mesoporous silica (MS) particles (200 nm) as templates and subsequent infiltration with pyridine dithioethylamine (PDA) modified poly(methacrylic acid) (PMAA-PDA). The infiltration of cysteamine (SH) modified PMAA (PMAASH) leads to a cross-linking by disulfide exchange followed by template removal. Further PEGylation of these PMAA nanogels did not affect their cellular association *in vitro*, but improved their lymphatic drainage *in vivo* (mice).
Similar to other nanoparticulate systems, the integration of stimuli responsive polymers promises access to carriers with local control of the cargo release. Recently, a new type of dual-responsive nanogel with tunable volume phase transition temperature and redox-labile properties was investigated.[548] The nanogel system is constructed from a copolymer based on vinylcaprolactam (VCL) and HPMA cross-linked with *N*,*N*'-*bis*(acryloyl)cystamine (P(VCL-s-s-HPMA)). The hydrophilicity of the nanogel allows a stable blood circulation at 37 °C. A higher temperature of the tumor tissue forces the nanogel to turn into a hydrophobic state which enhances its cell uptake. Upon the entrance into the tumor cells, a redox-triggered degradation of the nanogel (due to the presence of disulfide bonds) leads to a burst drug release. *In vivo* studies (A549 tumor-bearing mice) revealed that these nanogels can significantly limit the tumor growth with no side effects to normal tissues. These results underline the immense potential of the dual-responsive biodegradable nanogels for cancer therapy. Many other nanogel systems have been investigated *in vivo* based on polymers such as PMAA (drugs: DOX/TXL[549]), PEG (siRNA[550]), PEI (AZT 5'-triphosphate[551]), PEG-*b*-PGluA (17-AAG/DOX[552]; cisplatin/TXL[553]) and $PMEO_3MA$-*b*-PPFPMA (siRNA[554]). Considering the ongoing effort for the development of such carrier systems, we are certain that first nanogel materials will soon enter clinical trials.

Macroscopic drug carriers. They probably represent the most versatile application forms of pharmapolymers comprising the wide range of hydrogels and solid implants and inserts. The general trend is towards the creation of multiple functional systems. In our opinion, in particular the application of hydrogel systems will change significantly. Sensor and conditional release/activity can be established and are already shown for vaccination on animal trial stage.[555]

Hydrogels. The most common application form for hydrogels is certainly their use in contact lenses, but surprisingly they are not used as drug delivery vehicles so far, which is probably related to the loss of lens quality accompanied with the release. The recent development of new techniques to design contact lenses enables an extended drug release over a few weeks without any significant impact on the lens properties. Compared to alternative eye drops, these contact lenses revealed safety, efficacy and increased bioavailability in *in vivo* studies.[556] Corresponding contact lenses, placed on the cornea, release drugs into the post-lens (between lens and cornea) and reveal a prolonged contact time with the cornea.[557] The increased efficiency (35× higher than delivery with drops[558]) allows the delivery of drugs over extended time periods (which eliminates the need for multiple

dosing) while decreasing side effects since less drug amount is needed. Further ocular applications are the development of hydrogels based on poly(2-hydroxyethyl methacrylate) (PHEMA)[559] or poly(dimethyl siloxane) (PDMS),[560] which may serve as drug delivery agents for the anterior segment of the eye. The latter is also used for punctual plugs releasing cyclosporine A for a period of 3 months.[561] In the last years, immense effort has been put into the development of devices for ocular drug delivery,[562] and we are convinced that suitable systems will enter the market soon.

A real innovation is the non-hormonal contraceptive "Reversible inhibition of sperm under guidance" (RISUG®, Figure 28) for men developed by Guha and co-workers based on poly(styrene-*co*-maleic anhydride).[563] It represents a long acting and reversible alternative to a vasectomy as the polymer can be flushed with another injection of a dissolver.[564] It has been patented in several countries including India, China and the United States. While clinical phase III is already ongoing in India,[565] the Parsemus Foundation began to develop a similar polymer contraceptive inspired by RISUG® for the rest of the world in 2010 (Vasalgel™).[566] After one year of successful *in vivo* studies, they recently announced the start of first clinical trials in the second half of 2017 and a commercial launch in 2018.[567]

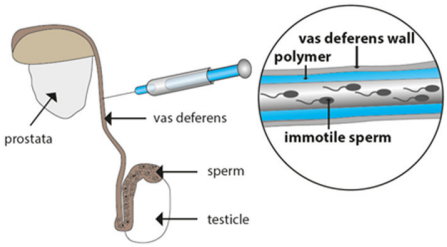

Figure 28. The work principle of "Reversible inhibition of sperm under guidance" (RISUG®): A) The hydrogel is injected into the vas deferens connected to each testicle; B) it coats the wall of the vas deferens. When sperm gets into contact with the wall it becomes unable to swim.

Besides the classic hydrogels, the development of so-called interpenetrating polymer networks (IPN) has expended enormously in the field of controlled release and targeted drug delivery in the last decades.[568] Introduced in 1960 by Miller,[569] IPN's are defined as "polymers comprising two or more networks which are at least partially interlaced on a molecular scale but not covalently bonded to each other and cannot be separated unless chemical bonds are broken" (IUPAC[570]). They represent a subgroup of physical gels. The blending of natural and/or synthetic polymers opens the field for the design of new controlled release systems for a variety of drugs and broadens the range of their properties.[571] IPNs reveal several advantages like an excellent swelling behavior, improved responsiveness and mechanical strength, which play an important role in drug delivery systems and differentiate them from single networks (such as hydrogels). Even if *in vitro* and *in vivo* data have been extensively studied and reviewed,[568, 571-572] and the number of patents on this technology is increasing frequently, IPN drug-loaded systems have not found their way into clinical studies up to now, and, hence, commercialization, so far. Their complexity due to the combination of various different properties has hindered a major breakthrough in pharmaceutical applications so far. The current research is still at the academic level, but in our opinion, IPNs are expected to receive much more attention in the future.

Coatings. Colon specific drug delivery has gained considerable attention not only considering colon associated diseases but also for the safe delivery of therapeutic peptides and proteins to the blood stream as the activity of proteolytic enzymes is far lower compared to the upper GI tract.[573] The marketed dosage forms that aim the site specific delivery of the drugs usually depend on the pH variations in the GI tract. However, the pH value difference between the small intestine and the colon is not high enough. This limits the efficient colon targeting in particular when the distal colon is targeted. Therefore, to achieve an efficient colon targeting, variations in the environment comparing the small and the large intestine are exploited in several *in vivo* studies, which include changes in the pH value, the different microbial enzymatic activity, the fluctuating intraluminal pressure or the transit time. Dosage forms which are coated with innovative colon targeting polymers have been extensively reviewed elsewhere.[574] However, it should be noted that novel polymers with unknown safety data always require additional safety assessment. Therefore, most of these studies use polymers with well-established safety profiles

for coatings. Hence, we do not envisage new marketed dosage forms with novel complex polymeric coatings in near future.

5. Concluding remark

The presented review attempted to provide a comprehensive overview of the current state of synthetic polymers used for drug delivery applications, so-called 'pharmapolymers'. Within the last decades, the impact of synthetic polymers has resulted in tremendous advances in chemical synthesis and analysis. The contribution highlights the current market situation and clinical status of respective polymers while paying attention to underlying chemical structures. In addition, we highlight upcoming trends in the development of new pharmapolymers, which in our opinion will have a tremendous impact on the market situation soon. However, we also summarize the obstacles these materials still have to overcome to the market for drug delivery applications. Our review comprises a detailed description of the most important polymer classes and their fields of application. Application forms like polymer-drug conjugates, drug carrier systems in scales ranging from nano- to macroscopic size, polymers as coatings and matrix excipients as well as polymeric drugs are described. We hope that providing a link between the properties and structures of these systems and their area of application helps scientists from different research fields where the systems are often just known by their trade names or abbreviations.

Acknowledgements

We acknowledge funding from the collaborative research center ChemBioSys (SFB 1127) by the German Science Foundation (DFG) and from the Thüringer Ministerium für Wirtschaft, Wissenschaft, und Digitale Gesellschaft (TMWWDG, ProExzellenz II, NanoPolar). M.G. is grateful for the funding by the DFG (GO 1100/4-1) and JB thanks the DFG for granting a fellowship (BR 4905/2-1). Furthermore, we thank Dr. Matthias Hartlieb for helpful comments.

Keywords

Pharmapolymers • drug delivery • market • clinical trials • structure-activity relationships

References

[1] A. S. Hoffman, *J. Control. Release* **2008**, *132*, 153-163.

[2] K. E. Uhrich, S. M. Cannizzaro, R. S. Langer, K. M. Shakesheff, *Chem. Rev.* **1999**, *99*, 3181-3198.

[3] a) P. J. Flory, *J. Am. Chem. Soc.* **1940**, *62*, 1561-1565; b) M. Szwarc, *Nature* **1956**, *178*, 1168-1169.

[4] A.-L. Brocas, C. Mantzaridis, D. Tunc, S. Carlotti, *Prog. Polym. Sci.* **2013**, *38*, 845-873.

[5] S. Penczek, M. Cypryk, A. Duda, P. Kubisa, S. Słomkowski, *Prog. Polym. Sci.* **2007**, *32*, 247-282.

[6] R. Hoogenboom*, Polyethers and Polyoxazolines*, in *Handbook of ring-opening polymerization* (Eds.: P. Dubois, O. Coulembier, J.-M. Raquez), Wiley-VCH, **2009**, pp. 141-164.

[7] a) B. Obermeier, F. Wurm, C. Mangold, H. Frey, *Angew. Chem. Int. Ed.* **2011**, *50*, 7988-7997; b) C. Mangold, F. Wurm, H. Frey, *Polym. Chem.* **2012**, *3*, 1714-1721; c) M. J. Barthel, T. Rudolph, S. Crotty, F. H. Schacher, U. S. Schubert, *J. Polym. Sci., Part A: Polym. Chem.* **2012**, *50*, 4958-4965.

[8] R. Kjellander, E. Florin, *J. Chem. Soc., Faraday Trans. 1* **1981**, *77*, 2053-2077.

[9] S. N. S. Alconcel, A. S. Baas, H. D. Maynard, *Polym. Chem.* **2011**, *2*, 1442-1448.

[10] a) A. Abuchowski, T. van Es, N. C. Palczuk, F. F. Davis, *J. Biol. Chem.* **1977**, *252*, 3578-3581; b) A. Abuchowski, J. R. McCoy, N. C. Palczuk, T. van Es, F. F. Davis, *J. Biol. Chem.* **1977**, *252*, 3582-3586.

[11] a) F. M. Veronese, *Biomaterials* **2001**, *22*, 405-417; b) F. M. Veronese, G. Pasut, *Drug Discovery Today* **2005**, *10*, 1451-1458; c) G. Pasut, F. M. Veronese, *Adv. Drug Delivery Rev.* **2009**, *61*, 1177-1188; d) M. J. Roberts, M. D. Bentley, J. M. Harris, *Adv. Drug Delivery Rev.* **2012**, *64*, 116-127.

[12] a) A. L. Klibanov, K. Maruyama, V. P. Torchilin, L. Huang, *FEBS Lett.* **1990**, *268*, 235-237; b) G. Blume, G. Cevc, *Biochim. Biophys. Acta Biomembr.* **1990**, *1029*, 91-97.

[13] S. Schöttler, G. Becker, S. Winzen, T. Steinbach, K. Mohr, K. Landfester, V. Mailänder, F. R. Wurm, *Nat. Nanotechnol.* **2016**, *11*, 372-377.

[14] a) V. P. Torchilin, V. S. Trubetskoy, *Adv. Drug Delivery Rev.* **1995**, *16*, 141-155; b) C. Monfardini, F. M. Veronese, *Bioconjugate Chem.* **1998**, *9*, 418-450.

[15] K. Knop, R. Hoogenboom, D. Fischer, U. S. Schubert, *Angew. Chem. Int. Ed.* **2010**, *49*, 6288-6308.

[16] a) A. Bendele, J. Seely, C. Richey, G. Sennello, G. Shopp, *Toxicol. Sci.* **1998**, *42*, 152-157; b) D. G. Rudmann, J. T. Alston, J. C. Hanson, S. Heidel, *Toxicol. Pathol.* **2013**, *41*, 970-983.

[17] D. A. Herold, K. Keil, D. E. Bruns, *Biochem. Pharmacol.* **1989**, *38*, 73-76.

[18] a) A. Chanan-Khan, J. Szebeni, S. Savay, L. Liebes, N. M. Rafique, C. R. Alving, F. M. Muggia, *Ann. Oncol.* **2003**, *14*, 1430-1437; b) J. Szebeni, *Toxicology* **2005**, *216*, 106-121.

[19] S. Dai, K. C. Tam, *Langmuir* **2004**, *20*, 2177-2183.

[20] S. Saeki, N. Kuwahara, M. Nakata, M. Kaneko, *Polymer* **1976**, *17*, 685-689.

[21] J. R. Fowles, M. I. Banton, L. H. Pottenger, *Crit. Rev. Toxicol.* **2013**, *43*, 363-390.

[22] M. Schömer, C. Schüll, H. Frey, *J. Polym. Sci., Part A: Polym. Chem.* **2013**, *51*, 995-1019.

[23] P. Kubisa, *J. Polym. Sci., Part A: Polym. Chem.* **2003**, *41*, 457-468.

[24] R. K. Kainthan, E. B. Muliawan, S. G. Hatzikiriakos, D. E. Brooks, *Macromolecules* **2006**, *39*, 7708-7717.

[25] M. A. Quadir, R. Haag, *J. Control. Release* **2012**, *161*, 484-495.

[26] A. Thomas, S. S. Müller, H. Frey, *Biomacromolecules* **2014**, *15*, 1935-1954.

[27] a) B. Klajnert, W. Walach, M. Bryszewska, A. Dworak, D. Shcharbin, *Cell Biol. Int.* **2006**, *30*, 248-252; b) R. K. Kainthan, J. Janzen, E. Levin, D. V. Devine, D. E. Brooks, *Biomacromolecules* **2006**, *7*, 703-709.

[28] M. I. Ul-Haq, B. F. L. Lai, R. Chapanian, J. N. Kizhakkedathu, *Biomaterials* **2012**, *33*, 9135-9147.

[29] K. Maruyama, S. Okuizumi, O. Ishida, H. Yamauchi, H. Kikuchi, M. Iwatsuru, *Int. J. Pharm.* **1994**, *111*, 103-107.

[30] O. Boussif, F. Lezoualc'h, M. A. Zanta, M. D. Mergny, D. Scherman, B. Demeneix, J. P. Behr, *Proc. Natl. Acad. Sci. U.S.A.* **1995**, *92*, 7297-7301.

[31] a) W. T. Godbey, K. K. Wu, A. G. Mikos, *J. Control. Release* **1999**, *60*, 149-160; b) W. T. Godbey, M. A. Barry, P. Saggau, K. K. Wu, A. G. Mikos, *J. Biomed. Mater. Res.* **2000**, *51*, 321-328.
[32] U. Lungwitz, M. Breunig, T. Blunk, A. Göpferich, *Eur. J. Pharm. Biopharm.* **2005**, *60*, 247-266.
[33] G. D. Jones, A. Langsjoen, S. M. M. C. Neumann, J. Zomlefer, *J. Org. Chem.* **1944**, *09*, 125-147.
[34] K. A. Gibney, I. Sovadinova, A. I. Lopez, M. Urban, Z. Ridgway, G. A. Caputo, K. Kuroda, *Macromol. Biosci.* **2012**, *12*, 1279-1289.
[35] a) T. Kagiya, S. Narisawa, T. Maeda, K. Fukui, *J. Polym. Sci. Part B* **1966**, *4*, 441-445; b) D. A. Tomalia, D. P. Sheetz, *J. Polym. Sci., Part A: Polym. Chem.* **1966**, *4*, 2253-2265.
[36] a) R. Tanaka, I. Ueoka, Y. Takaki, K. Kataoka, S. Saito, *Macromolecules* **1983**, *16*, 849-853; b) L. Tauhardt, K. Kempe, K. Knop, E. Altuntaş, M. Jäger, S. Schubert, D. Fischer, U. S. Schubert, *Macromol. Chem. Phys.* **2011**, *212*, 1918-1924.
[37] a) T. Saegusa, H. Ikeda, H. Fujii, *Macromolecules* **1972**, *5*, 108; b) T. Saegusa, S. Kobayashi, A. Yamada, *Macromolecules* **1975**, *8*, 390-396.
[38] T. Bus, C. Englert, M. Reifarth, P. Borchers, M. Hartlieb, A. Vollrath, S. Hoeppener, A. Traeger, U. S. Schubert, *J. Mater. Chem. B* **2017**, *5*, 1258-1274.
[39] K. Aoi, A. Motoda, M. Ohno, K. Tsutsumiuchi, M. Okada, T. Imae, *Polym. J.* **1999**, *31*, 1071-1078.
[40] a) J. H. Jeong, S. H. Song, D. W. Lim, H. Lee, T. G. Park, *J. Control. Release* **2001**, *73*, 391-399; b) H. M. L. Lambermont-Thijs, J. P. A. Heuts, S. Hoeppener, R. Hoogenboom, U. S. Schubert, *Polym. Chem.* **2011**, *2*, 313-322; c) H. P. C. Van Kuringen, J. Lenoir, E. Adriaens, J. Bender, B. G. De Geest, R. Hoogenboom, *Macromol. Biosci.* **2012**, *12*, 1114-1123.
[41] M. Jaeger, S. Schubert, S. Ochrimenko, D. Fischer, U. S. Schubert, *Chem. Soc. Rev.* **2012**, *41*, 4755-4767.
[42] a) A.-C. Albertsson, I. Varma, *Adv. Polym. Sci.* **2002**, *157*, 1-40; b) Q. Chen, G. Thouas, *Biomaterials: A Basic Introduction*, CRC Press (Taylor & Francis Group), Boca Raton, Florida, **2014**.
[43] B. Azimi, P. Nourpanah, M. Rabiee, S. Arbab, *J. Eng. Fiber. Fabr.* **2014**, *9*, 74-90.
[44] a) P. A. Gunatillake, R. Adhikari, *Eur. Cells Mater. J.* **2003**, *5*, 1-16; b) A. G. A. Coombes, S. C. Rizzi, M. Williamson, J. E. Barralet, S. Downes, W. A. Wallace, *Biomaterials* **2004**, *25*, 315-325; c) V. R. Sinha, K. Bansal, R. Kaushik, R. Kumria, A. Trehan, *Int. J. Pharm.* **2004**, *278*, 1-23; d) H. Sun, L. Mei, C. Song, X. Cui, P. Wang, *Biomaterials* **2006**, *27*, 1735-1740; e) X. Wei, C. Gong, M. Gou, S. Fu, Q. Guo, S. Shi, F. Luo, G. Guo, L. Qiu, Z. Qian, *Int. J. Pharm.* **2009**, *381*, 1-18.
[45] M. A. Woodruff, D. W. Hutmacher, *Prog. Polym. Sci.* **2010**, *35*, 1217-1256.
[46] M. Labet, W. Thielemans, *Chem. Soc. Rev.* **2009**, *38*, 3484-3504.
[47] C. Zhang, *Biodegradable polyesters: Synthesis, properties, applications*, in *Biodegradable polyesters*, Wiley-VCH, **2015**, pp. 1-24.
[48] K. Chavalitpanya, S. Phattanarudee, *Energy Procedia* **2013**, *34*, 542-548.
[49] a) A. Sarasam, S. V. Madihally, *Biomaterials* **2005**, *26*, 5500-5508; b) D. M. García Cruz, J. L. Gomez Ribelles, M. Salmerón Sánchez, *J. Biomed. Mater. Res. B* **2008**, *85*, 303-313.
[50] a) J. C. Middleton, A. J. Tipton, *Biomaterials* **2000**, *21*, 2335-2346; b) V. Singh, M. Tiwari, *Int. J. Polym. Sci.* **2010**, *2010*, 1-23; c) M. S. Lopes, A. L. Jardini, R. M. Filho, *Procedia Eng.* **2012**, *42*, 1402-1413.
[51] a) R. A. Jain, *Biomaterials* **2000**, *21*, 2475-2490; b) B. D. Ulery, L. S. Nair, C. T. Laurencin, *J. Polym. Sci., Part B: Polym. Phys.* **2011**, *49*, 832-864; c) H. K. Makadia, S. J. Siegel, *Polymer* **2011**, *3*, 1377-1397; d) B. Behera, *J. Med. Pharm. Innov.* **2013**, *1*, 1-5; e) B. Azimi, P. Nourpanah, M. Rabiee, S. Arbab, *J. Eng. Fiber. Fabr.* **2014**, *9*, 47-66.
[52] a) H. Tsuji, *Macromol. Biosci.* **2007**, *7*, 1299; b) P. Gentile, V. Chiono, I. Carmagnola, P. V. Hatton, *Int. J. Mol. Sci.* **2014**, *15*, 3640-3659.
[53] W. H. Carothers, G. L. Dorough, F. J. v. Natta, *J. Am. Chem. Soc.* **1932**, *54*, 761-772.

[54] C. C. Erbetta, R. J. Alves, J. M. Resende, R. F. Freitas, R. G. Sousa, *J. Biomater. Nanobiotechnol.* **2012**, *3*, 208-225.
[55] a) M. Jamshidian, E. A. Tehrany, M. Imran, M. Jacquot, S. Desobry, *Compr. Rev. Food Sci. Food Saf.* **2010**, *9*, 552-571; b) C. Engineer, J. Parikh, A. Raval, *Trends Biomater. Artif. Organs* **2011**, *25*, 79-85.
[56] S. W. Shalaby, D. D. Jamiolkowski, US 4140678 A, **1980**.
[57] a) S. J. Holland, B. J. Tighe, P. L. Gould, *J. Control. Release* **1986**, *4*, 155-180; b) J. Shin, K.-N. Yeh, *J. Appl. Polym. Sci.* **1999**, *74*, 921-936; c) L. Finelli, N. Lotti, A. Munari, *Eur. Polym. J.* **2002**, *38*, 1987-1993; d) S. Kim, K. Seong, O. Kim, S. Kim, H. Seo, M. Lee, G. Khang, D. Lee, *Biomacromolecules* **2010**, *11*, 555-560.
[58] J. J. Garcia, S. A. Miller, *Polym. Chem.* **2014**, *5*, 955-961.
[59] A. Einhorn, *Justus Liebigs Ann. Chem.* **1898**, *300*, 135-155.
[60] H. Schnell, *Angew. Chem.* **1956**, *68*, 633-640.
[61] D. Fox*, Polyesters: History*, in *High performance polymers: Their origin and development* (Eds.: R. B. Seymour, G. S. Kirshenbaum), Springer, **1986**, pp. 67-70.
[62] a) D. J. A. Cameron, M. P. Shaver, *Chem. Soc. Rev.* **2011**, *40*, 1761-1776; b) H. Seyednejad, A. H. Ghassemi, C. F. van Nostrum, T. Vermonden, W. E. Hennink, *J. Control. Release* **2011**, *152*, 168-176; c) Y. Zhang, H. F. Chan, K. W. Leong, *Adv. Drug Delivery Rev.* **2013**, *65*, 104-120.
[63] F. Suriano, O. Coulembier, J. L. Hedrick, P. Dubois, *Polym. Chem.* **2011**, *2*, 528-533.
[64] A. Cyriac, S. H. Lee, J. K. Varghese, E. S. Park, J. H. Park, B. Y. Lee, *Macromolecules* **2010**, *43*, 7398-7401.
[65] a) M. Taherimehr, P. P. Pescarmona, *J. Appl. Polym. Sci.* **2014**, *131*, 41141; b) R.-R. Ang, L. Tin Sin, S.-T. Bee, T.-T. Tee, A. A. H. Kadhum, A. R. Rahmat, B. A. Wasmi, *J. Cleaner Prod.* **2015**, *102*, 1-17.
[66] K. Sehanobish, T. Pham, H. C. P. Bosnyak, in *Polymeric Materials Encyclopedia, Vol. 8* (Ed.: J. C. Salamone), CRC Press (Taylor & Francis Group), **1996**, p. 5697.
[67] J. Xu, F. Prifti, J. Song, *Macromolecules* **2011**, *44*, 2660-2667.
[68] a) Y. Shibasaki, H. Sanada, M. Yokoi, F. Sanda, T. Endo, *Macromolecules* **2000**, *33*, 4316-4320; b) C. Yang, Z. Y. Ong, Y.-Y. Yang, P. L. R. Ee, J. L. Hedrick, *Macromol. Rapid Commun.* **2011**, *32*, 1826-1833; c) S. M. Guillaume, *Eur. Polym. J.* **2013**, *49*, 768-779; d) R. P. Brannigan, A. Walder, A. P. Dove, *J. Polym. Sci., Part A: Polym. Chem.* **2014**, *52*, 2279-2286.
[69] a) H. Wu, Y. Ji, Z. Li, X. Wang, Q. Zhang, S. Cui, W. Wu, J. Liu, K. Guo, *J. Polym. Sci., Part A: Polym. Chem.* **2015**, *53*, 729-736; b) C. Yang, S. Q. Liu, S. Venkataraman, S. J. Gao, X. Ke, X. T. Chia, J. L. Hedrick, Y. Y. Yang, *J. Control. Release* **2015**, *208*, 93-105.
[70] Z. Zhang, R. Kuijer, S. K. Bulstra, D. W. Grijpma, J. Feijen, *Biomaterials* **2006**, *27*, 1741-1748.
[71] a) M. Acemoglu, S. Bantle, T. Mindt, F. Nimmerfall, *Macromolecules* **1995**, *28*, 3030-3037; b) E. J. Vandenberg, D. Tian, *Macromolecules* **1999**, *32*, 3613-3619.
[72] T. F. Al-Azemi, K. S. Bisht, *Macromolecules* **1999**, *32*, 6536-6540.
[73] F. Sanda, J. Kamatani, T. Endo, *Macromolecules* **2001**, *34*, 1564-1569.
[74] P. G. Parzuchowski, M. Jaroch, M. Tryznowski, G. Rokicki, *Macromolecules* **2008**, *41*, 3859-3865.
[75] R. C. Pratt, F. Nederberg, R. M. Waymouth, J. L. Hedrick, *Chem. Commun.* **2008**, 114-116.
[76] J. Mindemark, T. Bowden, *Polymer* **2011**, *52*, 5716-5722.
[77] X. Zhang, Z. Zhong, R. Zhuo, *Macromolecules* **2011**, *44*, 1755-1759.
[78] a) Y. Shen, X. Chen, R. A. Gross, *Macromolecules* **1999**, *32*, 2799-2802; b) F. Suriano, R. Pratt, J. P. K. Tan, N. Wiradharma, A. Nelson, Y.-Y. Yang, P. Dubois, J. L. Hedrick, *Biomaterials* **2010**, *31*, 2637-2645.
[79] a) T. J. Deming, *Prog. Polym. Sci.* **2007**, *32*, 858-875; b) Y. Shen, X. Fu, W. Fu, Z. Li, *Chem. Soc. Rev.* **2015**, *44*, 612-622.

[80] a) A. Lavasanifar, J. Samuel, G. S. Kwon, *Adv. Drug Delivery Rev.* **2002**, *54*, 169-190; b) C. Li, *Adv. Drug Delivery Rev.* **2002**, *54*, 695-713; c) Y. Bae, K. Kataoka, *Adv. Drug Delivery Rev.* **2009**, *61*, 768-784; d) S. F. M. van Dongen, H.-P. M. de Hoog, R. J. R. W. Peters, M. Nallani, R. J. M. Nolte, J. C. M. van Hest, *Chem. Rev.* **2009**, *109*, 6212-6274; e) S. Hehir, N. R. Cameron, *Polym. Int.* **2014**, *63*, 943-954.
[81] H. Leuchs, *Ber. Deutsch. Chem. Ges.* **1906**, *39*, 857-861.
[82] a) H. R. Kricheldorf, *Angew. Chem. Int. Ed.* **2006**, *45*, 5752-5784; b) N. Hadjichristidis, H. Iatrou, M. Pitsikalis, G. Sakellariou, *Chem. Rev.* **2009**, *109*, 5528-5578; c) C. Deng, J. Wu, R. Cheng, F. Meng, H.-A. Klok, Z. Zhong, *Prog. Polym. Sci.* **2014**, *39*, 330-364.
[83] T. J. Deming, *J. Polym. Sci., Part A: Polym. Chem.* **2000**, *38*, 3011-3018.
[84] T. Aliferis, H. Iatrou, N. Hadjichristidis, *Biomacromolecules* **2004**, *5*, 1653-1656.
[85] a) I. Dimitrov, H. Schlaad, *Chem. Commun.* **2003**, 2944-2945; b) J.-F. Lutz, D. Schütt, S. Kubowicz, *Macromol. Rapid Commun.* **2005**, *26*, 23-28.
[86] H. Lu, J. Cheng, *J. Am. Chem. Soc.* **2007**, *129*, 14114-14115.
[87] a) C. He, X. Zhuang, Z. Tang, H. Tian, X. Chen, *Adv. Healthcare Mater.* **2012**, *1*, 48-78; b) H. Lu, J. Wang, Z. Song, L. Yin, Y. Zhang, H. Tang, C. Tu, Y. Lin, J. Cheng, *Chem. Commun.* **2014**, *50*, 139-155.
[88] A. Ogunleye, A. Bhat, V. U. Irorere, D. Hill, C. Williams, I. Radecka, *Microbiology* **2015**, *161*, 1-17.
[89] I.-L. Shih, Y.-T. Van, M.-H. Shen, *Mini-Rev. Med. Chem.* **2004**, *4*, 179-188.
[90] S. Roweton, S. J. Huang, G. Swift, *J. Environ. Polym. Degrad.* **1997**, *5*, 175-181.
[91] P. S. Farmer, E. J. Ariens, *Trends Pharmacol. Sci.* **1982**, *3*, 362-365.
[92] R. J. Simon, R. S. Kania, R. N. Zuckermann, V. D. Huebner, D. A. Jewell, S. Banville, S. Ng, L. Wang, S. Rosenberg, C. K. Marlowe, *Proc. Natl. Acad. Sci. U.S.A.* **1992**, *89*, 9367-9371.
[93] a) K. Kirshenbaum, A. E. Barron, R. A. Goldsmith, P. Armand, E. K. Bradley, K. T. V. Truong, K. A. Dill, F. E. Cohen, R. N. Zuckermann, *Proc. Natl. Acad. Sci. U.S.A.* **1998**, *95*, 4303-4308; b) R. N. Zuckermann, *Pept. Sci.* **2011**, *96*, 545-555.
[94] a) J. W. Robinson, H. Schlaad, *Chem. Commun.* **2012**, *48*, 7835-7837; b) J. Sun, R. N. Zuckermann, *ACS Nano* **2013**, *7*, 4715-4732; c) A. Birke, D. Huesmann, A. Kelsch, M. Weilbaecher, J. Xie, M. Bros, T. Bopp, C. Becker, K. Landfester, M. Barz, *Biomacromolecules* **2014**, *15*, 548-557; d) K. Klinker, R. Holm, P. Heller, M. Barz, *Polym. Chem.* **2015**, *6*, 4612-4623
[95] R. N. Zuckermann, J. M. Kerr, S. B. H. Kent, W. H. Moos, *J. Am. Chem. Soc.* **1992**, *114*, 10646-10647.
[96] a) R. M. J. Liskamp, D. T. S. Rijkers, J. A. W. Kruijtzer, J. Kemmink, *ChemBioChem* **2011**, *12*, 1626-1653; b) R. Luxenhofer, C. Fetsch, A. Grossmann, *J. Polym. Sci., Part A: Polym. Chem.* **2013**, *51*, 2731-2752; c) A. M. Rosales, R. A. Segalman, R. N. Zuckermann, *Soft Matter* **2013**, *9*, 8400-8414; d) A. S. Knight, E. Y. Zhou, M. B. Francis, R. N. Zuckermann, *Adv. Mater.* **2015**, *27*, 5665-5691; e) C. Secker, S. M. Brosnan, R. Luxenhofer, H. Schlaad, *Macromol. Biosci.* **2015**, *15*, 881-891.
[97] A. S. Culf, R. J. Ouellette, *Molecules* **2010**, *15*, 5282.
[98] H. K. Murnen, A. R. Khokhlov, P. G. Khalatur, R. A. Segalman, R. N. Zuckermann, *Macromolecules* **2012**, *45*, 5229-5236.
[99] S. M. Miller, R. J. Simon, S. Ng, R. N. Zuckermann, J. M. Kerr, W. H. Moos, *Bioorg. Med. Chem. Lett.* **1994**, *4*, 2657-2662.
[100] a) H. J. Olivos, P. G. Alluri, M. M. Reddy, D. Salony, T. Kodadek, *Org. Lett.* **2002**, *4*, 4057-4059; b) B. C. Gorske, S. A. Jewell, E. J. Guerard, H. E. Blackwell, *Org. Lett.* **2005**, *7*, 1521-1524.
[101] D. Zhang, S. H. Lahasky, L. Guo, C.-U. Lee, M. Lavan, *Macromolecules* **2012**, *45*, 5833-5841.
[102] a) M. Schneider, C. Fetsch, I. Amin, R. Jordan, R. Luxenhofer, *Langmuir* **2013**, *29*, 6983-6988; b) N. Gangloff, C. Fetsch, R. Luxenhofer, *Macromol. Rapid Commun.* **2013**, *34*, 997-1001.

[103] a) S. Lohan, G. S. Bisht, *Mini Rev. Med. Chem.* **2013**, *13*, 1073-1088; b) K. H. A. Lau, *Biomater. Sci.* **2014**, *2*, 627-633.
[104] a) C. M. Gao, A. Y. Yam, X. Wang, E. Magdangal, C. Salisbury, D. Peretz, R. N. Zuckermann, M. D. Connolly, O. Hansson, L. Minthon, H. Zetterberg, K. Blennow, J. P. Fedynyshyn, S. Allauzen, *PLoS ONE* **2010**, *5*, e15725; b) M. M. Reddy, R. Wilson, J. Wilson, S. Connell, A. Gocke, L. Hynan, D. German, T. Kodadek, *Cell* **2011**, *144*, 132-142.
[105] a) S. L. Seurynck, J. A. Patch, A. E. Barron, *Chem. Biol.* **2005**, *12*, 77-88; b) N. J. Brown, J. Johansson, A. E. Barron, *Acc. Chem. Res.* **2008**, *41*, 1409-1417.
[106] a) C. A. Olsen, *ChemBioChem* **2010**, *11*, 152-160; b) B.-C. Lee, R. N. Zuckermann, *ACS Chem. Biol.* **2011**, *6*, 1367-1374.
[107] J. Ulbricht, R. Jordan, R. Luxenhofer, *Biomaterials* **2014**, *35*, 4848-4861.
[108] a) W. Seeliger, E. Aufderhaar, W. Diepers, R. Feinauer, R. Nehring, W. Thier, H. Hellmann, *Angew. Chem. Int. Ed.* **1966**, *5*, 875-888; b) T. G. Bassiri, A. Levy, M. Litt, *J. Polym. Sci. Part B* **1967**, *5*, 871-879.
[109] a) F. Wiesbrock, R. Hoogenboom, C. H. Abeln, U. S. Schubert, *Macromol. Rapid Commun.* **2004**, *25*, 1895-1899; b) K. Kempe, C. R. Becer, U. S. Schubert, *Macromolecules* **2011**, *44*, 5825-5842; c) C. Englert, A. M. Schwenke, S. Hoeppener, C. Weber, U. S. Schubert, *Adv. Polym. Sci.* **2016**, *274*, 209-240.
[110] B. Guillerm, S. Monge, V. Lapinte, J.-J. Robin, *Macromol. Rapid Commun.* **2012**, *33*, 6000-6016.
[111] a) J. Kronek, Z. Kroneková, J. Lustoň, E. Paulovičová, L. Paulovičová, B. Mendrek, *J. Mater. Sci.: Mater. Med.* **2011**, *22*, 1725-1734; b) R. Luxenhofer, G. Sahay, A. Schulz, D. Alakhova, T. K. Bronich, R. Jordan, A. V. Kabanov, *J. Control. Release* **2011**, *153*, 73-82; c) M. Bauer, S. Schroeder, L. Tauhardt, K. Kempe, U. S. Schubert, D. Fischer, *J. Polym. Sci., Part A: Polym. Chem.* **2013**, *51*, 1816-1821.
[112] a) M. C. Woodle, C. M. Engbers, S. Zalipsky, *Bioconjugate Chem.* **1994**, *5*, 493-496; b) S. Zalipsky, C. B. Hansen, J. M. Oaks, T. M. Allen, *J. Pharm. Sci.* **1996**, *85*, 133-137.
[113] a) R. Hoogenboom, *Angew. Chem. Int. Ed.* **2009**, *48*, 7978-7994; b) R. Luxenhofer, Y. Han, A. Schulz, J. Tong, Z. He, A. V. Kabanov, R. Jordan, *Macromol. Rapid Commun.* **2012**, 1613-1631; c) V. R. de la Rosa, *J. Mater. Sci.: Mater. Med.* **2014**, *25*, 1211-1225.
[114] C. Weber, R. Hoogenboom, U. S. Schubert, *Prog. Polym. Sci.* **2012**, *37*, 686-714.
[115] R. Duncan, M. J. Vicent, *Adv. Drug Delivery Rev.* **2010**, *62*, 272-282.
[116] P. A. Vasey, S. B. Kaye, R. Morrison, C. Twelves, P. Wilson, R. Duncan, A. H. Thomson, L. S. Murray, T. E. Hilditch, T. Murray, S. Burtles, D. Fraier, E. Frigerio, J. Cassidy, *Clin. Cancer Res.* **1999**, *5*, 83-94.
[117] a) J. Kopeček, H. Bažilová, *Eur. Polym. J.* **1973**, *9*, 7-14; b) M. Teodorescu, K. Matyjaszewski, *Macromolecules* **1999**, *32*, 4826-4831; c) C. W. Scales, Y. A. Vasilieva, A. J. Convertine, A. B. Lowe, C. L. McCormick, *Biomacromolecules* **2005**, *6*, 1846-1850.
[118] a) M. Eberhardt, P. Théato, *Macromol. Rapid Commun.* **2005**, *26*, 1488-1493; b) M. I. Gibson, E. Fröhlich, H.-A. Klok, *J. Polym. Sci., Part A: Polym. Chem.* **2009**, *47*, 4332-4345.
[119] B. S. Tucker, B. S. Sumerlin, *Polym. Chem.* **2014**, *5*, 1566-1572.
[120] a) M. Heskins, J. E. Guillet, *J. Macromol. Sci. Chem. Ed.* **1968**, *A2*, 1441-1455; b) K. Dušek, D. Patterson, *J. Polym. Sci. Part. A-2* **1968**, *6*, 1209-1216.
[121] a) H. Wei, S.-X. Cheng, X.-Z. Zhang, R.-X. Zhuo, *Prog. Polym. Sci.* **2009**, *34*, 893-910; b) A. Halperin, M. Kröger, F. M. Winnik, *Angew. Chem. Int. Ed.* **2015**, *54*, 15342-15367.
[122] Z. M. O. Rzaev, S. Dinçer, E. Pişkin, *Prog. Polym. Sci.* **2007**, *32*, 534-595.
[123] T. Sun, G. Qing, *Adv. Mater.* **2011**, *23*, H57-H77.
[124] a) Y. Guan, Y. Zhang, *Soft Matter* **2011**, *7*, 6375-6384; b) Y. Lu, M. Ballauff, *Prog. Polym. Sci.* **2011**, *36*, 767-792; c) C. Li, Y. Ma, H. Niu, H. Zhang, *ACS Appl. Mater. Interfaces* **2015**, *7*, 27340–27350;

d) L. D. Blackman, D. B. Wright, M. P. Robin, M. I. Gibson, R. K. O'Reilly, *ACS Macro Lett.* **2015**, *4*, 1210-1214; e) H. Hathaway, D. R. Alves, J. Bean, P. P. Esteban, K. Ouadi, J. Mark Sutton, A. T. A. Jenkins, *Eur. J. Pharm. Biopharm.* **2015**, *96*, 437-441.
[125] H. M. Mansour, M. Sohn, A. Al-Ghananeem, P. P. DeLuca, *Int. J. Mol. Sci.* **2010**, *11*, 3298.
[126] a) F. Ganachaud, M. J. Monteiro, R. G. Gilbert, M.-A. Dourges, S. H. Thang, E. Rizzardo, *Macromolecules* **2000**, *33*, 6738-6745; b) G. Masci, L. Giacomelli, V. Crescenzi, *Macromol. Rapid Commun.* **2004**, *25*, 559-564.
[127] T. Steinbach, E. M. Alexandrino, C. Wahlen, K. Landfester, F. R. Wurm, *Macromolecules* **2014**, *47*, 4884-4893.
[128] J. Liu, W. Huang, Y. Pang, D. Yan, *Chem. Soc. Rev.* **2015**, *44*, 3942-3953.
[129] a) F. Marsico, M. Wagner, K. Landfester, F. R. Wurm, *Macromolecules* **2012**, *45*, 8511-8518; b) T. Steinbach, E. M. Alexandrino, F. R. Wurm, *Polym. Chem.* **2013**, *4*, 3800-3806.
[130] Y.-C. Wang, Y.-Y. Yuan, J.-Z. Du, X.-Z. Yang, J. Wang, *Macromol. Biosci.* **2009**, *9*, 1154-1164.
[131] L. Lieberman, *Ber. Chem.-Ges.* **1888**, *21*, 598-607.
[132] a) I. S. Kulaev, V. M. Vagabov, *Adv. Microb. Physiol* **1983**, *24*, 83-171; b) A. Kornberg, *J. Bacteriol.* **1995**, *177*, 491-496; c) I. S. Kulaev, V. M. Vagabov, T. V. Kulakovskaya, *The biochemistry of inorganic polyphosphates*, John Wiley & Sons, **1979**; d) T. Steinbach, F. R. Wurm, *Angew. Chem. Int. Ed.* **2015**, *54*, 6098-6108; e) X. Wang, H. C. Schröder, W. E. G. Müller, *Biotechnol. J.* **2016**, *11*, 11-30.
[133] a) A. Kornberg, S. R. Kornberg, E. S. Simms, *Biochim. Biophys. Acta* **1956**, *20*, 215-227; b) S. R. Kornberg, *Biochim. Biophys. Acta* **1957**, *26*, 294-300.
[134] a) R. P. Elliott, R. P. Straka, J. A. Garibaldi, *Appl. Microbiol.* **1964**, *12*, 517-522; b) A. Momeni, M. J. Filiaggi, *Langmuir* **2014**, *30*, 5256-5266.
[135] A. Kornberg, N. N. Rao, D. Ault-Riché, *Annu. Rev. Biochem.* **1999**, *68*, 89-125.
[136] J.-Z. Du, T.-M. Sun, S.-Q. Weng, X.-S. Chen, J. Wang, *Biomacromolecules* **2007**, *8*, 3375-3381.
[137] S. Zhang, A. Li, J. Zou, L. Y. Lin, K. L. Wooley, *ACS Macro Lett.* **2012**, *1*, 328-333.
[138] W.-J. Song, J.-Z. Du, N.-J. Liu, S. Dou, J. Cheng, J. Wang, *Macromolecules* **2008**, *41*, 6935-6941.
[139] J. Wang, H.-Q. Mao, K. W. Leong, *J. Am. Chem. Soc.* **2001**, *123*, 9480-9481.
[140] J. Liu, W. Huang, Y. Zhou, D. Yan, *Macromolecules* **2009**, *42*, 4394-4399.
[141] Y. Iwasaki, E. Yamaguchi, *Macromolecules* **2010**, *43*, 2664-2666.
[142] J. Libiszowski, K. Kałużynski, S. Penczek, *J. Polym. Sci. Polym. Chem. Ed.* **1978**, *16*, 1275-1283.
[143] J. A. Obritsch, D. Ryu, L. E. Lampila, L. B. Bullerman, *J. Food Prot.* **2008**, *71*, 1401-1405.
[144] A. S. Naidu, *Natural food antimicrobial systems*, CRC Press (Taylor & Francis Group), **2000**.
[145] E. Yilgör, I. Yilgör, *Prog. Polym. Sci.* **2014**, *39*, 1165-1195.
[146] a) L. Wilczek, J. Chojnowski, *Makromol. Chem.* **1983**, *184*, 77-90; b) A. Mitra, D. A. Atwood, *Polysiloxanes & polysilanes*, in *Encyclopedia of inorganic chemistry* (Ed.: R. B. King), John Wiley & Sons, **2006**.
[147] a) P. Cancouët, E. Daudet, G. Hélary, M. Moreau, G. Sauvet, *J. Polym. Sci., Part A: Polym. Chem.* **2000**, *38*, 826-836; b) A. Saxena, S. Rajaraman, M. Leatherman, *Macromolecules* **2007**, *40*, 752-755; c) M. D. Ninago, A. J. Satti, J. A. Ressia, A. E. Ciolino, M. A. Villar, E. M. Vallés, *J. Polym. Sci., Part A: Polym. Chem.* **2009**, *47*, 4774-4783.
[148] A. Colas, *Dow Corning, Life Sciences* **2005**.
[149] R. De Jaeger, M. Gleria, *Inorganic Polymers*, Nova Science Publishers, **2007**.
[150] H. Zhang, M. Chiao, *J. Med. Biol. Eng.* **2015**, *35*, 143-155.
[151] a) H. Schmolke, S. Demming, A. Edlich, V. Magdanz, S. Büttgenbach, E. Franco-Lara, R. Krull, C.-P. Klages, *Biomicrofluidics* **2010**, *4*, 44113; b) K. M. Kovach, J. R. Capadona, A. S. Gupta, J. A. Potkay, *J. Biomed. Mater. Res. A* **2014**, *102*, 4195-4205; c) M. A. Rufin, J. A. Gruetzner, M. J. Hurley, M. L. Hawkins, E. S. Raymond, J. E. Raymond, M. A. Grunlan, *J. Mater. Chem. B* **2015**, *3*, 2816-2825.

[152] C. Stevens, *Int. J. Cosmet. Sci.* **1998**, *20*, 296-304.
[153] M. H. Stenzel, L. Cummins, G. E. Roberts, T. P. Davis, P. Vana, C. Barner-Kowollik, *Macromol. Chem. Phys.* **2003**, *204*, 1160-1168.
[154] C. C. DeMerlis, D. R. Schoneker, *Food Chem. Toxicol.* **2003**, *41*, 319-326.
[155] I. Orienti, R. Trere, B. Luppi, F. Bigucci, T. Cerchiara, G. Zuccari, V. Zecchi, *Arch. Pharm.* **2002**, *335*, 89-93.
[156] S. M. More, R. V. Kulkarni, B. Sa, N. V. Kayane, *J. Appl. Polym. Sci.* **2010**, *116*, 1732-1738.
[157] G. Schröder*, Poly(vinyl ethers)*, in *Ullmann's encyclopedia of industrial chemistry*, Wiley-VCH, Weinheim, Germany, **2000**.
[158] M. G. Tardajos, M. Nash, Y. Rochev, H. Reinecke, C. Elvira, A. Gallardo, *Macromol. Chem. Phys* **2012**, *213*, 529-538.
[159] W. Reppe, *Angew. Chem.* **1953**, *65*, 577-578.
[160] V. G. Kadajji, G. V. Betageri, *Polymers* **2011**, *3*, 1972.
[161] V. Bühler, *Kollidon: Polyvinylpyrrolidone excipients for the pharmaceutical industry*, BASF, Ludwigshafen, Germany, **2008**.
[162] a) V. P. Torchilin, *J. Microencapsulation* **1998**, *15*, 1-19; b) Z. Zhu, C. Xie, Q. Liu, X. Zhen, X. Zheng, W. Wu, R. Li, Y. Ding, X. Jiang, B. Liu, *Biomaterials* **2011**, *32*, 9525-9535.
[163] F. Fischer, S. Bauer, *Chem. Unserer Zeit* **2009**, *43*, 376-383.
[164] a) F. Haaf, A. Sanner, F. Straub, *Polym. J.* **1985**, *17*, 143-152; b) M. B. Mohamed, M. K. Talari, M. Tripathy, A. B. A. Majeed, *Int. J. Drug Formulation Res.* **2012**, *3*, 13-28.
[165] W. Strohmeier, P. Hartmann, *Z. Naturforsch. B* **1964**, *19*, 655.
[166] a) P. S. Mohanachandran, P. G. Sindhumol, T. S. Kiran, *Int. J. Pharm. Sci. Rev. Res.* **2011**, *6*, 105-109; b) R. Bala, S. Khanna, P. Pawar, *Asian J. Pharm. Clin. Res.* **2012**, *5*, 8-14; c) M. Mangal, S. Thakral, M. Goswami, P. Ghai, *Int. J. Pharm. Pharm. Sci. Res.* **2012**, *2*, 26-35.
[167] M. Wytrwal, C. Leduc, M. Sarna, C. Goncalves, M. Kepczynski, P. Midoux, M. Nowakowska, C. Pichon, *Int. J. Pharm.* **2015**, *478*, 372-382.
[168] J. M. C. Lourenço, P. A. Ribeiro, A. M. Botelho do Rego, F. M. Braz Fernandes, A. M. C. Moutinho, M. Raposo, *Langmuir* **2004**, *20*, 8103-8109.
[169] K. Nollenberger, J. Albers, *Int. J. Pharm.* **2013**, *457*, 461-469.
[170] P. F. Holmes, M. Bohrer, J. Kohn, *Prog. Polym. Sci.* **2008**, *33*, 787-796.
[171] a) P. Kwiatkowski, J. Jurczak, J. Pietrasik, W. Jakubowski, L. Mueller, K. Matyjaszewski, *Macromolecules* **2008**, *41*, 1067-1069; b) E. Yoshida, *Colloid. Polym. Sci.* **2011**, *289*, 1625-1630; c) T. Yildirim, A. C. Rinkenauer, C. Weber, A. Traeger, S. Schubert, U. S. Schubert, *J. Polym. Sci., Part A: Polym. Chem.* **2015**, *53*, 2711-2721.
[172] F. Fleischhaker, A. P. Haehnel, A. M. Misske, M. Blanchot, S. Haremza, C. Barner-Kowollik, *Macromol. Chem. Phys.* **2014**, *215*, 1192-1200.
[173] K. Terao*, Poly(acrylic acid) (PAA)*, in *Encyclopedia of polymeric nanomaterials* (Eds.: Shiro Kobayashi, Klaus Müllen), Springer, Berlin, Heidelberg, Germany, **2014**, pp. 1-6.
[174] T. Swift, L. Swanson, M. Geoghegan, S. Rimmer, *Soft Matter* **2016**, *12*, 2542-2549.
[175] J. E. Elliott, M. Macdonald, J. Nie, C. N. Bowman, *Polymer* **2004**, *45*, 1503-1510.
[176] a) A. Bernkop-Schnürch, C. Egger, M. Elhassan Imam, A. H. Krauland, *J. Control. Release* **2003**, *93*, 29-38; b) G. M. Eichenbaum, P. F. Kiser, A. V. Dobrynin, S. A. Simon, D. Needham, *Macromolecules* **1999**, *32*, 4867-4878.
[177] S. Hochheiser, *Rohm and Haas: History of a chemical company*, University of Pennsylvania Press, Philadelphia, Pennsylvania, **1986**.
[178] U. Ali, K. J. B. A. Karim, N. A. Buang, *Polym. Rev.* **2015**, *55*, 678-705.
[179] a) F. Galli, S. Benedetti, U. Buoncristiani, M. Piroddi, C. Conte, F. Canestrari, E. Buoncristiani, A. Floridi, *Kidney Int.* **2003**, *64*, 748-755; b) T. G. Tihan, M. D. Ionita, R. G. Popescu, D. Iordachescu,

Mater. Chem. Phys. **2009**, *118*, 265-269; c) A. Gomaa, R. M. H. Lee, C. S. C. Liu, *Eye* **2011**, *25*, 1090-1093; d) M. Khandaker, M. B. Vaughan, T. L. Morris, J. J. White, Z. Meng, *Int. J. Nanomed.* **2014**, *9*, 2699-2712.

[180] A. Bhowmick, S. Banerjee, R. Kumar, P. Kundu, *Biomedicine and Nanotechnology* **2013**, *254*, 135-167.

[181] C. Migliaresi, L. Fambri, J. Kolarik, *Biomaterials* **1994**, *15*, 875-881.

[182] R. Yañez-Macias, I. Alvarez-Moises, I. Perevyazko, A. Lezov, R. Guerrero-Santos, U. S. Schubert, C. Guerrero-Sanchez, *Macromol. Chem. Phys.* **2017**, accepted.

[183] Y.-Z. You, D. S. Manickam, Q.-H. Zhou, D. Oupický, *J. Control. Release* **2007**, *122*, 217-225.

[184] T. Yildirim, A. Traeger, E. Preussger, S. Stumpf, C. Fritzsche, S. Hoeppener, S. Schubert, U. S. Schubert, *Macromolecules* **2016**, *49*, 3856-3868.

[185] B. Burns*, Polycyanoacrylates*, in *Encyclopedia of polymer science and technology* (Ed.: H. F. Mark), John Wiley & Sons, **2016**, pp. 1-27.

[186] J. M. Cracowski, V. Montembault, D. Bosc, B. Améduri, F. Odobel, L. Fontaine, *J. Polym. Sci., Part A: Polym. Chem.* **2009**, *47*, 1403-1411.

[187] H. Finkentscher, C. Heuck, DE 654989 C, **1930**.

[188] H. R. Clyde, US 2404713 A, **1946**.

[189] H. Dong, W. Tang, K. Matyjaszewski, *Macromolecules* **2007**, *40*, 2974-2977.

[190] M. Kopeć, P. Krys, R. Yuan, K. Matyjaszewski, *Macromolecules* **2016**, *49*, 5877-5883.

[191] a) P. Bajaj, K. Sen, S. H. Bahrami, *J. Appl. Polym. Sci.* **1996**, *59*, 1539-1550; b) P. Bajaj, T. V. Sreekumar, K. Sen, *J. Appl. Polym. Sci.* **2001**, *79*, 1640-1652; c) D. F. Grishin, I. D. Grishin, *Russ. Chem. Rev.* **2015**, *84*, 712.

[192] a) Y. Nakano, K. Hisatani, K. Kamide, *Polym. Int.* **1994**, *35*, 207-213; b) A. V. Novoselova, V. V. Shamanin, L. V. Vinogradova, *Polym. Sci. Ser. B Polym. Chem.* **2009**, *51*, 205-211.

[193] H. Ono, K. Hisatani, K. Kamide, *Polym. J.* **1993**, *25*, 245-265.

[194] M. L. Gupta, B. Gupta, W. Oppermann, G. Hardtmann, *J. Appl. Polym. Sci.* **2004**, *91*, 3127-3133.

[195] N. Arsalani, R. Rakh, E. Ghasemi, A. A. Entezami, *Iran. Polym. J.* **2009**, *18*, 623-632.

[196] S. K. Nataraj, K. S. Yang, T. M. Aminabhavi, *Prog. Polym. Sci.* **2012**, *37*, 487-513.

[197] C. Dizman, D. O. Demirkol, S. Ates, L. Torun, S. Sakarya, S. Timur, Y. Yagci, *Colloids Surf., B* **2011**, *88*, 265-270.

[198] M. Amirilargani, A. Sabetghadam, T. Mohammadi, *Polym. Adv. Technol.* **2012**, *23*, 398-407.

[199] O. Bayer, H. Rinke, W. Siefken, L. Orthner, H. Schild, DRP 728981 (13. Nov. 1937), I. G. Farben, Chem. Zbl., **1940**.

[200] a) P. A. Gunatillake, R. Adhikari, G. P. Felton*, Biodegradable polyurethanes: design, synthesis, properties and potential applications*, in *Biodegradable polymers: Processing, degradation and applications* (Ed.: Gary P. Felton), Nova Science Publishers, Hauppauge (New York), **2011**, pp. 431-470; b) G. T. Howard, *Int. Biodeterior. Biodegrad.* **2002**, *49*, 245-252; c) T. Thomson, *Polyurethanes as specialty chemicals: principles and applications*, CRC Press (Taylor & Francis Group), Boca Raton, Florida, **2005**.

[201] K. Uhlig, *Discovering polyurethanes*, Carl Hanser, München, Germany, **1999**.

[202] B. Tieke, *Makromolekulare Chemie: Eine Einführung*, John Wiley & Sons, **2014**.

[203] a) G. Natta, P. Corradini, I. W. Bassi, *Nuovo. Cima.* **1960**, *15*, 68-82; b) N. Ishihara, T. Seimiya, M. Kuramoto, M. Uoi, *Macromolecules* **1986**, *19*, 2464-2465.

[204] W. Kaminsky, *Metalorganic catalysts for synthesis and polymerization: recent results by Ziegler-Natta and metallocene investigations*, Springer Science & Business Media, Berlin, Germany, **1999**.

[205] P. Zinck, F. Bonnet, A. Mortreux, M. Visseaux, *Prog. Polym. Sci.* **2009**, *34*, 369-392.

[206] C. A. McNamara, M. J. Dixon, M. Bradley, *Chem. Rev.* **2002**, *102*, 3275-3300.

[207] J. Maul, B. G. Frushour, J. R. Kontoff, H. Eichenauer, K.-H. Ott, C. Schade*, Polystyrene and styrene copolymers*, in *Ullmann's encyclopedia of industrial chemistry*, Wiley-VCH, **2000**.
[208] http://plasticfoodservicefacts.com/Safety-of-Styrene-Based-Polymers-for-Food-Contact, last accessed 16.01.2017.
[209] N. Kumar, R. S. Langer, A. J. Domb, *Adv. Drug Delivery Rev.* **2002**, *54*, 889-910.
[210] A. Göpferich, J. Tessmar, *Adv. Drug Delivery Rev.* **2002**, *54*, 911-931.
[211] A. J. Domb, R. Langer, *J. Polym. Sci., Part A: Polym. Chem.* **1987**, *25*, 3373-3386.
[212] N. G. Gaylord, *J. Macromol. Sci., Rev. Macromol. Chem.* **1975**, *C13*, 235-261.
[213] G. J. Domski, J. M. Rose, G. W. Coates, A. D. Bolig, M. Brookhart, *Prog. Polym. Sci.* **2007**, *32*, 30-92.
[214] a) P. Cossee, *J. Catal.* **1964**, *3*, 80-88; b) G. Fink, R. Mülhaupt, H. H. Brintzinger, *Ziegler Catalysts: Recent Scientific Innovations and Technological Improvements*, Springer, Berlin, Heidelberg, Germany, **2012**.
[215] J. E. Puskas, Y. Chen, Y. Dahman, D. Padavan, *J. Polym. Sci., Part A: Polym. Chem.* **2004**, *42*, 3091-3109.
[216] A. J. Lovinger*, Poly(vinylidene fluoride)*, in *Developments in crystalline polymers, Vol. 1* (Ed.: D. C. Bassett), Springer, Dordrecht, Netherlands, **1982**, pp. 195-273.
[217] a) A. Grigoletto, K. Maso, A. Mero, A. Rosato, O. Schiavon, G. Pasut, *J. Drug Delivery Sci. Technol.* **2016**, *32*, 132–141; b) P. Mishra, B. Nayak, R. K. Dey, *Asian J. Pharm. Sci.*, *11*, 337–348.
[218] J. M. Harris, R. B. Chess, *Nat. Rev. Drug Discovery* **2003**, *2*, 214-221.
[219] A. Kolate, D. Baradia, S. Patil, I. Vhora, G. Kore, A. Misra, *J. Control. Release* **2014**, *192*, 67-81.
[220] V. B. Damodaran, C. J. Fee, *Eur. Pharm. Rev.* **2010**, *15*, 18.
[221] a) A. Kozlowski, J. Milton Harris, *J. Control. Release* **2001**, *72*, 217-224; b) P. L. Turecek, M. J. Bossard, F. Schoetens, I. A. Ivens, *J. Pharm. Sci.* **2016**, *105*, 460-475.
[222] a) I. Zundorf, T. Dingermann, *Die Pharmazie* **2014**, *69*, 323-326; b) M. A. Croyle, Q. C. Yu, J. M. Wilson, *Hum. Gene Ther.* **2000**, *11*, 1713-1722.
[223] S. DeFrees, Z.-G. Wang, R. Xing, A. E. Scott, J. Wang, D. Zopf, D. L. Gouty, E. R. Sjoberg, K. Panneerselvam, E. C. M. Brinkman-Van der Linden, R. J. Bayer, M. A. Tarp, H. Clausen, *Glycobiology* **2006**, *16*, 833-843.
[224] a) S. Brocchini, A. Godwin, S. Balan, J.-w. Choi, M. Zloh, S. Shaunak, *Adv. Drug Delivery Rev.* **2008**, *60*, 3-12; b) G. Pasut, F. M. Veronese, *J. Control. Release* **2012**, *161*, 461-472.
[225] E. W. M. Ng, D. T. Shima, P. Calias, E. T. Cunningham, D. R. Guyer, A. P. Adamis, *Nat. Rev. Drug Discovery* **2006**, *5*, 123-132.
[226] http://www.fda.gov/NewsEvents/Newsroom/PressAnnouncements/ucm472643.htm, last accessed 16.01.2017.
[227] a) I. A. Ivens, A. Baumann, T. A. McDonald, T. J. Humphries, L. A. Michaels, P. Mathew, *Haemophilia* **2013**, *19*, 11-20; b) M. V. Ragni, *Drugs* **2015**, *75*, 1587-1600; c) M. Laffan, *Br. J. Haematol.* **2016**, *172*, 23-31; d) R. Stidl, S. Fuchs, M. Bossard, J. Siekmann, P. L. Turecek, M. Putz, *Haemophilia* **2016**, *22*, 54-64.
[228] a) E. Blasko, L. Leong, D. S. Sim, L. Tang, E. Ho, J. Wu, K. Z. Kauser, B. Subramanyam, *Blood* **2014**, *124*, 1471-1471; b) T. T. Wynn, B. Gumuscu, *J. Blood Med.* **2016**, *7*, 121-128.
[229] H. R. Stennicke, M. Kjalke, D. M. Karpf, K. W. Balling, P. B. Johansen, T. Elm, K. Øvlisen, F. Möller, H. L. Holmberg, C. N. Gudme, E. Persson, I. Hilden, H. Pelzer, H. Rahbek-Nielsen, C. Jespersgaard, A. Bogsnes, A. A. Pedersen, A. K. Kristensen, B. Peschke, W. Kappers, F. Rode, L. Thim, M. Tranholm, M. Ezban, E. H. N. Olsen, S. E. Bjørn, *Blood* **2013**, *121*, 2108-2116.
[230] a) P. W. Collins, G. Young, K. Knobe, F. A. Karim, P. Angchaisuksiri, C. Banner, T. Gürsel, J. Mahlangu, T. Matsushita, E. P. Mauser-Bunschoten, J. Oldenburg, C. E. Walsh, C. Negrier, *Blood*

2014, *124*, 3880-3886; b) T. E. Coyle, M. T. Reding, J. C. Lin, L. A. Michaels, A. Shah, J. Powell, *J. Thromb. Haemost.* **2014**, *12*, 488-496.
[231] F. Peyvandi, I. Garagiola, S. Seregni, *J. Thromb. Haemost.* **2013**, *11*, 84-98.
[232] a) M. J. de Groot, M. Hoeksma, N. Blau, D. J. Reijngoud, F. J. van Spronsen, *Mol. Genet. Metab.* **2010**, *99*, S86-S89; b) J. B. Hennermann, S. Roloff, C. Gebauer, B. Vetter, A. von Arnim-Baas, E. Mönch, *Mol. Genet. Metab.* **2012**, *107*, 294-301.
[233] A. Bélanger-Quintana, A. Burlina, C. O. Harding, A. C. Muntau, *Mol. Genet. Metab.* **2011**, *104*, S19-S25.
[234] C. Sorli, *Am. J. Med.*, *127*, S39-S48.
[235] T. Hirose, *Diabetol. Int.* **2016**, *7*, 16-17.
[236] R. Haag, F. Kratz, *Angew. Chem. Int. Ed.* **2006**, *45*, 1198-1215.
[237] a) X. Pang, H.-L. Du, H.-Q. Zhang, Y.-J. Zhai, G.-X. Zhai, *Drug Discovery Today* **2013**, *18*, 1316-1322; b) W. Li, P. Zhan, E. De Clercq, H. Lou, X. Liu, *Prog. Polym. Sci.* **2013**, *38*, 421-444.
[238] M. Swierczewska, K. C. Lee, S. Lee, *Expert Opin. Emerging Drugs* **2015**, *20*, 531-536.
[239] http://fibromyalgianewstoday.com/2015/03/04/novel-drug-treats-chronic-pain-without-side-effects-danger-abuse/, last accessed 16.01.2017.
[240] http://www.nektar.com/pipeline/rd-pipeline/nktr-181, last accessed 16.01.2017.
[241] U. Hoch, C.-M. Staschen, R. K. Johnson, M. A. Eldon, *Cancer Chemother. Pharmacol.* **2014**, *74*, 1125-1137.
[242] A. Patnaik, K. P. Papadopoulos, A. W. Tolcher, M. Beeram, S. Urien, L. J. Schaaf, S. Tahiri, T. Bekaii-Saab, F. M. Lokiec, K. Rezaï, A. Buchbinder, *Cancer Chemother. Pharmacol.* **2013**, *71*, 1499-1506.
[243] http://www.nektar.com/pipeline/rd-pipeline/onzeald, last accessed 16.01.2017.
[244] a) http://www.fda.gov/downloads/AdvisoryCommittees/CommitteesMeetingMaterials/Drugs/OncologicDrugsAdvisoryCommittee/UCM426178.pdf, last accessed 16.01.2017; b) E. A. Perez, A. Awada, J. O'Shaughnessy, H. S. Rugo, C. Twelves, S.-A. Im, P. Gómez-Pardo, L. S. Schwartzberg, V. Diéras, D. A. Yardley, D. A. Potter, A. Mailliez, A. Moreno-Aspitia, J.-S. Ahn, C. Zhao, U. Hoch, M. Tagliaferri, A. L. Hannah, J. Cortes, *Lancet Oncol.* **2015**, *16*, 1556-1568.
[245] Z. Hong, *Curr. Bioact. Compd.* **2011**, *7*, 3-7.
[246] E. C. Emery, A. P. Luiz, J. N. Wood, *Expert Opin. Ther. Targets* **2016**, *20*, 975-983.
[247] a) E. M. Pelegri-O'Day, E.-W. Lin, H. D. Maynard, *J. Am. Chem. Soc.* **2014**, *136*, 14323-14332; b) Y. Qi, A. Chilkoti, *Curr. Opin. Chem. Biol.* **2015**, *28*, 181-193.
[248] S. Shah, T. Prematta, N. F. Adkinson, F. T. Ishmael, *J. Clin. Pharmacol.* **2013**, *53*, 352-355.
[249] R. Duncan, *Nat. Rev. Cancer* **2006**, *6*, 688-701.
[250] A. Godwin, K. Bolina, M. Clochard, E. Dinand, S. Rankin, S. Simic, S. Brocchini, *J. Pharm. Pharmacol.* **2001**, *53*, 1175-1184.
[251] a) H. Maeda, J. Takeshita, R. Kanamaru, *Int. J. Pept. Protein Res.* **1979**, *14*, 81-87; b) H. Maeda, M. Ueda, T. Morinaga, T. Matsumoto, *J. Med. Chem.* **1985**, *28*, 455-461.
[252] N. Ohtsuka, T. Konno, Y. Miyauchi, H. Maeda, *Cancer* **1987**, *59*, 1560-1565.
[253] T. Konno, H. Maeda*, Targeting chemotherapy of hepatocellular carcinoma*, in *Neoplasms of the liver* (Eds.: Kunio Okuda, Kamal G. Ishak), Springer, Tokyo, Japan, **1987**, pp. 343-352.
[254] P. Caliceti, F. M. Veronese, *Adv. Drug Delivery Rev.* **2003**, *55*, 1261-1277.
[255] Y. Matsumura, H. Maeda, *Cancer Res.* **1986**, *46*, 6387-6392.
[256] H. Ishii, J. Furuse, M. Nagase, Y. Maru, M. Yoshino, T. Hayashi, *Jpn. J. Clin. Oncol.* **2003**, *33*, 570-573.
[257] T. Taguchi, T. Saito, J. Ota, I. Nakao, K. Ohashi, H. Nakamura, T. Konno, *Gan to kagaku ryoho* **1991**, *18*, 1665-1675.
[258] M. J. Vicent, R. Duncan, *Trends Biotechnol.* **2006**, *24*, 39-47.

[259] a) B. Rihova, M. Bilej, V. Vetvicka, K. Ulbrich, J. Strohalm, J. Kopecek, R. Duncan, *Biomaterials* **1989**, *10*, 335-342; b) B. Rihova, K. Ulbrich, J. Kopecek, P. Mancal, *Folia Microbiol.* **1983**, *28*, 217-227.
[260] P. M. Loadman, M. C. Bibby, J. A. Double, W. M. Al-Shakhaa, R. Duncan, *Clin. Cancer Res.* **1999**, *5*, 3682-3688.
[261] P. Rejmanová, J. Kopeček, R. Duncan, J. B. Lloyd, *Biomaterials* **1985**, *6*, 45-48.
[262] J. Cassidy, R. Duncan, G. J. Morrison, J. Strohalm, D. Plocova, J. Kopecek, S. B. Kaye, *Biochem. Pharmacol.* **1989**, *38*, 875-879.
[263] R. Duncan, L. C. Seymour, L. Scarlett, J. B. Lloyd, P. Rejmanová, J. Kopecek, *Biochim. Biophys. Acta* **1986**, *880*, 62-71.
[264] L. W. Seymour, D. R. Ferry, D. Anderson, S. Hesslewood, P. J. Julyan, R. Poyner, J. Doran, A. M. Young, S. Burtles, D. J. Kerr, *J. Clin. Oncol.* **2002**, *20*, 1668-1676.
[265] E. Gianasi, M. Wasil, E. G. Evagorou, A. Keddle, G. Wilson, R. Duncan, *Eur. J. Cancer* **1999**, *35*, 994-1002.
[266] X. Lin, Q. Zhang, J. R. Rice, D. R. Stewart, D. P. Nowotnik, S. B. Howell, *Eur. J. Cancer* **2004**, *40*, 291-297.
[267] a) http://www.prnewswire.com/news-releases/access-expands-its-polymer-platinate-program-71728437.html, last accessed 16.01.2017; b) R. Tong, J. Cheng, *Polym. Rev.* **2007**, *47*, 345-381.
[268] D. P. Nowotnik, E. Cvitkovic, *Adv. Drug Delivery Rev.* **2009**, *61*, 1214-1219.
[269] D. P. Nowotnik, *Curr. Bioact. Compd.* **2011**, *7*, 21-26.
[270] https://www.clinicaltrialsregister.eu/ctr-search/search?query=2010-020030-25, last accessed 16.01.2017.
[271] J. M. Meerum Terwogt, W. W. ten Bokkel Huinink, J. H. Schellens, M. Schot, I. A. Mandjes, M. G. Zurlo, M. Rocchetti, H. Rosing, F. J. Koopman, J. H. Beijnen, *Anticancer drugs* **2001**, *12*, 315-323.
[272] a) N. E. Schoemaker, C. van Kesteren, H. Rosing, S. Jansen, M. Swart, J. Lieverst, D. Fraier, M. Breda, C. Pellizzoni, R. Spinelli, M. G. Porro, J. H. Beijnen, J. H. M. Schellens, W. W. ten Bokkel Huinink, *Br. J. Cancer* **2002**, *87*, 608-614; b) D. Bissett, J. Cassidy, J. S. de Bono, F. Muirhead, M. Main, L. Robson, D. Fraier, M. L. Magnè, C. Pellizzoni, M. G. Porro, R. Spinelli, W. Speed, C. Twelves, *Br. J. Cancer* **2004**, *91*, 50-55; c) F. M. Wachters, H. J. M. Groen, J. G. Maring, J. A. Gietema, M. Porro, H. Dumez, E. G. E. de Vries, A. T. van Oosterom, *Br. J. Cancer* **2004**, *90*, 2261-2267.
[273] a) X.-M. Liu, S. C. Miller, D. Wang, *Adv. Drug Delivery Rev.* **2010**, *62*, 258; b) J. Kopeček, P. Kopečková, *Adv. Drug Delivery Rev.* **2010**, *62*, 122-149.
[274] a) H. Ross, P. Bonomi, C. Langer, M. O'Brien, K. O'Byrne, L. Paz-Ares, A. Sandler, M. Socinski, F. Oldham, J. Singer, *J. Clin. Oncol.* **2006**, *24*, abstr. 7039; b) C. J. Langer, K. J. O'Byrne, M. A. Socinski, S. M. Mikhailov, K. Leśniewski-Kmak, M. Smakal, T. E. Ciuleanu, S. V. Orlov, M. Dediu, D. Heigener, A. J. Eisenfeld, L. Sandalic, F. B. Oldham, J. W. Singer, H. J. Ross, *J. Thorac. Oncol.* **2008**, *3*, 623-630; c) M. E. R. O'Brien, M. A. Socinski, A. Y. Popovich, I. N. Bondarenko, A. Tomova, B. T. Bilynsky˘ı, Y. S. Hotko, V. L. Ganul, I. Y. Kostinsky, A. J. Eisenfeld, L. Sandalic, F. B. Oldham, B. Bandstra, A. B. Sandler, J. W. Singer, *J. Thorac. Oncol.* **2008**, *3*, 728-734.
[275] P. Bonomi, *Expert Rev. Anticancer Ther.* **2007**, *7*, 415-422.
[276] http://www.prnewswire.com/news-releases/european-regulatory-agency-accepts-cell-therapeutics-incs-marketing-authorization-application-for-xyotaxtm-for-lung-cancer-for-review-56983987.html, last accessed 16.01.2017.
[277] J. Homsi, G. R. Simon, C. R. Garrett, G. Springett, R. De Conti, A. A. Chiappori, P. N. Munster, M. K. Burton, S. Stromatt, C. Allievi, P. Angiuli, A. Eisenfeld, D. M. Sullivan, A. I. Daud, *Clin. Cancer Res.* **2007**, *13*, 5855-5861.

[278] K. L. Eskow Jaunarajs, D. G. Standaert, T. X. Viegas, M. D. Bentley, Z. Fang, B. Dizman, K. Yoon, R. Weimer, P. Ravenscroft, T. H. Johnston, M. P. Hill, J. M. Brotchie, R. W. Moreadith, *Mov. Disord.* **2013**, *28*, 1675-1682.
[279] http://serinatherapeutics.com/, last accessed 16.01.2017.
[280] D. H. Wakefield, J. J. Klein, J. A. Wolff, D. B. Rozema, *Bioconjugate Chem.* **2005**, *16*, 1204-1208.
[281] D. B. Rozema, D. L. Lewis, D. H. Wakefield, S. C. Wong, J. J. Klein, P. L. Roesch, S. L. Bertin, T. W. Reppen, Q. Chu, A. V. Blokhin, J. E. Hagstrom, J. A. Wolff, *Proc. Natl. Acad. Sci. U.S.A.* **2007**, *104*, 12982-12987.
[282] J. M. Rademaker-Lakhai, C. Terret, S. B. Howell, C. M. Baud, R. F. de Boer, D. Pluim, J. H. Beijnen, J. H. M. Schellens, J.-P. Droz, *Clin. Cancer Res.* **2004**, *10*, 3386-3395.
[283] V.-T. Tran, J.-P. Benoît, M.-C. Venier-Julienne, *Int. J. Pharm.* **2011**, *407*, 1-11.
[284] M. Vert, K.-H. Hellwich, M. Hess, P. Hodge, P. Kubisa, M. Rinaudo, F. Schué, *Pure Appl. Chem.* **2012**, *84*, 377-410.
[285] D. S. Kohane, *Biotechnol. Bioeng.* **2007**, *96*, 203-209.
[286] J. Renukuntla, A. D. Vadlapudi, A. Patel, S. H. S. Boddu, A. K. Mitra, *Int. J. Pharm.* **2013**, *447*, 75-93.
[287] A. C. Hunter, J. Elsom, P. P. Wibroe, S. M. Moghimi, *Nanomed. Nanotechnol. Biol. Med.* **2012**, *8, Supplement 1*, S5-S20.
[288] F. Ungaro, I. d' Angelo, A. Miro, M. I. La Rotonda, F. Quaglia, *J. Pharm. Pharmacol.* **2012**, *64*, 1217-1235.
[289] K. Letchford, H. Burt, *Eur. J. Pharm. Biopharm.* **2007**, *65*, 259-269.
[290] T. W. Prow, J. E. Grice, L. L. Lin, R. Faye, M. Butler, W. Becker, E. M. T. Wurm, C. Yoong, T. A. Robertson, H. P. Soyer, M. S. Roberts, *Adv. Drug Delivery Rev.* **2011**, *63*, 470-491.
[291] A. Firooz, S. Nafisi, H. I. Maibach, *Int. J. Pharm.* **2015**, *495*, 599-607.
[292] V. Lassalle, M. L. Ferreira, *Macromol. Biosci.* **2007**, *7*, 767-783.
[293] G. Singh, T. Kaur, R. Kaur, A. Kaur, *Int. J. Pharm. Pharm. Sci.* **2014**, *1*, 30-42.
[294] http://www.rovi.es/ficheros/notas/ingles/185i.pdf., last accessed 16.01.2017.
[295] W. Dang, I. R. Garver, DE 60023138 T2, **2006**.
[296] D. K. Armstrong, G. F. Fleming, M. Markman, H. H. Bailey, *Gynecol. Oncol.* **2006**, *103*, 391-396.
[297] S. Kaity, S. Maiti, A. Ghosh, D. Pal, A. Ghosh, S. Banerjee, *J. Adv. Pharm. Technol. Res.* **2010**, *1*, 283-290.
[298] T. Nicolai, O. Colombani, C. Chassenieux, *Soft Matter* **2010**, *6*, 3111-3118.
[299] G. Riess, *Prog. Polym. Sci.* **2003**, *28*, 1107-1170.
[300] M. Talelli, M. Barz, C. J. F. Rijcken, F. Kiessling, W. E. Hennink, T. Lammers, *Nano Today* **2015**, *10*, 93-117.
[301] E. Pérez-Herrero, A. Fernández-Medarde, *Eur. J. Pharm. Biopharm.* **2015**, *93*, 52-79.
[302] Y. Min, J. M. Caster, M. J. Eblan, A. Z. Wang, *Chem. Rev.* **2015**, *115*, 11147-11190.
[303] C. Oerlemans, W. Bult, M. Bos, G. Storm, J. F. W. Nijsen, W. E. Hennink, *Pharm. Res.* **2010**, *27*, 2569-2589.
[304] http://www.samyangbiopharm.com/eng/productintroduce/injection01, last accessed 16.01.2017.
[305] S.-W. Lee, M.-H. Yun, S. W. Jeong, C.-H. In, J.-Y. Kim, M.-H. Seo, C.-M. Pai, S.-O. Kim, *J. Control. Release* **2011**, *155*, 262-271.
[306] K. Kato, K. Chin, T. Yoshikawa, K. Yamaguchi, Y. Tsuji, T. Esaki, K. Sakai, M. Kimura, T. Hamaguchi, Y. Shimada, Y. Matsumura, R. Ikeda, *Invest. New Drugs* **2012**, *30*, 1621-1627.
[307] J. W. Valle, A. Armstrong, C. Newman, V. Alakhov, G. Pietrzynski, J. Brewer, S. Campbell, P. Corrie, E. K. Rowinsky, M. Ranson, *Invest. New Drugs* **2011**, *29*, 1029-1037.

[308] J. Hrkach, D. Von Hoff, M. M. Ali, E. Andrianova, J. Auer, T. Campbell, D. De Witt, M. Figa, M. Figueiredo, A. Horhota, S. Low, K. McDonnell, E. Peeke, B. Retnarajan, A. Sabnis, E. Schnipper, J. J. Song, Y. H. Song, J. Summa, D. Tompsett, G. Troiano, T. Van Geen Hoven, J. Wright, P. LoRusso, P. W. Kantoff, N. H. Bander, C. Sweeney, O. C. Farokhzad, R. Langer, S. Zale, *Sci. Transl. Med.* **2012**, *4*, 128ra139-128ra139.

[309] S. Ashton, Y. H. Song, J. Nolan, E. Cadogan, J. Murray, R. Odedra, J. Foster, P. A. Hall, S. Low, P. Taylor, R. Ellston, U. M. Polanska, J. Wilson, C. Howes, A. Smith, R. J. A. Goodwin, J. G. Swales, N. Strittmatter, Z. Takáts, A. Nilsson, P. Andren, D. Trueman, M. Walker, C. L. Reimer, G. Troiano, D. Parsons, D. De Witt, M. Ashford, J. Hrkach, S. Zale, P. J. Jewsbury, S. T. Barry, *Sci. Transl. Med.* **2016**, *8*, 325ra317.

[310] a) L. Cadzow, K. Arnold, D. Thrasher, J. Nolan, A. Horhota, E. Lewis-Clark, J. Wright, S. Low, *Mol. Cancer Ther.* **2015**, *14*, C184; b) http://www.businesswire.com/news/home/20150924005171/en/BIND-Therapeutics-Announces-Pfizer-Exercises-Option-Advance, last accessed 16.01.2017.

[311] Y. Matsumura, T. Hamaguchi, T. Ura, K. Muro, Y. Yamada, Y. Shimada, K. Shirao, T. Okusaka, H. Ueno, M. Ikeda, N. Watanabe, *Br. J. Cancer* **2004**, *91*, 1775-1781.

[312] L. Pittet, D. Altreuter, P. Ilyinskii, C. Fraser, Y. Gao, S. Baldwin, M. Keegan, L. Johnston, T. Kishimoto, *J. Immunol.* **2012**, *188*, 75.11.

[313] R. A. Maldonado, R. A. LaMothe, J. D. Ferrari, A. H. Zhang, R. J. Rossi, P. N. Kolte, A. P. Griset, C. O'Neil, D. H. Altreuter, E. Browning, L. Johnston, O. C. Farokhzad, R. Langer, D. W. Scott, U. H. von Andrian, T. K. Kishimoto, *Proc. Natl. Acad. Sci. U.S.A.* **2015**, *112*, E156-165.

[314] T. Ueno, K. Endo, K. Hori, N. Ozaki, A. Tsuji, S. Kondo, N. Wakisaka, S. Murono, K. Kataoka, Y. Kato, T. Yoshizaki, *Int. J. Nanomed.* **2014**, *9*, 3005-3012.

[315] S. Eliasof, D. Lazarus, C. G. Peters, R. I. Case, R. O. Cole, J. Hwang, T. Schluep, J. Chao, J. Lin, Y. Yen, H. Han, D. T. Wiley, J. E. Zuckerman, M. E. Davis, *Proc. Natl. Acad. Sci. U.S.A.* **2013**, *110*, 15127-15132.

[316] D. Lazarus, S. Kabir, S. Eliasof, *Cancer Res.* **2012**, *72*, 5643.

[317] S. Wohlfart, A. S. Khalansky, C. Bernreuther, M. Michaelis, J. Cinatl Jr, M. Glatzel, J. Kreuter, *Int. J. Pharm.* **2011**, *415*, 244-251.

[318] Q. Zhou, X. Sun, L. Zeng, J. Liu, Z. Zhang, *Nanomed. Nanotechnol. Biol. Med.* **2009**, *5*, 419-423.

[319] B. S. Pattni, V. V. Chupin, V. P. Torchilin, *Chem. Rev.* **2015**, *115*, 10938-10966.

[320] https://www.doxil.com/, last accessed 16.01.2017.

[321] http://www.fda.gov/drugs/informationondrugs/approveddrugs/ucm292721.htm, last accessed 16.01.2017.

[322] http://www.ciplamed.com/content/oncodox-peg-injection, last accessed 16.01.2017.

[323] G. P. Stathopoulos, *Anti-Cancer Drugs* **2010**, *21*, 732-736.

[324] G. P. Stathopoulos, D. Antoniou, J. Dimitroulis, P. Michalopoulou, A. Bastas, K. Marosis, J. Stathopoulos, A. Provata, P. Yiamboudakis, D. Veldekis, N. Lolis, N. Georgatou, M. Toubis, C. Pappas, G. Tsoukalas, *Ann. Oncol.* **2010**, *21*, 2227-2232.

[325] U. Lächelt, E. Wagner, *Chem. Rev.* **2015**, *115*, 11043-11078.

[326] Y. Lee, K. Kataoka, *Adv. Polym. Sci.* **2012**, 95-134.

[327] a) R. Kanasty, J. R. Dorkin, A. Vegas, D. Anderson, *Nat. Mater.* **2013**, *12*, 967-977; b) H. Yin, R. L. Kanasty, A. A. Eltoukhy, A. J. Vegas, J. R. Dorkin, D. G. Anderson, *Nat. Rev. Genet.* **2014**, *15*, 541-555.

[328] C. A. Taylor, Z. Liu, T. C. Tang, Q. Zheng, S. Francis, T.-W. Wang, B. Ye, J. A. Lust, R. Dondero, J. E. Thompson, *Mol. Ther.* **2012**, *20*, 1305-1314.

[329] L. Buscail, B. Bournet, F. Vernejoul, G. Cambois, H. Lulka, N. Hanoun, M. Dufresne, A. Meulle, A. Vignolle-Vidoni, L. Ligat, N. Saint-Laurent, F. Pont, S. Dejean, M. Gayral, F. Martins, J. Torrisani, O.

Barbey, F. Gross, R. Guimbaud, P. Otal, F. Lopez, G. Tiraby, P. Cordelier, *Mol. Ther.* **2015**, *23*, 779-789.
[330] http://www.biocancell.com/lead-program/bc-819/, last accessed 16.01.2017.
[331] I. J. Matouk, D. Halle, M. Gilon, A. Hochberg, *J. Transl. Med.* **2015**, *13*, 1-12.
[332] J. G. Fewell, M. Matar, G. Slobodkin, S.-O. Han, J. Rice, B. Hovanes, D. H. Lewis, K. Anwer, *J. Control. Release* **2005**, *109*, 288-298.
[333] R. D. Alvarez, M. W. Sill, S. A. Davidson, C. Y. Muller, D. P. Bender, R. L. DeBernardo, K. Behbakht, W. K. Huh, *Gynecol. Oncol.* **2014**, *133*, 433-438.
[334] http://celsion.com/pages/pipeline, last accessed 16.01.2017.
[335] M. E. Davis, *Mol. Pharmaceutics* **2009**, *6*, 659-668.
[336] M. E. Davis, J. E. Zuckerman, C. H. J. Choi, D. Seligson, A. Tolcher, C. A. Alabi, Y. Yen, J. D. Heidel, A. Ribas, *Nature* **2010**, *464*, 1067-1070.
[337] H. B. Levy, G. Baer, S. Baron, C. E. Buckler, C. J. Gibbs, M. J. Iadarola, W. T. London, J. Rice, *J. Infect. Dis.* **1975**, *132*, 434-439.
[338] A. S. Levine, H. B. Levy, *Cancer Treat. Rep.* **1978**, *62*, 1907-1912.
[339] M. W. Konstan, P. B. Davis, J. S. Wagener, K. A. Hilliard, R. C. Stern, L. J. H. Milgram, T. H. Kowalczyk, S. L. Hyatt, T. L. Fink, C. R. Gedeon, S. M. Oette, J. M. Payne, O. Muhammad, A. G. Ziady, R. C. Moen, M. J. Cooper, *Hum. Gene Ther.* **2004**, *15*, 1255-1269.
[340] F. Lori, J. Trocio, N. Bakare, L. M. Kelly, J. Lisziewicz, *Vaccine* **2005**, *23*, 2030-2034.
[341] a) J. Hartikka, A. Geall, V. Bozoukova, D. Kurniadi, D. Rusalov, J. Enas, J.-H. Yi, A. Nanci, A. Rolland, *J. Gene Med.* **2008**, *10*, 770-782; b) M. A. Kharfan-Dabaja, T. Nishihori, *Expert Rev. Vaccines* **2015**, *14*, 341-350.
[342] A. L. Sisson, R. Haag, *Soft Matter* **2010**, *6*, 4968-4975.
[343] A. V. Kabanov, S. V. Vinogradov, *Angew. Chem. Int. Ed.* **2009**, *48*, 5418-5429.
[344] A. L. Lewis, M. V. Gonzalez, S. W. Leppard, J. E. Brown, P. W. Stratford, G. J. Phillips, A. W. Lloyd, *J. Mater. Sci. Mater. Med.* **2007**, *18*, 1691-1699.
[345] G. Bruixola, R. García, F. Gomez, C. Escoín, L. Palomar, H. de la Cueva, J. J. Martínez, A. Santaballa, *Ann. Oncol.* **2015**, *26*, iii6-ii9.
[346] O. K. Akinwande, P. Philips, P. Duras, S. Pluntke, C. Scoggins, R. C. Martin, *Cardiovasc. Interv. Radiol.* **2015**, *38*, 361-371.
[347] A. L. Lewis, M. R. Dreher, V. O'Byrne, D. Grey, M. Caine, A. Dunn, Y. Tang, B. Hall, K. D. Fowers, C. G. Johnson, K. V. Sharma, B. J. Wood, *J. Mater. Sci. Mater. Med.* **2016**, *27*, 13.
[348] M. Boulin, P. Hillon, J. P. Cercueil, F. Bonnetain, S. Dabakuyo, A. Minello, J. L. Jouve, C. Lepage, M. Bardou, M. Wendremaire, P. Guerard, A. Denys, A. Grandvuillemin, B. Chauffert, L. Bedenne, B. Guiu, *Alimentary Pharmacology & Therapeutics* **2014**, *39*, 1301-1313.
[349] R. Duran, K. Sharma, M. R. Dreher, K. Ashrafi, S. Mirpour, M. Lin, R. E. Schernthaner, T. R. Schlachter, V. Tacher, A. L. Lewis, S. Willis, M. den Hartog, A. Radaelli, A. H. Negussie, B. J. Wood, J.-F. H. Geschwind, *Theranostics* **2016**, *6*, 28-39.
[350] https://www.btgplc.com/media/press-releases/first-patient-treated-with-lc-bead-lumi-radiopaque-embolic-bead-supported-by-philips-live-image-guidance/, last accessed 16.01.2017.
[351] U. Fritz, O. Fritz, T. A. Gordy, R. Wojcik, J. Blummel, A. Kuller, US 9107850 B2, **2009**.
[352] B. Guiu, A. Schmitt, S. Reinhardt, A. Fohlen, T. Pohl, M. Wendremaire, A. Denys, J. Blümmel, M. Boulin, *J. Vasc. Interv. Radiol.* **2015**, *26*, 262-270.
[353] E. de Luis, J. I. Bilbao, J. A. G. J. Ciércoles, A. Martínez-Cuesta, A. de Martino Rodríguez, M. D. Lozano, *Cardiovasc. Interv. Radiol.* **2008**, *31*, 367-376.
[354] K. Malagari, A. Pomoni, D. Filippiadis, D. Kelekis, *Hepat. Oncol.* **2015**, *2*, 147-157.

[355] http://www.terumo-europe.com/en-emea/interventional-oncology/loco-regional-treatment/drug-elutable-microspheres-tace/lifepearl%C2%AE-microspheres, last accessed 16.01.2017.
[356] http://www.marketwired.com/press-release/biolex-sells-lex-system-to-synthon-and-initiates-sale-of-locteron-1653466.htm, last accessed 16.01.2017.
[357] J. Alemán, A. V. Chadwick, J. He, M. Hess, K. Horie, R. G. Jones, P. Kratochvíl, I. Meisel, I. Mita, G. Moad, *Pure Appl. Chem.* **2007**, *79*, 1801-1829.
[358] a) M. Hamidi, A. Azadi, P. Rafiei, *Adv. Drug Delivery Rev.* **2008**, *60*, 1638-1649; b) K. S. Soni, S. S. Desale, T. K. Bronich, *J. Control. Release* **2016**, *240*, 109-126.
[359] http://www.avadel.com/research-pipeline/innovative-technologies/medusa-/, last accessed 16.01.2017.
[360] Y. P. Chan, R. Meyrueix, R. Kravtzoff, F. Nicolas, K. Lundstrom, *Expert Opin. Drug Deliv.* **2007**, *4*, 441-451.
[361] L. Jorgensen, H. M. Nielson, *Delivery Technologies for Biopharmaceuticals: Peptides, Proteins, Nucleic Acids and Vaccines*, JohnWiley & Sons, West Sussex (U. K.), **2009**.
[362] http://www.marketwired.com/press-release/flamel-technologies-medusar-formulated-interferon-alpha-demonstrates-favorable-antiviral-nasdaq-flml-1673013.htm, last accessed 16.01.2017.
[363] http://adisinsight.springer.com/drugs/800040952, last accessed 16.01.2017.
[364] http://www.ocutx.com/pipeline/dexamethasone-punctum-plug, last accessed 16.01.2017.
[365] https://www.drugs.com/clinical_trials/ocular-therapeutix-announces-successful-topline-results-both-inflammation-pain-primary-efficacy-17243.html, last accessed 16.01.2017.
[366] C. Blizzard, A. Desai, A. Driscoll, *J. Ocul. Pharmacol. Ther.* **2016**, *32*, 595-600.
[367] E. Caló, V. V. Khutoryanskiy, *Eur. Polym. J.* **2015**, *65*, 252-267.
[368] http://www.ferringusa.com/pi/cervidil., last accessed 16.01.2017.
[369] P. Gupta, K. Vermani, S. Garg, *Drug Discovery Today* **2002**, *7*, 569-579.
[370] http://www.businesswire.com/news/home/20080225005425/en/Marillion-Pharmaceuticals-Cytokine-PharmaSciences-Announce-License-Agreement, last accessed 16.01.2017.
[371] J. Gibson, J. A. Halliday, K. Ewert, S. Robertson, *Br. Dent. J.* **2007**, *202*, E17.
[372] http://adisinsight.springer.com/drugs/800020054, last accessed 16.01.2017.
[373] https://docetp.mpa.se/LMF/Misodel%20vaginal%20delivery%20system%20ENG%20PAR.pdf, last accessed 16.01.2017.
[374] http://www.supprelinla.com/, last accessed 16.01.2017.
[375] L. A. Silverman, E. K. Neely, G. B. Kletter, K. Lewis, S. Chitra, O. Terleckyj, E. A. Eugster, *J. Clin. Endocrinol. Metab.* **2015**, *100*, 2354-2363.
[376] http://www.vantasimplant.com/, last accessed 16.01.2017.
[377] http://www.hydromer.com/cosmetic/aquamere.pdf, last accessed 16.01.2017.
[378] http://www.hydromer.com/cosmetic/aquatrix.pdf, last accessed 16.01.2017.
[379] V. A. Stoy, *J. Biomater. Appl.* **1988**, *3*, 552-604.
[380] http://www.bloomberg.com/research/stocks/private/snapshot.asp?privcapId=711690, last accessed 16.01.2017.
[381] R. C. Rathi, J. Bark, K. D. Fowers*, SQZgelTM*, in *Modified-release drug delivery technology* (Eds.: M. J. Rathbone, J. Hadgraft, M. S. Roberts, M. E. Lane), CRC Press (Taylor & Francis Group), Salt Lake City, Utah, **2008**, pp. 153-162.
[382] https://hum-molgen.org/companies/profile.php3/413-gelmed, last accessed 16.01.2017.
[383] D. E. Newton, *Chemistry of New Materials*, Facts On File, New York, **2007**.
[384] N. L. Elstad, K. D. Fowers, *Adv. Drug Delivery Rev.* **2009**, *61*, 785-794.

[385] B. Tyler, K. D. Fowers, K. W. Li, V. R. Recinos, J. M. Caplan, A. Hdeib, R. Grossman, L. Basaldella, K. Bekelis, G. Pradilla, F. Legnani, H. Brem, *J. Neurosurg.* **2010**, *113*, 210-217.
[386] G. Bonacucina, M. Cespi, G. Mencarelli, G. Giorgioni, G. F. Palmieri, *Polymers* **2011**, *3*, 779-811.
[387] M. McKenzie, D. Betts, A. Suh, K. Bui, L. D. Kim, H. Cho, *Molecules* **2015**, *20*, 20397-20408.
[388] S. J. Vukelja, S. P. Anthony, J. C. Arseneau, B. S. Berman, C. Casey Cunningham, J. J. Nemunaitis, W. E. Samlowski, K. D. Fowers, *Anticancer Drugs* **2007**, *18*, 283-289.
[389] G. A. DuVall, D. Tarabar, R. H. Seidel, N. L. Elstad, K. D. Fowers, *Anticancer Drugs* **2009**, *20*, 89-95.
[390] http://www.scripintelligence.com/researchdevelopment/BTG-discontinues-paclitaxel-gel-after-Phase-IIb-failure-313595, last accessed 16.01.2017.
[391] http://ipmglobal.org/our-work/our-products/dapivirine-ring/phase-iii-results, last accessed 16.01.2017.
[392] http://pipeline.ctiexchange.org/products/upa-vaginal-ring, last accessed 16.01.2017.
[393] J. T. Clark, M. R. Clark, N. B. Shelke, T. J. Johnson, E. M. Smith, A. K. Andreasen, J. S. Nebeker, J. Fabian, D. R. Friend, P. F. Kiser, *PLoS ONE* **2014**, *9*, e88509.
[394] S. R. Ugaonkar, A. Wesenberg, J. Wilk, S. Seidor, O. Mizenina, L. Kizima, A. Rodriguez, S. Zhang, K. Levendosky, J. Kenney, M. Aravantinou, N. Derby, B. Grasperge, A. Gettie, J. Blanchard, N. Kumar, K. Roberts, M. Robbiani, J. A. Fernández-Romero, T. M. Zydowsky, *J. Control. Release* **2015**, *213*, 57-68.
[395] http://www.tevapharm.com/news/phase_iii_study_of_teva_s_milprosa_progesterone_vaginal_ring_published_in_fertility_and_sterility_03_13.aspx, last accessed 16.01.2017.
[396] http://www.ipmglobal.org/content/ipms-dapivirine-ring-may-offer-significant-hiv-protection-when-used-consistently-new-data, last accessed 16.01.2017.
[397] D. Ramchandran, U. D. Upadhyay, *Population Reports* **2007**, 1-19.
[398] A. Lendvay, R. Otieno-Masaba, S. K. Azmat, A. Wheeless, W. Hameed, B. T. Shaikh, S. Kuria, M. J. Steiner, M. Chen, P. J. Feldblum, *Contraception* **2014**, *89*, 197-203.
[399] http://www.dahua-sh.com/, last accessed 16.01.2017.
[400] S. Palomba, A. Falbo, A. Di Cello, C. Materazzo, F. Zullo, *Gynecol. Endocrinol.* **2012**, *28*, 710-721.
[401] https://pipeline.ctiexchange.org/fillpdf?fid=105&nid=869, last accessed 16.01.2017.
[402] V. Halpern, R. M. Stalter, D. H. Owen, L. J. Dorflinger, A. Lendvay, K. H. Rademacher, *Contraception* **2015**, *92*, 3-9.
[403] http://www.fda.gov/NewsEvents/Newsroom/PressAnnouncements/ucm503719.htm, last accessed 16.01.2017.
[404] E. Dolgin, *Nat. Med.* **2014**, *20*, 9-11.
[405] http://www.medicinenet.com/pilocarpine-ophthalmic_ocular_system/article.htm, last accessed 16.01.2017.
[406] D. B. Troy, J. P. Remington, P. Beringer, *Remington: The science and practice of pharmacy*, Lippincott Williams & Wilkins, Philadelphia, Pennsylvania, **2006**.
[407] J. Wang, A. Jiang, M. Joshi, J. Christoforidis, *Mediators Inflammation* **2013**, *2013*, 780634.
[408] W. A. Pearce, S. Yeh, H. F. Fine, *Ophthalmic surgery, lasers & imaging retina* **2016**, *47*, 103-107.
[409] A. C. Anselmo, S. Mitragotri, *J. Control. Release* **2014**, *190*, 15-28.
[410] M. Cabrera, S. Yeh, T. A. Albini, *J. Ophthalmol.* **2014**, *2014*, 5.
[411] a) Q. D. Nguyen, E. B. Rodrigues, M. E. Farah, W. F. Mieler, D. V. Do*, Retinal pharmacotherapeutics: Retinal pharmacotherapeutics*, in *Developments in ophthalmology* (Ed.: F. Bandello), Karger, **2016**; b) N. Kuno, S. Fujii, *Ocular Drug Delivery Systems for the Posterior Segment: A Review*, Retina Today May/June, **2012**.
[412] http://www.gliadel.com/, last accessed 16.01.2017.
[413] http://propelopens.com/, last accessed 16.01.2017.

[414] T. Golan, E. Z. Khvalevsky, A. Hubert, R. M. Gabai, N. Hen, A. Segal, A. Domb, G. Harari, E. B. David, S. Raskin, Y. Goldes, E. Goldin, R. Eliakim, M. Lahav, Y. Kopleman, A. Dancour, A. Shemi, E. Galun, *Oncotarget* **2015**, *6*, 24560-24570.
[415] http://www.drug-dev.com/Main/Back-Issues/ADVANCED-DELIVERY-DEVICES-Implantable-DrugEluting-1006.aspx, last accessed 16.01.2017.
[416] http://sinusys.com/, last accessed 16.01.2017.
[417] M. J. Cima, H. Lee, K. Daniel, L. M. Tanenbaum, A. Mantzavinou, K. C. Spencer, Q. Ong, J. C. Sy, J. Santini, C. M. Schoellhammer, D. Blankschtein, R. S. Langer, *J. Control. Release* **2014**, *190*, 157-171.
[418] S. V. Sastry, J. R. Nyshadham, J. A. Fix, *Pharm. Sci. Technol. Today* **2000**, *3*, 138-145.
[419] M. W. Tibbitt, J. E. Dahlman, R. Langer, *J. Am. Chem. Soc.* **2016**, *138*, 704-717.
[420] G. Traverso, R. Langer, *Nature* **2015**, *519*, S19.
[421] a) F. Kong, R. P. Singh, *J. Food Sci.* **2008**, *73*, R67-R80; b) F. J. O. Varum, G. B. Hatton, A. W. Basit, *Int. J. Pharm.* **2013**, *457*, 446-460.
[422] C. S. Leopold, *Pharm. Sci. Technol. Today* **1999**, *2*, 197-204.
[423] S. D. Hussan, R. Santanu, P. Verma, V. Bhandari, *IOSR J. Pharm.* **2012**, *2*, 5-11.
[424] a) S. Thakral, N. K. Thakral, D. K. Majumdar, *Expert Opin. Drug Deliv.* **2013**, *10*, 131-149; b) C. Lautenschläger, C. Schmidt, D. Fischer, A. Stallmach, *Adv. Drug Delivery Rev.* **2014**, *71*, 58-76.
[425] S. Joshi, H. U. Petereit, *Int. J. Pharm.* **2013**, *457*, 395-406.
[426] T. Yoshida, T. C. Lai, G. S. Kwon, K. Sako, *Expert Opin. Drug Deliv.* **2013**, *10*, 1497-1513.
[427] M. A. Hanson, M. T. Fareed, S. L. Argenio, A. O. Agunwamba, T. R. Hanson, *Prim. Care* **2013**, *40*, 1-16.
[428] T. Hu, J. Yang, K. Cui, Q. Rao, T. Yin, L. Tan, Y. Zhang, Z. Li, G. Wang, *ACS Appl. Mater. Interfaces* **2015**, *7*, 11695-11712.
[429] Y. Huang, H. C. A. Ng, X. W. Ng, V. Subbu, *J. Control. Release* **2014**, *193*, 188-201.
[430] W. Khan, S. Farah, A. J. Domb, *J. Control. Release* **2012**, *161*, 703-712.
[431] J. Iqbal, J. Gunn, P. W. Serruys, *Br. Med. Bull.* **2013**, *106*, 193-211.
[432] A. E. Alahmar, A. D. Grayson, M. Andron, M. Egred, E. D. Roberts, B. Patel, R. K. G. Moore, K. Albouaini, M. Jackson, R. A. Perry, *Int. J. Cardiol.* **2009**, *132*, 398-404.
[433] T. Palmerini, G. Biondi-Zoccai, D. Della Riva, A. Mariani, P. Genereux, A. Branzi, G. W. Stone, *J. Am. Coll. Cardiol.* **2013**, *62*, 1915-1921.
[434] S. L. Chin-Quee, S. H. Hsu, K. L. Nguyen-Ehrenreich, J. T. Tai, G. M. Abraham, S. D. Pacetti, Y. F. Chan, G. Nakazawa, F. D. Kolodgie, R. Virmani, N. N. Ding, L. A. Coleman, *Biomaterials* **2010**, *31*, 648-657.
[435] a) D. M. Martin, F. J. Boyle, *Med. Eng. Phys.* **2011**, *33*, 148-163; b) T. Tada, R. A. Byrne, S. Cassese, L. King, S. Schulz, J. Mehilli, A. Schömig, A. Kastrati, *Am. Heart J.* **2013**, *165*, 80-86; c) B. D. Gogas, M. McDaniel, H. Samady, S. B. I. King, *Trends Cardiovasc. Med.* **2014**, *24*, 305-313.
[436] A. M. Sammel, D. Chen, N. Jepson, *Heart, Lung and Circulation* **2013**, *22*, 495-506.
[437] a) G. G. Stefanini, B. Kalesan, P. W. Serruys, D. Heg, P. Buszman, A. Linke, T. Ischinger, V. Klauss, F. Eberli, W. Wijns, M.-C. Morice, C. Di Mario, R. Corti, D. Antoni, H. Y. Sohn, P. Eerdmans, G.-A. van Es, B. Meier, S. Windecker, P. Jüni, *Lancet* **2011**, *378*, 1940-1948; b) K. Upendra, B. Sanjeev, *Minerva Cardioangiol.* **2012**, *60*, 23-31; c) P. A. Lemos, I. Bienert, *Expert Rev. Med. Devices* **2013**, *10*, 295-300; d) D. J. Kereiakes, I. T. Meredith, S. Windecker, R. Lee Jobe, S. R. Mehta, I. J. Sarembock, R. L. Feldman, B. Stein, C. Dubois, T. Grady, S. Saito, T. Kimura, T. Christen, D. J. Allocco, K. D. Dawkins, *Circ. Cardiovasc. Interv.* **2015**, *8*, e002372; e) L. O. Jensen, P. Thayssen, M. Maeng, J. Ravkilde, H. S. Hansen, S. E. Jensen, H. E. Bøtker, K. Berencsi, J. F. Lassen, E. H. Christiansen, *Am. Heart J.* **2015**, *170*, 210-215.
[438] W. Chen, T. C. J. Habraken, W. E. Hennink, R. J. Kok, *Bioconjugate Chem.* **2015**, *26*, 1277-1288.

[439] B. D. Gogas, V. Farooq, Y. Onuma, P. W. Serruys, *Hellenic J. Cardiol.* **2012**, *53*, 301-309.
[440] https://www.drugs.com/inactive/, last accessed 16.01.2017.
[441] http://www.accessdata.fda.gov/scripts/cder/iig/index.cfm, last accessed 16.01.2017.
[442] H. Sohi, Y. Sultana, R. K. Khar, *Drug Dev. Ind. Pharm.* **2004**, *30*, 429-448.
[443] B. Karolewicz, *Saudi Pharm. J.* **2016**, *24*, 525-536.
[444] K. Babiuch, M. Gottschaldt, O. Werz, U. S. Schubert, *RSC Advances* **2012**, *2*, 10427-10465.
[445] G. L. Amidon, H. Lennernas, V. P. Shah, J. R. Crison, *Pharm. Res.* **1995**, *12*, 413-420.
[446] http://www.fda.gov/downloads/Drugs/Guidances/ucm070246.pdf., last accessed 16.01.2017.
[447] S. Baghel, H. Cathcart, N. J. O'Reilly, *J. Pharm. Sci.* **2016**, *105*, 2527-2544.
[448] O. M. Y. Koo, *Pharmaceutical Excipients: Properties, Functionality, and Applications in Research and Industry*, John Wiley & Sons, **2016**.
[449] a) A. K. Singla, M. Chawla, A. Singh, *Drug Dev. Ind. Pharm.* **2000**, *26*, 913-924; b) G. P. Andrews, T. P. Laverty, D. S. Jones, *Eur. J. Pharm. Biopharm.* **2009**, *71*, 505-518.
[450] Z. Zhu, Y. Zhai, N. Zhang, D. Leng, P. Ding, *Asian J. Pharm. Sci.* **2013**, *8*, 218-227.
[451] a) R. P. Gullapalli, C. L. Mazzitelli, *Int. J. Pharm.* **2015**, *496*, 219-239; b) A. D'Souza A, R. Shegokar, *Expert Opin. Drug Deliv.* **2016**, *13*, 1257-1275.
[452] E. T. Cole, D. Cadé, H. Benameur, *Adv. Drug Deliv. Rev.* **2008**, *60*, 747-756.
[453] T. Schettler, S. Paris, M. Pellett, S. Kidner, D. Wilkinson, *Clin. Drug Investig.* **2001**, *21*, 73-78.
[454] Q. T. Shubhra, J. Tóth, J. Gyenis, T. Feczkó, *Polym. Rev.* **2014**, *54*, 112-138.
[455] a) G. Dumortier, J. L. Grossiord, F. Agnely, J. C. Chaumeil, *Pharm. Res.* **2006**, *23*, 2709-2728; b) J. J. Escobar-Chávez, M. López-Cervantes, A. Naik, Y. Kalia, D. Quintanar-Guerrero, A. Ganem-Quintanar, *J. Pharm. Pharm. Sci.* **2006**, *9*, 339-358.
[456] a) A. V. Kabanov, E. V. Batrakova, V. Y. Alakhov, *J. Control. Release* **2002**, *82*, 189-212; b) E. V. Batrakova, A. V. Kabanov, *J. Control. Release* **2008**, *130*, 98-106.
[457] E. A. Yapar, O. Ynal, *Trop. J. Pharm. Res.* **2012**, *11*, 855-866.
[458] A. Al-Khattawi, A. R. Mohammed, *Expert Opin. Drug Deliv.* **2013**, *10*, 651-663.
[459] N. Krishna, F. Brow, *Am. J. Ophthalmol.* **1964**, *57*, 99-106.
[460] N. Debotton, A. Dahan, *Med. Res. Rev.* **2017**, *37*, 52-97.
[461] A. Dahan, J. M. Miller, *AAPS J.* **2012**, *14*, 244-251.
[462] C. G. Wermuth, D. Aldous, P. Raboisson, D. Rognan, *The Practice of Medicinal Chemistry*, Academic Press, Elsevier Science, San Diego, California, **1996**.
[463] L. Shargel, I. Kanfer, *Generic drug product development: Specialty dosage forms*, CRC Press (Taylor & Francis Group), **2016**.
[464] S. Garg, K. R. Tambwekar, K. Vermani, A. Garg, C. L. Kaul, L. J. Zaneveld, *Pharm. Technol.* **2001**, 15.
[465] J. das Neves, M. F. Bahia, *Int. J. Pharm.* **2006**, *318*, 1-14.
[466] M. Justin-Temu, F. Damian, R. Kinget, G. Van Den Mooter, *J. Womens Health (Larchmt.)* **2004**, *13*, 834-844.
[467] C. M. Caramella, S. Rossi, F. Ferrari, M. C. Bonferoni, G. Sandri, *Adv. Drug Delivery Rev.* **2015**, *92*, 39-52.
[468] J. H. Guo, *Drug Deliv. Technol.* **2003**, *3*.
[469] D. R. Devi, P. Sandhya, B. N. V. Hari, *J. Pharm. Sci. Res.* **2013**, *5*, 159-165.
[470] H. Almeida, M. H. Amaral, P. Lobao, J. M. Lobo, *Drug Discov. Today* **2014**, *19*, 400-412.
[471] P. Mahlumba, Y. Choonara, P. Kumar, L. du Toit, V. Pillay, *Molecules* **2016**, *21*, 1002.
[472] P. Dhal, S. R. Holmes-Farley, C. Huval, T. Jozefiak, *Adv. Polym. Sci.* **2006**, *192*, 9-58.
[473] B. B. Gerstman, R. Kirkman, R. Platt, *Am. J. Kidney Dis.* **1992**, *20*, 159-161.
[474] Z. Harel, S. Harel, P. S. Shah, R. Wald, J. Perl, C. M. Bell, *Am. J. Med.* **2013**, *126*, 264.e269-224.

[475] M. R. Weir, G. L. Bakris, D. A. Bushinsky, M. R. Mayo, D. Garza, Y. Stasiv, J. Wittes, H. Christ-Schmidt, L. Berman, B. Pitt, *N. Engl. J. Med.* **2015**, *372*, 211-221.
[476] E. A. Slatopolsky, S. K. Burke, M. A. Dillon, *Kidney Int.* **1999**, *55*, 299-307.
[477] W. H. Mandeville, D. I. Goldberg, *Curr. Pharm. Des.* **1997**, *3*, 15-28
[478] a) M. H. Davidson, *Expert Opin. Pharmacother.* **2007**, *8*, 2569-2578; b) T. Suzuki, K. Oba, Y. Igari, N. Matsumura, K. Watanabe, S. Futami-Suda, H. Yasuoka, M. Ouchi, K. Suzuki, Y. Kigawa, H. Nakano, *J. Nippon Med. Sch.* **2013**, *80*, 211-217.
[479] T. J. Louie, J. Peppe, C. K. Watt, D. Johnson, R. Mohammed, G. Dow, K. Weiss, S. Simon, J. F. John, G. Garber, S.-C. Taber, D. M. Davidson, *Clin. Infect. Dis.* **2006**, *43*, 411-420.
[480] E. M. Nestorovich, S. M. Bezrukov, *Expert Opin. Drug Discovery* **2014**, *9*, 299-318.
[481] J. D. Reuter, A. Myc, M. M. Hayes, Z. Gan, R. Roy, D. Qin, R. Yin, L. T. Piehler, R. Esfand, D. A. Tomalia, J. R. Baker, *Bioconjugate Chem.* **1999**, *10*, 271-278.
[482] J. Balzarini, L. Van Damme, *Lancet* **2007**, *369*, 787-797.
[483] D. Concagh, V. R. Garigapati, S. R. Holmes-Farley, C. C. Huval, T. H. Jozefiak, W. H. Mandeville, K. K. Shackett, WO 2001005408 A1, **2001**.
[484] I. Melnikova, D. Wages, *Nat. Rev. Drug Discovery* **2006**, *5*, 369-370.
[485] A. Colas, L. Aguadisch, *Chim. Nouv.* **1997**, *15*, 1779.
[486] K. Mojsiewicz-Pieńkowska*, Review of current pharmaceutical applications of polysiloxanes (silicones)*, in *Handbook of polymers for pharmaceutical technologies* (Eds.: V. K. Thakur, M. K. Thakur), John Wiley & Sons, **2015**, pp. 363-381.
[487] M. Ahsan, L. Babaei, A. Gholamrezaei, M. H. Emami, *Diagn. Ther. Endosc.* **2011**, *2011*, 4.
[488] N. J. Carter, G. M. Keating, *Drugs* **2012**, *70*, 1545-1577.
[489] A. Djukic, J. Feldman, H. P. Frey, J. Jankowski, R. Holtzer, S. Moshe, H. Muzumdar, S. Rose, R. Shinnar, S. Shinnar, *Eur. J. Paediatr. Neurol.* **2015**, *19*, S8.
[490] G. Landa, O. Butovsky, J. Shoshani, M. Schwartz, A. Pollack, *Curr. Res.* **2008**, *33*, 1011-1013.
[491] J. Kovalchin, J. Krieger, M. Genova, K. Collins, M. Augustyniak, A. Masci, T. Hittinger, B. Kuca, G. Edan, C. Braudeau, M. Rimbert, U. Patel, E. Mascioli, E. Zanelli, *J. Neuroimmunol.* **2010**, *225*, 153-163.
[492] E. P. Orringer, J. F. Casella, K. I. Ataga, M. Koshy, P. Adams-Graves, L. Luchtman-Jones, T. Wun, M. Watanabe, F. Shafer, A. Kutlar, M. Abboud, M. Steinberg, B. Adler, P. Swerdlow, C. Terregino, S. Saccente, B. Files, S. Ballas, R. Brown, S. Wojtowicz-Praga, J. M. Grindel, *JAMA* **2001**, *286*, 2099-2106.
[493] R. Ghadi, A. Jain, W. Khan, A. Domb, *Wound Healing Biomaterials-Volume 2: Functional Biomaterials* **2016**, 203.
[494] A. Nan, S. L. Croft, V. Yardley, H. Ghandehari, *J. Control. Release* **2004**, *94*, 115-127.
[495] http://arrowheadpharma.com/pipeline/, last accessed 16.01.2017.
[496] M. Miyamoto, K. Naka, M. Tokumizu, T. Saegusa, *Macromolecules* **1989**, *22*, 1604-1607.
[497] F. Manzenrieder, R. Luxenhofer, M. Retzlaff, R. Jordan, M. G. Finn, *Angew. Chem. Int. Ed.* **2011**, *50*, 2601-2605.
[498] A. Mero, G. Pasut, L. D. Via, M. W. M. Fijten, U. S. Schubert, R. Hoogenboom, F. M. Veronese, *J. Control. Release* **2008**, *125*, 87-95.
[499] a) J. Tong, R. Luxenhofer, X. Yi, R. Jordan, A. V. Kabanov, *Mol. Pharmaceutics* **2010**, *7*, 984-992; b) A. Mero, Z. Fang, G. Pasut, F. M. Veronese, T. X. Viegas, *J. Control. Release* **2012**, *159*, 353-361.
[500] a) S. Konieczny, C. P. Fik, N. J. H. Averesch, J. C. Tiller, *J. Biotechnol.* **2012**, *159*, 195-203; b) S. Konieczny, C. Krumm, D. Doert, K. Neufeld, J. C. Tiller, *J. Biotechnol.* **2014**, *181*, 55-63.
[501] T. Lühmann, M. Schmidt, M. N. Leiske, V. Spieler, T. C. Majdanski, M. Grube, M. Hartlieb, I. Nischang, S. Schubert, U. S. Schubert, L. Meinel, *ACS Biomater. Sci. Eng.* **2017**, *3*, 304–312.

[502] M. Schmitz, M. Kuhlmann, O. Reimann, C. P. R. Hackenberger, J. Groll, *Biomacromolecules* **2015**, *16*, 1088-1094.
[503] W. H. Velander, R. D. Madurawe, A. Subramanian, G. Kumar, G. Sinai-Zingde, J. S. Riffle, C. L. Orthner, *Biotechnol. Bioeng.* **1992**, *39*, 1024-1030.
[504] T. X. Viegas, M. D. Bentley, J. M. Harris, Z. Fang, K. Yoon, B. Dizman, R. Weimer, A. Mero, G. Pasut, F. M. Veronese, *Bioconjugate Chem.* **2011**, *22*, 976-986.
[505] M. Schmidt, S. Harmuth, E. R. Barth, E. Wurm, R. Fobbe, A. Sickmann, C. Krumm, J. C. Tiller, *Bioconjugate Chem.* **2015**, *26*, 1950-1962.
[506] M. Bauer, C. Lautenschlaeger, K. Kempe, L. Tauhardt, U. S. Schubert, D. Fischer, *Macromol. Biosci.* **2012**, *12*, 986-998.
[507] B. Cao, Q. Tang, G. Cheng, *J. Biomater. Sci., Polym. Ed.* **2014**, *25*, 1502-1513.
[508] X. Wang, X. Sun, G. Jiang, R. Wang, R. Hu, X. Xi, Y. Zhou, S. Wang, T. Wang, *J. Appl. Polym. Sci.* **2013**, *128*, 3289-3294.
[509] Z. Wang, G. Ma, J. Zhang, W. Lin, F. Ji, M. T. Bernards, S. Chen, *Langmuir* **2014**, *30*, 3764-3774.
[510] W. Lin, H. Zhang, J. Wu, Z. Wang, H. Sun, J. Yuan, S. Chen, *J. Mater. Chem. B* **2013**, *1*, 2482-2488.
[511] Z. Zhao, J. Wang, H.-Q. Mao, K. W. Leong, *Adv. Drug Delivery Rev.* **2003**, *55*, 483-499.
[512] T. Steinbach, F. R. Wurm, *Biomacromolecules* **2016**, *17*, 3338-3346.
[513] S. Zhang, J. Zou, M. Elsabahy, A. Karwa, A. Li, D. A. Moore, R. B. Dorshow, K. L. Wooley, *Chem. Sci.* **2013**, *4*, 2122-2126.
[514] J.-Z. Du, X.-J. Du, C.-Q. Mao, J. Wang, *J. Am. Chem. Soc.* **2011**, *133*, 17560-17563.
[515] E. Falco, M. Patel, J. Fisher, *Pharm. Res.* **2008**, *25*, 2348-2356.
[516] S. Tempelaar, L. Mespouille, O. Coulembier, P. Dubois, A. P. Dove, *Chem. Soc. Rev.* **2013**, *42*, 1312-1336.
[517] D. P. Sanders, K. Fukushima, D. J. Coady, A. Nelson, M. Fujiwara, M. Yasumoto, J. L. Hedrick, *J. Am. Chem. Soc.* **2010**, *132*, 14724-14726.
[518] A. C. Engler, X. Ke, S. Gao, J. M. W. Chan, D. J. Coady, R. J. Ono, R. Lubbers, A. Nelson, Y. Y. Yang, J. L. Hedrick, *Macromolecules* **2015**, *48*, 1673-1678.
[519] J. M. W. Chan, X. Ke, H. Sardon, A. C. Engler, Y. Y. Yang, J. L. Hedrick, *Chem. Sci.* **2014**, *5*, 3294-3300.
[520] a) Z. Y. Ong, K. Fukushima, D. J. Coady, Y.-Y. Yang, P. L. R. Ee, J. L. Hedrick, *J. Control. Release* **2011**, *152*, 120-126; b) J. Feng, R.-X. Zhuo, X.-Z. Zhang, *Prog. Polym. Sci.* **2012**, *37*, 211-236; c) W. Chen, F. Meng, R. Cheng, C. Deng, J. Feijen, Z. Zhong, *J. Control. Release* **2014**, *190*, 398-414.
[521] S. D. Allison, *Expert Opin. Drug Deliv.* **2008**, *5*, 615-628.
[522] S. Wilhelm, A. J. Tavares, Q. Dai, S. Ohta, J. Audet, H. F. Dvorak, W. C. W. Chan, *Nat. Rev. Mater.* **2016**, *1*, 16014.
[523] http://www.nanopartikel.info/en/, last accessed 16.01.2017.
[524] http://inbs.med.utoronto.ca/cnr/, last accessed 16.01.2017.
[525] H. Otsuka, Y. Nagasaki, K. Kataoka, *Adv. Drug Delivery Rev.* **2003**, *55*, 403-419.
[526] R. Rietscher, J. A. Czaplewska, T. C. Majdanski, M. Gottschaldt, U. S. Schubert, M. Schneider, C.-M. Lehr, *Int. J. Pharm.* **2016**, *500*, 187-195.
[527] a) T. Sun, Y. S. Zhang, B. Pang, D. C. Hyun, M. Yang, Y. Xia, *Angew. Chem. Int. Ed.* **2014**, *53*, 12320-12364; b) N. Kamaly, B. Yameen, J. Wu, O. C. Farokhzad, *Chem. Rev.* **2016**, *116*, 2602-2663.
[528] M. Karimi, A. Ghasemi, P. S. Zangabad, R. Rahighi, S. M. M. Basri, H. Mirshekari, M. Amiri, Z. S. Pishabad, A. Aslani, M. Bozorgomid, *Chem. Soc. Rev.* **2016**, *45*, 1457-1501.
[529] J. E. Zuckerman, M. E. Davis, *Nat. Rev. Drug Discovery* **2015**, *14*, 843-856.
[530] J. W. Choi, J.-H. Park, S. Y. Baek, D.-D. Kim, H.-C. Kim, H.-J. Cho, *Colloids Surf., B* **2015**, *132*, 305-312.
[531] D. Y. Wong, S. J. Hollister, P. H. Krebsbach, C. Nosrat, *Tissue Engineer.* **2007**, *13*, 2515-2523.

[532] D. Mondal, M. Griffith, S. S. Venkatraman, *Int. J. Polym. Mater.* **2016**, *65*, 255-265.
[533] S. Kalita, B. Devi, R. Kandimalla, K. K. Sharma, A. Sharma, K. Kalita, A. C. Kataki, J. Kotoky, *Int. J. Nanomed.* **2015**, *10*, 2971-2984.
[534] a) A. Takahashi, Y. Yamamoto, M. Yasunaga, Y. Koga, J.-i. Kuroda, M. Takigahira, M. Harada, H. Saito, T. Hayashi, Y. Kato, T. Kinoshita, N. Ohkohchi, I. Hyodo, Y. Matsumura, *Cancer Sci.* **2013**, *104*, 920-925; b) Y. Matsumura, *Jpn. J. Clin. Oncol.* **2014**, *44*, 515-525.
[535] A. Sugaya, I. Hyodo, Y. Koga, Y. Yamamoto, H. Takashima, R. Sato, R. Tsumura, F. Furuya, M. Yasunaga, M. Harada, R. Tanaka, Y. Matsumura, *Cancer Sci.* **2016**, *107*, 335-340.
[536] S. Y. Wong, J. M. Pelet, D. Putnam, *Prog. Polym. Sci.* **2007**, *32*, 799-837.
[537] a) C.-H. Ahn, S. Y. Chae, Y. H. Bae, S. W. Kim, *J. Control. Release* **2002**, *80*, 273-282; b) M. L. Forrest, J. T. Koerber, D. W. Pack, *Bioconjugate Chem.* **2003**, *14*, 934-940; c) C. Englert, M. Hartlieb, P. Bellstedt, K. Kempe, C. Yang, S. K. Chu, X. Ke, J. M. García, R. J. Ono, M. Fevre, R. J. Wojtecki, U. S. Schubert, Y. Y. Yang, J. L. Hedrick, *Macromolecules* **2015**, *48*, 7420-7427.
[538] a) S. Taranejoo, J. Liu, P. Verma, K. Hourigan, *J. Appl. Polym. Sci.* **2015**, *132*, 42096; b) C. Englert, M. Fevre, R. J. Wojtecki, W. Cheng, Q. Xu, C. Yang, X. Ke, M. Hartlieb, K. Kempe, J. M. Garcia, R. J. Ono, U. S. Schubert, Y. Y. Yang, J. L. Hedrick, *Polym. Chem.* **2016**, *7*, 5862-5872.
[539] C. Englert, A.-K. Trützschler, M. Raasch, T. Bus, P. Borchers, A. S. Mosig, A. Traeger, U. S. Schubert, *J. Control. Release* **2016**, *241*, 1-14.
[540] S. Agarwal, Y. Zhang, S. Maji, A. Greiner, *Mater. Today* **2012**, *15*, 388-393.
[541] Y. Qian, Y. Zha, B. Feng, Z. Pang, B. Zhang, X. Sun, J. Ren, C. Zhang, X. Shao, Q. Zhang, X. Jiang, *Biomaterials* **2013**, *34*, 2117-2129.
[542] L. Bédouet, F. Pascale, L. Moine, M. Wassef, S. H. Ghegediban, V.-N. Nguyen, M. Bonneau, D. Labarre, A. Laurent, *Int. J. Pharm.* **2013**, *456*, 536-544.
[543] C. Sonnet, C. L. Simpson, R. M. Olabisi, K. Sullivan, Z. Lazard, Z. Gugala, J. F. Peroni, J. M. Weh, A. R. Davis, J. L. West, E. A. Olmsted-Davis, *J. Orthop. Res.* **2013**, *31*, 1597-1604.
[544] M. Molina, M. Asadian-Birjand, J. Balach, J. Bergueiro, E. Miceli, M. Calderon, *Chem. Soc. Rev.* **2015**, *44*, 6161-6186.
[545] Y. Tahara, K. Akiyoshi, *Adv. Drug Delivery Rev.* **2015**, *95*, 65-76.
[546] A. Sharma, T. Garg, A. Aman, K. Panchal, R. Sharma, S. Kumar, T. Markandeywar, *Artif. Cells Nanomed. Biotechnol.* **2016**, *44*, 165-177.
[547] S. De Koker, J. Cui, N. Vanparijs, L. Albertazzi, J. Grooten, F. Caruso, B. G. De Geest, *Angew. Chem. Int. Ed.* **2016**, *55*, 1334-1339.
[548] Y. Tian, Y. Wang, S. Shen, X. Jiang, Y. Wang, W. Yang, *Part. Part. Syst. Charact.* **2015**, *32*, 1092-1101.
[549] S. Jin, J. Wan, L. Meng, X. Huang, J. Guo, L. Liu, C. Wang, *ACS Appl. Mater. Interfaces* **2015**, *7*, 19843-19852.
[550] M. Da, S. M. Tian, J. Baryza, J. C. Luft, J. M. DeSimone, *Mol. Pharmaceutics* **2015**, *12*, 3518-3526.
[551] T. Gerson, E. Makarov, T. H. Senanayake, S. Gorantla, L. Y. Poluektova, S. V. Vinogradov, *Nanomed. Nanotechnol. Biol. Med.* **2014**, *10*, 177-185.
[552] S. S. Desale, S. M. Raja, J. O. Kim, B. Mohapatra, K. S. Soni, H. Luan, S. H. Williams, T. A. Bielecki, D. Feng, M. Storck, V. Band, S. M. Cohen, H. Band, T. K. Bronich, *J. Control. Release* **2015**, *208*, 59-66.
[553] S. S. Desale, K. S. Soni, S. Romanova, S. M. Cohen, T. K. Bronich, *J. Control. Release* **2015**, *220, Part B*, 651-659.
[554] L. Kaps, L. Nuhn, M. Aslam, A. Brose, F. Foerster, S. Rosigkeit, P. Renz, R. Heck, Y. O. Kim, I. Lieberwirth, D. Schuppan, R. Zentel, *Adv. Healthcare Mater.* **2015**, *4*, 2809-2815.
[555] P. Tomakidi, T. Steinberg, W. Weber, D. Laird, R. Gübeli, EP 2455104 B1, **2013**.
[556] K. H. Hsu, S. Gause, A. Chauhan, *J. Drug Delivery Sci. Technol.* **2014**, *24*, 123-135.

[557] L. Xinming, C. Yingde, A. W. Lloyd, S. V. Mikhalovsky, S. R. Sandeman, C. A. Howel, L. Liewen, *Cont. Lens Anterior Eye* **2008**, *31*, 57-64.
[558] C.-C. Li, A. Chauhan, *Ind. Eng. Chem. Res.* **2006**, *45*, 3718-3734.
[559] A. Ribeiro, F. Veiga, D. Santos, J. J. Torres-Labandeira, A. Concheiro, C. Alvarez-Lorenzo, *Biomacromolecules* **2011**, *12*, 701-709.
[560] C.-C. Peng, A. Chauhan, *J. Control. Release* **2011**, *154*, 267-274.
[561] C. Gupta, A. Chauhan, *J. Control. Release* **2011**, *150*, 70-76.
[562] a) A. M. Ribeiro, A. Figueiras, F. Veiga, *J. Pharm. Pharm. Sci.* **2015**, *18*, 683-695; b) S. Kirchhof, A. M. Goepferich, F. P. Brandl, *Eur. J. Pharm. Biopharm.* **2015**, *95*, 227-238.
[563] S. K. Guha, US 5488075 A, **1996**.
[564] N. K. Lohiya, I. Alam, M. Hussain, S. R. Khan, A. S. Ansari, *Indian. J. Med. Res.* **2014**, *140*, 63-72.
[565] N. K. Lohiya, R. Suthar, A. Khandelwal, S. Goyal, A. S. Ansari, B. Manivannan, *Int. J. Androl.* **2010**, *33*, e198-e206.
[566] https://www.parsemusfoundation.org/projects/vasalgel/, last accessed 16.01.2017.
[567] https://www.parsemusfoundation.org/contraceptives/two-steps-forward/, last accessed 16.01.2017.
[568] A. Lohani, G. Singh, S. S. Bhattacharya, A. Verma, *J. Drug Delivery* **2014**, *2014*, 11.
[569] J. R. Millar, *J. Chem. Soc.* **1960**, 1311-1317.
[570] A. D. Jenkins, P. Kratochvíl, R. F. T. Stepto, U. W. Suter, *Pure Appl. Chem.* **1996**, *68*, 2287.
[571] T. M. Aminabhavi, M. N. Nadagouda, U. A. More, S. D. Joshi, V. H. Kulkarni, M. N. Noolvi, P. V. Kulkarni, *Expert Opin. Drug Deliv.* **2015**, *12*, 669-688.
[572] E. S. Dragan, *Chem. Eng. J.* **2014**, *243*, 572-590.
[573] L. F. A. Asghar, S. Chandran, *J. Pharm. Pharm. Sci.* **2006**, *9*, 327-338.
[574] a) L. Palugan, M. Cerea, L. Zema, A. Gazzaniga, A. Maroni, *J. Drug Delivery Sci. Technol.* **2015**, *25*, 1-15; b) A. Maroni, M. D. Del Curto, L. Zema, A. Foppoli, A. Gazzaniga, *Int. J. Pharm.* **2013**, *457*, 372-394.

PUBLICATION 2

Enhancing the biocompatibility and biodegradability of linear poly(ethylene imine) through controlled oxidation

C. Englert, M. Hartlieb, P. Bellstedt, K. Kempe, C. Yang, S. K. Chu, X. Ke, J. M. García, R. J. Ono, M. Fevre, R. J. Wojtecki, U. S. Schubert, Y. Y. Yang, J. L. Hedrick

Macromolecules **2015**, *48*, 7420-7427

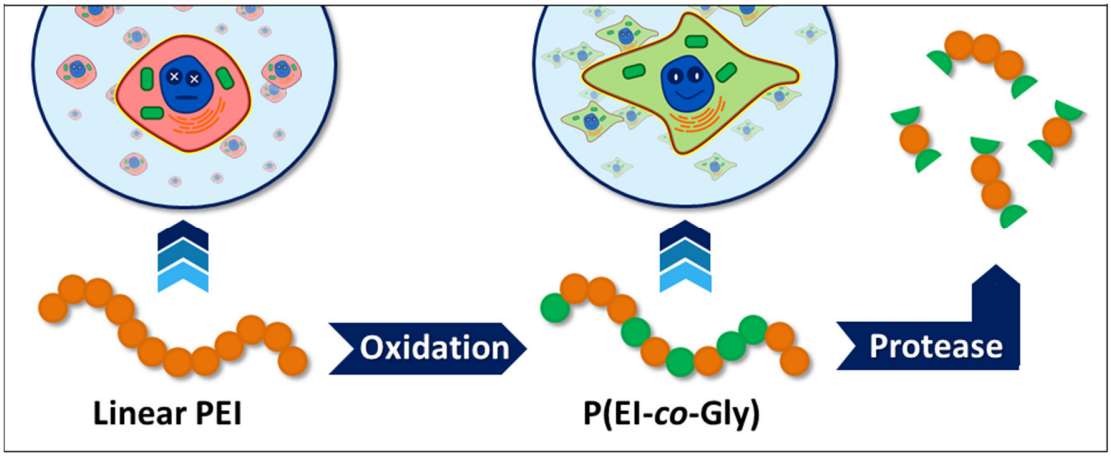

Macromolecules

Article

pubs.acs.org/Macromolecules

Enhancing the Biocompatibility and Biodegradability of Linear Poly(ethylene imine) through Controlled Oxidation

Christoph Englert,[†,‡,§] Matthias Hartlieb,[†,‡] Peter Bellstedt,[†] Kristian Kempe,[†,‡] Chuan Yang,[∥] Swee Kwang Chu,[∥] Xiyu Ke,[∥] Jeannette M. García,[§] Robert J. Ono,[§] Mareva Fevre,[§] Rudy J. Wojtecki,[§] Ulrich S. Schubert,*[,†,‡] Yi Yan Yang,*[,∥] and James L. Hedrick*[,§]

[†]Laboratory of Organic and Macromolecular Chemistry (IOMC), Friedrich Schiller University Jena, Humboldtstrasse 10, 07743 Jena, Germany

[‡]Jena Center for Soft Matter (JCSM), Friedrich Schiller University Jena, Philosophenweg 7, 07743 Jena, Germany

[§]IBM Almaden Research Center, 650 Harry Road, San Jose, California 95120, United States

[∥]Institute of Bioengineering and Nanotechnology, 31 Biopolis Way, The Nanos, Singapore 138669, Singapore

Supporting Information

ABSTRACT: (Bio)degradable poly(ethylene imine-*co*-glycine)s (P(EI-*co*-Gly)) were synthesized through efficient and controlled oxidation of linear poly(ethylene imine) (LPEI) using hydrogen peroxide in a methanol/water mixture. Temperature, peroxide concentration, and reaction time were varied to adjust the degree of oxidation (DO). At low temperatures, the oxidation process was found to be well-controlled with almost 85% of ethylene imine units converted to the corresponding amide. Importantly, oxidation of more than 10% of the LPEI rendered the polymers water-soluble. The oxidation reaction and molecular structure of P(EI-*co*-Gly)s were studied in detail by various nuclear magnetic resonance (NMR) methods, infrared (IR) spectroscopy, and size exclusion chromatography (SEC). The introduction of backbone amide groups to the P(EI-*co*-Gly)s facilitated its (bio)degradation under acidic conditions or by proteases. Moreover, the P(EI-*co*-Gly)s exhibited negligible cytotoxicity, particularly relative to LPEI. The interaction of the copolymers with serum-containing medium was investigated showing no indication of coagulation. Preliminary studies indicate that P(EI-*co*-Gly) is a promising biodegradable polymer with negligible toxicity in human cell lines.

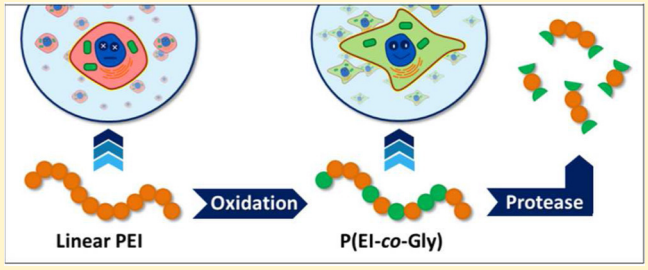

INTRODUCTION

Poly(ethylene imine) (PEI) is one of the most successfully and widely studied vectors in nonviral gene delivery and is considered the gold standard for gene transfection.[1,2] The repeating ethylene amine structure of PEI can electrostatically interact with the DNA/RNA phosphate groups and form so-called polyplexes.[3−5] The polymer exists in branched or linear architecture, which influences the transfection behavior.[6,7] However, PEI suffers from several drawbacks such as cytotoxicity,[8−10] low hemocompatibility,[11] and nonbiodegradability,[12,13] which limits its clinical applications.

In the past decade, the chemical modification of PEI has garnered tremendous interest, with the primary objective of reducing cytotoxicity, increasing transfection efficiency and cell selectivity.[2,14−16] Most biological studies have focused on partially modified PEI conjugates.[17−19] Procedures have involved chemical transformation of the amine groups of PEI via alkylation, ring-opening of epoxides, and Michael addition, among others.[2]

Previously, MacDonald and co-workers reported the oxidation of branched PEI by hydrogen peroxide.[20] The authors demonstrated that the modification of the PEI backbone proceeds via the following intermediate species: hydroxylamine (**2**),[21] nitrone (**3**),[22,23] and oxaziridine (**4**)[23−25] (Scheme 1). The ring-opening of the oxaziridine, as postulated by MacDonald, leads to a Beckmann-type rearrangement product[26] and, subsequently, to the formation of the thermodynamic product, a stable amide group (**5**). The resulting structure resembles the repeating unit of poly(glycine) (PGly), which renders the polymers potentially biocompatible and degradable. However, this report claimed the oxidation to be accompanied by partial chain degradation, mainly referring to the appearance of carboxylic acid and aldehyde signals. These signals can, among others, occur from the oxidation (and subsequent hydrolysis) of primary amines present in branched PEI.[20] To this end, we utilize linear PEI for the presented study to prevent the influence of primary amines. Furthermore, the use of a linear polymer precursor simplifies the characterization due to the absence of primary and tertiary amines. Using

Received: September 3, 2015
Revised: September 29, 2015
Published: October 13, 2015

DOI: 10.1021/acs.macromol.5b01940
Macromolecules 2015, 48, 7420−7427

Scheme 1. Schematic Representation of the Oxidation Mechanism of a Secondary Amine (1) via Hydroxylamine (2), Nitrone (3), and Oxaziridine (4) Intermediates To Form the Final Amide Group (5), As Proposed by MacDonald et al.[20]

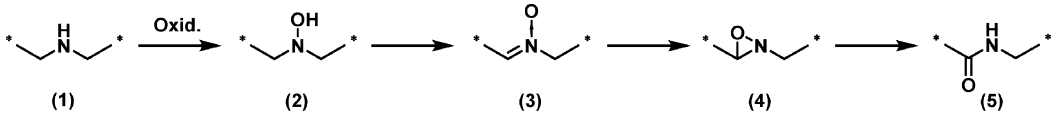

Table 1. Different Approaches for the Oxidation of Linear Poly(ethylene imine)

Oxidizing agent	Structure	Equivalents per EI unit	Solvent	Temperature [°C]	Time [h]	Degree of oxidation [%] (^{1}H NMR)
Oxone[29]	$KHSO_5$/ $KHSO_4$/ K_2SO_4	1.1	MeOH	18	16	degradation
White catalyst[30], O_2	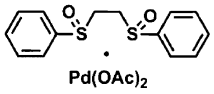	0.1	MeOH	45	7	no oxidation
MCPBA	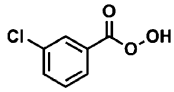	1.0	$CHCl_3$	18	16	no oxidation
Aq. H_2O_2		4.0	MeOH	18	16	80

modern characterization techniques and careful kinetic studies, we show that polymer degradation is minimal.

Surprisingly, since the initial report of the PEI oxidation, few (if any) similar reports have appeared in the past 40 years. The controlled oxidation of PEI represents a highly useful method for the modification of PEI and offers a unique opportunity to facilitate biocompatibility and degradability of an otherwise toxic PEI. Such an improvement would enable, for the first time, *in vivo* studies especially for applicability in gene delivery. Recently, Hauser and co-workers demonstrated that the oxidation of an already formed PEI/DNA polyplex would decrease the amount of cationic charges.[27] However, this contribution focused on the biological performance of these altered polyplexes and lacked details on the chemical nature of the modification.

The goal of the present work was to understand the oxidation of PEI, to identify the optimal reagents/conditions to gain control over the oxidation process, and to evaluate the structure of the resulting polymers in detail. Therefore, we investigated the influence of several parameters, including time, temperature, and concentration, as well as the nature of the oxidizing agent in order to identify optimized conditions. A series of four P(EI-*co*-Gly) copolymers were synthesized and extensively analyzed. The degradation of the polymers was examined using HCl or trypsin and underlined the potential of the presented macromolecular system. Furthermore, serum stability and cytotoxicity were evaluated and found to be superior as compared to unmodified PEI.

RESULTS AND DISCUSSION

Oxidation of Linear Poly(ethylene imine). The first parameter investigated in the oxidation process of LPEI[28] was the oxidizing agent. Initial experiments focused on evaluating the suitability of various oxidizing agents (Table 1), where the degree of oxidation (DO) was assessed by ^{1}H NMR spectroscopy. Interestingly, the use of common oxidizing agents such as oxone, *m*-chloroperoxybenzoic acid (*m*CPBA), or the White catalyst (a palladium coordination complex) led to no measurable DO and, in some cases, degradation of the polymer. The oxidation of LPEI with hydrogen peroxide, however, led to oxidized species with a DO of up to 80%. The modified polymers exhibited an extraordinarily high water solubility for DOs > 10%. The simplicity of the oxidation reaction together with the ease of purification (precipitation in diethyl ether followed by freeze-drying) makes this procedure straightforward. For these reasons, hydrogen peroxide oxidation was the method used for all following investigations.

In the mechanism described above (Scheme 1), the oxidation of LPEI converts the latter into a partially oxidized poly(ethylene imine-*co*-glycine) (P(EI-*co*-Gly)) (Scheme 2), which

Scheme 2. Schematic Representation of the Oxidation of Commercial LPEI to P(EI-*co*-Gly) by Hydrogen Peroxide

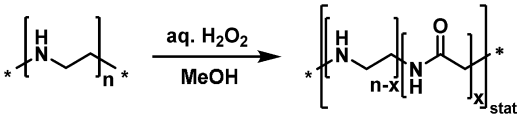

consists of unaffected ethylene imine (EI) and newly formed glycine (Gly) units. Because of incomplete hydrolysis during its industrial synthesis process, the starting LPEI contains up to 5% 2-ethyl-2-oxazoline units.[31] These groups remain unaffected during the oxidation, which is shown by oxidation experiments of poly(2-ethyl-2-oxazoline) homopolymer (Supporting Information, Figure S1). Furthermore, the unaffected 2-ethyl-2-oxazoline (EtOx) repeating units were also used to quantify the DO. Since the signals of EI and Gly repeating units, respectively, are not entirely baseline separated, the error of the quantification of the DO is estimated as ±5%. The sharp signal at ∼8.30 ppm could be attributed to degraded species or

DOI: 10.1021/acs.macromol.5b01940
Macromolecules 2015, 48, 7420−7427

solvent impurities. However, the integral of the peak is lower than 2% as compared to the polymer signals.

The successful oxidation is exemplified by ^{1}H NMR analysis in Figure 1, which shows an overlay of LPEI and P(EI-*co*-Gly$_{67\%}$) spectra. As verified by HSQC NMR measurements (Figure S2), the newly formed signal F can be primarily ascribed to the CH_2 group of the glycine backbone. Signal E indicates the formation of an amide group showing no coupling to polymer associated carbon signals (see Figure S2).[32] Its appearance is rather surprising and cannot be used for quantification of the degree of oxidation (DO) due to proton exchange processes in D_2O. The ^{13}C NMR signal at ~170 ppm corresponds to the amide carbonyl group (no coupling was observed by heteronuclear NMR, HSQC). The DO was calculated from the integration of the ^{1}H NMR signals of the copolymer backbones via eq 1 (Experimental Section).

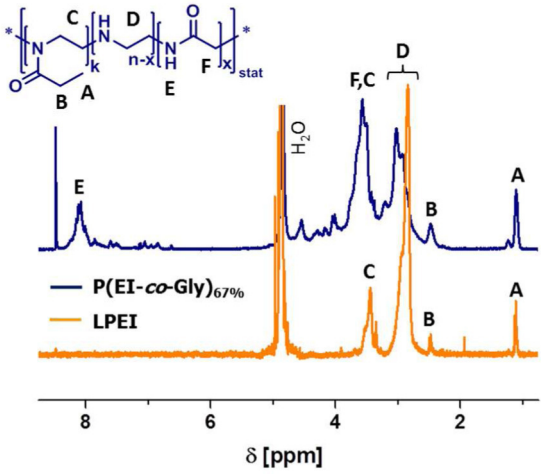

Figure 1. Comparison of ^{1}H NMR spectra of LPEI and P(EI-*co*-Gly) (including unaffected EtOx units, <5%) with a degree of oxidation of about 67% (D_2O, 400 MHz).

Kinetic Investigations. Synthetic control over the oxidation process is critical, so the oxidation reaction was investigated as a function of the concentration of peroxide, the temperature, and reaction time. First, the oxidation was performed with varying concentrations of hydrogen peroxide (0−1 equiv of H_2O_2 per EI repeating unit) for 20 h at 18 °C, the optimized time/temperature to observe a maximum DO (Figure S3). The increase in peroxide concentration resulted in a nearly linear increase of the DOs and represents a simple and effective method to control the DO. Moreover, with 0.9 equiv of H_2O_2 per EI unit, the DO reaches a maximum of 60%, whereas an excess of H_2O_2 (4 equiv) enables the oxidation of almost 85% of EI units. For this reason, excess of H_2O_2 was used for the following kinetic studies.

Starting from identical mixtures of LPEI, methanol, and H_2O_2, the oxidation reaction was performed at various temperatures and reaction times. The determined DOs from temperature- and time-dependent investigations (by ^{1}H NMR) resulted in the kinetic curves depicted in Figure 2. Increasing temperature led to faster oxidation and, hence, higher DOs. The short recording times of the curve associated with the reaction conducted at 0 °C is due to technical limitations, as it was difficult to maintain this temperature for longer time periods. Higher temperatures were also explored; a similar experiment at 55 °C resulted in a multitude of sharp signals in the ^{1}H NMR spectrum of the products, which are not typical for polymers with broad molar mass distributions, suggesting degradation to low molar mass species (Figure S4). We therefore concluded that ambient temperature (18 °C in our case) was sufficient for attaining high DOs of up to 85% without causing polymer degradation. In summary, adjusting the H_2O_2 concentration, time, and temperature represents a simple and effective method to control the DO.

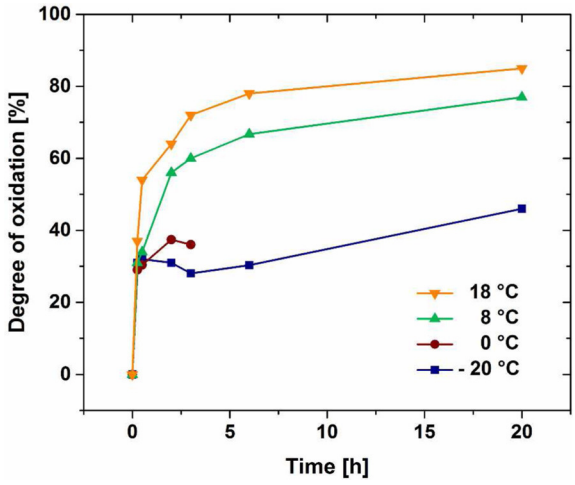

Figure 2. Kinetic studies of the oxidation of LPEI at different temperatures with a 4-fold excess of H_2O_2. Degrees of oxidation were calculated from ^{1}H NMR spectra (D_2O, 400 MHz).

P(EI-*co*-Gly) with Varying DOs. The ability to adjust the DO via temperature and time enabled the synthesis of a series of P(EI-*co*-Gly)s with varying amounts of glycine units (Table 2, **1**−**4**). To avoid the investigation of potential degradation products, centrifugal concentration was performed for all P(EI-*co*-Gly) samples using disposable Vivaspin 20 ultrafiltration devices with a molar mass cutoff (MWCO) of 3000 g mol^{-1}.

Larger H_2O_2 concentrations and higher temperatures resulted in a faster and less controllable oxidation. Therefore, to achieve polymers with lower DOs (e.g., **1** and **2**), the reaction was performed at 0 °C. Higher oxidation degrees (**3** and **4**) were obtained at 18 °C followed by purification through precipitation and freeze-drying.

An overlay of the ^{1}H NMR spectra of **1**−**4** can be found in Figure 3. A downfield shift of the LPEI backbone signal D to signal F as well as the appearance of the amide signal around 7.90 ppm (E) indicates a successful oxidation.

Diffusion-ordered NMR spectroscopy (DOSY NMR) confirms the presence of a single (polymeric) species, as indicated by the diffusion coefficient and, hence, the absence of degradation (Figure S5). Diffusion coefficients are specified in Table 2. Missing Mark−Houwink values, α and K, for the copolymers hinder the calculation of the molar weights via the Mark−Houwink equation. For LPEI, the molar mass (M_n) was determined as 4200 g mol^{-1} by viscosity measurements using literature values.[33] The viscosity of methanol (determined by viscosity measurements using a capillary/ball combination) and the diffusion coefficients were used to calculate the hydrodynamic radii R_0 of the (co)polymers via the Einstein−Smoluchowski relation (Table 2). Because of equipment dependent data, the diffusion coefficient from the residual water peak was used to "standardize" R_0 values of the (co)polymers by simple correction to literature reported value of D_{H_2O}.

DOI: 10.1021/acs.macromol.5b01940
Macromolecules 2015, 48, 7420−7427

Table 2. Parameters for P(EI-*co*-Gly)s 1−4 and Starting LPEI at 25 °C: Degree of Oxidation (DO), Number-Averaged Molar Mass M_n (NMR, SEC), Diffusion Coefficient D (DOSY), Intrinsic Viscosity μ_{int}, and Hydrodynamic Radius R_0 According to the Einstein−Smoluchowski Relation

			M_n [g mol^{-1}]				
no.	composition	DO[a] [%]	NMR[b]	SEC (DMAc)[c,g]	D[d] [10^{-10} m^2 s^{-1}]	μ_{int}[e] [mL g^{-1}]	R_0[f] [nm]
	LPEI		6500[36]	1100	2.8	28.6	3.07
1	P(EI$_{80}$-*co*-Gly$_{20}$)	20	6900	1500	6.3	6.9	1.37
2	P(EI$_{60}$-*co*-Gly$_{40}$)	40	7300	1400	8.9	8.0	0.97
3	P(EI$_{33}$-*co*-Gly$_{67}$)	67	7900	1700	6.8	8.6	1.27
4	P(EI$_{15}$-*co*-Gly$_{85}$)	85	8200	1600	7.9	8.3	1.09

[a]Percentage of formed GLY units determined by ^{1}H NMR spectroscopy. [b]Determined by ^{1}H NMR (calculated from LPEI: 6500 g mol^{-1},[36] ratio of PEI and GLY). [c]Determined by SEC (eluent: DMAc + 0.21% LiCl, calibration against polystyrene standard). [d]Determined by diffusion-ordered NMR spectroscopy (DOSY, D_2O, 400 MHz, 25 °C, see Figure S4). [e]Determined by viscosity measurements (MeOH, 25 °C). [f]Calculated by Einstein−Smoluchowski relation by means of $\eta_{0,MeOH}$ = 0.61 × 10^{-3} kg m^{-1} s^{-1} (Experimental Section, eq 2).[37] The diffusion coefficient from residual water peak (D_{H_2O} = 5.60 × 10^{-9} m^2 s^{-1} (25 °C)) was used to "standardize" R_0 values by simple correction to literature reported value of $D_{H_2O,Lit}$ = 2.30 × 10^{-9} m^2 s^{-1} (25 °C).[38] [g]All samples are hardly soluble in the SEC eluent DMAc. Unfortunately, there is no calibration standard available for cationic polymers like LPEI and derivatives.

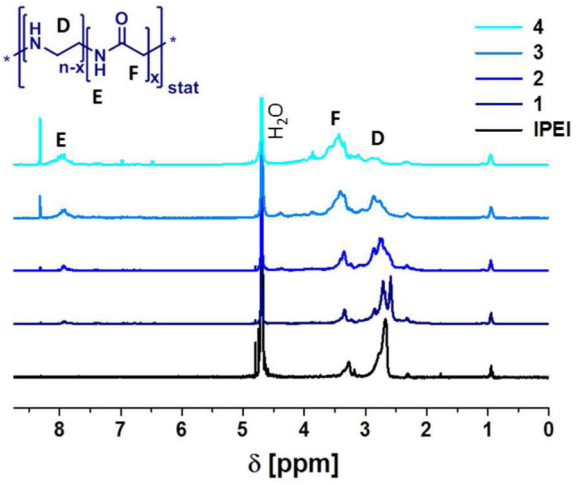

Figure 3. ^{1}H NMR spectra of LPEI and P(EI-*co*-Gly)s **1−4** (D_2O, 400 MHz).

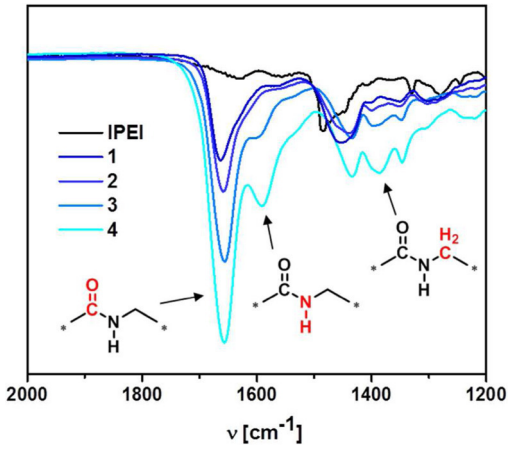

Figure 4. IR spectra of P(EI-*co*-Gly)s **1−4** and LPEI in the wavenumber range from 1200 to 2000 cm^{-1}.

A difference in R_0 of LPEI and P(EI-*co*-Gly)s can be explained by two factors: first, hydrogen bonding, which occurs due to the presence of the newly formed amide groups, and second, decreasing charges owing to the disappearance of secondary amines. This allows an entanglement of the polymer chains, and as a result, smaller hydrodynamic radii are observed for the oxidized species. However, the larger R_0 of LPEI could also be attributed to the formation of aggregates as the polymer is known to form hydrogen bonds in aqueous solution.[34] Unfortunately, asymmetric flow field flow fractionation (AF4, RC membrane with MWCO of 10 000 g mol^{-1}), a well-established method for the detailed characterization of cationic polymers,[35] was not successful due to the low molar masses of the starting LPEI and the corresponding oxidized copolymers (<10 000 g mol^{-1}).

The IR spectra (in the wavenumber region between 1200 and 2000 cm^{-1}) of LPEI and **1−4** are shown in Figure 4. Numerous investigations regarding IR spectroscopy of polyglycine are known from the literature.[39−41] The vibration at 1660 cm^{-1} results from the carbonyl stretching vibration of the secondary amide group in P(EI-*co*-Gly).[20,42] This signifies a successful oxidation. Signals attributable to carboxylic acid derivatives, as possible degradation products, are expected to appear at higher wavenumbers (>1700 cm^{-1});[43] however, they are not observed. Starting from LPEI (no carbonyl vibration), increased DOs lead to more intense carbonyl bands. The signal at 1600 cm^{-1} is likewise assigned to amide mode. The vibrations between 1400 and 1340 cm^{-1} can be assigned to the CH_2 bending and wagging mode of the formed glycine, respectively. The 1480 cm^{-1} band of the LPEI-CH_2 backbone gradually decreases in wavenumber (to 1435 cm^{-1}) with an increase of DO.

Poor solubility in common solvents and expected interactions of the cationic polymer with the column material in the case of aqueous SEC setups prohibit successful determination of molar masses of the P(EI-*co*-Gly) by size exclusion measurements. However, LPEI and copolymers **1−4** could be dissolved in *N*,*N*-dimethylacetamide (DMAc) at low concentrations. The appearance of the LPEI signal at higher elution volumes, and hence at lower molar masses, compared to the P(EI-*co*-Gly)s is another indication for the absence of quantitative degradation during oxidation (Figure S6). Unfortunately, a calibration for cationic polymers is not available, which complicates the determination of accurate molar masses by SEC.

Degradation Studies. One potential advantage of P(EI-*co*-Gly) compared to unmodified LPEI is the possibility of biodegradation due to the incorporation of amide bonds in the

DOI: 10.1021/acs.macromol.5b01940
Macromolecules 2015, 48, 7420−7427

polymer backbone. To investigate the decomposition behavior, P(EI-*co*-Gly$_{67\%}$) (**3**) was chosen as a model polymer and subjected to acidic (6 mol L^{-1} HCl) and enzymatic (trypsin) conditions. While the pure LPEI showed no changes under these conditions, the ^{1}H NMR spectra of the oxidized species revealed sharp and undefined signals (comparable to the oxidation reactions at high temperatures), usually atypical for polymers with broad molar mass distributions and chain lengths of around 150 units (Figure 5). Further evidence of a

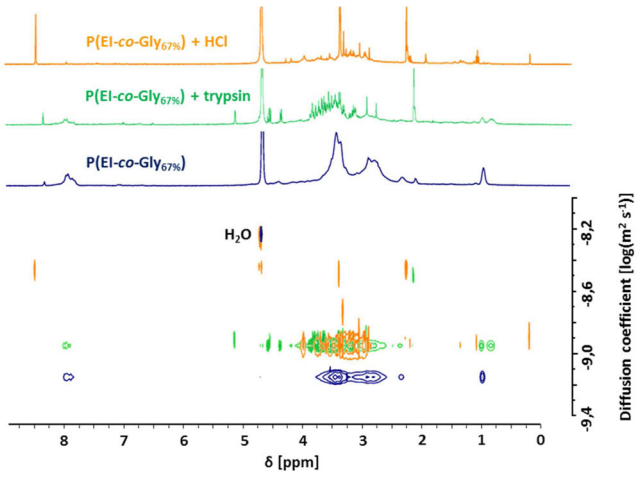

Figure 5. DOSY NMR of **3** before (blue) and after treatment with 6 mol L^{-1} aqueous hydrogen chloride (orange) and peptidase (trypsin) (green) (D_2O, 400 MHz, 25 °C).

successful degradation is given by the splitting of the signals of the EtOx side chain and the reduction in the peak intensity of the amide bond at 7.9 ppm, which completely disappeared upon the treatment with HCl. Simultaneously, the intensity of the sharp signal at 8.45 ppm increases, validating the earlier assumption of this signal being attributed to degradation products. Furthermore, successful degradation was confirmed utilizing DOSY NMR (Figure 5). Polymer degradation results in increased diffusion coefficients as well as a fractionation of the signals. The signal of water was used for calibration.

Size exclusion chromatography in DMAc confirmed the successful degradation (Figure S7). The improved solubility and the shift to lower molar masses further support our claim.

Cytotoxicity and Serum Stability. Another important parameter for a candidate polymer for biomedical applications is its biocompatibility. Pure PEI, although known as a gold standard for nonviral gene delivery,[1,2] possesses a high cytotoxicity due to its high cationic charge density. Since oxidation of LPEI results in repeating units similar to natural occurring peptides, we hypothesized that the cytocompatibility of oxidized LPEI (i.e., P(EI-*co*-Gly)) should exceed that of PEI. Such an improvement would enable *in vivo* studies especially for gene delivery applications. In order to evaluate this parameter, cytotoxicity was investigated by 3-[4,5-dimenthylthiazol-2-yl]-2,5-diphenyltetrazolium bromide (MTT) assay using human embryonic kidney 293 cell line (HEK 293) (Figure 6A).

While LPEI induces a toxic effect already at very low concentrations (<6.25 mg L^{-1}), all copolymers investigated are cytocompatible up to a concentration of 25 mg L^{-1}. Furthermore, a noticeable effect of the DO on the cell viability can be observed. For example, while cell viability values drop below 60% after incubation with P(EI-*co*-Gly$_{20\%}$) (**1**) at 50 mg L^{-1} for 48 h, P(EI-*co*-Gly$_{85\%}$) (**4**) still does not induce harmful effects, with ∼80% cell viability even at relatively high concentrations (200 mg L^{-1}).

A second important parameter, the interactions of polymers with serum proteins, was assessed by DLS measurements of P(EI-*co*-Gly)s after treatment with fetal bovine serum (FBS) (Figure 6B). All investigated copolymers resulted in *Z*-average values that were indistinguishable from the untreated control sample (pure FBS), indicating no further aggregation and, hence, polymer stability in the presence of serum proteins over 48 h. LPEI itself could not be investigated since its addition to serum resulted in an immediate precipitation of protein components. It should be noted that this investigation does only demonstrate the absence of serum coagulation, while an interaction of protein and polymer is still possible. In conclusion, it can be stated that even a low DO is able to shield the copolymer from interacting with cell membrane/proteins and therefore significantly reduces harmful effects on cells, as shown by the cytotoxicity investigations.

EXPERIMENTAL SECTION

Materials. Reagents were used as received unless otherwise noted. LPEI (MW 25 000 g mol^{-1}) was obtained from Polysciences. Aqueous hydrogen peroxide solution (30% w/w) and methanol were purchased from Sigma-Aldrich (USA). Poly(2-ethyl-2-oxazoline) with a degree of polymerization of 95 was synthesized according to the literature starting from 2-ethyl-2-oxazoline (Sigma-Aldrich).[44] Hydrochloric acid and trypsin were purchased from Sigma-Aldrich. Centrifugal

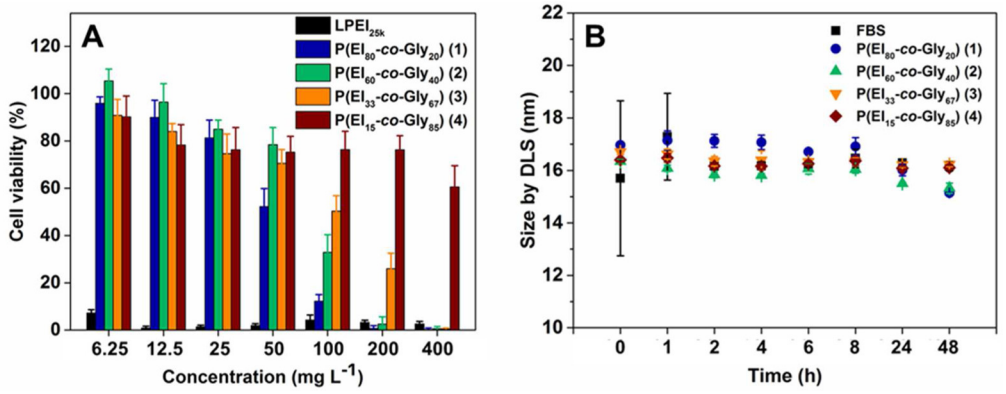

Figure 6. (A) Cytotoxicity of LPEI as well as P(EI-*co*-Gly)s **1**−**4** by MTT assay on HEK 293 cells. (B) Serum stability by time-dependent DLS measurements of FBS in the presence of P(EI-*co*-Gly)s **1**−**4**.

DOI: 10.1021/acs.macromol.5b01940
Macromolecules 2015, 48, 7420−7427

concentration was performed using disposable Vivaspin 20 ultrafiltration devices with a molar mass cutoff (MWCO) of 3000 g mol^{-1}.

General Methods and Instrumentation. Proton (^{1}H) nuclear magnetic resonance (NMR) and carbon (^{13}C) NMR spectra were acquired in D_2O, at room temperature using a Bruker AC 400 MHz or a Bruker AC 300 MHz (100 MHz ^{13}C); chemical shifts (δ) are expressed in parts per million relative to TMS. ^{1}H NMR measurements were carried out with an acquisition time of 3.2 s, a pulse repetition time of 2.0 s, a 30° pulse width, 5208 Hz spectral width, and 32K data points.

The degree of oxidation (DO) was calculated from the integrals of the ^{1}H NMR signals of the copolymer backbones (see Figure 1 and Figure S2) using eq 1

$$\mathrm{DO} = \frac{2\left(F - \frac{4}{3}A\right)}{2\left(F - \frac{4}{3}A\right) + D} \quad (1)$$

where F is the integral of NH−CO−CH_2, A is the integral of CH_2−CH_3 (provided that $A \ll F$), and D is the integral of NH−CH_2−CH_2. Diffusion-ordered NMR spectroscopy (DOSY) was performed on a Bruker 400 MHz Avance I NMR system equipped with a BBO z-gradient probehead. 2D spectra were recorded using a pulse programm (Bruker: "ledbpgp2s") with bipolar gradient pulses and two spoil gradients.[45] Experimental parameters were optimized once using a 1D version of the aforementioned pulse sequence and then kept constant for all samples: 32 number of scans, recycle delay of 2 s, acquisition time of 1.7 s, diffusion time ($d20$) of 75 ms, a gradient pulse length ($p30$) of 2.5 ms, and a linear gradient amplitude ramp ranging from 5 to 95% (with respect to the maximum strength of 53.5 G/cm) with 64 increments. Sample temperature was set to 25 °C. Standard DOSY processing algorithms provides by TopSpin were utilized to obtain the final DOSY spectra and to extract the diffusion coefficients.

Size exclusion chromatographies (SEC) were performed on an Agilent Technologies 1200 Series gel permeation chromatography system equipped with a G1329A autosampler, a G131A isocratic pump, a G1362A refractive index detector, and both a PSS Gram 30 and a PSS Gram 1000 column placed in series. As eluent, a 0.21% LiCl solution in *N*,*N*-dimethylacetamide (DMAc) was used at 1 mL min^{-1} flow rate and a column oven temperature of 40 °C. Molar masses were calculated using poly(styrene) standard.

Fourier transform infrared (FT-IR) spectra were recorded on a Thermo Nicolet Nexus 670 FT-IR spectrometer, using the attenuated total reflectance (ATR) method.

Viscosity measurements were conducted using an AMVn viscometer (Anton Paar, Graz, Austria), with the capillary/ball combination of the measuring system. The respective flow times for the solvent (methanol) and polymer solutions, τ_0 and t, were measured at 25 °C, with relative viscosities $\eta_r = t/\tau_0$ in the range of 1.1−1.8, which corresponds to dilute solutions.

The hydrodynamic radius R_0 was calculated from diffusion coefficients D (DOSY) and liquids viscosity η_0 by eq 2, the Einstein−Smoluchowski relation.

$$R_0 = \frac{k_B T}{6\pi\eta_0 D} \quad (2)$$

where k_B is the Boltzmann constant, T is the temperature, η_0 is the liquid's viscosity, and D is the diffusion coefficient.

Oxidation of Linear Poly(ethylene imine). The synthesis is exemplified by the P(EI-*co*-$Gly_{67\%}$) with a degree of oxidation (DO) about 67%. LPEI (0.025 g) was dissolved in methanol (V = 0.63 mL). After stirring for 5 min, aqueous hydrogen peroxide solution (4 equiv per EI unit, 0.125 mL, 30% w/w) was added dropwise into the stirring polymer mixture at room temperature (water bath, 18 °C). After 2 h, the mixture was precipitated two times into 15 mL of ice-cold diethyl ether. The oxidized polymer was filtered off and washed with 5 mL of diethyl ether. The residue was dissolved in 3 mL distilled water and freeze-dried overnight (yield: 95%).

LPEI. ^{1}H NMR (400 MHz, D_2O): δ 3.46−3.28 (NH−CH_2−CH_2), 3.00−2.60 (NH−CH_2), 2.35 (CH_2 EtOx), 0.99 (CH_3 EtOx) ppm. ^{13}C NMR (100 MHz, D_2O): δ 148.5 (CO−CH_2−CH_3), 47.1 (NH−CH_2−CH_2), 25.1 (CH_2−CH_3), 9.8 (CH_2−CH_3) ppm. FT-IR: $\tilde{\nu}$ 3180 (OH, NH), 2870 (CH asym/sym str), 1480 (C−H def), 1280, 1125 (C−N str), 1045 (C−N) cm^{-1}.

P(EI-co-GLY$_{67\%}$). DO = 67%, μ_{Int} = 8.6 mL g^{-1}. ^{1}H NMR (400 MHz, D_2O): δ 8.30, 8.05−7.75 (NH−CO−CH_2), 3.75−3.18 (NH−CO−CH_2), 3.14−2.41 (NH−CH_2−CH_2), 2.30 (CH_2−CH_3), 1.94 (CH_2−CH_3) ppm. ^{13}C NMR (100 MHz, D_2O): δ 171.1 (NH−CO−CH_2), 166.5, 140.5 (CO−CH_2−CH_3), 47.0−34.7 (NH−CH_2−CH_2, NH−CO−CH_2), 25.2 (CH_2−CH_3), 8.5 (CH_2−CH_3) ppm. FT-IR: $\tilde{\nu}$ 3260 (OH, NH), 2870 (CH asym/sym str), 1658 (C═O), 1600 (NH bending), 1435 (C−H def), 1395, 1340 ($CH_{2,Gly}$ asym/sym str), 1155 (C−N str), 1065 (C−N) cm^{-1}.

Kinetic Investigations. The peroxide concentration dependent oxidation of linear poly(ethylene imine) was performed according to the general procedure described above. For further kinetic investigations, the H_2O_2 concentration was set constant to 4 equiv per EI unit to reach a maximum level of oxidation. To investigate the influence of temperature, five analogue stock solutions of LPEI, ethanol, and H_2O_2 were prepared and stirred at selected temperatures (ranging from −20 to 55 °C). After defined time ranges (ranging from 0.5 to 20 h) aliquots were taken and purified by precipitation. After washing with diethyl ether the samples were freeze-dried. The degree of oxidation was determined by proton nuclear magnetic resonance measurements (^{1}H NMR).

P(EI-*co*-Gly) with Varying DOs. The oxidation of linear poly(ethylene imine) was performed in larger scales according to the general procedure described above. Since larger amounts of H_2O_2 lead to higher generation of heat and, hence, to a faster and more uncontrollable oxidation, the reaction for lower oxidation samples **1** and **2** was performed at 0 °C. Higher oxidation degrees (**3** and **4**) were obtained at room temperature (18 °C).

Degradation Studies. Polymer **1** (DO 67%, 20 mg) was dissolved in 6 mol L^{-1} HCl (2 mL) and stirred for 20 h at 70 °C. Subsequently, the mixture was neutralized with sodium hydroxide and freeze-dried. A second approach was the addition of the protease Trypsin (0.5 mL) to an aqueous solution of **1** (5 mg in 1 mL of H_2O). After stirring for 20 h at 37 °C, the mixture was freeze-dried. Both products were analyzed by ^{1}H and DOSY NMR and SEC.

Cytotoxicity. HEK 293 cells were cultured in RPMI-1640 supplied with 10% fetal bovine serum (FBS) and 1% penicillin−streptomycin. HEK 293 cells were seeded onto 96-well plates at a density of 10 000 cells/well. The cells were incubated at 37 °C, 5% CO_2. After 24 h, the medium was replaced with fresh medium containing polymer at various concentrations. After incubation for 48 h, 100 μL of fresh medium and 20 μL of 5 mg/mL MTT solution were used to replace the sample medium. After 4 h of incubation, the medium was removed, and DMSO (150 μL) was added to each well to dissolve the formazan crystals. The absorbance of each well was measured with a microplate reader (Power-Wave X, Biotek Instruments, USA) at 690 nm as reference and subtracted from the absorbance of the same well at 550 nm. The results were presented as a percentage of absorbance of the blank control.

Serum Stability. Polymers were dissolved in PBS containing 10% FBS. The particle sizes within the polymer solutions were analyzed using a Zetasizer 3000 HAS (Malvern Instrument Ltd., Malvern, UK) equipped with a He−Ne laser beam at 658 nm (scattering angle: 90°) over 48 h. The concentration of the polymers was 500 mg/L. Each sample was measured three times, and an average particle size was obtained.

CONCLUSION

A method for the tailored oxidation of commercially available linear poly(ethylene imine) (LPEI) was developed. The 1972 report by MacDonald et al. on the oxidation of branched poly(ethylene imine) was revisited by means of extensive kinetic studies and characterizations of the modified LPEIs (NMR, DOSY, IR, SEC, viscometry). Concentration as well as temperature proved efficient parameters to control the degree

DOI: 10.1021/acs.macromol.5b01940
Macromolecules 2015, 48, 7420−7427

of oxidation of poly(ethylene imine-*co*-glycine)s (P(EI-*co*-Gly)) copolymers. At low temperatures, the oxidation process was found to be well-controlled, and a maximum of 85% oxidized EI units could be reached. Notably, oxidation of only 10% of the LPEI led to water-soluble polymers. The formed amide groups render the copolymers (bio)degradable, as shown by the decomposition experiments using aqueous hydrogen chloride and trypsin. Finally, the biocompatibility improvement of P(EI-*co*-Gly)s compared to LPEI was demonstrated by cytotoxicity investigations and serum stability measurements.

The controlled oxidation of LPEI, as shown in this contribution, enables the specific improvement of the (bio)-properties, such as biodegradation and biocompatibility, and hence helps to overcome the main drawbacks of the initial material. It can be assumed that there is an optimal composition of copolymers to reach high transfection efficiencies (EI content) while showing good cytocompatibility (Gly content). However, the investigation of the transfection abilities will be the focus of further studies.

■ ASSOCIATED CONTENT

Ⓢ Supporting Information

The Supporting Information is available free of charge on the ACS Publications website at DOI: 10.1021/acs.macromol.5b01940.

Figures S1−S7 (PDF)

■ AUTHOR INFORMATION

Corresponding Authors

*E-mail: ulrich.schubert@uni-jena.de (U.S.S.).
*E-mail: yyyang@ibn.a-star.edu.sg (Y.Y.Y.).
*E-mail: hedrick@us.ibm.com (J.L.H.).

Present Address

K.K. and M.H.: Department of Chemistry, University of Warwick, Gibbet Hill Road, Coventry CV4 7AL, UK.

Notes

The authors declare no competing financial interest.

■ ACKNOWLEDGMENTS

C.E. is grateful to the Deutscher Akademischer Austauschdienst (DAAD) for financial support. Furthermore, this work was supported by the Institute of Bioengineering and Nanotechnology "Biomedical Research Council, Agency for Science, Technology and Research, Singapore", and IBM Almaden Research Center, USA. M.H. gratefully acknowledges the German Research Foundation (DFG, GZ: HA 7725/1-1) for funding.

■ REFERENCES

(1) Mintzer, M. A.; Simanek, E. E. *Chem. Rev.* **2009**, *109*, 259−302.
(2) Jaeger, M.; Schubert, S.; Ochrimenko, S.; Fischer, D.; Schubert, U. S. *Chem. Soc. Rev.* **2012**, *41*, 4755−4767.
(3) Brissault, B.; Kichler, A.; Guis, C.; Leborgne, C.; Danos, O.; Cheradame, H. *Bioconjugate Chem.* **2003**, *14*, 581−587.
(4) Boussif, O.; Lezoualch, F.; Zanta, M. A.; Mergny, M. D.; Scherman, D.; Demeneix, B.; Behr, J. P. *Proc. Natl. Acad. Sci. U. S. A.* **1995**, *92*, 7297−7301.
(5) Godbey, W. T.; Wu, K. K.; Mikos, A. G. *J. Controlled Release* **1999**, *60*, 149−160.
(6) Wightman, L.; Kircheis, R.; Roessler, V.; Carotta, S.; Ruzicka, R.; Kursa, M.; Wagner, E. *J. Gene Med.* **2001**, *3*, 362−372.
(7) Lungwitz, U.; Breunig, M.; Blunk, T.; Goepferich, A. *Eur. J. Pharm. Biopharm.* **2005**, *60*, 247−266.
(8) Hunter, A. C. *Adv. Drug Delivery Rev.* **2006**, *58*, 1523−1531.
(9) Moghimi, S. M.; Symonds, P.; Murray, J. C.; Hunter, A. C.; Debska, G.; Szewczyk, A. *Mol. Ther.* **2005**, *11*, 990−995.
(10) Fischer, D.; Li, Y.; Ahlemeyer, B.; Krieglstein, J.; Kissel, T. *Biomaterials* **2003**, *24*, 1121−1131.
(11) Fischer, D.; Bieber, T.; Li, Y.; Elsaesser, H.-P.; Kissel, T. *Pharm. Res.* **1999**, *16*, 1273−1279.
(12) Jere, D.; Jiang, H.; Arote, R.; Kim, Y.; Choi, Y.; Cho, M.; Akaike, T.; Cho, C. *Expert Opin. Drug Delivery* **2009**, *6*, 827−834.
(13) Wen, Y.; Pan, S.; Luo, X.; Zhang, X.; Zhang, W.; Feng, M. *Bioconjugate Chem.* **2009**, *20*, 322−332.
(14) Neu, M.; Fischer, D.; Kissel, T. *J. Gene Med.* **2005**, *7*, 992−1009.
(15) Kobayashi, S.; Gros, L.; Muacevic, G.; Ringsdorf, H. *Makromol. Chem.* **1983**, *184*, 793−801.
(16) Fernandes, J. C.; Qiu, X.; Winnik, F. M.; Benderdour, M.; Zhang, X.; Dai, K.; Shi, Q. *Int. J. Nanomed.* **2013**, *8*, 4091−4102.
(17) Strehblow, C.; Schuster, M.; Moritz, T.; Kirch, H.-C.; Opalka, B.; Petri, J. B. *J. Controlled Release* **2005**, *102*, 737−747.
(18) Li, D.; Tang, G. P.; Li, J. Z.; Kong, Y.; Huang, H. L.; Min, L. J.; Zhou, J.; Shen, F. P.; Wang, Q. Q.; Yu, H. *J. Biomater. Sci., Polym. Ed.* **2007**, *18*, 545−560.
(19) Elfinger, M.; Geiger, J.; Hasenpusch, G.; Üzgün, S.; Sieverling, N.; Aneja, M. K.; Maucksch, C.; Rudolph, C. *J. Controlled Release* **2009**, *135*, 234−241.
(20) Haas, H. C.; Schuler, N. W.; Macdonald, R. L. *J. Polym. Sci., Part A-1: Polym. Chem.* **1972**, *10*, 3143−3158.
(21) Murahashi, S.; Mitsui, H.; Shiota, T.; Tsuda, T.; Watanabe, S. *J. Org. Chem.* **1990**, *55*, 1736−1744.
(22) Cicchi, S.; Marradi, M.; Goti, A.; Brandi, A. *Tetrahedron Lett.* **2001**, *42*, 6503−6505.
(23) Mare, H. E. D. L.; Coppinger, G. M. *J. Org. Chem.* **1963**, *28*, 1068−1070.
(24) Kamlet, M.; Kaplan, L. *J. Org. Chem.* **1957**, *22*, 576−578.
(25) Splitter, J.; Calvin, M. *J. Org. Chem.* **1958**, *23*, 651−651.
(26) Just, G.; Cunningham, M. *Tetrahedron Lett.* **1972**, *13*, 1151−1153.
(27) Seow, W. Y.; Liang, K.; Kurisawa, M.; Hauser, C. A. E. *Biomacromolecules* **2013**, *14*, 2340−2346.
(28) All investigations were performed using commercially available LPEI. The molar mass indicated by the supplier (PolySciences, 25 000 g mol^{-1}) is misleading. The real molar mass M_n is around 6500 g mol^{-1} according to the literature,[35] which corresponds to a LPEI with 150 repeating units.
(29) Travis, B. R.; Sivakumar, M.; Hollist, G. O.; Borhan, B. *Org. Lett.* **2003**, *5*, 1031−1034.
(30) Fraunhoffer, K. J.; White, M. C. *J. Am. Chem. Soc.* **2007**, *129*, 7274−7276.
(31) Tauhardt, L.; Kempe, K.; Knop, K.; Altuntaş, E.; Jaeger, M.; Schubert, S.; Fischer, D.; Schubert, U. S. *Macromol. Chem. Phys.* **2011**, *212*, 1918−1924.
(32) Ijare, O. B.; Somashekar, B. S.; Gowda, G. A. N.; Sharma, A.; Kapoor, V. K.; Khetrapal, C. L. *Magn. Reson. Med.* **2005**, *53*, 1441−1446.
(33) Weyts, K. F.; Goethals, E. J.; Bunge, W. M.; Bloys van Treslong, C. J. *Eur. Polym. J.* **1990**, *26*, 445−447.
(34) Gembitskii, P. A.; Kleshcheva, N. A.; Golitsyna, T. L.; Nikolaev, G. M.; Zhuk, D. S. *Bull. Acad. Sci. USSR, Div. Chem. Sci.* **1975**, *24*, 2516−2516.
(35) Wagner, M.; Pietsch, C.; Tauhardt, L.; Schallon, A.; Schubert, U. S. *J. Chromatogr. A* **2014**, *1325*, 195−203.
(36) Gibney, K.; Sovadinova, I.; Lopez, A. I.; Urban, M.; Ridgway, Z.; Caputo, G. A.; Kuroda, K. *Macromol. Biosci.* **2012**, *12*, 1279−1289.
(37) Lindsay, S. *Introduction to Nanoscience*; Oxford University Press: Oxford, 2009.
(38) Holz, M.; Heil, S. R.; Sacco, A. *Phys. Chem. Chem. Phys.* **2000**, *2*, 4740−4742.
(39) Fukushima, K.; Ideguchi, Y.; Miyazawa, T. *Bull. Chem. Soc. Jpn.* **1963**, *36*, 1301−1307.

DOI: 10.1021/acs.macromol.5b01940
Macromolecules 2015, 48, 7420−7427

(40) Suzuki, S.; Iwashita, Y.; Shimanouchi, T.; Tsuboi, M. *Biopolymers* **1966**, *4*, 337−350.
(41) Gupta, V. D.; Trevino, S.; Boutin, H. *J. Chem. Phys.* **1968**, *48*, 3008−3015.
(42) Taga, K.; Sowa, M. G.; Wang, J.; Etori, H.; Yoshida, T.; Okabayashi, H.; Mantsch, H. H. *Vib. Spectrosc.* **1997**, *14*, 143−146.
(43) Ojamäe, L.; Aulin, C.; Pedersen, H.; Käll, P.-O. *J. Colloid Interface Sci.* **2006**, *296*, 71−78.
(44) Wiesbrock, F.; Hoogenboom, R.; Leenen, M.; van Nispen, S. F. G. M.; van der Loop, M.; Abeln, C. H.; van den Berg, A. M. J.; Schubert, U. S. *Macromolecules* **2005**, *38*, 7957−7966.
(45) Wu, D. H.; Chen, A. D.; Johnson, C. S. *J. Magn. Reson., Ser. A* **1995**, *115*, 260−264.

DOI: 10.1021/acs.macromol.5b01940
Macromolecules 2015, 48, 7420−7427

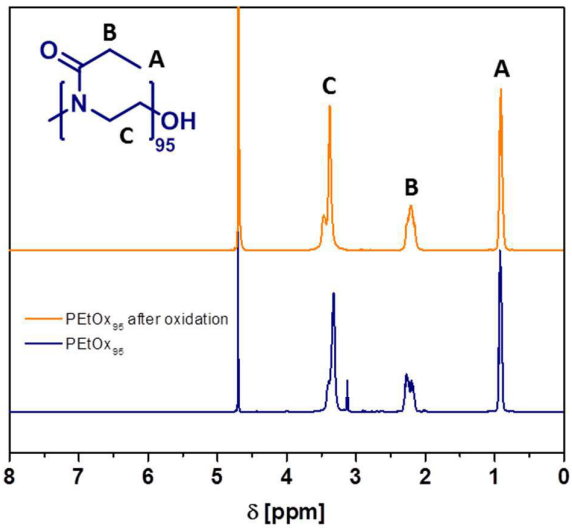

Figure S1. ^{1}H NMR spectra of poly(2-ethyl-2-oxazoline) (DP 95) before and after oxidation with hydrogen peroxide (4 equiv.) at room temperature (18 °C) for 20 hours (D_2O, 400 MHz).

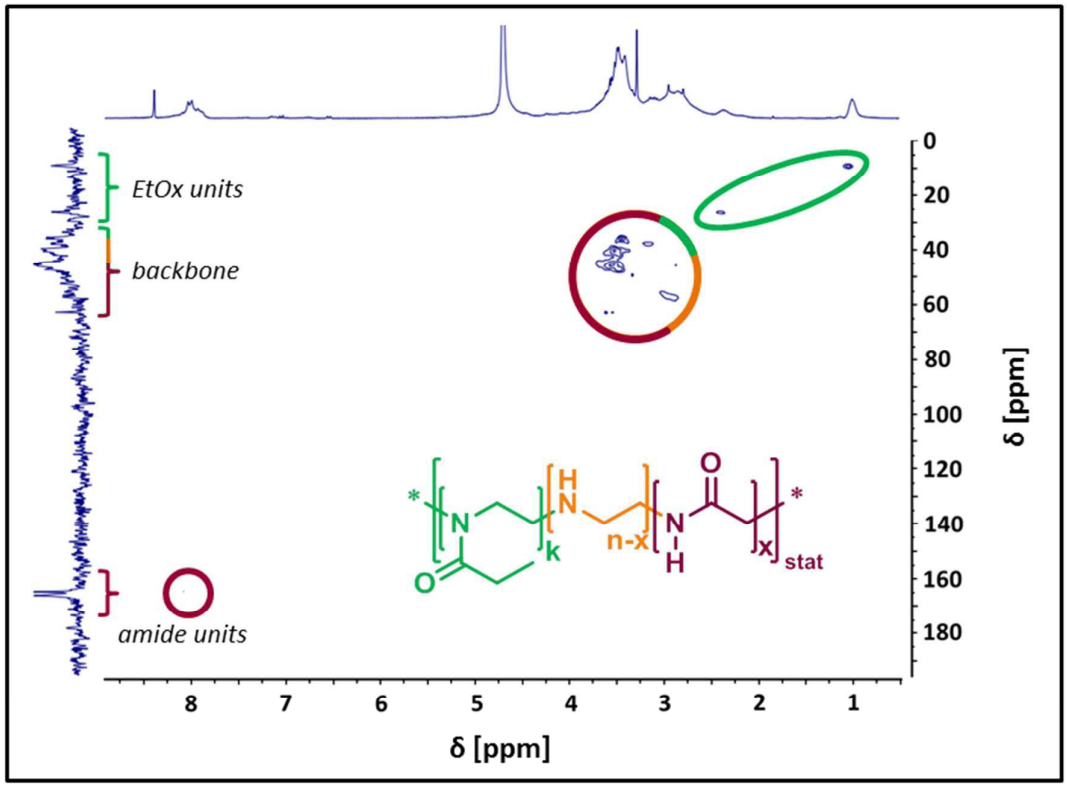

Figure S2. HSQC NMR of P(EI-*co*-Gly) (including unaffected EtOx units, < 5%) with a degree of oxidation of about 67% (D_2O, 400 MHz).

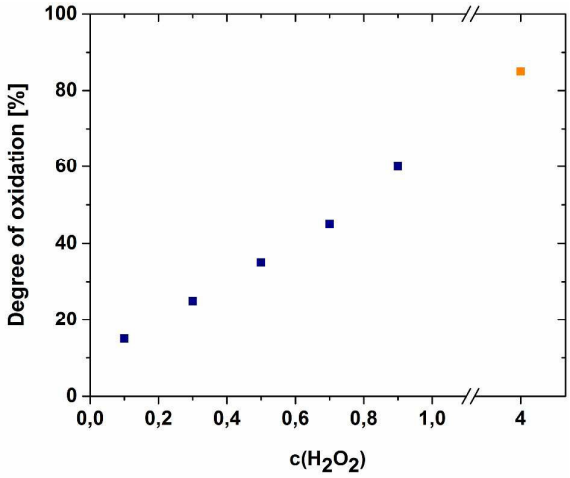

Figure S3. Kinetic studies of the oxidation of LPEI in methanol dependent on H_2O_2 concentration ($0 < c(H_2O_2) < 0.9$ equiv. per EI unit). For comparison, the DO of LPEI oxidized with a 4-fold excess of H_2O_2 is added (orange).

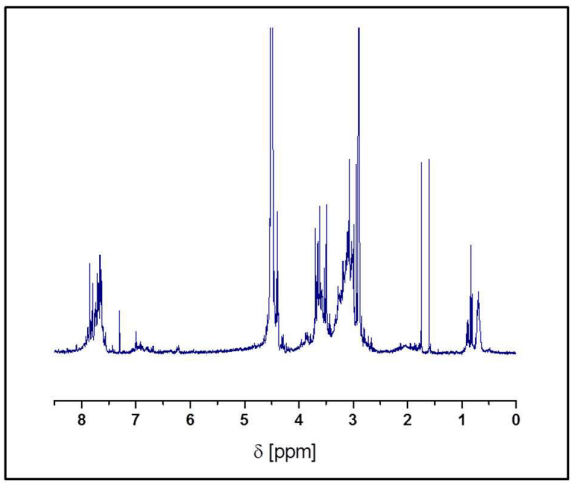

Figure S4. ^{1}H NMR spectrum of degraded P(EI-*co*-Gly), while performing the oxidation of LPEI at 55 °C for 20 minutes (D_2O, 400 MHz).

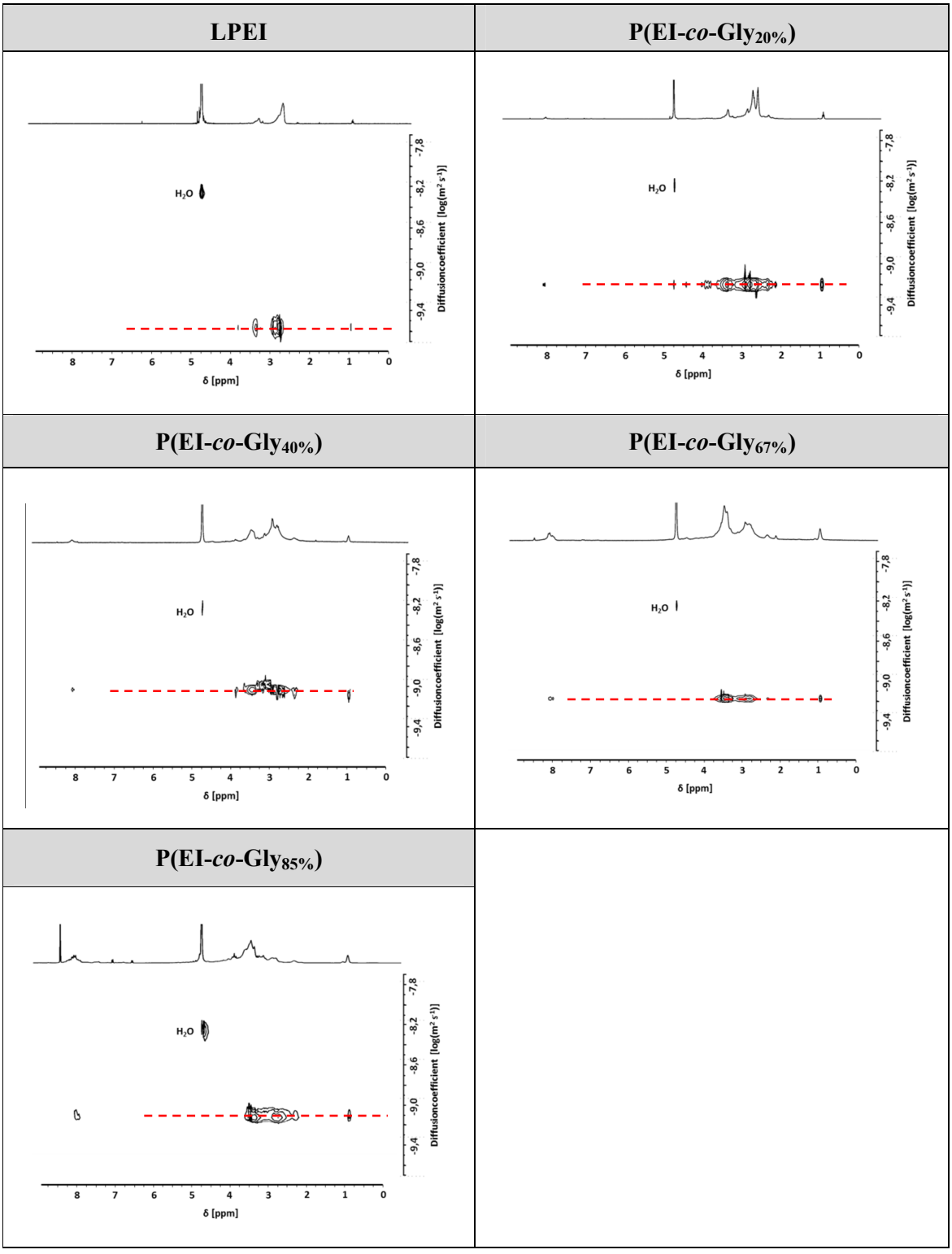

Figure S5. DOSY NMR spectra of LPEI and **1-4** with different DOs (D_2O, 400 MHz, 25 °C).

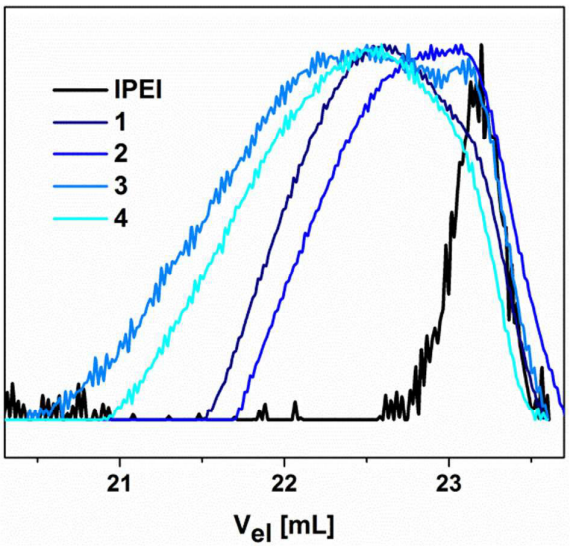

Figure S6. SEC traces of P(EI-*co*-Gly)s **1-4** and LPEI (*N*,*N*-dimethylacetamide, 0.21% LiCl).

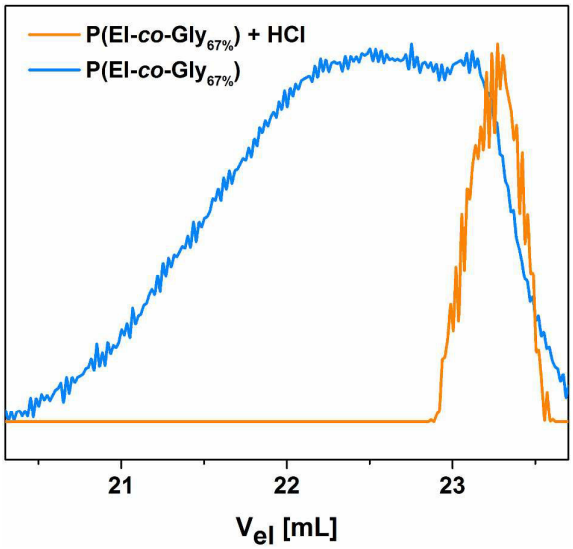

Figure S7. SEC traces of P(EI-*co*-$Gly_{67\%}$) before and after degradation with 6 mol L^{-1} aqueous hydrogen chloride (DMAc, 0.21% LiCl).

PUBLICATION 3

Facile carbohydrate-mimetic modifications of poly(ethylene imine) carriers for gene delivery applications

C. Englert, M. Fevre, R. J. Wojtecki, W. Cheng, Q. Xu, C. Yang, X. Ke, M. Hartlieb, K. Kempe, J. M. García, R. J. Ono, U. S. Schubert, Y. Y. Yang, J. L. Hedrick

Polym. Chem. **2016**, *7*, 5862-5872

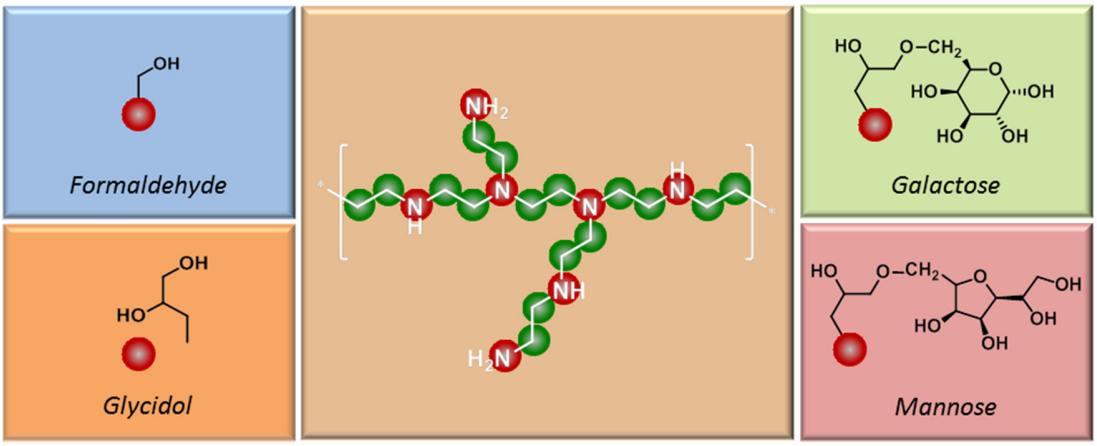

Polymer Chemistry

PAPER

View Article Online
View Journal | View Issue

Cite this: *Polym. Chem.*, 2016, **7**, 5862

Facile carbohydrate-mimetic modifications of poly(ethylene imine) carriers for gene delivery applications†

Christoph Englert,[a,b,c] Mareva Fevre,[a] Rudy J. Wojtecki,[a] Wei Cheng,[d] Qingxing Xu,[d] Chuan Yang,[d] Xiyu Ke,[d] Matthias Hartlieb,‡[b,c] Kristian Kempe,‡[b,c] Jeannette M. García,[a] Robert J. Ono,[a] Ulrich S. Schubert,*[b,c] Yi Yan Yang*[d] and James L. Hedrick*[a]

Received 2nd June 2016,
Accepted 16th August 2016

DOI: 10.1039/c6py00940a

www.rsc.org/polymers

Commercially-available linear and branched PEIs (LPEI and BPEI) were chemically-modified with carbohydrates and carbohydrate-mimetics to improve biocompatibility. Hydroxyl moieties were installed in a close proximity *via* reaction of PEI's amines with paraformaldehyde (pF) or glycidol. Mixing PEI with pF led to the formation of hemiaminal moieties as well as *N*-methylation of the backbone through an Eschweiler–Clarke-type rearrangement. The amount of attached hydroxyl groups depended on the initial amount of pF and the results were in agreement with NMR studies on model reactions with primary and secondary amines. The primary amines of BPEI triggered the ring-opening of glycidol and sugar-containing epoxides, in methanol and at room temperature. PEI chains modified with pF displayed the same cytotoxicity as the parent polymer, unless a sufficient amount of pF was added to trigger *N*-methylation of the backbone. In contrast, glycidol and sugar-functionalized BPEIs exhibited lower toxicity but similar (if not higher) transfection efficiency as compared to unmodified BPEI.

Introduction

Nucleic acid-based gene therapy holds great promise in treating human diseases by replacement of defective genes or repression of redundant gene expression to normal levels by the use of RNA interference.[1] Gene delivery vectors are commonly classified as viral or non-viral. Although viral vectors have superior transduction capabilities, their clinical applications have been limited owing to their immunogenic and oncogenic potentials.[2,3] To circumvent this problem, a number of non-viral gene delivery systems have been reported, which include (1) complexes of nucleic acids with various cationic molecules including lipids,[4] polymers[5] and peptides[6] and (2) conjugates of nucleic acids with natural ligands such as cholesterol,[7] as well as cell-penetrating peptides.[8]

The successful clinical application of gene delivery vectors depends mainly on three factors: (1) high gene transfection efficiency, (2) low toxicity and (3) the ability of the vectors to overcome numerous biological barriers after systemic or local administration. Among the various types of non-viral vectors, poly(ethylene imine) (PEI) has been used as the gold standard.[9] Indeed, linear PEI (LPEI) and branched PEI (BPEI) possess one of the highest cationic charge density potential of all organic macromolecules.[10] Every third atom is an amine, of which every sixth nitrogen atom is protonated under physiological conditions.[10] In this way, PEI is able to interact with the phosphate groups of deoxyribonucleic acid (DNA), as well as ribonucleic acid (RNA) to form toroidal complexes that are readily endocytosed by cells.[11,12] Therefore, PEI demonstrates an extremely high gene transfection efficiency *in vitro*.[10,13–16] However, the net positive charge of PEI/polyplexes led to major drawbacks associated with toxicity, aggregation and undesired non-specific interactions with cellular and non-cellular components, particularly *in vivo*.[17] Notably, since LPEI shows various advantages over BPEI, both from a synthetic (more defined products, easier to characterize)[13] and from a biological/clinical side (increased

[a]*IBM Almaden Research Center, 650 Harry Road, San Jose, CA 95120, USA. E-mail: hedrick@us.ibm.com*
[b]*Laboratory of Organic and Macromolecular Chemistry (IOMC), Friedrich Schiller University Jena, Humboldtstrasse 10, 07743 Jena, Germany. E-mail: ulrich.schubert@uni-jena.de*
[c]*Jena Center for Soft Matter (JCSM), Friedrich Schiller University Jena, Philosophenweg 7, 07743 Jena, Germany*
[d]*Institute of Bioengineering and Nanotechnology, 31 Biopolis Way, The Nanos, Singapore 138669, Singapore. E-mail: yyyang@ibn.a-star.edu.sg*
†Electronic supplementary information (ESI) available. See DOI: 10.1039/c6py00940a
‡Current address: Department of Chemistry, University of Warwick, Gibbet Hill Road, Coventry, CV4 7AL, UK.

biocompatibility),[18] it has been the focus of multiple clinical trials for years.[19–23]

The most common method for the synthesis of LPEI is the acidic[24–26] or basic[27,28] hydrolysis of poly(2-alkyl-2-oxazoline)s (POx). In contrast, branched poly(ethylene imine) can be synthesized by the ring-opening polymerization of unsubstituted aziridines leading to branched chains with primary, secondary, and tertiary amino groups.[29] Current research focuses on the design of biodegradable[30–34] and more biocompatible derivatives[35,36] by modifying the PEI backbone and/or side chains. Various chemical transformations of the amino groups of PEI have been reviewed,[13] and can be categorized as follows: reductive *N*-methylation,[37,38] nucleophilic substitution with alkylhalogenids,[39] ring-opening of epoxides and carbonates,[40–43] conjugate addition[31,44] and acylation resulting in carbamates[45] or pseudo-poly(2-oxazoline)s.[43,46,47] Synthetic post-polymerization functionalization methods for enhanced biocompatibility of BPEI are summarized in Table 1.

Considerable efforts have focused on the attachment of carbohydrate-containing moieties, owing to the non-toxicity of such molecules, as well as the potential to target cells exhibiting carbohydrate-receptors. For instance, saccharides such as oligo-maltose,[53] chitosan,[54] galactose[55] and mannose[56] have been grafted onto PEI. Recently, we reported on the modification of the primary amines of BPEI using a single ring-opening step of mannose-functionalized cyclic carbonates.[52] This transformation mitigated PEI cytotoxicity and non-specific interactions, as well as enhanced the gene transfection efficiency. However, most of these modifications required multi-step syntheses or harsh experimental conditions, often resulting in poor control over the final polymer composition.

Herein, in an effort to devise a facile and economical synthetic strategy to carbohydrate-like modification of PEI, we focused on the installation of hydroxyl moieties in close proximity to the PEI backbone, in an effort to mimic the vicinal diols of sugars. Towards this goal, PEI was functionalized by a single-step transformation with hemiaminal moieties using paraformaldehyde and by ring-opening of glycidol or galactose- and mannose-functionalized epoxides. All reagents were either commercially available or easily synthesized. Detailed nuclear magnetic resonance (NMR) investigations allowed for the accurate characterization of the structure of the modified PEI. The relevance of these modifications for the use of PEI as a gene delivery vector was validated by cytotoxicity and gene transfection efficiency assays.

Results and discussion

Functionalization with formaldehyde

Hydroxyl functional groups were installed on both LPEI and BPEI by modification of the polymer with paraformaldehyde (pF). In the case of BPEI, both the primary and secondary amines could be successfully reacted to obtain a polymer with

Table 1 Synthetic post-polymerization modification methods for enhanced biocompatibility of branched PEI

	Functionalized				
Reagent(s)	–NH_2	–NH–	Product(s)	Transfection	Ref.
mPEG–NCO	✓		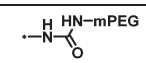	n.d.[a]	45
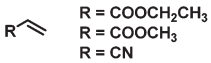 R = $COOCH_2CH_3$, R = $COOCH_3$, R = CN	✓		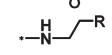	pDNA siRNA	44 and 48
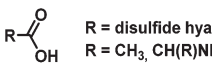 R = disulfide hyaluronic acid, R = CH_3, $CH(R)NH_2$	✓	✓	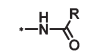	pDNA pDNA	49 and 50
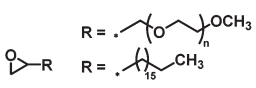 R = OCH_3, R = CH_3, R = OH	✓	✓	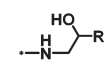	pDNA siRNA n.d.	40, 41 and 43
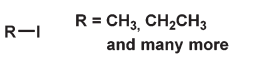 R = CH_3, CH_2CH_3 and many more	✓	✓	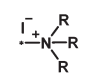	pDNA	50
	✓	✓	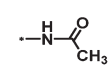	siRNA n.d.	48 and 43
	✓	✓	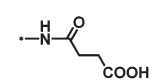	siRNA n.d.	48 and 43
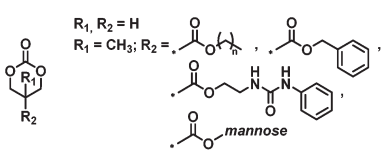 $R_1, R_2 = H$; $R_1 = CH_3$; R_2 = ..., mannose	✓		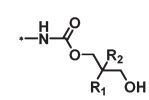	pDNA pDNA pDNA	42, 51 and 52

[a] n.d. – not determined.

a high degree of functionalization. BPEI is a hyperbranched polymer that contains primary ($pK_a \sim 9.6$, measured in 0.5 M NaCl/H_2O), secondary ($pK_a \sim 8.6$) and tertiary ($pK_a \sim 7.5$) amine groups in a theoretical ratio of 1 : 2 : 1.[57] However, the experimental ratio was found to be 1 : 1 : 1 for commercially-available BPEI,[58] with only about 20% of the amine moieties protonated under physiological conditions.[59] Therefore, when the primary and secondary amine moieties are functionalized quantitatively, tertiary amines are available for protonation in the endosome to facilitate endosomal escape through the "proton sponge effect".[10,60–62] Moreover, the decoration of the amine groups also mitigates the toxicity of PEI, enabling higher dosing and nitrogen/phosphorus ratios.

We recently reported that hemiaminal and bis-hemiaminals were intermediates in the reaction of amino-functionalized poly(ethylene glycol) with pF[63] and that transient species were kinetically captured when stoichiometric or an excess of pF was used with respect to the amine groups.[64,65] Preliminary experiments with BPEI and super-stoichiometric amounts of pF (10 equiv. per amine functionality, including primary, secondary and tertiary amine groups) resulted in the formation of an insoluble gel after <1 min stirring at 90 °C, attesting of the crosslinking of the BPEI chains. Model ^{1}H NMR studies on small molecule primary amines showed that variable species were produced depending on the electronics and solubility of the model compound in D_2O. Moreover, as already established while reacting diamino-functionalized PEG and pF in organic solvents,[64,65] transient species are kinetically-quenched to form gels, owing to the polymeric nature of the amine. Both these observations precluded accurate identification of the crosslinks with PEI in aqueous conditions, which was most likely a mixture of aminals and hemiaminal ethers as previously reported for melamine/formaldehyde resins[66,67] and possibly a small quantity of hexahydrotriazine crosslinks.[63,64] NMR experiments on the reaction of LPEI with >0.5 equiv. pF showed the appearance of a new signal in the ^{1}H NMR spectrum of the product at ~2.1 ppm. This signal was identified by DEPT 135/90 to correspond to a *N*-methyl group, attributed to the methylation of the PEI backbone, likely according to an Eschweiler–Clarke-type rearrangement (see Scheme S1†),[37,68] where iminium intermediate forms as secondary amines are reduced to the corresponding tertiary amines. This side reaction with excess formaldehyde therefore limited the amount of hemiaminal moieties that could be attached to the PEI backbone. However, the *N*-methylation of PEI was shown to reduce the cytotoxicity by lowering the net positive charge of the PEI/polyplexes under physiological conditions, but also to decrease the transfection efficiency.[69]

Therefore, the concentration of pF was decreased and varied from 0.05 to 1.20 equivalents (per amine functionality, see Table 2), to mitigate the occurrence of crosslinking of BPEI (**B1** to **B4**) and *N*-methylation of the backbone of LPEI (**L1** to **L5**) (see Scheme 1). The reactions were carried out for 15 h at 90 °C to accommodate for the diminished reactivity of sterically-encumbered amino groups of BPEI. In the case of BPEI, a viscosity increase was observed with increasing formaldehyde concentration and, eventually, the reaction mixture turned into a completely insoluble gel for initial formaldehyde loadings greater than 0.5 equiv.

Table 2 Overview of modified poly(ethylene imine)s obtained by varying the paraformaldehyde (pF) content

Polymer structure	Functional. agent	Polymer	Equiv. pF[a]
Linear poly(ethylene imine)		**L1**	0.15
		L2	0.30
		L3	0.50
		**L4**	0.75
		L5	1.20
Branched poly(ethylene imine)		**B1**	0.05
		B2	0.15
		B3	0.30
		B4	0.50

[a] Per amine functionality, including primary, secondary and tertiary amine groups.

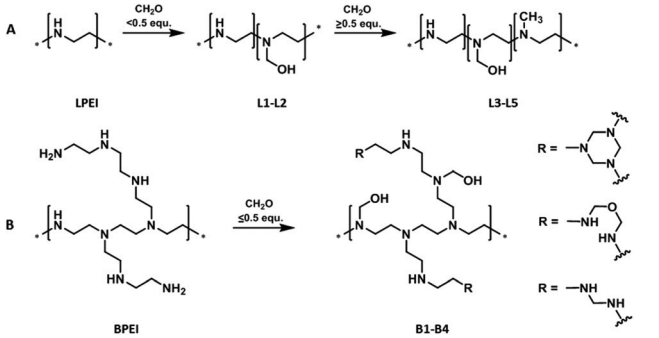

Scheme 1 Schematic representation of the functionalization of (A) linear poly(ethylene imine) (**L1** to **L5**) and (B) branched poly(ethylene imine) (**B1** to **B4**) with paraformaldehyde; wavy lines represent network's formation (R represents possible crosslinking groups, ratio not determined).

Fig. 1 depicts the ^{1}H NMR spectra of linear and branched PEI modified with increasing pF concentration. The integration values of signal C, attributed to network formation (C′, for BPEI) and hemiaminal species, increased with formaldehyde concentration for both polymer architectures. With 0.50 equiv. of pF (**L3**, **B4**) or higher (**L4**, **L5**), methylation of the PEI backbone was also observed.[37] These data are in agreement with model reactions performed using *n*-propylamine (to model primary amine reactivity) and dipropylamine (to model secondary amines) with 0.50 equiv. pF in d_6-DMSO (see Fig. S2†).

Diffusion-ordered NMR (DOSY) spectra of LPEI and BPEI reacted with 0.50 (**L3**) and 0.05 equiv. pF (**B1**), respectively, are displayed in Fig. 2 (the signal of methanol was used as an internal standard). A single diffusion coefficient was observed for both functionalized species. The diffusion coefficients of **L3** and **B1** were larger than the unmodified counterparts, indicating that the functionalization of PEI with formaldehyde led to a decrease of the hydrodynamic radius of the polymer in solution. The absence of sharp signals on the ^{1}H NMR spectra of **L3** and **B1**, as well as the detection of a single diffusion

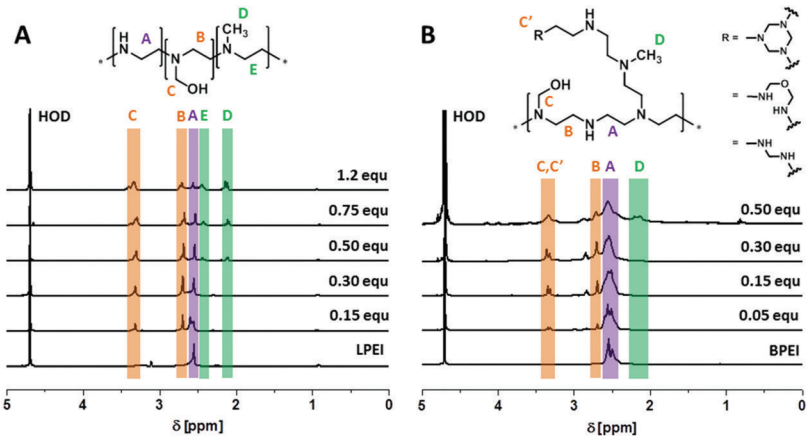

Fig. 1 ^{1}H NMR spectra of (A) linear (**L1** to **L5**) and (B) branched (**B1** to **B4**) poly(ethylene imine)s modified with varying contents of pF; wavy lines represent network's formation (D_2O, 400 MHz).

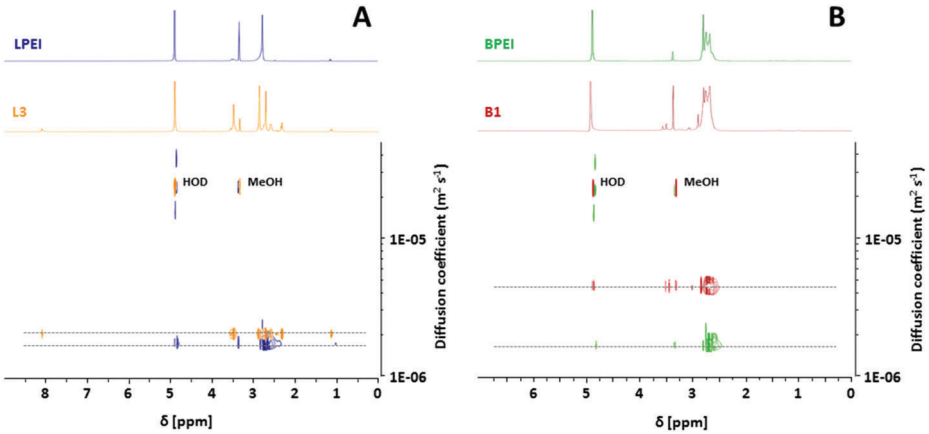

Fig. 2 Diffusion ordered NMR spectra (MeOD, 400 MHz, 25 °C) of (A) LPEI and corresponding hemiaminal-functionalized **L3** (0.5 equiv. pF *vs.* –NH), and, (B) BPEI and corresponding hemiaminal-functionalized **B1** (0.05 equiv. pF per amine functionality, including primary, secondary and tertiary amine groups).

coefficient ruled out any backbone degradation. However, the functionalization of amino moieties of PEI using paraformaldehyde leads to (i) a decrease of charged species per chain owing to increased *N*-substitution, and (ii) the introduction of hydroxyl groups that can create intramolecular H-bonding. Both phenomena could cause the formation of more compact particles in solution and could explain the observed smaller hydrodynamic radii exhibited by the functionalized PEI chains.

Modification with epoxides

Glycidol, as well as, mannose- and galactose-functionalized epoxides were used to modify PEI through a straightforward ring-opening reaction under mild and catalyst-free conditions (see Table 3).

Glycidol was employed as a control carbohydrate-mimetic to facilitate comparison with the hemiaminal modification (Scheme 2, **L6** to **L10** and **B5** to **B9**). Noteworthy, hemiaminal moieties exhibited poor stability under acidic conditions, while ring-opened glycidol moieties are stable in biological environments.[43] Efficient polymer functionalization was verified by ^{1}H NMR (see Fig. S3†) and DOSY NMR experiments of **L8** and **B7** (see Fig. S4†). Mannose and galactose have already been used as efficient modifiers to decrease the toxicity of PEI while allowing for targeting of cells exhibiting either mannose[52,56] or galactose[55] receptors. However, as already mentioned, the sugar-functionalization of PEI usually involves tedious synthetic work.[70]

Epoxides bearing pendant sugars were prepared by a one-step nucleophilic substitution of commercially-available protected sugars with epichlorohydrin in THF. To modify the polymers, ring-opening reactions were carried out in MeOH at room temperature (see Scheme 2B), followed by hydrolysis of the acetal protecting groups for the sugar-containing polymers (Galactose: **B10**, Mannose: **B11**). Efficient polymer functionalization was verified by ^{1}H NMR experiments (see Fig. S5† for galactose, Fig. S6† for mannose functionalization). Due to the overlapping of the ^{1}H NMR signals in the 2.5 to 4.0 ppm region for the deprotected sugar-functionalized BPEI, compo-

Table 3 Overview of modified poly(ethylene imine)s obtained by varying the glycidol, mannose and galactose contents

Polymer structure	Functional agent	Polymer	Equiv. epoxide[a]
Linear poly(ethylene imine)		**L6**	0.15
		L7	0.30
		L8	0.50
		L9	0.75
		L10	1.20
Branched poly(ethylene imine)	*Glycidol*	**B5**	0.05
		B6	0.15
		B7	0.30
		B8	0.50
		B9	0.75
Branched poly(ethylene imine)		**B10**	0.09
Branched poly(ethylene imine)		**B11**	0.09

[a] Per amine functionality, including primary, secondary and tertiary amine groups.

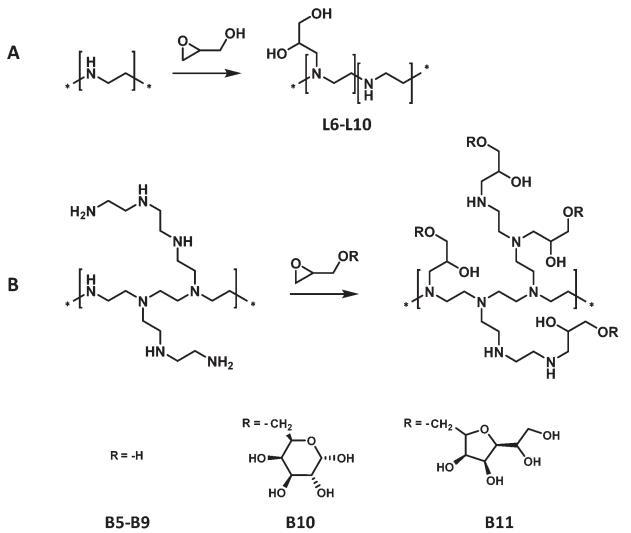

Scheme 2 Schematic representation of the functionalization of (A) linear poly(ethylene imine) with glycidol (**L6** to **L10**) and (B) branched poly(ethylene imine) with glycidol (**B5** to **B9**), galactose (**B10**) and mannose (**B11**) sugar moieties.

sition of these polymers was calculated on dialyzed samples prior to hydrolysis.

Biocompatibility and transfection experiments

As previously mentioned, one of the major disadvantages of PEI is its inherent cytotoxicity. *In vitro* studies were performed on hemiaminal, glycidol and sugar-functionalized PEIs to evaluate their biocompatibility and gene transfection efficiency in a model mammalian cell line HEK293.

The modification of LPEI and BPEI with pF did not allow for any improvement of the toxicity, except when LPEI was modified with higher amounts of pF (see Fig. S8†). Mixing more than 0.5 equiv. pF (*vs.* –NH) with LPEI induced *N*-methylation of the backbone, which is thought to reduce the toxicity of PEI through a decrease of the extent of positive charges per chain.[69] In addition, the hemiaminal moieties proved unstable in acidic pH values, releasing formaldehyde under endosomal conditions.[71] This effect could account for the similar toxicity of pF-modified samples compared to pure PEI (see Fig. S7† for cytotoxicity assays of pF-modified PEI). For this reason, pF-functionalized samples were not used in transfection studies and the biological assessment was focused on epoxide-modified PEI.

The positive charges of glycidol and sugar-functionalized BPEIs were used to condense anionic DNA in order to prepare PEI/DNA nanocomplexes. The size, charge, cytotoxicity and ability to bind as well as transfect a luciferase-reporter gene *in vitro* of the DNA polyplexes of **B6** (0.15 equiv. glycidol), **B9** (0.75 equiv. glycidol), **B10** (0.09 equiv. galactose), and **B11** (0.09 equiv. mannose) were analysed. All polymers were able to bind DNA effectively at N/P 5 and above, where complete retardation of DNA mobility was achieved as demonstrated in gel electrophoresis assays (Fig. S8†). The DNA molecules were fully complexed with **B6**, and retardation of DNA mobility achieved at N/P 1 and above. Increasing the number of glycidol decreased polymer/DNA interaction (**B6** *vs.* **B9**) as the number of primary amine groups, which were responsible for DNA binding, was reduced. **B6** had higher DNA binding ability than unmodified BPEI. Although the number of galactose and mannose attached onto PEI was slightly lower than that of glycidol (**B10** and **B11** *vs.* **B6**), **B6**/DNA interaction was still stronger than **B10** or **B11**/DNA interaction, most probably owing to steric hindrance provided by mannose and galactose moieties.

Nanoparticle sizes below 200 nm are commonly desirable for effective cellular uptake.[72] As depicted in Fig. 3A, the size of the polymer/DNA complexes inversely correlated with N/P ratio, suggesting more compact complexes formed *via* strong electrostatic interaction between functionalized BPEIs and anionic DNA at higher N/P ratios. The size of the complexes dropped from over 200 nm at N/P 10 to 89, 96, 90 and 129 nm at N/P 50 for **B6**, **B9**, **B10** and **B11**, respectively. Moreover, the size distributions of **B6**/DNA, **B9**/DNA, **B10**/DNA and **B11**/DNA complexes were narrow with polydispersity indices (PDI) of 0.10, 0.11, 0.16 and 0.15, respectively. DNA complexes formed with unmodified BPEI at N/P 10 displayed a similar size (~84 nm) and PDI (0.12). These results suggest that except for **B9** the lower charge density of the modified BPEI did not significantly affect its ability to complex DNA as compared to unmodified BPEI.

The surface charge of polymer/DNA complexes plays a key role in determining toxicity and gene transfection efficiency.[73] It has been reported that positively charged particles are prone to undesired interactions with plasma proteins and erythrocytes, a process called opsonization, which triggers a rapid clearance by the reticuloendothelial system (RES), limiting *in vivo* applications.[74] The high positive charge of PEI is also thought to induce side effects such as liver necrosis, and

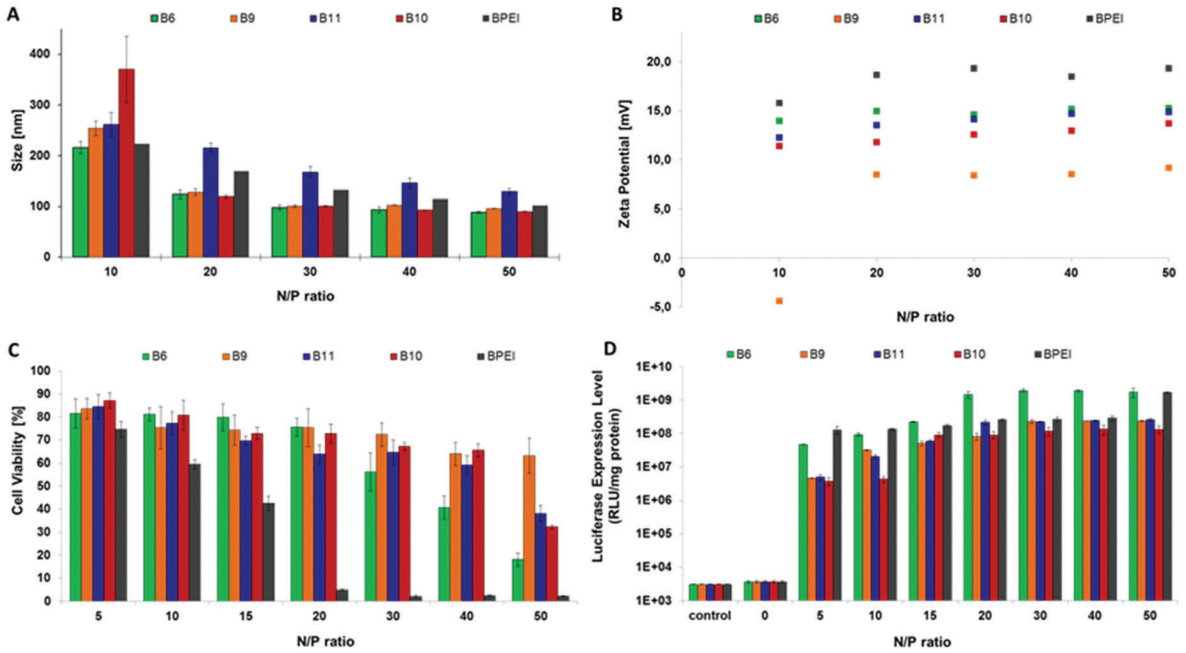

Fig. 3 (A) Particle size and (B) zeta potential of polymer/DNA complexes at various N/P ratios. (C) Viability of HEK293 cells after incubation for 4 h with polymer/DNA complexes at various N/P ratios in comparison to BPEI/DNA complexes. Results represent mean ± standard deviation of 6 replicates. Polymer concentrations in the order of N/P ratios specified: **B6** – 3.1, 6.3, 9.4, 12.5, 18.8, 25.1, and 31.4 mg L^{-1}. **B9** – 3.8, 7.6, 11.4, 15.2, 22.9, 30.5, and 38.1 mg L^{-1}. **B10** – 4.3, 8.7, 13.0, 17.4, 26.0, 34.7, and 43.4 mg L^{-1}. **B11** – 4.3, 8.5, 12.8, 17.0, 25.5, 34.0, and 42.5 mg L^{-1}. BPEI – 2.9, 5.7, 8.6, 11.5, 17.2, 22.9, and 28.6 mg L^{-1}. (D) *In vitro* luciferase expression levels in HEK293 cells, mediated by polymers at various N/P ratios. Results represent mean ± standard deviation of triplicates. Polymer concentrations in the order of N/P ratios specified: **B6** – 0, 3.1, 6.3, 9.4, 12.5, 18.8, 25.1, and 31.4 mg L^{-1}. **B9** – 0, 3.8, 7.6, 11.4, 15.2, 22.9, 30.5, and 38.1 mg L^{-1}. **B10** – 0, 4.3, 8.7, 13.0, 17.4, 26.0, 34.7, and 43.4 mg L^{-1}. **B11** – 0, 4.3, 8.5, 12.8, 17.0, 25.5, 34.0, and 42.5 mg L^{-1}. BPEI – 0, 2.9, 5.7, 8.6, 11.5, 17.2, 22.9, and 28.6 mg L^{-1}.

shock after systemic injection of high doses.[17,74] Therefore, a reduction of the zeta potential of PEI/DNA complexes would be beneficial for gene delivery applications. **B6**, **B10**, and **B11**/DNA complexes exhibited reduced cationic charge density on the surface at N/P 10 to 50 as compared to BPEI/DNA complexes at N/P 10 (Zeta potential: ~11 to 15 mV for **B6**, **B10** and **B11**/DNA complexes and ~16 mV for BPEI/DNA complexes, Fig. 3A). **B9**/DNA complexes presented a significantly lower cationic charge density on the surface than other complexes at N/P 10 to 50 (zeta potential: ~−4 to 9 mV). Indeed, a higher degree of functionalization provided more hydroxyl groups effectively shielding the surface charge of the polymer/DNA nanocomplexes, as well as, lowered the amount of cationic charges owing to the pK_a decrease of amines with substitution.

The cytotoxicity of modified BPEI/DNA and control BPEI/DNA complexes was evaluated by MTT assay using HEK293 cells. BPEI is thought to aggregate on cell surfaces and initiate hole formation in the cell membrane, leading to leakage of vital cellular contents and cell death, limiting potential *in vivo* applications.[75] As shown in Fig. 3C, the high cytotoxicity associated with BPEI caused less than 10% cell viability for N/P higher than 20. In a sharp contrast, all the glycidol- and sugar-functionalized PEI/DNA complexes were much less cytotoxic at all N/P ratios tested. For instance, at N/P ratio of 20, more than 75% and 60% cells were viable upon 4 h treatment with glycidol-modified **B6** and **B9**/DNA and sugar-modified **B10** and **B11**/DNA complexes, respectively (*vs.* only 5% viable cells in the BPEI/DNA complexes-treated group). Even at N/P ratio 50, **B10** and **B11**/DNA complexes demonstrated more than 30% cell viability, and more than 63% cells survived upon **B9**/DNA treatment. Therefore, cytotoxicity was efficiently mitigated by the installation of hydroxyl groups on BPEI by ring opening of glycidol- or sugar-functionalized epoxides, owing to both higher substitution degrees of amines and shielding of BPEI positive charges from hydroxyl moieties.

To assess the suitability of these polymers as gene delivery vectors, *in vitro* luciferase gene transfection assays were performed on HEK293 cells. BPEI achieved high gene transfection efficiency of 1.3×10^8 RFU mg^{-1} protein at N/P 10 with cell viability of ~60% (Fig. 3D). Increasing N/P ratio to 20 led to significant cytotoxicity, as evidenced by cell viability <45%. At N/P 30, both **B10** and **B11** achieved high transfection efficiency (1.16×10^8 CFU mg^{-1} protein and 2.2×10^8 CFU mg^{-1} protein, respectively, comparable to that induced by unmodified BPEI), while exhibiting lower cytotoxicity (cell viability was ~65%), in contrast to BPEI/DNA complexes. At N/P 20, **B6** exhibited a 10-time higher luciferase transfection efficiency than unmodified BPEI (1.5×10^9 RFU mg^{-1} protein *vs.* 2.6×10^8 RFU mg^{-1} protein, respectively) and tremendously lower cytotoxicity (~76% cell viability *vs.* 5% for unmodified BPEI). **B9** displayed a lower transfection efficiency than **B6**, evidencing that the incorporation of a higher number of hydroxyl groups led to

lower surface charge (Fig. 3B) and transfection efficiency of polymer/DNA complexes. Overall, owing to the lower cytotoxicity of modified BPEIs, higher N/P ratios could be used, leading, in the case of **B6**, to a 10-fold increase in gene transfection efficiency, as compared to non-functionalized BPEI.

Conclusion

Poly(ethylene imine) (PEI) is one of the most widely used polymeric transfection vectors. Although PEI allows for an extremely high transfection efficiency, its cytotoxicity is still a major issue in the context of biomedical applications. Here, commercially-available poly(ethylene imine) was modified by the attachment of hydroxyl groups through hemiaminal chemistry or *via* ring opening of glycidol or of sugar-containing epoxides. The initial stoichiometry of paraformaldehyde (pF) *vs.* PEI had a tremendous impact on the composition of the product: at low pF concentrations, hemiaminal decorated-PEI was formed, while partially *N*-methylated polymers due to an Eschweiler–Clarke-type rearrangement, and/or crosslinked materials were obtained when using higher amounts of pF. Primary amines present in BPEI were found to readily ring-open glycidol and epoxides modified through a one-step procedure with mannose and galactose, allowing for the easy decoration of PEI with vicinal diols and sugar moieties. Hemiaminal functionalized PEI exhibited limited stability in acidic conditions, leading to toxicity similar to the parent PEI unless *N*-methylation of the backbone was induced. In contrast, attachment of glycidol or sugar groups allowed mitigating toxicity with minimal loss in efficacy, with only 9% amine functionalization in the case of sugars. The most promising candidate for gene delivery applications was obtained by reacting 0.15 equiv. of glycidol with BPEI, which led to a 10-fold increase in luciferase expression level as compared to unmodified BPEI, while maintaining a cell survival higher than 65%.

Experimental

Materials

Paraformaldehyde, *n*-propylamine, dipropylamine, glycidol, epichlorohydrin, 2,3:5,6-di-*O*-isopropylidene-α-D-mannofuranose, 1,2:3,4-di-*O*-isopropylidene-α-D-galactopyra-nose, and sodium hydride were purchased from Sigma Aldrich. d_6-DMSO was obtained from Cambridge Isotope Labs (CIO). LPEI (MW 25 000 g mol^{-1}) was obtained from Polysciences and BPEI (MW 10 000 g mol^{-1}) was purchased from Sigma Aldrich (USA). All reagents were used as received unless otherwise noted.

General methods and instrumentation

Proton (^{1}H) nuclear magnetic resonance (NMR) and carbon (^{13}C) NMR spectra were acquired at room temperature using a Bruker AC 400 MHz or a Bruker AC 300 MHz spectrometer (100 MHz ^{13}C); chemical shifts (δ) are expressed in parts per million relative to TMS. ^{1}H NMR measurements were carried out with an acquisition time of 3.2 s, a pulse repetition time of 2.0 s, a 30° pulse width, 5208 Hz spectral width, and 32k data points.

Model reactions

The model reactions were performed in a 3 mol% solution of *n*-propylamine (20.0 μL) or dipropylamine (20.0 μL) with 0.5 equiv. paraformaldehyde (3.6 mg and 2.2 mg respectively, pF) in d_6-DMSO (0.7 mL) at 90 °C for 2 h. The reaction mixtures were then analyzed by ^{1}H NMR (see Fig. S2†).

pF-Propylamine. 0.5 equiv. formaldehyde, ^{1}H NMR (400 MHz, d_6-DMSO): δ 3.80–2.70 (–N$H_{2\ (precursor)}$, –NH_2–CH_2–NH_2–, pF fragments), 2.48 (–CH_2–NH_2), 2.30 (–CH_2–NH_2), 1.35 (CH_3–CH_2), 0.85 (CH_3–CH_2) ppm.

pF-Dipropylamine. 0.5 equiv. formaldehyde, ^{1}H NMR (400 MHz, d_6-DMSO): δ 3.60–3.10 (CH_2–N*H*–CH_2, pF fragments), 2.95 (–NH_2–CH_2–OH), 2.43 (–CH_2–NHR), 2.38 (CH_2–NR–CH_2OH), 1.38 (CH_3–CH_2), 0.84 (CH_3–CH_2) ppm.

Modification of linear poly(ethylene imine) with formaldehyde (L1 to L5)

Commercial LPEI (1.00 g, 25 kDa, PolySciences) was reacted with varying equivalents of paraformaldehyde (from 0.094 g to 0.742 g, 0.50 to 1.20 equivalents) in deionized water (V_{total} = 30 mL, 3.3 wt%). The reaction mixture was heated to 90 °C in an oil bath. After 15 hours, the water was removed under reduced pressure and the residue dissolved in methanol (*ca.* 10.0 mL). Subsequently, the mixture was precipitated two times into 250 mL ice-cold diethyl ether. The functionalized LPEI was filtered off and washed with 50.0 mL diethyl ether. The residue was dissolved in 10 mL water and freeze-dried (yield: 70 to 85%).

LPEI: ^{1}H NMR (400 MHz, D_2O): δ 3.46–3.28 (NH–CH_2–CH_2), 3.00–2.60 (NH–CH_2), 2.35 (CH_2 EtOx), 0.99 (CH_3 EtOx) ppm; ^{13}C NMR (100 MHz, D_2O): δ 148.5 (*C*O–CH$_2$–CH$_3$), 47.1 (NH–*C*H$_2$–*C*H$_2$), 25.1 (CH_2–CH$_3$), 9.8 (CH$_2$–CH_3) ppm.

L2: 0.3 equiv. formaldehyde, ^{1}H NMR (400 MHz, D_2O): δ 8.32, 7.92, 3.33 (Hem: NR$_2$–CH_2–OH), 2.72 (RN$_{Hem}$–CH_2–CH_2), 2.67, 2.57 (RNH–CH_2–CH_2), 2.32 (CH_2 EtOx), 0.95 (CH_3 EtOx) ppm; ^{13}C NMR (100 MHz, D_2O): δ 75.4 (Hem: NR$_2$–*C*H$_2$–OH), 53.7–52.9 (RNH–*C*H$_2$–*C*H$_2$), 51.7 (RN$_{Hem}$–*C*H$_2$–*C*H$_2$), 47.1–46.6 (RNH–*C*H$_2$–*C*H$_2$), 26.1 (*C*H$_2$–CH$_3$), 9.0 (CH$_2$–*C*H$_3$) ppm.

L4: 0.75 equiv. formaldehyde, ^{1}H NMR (400 MHz, D_2O): δ 4.74, 3.33 (Hem: NR$_2$–CH_2–OH), 2.71 (RN$_{Hem}$–CH_2–CH_2), 2.57 (RNH–CH_2–CH_2), 2.46 (RN(CH$_3$)–CH_2–CH_2), 2.30 (CH_2 EtOx), 2.15, 2.12 (NR$_2$–CH_3), 0.95 (CH_3 EtOx) ppm; ^{13}C NMR (100 MHz, D_2O): δ 75.3 (Hem: NR$_2$–*C*H$_2$–OH), 53.7 (RN(CH$_3$)–*C*H$_2$–*C*H$_2$), 53.2 (RNH–*C*H$_2$–*C*H$_2$), 51.8 (RN$_{Hem}$–*C*H$_2$–*C*H$_2$), 41.6 (NR$_2$–*C*H$_3$), 26.1 (*C*H$_2$–CH$_3$), 9.1 (CH$_2$–*C*H$_3$) ppm.

Modification of branched poly(ethylene imine) with formaldehyde (B1 to B4)

The formaldehyde functionalization of commercial BPEI was performed analog to LPEI functionalization. Therefore, BPEI (1.50 g, 10 kDa, Sigma Aldrich) was reacted with varying

equivalents of paraformaldehyde (from 0.570 g to 0.843 g, 0.05 to 0.50 equiv.) in deionized water (V_{total} = 30 mL, 5 wt%). The reaction mixture was heated to 90 °C in an oil bath. After 15 hours, the water was removed under reduced pressure and the residue dissolved in methanol (*ca.* 10 mL). Subsequently, the mixture was precipitated two times into 250 mL ice-cold diethyl ether. The functionalized BPEI was filtered off and washed with 50 mL diethyl ether. The residue was dissolved in 10 mL warm water and freeze-dried. For higher functionalization degrees, gelation occurred. For these samples, the swollen gel was washed with 50 mL water, and, subsequently, freeze-dried (yield: 75 to 90%).

BPEI: ^{1}H NMR (400 MHz, MeOD): δ 2.81–2.54 (BPEI backbone) ppm, ^{13}C NMR (100 MHz, MeOD): δ 56.1, 53.1, 51.0, 50.7, 47.6, 45.5, 39.8, 37.7 (BPEI backbone) ppm.

B2: 0.15 equiv. formaldehyde, ^{1}H NMR (400 MHz, MeOD): δ 3.41–3.27 (NR_2–CH_2–OH, NR_2–CH_2–NR_2), 2.84, 2.70 (RN_{Hem}–CH_2–CH_2), 2.80–2.30 (BPEI backbone) ppm; ^{13}C NMR (100 MHz, MeOD): δ 76.2 (NR_2–*C*H_2–NR_2), 69.5 (NR_2–*C*H_2–OH), 51.8 (NR_2–*C*H_2–CH_2, RN_{Hem}–*C*H_2–*C*H_2), 43.8 (NR_2–*C*H_2–CH_2, RN_{Hem}–*C*H_2–*C*H_2), 56.0, 53.0, 51.1, 48.1, 46.9, 40.2, 38.92 (BPEI backbone) ppm.

B4: 0.5 equiv. formaldehyde, ^{1}H NMR (400 MHz, MeOD): δ 3.77–3.39 (NR_2–CH_2–OH; NR_2–CH_2–NR_2), 3.10–2.90 (RN_{Hem}–CH_2–CH_2), 2.86–2.63 (BPEI backbone), 2.59 (RN(CH_3)–CH_2–CH_2), 2.35 (NR_2–CH_3), 1.33 ppm; ^{13}C NMR (100 MHz, MeOD): δ 76.1 (NR_2–*C*H_2–NR_2), 69.4 (NR_2–*C*H_2–OH), 55.6 (RN(CH_3)–*C*H_2–*C*H_2), 51.7 (NR_2–*C*H_2–CH_2, RN_{Hem}–*C*H_2–*C*H_2), 44.2 (NR_2–*C*H_3), 43.6 (NR_2–*C*H_2–CH_2, RN_{Hem}–*C*H_2–*C*H_2), 55.4, 52.7, 52.2, 51.7, 46.3 (BPEI backbone) ppm.

Modification of linear poly(ethylene imine) with glycidol (L6 to L10)

Commercial LPEI (1.0 g, 25k Da, PolySciences) was reacted with varying equivalents of glycidol (from 240 μL to 1.89 mL) in methanol (V_{total} = 20.0 mL, 5 wt%) according to literature.[43] The reaction mixture was stirred at room temperature for 20 hours. Subsequently, the mixture was concentrated under reduced pressure (to 10.0 mL) and precipitated two times into 250 mL of ice-cold diethyl ether. The functionalized LPEI was filtered off and washed with 50.0 mL diethyl ether. The residue was dissolved in 10 mL water and freeze-dried (yield: 80–90%).

LPEI: ^{1}H NMR (400 MHz, MeOD): δ 3.57–3.40, 2.97–2.71 (NH–CH_2–CH_2), 2.48 (CH_2 EtOx), 1.15 (CH_3 EtOx) ppm; ^{13}C NMR (100 MHz, MeOD): δ 48.2, 46.8 (NH–*C*H_2–*C*H_2), 25.7 (*C*H_2–CH_3), 8.7 (CH_2–*C*H_3) ppm.

L8: 0.5 equiv. glycidol, ^{1}H NMR (400 MHz, MeOD): δ 3.97–3.71 (RCH_2–C*H*OH–CH_2–OH), 3.64–3.42 (RCH_2–CHOH–CH_2–OH), 2.96–2.65 (RNH–CH_2–CH_2), 2.65–2.50 (RNGly–CH_2–CH_2), 2.47 (CH_2 EtOx), 1.15 (CH_3 EtOx) ppm; ^{13}C NMR (100 MHz, MeOD): δ 73.8, 72.6 (RCH_2–CHOH–*C*H_2–OH), 70.9, 69.9 (CH_2–*C*HOH–CH_2), 64.4, 63.0 (RCH_2–CHOH–CH_2–OH), 57.4, 53.9, 52.7 (RNGly–*C*H_2–*C*H_2), 48.5–46.3 (RNH–*C*H_2–*C*H_2), 25.8 (*C*H_2–CH_3), 8.8 (CH_2–*C*H_3) ppm.

Modification of branched poly(ethylene imine) with glycidol (B5 to B9)

The glycidol functionalization of commercial BPEI was performed analog to LPEI functionalization. Therefore, BPEI (1.00 g, 10 kDa, Sigma Aldrich) was reacted with varying equivalents of glycidol (from 90.0 μL to 1.25 mL) in methanol (V_{total} = 20.0 mL, 5 wt%) according to literature.[43] The reaction mixture was stirred at room temperature for 20 hours. Subsequently, the mixture was concentrated under reduced pressure (to 10 mL) and precipitated two times into 250 mL ice-cold diethyl ether. The functionalized BPEI was filtered off and washed with 50 mL diethyl ether. The residue was dissolved in 10.0 mL water and freeze-dried (yield: 70–90%).

BPEI: ^{1}H NMR (400 MHz, MeOD): δ 2.81–2.54 (BPEI backbone) ppm, ^{13}C NMR (100 MHz, D_2O): δ 56.1, 53.1, 51.0, 50.7, 47.6, 45.5, 39.8, 37.7 (BPEI backbone) ppm.

B7: 0.3 equiv. glycidol, ^{1}H NMR (400 MHz, MeOD): δ 3.96–3.70 (CH_2–C*H*OH–CH_2–OH), 3.63–3.44 (RCH_2–CHOH–CH_2–OH), 2.88–2.44 (BPEI backbone, RNGly–CH_2–CH_2) ppm; ^{13}C NMR (100 MHz, MeOD): δ 73.9, 72.6 (RCH_2–CHOH–*C*H_2–OH), 71.4–68.4 (CH_2–*C*HOH–CH_2), 64.6, 63.1 (RCH_2–CHOH–CH_2–OH), 54.7–51.2, 49.1–46.3, 40.5, 38.8 (BPEI backbone, RNGly–CH_2–CH_2) ppm.

Modification of branched poly(ethylene imine) with sugar-functionalized epoxides (B10, B11)

1,2:3,4-Di-*O*-isopropylidene-α-D-galactopyranose glycidyl ether. 6.14 g 1,2:3,4-Di-*O*-isopropylidene-α-D-galactopyranose (23.59 mmol) and 1.88 mL epichlorohydrin (24.1 mmol, 1.02 equiv.) were dissolved in 60 mL dry THF in a 250 mL round bottom flask. 1.13 g NaH (60 wt% dispersion in mineral oil, 28.3 mmol, 1.20 equiv.) was next added at 0 °C. The mixture was stirred at room temperature for 1 h and refluxed overnight. The reaction was cooled down and quenched with excess MeOH and H_2O. The solvent was evaporated and the crude product redissolved in EtOAc (150 mL) and washed with water (100 mL) twice. Purification by column chromatography (silica, 4 : 1 CH_2Cl_2/EtOAc) provided the desired product as a colorless oil (yield: 43%).

^{1}H NMR (400 MHz, $CDCl_3$): δ 5.47 (m, 1H, C$H_{ringGal}$), 4.54 (m, 1H, C$H_{ringGal}$), 4.25 (m, 1H, C$H_{ringGal}$), 4.19 (t, 1H, C$H_{ringGal}$), 3.92 (t, 1H, C$H_{ringGal}$), 3.82–3.32 (m, 4H, –CH_2–O–CH_2–), 3.11 (m, 1H, C$H_{epoxide}$), 2.73 (t, 1H, C$H_{2epoxide}$), 2.55 (m, 1H, C$H_{2epoxide}$), 1.48 (s, 3H, CH_3), 1.38 (s, 3H, CH_3), 1.26 (s, 6H, CH_3) ppm.

isoB10: 1,2:3,4-Di-*O*-isopropylidene-α-D-galactopyranose glycidyl ether (0.30 g, 0.94 mmol, 25 equiv.) and BPEI (0.38 g, 10 kDa, Sigma Aldrich) were stirred in MeOH (3 mL) at room temperature for three days. A 0.2 mL aliquot was dialyzed *vs.* MeOH for quantification of the attached amount of sugar (three MeOH changes, MWCO: 1000 g mol^{-1}) by ^{1}H NMR (see Fig. S5,† 20 galactose moieties attached). To the rest of the reaction mixture were added 9 mL H_2O, 7 mL MeOH and 1 mL 37% HCl (final HCl concentration: 0.5 M). Hydrolysis of the isopropylidene groups was carried out for 2 h at reflux. The

reaction mixture was cooled down to room temperature and dialyzed *vs.* H_2O (three H_2O changes, MWCO: 1000 g mol^{-1}) and finally lyophilized (see Fig. S5† for ^1H NMR spectrum attesting of the full hydrolysis).

^1H NMR (400 MHz, $CDCl_3$): δ 5.60–3.35 (isoGalBPEI), 3.35–2.10 (isoGalBPEI), 1.60–1.29 (isoGalBPEI) ppm.

2,3:5,6-Di-*O*-isopropylidene-α-D-mannofuranose glycidyl ether. 2,3:5,6-Di-*O*-isopropylidene-α-D-mannofuranose glycidyl ether was prepared using a similar procedure.

^1H NMR (400 MHz, $CDCl_3$): δ 5.05 (d, 1H, CH_{Man}), 4.81 (t, 1H, CH_{Man}), 4.66 (t, 1H, CH_{Man}), 4.42 (m, 1H, CH_{Man}), 4.13 (m, 1H, CH_{Man}), 4.06 (m, 1H, CH_{Man}), 3.99 (m, 1H, CH_{Man}), 3.88–3.37 (m, 2H, $-CH_2-O-$), 3.16 (br, 1H, $CH_{epoxide}$), 2.83 (t, 1H, $CH_{2epoxide}$), 2.65–2.60 (m, 1H, $CH_{2epoxide}$), 1.47 (s, 3H, CH_3), 1.40 (s, 3H, CH_3), 1.34 (s, 6H, CH_3) ppm.

isoB11: Mannose-functionalized BPEI was prepared using a similar procedure (see Fig. S6† for ^1H NMR spectrum attesting of the full hydrolysis).

0.09 equiv. mannose, ^1H NMR (400 MHz, $CDCl_3$): δ 5.06–3.31 (isoManBPEI), 3.26–2.12 (isoManBPEI), 1.55–1.21 (isoManBPEI) ppm.

Preparation and characterization of polymer/DNA complexes

The polymer was dissolved in DNase/RNase-free water (Fermentas, Singapore). Subsequently, an equivolume solution of DNA (pCMV-luciferase, Carl Wheeler, Vival, San Diego, CA, USA) was dripped into the polymer solution to achieve the intended N/P ratios (molar ratio of nitrogen content in the polymer to the phosphorus content of the nucleic acids) under gentle vortexing for about 5 s. The resulting mixture solution was equilibrated for 30 min at room temperature to allow complete electrostatic interaction between the polymer and DNA.

The particle sizes and zeta potentials of the polymer/DNA complexes were measured by Zetasizer (Malvern Instrument Ltd, Worcestershire, UK). Immediately prior to the measurement, the polymer/DNA complexes were diluted 10 times in PBS to mimic the dilution in the physiological environment after i.v. administration. Particle size and zeta potential measurements were repeated for three runs per sample and reported as the mean ± standard deviation of three readings.

Gel retardation assay

Polymer/DNA complexes were prepared as described above with N/P ratios ranging from 1 to 50. 20 μL of the post equilibrated complexes were used for electroporation on ethidium bromide stained 1% agarose gel in 1× TBE buffer (Biopolis Shared Facilities, A*STAR, Singapore) at 110 V for 50 min. The gel was then viewed under a UV illuminator (Chemi Genius, Evolve, Singapore), and the N/P ratio where complete binding and retardation of the free DNA plasmid occurred were noted.

Cell culture

HEK293 cells (ATCC, USA) were cultured in Dulbecco's Modified Eagle Medium (DMEM, Invitrogen, Singapore). The media were supplemented with 10% (v/v) fetal bovine serum (FBS, Invitrogen, Singapore), streptomycin at 100 μg mL^{-1}, penicillin at 100 U mL^{-1}, L-glutamine at 2 mM, and 1 mM sodium pyruvate (Sigma-Aldrich, Singapore). Cells were cultured at 37 °C, under an atmosphere of 5% CO_2 and 95% humidified air. Cells were split using Trypsin/EDTA medium (Invitrogen, Singapore) when reached 90% confluence.

In vitro gene transfection efficiency

The *in vitro* gene transfection efficiency of the polymer/DNA complexes was investigated using HEK293 cells. Cells were seeded onto 24-well plates (Nunc, Thermo Fisher Scientific, Singapore) at a density of 1×10^5 cells per 500 μL per well for luciferase gene delivery. After 24 h, the plating media were replaced with fresh growth media, followed by the drop-wise addition of 50 μL of complex solution (containing 2.5 μg luciferase plasmid DNA) at various N/P ratios. Following 4 h of incubation, free complexes were removed by replacing the medium in each well with fresh medium. After a further 68 h of incubation, the cell culture medium in each well was removed and the cells were rinsed once with 0.5 mL of phosphate-buffered saline (PBS, pH 7.4). Reporter lysis buffer (0.2 mL) was added to each well. The cell lysate collected after two cycles of freezing (−80 °C, 30 min) and thawing (room temperature, 30 min) was cleared by centrifugation at 14 000 rpm for 5 min. After that, 20 μL of supernatant was mixed with 100 μL of luciferase substrate for the determination of relative light units (RLU) using a luminometer (Lumat LB9507, Berthold, Germany). The RLU readings were normalized against the protein concentration of the supernatant determined using the Pierce™ BCA Protein Assay Kit (Thermo Fisher Scientific, Singapore) to give the overall luciferase expression efficiency. In all *in vitro* gene expression experiments, naked DNA was used as a negative control. Data were expressed as mean ± standard deviations of three replicates.

Cell viability

The cytotoxicity of the polymer/DNA complexes was studied using the standard MTT assay protocol. Briefly, HEK293 cells were seeded onto 96-well plates at a density of 10 000 cells per well, and allowed to grow to 60 to 70% confluence before treatment. After 24 h, the medium was replaced with fresh medium. The cells in each well were subsequently incubated with growth medium comprising of 10 μL of polymer/DNA complexes and 100 μL of fresh medium for 4 h at 37 °C. Following incubation, the medium was replaced with fresh growth medium and incubated further for 68 h. Subsequently, 100 μL of growth medium and 20 μL of MTT solution (5 mg mL^{-1} in PBS, Merck, Singapore) were added to each well and the cells were incubated for 4 h at 37 °C. Formazan crystals formed in each well were solubilized using 150 μL of DMSO upon removal of growth media. A 100 μL aliquot from each well was then transferred to a new 96-well plate for determination of absorbance using a microplate spectrophotometer at wavelengths of 550 nm and 690 nm. Relative cell viability was expressed as $[(A_{550} - A_{690})_{sample}/(A_{550} - A_{690})_{control}] \times 100\%$. Data were expressed as mean ± standard deviations of eight replicates per N/P ratio.

Acknowledgements

This work was supported by the Institute of Bioengineering and Nanotechnology (Biomedical Research Council, Agency for Science, Technology and Research, Singapore), and IBM Almaden Research Center, USA. C. E. is grateful to the Deutscher Akademischer Austauschdienst (DAAD) for financial support. Furthermore, the funding of the collaborative research center ChemBioSys (SFB 1127) by the Deutsche Forschungsgemeinschaft (DFG) is highly acknowledged.

References

1 J. A. Broderick and P. D. Zamore, *Gene Ther.*, 2011, **18**, 1104–1110.
2 W. Walther and U. Stein, *Drugs*, 2000, **60**, 249–271.
3 R. Gardlík, R. Pálffy, J. Hodosy, J. Lukács, J. Turna and P. Celec, *Med. Sci. Monit. Basic Res.*, 2005, **11**, RA110–RA121.
4 C. R. Dass, *Int. J. Pharm.*, 2002, **241**, 1–25.
5 J.-L. Merlin, A. N'Doye, T. Bouriez and G. Dolivet, *Drug News Perspect.*, 2002, **15**, 445.
6 R. I. Mahato, *J. Drug Targeting*, 1999, **7**, 249–268.
7 J. Soutschek, A. Akinc, B. Bramlage, K. Charisse, R. Constien, M. Donoghue, S. Elbashir, A. Geick, P. Hadwiger, J. Harborth, M. John, V. Kesavan, G. Lavine, R. K. Pandey, T. Racie, K. G. Rajeev, I. Rohl, I. Toudjarska, G. Wang, S. Wuschko, D. Bumcrot, V. Koteliansky, S. Limmer, M. Manoharan and H.-P. Vornlocher, *Nature*, 2004, **432**, 173–178.
8 M. Mäe, S. E. Andaloussi, T. Lehto and Ü. Langel, *Expert Opin. Drug Delivery*, 2009, **6**, 1195–1205.
9 M. A. Mintzer and E. E. Simanek, *Chem. Rev.*, 2009, **109**, 259–302.
10 O. Boussif, F. Lezoualc'h, M. A. Zanta, M. D. Mergny, D. Scherman, B. Demeneix and J.-P. Behr, *Proc. Natl. Acad. Sci. U. S. A.*, 1995, **92**, 7297–7301.
11 W. T. Godbey, M. A. Barry, P. Saggau, K. K. Wu and A. G. Mikos, *J. Biomed. Mater. Res.*, 2000, **51**, 321–328.
12 W. T. Godbey, K. K. Wu and A. G. Mikos, *J. Controlled Release*, 1999, **60**, 149–160.
13 M. Jaeger, S. Schubert, S. Ochrimenko, D. Fischer and U. S. Schubert, *Chem. Soc. Rev.*, 2012, **41**, 4755–4767.
14 D. D. Dunlap, A. Maggi, M. R. Soria and L. Monaco, *Nucleic Acids Res.*, 1997, **25**, 3095–3101.
15 T. Reschel, Č. Koňák, D. Oupický, L. W. Seymour and K. Ulbrich, *J. Controlled Release*, 2002, **81**, 201–217.
16 J. W. Wiseman, C. A. Goddard, D. McLelland and W. H. Colledge, *Gene Ther.*, 2003, **10**, 1654–1662.
17 P. Chollet, M. C. Favrot, A. Hurbin and J.-L. Coll, *J. Gene Med.*, 2002, **4**, 84–91.
18 M. Neu, D. Fischer and T. Kissel, *J. Gene Med.*, 2005, **7**, 992–1009.
19 M.-E. Bonnet, P. Erbacher and A.-L. Bolcato-Bellemin, *Pharm. Res.*, 2008, **25**, 2972–2982.
20 B. D. Goula, S. Mantero, G. Merlo, G. Levi and B. A. Demeneix, *Gene Ther.*, 1998, **5**, 1291–1295.
21 L. Wightman, R. Kircheis, V. Rössler, S. Carotta, R. Ruzicka, M. Kursa and E. Wagner, *J. Gene Med.*, 2001, **3**, 362–372.
22 P. Zhang, N. Xu, L. Zhou, X. Xu, Y. Wang, K. Li, Z. Zeng, X. Wang, X. Zhang and C. Bai, *Transl. Respir. Med.*, 2013, **1**, 1–11.
23 S.-M. Zou, P. Erbacher, J.-S. Remy and J.-P. Behr, *J. Gene Med.*, 2000, **2**, 128–134.
24 J. H. Jeong, S. H. Song, D. W. Lim, H. Lee and T. G. Park, *J. Controlled Release*, 2001, **73**, 391–399.
25 H. M. L. Lambermont-Thijs, F. S. van der Woerdt, A. Baumgaertel, L. Bonami, F. E. Du Prez, U. S. Schubert and R. Hoogenboom, *Macromolecules*, 2010, **43**, 927–933.
26 L. Tauhardt, K. Kempe, K. Knop, E. Altuntaş, M. Jaeger, S. Schubert, D. Fischer and U. S. Schubert, *Macromol. Chem. Phys.*, 2011, **212**, 1918–1924.
27 T. Saegusa, H. Ikeda and H. Fujii, *Macromolecules*, 1972, **5**, 108–108.
28 T. Saegusa, S. Kobayashi and A. Yamada, *Macromolecules*, 1975, **8**, 390–396.
29 G. D. Jones, A. Langsjoen, S. M. M. C. Neumann and J. Zomlefer, *J. Org. Chem.*, 1944, **9**, 125–147.
30 C.-H. Ahn, S. Y. Chae, Y. H. Bae and S. W. Kim, *J. Controlled Release*, 2002, **80**, 273–282.
31 M. L. Forrest, J. T. Koerber and D. W. Pack, *Bioconjugate Chem.*, 2003, **14**, 934–940.
32 M. Thomas, Q. Ge, J. J. Lu, J. Chen and A. Klibanov, *Pharm. Res.*, 2005, **22**, 373–380.
33 W. Y. Seow, K. Liang, M. Kurisawa and C. A. E. Hauser, *Biomacromolecules*, 2013, **14**, 2340–2346.
34 C. Englert, M. Hartlieb, P. Bellstedt, K. Kempe, C. Yang, S. K. Chu, X. Ke, J. M. García, R. J. Ono, M. Fevre, R. J. Wojtecki, U. S. Schubert, Y. Y. Yang and J. L. Hedrick, *Macromolecules*, 2015, **48**, 7420–7427.
35 A. C. Rinkenauer, L. Tauhardt, F. Wendler, K. Kempe, M. Gottschaldt, A. Traeger and U. S. Schubert, *Macromol. Biosci.*, 2015, **15**, 414–425.
36 S. Taranejoo, J. Liu, P. Verma and K. Hourigan, *J. Appl. Polym. Sci.*, 2015, **132**, 42096.
37 R. Tanaka, M. Koike, T. Tsutsui and T. Tanaka, *J. Polymer Sci., Polym. Lett. Ed.*, 1978, **16**, 13–19.
38 R. Tanaka, I. Ueoka, Y. Takaki, K. Kataoka and S. Saito, *Macromolecules*, 1983, **16**, 849–853.
39 G. Nöding and W. Heitz, *Macromol. Chem. Phys.*, 1998, **199**, 1637–1644.
40 S.-J. Sung, S. H. Min, K. Y. Cho, S. Lee, Y.-J. Min, Y. I. Yeom and J.-K. Park, *Biol. Pharm. Bull.*, 2003, **26**, 492–500.
41 A. Schroeder, J. E. Dahlman, G. Sahay, K. T. Love, S. Jiang, A. A. Eltoukhy, C. G. Levins, Y. Wang and D. G. Anderson, *J. Controlled Release*, 2012, **160**, 172–176.
42 C. Yang, W. Cheng, P. Y. Teo, A. C. Engler, D. J. Coady, J. L. Hedrick and Y. Y. Yang, *Adv. Healthcare Mater.*, 2013, **2**, 1304–1308.

43 S. Wen, F. Zheng, M. Shen and X. Shi, *J. Appl. Polym. Sci.*, 2012, **128**, 3807–3813.
44 M. Krämer, J.-F. Stumbé, G. Grimm, B. Kaufmann, U. Krüger, M. Weber and R. Haag, *ChemBioChem*, 2004, **5**, 1081–1087.
45 H. Petersen, P. M. Fechner, D. Fischer and T. Kissel, *Macromolecules*, 2002, **35**, 6867–6874.
46 K. Kunath, T. Merdan, O. Hegener, H. Häberlein and T. Kissel, *J. Gene Med.*, 2003, **5**, 588–599.
47 C. Englert, L. Tauhardt, M. Hartlieb, K. Kempe, M. Gottschaldt and U. S. Schubert, *Biomacromolecules*, 2014, **15**, 1124–1131.
48 A. Zintchenko, A. Philipp, A. Dehshahri and E. Wagner, *Bioconjugate Chem.*, 2008, **19**, 1448–1455.
49 P.-H. Yeh, J.-S. Sun, H.-C. Wu, L.-H. Hwang and T.-W. Wang, *RSC Adv.*, 2013, **3**, 12922–12932.
50 M. Thomas and A. M. Klibanov, *Proc. Natl. Acad. Sci. U. S. A.*, 2002, **99**, 14640–14645.
51 P. Y. Teo, C. Yang, J. L. Hedrick, A. C. Engler, D. J. Coady, S. Ghaem-Maghami, A. J. T. George and Y. Y. Yang, *Biomaterials*, 2013, **34**, 7971–7979.
52 W. Cheng, C. Yang, J. L. Hedrick, D. F. Williams, Y. Y. Yang and P. G. Ashton-Rickardt, *Biomaterials*, 2013, **34**, 3697–3705.
53 D. Gutsch, D. Appelhans, S. Höbel, B. Voit and A. Aigner, *Mol. Pharmaceutics*, 2013, **10**, 4666–4675.
54 K. Wong, G. Sun, X. Zhang, H. Dai, Y. Liu, C. He and K. W. Leong, *Bioconjugate Chem.*, 2006, **17**, 152–158.
55 K. Kunath, A. von Harpe, D. Fischer and T. Kissel, *J. Controlled Release*, 2003, **88**, 159–172.
56 S. S. Diebold, M. Kursa, E. Wagner, M. Cotten and M. Zenke, *J. Biol. Chem.*, 1999, **274**, 19087–19094.
57 M. Borkovec and G. J. M. Koper, *Macromolecules*, 1997, **30**, 2151–2158.
58 A. von Harpe, H. Petersen, Y. Li and T. Kissel, *J. Controlled Release*, 2000, **69**, 309–322.
59 J. Suh, H. J. Paik and B. K. Hwang, *Bioorg. Chem.*, 1994, **22**, 318–327.
60 J.-P. Behr, *Chimia*, 1997, **51**, 34–36.
61 A. Akinc, M. Thomas, A. M. Klibanov and R. Langer, *J. Gene Med.*, 2005, **7**, 657–663.
62 R. V. Benjaminsen, M. A. Mattebjerg, J. R. Henriksen, S. M. Moghimi and T. L. Andresen, *Mol. Ther.*, 2013, **21**, 149–157.
63 G. O. Jones, J. M. García, H. W. Horn and J. L. Hedrick, *Org. Lett.*, 2014, **16**, 5502–5505.
64 C. H. Fox, G. M. ter Hurrne, R. J. Wojtecki, G. O. Jones, H. W. Horn, E. W. Meijer, C. W. Frank, J. L. Hedrick and J. M. Garcia, *Nat. Commun.*, 2015, **6**, 7417.
65 M. Fevre, G. O. Jones, M. Zhang, J. M. García and J. L. Hedrick, *Adv. Mater.*, 2015, **27**, 4714–4718.
66 K. Siimer, P. Christjanson, T. Kaljuvee, T. Pehk, I. Lasn and I. Saks, *J. Therm. Anal. Calorim.*, 2008, **92**, 19–27.
67 L. M. Zhou, Q. Xu and D. N. Wang, *J. Appl. Polym. Sci.*, 2006, **100**, 2832–2837.
68 N. Matubayasi and M. Nakahara, *J. Chem. Phys.*, 2005, **122**, 074509.
69 M. Breunig, U. Lungwitz, J. Klar, A. Kurtz, T. Blunk and A. Goepferich, *J. Nanosci. Nanotechnol.*, 2004, **4**, 512–520.
70 F. Suriano, R. Pratt, J. P. K. Tan, N. Wiradharma, A. Nelson, Y. Y. Yang, P. Dubois and J. L. Hedrick, *Biomaterials*, 2010, **31**, 2637–2645.
71 J. M. García, G. O. Jones, K. Virwani, B. D. McCloskey, D. J. Boday, G. M. ter Huurne, H. W. Horn, D. J. Coady, A. M. Bintaleb, A. M. S. Alabdulrahman, F. Alsewailem, H. A. A. Almegren and J. L. Hedrick, *Science*, 2014, **344**, 732–735.
72 F. Jacobs, E. Wisse and B. De Geest, *Am. J. Pathol.*, 2010, **176**, 14–21.
73 Z. Y. Ong, K. Fukushima, D. J. Coady, Y. Y. Yang, P. L. R. Ee and J. L. Hedrick, *J. Controlled Release*, 2011, **152**, 120–126.
74 M. Ogris, S. Brunner, S. Schüller, R. Kircheis and E. Wagner, *Gene Ther.*, 1999, **6**, 595–605.
75 S. Hong, P. R. Leroueil, E. K. Janus, J. L. Peters, M.-M. Kober, M. T. Islam, B. G. Orr, J. R. Baker and M. M. Banaszak Holl, *Bioconjugate Chem.*, 2006, **17**, 728–734.

SUPPORTING INFORMATION

Facile Carbohydrate-Mimetic Modifications of Poly(ethylene imine) Carriers for Gene Delivery Applications

Christoph Englert,[a,b,c] Mareva Fevre,[a] Rudy J. Wojtecki,[a] Wei Cheng,[d] Qingxing Xu,[d] Chuan Yang,[d] Xiyu Ke,[d] Matthias Hartlieb,[b,c,#] Kristian Kempe,[b,c,#] Jeannette M. García,[a] Robert J. Ono,[a] Ulrich S. Schubert,[b,c,] Yi Yan Yang,[d,]* James L. Hedrick[a,]**

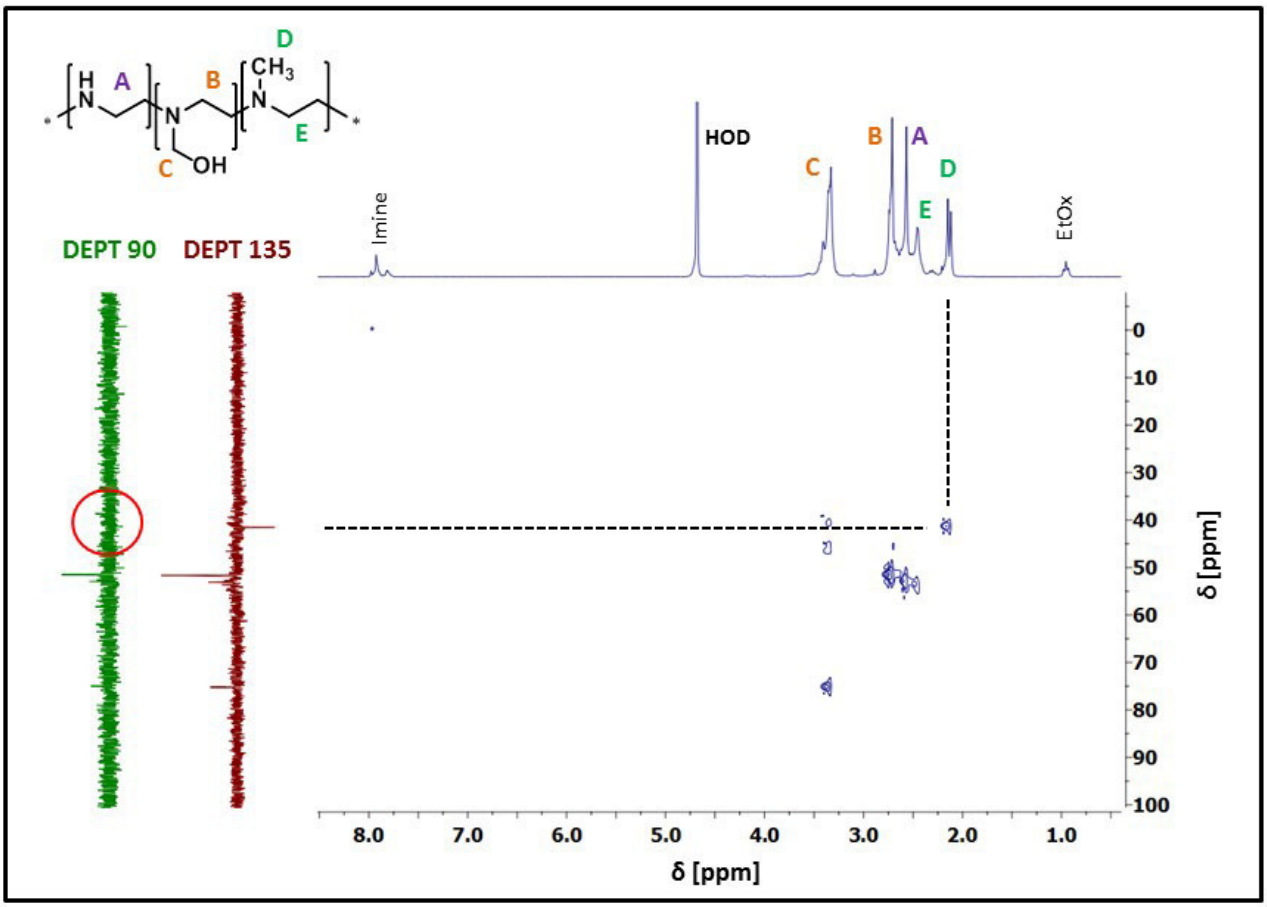

Figure S1. HSQC-DEPT-NMR spectra of **L4** (0.75 equiv. formaldehyde). The appearance of a negative signal in the DEPT 135 experiment that disappears in DEPT 90 indicated the presence of a N-CH_3 group and, therefore, the methylation of LPEI (D_2O, 400 MHz).

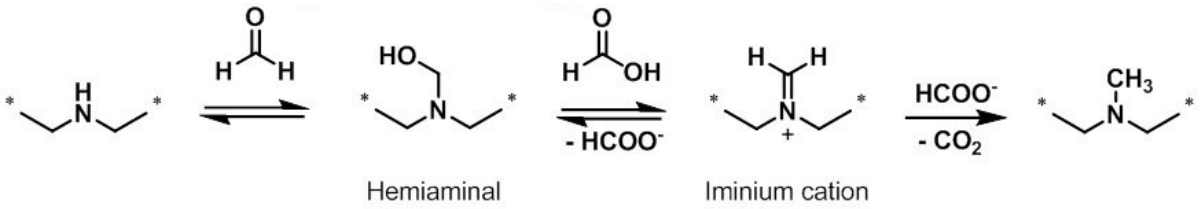

Scheme S1. Mechanism for Eschweiler-Clarke rearrangement leading to the methylation of secondary amines.[37,69]

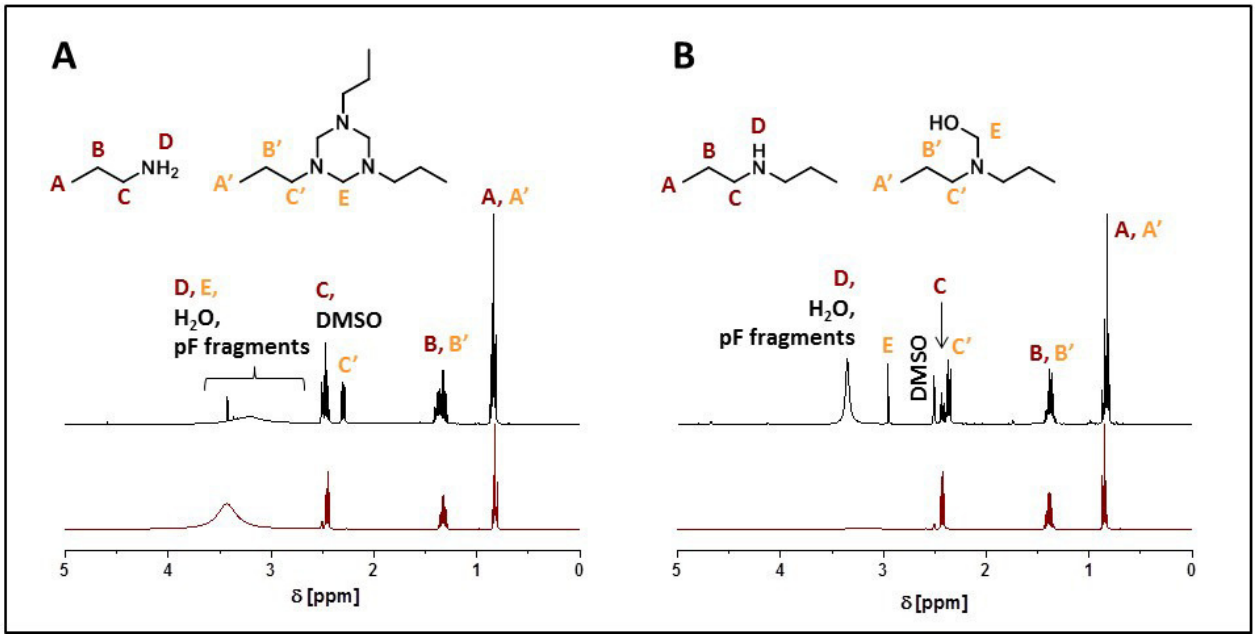

Figure S2. ^{1}H NMR spectra (d_6-DMSO, 400 MHz) of the reaction mixture of A) *n*-propylamine and 0.5 equiv. paraformaldehyde in d_6-DMSO (0.7 mL) after stirring at 90 °C for 2 h, and, B) dipropylamine and 0.5 equiv. paraformaldehyde in d_6-DMSO (0.7 mL) after stirring at 90 °C for 2 h.

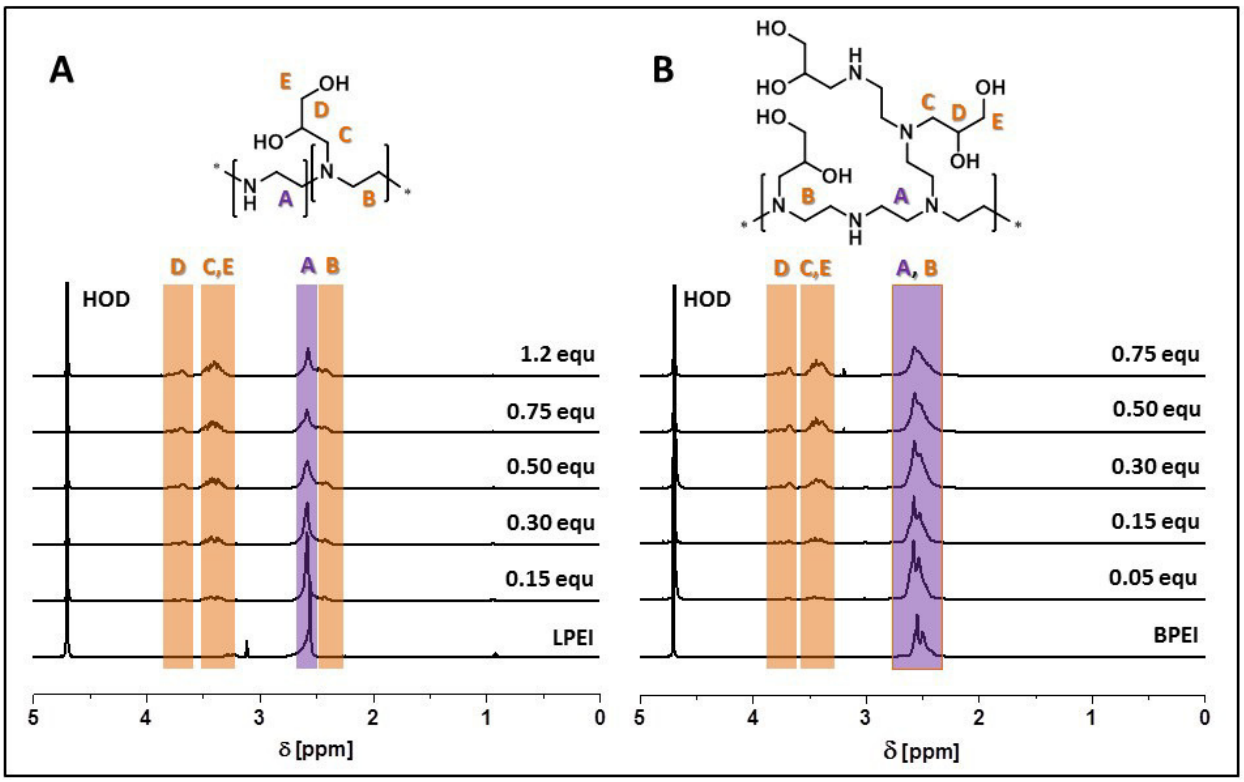

Figure S3. ^{1}H NMR spectra of (A) linear (**L6-L10**) and (B) branched PEI, modified with varying contents of glycidol (**B5-B9**) (D_2O, 400 MHz).

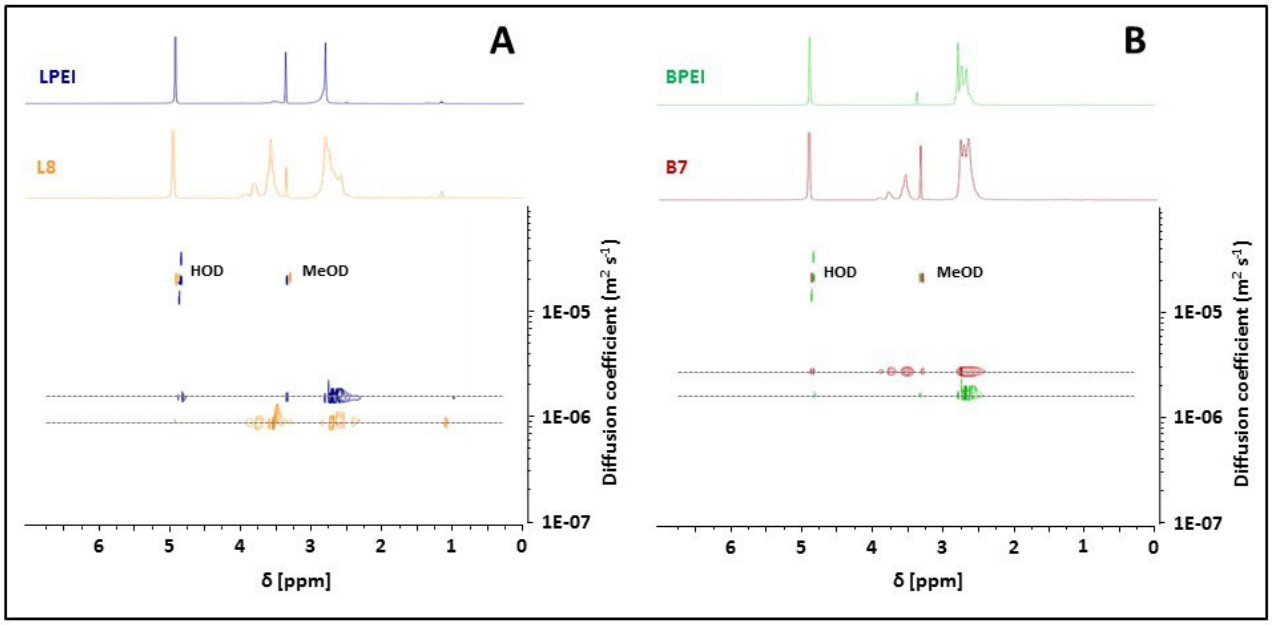

Figure S4. Diffusion ordered NMR spectra (MeOD, 400 MHz, 25 °C) of (A) LPEI and corresponding glycidol-functionalized **L8** (0.5 equiv. glycidol *vs.* -NH), and, (B) BPEI and corresponding glycidol-functionalized species **B7** (0.3 equiv. glycidol per amine functionality, including primary, secondary and tertiary amine groups).

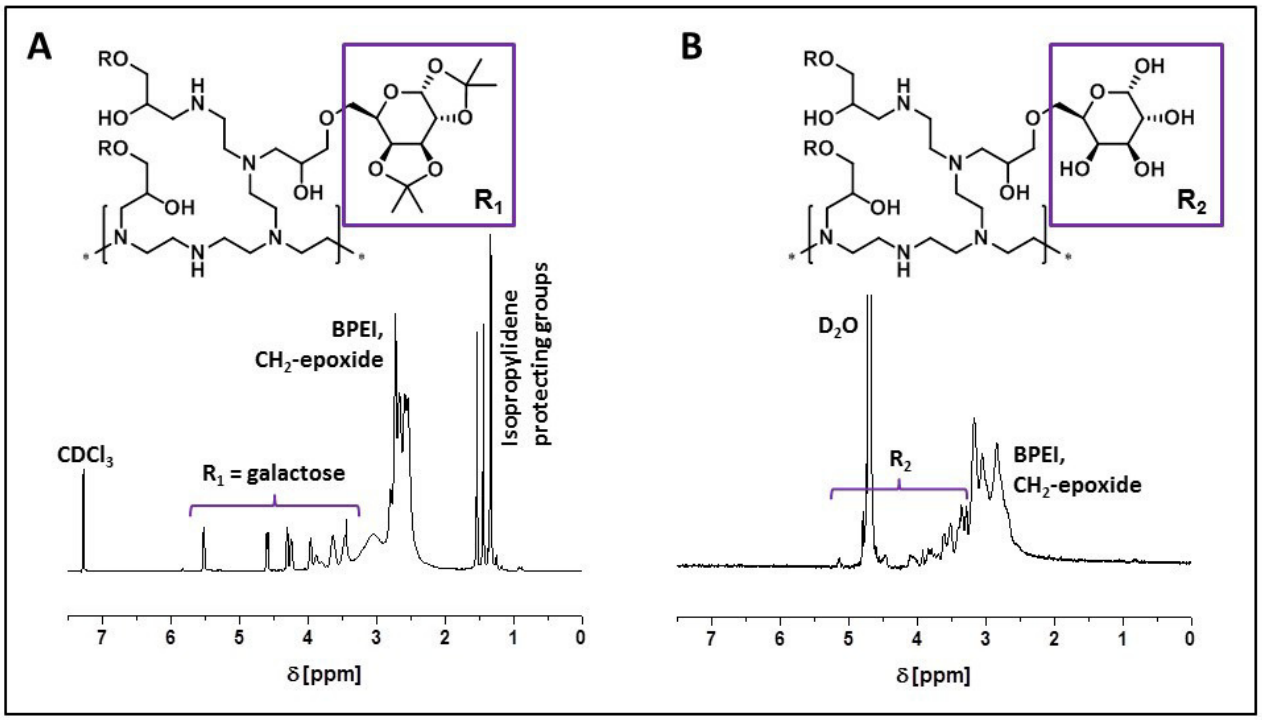

Figure S5. ^{1}H NMR spectra of A) a dialyzed aliquot of ***iso*B10** ($CDCl_3$, 400 MHz), and, B) the dialyzed aliquot of **B10** after hydrolysis (D_2O, 400 MHz).

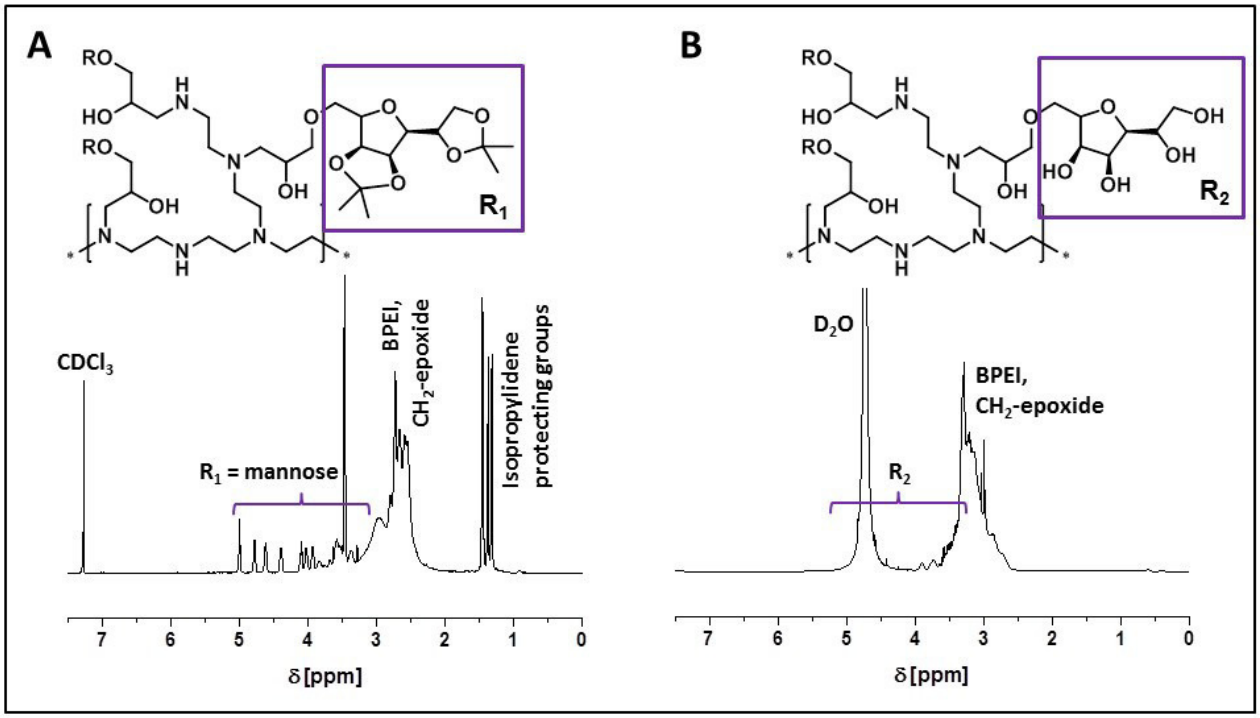

Figure S6. ^{1}H NMR spectra of A) a dialyzed aliquot of ***iso*B11** ($CDCl_3$, 400 MHz), and, B) the dialyzed aliquot of **B11** after hydrolysis (D_2O, 400 MHz).

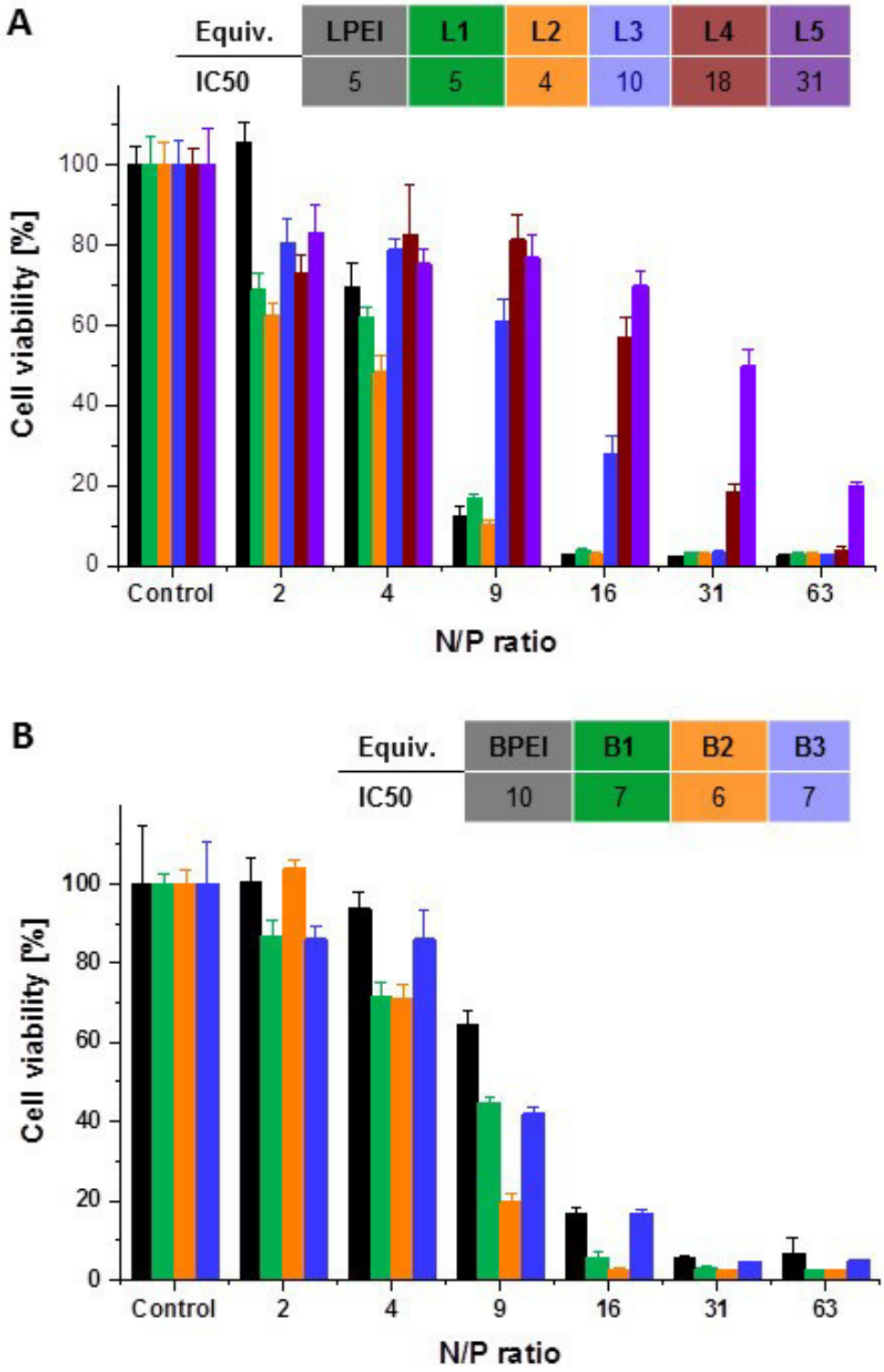

Figure S7. Cytotoxicity of formaldehyde functionalized A) LPEI (**L1**-**L5**) and B) BPEI (**B1**-**B3**) by MTT assay on HEK 293 cells.

B6 (0.15 equiv. glycidol)

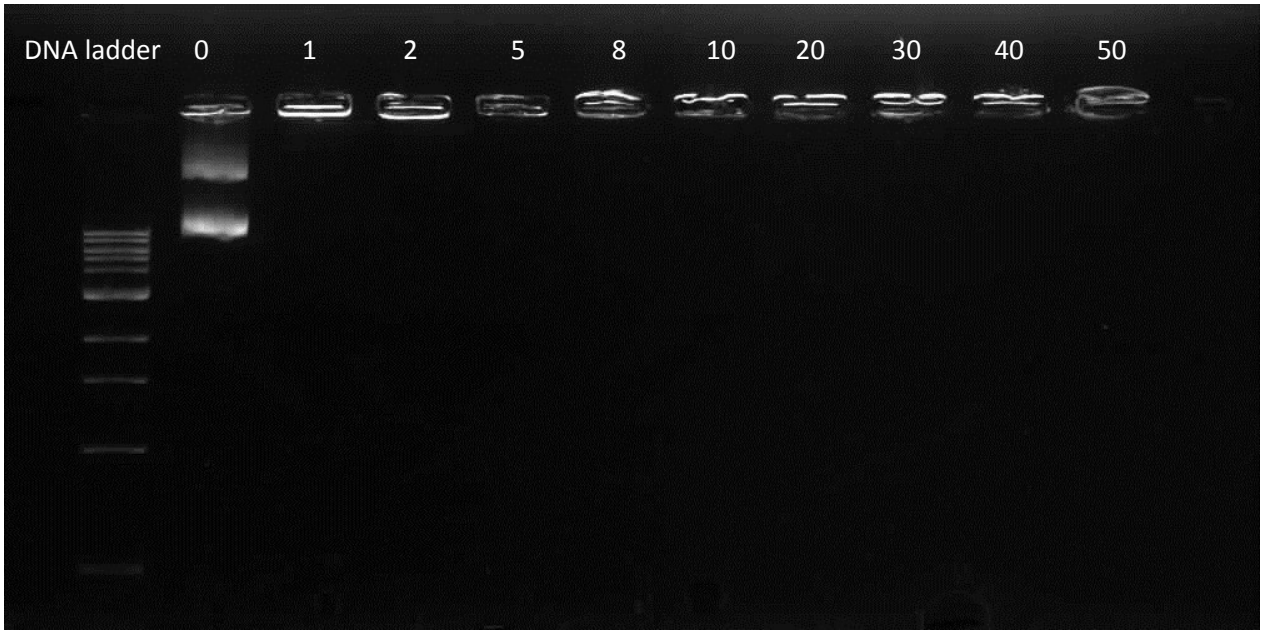

B9 (0.75 equiv. glycidol)

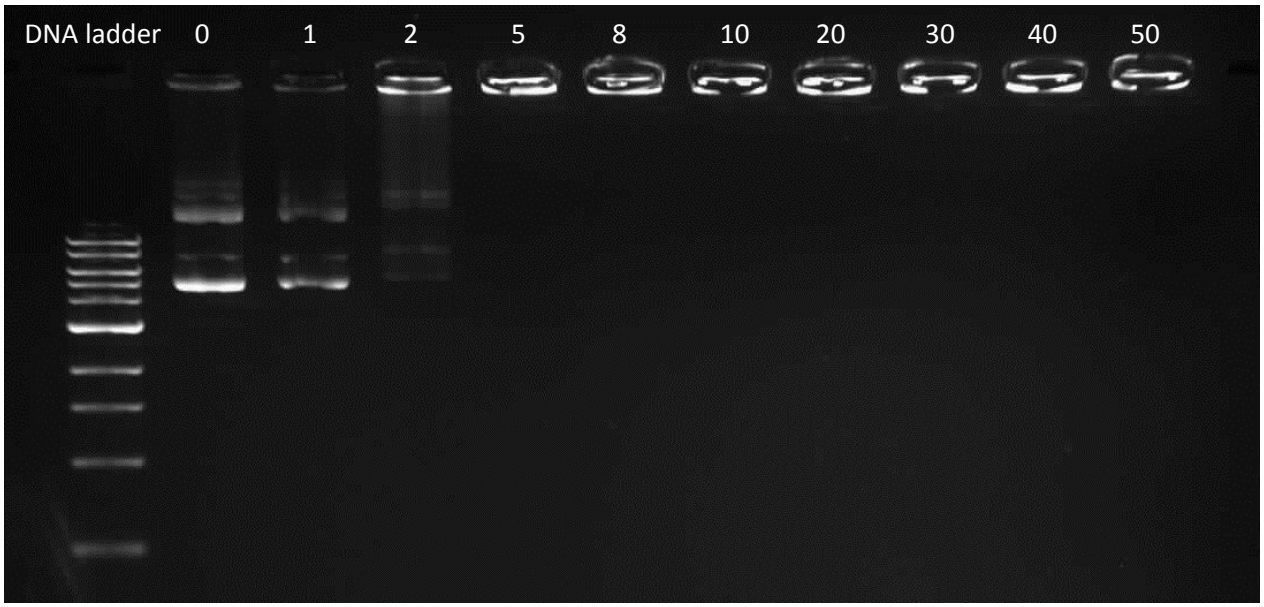

B10 (0.09 equiv. galactose)

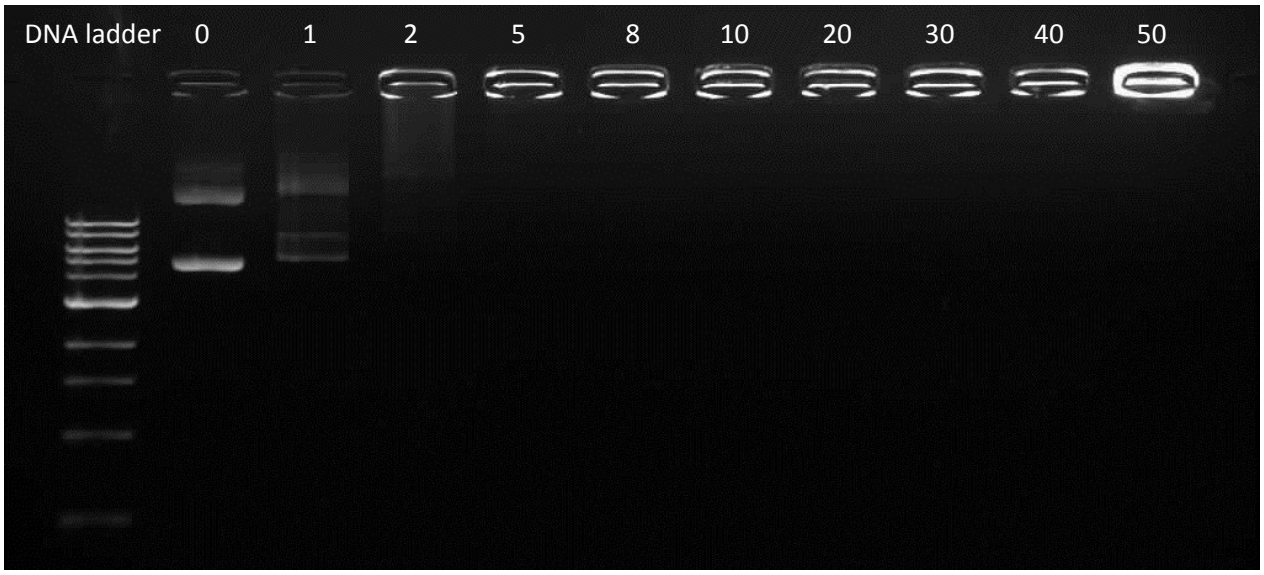

B11 (0.09 equiv. mannose)

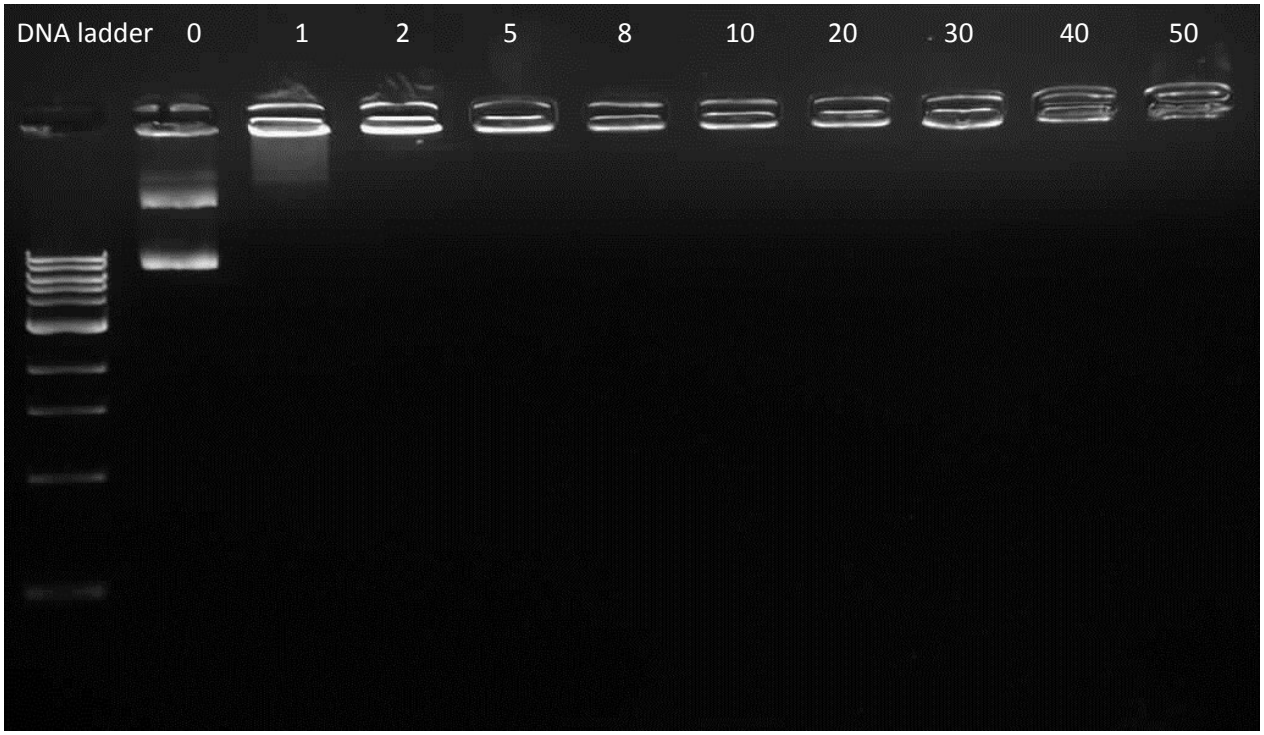

BPEI

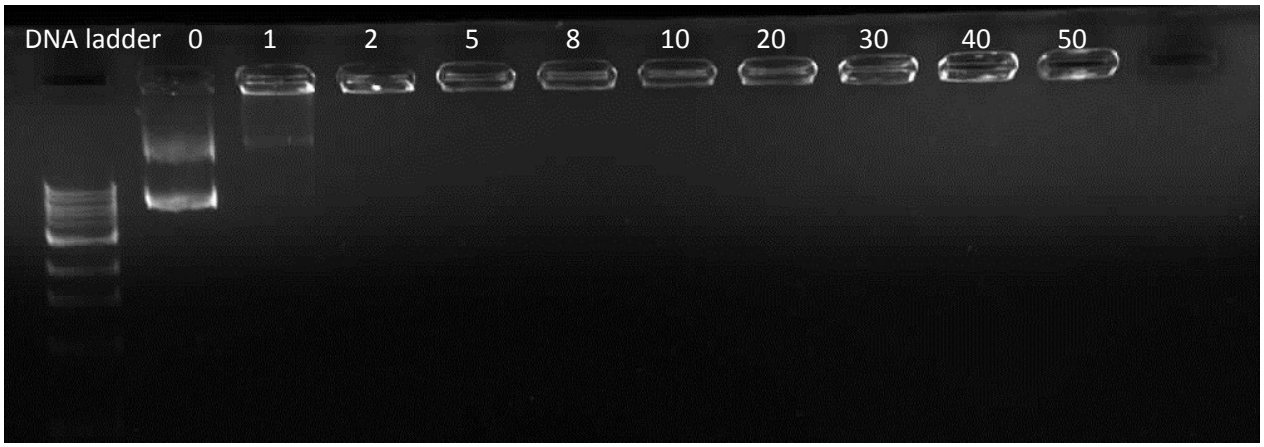

Figure S8. Electrophoretic mobility of DNA in polymer/DNA complexes.

PUBLICATION 4

Microwave-assisted polymer modifications

C. Englert, A. M. Schwenke, S. Hoeppener, C. Weber, U. S. Schubert

Adv. Polym. Sci. **2015**, *274*, 209-240

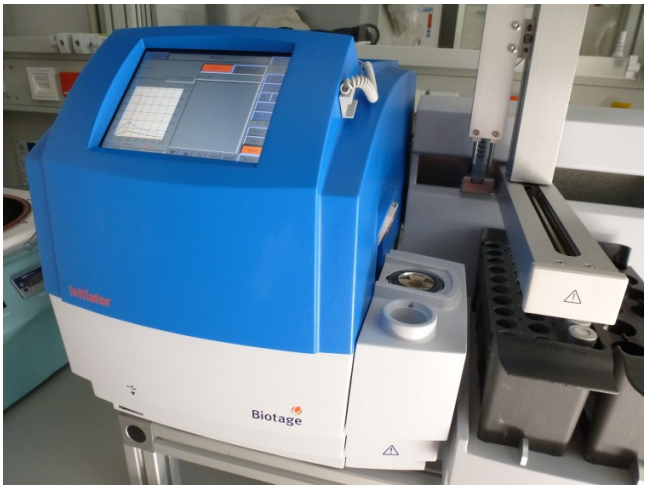

Adv Polym Sci (2016) 274: 209–240
DOI: 10.1007/12_2015_347

Published online: 14 February 2016

Microwave-Assisted Polymer Modifications

Christoph Englert, Almut M. Schwenke, Stephanie Hoeppener, Christine Weber, and Ulrich S. Schubert

Abstract Modern microwave synthesizers allow a detailed adjustment and control of temperature and power, such that many polymer modification reactions are performed nowadays using established synthesis protocols. This chapter provides a broad overview of post-polymerization modification reactions where these advantages are exploited for functionalization of synthetic and natural polymers. Selected examples are discussed in detail to demonstrate the versatility of the technique but also to address the challenges of screening approaches often applied to identify the optimum reaction conditions. While microwave synthesizers are regarded as efficient heating devices in the field of synthetic chemistry, selective heating of, for example, conjugated polymers has opened non-standard opportunities for the development of novel nanomaterials.

Keywords Carbon nanomaterials • Microwave-assisted synthesis • Poly(ethylene imine) • Polymer modification • Polysaccharide • Post-polymerization modification

Contents

C. Englert, A.M. Schwenke, S. Hoeppener, C. Weber (✉), and U.S. Schubert (✉)
Laboratory for Organic and Macromolecular Chemistry (IOMC), Friedrich Schiller University Jena, Humboldtstrasse 10, 07743 Jena, Germany

Jena Center for Soft Matter (JCSM), Friedrich Schiller University Jena, Philosophenweg 7, 07743 Jena, Germany
e-mail: christine.weber@uni-jena.de; ulrich.schubert@uni-jena.de

Abbreviations

ATRP	Atom transfer radical polymerization
bipy	Bipyridine
C-dots	Carbon dots
CL	ε-Caprolactone
DMF	*N*,*N*-Dimethylformamide
DMSO	Dimethylsulfoxide
DP	Degree of polymerization
dppp	Diphosphine 1,3-bis(diphenylphosphino)propane
DS	Degree of substitution
EDTA	Ethylenediaminetetraacetic acid
FRP	Free radical polymerization
LPEI	Linear poly(ethylene imine)
NBS	*N*-Bromosuccinimide
NMP	*N*-Methyl pyrrolidone
PAA	Poly(acrylic acid)
PCL	Poly(ε-caprolactone)
PE	Polyethylene
PEI	Poly(ethylene imine)
PEO	Poly(ethylene oxide)
PEtOx	Poly(2-ethyl-2-oxazoline)
PMeOx	Poly(2-methyl-2-oxazoline)
POx	Poly(2-oxazoline)
PPhOx	Poly(2-phenyl-2-oxazoline)
PPO	Poly(propylene oxide)
PS	Polystyrene
pTosOH	*p*-Toluene sulfonic acid
ROP	Ring-opening polymerization
SEM	Scanning electron microscopy
TEA	Triethylamine
TEBA	Triethyl benzyl ammonium chloride
TEM	Transmission electron microscopy
wt%	Weight percent

1 Introduction

Nature provides a vast and cheap amount of resources for polymer science. Naturally occurring polymers, i.e., biopolymers such as cellulose are readily available in large quantities and represent raw materials for many applications, in packaging, paper, or textile industry. However, the properties of these natural precursors often have to be tailored to make them suitable for specialized applications. Polymer modification reactions are ideally suited for this purpose. A major part of this chapter covers the microwave-assisted functionalization of polysaccharides. Functional moieties in synthetic polymers are often introduced by polymerization with functional monomers, initiators, or direct end-capping reagents. For such microwave-assisted polymerizations, the reader is referred to the respective chapters in this book [1–5]. Besides, microwave-assisted approaches also have been used for post-polymerization modification of synthetic polymers, which is the focus in this chapter.

From the perspective of material sciences, microwave irradiation is used for two kinds of polymer modifications. On the one hand, the morphology of solid polymers and their blends can be affected, as has been reported for both natural [6–8] and synthetic [9–13] polymers. Furthermore, polymer solutions and solid polymer structures can be treated with microwave irradiation, to obtain solid carbon materials. The latter is discussed at the beginning of this chapter. Subsequently, the chemical functionalization of natural and synthetic polymers via microwave-assisted approaches is summarized.

2 Microwave-Assisted Formation of Carbon Materials from Polymeric Precursors

The microwave-assisted heating of solutions containing a polymer can not only be used to introduce functionalities but can also induce reactions that result in the formation of carbon materials. Such processes are often accompanied by a color change to yellowish-brown as a result of the formation of carbon nanoparticles. The so-called carbon dots (C-dots), which often possess fluorescent properties, are highly useful for applications, for example as optical-imaging agents for life-science applications. Various carbonaceous precursors are reported to yield such C-dots in straightforward and rapid one-step synthesis protocols. For example a triblock copolymer composed of a poly(propylene oxide) central block and two poly(ethylene oxide) blocks (PEO-PPO-PEO) was irradiated in the presence of phosphoric acid for only 4 min, resulting in carbon particles with diameters of 5–20 nm [14]. By applying a microwave-assisted hydrothermal process (180 °C for

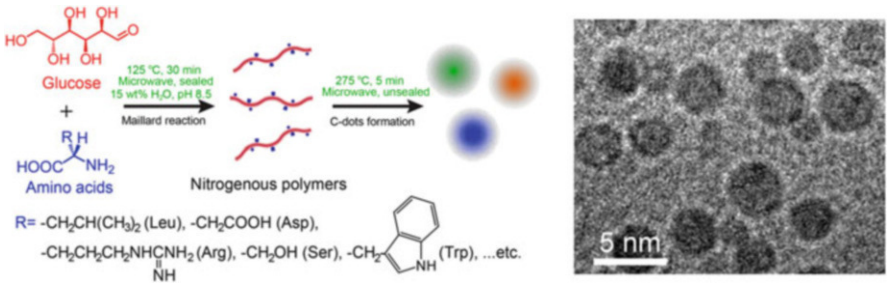

Fig. 1 Synthesis scheme and TEM image of nitrogen-doped C-dots with tunable emission color [17]. Reprinted with permission of Macmillan Publishers Ltd: Scientific Reports 2014, 4, 3564, copyright 2014

20 min), aqueous solutions of natural resources such as flour yielded C-dots with diameters ranging from 1 to 4 nm [15]. Although the detailed mechanism remains unclear to date, the proposed pathway of the formation of C-dots from carbohydrate-based materials includes the decomposition of the precursor via hydrolysis and dehydration. The soluble compounds obtained are believed to polymerize via polycondensation reactions to yield different soluble polymeric products. Finally, the C-dots would be formed by subsequent aromatization and carbonization [16].

The synthesis of C-dots doped with hetero atoms can be accomplished by utilization of nitrogen or phosphorus-containing precursors. Therefore, precursor polymers were synthesized from a mixture of glucose and amino acids in a microwave-assisted synthesis via the Maillard reaction. Subsequently, an open vessel microwave treatment for 5 min at 275 °C resulted in the formation of nitrogen-doped C-dots with tunable multicolor luminescence (Fig. 1) [17]. The irradiation of a tannin–melamine–hexamine polymer in the presence of polyphosphoric acid yielded nitrogen and phosphorus co-doped mesoporous carbon. Spherical structures were obtained after 10–30 min of irradiation [18].

Chains of graphitic carbon particles in the range from 340 to 620 nm were obtained from poly(ethylene glycol) by microwave-assisted heating in a hydrothermal setup (mixture of ethanol, water, and sodium hydroxide) [19]. After a prolonged irradiation (2 h at 220 °C), as well fibrous carbon structures were obtained.

When polymer structures are heated by microwave irradiation in the solid state, even the transformation of the polymer backbone into a more or less pure carbon material can be achieved. Because microwave radiation provides direct heating of the reactants and strongly interacts with specific types of materials, carbonization can occur within a short irradiation period of just a few minutes [20]. In particular, exceptional fast heating is observed when conductive polymer structures are irradiated, which efficiently absorb the microwave irradiation. Zhang and co-workers [21, 22] prepared nanostructured chlorine-doped polypyrrole precursors of different shapes including fibers, tubes, and spherical particles (Fig. 2). The structures were

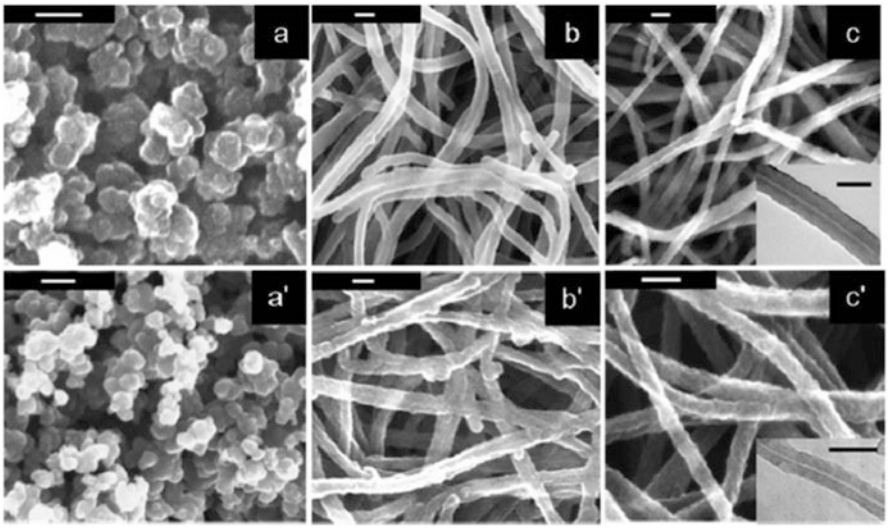

Fig. 2 Microwave-assisted synthesis of nanostructured carbon from doped polypyrrole structures. SEM and TEM images before (**a–c**) and after (**a'–c'**) heating. *Scale*: 100 nm. Reproduced from [22] with permission of The Royal Society of Chemistry

carbonized within 3–5 min when subjected to microwave radiation. Thereby, a weight loss of 50% occurred, and the carbon content of the material was increased from 56% to more than 90%. Despite being performed under non-inert conditions, no oxidation of the backbone took place, which is most likely prevented because of the very rapid heating and carbonization process. The morphology of the nanostructures was retained even though a slight shrinkage occurred.

Structures composed of non-conducting polymers can be as well carbonized by microwave irradiation although longer heating times are required. For example, poly(acrylonitrile) fibers were graphitized by a microwave plasma process in an argon atmosphere [23]. Biowaste materials such as cotton, wood, or filter paper could also be graphitized when polypyrrole was added as filler material to increase the heating efficiency. The morphology and porosity of the biowaste precursors was retained, but the materials exhibited a graphitic structure after the microwave-assisted treatment [24].

Additionally, graphitic materials with high crystallinity were prepared by microwave-supported heating and can be exfoliated into graphene in a two-step microwave protocol [25]. First, metal phthalocyanine was synthesized, which was carbonized at 450 °C in a second step. Direct quenching with a mixture of water and ice or with liquid nitrogen resulted in the exfoliation to graphene with typically one to eight layers [25].

3 Microwave-Assisted Modification of Polysaccharides

The manifold functional biopolymer moieties that nature has been developing over millions of years represent a rich pool of which synthetic chemists can take advantage. Microwave irradiation has been exploited for the functionalization of these raw materials since the 1980s. However, some of these functional moieties and their stereochemistry are exactly the reason that make natural polymers often difficult to dissolve in common solvents because of the presence of strong inter- or intramolecular hydrogen bonds. Because solubility represents a prerequisite for homogeneous functionalization reactions, the development of optimum reaction conditions is often challenging and requires harsh conditions or very aggressive solvents such as concentrated acids. The main advantages of the application of microwave irradiation in this respect are the high temperatures that can be applied (along with the opportunity to heat above the boiling point of the solvent in closed reaction vessels) and the very efficient heating of special solvents such as ionic liquids. However, the dissolution of barely soluble materials under rather drastic conditions can still be accompanied by a degradation of the polymeric materials, a fact that has been exploited for the tailored synthesis of polysaccharides with lower degrees of polymerization.

3.1 Dissolution and Degradation

Starch consists of mainly two polysaccharide fractions. Although amylose is a linear polymer where the α-D-glucose monomers are linked 1,4-glycosidically, additional 1,6-glycosidic linkages result in a branched structure and higher molar mass of the second component amylopectin (Scheme 1). Because starch is a natural product, its composition is prone to variation depending on the resource from which it was isolated. A large amount of different starches could be dissolved in dimethylsulfoxide (DMSO) without degradation using microwave irradiation [26]. At a constant power of 900 W, a few seconds of heating time were sufficient to dissolve the entire starch samples without noticeable degradation in most cases (35 s, maximum temperature 143 °C). On the other hand, microwave reactors can be used to tailor the degradation of starch during acidic hydrolysis. In a semi-dry process, the molar mass of granular starch was efficiently reduced in less than 2 min [27]. In particular, the amylopectin fraction was affected, and the final degree of polymerization (DP) could be tuned by the reaction temperature (60–85 °C) and the amount of hydrochloric acid catalyst. Higher reaction temperatures (up to 100 °C) resulted in the formation of dextrins, i.e., poly(α-D-glucose)s with much lower molar masses.

Because cellulose consists of β-D-glucose repeating units linked 1,4-glycosidically, strong hydrogen bonds are present that ultimately lead to its fibrous structure but make its dissolution extremely difficult. Applying ionic liquids

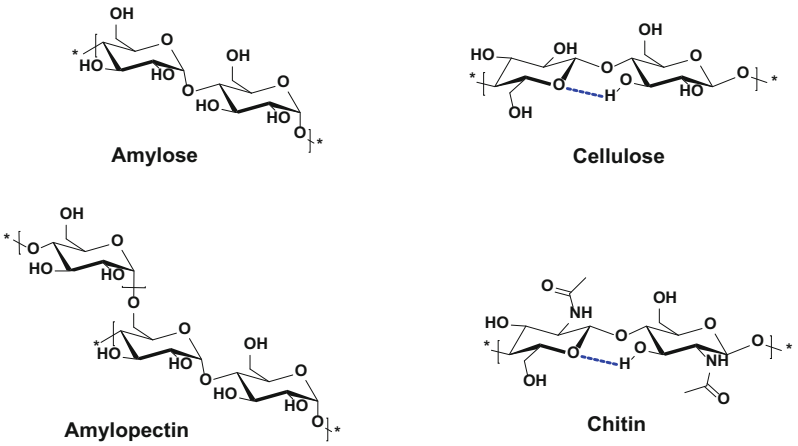

Scheme 1 Schematic representation of the structure of selected polysaccharides. The *dashed blue lines* represent the hydrogen bonds that complicate the dissolution of polymers based on *β*-D-glucopyranose

in a screening approach using varying microwave settings proved suitable to dissolve up to 10 wt% of cellulose. Thereby, the DP was decreased by roughly a third in some cases [28]. Because the *N*-acetyl-*β*-D-glucopyramin repeating units of chitin are linked in a similar fashion, its solubilization is also challenging [29]. As for cellulose, the combination of ionic liquids and microwave-assisted heating is helpful to overcome the tight hydrogen bonds of this polysaccharide. Hence, it is possible to prepare 20 wt% solutions [30]. Chitosan, i.e., partially deacetylated chitin, represents one of the few cationic polymers directly available from natural resources [31]. However, its solubility in water (which is often required for applications or further functionalization under mild conditions) is limited to polymers with a low DP [32]. Such oligomeric chitosans are obtained via degradation of high molar mass polymers using different methods. A mild treatment with hydrogen peroxide under microwave irradiation is highly reproducible and prevents the occurrence of undesired side reactions [33]. Appropriate adjustment of the reaction conditions even enables the tailoring of the DP of the oligomers [34].

Similarly, microwave-supported treatment has been reported for the preparation of sulfonated polysaccharides based on galactose with defined molar masses. Factors such as pH value, adjustment of microwave power, or heating time were varied to obtain both *λ*- and *κ*-carrageenan oligomers [35, 36].

3.2 *Modification of Polysaccharide Hydroxyl Groups*

All polysaccharides possess multiple hydroxyl functionalities, which can be used to modify the polymers' nature. Scheme 2 outlines the synthetic possibilities that have

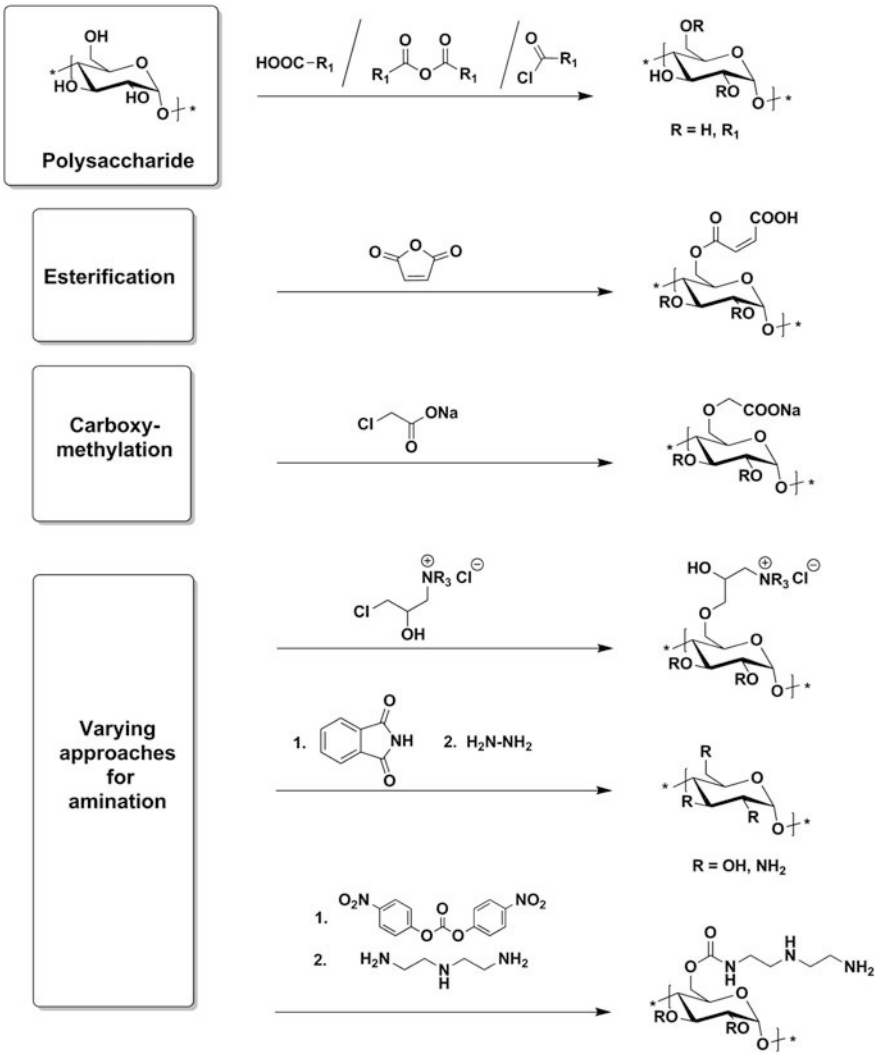

Scheme 2 Schematic representation of microwave-assisted modifications of polysaccharides by utilization of hydroxyl functionalities. It should be noted that the polysaccharide structure is exemplary and varies as described in the text

been exploited using microwave-assisted synthetic approaches, which are summarized in the following section.

Among these, the most well-known strategy is the esterification of the –OH moieties. Similar to protocols utilizing traditional heating, common microwave-assisted approaches include enzymatically catalyzed esterification using simple carboxylic acids, acid chlorides, and the use of anhydrides with or without additional catalyst. Table 1 provides an overview of selected microwave-assisted

Table 1 Esterification of polysaccharides using microwave-assisted chemistry

Poly-saccharide	Method	Product	Conditions	DS	References
Starch	Carboxylic acid/lipase	Acetate Laurate Stearate	DMF/DMSO 80/160 mW g^{-1a} 60/120 min	0.03–0.51	[37]
Starch	Carboxylic acid/lipase	Acetate Laurate Stearate	DMF/DMSO 25/80°C 120/300 min	0.01–0.43	[37]
Starch	Anhydride	Acetate Succinate	NaOH/NaOAc 260–1,300 W 1–5 min	≤0.37	[38]
Starch	Anhydride Carboxylic acid	Acetate	Max. 650 W 150°C, 4–7 min Variable defined temperature programs	0.19–0.78	[39]
Starch	Anhydride Carboxylic acid	Acetate	I_2 catalysis 100 W, 100°C 2–10 min	0.02–1.27	[40]
Konjac	Anhydride	Succinate	600 W 100 s	0.17–0.24	[38]
Cellulose	Anhydride	Acetate Propanoate Butyrate Pentanoate Hexanoate	Ionic liquid 30 W 80°C 8–12 h	1.5–2.9	[41]
Cellulose	Anhydride	Acetate	0.01–0.15 equiv. I_2 300–800 W, 80–130°C, 5–45 min	0.48–2.8	[42]
Pectin	Anhydride	Linolate Oleate Palmitate	0.1 equiv. K_2CO_3 900 W 3–6 min	N/A	[43]
Carboxy-methyl starch	Anhydride	Octenyl-succinate	DMSO, 0.1 equiv. *p*TosOH 1–5 min, 140 W 90–160°C	0.05–0.55	[44]
Hemi-cellulose	Acid chloride	Propionate Octanoate Laurate Oleate	DMF, 0.05 equiv. NBS 300 W, 78°C, 5 min	0.67–1.28	[45]
Hemi-cellulose	Acid chloride	Laurate	DMF, LiCl, TEA, various catalysts 300 W, 78°C, 1–8 min	0.77–1.64	[46]

[a]With reference to the amount of sample

synthesis conditions and the degrees of substitution (DS) that could be achieved, although a direct comparison is difficult because of the various types of microwave synthesizers that were applied in different modes. Despite the versatility modern (automatized) microwave synthesizers offer and the unique possibilities to design experiments design of experiments [40] with respect to the optimization of reaction

conditions, these opportunities should not replace critical thinking. It must be noted that the applied reaction conditions sometimes impose a strong influence on the materials obtained. Short reaction times are often reported at the expenses of high DS. Nevertheless, the efficiency of a careful adjustment of the reaction conditions in the microwave synthesizer was demonstrated by Possidonio et al., who could achieve very high and tailored DS values by reacting cellulose with a range of anhydrides in ionic liquids under microwave irradiation with negligible degradation of the polysaccharide [41].

Because of the manifold esters that can be obtained (ranging from acetates to fatty acid esters), this method offers access to polymers from renewable resources featuring a variety of properties. Besides the adjustment of hydrophobicity and the resulting variation of mechanical properties [47], the introduction of further functional moieties such as double bonds derived from fatty acids [43] or carboxylic acids has also been reported. The latter is easily possible in a one-step reaction by conversion of the polysaccharide hydroxyl groups with a cyclic anhydride such as succinic [38] or maleic [48] anhydride. Using appropriately designed anhydrides, the combination of both has been reported simultaneously in a one-step synthesis [44]. On the other hand, the selective esterification of the hydroxyl moieties of pectin, a polysaccharide which already contains carboxylic acid functionalities, has also been reported [43].

Carboxymethylation represents a common method to introduce carboxylic acid functionalities to polysaccharides using chloracetic acid under alkaline conditions. This reaction has been performed under microwave irradiation with several natural polysaccharides, such as konjac [38], agarose [49], and hemicellulose [50]. In comparison to conventional heating, similar DS values could be achieved, although shorter reaction times were sufficient during microwave-assisted syntheses.

The utilization of analogous reactants (Scheme 2) makes it possible to introduce amine functionalities to polysaccharides via the hydroxyl groups already present. For starch, microwave irradiation proved superior to conventional heating in both reaction time and DS [38]. However, when the fraction of amines in chitosan was increased, conventional heating resulted in much higher DS because of the evaporation of the solvent in the microwave reactor [38]. This problem would probably be avoided by application of modern synthesizers which enable the use of closed reaction vessels nowadays.

An alternative approach towards amino-functional agarose involves the conversion of the agarose hydroxyl functionalities with phthalimide and subsequent hydrazinolysis [51]. During both steps of the Gabriel-like synthesis, optimized microwave-assisted procedures gave rise to DS of around 0.9. Activation of inulin using bis(4-nitrophenyl) carbonate via microwave-assisted chemistry represents another possibility to include amine moieties to a polysaccharide the basis of which functional groups are alcohols [52].

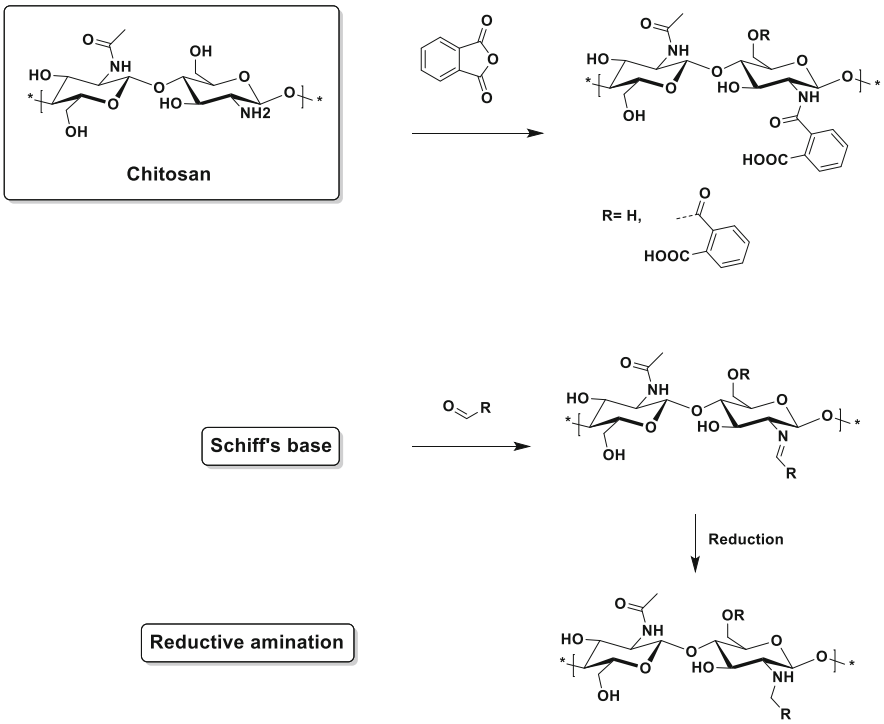

Scheme 3 Schematic representation of the main strategies for microwave-assisted modifications of chitosan amine moieties

3.3 Modification of Chitosan Amine Moieties

The nucleophilicity of the primary amine functionalities of chitosan offers several ways for polymer modification (Scheme 3). However, in the case of unselective reactants, the polysaccharide hydroxyl groups are prone to reaction as well. One example is the application of phthalic anhydride, which was well investigated in terms of microwave-assisted as well as conventional heating [53]. Optimized reaction conditions in the microwave synthesizer (DMF, 500 W, 3 min) resulted in a DS value of 1.4, almost without degradation of the chitosan. To achieve a similar DS value by conventional heating, a reaction time of 5 h was necessary, which caused significant polymer degradation.

In contrast, the formation of Schiff's bases is a possibility to functionalize selectively the primary amine moieties of chitosan. If a reducing agent such as sodium boron hydride is added in situ, the selective alkylation is possible via the so-called reductive amination approach. This reaction has been studied by Petit et al., who compared the alkylation yields achievable via microwave-assisted synthesis in detail to conventional heating using octanal as an exemplary aldehyde reactant [54]. As depicted in Fig. 3, the microwave setup proved superior in terms

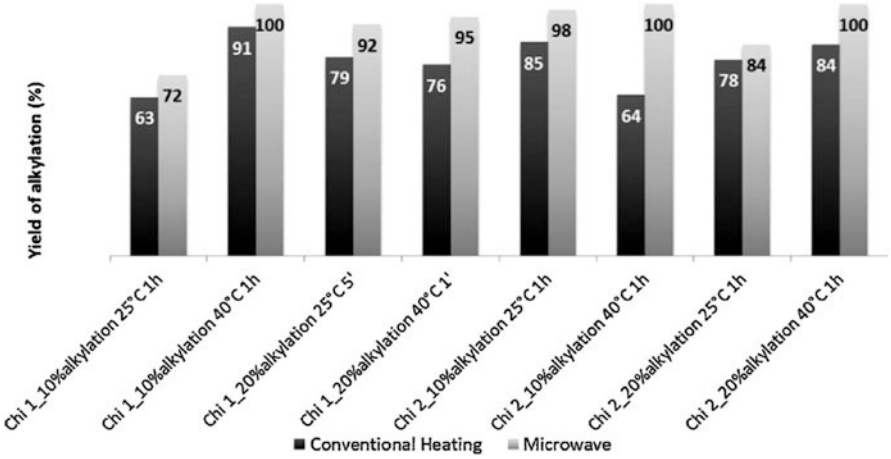

Fig. 3 Comparison of yields obtained for the synthesis of alkylchitosan using conventional heating and microwave irradiation. Reprinted from Carbohydrate Polymers 116, C. Petit et al., Amphiphilic derivatives of chitosan using microwave irradiation: towards an eco-friendly process to chitosan derivatives, 26–33, Copyright 2015, with permission from Elsevier [54]

of alkylation yield, in particular when short reaction times were used. The rheological and surface active properties of the alkylated chitosan derivatives were similar to those of materials prepared by conventional methods.

To obtain scavenger materials for lead and mercury ions, the Schiff's base route was applied to prepare crosslinked chitosan using a double aldehyde functional crown ether via microwave irradiation (800 W, 10 min) [55]. On the other hand, this type of chemistry was reported useful to protect the amine functionalities of chitosan prior to crosslinking with epichlorohydrin [56]. Subsequent deprotection of the Schiff's bases from benzaldehyde under acidic conditions yielded the amino functionalities, which were then functionalized with EDTA via the anhydride method. Microwave-assisted chemistry was exploited in all of these five synthetic steps. A much simpler method to prepare crosslinked copper complexes from chitosan involves the direct complexation of chitosan amine functions followed by Schiff's base formation using glutaraldehyde to include covalent junctions in the network [57]. Both steps comprised the use of microwave synthesizers.

3.4 Modification of Carboxylic Acid Functional Polysaccharides

Alginic acid represents a polysaccharide based on α-L-guluronic acid and β-D-mannuronic acid that naturally contains carboxylic acid functionalities which have been exploited for further modification of the biopolymer. The deprotonated alginate can be crosslinked by addition of calcium ions, a reaction which can also be

used for co-precipitation of proteins. The selectivity of this so-called affinity precipitation can be enhanced by pre-treatment of the native alginic acid [58]. In addition, sodium alginate was successfully applied as a stabilizing agent during the microwave-assisted synthesis of copper nanoparticles [59]. Besides the mere use of the carboxylic acid moieties for the formation of salts, their existence provides the opportunity for further chemical modification by amidation using amines. Without further activation of the carboxylic acid groups, DS between 0.5 and 1.0 could be achieved after reaction with an excess of varying diamines at 100 °C for 10 min using 300 W microwave irradiation, even in aqueous media [60]. The resulting amino-functional alginates were subsequently crosslinked using the natural fluorescent dye genipin. In a similar approach, the modified biopolymer carboxymethylated cellulose (see above) was reacted with ethylene diamine and subsequently crosslinked with alginic acid using the same reaction conditions [61]. Interestingly, microwave irradiation (800 W, 1 min) alone has been reported to be sufficient to crosslink carboxymethylated starch via formation of anhydrides because of dehydration during the heating process [62].

In an alternative approach, carboxymethylated cellulose was applied for transesterification of methyl esters derived from rapeseed oil via microwave-assisted heating [63]. Although the DS values achievable were moderate ($DS < 0.1$), the environmentally benign synthetic approach using a mixture of water and DMF required only reaction times of a few minutes to produce efficient emulsifiers from almost entirely natural resources.

3.5 Grafted Polysaccharides

Singh and Sanghi have reviewed the microwave-assisted grafting of polysaccharides in 2012 based on a distinction between the different types of polysaccharides [64]. Hence, this topic is only briefly discussed here from a viewpoint that distinguishes the type of grafting mechanism based on the functional groups present in the polysaccharides and monomers used for the grafting (Scheme 4).

Because alcohols represent initiators for various ring-opening polymerizations (ROP) of lactones to yield polyesters, polysaccharides with their multiple hydroxyl groups seem to be ideal starting materials for grafting-from approaches. Microwave irradiation is especially favorable because the standard catalyst for this type of ROP, tin octoate, requires high reaction temperatures to promote the polymerization of, for example, the quite robust monomer ε-caprolactone (CL). However, the large difference in hydrophilicity between unmodified polysaccharides and the hydrophobic CL and PCL gives rise to complications because of miscibility in bulk polymerizations. Only when unmodified starch was swollen in water microwave-induced polymerization of the monomer could be observed [38]. The grafting of PCL from the more hydrophobic acetylated konjac was reported to be more successful. In any case, water can initiate the ROP of CL as well, leading to the formation of PCL homopolymers, which requires exhaustive purification of the

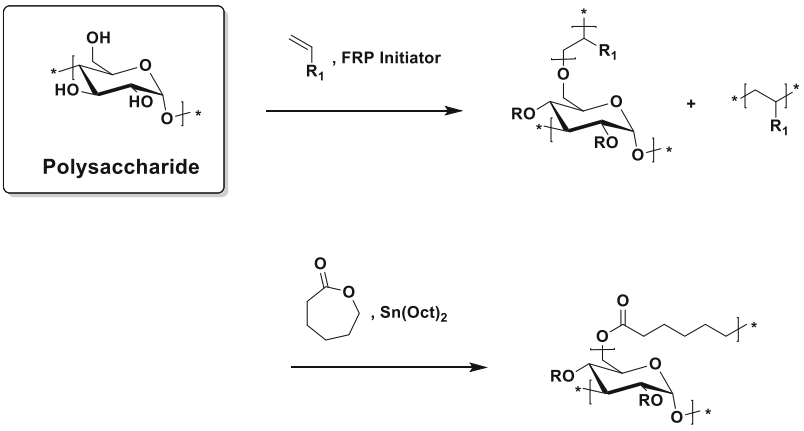

Scheme 4 Schematic representation of microwave-assisted grafting modifications of polysaccharides using ε-caprolactone (*bottom*) and FRP of vinylic monomers (*top*). It should be noted that the polysaccharide structure is exemplary and varies as described in the text

graft copolymers [65]. In addition, the exact determination of the composition of the isolated products by spectroscopic means is difficult, although the microwave-assisted bulk synthesis and purification of PCL grafted cellulose [65] and chitin [66] whiskers was achieved successfully in general. The grafting of PCL from chitosan is further complicated by the presence of amine functionalities, which have to be protected prior to the ROP [67]. Phthalic anhydride has been used for this purpose, although the subsequent deprotection via hydrazine can easily induce a degradation of the grafted PCL chains.

The grafting of polymers from vinylic monomers onto or from polysaccharides via microwave-assisted synthesis protocols is mainly performed using various initiator systems able to generate radicals on the polysaccharide. In particular, redox initiators and persulfates are utilized frequently. Hence, this represents a free radical polymerization (FRP), further complicated by the fact that the radical initiator systems are not only capable of creating active radical species on the polysaccharides but can also simply initiate polymerization of the vinylic monomers on their own [68]. This can be compensated to some extent by an addition of monomer subsequent to an "activation step" in which only the polysaccharide and the initiator are heated. It should be clearly stated that the combination of both FRP and unselective initiation results in the formation of considerable amounts of non-grafted synthetic polymer chains, which can be difficult to remove from the graft copolymer. However, optimization of microwave-assisted synthesis was suitable to reach high monomer conversions of acrylonitrile in very short reaction times of a few minutes [69]. On the other hand, longer reaction times (2 h) were reported to be more favorable as soon as the graft copolymers are purified and characterized thoroughly, as shown for alginate-*g*-poly(vinylpyrrolidone) [70].

The homopolymer removal plays a minor role when the surfaces of polysaccharide fibers [71, 72] or other solid materials based on cellulose (pine needles) [73] are

directly modified via such methods, because the separation of ungrafted polymer chains can easily be accomplished in this case. Bifunctional vinylic monomers are often added as crosslinkers, which results in the formation of hydrogels, i.e., insoluble materials that are again easy to purify [74–77].

4 Microwave-Assisted Modification of Synthetic Polymers

Microwave-assisted approaches for the modification of synthetic polymers comprise a wide field, ranging from recycling of commodity polymers over the introduction of functional moieties, which can be pendant or at the chain end groups, to the functionalization of resins or surfaces. Hence, we first provide an overview about the general possibilities and approaches that can be and have been applied. Subsequently, selected examples are discussed in more detail, in particular those where extensive investigations on the microwave-assisted syntheses were made and resulted in the establishment of optimized synthesis protocols.

4.1 General Approaches for the Microwave-Assisted Modification of Synthetic Polymers

A wide range of reaction types have been performed under microwave irradiation, ranging from "simple" modifications of commodity polymers to the precise adjustment of functionalities in speciality polymers (see Table 2). One of the first modifications reported is the rapid surface oxidation of polyethylene (PE) with potassium permanganate, which leads to the formation of vinyl and hydroxyl moieties [78]. This method represents an environmentally friendly technique without affecting the thermal properties of the PE and without the formation of hydroperoxy groups.

An additional application of microwave irradiation is the conversion of expanded polystyrene (PS) waste into polymeric flocculants by a sulfonation reaction using sulfuric acid in the presence of the catalyst silver sulfate [79]. The product revealed similar properties to the modified PS obtained after conventional heating and the reaction time could be significantly reduced (from 1 h to 15 min). The phosphonation of branched poly(ethylene imine) (PEI) via microwave-assisted synthesis using formaldehyde and phosphorous acid also provides similar products as conventional heating [80]. Although the DS could be well tailored in both methods, microwave-assisted heating proved faster and easier once more.

Taking advantage of the high temperatures that can be achieved, even in low-boiling solvents in closed reactions vessels, microwave-assisted approaches are especially useful for hetero-Diels–Alder reactions. The deprotection of furan–maleimide adducts pendant to PEO-based copolymers was only possible after

Table 2 Overview of general possibilities for microwave-assisted polymer modifications

Polymer	Reactant	Solvent, catalyst	Microwave		References
			t (min)	*T*/Power	
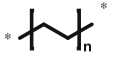	$KMnO_4$	–	0.3–1.5	900 W	[78]
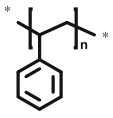	H_2SO_4	Ag_2SO_4	5–30	80–110 °C	[79]
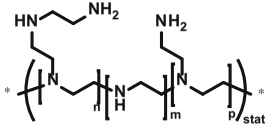	CH_2O, H_3PO_3	HCl	8	150 W	[80]
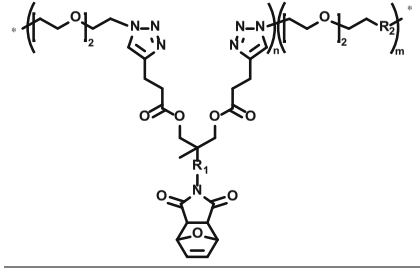	–	$CHCl_3$, CH_3CN	60	110 °C	[81]

subjecting the protected polymers to microwave-supported heating in a chloroform–acetonitrile mixture, and attempts to use conventional heating failed [81]. Within 1 h, the complete removal of the furan protecting groups was achieved, and the copolymer itself remained intact.

4.2 Polymer Functionalization Using Nucleophilic Reagents

Nucleophiles such as amines, phenolates, or thiolates represent valuable reagents to introduce further functionalities or to simply modify the properties of a precursor polymer. In the following, suitable precursor polymer types are discussed, structured according to the underlying chemical reaction mechanisms. Table 3 provides an overview of the respective microwave-assisted polymer modifications, along with a general description of the utilized reaction conditions.

The nucleophilic ring opening of cyclic ethers represents an early example where microwave irradiation was studied as synthetic tool for further modification of polymers. In the easiest case, suitable polymers for this purpose can simply be epoxidized liquid natural rubber, as reported by Huy et al., who used α-naphthyl acetic acid as nucleophilic reagent to open the three-membered ring [82]. As for many other reactions discussed above, microwave-assisted approaches resulted in higher conversions at shorter reaction time compared to conventional heating. The ring opening of oxetanes as the analogous four-membered rings with amines was successfully employed in a similar fashion to functionalize various polymers based on bisphenols [83]. Microwave-assisted synthesis approaches alone already gave rise to higher conversions. The addition of zinc chloride as catalyst enhanced this effect even further, presumably because its polarity made it an efficient microwave absorber [84].

The microwave-assisted amidation and esterification of various carboxylic acid-functional polymers has been thoroughly studied by Ritter and co-workers. A poly (acrylic acid) (PAA) homopolymer could be functionalized with various adamantyl moieties simply by mixing with the respective adamantyl-functional amine and subsequent use of microwave irradiation [85]. Without the requirement of solvents or coupling agents, copolymers with 5 mol% of adamantyl units were obtained, whose sodium salts were used to form hydrogels produced by the intermolecular association of the hydrophobic side chains. Utilizing *p*-toluenesulfonic acid (pTos–OH) as catalyst, poly[ethylene-*co*-(acrylic acid)] (PE-*co*-PAA) could be modified with phenol derivatives under solvent-free conditions [86]. In a direct comparison with conventional oil bath heating, the microwave irradiation was shown to promote effectively the esterification of the copolymer. A reaction within a few minutes resulted in a high level of reproducibility and conversion. An analogous approach proved suitable for the amidation of PE-*co*-PAA with (2-aminoethoxy) ethanol in a single step to obtain a polyinitiator for the ROP of CL [87]. Subsequently, the results were transferred to poly(ether sulfone)s as alternative polymer

Table 3 Overview of microwave-assisted nucleophilic polymer modifications

Polymer	Reactant	Solvent, catalyst	Microwave		References
			t (min)	*T* (°C)	
	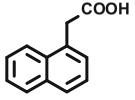	Chlorobenzene, TEBA	5–15	150–240 W	[82]
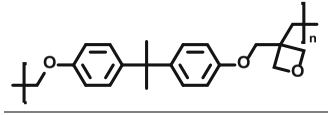	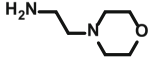	DMF	60–180	200–800 W	[83]
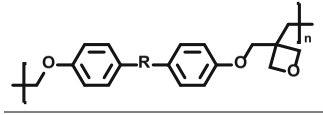		DMF, $ZnCl_2$	20	100	[84]
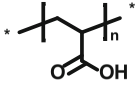	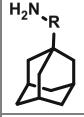	–	20	220	[85]
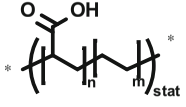	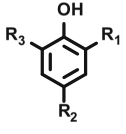	pTosOH	5	165	[86]
	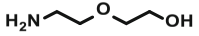	Toluene	90	220	[87]

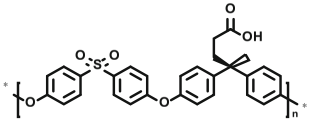	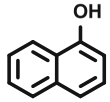	pTosOH	3	200	[88]
	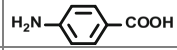	NMP	20	190	
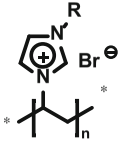		–	180	200	[89]
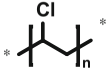	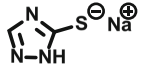	Cyclo-hexanone	30–2,880	40–80	[90]
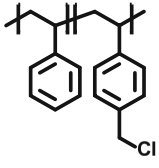	NBu_3	DMF	15	195 W	[91]
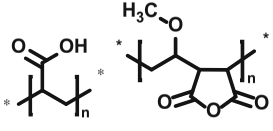	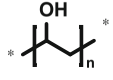	H_2O	20	100–150	[92]

type, which could be successfully functionalized with 1-naphthol as well as 4-aminobenzoic acid, even in an apolar solvent such as xylene [88].

DMF can act as an excellent source for dimethylamine and carbon monoxide under microwave irradiation [89]. The in situ generation of these gases is especially advantageous for small-scale reactions where the direct use is impractical, as shown by the modification of poly(vinylimidazolium) salts. The proposed final copolymer structure contains mainly units of 1-vinylimidazole and some units of amines, formamides, and alkenes.

Microwave-assisted modifications of synthetic polymers are not limited to speciality polymers but have also proved to be useful for the functionalization of commodity polymers such as poly(vinyl chloride) [90]. A series of copolymers was obtained by nucleophilic substitution with 1,2,4-triazol-5-yl-sulfanyl groups. Using microwave irradiation as heating source, the reaction could be performed with the highest level of conversion, a significant decrease in reaction times and without the occurrence of secondary reactions. In a similar fashion, a copolymer of styrene and chloromethyl styrene was quaternized with tributyl amine to serve as phase transfer catalyst [91].

When a polymeric nucleophile such as poly(vinylalcohol) is used, hydrogels can be prepared directly from suitable precursor polymers such as PAA or poly(methyl vinyl ether-*alt*-maleic anhydride), taking advantage of the excellent microwave absorption of water [92]. Irradiation of appropriate combinations of polymers in aqueous solutions directly resulted in sterile hydrogels with high swelling ratios, which did not require further purification steps because the use of monomers could be omitted during the synthetic approach.

4.3 Hydrolysis of Poly(2-Oxazoline)s

PEI represents the "gold standard" for non-viral gene transfection and, thus, is of major importance in pharmaceutical research [93, 94]. However, the direct polymerization of its monomer aziridin results in the formation of branched polymers. Thus, linear PEIs (LPEIs) with defined molar masses are usually prepared by hydrolysis of its *N*-acyl derivatives, i.e., poly(2-oxazoline)s (POx). Although the required time for acidic hydrolysis ranges from a few hours to several days under conventional heating (depending on the substituent of the POx), the alkaline hydrolysis is even slower. Because drastic reaction conditions are frequently applied, intensive investigations have been carried out regarding the use of microwave-assisted synthetic approaches under several hydrolysis conditions to accelerate this type of reaction (Table 4).

The first reports relied on the use of the hydrophilic POx, i.e., poly(2-methyl-2-oxazoline) (PMeOx) and poly(2-ethyl-2-oxazoline) (PEtOx) [95]. Thereby, kinetic investigations during the microwave-assisted acidic hydrolysis revealed that 2 h were sufficient to reach conversions above 90%, even for the slightly more hydrophobic PEtOx. Subsequent optimization of the hydrolysis and purification

Table 4 Overview of microwave-assisted hydrolysis of poly(2-oxazoline)s

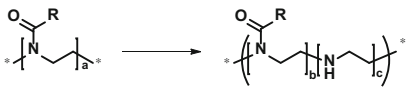

Starting (co-) polymer	R_1	R_2	a (units)	Ox_1:Ox_2: EI (%)[a]	Hydrolysis conditions	References
Homo	CH_3	–	5–200	1:99	HCl (16 wt%), 100 °C	[95]
	C_2H_5					
Homo	C_2H_5	–	10–200	1:99	HCl (16 wt%), 130 °C	[96]
Homo	C_2H_5	–	30, 500	5:95	HCl (3 wt%), 180 °C	[97]
Statistical	CH_3	C_6H_5	$a_1 = 60$ $a_2 = 40$	0:2:98	HCl (16 wt%), 100 °C	[98]
				20:21:59	NaOH	
Block				0:16:84	HCl (16 wt%), 100 °C	
				23:36:42	NaOH	
Homo	CH_3	–	100	5:95	HCl (12 wt%), 100 °C, EtOH:H_2O 4:1	[99]
	C_2H_5			68:22		
	C_6H_5			87:13		
Block	CH_3	C_2H_5	$a_1 = 50$ $a_2 = 50$	15:37:48		
		C_6H_5	$a_1 = 60$ $a_2 = 15$	4:18:78		
Homo	C_2H_5	–	100	5:95	HCl (16 wt%), 160 °C	[100]
	n-C_9H_{19}			13:87		

[a]The maximum degree of hydrolysis can be determined only within the limits of the ^{1}H NMR accuracy

procedure proved that even a reaction time of 1 h is sufficient if the reaction is performed at 130 °C [96]. An effective way to accelerate further the hydrolysis of PEtOx is to increase the reaction temperature while using comparatively low acid concentrations [97]. Detailed kinetic investigations, along with the determination of the Arrhenius parameters, revealed the best results at 180 °C with a low-concentrated aqueous solution of HCl. Further increase of the temperature resulted in main chain degradation.

The fact that the hydrolysis rate of hydrophilic POx is significantly enhanced compared to hydrophobic POx has been exploited to prepare gradient and block copolymers, where preferentially the hydrophilic block is transformed to PEI [98]. The preferential cleavage of the PMeOx block in block copolymers with poly(2-phenyl-2-oxazoline) (PPhOx) enabled the synthesis of novel PEI-PPhOx copolymers which exhibit thermoresponsive micellization behavior, and, in some cases, pH responsive micellization. Utilizing an ethanol–water mixture, the selectivity of the hydrolysis could be further enhanced, even allowing a certain differentiation of the hydrophilic PMeOx and PEtOx [99]. Similarly, the hydrolysis rate of PEtOx is higher than that of the hydrophobic poly(2-*n*-nonyl-2-oxazoline) under the same conditions, presumably because the *n*-nonyl chains collapse around the

polymer backbone in aqueous HCl [100]. Nevertheless, the degree of hydrolysis of both POx could be well controlled by adjustment of the reaction time. Hence, a range of copolymers with antimicrobial activity was obtained.

4.4 Modification of Polymer End Groups

The fact that many polymers with defined end groups are accessible from living and controlled polymerizations has brought these "tiny" parts of the polymer chains into the focus of research. Although a range of polymers from microwave-assisted polymerizations can be end-functionalized in situ [101, 102], we only discuss end-group modifications here, where microwave-assisted synthesis approaches have actually been applied for the end-group modification (Table 5).

As a prominent polymer for life science applications, PEO and its copolymer with propylene oxide, PEO-*b*-PPO, have long been commercially available with hydroxyl end groups and with various architectures. Hence, these precursors are often applied to introduce further functionalities. In a two-step microwave-assisted approach, PEO-OH was functionalized with piperazinyl and diazepanyl moieties to serve as support for further preparation of guanidium derivatives [103].

PEO-diol and star-shaped PEO were also easily and quickly functionalized with methacrylate moieties on both end groups. The very simple and well described microwave-assisted procedure can also be adapted for functionalization of the *N*-termini of peptides [104]. The attachment of glucose to the end groups of PEO-*b*-PPO-*b*-PEO via microwave-assisted ring-opening of the sugar's lactone represents another example where microwave synthesizers were applied successfully for a reaction that typically requires high temperatures [105].

Bromo end groups derived from atom transfer radical polymerization (ATRP) or from the synthesis of polythiophenes represent another type of end functionality that has been further functionalized using microwave-assisted approaches. Thus, telechelic PS and poly(methyl methacrylate) functionalized with C_{60} were prepared with an increased degree of functionalization in comparison to conventional heating, both polymer types remaining intact [106]. The coupling of highly regioregular poly(thiophene)-based multiblock copolymers can also be achieved and improved under microwave conditions taking advantage of active nickel complexes present as end groups of the individual blocks [107].

The azide-alkyne 1,3-dipolar cycloaddition has become a valuable tool in synthetic polymer chemistry. Microwave-assisted approaches make use of its versatility for step-growth polymerizations [110, 111], for dendrimer synthesis [112, 113], and for monomer preparation [114]. In terms of modification of polymer end groups, alkyne functional PCL has been utilized to synthesize star-shaped PCL with a β-cyclodextrin core via microwave-assisted "click" chemistry in a core-first approach [108]. The same PCL was also coupled to 3,6-di(pyridine-2-yl)pyridazine via a Diels–Alder reaction with inverse-electron-demand to give access to [2 × 2] grid-like metal complexes.

Table 5 Overview of microwave-assisted polymer end-group modifications

Polymer	Functional unit	Solvent, catalyst	Microwave		References
			t (min)	T/Power	
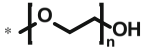	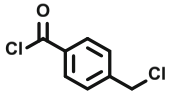	Toluene pyridine	10	200	[103]
	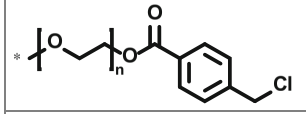	CH_2Cl_2	5	120 W	
	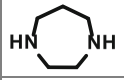				
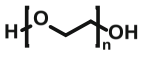	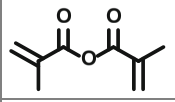	–	5	Max	[104]
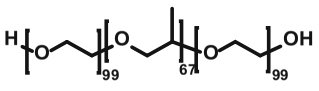	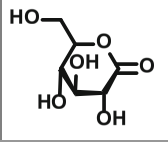	DMF, $Sn(Oct)_2$	15	90–270 W	[105]

(continued)

Table 5 (continued)

Polymer	Functional unit	Solvent, catalyst	Microwave		References
			t (min)	T/Power	
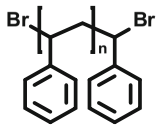		Toluene, DMF	20	300 W	[106]
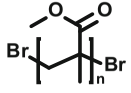		CuBr, bipy	15		
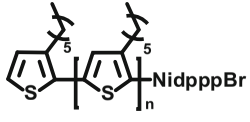	–	THF	10	120 °C	[107]
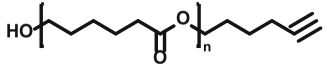	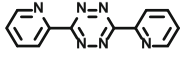		150	150 °C	[108]
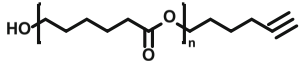	β-Cyclodextrin–N_3	DMF, Cu_2SO_4, Na-ascorbate	15	100 °C	
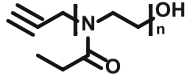	Surface–N_3	H_2O, EtOH, Cu_2SO_4, Na-ascorbate	15–25	120 °C	[109]

Microwave-assisted "click" chemistry on polymer end groups is not limited to reactions in solution. Relying on the azide-alkyne 1,3-dipolar cycloaddition, propargyl-end functional PEtOx was coupled to surfaces functionalized with azide-carrying monolayers in a microwave setup modified to fit silicon substrates inside the common reaction vessels [109]. Vice versa, silica surfaces with an immobilized polymer, i.e., poly(PEO-methacrylate) tethered with both azide and alkyne moieties obtained from surface-initiated ATRP, were subjected to this type of reaction with small molecules as counterparts to functionalize the surfaces further [115].

4.5 Modification of Polymeric Resins

Merrifield resins represent very common substrates for a wide range of reactions on solid polymeric supports and are well known, for instance, in the field of solid phase peptide synthesis. Consisting of crosslinked PS with varying fractions of incorporated chloromethyl styrene, the benzyl chloride groups provide the reactive positions prone to attack by nucleophiles.

Microwave-assisted heating proved superior in comparison to conventional heating during the conversion of the resin's chloride functionalities with PEO under alkaline conditions [116]. Even in 2 min, higher DS values of the resin were achieved than after 35 min during conventional heating, although the thermal degradation of the PEO was significantly reduced. Amines are the more common nucleophiles used with Merrifield resins, but thiols and imidazoles were also immobilized via microwave-assisted approaches [117]. Careful investigations of the obtained products from immobilization of *N*-methyl-D-glucanamine revealed that chemistry using microwave synthesizers is not superior to conventional methods in any case, a fact which is often disregarded upon selling novel synthetic approaches [118]. However, the direct volumetric heating and the possibility to work at higher temperatures than the boiling points of the solvents certainly are advantages which can help to improve reaction times and homogeneity. As such, microwave-assisted synthesis protocols can be very effective during the synthesis of peptides if the reaction conditions are thoroughly adjusted [119]. This also enables the custom-made synthesis of specially designed glycopeptides in a much faster fashion than under conventional heating [120, 121].

5 Summary, Conclusions, and Outlook

Since microwave synthesizers have found their way into synthetic chemical laboratories, a wide range of natural and synthetic polymers have been subjected to microwave-assisted modification reactions. However, the way these heating sources are applied has significantly changed since the 1990s. The pioneers had

to rely on household microwave ovens or self-built equipment and merely compared the properties of modified polymers derived from microwave-supported heating to those obtained by established synthesis protocols. In contrast, the modern microwave synthesizers allow a detailed adjustment and control of temperature and power, so that many microwave-assisted polymer modification reactions are performed nowadays using optimized synthesis protocols that could be established. In those fields, microwave synthesizers are recognized as common synthetic tools because of advantages such as fast and homogenous heating, the possibility to perform reactions at high temperatures and under pressure, and their ease of handling.

Other fields of research still struggle with the identification of optimum reaction conditions and questions of special microwave effects beyond more effective heating. Unfortunately, some of these investigations tend to lack critical judgment of the chemistry performed and merely highlight the systematic workflows applied. However, also in these fields detailed structural investigations of the products obtained will lead to reasonable synthetic approaches so that microwave synthesizers will become standard equipment for more synthetic polymer chemists in the future.

On the other hand, selective heating of, for example, conjugated polymers by microwave irradiation has opened non-classical opportunities in materials science. Hence, more developments of novel nanomaterials prepared from polymers via microwave-assisted approaches are to be discovered in this still vital field of research.

Acknowledgement The authors acknowledge the Carl-Zeiss-Foundation and the Thuringian Ministry of Economic Affairs, Science and Digital Society (TMWWdG).

References

1. Fang L, Han G, Zhang H (2015) Microwave-assisted free radical polymerizations. Adv Polym Sci. doi:10.1007/12_2013_276
2. Fimberger M, Wiesbrock F (2015) Microwave-assisted synthesis of polyesters and polyamides by ring-opening polymerization. Adv Polym Sci. doi:10.1007/12_2014_293
3. Luef KP, Hoogenboom R, Schubert US, Wiesbrock F (2015) Microwave-assisted cationic ring-opening polymerization of 2-oxazolines. Adv Polym Sci. doi:10.1007/12_2015_340
4. Mallakpour S, Zadehnazari A (2013) Microwave-assisted step-growth polymerizations (From polycondensation to C–C coupling). Adv Polym Sci. doi:10.1007/12_2013_275
5. Reynaud S, Grassl B (2015) Microwave-assisted controlled radical polymerization. Adv Polym Sci. doi:10.1007/12_2014_302
6. Ibrahim NA, Abou Elmaaty TM, Eid BM, Abd El-Aziz E (2013) Combined antimicrobial finishing and pigment printing of cotton/polyester blends. Carbohydr Polym 95:379–388
7. Jacquot C, Jacquot M, Marques P, Jasniewski J, Akhtar MJ, Didelot A-S, Desobry S (2014) Influence of microwave heating time on the structure and properties of chitosan films. J Appl Polym Sci 131:40779
8. Felix J, Gatenholm P, Schreiber HP (1994) Plasma modification of cellulose fibers – effects on some polymer composite properties. J Appl Polym Sci 51:285–295

9. Dinesh M, Chikkakuntappa R (2013) Microwave irradiation induced modifications on the interfaces in SAN/EVA/PVC and PVAc/BPA/PVP ternary polymer blends: positron lifetime study. Nucl Instrum Meth B 310:67–74
10. Manjula MK, Rai KML, Raj JM, Siddaramaiah CSM, Ranganathaiah C (2010) Microwave assisted improvement in physico-mechanical properties of poly(vinyl alcohol)/poly(ethylene imine)/gelatin blends. J Polym Res 17:89–98
11. Raj JM, Altaweel AMAM, Chandrashekara MN, Ramya P, Ravikumar HB, Ranganathaiah C (2011) An effective tool to characterize adhesion at the interface of binary polymer blends: a free volume study. J Polym Eng 31:93–96
12. Raj JM, Ranganathaiah C (2009) A new method of stabilization and characterization of the interface in binary polymer blends by irradiation: a positron annihilation study. J Polym Sci B Polym Phys 47:619–632
13. Raj JM, Ranganathaiah C, Ganesh S (2008) Interfacial modifications in PS/PMMA and PVC/EVA blends by e-beam and microwave irradiation: a free volume study. Polym Eng Sci 48:1495–1503
14. Mitra S, Chandra S, Kundu T, Banerjee R, Pramanik P, Goswami A (2012) Rapid microwave synthesis of fluorescent hydrophobic carbon dots. RSC Adv 2:12129–12131
15. Qin X, Lu W, Asiri AM, Al-Youbi AO, Sun X (2013) Microwave-assisted rapid green synthesis of photoluminescent carbon nanodots from flour and their applications for sensitive and selective detection of mercury(II) ions. Sens Actuator B Chem 184:156–162
16. Liu Y, Xiao N, Gong N, Wang H, Shi X, Gu W, Ye L (2014) One-step microwave-assisted polyol synthesis of green luminescent carbon dots as optical nanoprobes. Carbon 68:258–264
17. Wei W, Xu C, Wu L, Wang J, Ren J, Qu X (2014) Non-enzymatic-browning-reaction: a versatile route for production of nitrogen-doped carbon dots with tunable multicolor luminescent display. Sci Rep 4:3564
18. Bairi VG, Bourdo SE, Nasini UB, Ramasahayam SK, Watanabe F, Berry BC, Viswanathan T (2013) Microwave-assisted synthesis of nitrogen and phosphorus co-doped mesoporous carbon and their potential application in alkaline fuel cells. Sci Adv Mater 5:1275–1281
19. Harris AT, Deshpande S, Kefeng X (2009) Synthesis of graphitic carbon particle chains at low temperatures under microwave irradiation. Mater Lett 63:1390–1392
20. Schwenke AM, Hoeppener S, Schubert US (2015) Synthesis and modification of carbon nanomaterials utilizing microwave heating. Adv Mater 27:4113–4141
21. Zhang X, Liu Z (2012) Recent advances in microwave initiated synthesis of nanocarbon materials. Nanoscale 4:707–714
22. Zhang X, Manohar SK (2006) Microwave synthesis of nanocarbons from conducting polymers. Chem Commun 2477–2479
23. Kim S-Y, Kim SY, Lee S, Jo S, Im Y-H, Lee H-S (2015) Microwave plasma carbonization for the fabrication of polyacrylonitrile-based carbon fiber. Polymer 56:590–595
24. Wang C, Ma D, Bao X (2008) Transformation of biomass into porous graphitic carbon nanostructures by microwave irradiation. J Phys Chem C 112:17596–17602
25. Xu Z, Li H, Li W, Cao G, Zhang Q, Li K, Fu Q, Wang J (2011) Large-scale production of graphene by microwave synthesis and rapid cooling. Chem Commun 47:1166–1168
26. Bello-Perez LA, Roger P, Baud B, Colonna P (1998) Macromolecular features of starches determined by aqueous high-performance size exclusion chromatography. J Cereal Sci 27: 267–278
27. Klingler R, Busch KG, Vahedi B (1997) Acid modification of starch in a semi-dry process. Starch 49:391–395
28. Vitz J, Erdmenger T, Haensch C, Schubert US (2009) Extended dissolution studies of cellulose in imidazolium based ionic liquids. Green Chem 11:417–424
29. Jaworska MM, Kozlecki T, Gorak A (2012) Review of the application of ionic liquids as solvents for chitin. J Polym Eng 32:67–69

30. Qin Y, Lu X, Sun N, Rogers RD (2010) Dissolution or extraction of crustacean shells using ionic liquids to obtain high molecular weight purified chitin and direct production of chitin films and fibers. Green Chem 12:968–971
31. Wang J, Chen C (2014) Chitosan-based biosorbents: modification and application for biosorption of heavy metals and radionuclides. Bioresour Technol 160:129–141
32. Illy N, Robitzer M, Auvergne R, Caillol S, David G, Boutevin B (2014) Synthesis of water-soluble allyl-functionalized oligochitosan and its modification by thiol-ene addition in water. J Polym Sci Part A Polym Chem 52:39–48
33. Shao J, Yang Y, Zhong Q (2003) Studies on preparation of oligoglucosamine by oxidative degradation under microwave irradiation. Polym Degrad Stab 82:395–398
34. Sun T, Zhou D, Xie J, Mao F (2007) Preparation of chitosan oligomers and their antioxidant activity. Eur Food Res Technol 225:451–456
35. Zhou G, Yao W, Wang C (2006) Kinetics of microwave degradation of λ-carrageenan from Chondrus ocellatus. Carbohydr Polym 64:73–77
36. Tang F, Chen F, Li F (2013) Preparation and potential in vivo anti-influenza virus activity of low molecular-weight kappa-carrageenans and their derivatives. J Appl Polym Sci 127: 2110–2115
37. Lukasiewicz M, Kowalski S (2012) Low power microwave-assisted enzymatic esterification of starch. Starch 64:188–197
38. Koroskenyi B, McCarthy S (2002) Microwave-assisted solvent-free or aqueous-based synthesis of biodegradable polymers. J Polym Environ 10:93–104
39. Shogren RL, Biswas A (2006) Preparation of water-soluble and water-swellable starch acetates using microwave heating. Carbohyd Polym 64:16–21
40. Soetaredjo FE, Ismadji S, Huynh LH, Kasim NS, Tran-Thi NY, Ayucitra A, Ju Y-H (2012) Facile preparation of sago starch esters using full factorial design of experiment. Starch 64: 590–597
41. Possidonio S, Fidale LC, El Seoud OA (2010) Microwave-assisted derivatization of cellulose in an ionic liquid: an efficient, expedient synthesis of simple and mixed carboxylic esters. J Polym Sci A Polym Chem 48:134–143
42. Li J, Zhang L-P, Peng F, Bian J, Yuan T-Q, Xu F, Sun R-C (2009) Microwave-assisted solvent-free acetylation of cellulose with acetic anhydride in the presence of iodine as a catalyst. Molecules 14:3551
43. Calce E, Bugatti V, Vittoria V, De Luca S (2012) Solvent-free synthesis of modified pectin compounds promoted by microwave irradiation. Molecules 17:12234–12242
44. Čížová A, Sroková I, Sasinková V, Malovíková A, Ebringerová A (2008) Carboxymethyl starch octenylsuccinate: microwave- and ultrasound-assisted synthesis and properties. Starch 60:389–397
45. Xu F, Jiang J-X, Sun R-C, She D, Peng B, Sun J-X, Kennedy JF (2008) Rapid esterification of wheat straw hemicelluloses induced by microwave irradiation. Carbohydr Polym 73:612–620
46. Ren J-L, Xu F, Sun R-C, Peng B, Sun J-X (2008) Studies of the lauroylation of wheat straw hemicelluloses under heating. J Agric Food Chem 56:1251–1258
47. Suchaiya V, Aht-Ong D (2014) Microwave-assisted modification of cellulose as a compatibilizer for PLA and MCC biocomposite film: effects of side chain length and content on mechanical and thermal properties. Polym Polym Compos 22:613–624
48. Aime S, Gianolio E, Uggeri F, Tagliapietra S, Barge A, Cravotto G (2006) New paramagnetic supramolecular adducts for MRI applications based on non-covalent interactions between Gd (III)-complexes and beta- or gamma-cyclodextrin units anchored to chitosan. J Inorg Biochem 100:931–938
49. Chaudhary JP, Kondaveeti S, Gupta V, Prasad K, Meena R (2014) Preparation and functional evaluation of agarose derivatives. J Appl Polym Sci 131:40630
50. Peng X-W, Ren J-L, Zhong L-X, Cao X-F, Sun R-C (2011) Microwave-induced synthesis of carboxymethyl hemicelluloses and their rheological properties. J Agric Food Chem 59: 570–576

51. Kondaveeti S, Mehta GK, Siddhanta AK (2014) Modification of agarose: 6-aminoagarose mediated syntheses of fluorogenic pyridine carboxylic acid amides. Carbohydr Polym 106: 365–373
52. Sardo C, Farra R, Licciardi M, Dapas B, Scialabba C, Giammona G, Grassi M, Grassi G, Cavallaro G (2015) Development of a simple, biocompatible and cost-effective inulin-diethylenetriamine based siRNA delivery system. Eur J Pharm Sci 75:60–71
53. Liu L, Li Y, Li Y, Fang Y-E (2004) Rapid N-phthaloylation of chitosan by microwave irradiation. Carbohydr Polym 57:97–100
54. Petit C, Reynaud S, Desbrieres J (2015) Amphiphilic derivatives of chitosan using microwave irradiation. Toward an eco-friendly process to chitosan derivatives. Carbohydr Polym 116:26–33
55. Radwan AA, Alanazi FK, Alsarra IA (2010) Microwave irradiation-assisted synthesis of a novel crown ether crosslinked chitosan as a chelating agent for heavy metal ions (M + n). Molecules 15:6257
56. Ge H, Huang S (2010) Microwave preparation and adsorption properties of EDTA-modified cross-linked chitosan. J Appl Polym Sci 115:514–519
57. Cao Z, Ge H, Lai S (2001) Studies on synthesis and adsorption properties of chitosan cross-linked by glutaraldehyde and Cu(II) as template under microwave irradiation. Eur Polym J 37:2141–2143
58. Mondal K, Mehta P, Gupta MN (2004) Affinity precipitation of Aspergillus niger pectinase by microwave-treated alginate. Protein Expr Purif 33:104–109
59. Diaz-Visurraga J, Daza C, Pozo C, Becerra A, von Plessing C, Garcia A (2012) Study on antibacterial alginate-stabilized copper nanoparticles by FT-IR and 2D-IR correlation spectroscopy. Int J Nanomedicine 7:3597–3612
60. Chhatbar MU, Meena R, Prasad K, Chejara DR, Siddhanta AK (2011) Microwave-induced facile synthesis of water-soluble fluorogenic alginic acid derivatives. Carbohydr Res 346: 527–533
61. Sanandiya ND, Siddhanta AK (2013) Facile synthesis of a new fluorogenic metal scavenging interpolymeric diamide based on cellulose and alginic acids. Carbohydr Res 381:93–100
62. Grabowska B, Sitarz M, Olejnik E, Kaczmarska K (2015) FT-IR and FT-Raman studies of cross-linking processes with Ca2+ ions, glutaraldehyde and microwave radiation for polymer composition of poly(acrylic acid)/sodium salt of carboxymethyl starch – part I. Spectrochim Acta A 135:529–535
63. Tomanová V, Pielichowski K, Sroková I, Žoldaková A, Sasinková V, Ebringerová A (2008) Microwave-assisted synthesis of carboxymethylcellulose – based polymeric surfactants. Polym Bull 60:15–25
64. Singh V, Kumar P, Sanghi R (2012) Use of microwave irradiation in the grafting modification of the polysaccharides - a review. Prog Polym Sci 37:340–364
65. Lin N, Chen G, Huang J, Dufresne A, Chang PR (2009) Effects of polymer-grafted natural nanocrystals on the structure and mechanical properties of poly(lactic acid): a case of cellulose whisker-graft-polycaprolactone. J Appl Polym Sci 113:3417–3425
66. Feng L, Zhou Z, Dufresne A, Huang J, Wei M, An L (2009) Structure and properties of new thermoforming bionanocomposites based on chitin whisker-graft-polycaprolactone. J Appl Polym Sci 112:2830–2837
67. Liu L, Li Y, Fang Y, Chen LX (2005) Microwave-assisted graft copolymerization of epsilon-caprolactone onto chitosan via the phthaloyl protection method. Carbohydr Polym 60: 351–356
68. Das R, Das D, Ghosh P, Ghosh A, Dhara S, Panda AB, Pal S (2015) Novel pH-responsive graft copolymer based on HPMC and poly(acrylamide) synthesised by microwave irradiation: application in controlled release of ornidazole. Cellulose 22:313–327
69. Meenkashi, Ahuja M, Verma P (2014) MW-assisted synthesis of carboxymethyl tamarind kernel polysaccharide-g-polyacrylonitrile: optimization and characterization. Carbohyd Polym 113:532–538

70. Yiğitoğlu M, Aydın G, Işıklan N (2014) Microwave-assisted synthesis of alginate-g-polyvinylpyrrolidone copolymer and its application in controlled drug release. Polym Bull 71:385–414
71. Kalia S, Sheoran R (2011) Modification of ramine fibers using microwave-assisted and cellulase enzyme-assisted biopolishing: a comparative study of morphology, thermal stability, and crystallinity. Int J Polym Anal Ch 16:307–318
72. Kalia S, Vashistha S (2012) Surface modification of sisal fibers (Agave sisalana) using bacterial cellulase and methyl methacrylate. J Polym Environ 20:142–151
73. Thakur VK, Thakur MK, Gupta RK (2013) Graft copolymers from cellulose: synthesis, characterization and evaluation. Carbohydr Polym 97:18–25
74. Sorour MH, El Sayed MM, Abd El Moneem NM, Talaat HA, Shaalan HF, El Marsafy SM (2013) Process and financial considerations pertinent to hydrogel manufacture. Starch 65:527–534
75. Sorour M, El-Sayed M, Abd El Moneem N, Talaat HA, Shalaan H, El Marsafy S (2013) Characterization of hydrogel synthesized from natural polysaccharides blend grafted acrylamide using microwave (MW) and ultraviolet (UV) techniques. Starch 65:172–178
76. Wei X, Chang G, Li J, Wang F, Cui L, Fu T, Kong L (2014) Preparation of pH- and salinity-responsive cellulose copolymer in ionic liquid. J Polym Res 21:535
77. Likhitha M, Sailaja RRN, Priyambika VS, Ravibabu MV (2014) Microwave assisted synthesis of guar gum grafted sodium acrylate/cloisite superabsorbent nanocomposites: reaction parameters and swelling characteristics. Int J Biol Macromol 65:500–508
78. Mallakpour SE, Hajipour AR, Mahdavian AR, Zadhoush A, Ali-Hosseini F (2001) Microwave assisted oxidation of polyethylene under solid-state conditions with potassium permanganate. Eur Polym J 37:1199–1206
79. Sulkowski WW, Wolinska A, Sulkowska A, Nowak K, Bogdal D (2008) Sulphonation of expanded polystyrene waste under microwave irradiation. E Polymers 7:65–71
80. Monteil C, Bar N, Moreau B, Retoux R, Bee A, Talbot D, Villemin D (2014) Phosphonated polyethylenimine-coated nanoparticles: size- and zeta-potential-adjustable nanomaterials. Part Part Syst Charact 31:219–227
81. Arslan M, Gok O, Sanyal R, Sanyal A (2014) Clickable poly(ethylene glycol)-based copolymers using azide-alkyne click cycloaddition-mediated step-growth polymerization. Macromol Chem Phys 215:2237–2247
82. Huy HT, Buu TN, Dung TTK, Han TN, VanQuang P (1996) Fixation of alpha-naphthyl acetic acid onto epoxidized liquid natural rubber in microwave reactor (monomode system). J Macromol Sci Pure Appl Chem 1957–1962
83. Hurduc N, Buisine JM, Decock P, Talewee J, Surpateanu G (1996) Influence of microwaves irradiation on modification of oxetane based polymers with 4-(2-amino-ethyl)morpholine. Polym J 28:550–552
84. Baudel V, Cazier F, Woisel P, Surpateanu G (2002) Synthesis and modification of oxetane based oligomers with 3-ethoxypropylamine by focused microwave irradiation. Eur Polym J 38:615–618
85. Kretschmann O, Schmitz S, Ritter H (2007) Microwave-assisted synthesis of associative hydrogels. Macromol Rapid Commun 28:1265–1269
86. Bezdushna E, Ritter H (2007) Microwave-assisted esterification of methacrylic acid and polymer-analogous esterification of poly[ethylene-co-(acrylic acid)] with dissimilar phenols. Macromol Rapid Commun 28:443–448
87. Sinnwell S, Ritter H (2007) Microwave assisted hydroxyalkylamidation of poly(ethylene-co-acrylic acid) and formation of grafted poly(ϵ-caprolactone) side chains. J Polym Sci A Polym Chem 45:3659–3667
88. Bezdushna E, Ritter H (2008) Microwave promoted polymer analogous amidation and esterification of poly(ether sulfone) bearing free carboxylic groups. Macromol Chem Phys 209:1942–1947

89. Dickmeis M, Ritter H (2009) Microwave-assisted modification of poly(vinylimidazolium salts) via N, N-dimethylformamide decomposition. Macromol Chem Phys 210:776–782
90. Lamanna M, D'Accorso N (2011) New copolymers with heterocyclic pendant groups obtained from PVC using microwave-assisted process. J Appl Polym Sci 121:951–956
91. Chen ZX, Xu GY, Yang GC, Wang W (2004) Preparation of non-cross-linked polystyrene-supported quaternary ammonium salts and use as phase transfer catalysts under microwave. React Funct Polym 61:139–146
92. Cook JP, Goodall GW, Khutoryanskaya OV, Khutoryanskiy VV (2012) Microwave-assisted hydrogel synthesis: a new method for crosslinking polymers in aqueous solutions. Macromol Rapid Commun 33:332–336
93. Englert C, Tauhardt L, Hartlieb M, Kempe K, Gottschaldt M, Schubert US (2014) Linear poly (ethylene imine)-based hydrogels for effective binding and release of DNA. Biomacromolecules 15:1124–1131
94. Rinkenauer AC, Vollrath A, Schallon A, Tauhardt L, Kempe K, Schubert S, Fischer D, Schubert US (2013) Parallel high-throughput screening of polymer vectors for nonviral gene delivery: evaluation of structure–property relationships of transfection. ACS Comb Sci 15: 475–482
95. Lambermont-Thijs HM, van der Woerdt FS, Baumgaertel A, Bonami L, Du Prez FE, Schubert US, Hoogenboom R (2009) Linear poly (ethylene imine)s by acidic hydrolysis of poly(2-oxazoline)s: kinetic screening, thermal properties, and temperature-induced solubility transitions. Macromolecules 43:927–933
96. Tauhardt L, Kempe K, Knop K, Altuntas E, Jaeger M, Schubert S, Fischer D, Schubert US (2011) Linear polyethyleneimine: optimized synthesis and characterization - on the way to "pharmagrade" batches. Macromol Chem Phys 212:1918–1924
97. de la Rosa VR, Bauwens E, Monnery BD, De Geest BG, Hoogenboom R (2014) Fast and accurate partial hydrolysis of poly(2-ethyl-2-oxazoline) into tailored linear polyethylenimine copolymers. Polym Chem 5:4957–4964
98. Lambermont-Thijs HML, Heuts JPA, Hoeppener S, Hoogenboom R, Schubert US (2011) Selective partial hydrolysis of amphiphilic copoly(2-oxazoline)s as basis for temperature and pH responsive micelles. Polym Chem 2:313–322
99. van Kuringen HPC, de la Rosa VR, Fijten MWM, Heuts JPA, Hoogenboom R (2012) Enhanced selectivity for the hydrolysis of block copoly(2-oxazoline)s in ethanol–water resulting in linear poly(ethylene imine) copolymers. Macromol Rapid Commun 33:827–832
100. Kelly AM, Kaltenhauser V, Mühlbacher I, Rametsteiner K, Kren H, Slugovc C, Stelzer F, Wiesbrock F (2013) Poly(2-oxazoline)-derived contact biocides: contributions to the understanding of antimicrobial activity. Macromol Biosci 13:116–125
101. Tauhardt L, Frant M, Pretzel D, Hartlieb M, Bucher C, Hildebrand G, Schroter B, Weber C, Kempe K, Gottschaldt M, Liefeith K, Schubert US (2014) Amine end-functionalized poly (2-ethyl-2-oxazoline) as promising coating material for antifouling applications. J Mater Chem B 2:4883–4893
102. Weber C, Czaplewska JA, Baumgaertel A, Altuntas E, Gottschaldt M, Hoogenboom R, Schubert US (2012) A sugar decorated macromolecular bottle brush by carbohydrate-initiated cationic ring-opening polymerization. Macromolecules 45:46–55
103. Chen C-H, Tung C-L, Sun C-M (2012) Microwave-assisted synthesis of highly functionalized guanidines on soluble polymer support. Tetrahedron Lett 53:3959–3962
104. Van Hove AH, Wilson BD, Benoit DSW (2013) Microwave-assisted functionalization of poly(ethylene glycol) and on-resin peptides for use in chain polymerizations and hydrogel formation. J Vis Exp 80, e50890
105. Glisoni RJ, Sosnik A (2014) Novel poly(ethylene oxide)-b-poly(propylene oxide) copolymer-glucose conjugate by the microwave-assisted ring opening of a sugar lactone. Macromol Biosci 14:1639–1651
106. Wu H, Li F, Lin Y, Yang M, Chen W, Cai R (2006) Synthesis of telechelic C60 end-capped polymers under microwave irradiation. J Appl Polym Sci 99:828–834

107. Ouhib F, Desbief S, Lazzaroni R, De Winter J, Gerbaux P, Jerome C, Detrembleur C (2012) Thermally induced coupling of poly(thiophene)-based block copolymers prepared by Grignard metathesis polymerization: a straightforward route toward highly regioregular multiblock conjugated copolymers. Macromolecules 45:6796–6806
108. Hoogenboom R, Moore BC, Schubert US (2006) Synthesis of star-shaped poly(ε-caprolactone) via "click" chemistry and "supramolecular click" chemistry. Chem Commun 4010–4012
109. Haensch C, Erdmenger T, Fijten MWM, Hoeppener S, Schubert US (2009) Fast surface modification by microwave assisted click reactions on silicon substrates. Langmuir 25: 8019–8024
110. Gloecklhofer F, Lumpi D, Kohlstaedt M, Yurchenko O, Wuerfel U, Froehlich J (2015) Towards continuous junction (CJ) organic electronic devices: fast and clean post-polymerization modification by oxidation using dimethyldioxirane (DMDO). React Funct Polym 86:16–26
111. Gloecklhofer F, Lumpi D, Stoeger B, Froehlich J (2014) Multigram synthesis of bis (trimethylsilyl)ethynyl benzenes suitable for post-polymerization modification. New J Chem 38:2229–2232
112. Malkoch M, Schleicher K, Drockenmuller E, Hawker CJ, Russell TP, Wu P, Fokin VV (2005) Structurally diverse dendritic libraries: a highly efficient functionalization approach using click chemistry. Macromolecules 38:3663–3678
113. Rijkers DTS, van Esse GW, Merkx R, Brouwer AJ, Jacobs HJF, Pieters RJ, Liskamp RMJ (2005) Efficient microwave-assisted synthesis of multivalent dendrimeric peptides using cycloaddition reaction (click) chemistry. Chem Commun 4581–4583
114. Trellenkamp T, Ritter H (2010) Poly(N-vinylpyrrolidone) bearing covalently attached cyclodextrin via click-chemistry: synthesis, characterization, and complexation behavior with phenolphthalein. Macromolecules 43:5538–5543
115. Liu X, Zheng H-N, Ma Y-Z, Yan Q, Xiao S-J (2011) Microwave irradiated click reactions on silicon surfaces via derivertization of covalently grafted poly(PEGMA) brushes. J Colloid Interface Sci 358:116–122
116. Yaylayan VA, Siu M, Belanger JMR, Pare JRJ (2002) Microwave-assisted PEGylation of Merrifield resins. Tetrahedron Lett 43:9023–9025
117. Pilsniak M, Trochimczuk AW (2007) Synthesis and characterization of polymeric resins with aliphatic and aromatic amino ligands and their sorption behavior towards gold from ammonium hydroxide solutions. React Funct Polym 67:1570–1576
118. Wolska J, Bryjak M (2011) Preparation of polymeric microspheres for removal of boron by means of sorption-membrane filtration hybrid. Desalination 283:193–197
119. Matsushita T, Hinou H, Kurogochi M, Shimizu H, Nishimura S-I (2005) Rapid microwave-assisted solid-phase glycopeptide synthesis. Org Lett 7:877–880
120. Izumi R, Matsushita T, Fujitani N, Naruchi K, Shimizu H, Tsuda S, Hinou H, Nishimura S-I (2013) Microwave-assisted solid-phase synthesis of antifreeze glycopeptides. Chem Eur J 19: 3913–3920
121. Matsushita T, Hinou H, Fumoto M, Kurogochi M, Fujitani N, Shimizu H, Nishimura S-I (2006) Construction of highly glycosylated mucin-type glycopeptides based on microwave-assisted solid-phase syntheses and enzymatic modifications. J Org Chem 71:3051–3063

PUBLICATION 5

3rd generation poly(ethylene imine)s for gene delivery

T. Bus,‡ C. Englert,‡ M. Reifarth, P. Borchers, M. Hartlieb, A. Vollrath,
S. Hoeppener, A. Traeger, U. S. Schubert

J. Mater. Chem. B **2017**, *5*, 1258-1274

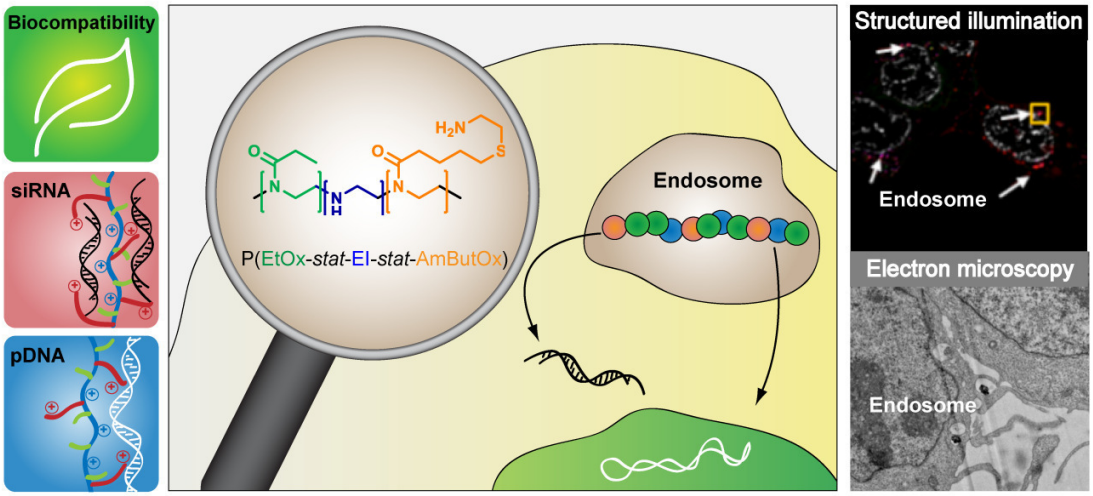

‡ Authors contributed equally.

Journal of Materials Chemistry B

PAPER

View Article Online
View Journal | View Issue

Cite this: J. Mater. Chem. B, 2017, 5, 1258

3rd generation poly(ethylene imine)s for gene delivery†

Tanja Bus,‡[ab] Christoph Englert,‡[ab] Martin Reifarth,[abcd] Philipp Borchers,[ab] Matthias Hartlieb,§[ab] Antje Vollrath,[ab] Stephanie Hoeppener,[ab] Anja Traeger*[ab] and Ulrich S. Schubert*[ab]

Received 4th October 2016,
Accepted 20th December 2016

DOI: 10.1039/c6tb02592g

www.rsc.org/MaterialsB

Cationic polymers play a crucial role within the field of gene delivery offering the possibility to circumvent (biological) barriers in an elegant way. However, polymers are accompanied either by a high cytotoxicity or low efficiency. In this study, a series of high molar mass poly(2-oxazoline)-based copolymers was synthesized introducing 2-ethyl-2-oxazoline, ethylene imine, and primary amine bearing monomer units representing a new generation of poly(ethylene imine) (PEI). The potential of these modified PEIs as non-viral gene delivery agents was assessed and compared to linear PEI by studying the cytotoxicity, the polyplex characteristics, the transfection efficiency, and the cellular uptake using plasmid DNA (pDNA) as well as small interfering RNA (siRNA). High transfection efficiencies, even in serum containing media, were achieved using pDNA without revealing any cytotoxic effects on the cell viability at concentrations up to 1 mg mL^{-1}. The delivery potential for siRNA was further investigated showing the importance of polymer composition for different genetic materials. To elucidate the origins for this superior performance, super-resolution and electron microscopy of transfected cells were used, identifying the endosomal release of the polymers as well as a reduced protein interaction as the main difference to PEI-based transfection processes. In this respect, the investigated copolymers represent remarkable alternatives as non-viral gene delivery agents.

Introduction

Within the last decades synthetic polymers emerged as versatile tools in the field of gene delivery.[1] They represent promising alternatives to viral vectors or lipid-based, non-viral transfection agents, since they combine the advantages of large scale production, simple storage conditions, and the availability of a variety of architectures with tailored properties, *e.g.* defined molar masses, end groups, and functionalities.[2] The most prominent representative of synthetic, cationic polymers utilized for nucleic acid delivery is the gold standard poly(ethylene imine) (PEI).[3,4] Subdivided into a linear (lPEI) and a branched (bPEI) topology, it reveals one of the highest cationic-charge-densities of all organic macromolecules.[5] Under physiological conditions, every sixth nitrogen (N) is protonated[6] and able to interact with the phosphate groups (P) of deoxyribonucleic acid (DNA) as well as ribonucleic acid (RNA) to form nanoscale interelectrolyte complexes, so-called polyplexes.[7–9]

lPEI offers the benefit to be synthesized by hydrolysis of poly(2-alkyl-2-oxazoline)s (POx) using a living polymerization process resulting in well-defined structures.[10] However, these advantages are accompanied by a severe cytotoxicity and undesired non-specific interactions with cellular and non-cellular components, both *in vitro* and *in vivo*.[11–13] Various attempts have been made to optimize PEI by focusing on the design of biodegradable[14–16] and biocompatible[17,18] derivatives, which represent the 2nd generation of PEI-based polymers. Carbohydrates, *e.g.* dextran[19] or hydroxyethyl starch (HES),[20] as well as stealth polymers like poly(ethylene glycol) (PEG)[21,22] are extensively studied.[23] Approaches as the introduction of biodegradable linkers, such as disulfide bonds,[24–26] the combination with liposomes[27,28] or the utilization of micelles or nanoparticles in combination with PEI[29,30] are further concepts partially fulfilling the complex requirements. Besides the post-modification of the PEI backbone, the partial hydrolysis of POx, resulting in P(Ox-*stat*-EI) copolymers, represents a

[a] Laboratory of Organic and Macromolecular Chemistry (IOMC), Friedrich Schiller University Jena, Humboldtstrasse 10, 07743 Jena, Germany. E-mail: ulrich.schubert@uni-jena.de, anja.traeger@uni-jena.de
[b] Jena Center for Soft Matter (JCSM), Friedrich Schiller University Jena, Philosophenweg 7, 07743 Jena, Germany
[c] Institute of Physical Chemistry and Abbe Center of Photonics, Friedrich Schiller University Jena, Helmholtzweg 4, 07743 Jena, Germany
[d] Leibniz Institute of Photonic Technology, Albert-Einstein-Strasse 9, 07745 Jena, Germany

† Electronic supplementary information (ESI) available: Fig. S1–S21. See DOI: 10.1039/c6tb02592g

‡ The authors contributed equally to this work.

§ Current address: Department of Chemistry, University of Warwick, Gibbet Hill Road, Coventry, CV4 7AL, UK.

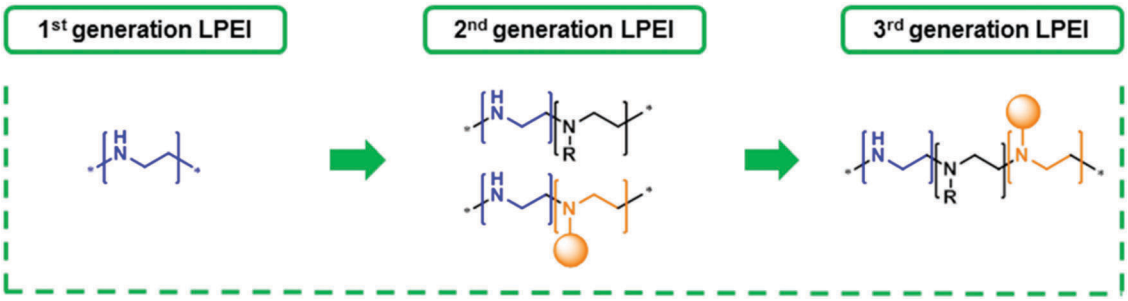

Fig. 1 Overview of different generations of linear poly(ethylene imine) (lPEI). Compared to the original lPEI (1st generation), which has been established over the last decades, the 2nd generation lPEI contains functional monomer units (black or orange) besides the present ethylene imine units (blue). The 3rd generation lPEI describes the presence of multiple functional units comprising cationic functionalities (blue), functional groups to increase cell viability (black) as well as a third group of functionalities (orange, *e.g.* primary amine functionalities or targeting molecules).

promising approach.[31,32] The "stealth behavior" of POx, comparable to PEG, facilitates a reduction of cytotoxicity.[32,33] Although the cytotoxicity problem might be solved, the modifications often result in inefficient gene delivery presumably due to weak DNA complexation and decreased cell interaction.[34] Hence, the design criteria for a perfect polymeric vector are still unknown and other polymer characteristics, *i.e.* the degree of hydrophobicity or synergistic effects of different polycationic species within one polymeric vector, have to be considered.[17,35]

The present contribution focusses on the synthesis of high molar mass copolymers of lPEI and POx. A combination of primary and secondary amines as well as non-charged 2-ethyl-2-oxazoline (EtOx) units was aspired. While different amine species were used to support the polyplex formation, biocompatibility is achieved *via* the integration of EtOx. To realize the synthesis of the targeted polymer structure, a post-polymerization functionalization of partially hydrolyzed high molar mass poly(2-ethyl-2-oxazoline) (PEtOx) was used. The insertion of alkenes is followed by the functionalization *via* thiol–ene click chemistry. This extraordinary combination of modification techniques offers a new platform of copolymers which marks the beginning of a new generation – the 3rd generation of PEI (see Fig. 1).

The designed copolymers were investigated concerning their *in vitro* transfection potential including polyplex characterization, competitor/serum interaction and the cellular uptake mechanism using plasmid DNA as well as siRNA. For a detailed understanding of the mechanism during the gene delivery process super-resolution fluorescence as well as electron microscopy were utilized.

Materials and methods

Materials

2-Ethyl-2-oxazoline (EtOx) and methyl tosylate were obtained from Acros Organics, distilled to dryness (over barium oxide in the case of EtOx), and stored under argon atmosphere. Pyridine, methanol, dichloromethane, 4-*N*,*N*-dimethylaminopyridine (DMAP), 2-(boc-amino)ethanethiol, 2,2-dimethoxy-2-phenylacetophenone (DMPA), trifluoroacetic acid and Amberlyst® A21 (free base) were obtained from Sigma Aldrich (Steinhausen, Germany) and are of analytical grade and were used without further purification. Acetonitrile was purified on a MBraun solvent purification system (MB SPS-800). The dye Cy5 was purchased from Lumiprobe GmbH (Hannover, Germany). *N*-Succinimidyl-4-pentenate was prepared according to literature procedures.[36] The commercially available poly(ethylene imine)s, both the branched (bPEI) as well as the linear (lPEI) type, were purchased from Polysciences (USA). Poly(methacrylic acid) (PMAA, DP = 200) was synthesized according to literature procedures.[37] The transfection reagent jetPRIME, used as positive control for siRNA delivery, was obtained from Polyplus (Polyplus transfection SA, USA). 5-(*N*-Ethyl-*N*-isopropyl)amiloride (EIPA) was purchased from Sigma-Aldrich (Merck, Darmstadt). Ethidium bromide solution (1%, 10 mg mL^{-1}) was purchased from Carl Roth (Karlsruhe, Germany). AlamarBlue, YOYO-1 iodide, Hoechst 33342 trihydrochloride as well as all other indicated CLSM dyes were obtained from Life Technologies (Thermo Fisher Scientific, Germany). If not stated otherwise, cell culture media and solutions (L-glutamine, antibiotics) were obtained from Biochrom (Berlin, Germany). Plasmid pEGFP-N1 (4.7 kb, Clontech, USA) encoding green fluorescent protein (EGFP) was isolated with the Giga Plasmid Kit provided by Qiagen (Hilden, Germany). The siRNA negative controls (scrambled siRNA, 21 nucleotides, double-stranded) and the siRNA against *egfp* (sense 5′-GCAAGCTGACCCTGAAGTTCAT-3′, antisense 5′-ATGAACTTCAGGGTCAGCTTGC-3′) were purchased from Eurogentech (Seraing, Belgium).

General methods and instrumentation

An Initiator Sixty single-mode microwave synthesizer from Biotage, equipped with a noninvasive IR sensor (accuracy: 2%), was used for polymerizations and hydrolyses under microwave irradiation.

Proton (^{1}H) nuclear magnetic resonance (NMR) spectra were acquired in deuterated methanol, at room temperature using a Bruker AC 300 MHz spectrometer; chemical shifts (δ) are expressed in parts per million relative to TMS.

Size exclusion chromatography (SEC) was performed using an Agilent Technologies 1200 Series gel permeation chromatography system equipped with a G1329A auto sampler, a G131A isocratic pump, a G1362A refractive index detector, and both a PSS Gram 30 and a PSS Gram 1000 column placed in series. As eluent a 0.21% LiCl solution in *N*,*N*-dimethylacetamide (DMAc) was used at 1 mL min^{-1} flow rate and a column oven temperature of 40 °C. Molar masses were calculated using a poly(styrene) calibration.

Asymmetric flow field-flow fractionation (AF4) was performed on an AF2000 MT System (Postnova Analytics, Landsberg, Germany) coupled to an UV (PN3211, 260 nm (Postnova)), RI (PN3150), multi-angle light scattering (MALLS, PN3070, 633 nm (Postnova)) and DLS (ZetaSizer Nano ZS; Malvern) detector. The eluent was delivered by three different pumps (tip, focus, cross-flow) and the sample was injected by an autosampler (PN5300) into the channel. The channel has a trapezoidal geometry and an overall area of 31.6 cm^2. The nominal height of the spacer was 500 μm. A regenerated cellulose membrane with a molar mass cut-off of 10 kDa served as accumulation wall. All experiments were carried out at 25 °C with pure water as eluent. A sample of 10 μL (1 mg mL^{-1}) was injected with an injection flow rate of 0.2 mL min^{-1} and a cross-flow rate of 1.2 mL min^{-1} for 7 min (detector flow rate 0.5 ml min^{-1}, focus flow rate 1.5 mL min^{-1}). After the focusing step, the cross-flow rate was reduced under an exponential gradient (0.4) within 10 min to 0 mL min^{-1}. The cross-flow was kept constant at 0 mL min^{-1} for 40 min to ensure complete elution. All measurements were in triplicate.

For the acid/base titration the copolymers **P1** to **P3** ($m \sim 20$ mg) were dissolved in 4 mL deionized water, and 20 μL conc. hydrochloric acid were added (0.06 M). The titration was performed against 0.1 M aqueous sodium hydroxide solution using a 765 Dosimat from Metrohm, a digital pH/mV-thermometer GMH 3530 from Greisinger electronic, and the EBS9 M Recorder software.

Synthesis of poly(2-ethyl-2-oxazoline) (PEtOx)

The monomer 2-ethyl-2-oxazoline (3.965 g) and the initiator methyl tosylate (12.42 mg, 0.067 mmol) were dissolved in dry acetonitrile (6.0 mL) in a microwave vial within a glovebox under nitrogen atmosphere. After stirring for 2 minutes the vessel was transferred to a microwave synthesizer and heated for 128 min at 140 °C. After cooling to room temperature, a sample was taken to determine the chain length by ^{1}H NMR. The polymerization mixture was diluted with 5 mL of dichloromethane, followed by precipitation in 250 mL ice-cold diethyl ether. The precipitate was filtered off, dissolved in deionized water and lyophilized (yield: 3.720 g, 94%).

PEtOx. DP = 575. ^{1}H NMR (300 MHz, D_2O): δ 3.70–3.20 (–NR–CH_2–CH_2), 2.41–2.08 (CH_2–CH$_3$), 1.09–0.79 (CH$_2$–CH_3) ppm. SEC (DMAc, LiCl): M_n = 69 000 g mol^{-1}, $Đ$ = 1.3. AF4: M_n = 57 000 g mol^{-1}, $Đ$ = 1.23.

Synthesis of poly(2-ethyl-2-oxazoline-*stat*-ethylene imine) (P(EtOx-*stat*-EI))

To obtain a specific degree of hydrolysis of **P(EtOx-*stat*-EI)**, kinetic studies were performed previously according to literature procedures.[38] The results were used to synthesize PEtOx with defined degree of hydrolysis in larger scale. Accordingly, **PEtOx** (3.510 g, 0.062 mmol) was dissolved in 6 M hydrochloric acid (36 mL). The reaction mixture was heated in a microwave synthesizer at 100 °C for 100 min. Subsequently, the excess of HCl and the resulting propionic acid were distilled off and the residue was dissolved in 15 mL water. The obtained solution was neutralized with 3 M aqueous NaOH to a pH value >8, and the remaining solvent was removed under reduced pressure. The residue was dissolved in DMF and the filtered polymer solution was precipitated two times in 500 mL cold diethyl ether. The obtained product was dried at 85 °C under reduced pressure. ^{1}H NMR spectroscopy was used to determine the conversion of the PEtOx to lPEI. Therefore, the signals from the released lPEI backbone and the signals from the remaining CH_3 group in the side chain of PEtOx were used (yield: 2.350 g, 91%).

P(EtOx-*stat*-EI). EtOx : EI [%] = 54 : 46. ^{1}H NMR (300 MHz, MeOD): δ 3.69–3.41 (NR–CH_2–CH_2), 2.93–2.63 (NH–CH_2–CH_2), 2.55–2.31 (CH_2–CH$_3$), 1.19–1.03 (CH$_2$–CH_3) ppm. SEC (DMAc, LiCl): M_n = 48 000 g mol^{-1}, $Đ$ = 1.28. AF4: M_n = 31 300 g mol^{-1}, $Đ$ = 1.03.

Synthesis of P(EtOx-*stat*-EI-*stat*-ButEnOx) (preP1 to preP3)

The partially hydrolyzed PEtOx, **P(EtOx-*stat*-EI)** (**1**: 659 mg, **2**: 654 mg, **3**: 647 mg), and the catalyst 4-*N*,*N*-dimethylaminopyridine (DMAP, 100 mg, 0.82 mmol) were dissolved in a microwave vial in pyridine (V = 8 mL) at 80 °C. In a second vial, a defined quantity of *N*-succinimidyl-4-pentenate (645 mg, 483 mg, 318 mg) was dissolved in the same solvent (4 mL) and heated up to 80 °C. The two solutions were combined and solvent was added (3 mL) to yield a 4 wt% mixture of **P(EtOx-*stat*-EI)**. The reaction mixture was stirred for 20 h at 80 °C. After cooling to room temperature the sample was filtered and precipitated into 400 mL ice-cold diethyl ether. The copolymer was filtered off and washed with 40 mL of diethyl ether. Due to the negligible effect of the side product *N*-hydroxysuccinimide on subsequent reaction steps, no further purification steps were required. The residue was dried under reduced pressure to constant weight (yield: **1**: 619 mg, 68%, **2**: 650 mg, 75%, **3**: 625 mg, 77%).

preP1. EtOx : EI : ButEnOx = 54 : 12 : 34%. ^{1}H NMR (300 MHz, MeOD): δ 6.00–5.77 (*H*C═CH$_2$), 5.18–4.95 (HC═C*H*$_2$), 3.81–3.40 (NR–CH_2–CH_2), 3.00–2.74 (NH–CH_2–CH_2), 2.67 (NHS), 2.60–2.20 (CH_2–CH$_3$, CH_2–CH_2–C$_2$H$_3$), 1.20–0.97 (CH$_2$–CH_3) ppm. SEC (DMAc, LiCl): M_n = 36 000 g mol^{-1}, $Đ$ = 2.12. AF4: M_n = 25 500 g mol^{-1}, $Đ$ = 1.41.

preP2. EtOx : EI : ButEnOx = 54 : 17 : 29%. ^{1}H NMR (300 MHz, MeOD): δ 6.00–5.78 (*H*C═CH$_2$), 5.17–4.95 (HC═C*H*$_2$), 3.81–3.40 (NR–CH_2–CH_2), 2.95–2.68 (NH–CH_2–CH_2), 2.59 (NHS), 2.57–2.21 (CH_2–CH$_3$, CH_2–CH_2–C$_2$H$_3$), 1.21–1.00 (CH$_2$–CH_3) ppm. SEC (DMAc, LiCl): M_n = 34 500 g mol^{-1}, $Đ$ = 1.63. AF4: M_n = 30 900 g mol^{-1}, $Đ$ = 1.33.

preP3. EtOx : EI : ButEnOx = 54 : 23 : 23%. ^{1}H NMR (300 MHz, MeOD): δ 5.99–5.76 (*H*C═CH$_2$), 5.19–4.96 (HC═C*H*$_2$), 3.81–3.40 (NR–CH_2–CH_2), 2.94–2.66 (NH–CH_2–CH_2), 2.57 (NHS), 2.55–2.25 (CH_2–CH$_3$, CH_2–CH_2–C$_2$H$_3$), 1.22–0.99 (CH$_2$–CH_3) ppm. SEC (DMAc, LiCl): M_n = 36 000 g mol^{-1}, $Đ$ = 1.55. AF4: M_n = 30 400 g mol^{-1}, $Đ$ = 1.33.

Synthesis of P(EtOx-*stat*-EI-*stat*-bocAmButOx) *via* thiol–ene functionalization (*boc*P1 to *boc*P3)

In a microwave vial, **P(EtOx-*stat*-EI-*stat*-ButEnOx)** (**preP1**: 253 mg, **preP2**: 351 mg, **preP3**: 360 mg) was dissolved in methanol (2 mL). In a second vial, the photoinitiator 2,2-dimethoxy-2-phenylacetophenone (DMPA, 49 ± 0.5 mg, 0.19 mmol) and a 1.3-fold excess per double bond of 2-(boc-amino)ethanethiol (193 μL, 239 μL, 205 μL)

were dissolved in methanol (2 mL), likewise. The combined solutions (10 wt%) were degassed with nitrogen for 20 min and the clear solution was stirred in a UV chamber (λ = 365 nm) overnight. Subsequently, the copolymer was precipitated in 200 mL ice-cold diethyl ether. After filtration, the copolymer was dried under reduced pressure for two days (yield: ***boc*P1**: 361 mg, 89%, ***boc*P2**: 493 mg, 92%, ***boc*P3**: 476 mg, 92%).

***boc*P1.** EtOx : EI : bocAmButOx = 54 : 12 : 34%. ^{1}H NMR (300 MHz, MeOD): δ 3.81–3.40 (NR–CH_2–CH_2), 3.27–3.16 (S–CH_2–CH_2), 3.00–2.74 (NH–CH_2–CH_2), 2.64 (NHS), 2.63–2.55 (S–CH_2–CH_2), 2.54–2.27 (CH_2–CH$_3$, CH_2–C$_2$H$_4$–CH_2), 1.82–1.57 (CH$_2$–C$_2$$H_4$–CH$_2$), 1.55–1.39 (C(C$H_3$)$_3$), 1.21–1.00 (CH$_2$–C$H_3$) ppm.

***boc*P2.** EtOx : EI : bocAmButOx = 54 : 17 : 29%. ^{1}H NMR (300 MHz, MeOD): δ 3.81–3.41 (NR–CH_2–CH_2), 3.28–3.16 (S–CH_2–CH_2), 2.92–2.72 (NH–CH_2–CH_2), 2.69–2.59 (S–CH_2–CH$_2$), 2.58 (NHS), 2.54–2.29 (CH_2–CH$_3$, CH_2–C$_2$H$_4$–CH_2), 1.82–1.56 (CH$_2$–C$_2$$H_4$–CH$_2$), 1.55–1.39 (C(C$H_3$)$_3$), 1.21–1.03 (CH$_2$–C$H_3$) ppm.

***boc*P3.** EtOx : EI : bocAmButOx = 54 : 23 : 23%. ^{1}H NMR (300 MHz, MeOD): δ 3.79–3.41 (NR–CH_2–CH_2), 3.27–3.17 (S–CH_2–CH_2), 2.91–2.71 (NH–CH_2–CH_2), 2.67–2.59 (S–CH_2–CH$_2$), 2.58 (NHS), 2.54–2.29 (CH_2–CH$_3$, CH_2–C$_2$H$_4$–CH_2), 1.80–1.56 (CH$_2$–C$_2$$H_4$–CH$_2$), 1.55–1.39 (C(C$H_3$)$_3$), 1.20–1.02 (CH$_2$–C$H_3$) ppm.

Synthesis of P(EtOx-*stat*-EI-*stat*-AmButOx) *via* deprotection (P1 to P3)

The copolymer **P(EtOx-*stat*-EI-*stat*-bocAmButOx)** (***boc*P1**: 321 mg, ***boc*P2**: 402 mg, ***boc*P3**: 420 mg) was dissolved in dichloromethane (3 mL). Trifluoroacetic acid was added (5 mL) and the reaction mixture was stirred overnight at room temperature. The copolymer was precipitated in 400 mL ice-cold diethyl ether. The precipitate was filtered, washed with 40 mL diethyl ether, dissolved in methanol and shaken overnight with Amberlyst A21 (free base) ($\sim$0.5 g). The solvent was removed and the copolymer lyophilized (yield: **P1**: 240 mg, 95%, **P2**: 293 mg, 91%, **P3**: 330 mg, 95%).

P1. EtOx : EI : bocAmButOx = 54 : 12 : 34%. ^{1}H NMR (300 MHz, MeOD): δ 3.76–3.29 (NR–CH_2–CH_2), 3.11–2.98 (S–CH_2–CH_2), 2.84–2.65 (NH–CH_2–CH_2), 2.58 (NHS), 2.57–2.46 (S–CH_2–CH$_2$), 2.45–2.16 (CH_2–CH$_3$, CH_2–C$_2$H$_4$–CH_2), 1.83–1.44 (CH$_2$–C$_2$$H_4$–CH$_2$), 1.10–0.89 (CH$_2$–C$H_3$) ppm. SEC (DMAc, LiCl): M_n = 30 500 g mol^{-1}, $Đ$ = 1.60. AF4: M_n = 35 300 g mol^{-1}, $Đ$ = 1.74.

P2. EtOx : EI : bocAmButOx = 54 : 17 : 29%. ^{1}H NMR (300 MHz, MeOD): δ 3.68–3.21 (NR–CH_2–CH_2), 3.01–2.87 (S–CH_2–CH_2), 2.72–2.56 (NH–CH_2–CH_2), 2.50 (NHS), 2.48–2.37 (S–CH_2–CH$_2$), 2.37–2.08 (CH_2–CH$_3$, CH_2–C$_2$H$_4$–CH_2), 1.70–1.36 (CH$_2$–C$_2$$H_4$–CH$_2$), 1.03–0.82 (CH$_2$–C$H_3$) ppm. SEC (DMAc, LiCl): M_n = 39 000 g mol^{-1}, $Đ$ = 1.58. AF4: M_n = 43 700 g mol^{-1}, $Đ$ = 1.72.

P3. EtOx : EI : bocAmButOx = 54 : 23 : 23%. ^{1}H NMR (300 MHz, MeOD): δ 3.87–3.40 (NR–CH_2–CH_2), 3.23–3.03 (S–CH_2–CH_2), 2.97–2.75 (NH–CH_2–CH_2), 2.74–2.57 (S–CH_2–CH$_2$), 2.56–2.28 (CH_2–CH$_3$, CH_2–C$_2$H$_4$–CH_2), 1.88–1.56 (CH$_2$–C$_2$$H_4$–CH$_2$), 1.22–0.98 (CH$_2$–C$H_3$) ppm. SEC (DMAc, LiCl): M_n = 31 500 g mol^{-1}, $Đ$ = 1.45. AF4: M_n = 30 500 g mol^{-1}, $Đ$ = 1.62.

Copolymer labeling with Cy5

Copolymer **P3** (40 mg) and triethylamine (150 μL) were dissolved in DMF (10 mL). After addition of the cyanine-5-NHS-ester (0.4 mg) the reaction was stirred at room temperature overnight. The labeled copolymer was precipitated in 500 mL ice-cold diethyl ether, filtered and re-dissolved in H_2O (15 mL). Further purification was performed by dialysis against water using a Spectra/Por 3 dialysis membrane (3500 g mol^{-1} cut-off). Finally, the product was lyophilized and obtained as a blue powder. The calculated labeling efficiency (*via* UV-Vis) for conjugation was 65% for **P3–Cy5** (yield: 27 mg, 67%). **lPEI** was treated likewise but dialyzed against a water/methanol mixture and dried under reduced pressure, subsequently (yield: 2.6 mg, 26%; labeling efficiency: 2%).

Synthesis of linear poly(ethylene imine) (lPEI)

The synthesized copolymer **P(EtOx-*stat*-EI)** (DP = 575, 100 mg) was treated with an excess of 6 M aqueous hydrochloric acid (1.5 mL) for 2 hours at 100 °C in a microwave synthesizer to yield a hydrolyzed linear poly(ethylene imine) (DP = 575). Neutralization and purification *via* precipitation were performed analogous to the described synthesis of **P(EtOx-*stat*-EI)** (see above). The product **lPEI** was dried at 85 °C under high vacuum for 2 days and the degree of hydrolysis was determined by ^{1}H NMR by correlating the integrals of the PEI backbone and the remaining methyl group of the PEtOx side chain (yield: 51 mg, 87%).

lPEI. EtOx : EI [%] = 5 : 95. ^{1}H NMR (300 MHz, MeOD): δ 3.58–3.41 (NR–CH_2–CH_2), 2.91–2.61 (NH–CH_2–CH_2), 2.56–2.36 (CH_2–CH$_3$), 1.18–1.06 (CH$_2$–CH_3) ppm.

Polyplex preparation

Polyplexes of pDNA and polymers were prepared by mixing stock solutions of 15 μg mL^{-1} pDNA and different amounts of polymers (1 mg mL^{-1}) to obtain various N/P ratios (nitrogen of polymer to phosphate of pDNA) in HBG buffer (20 mM 4-(2-hydroxyethyl)piperazine-1-ethanesulfonic acid (HEPES) and 5% (w/v) glucose, pH 7.2). The solutions were vortexed for 10 s at maximal speed and incubated at room temperature for 20 min to ensure complex formation. For the preparation of polyplexes with siRNA, 1 μM siRNA (final concentration) was used as described above.

Ethidium bromide quenching assay

The formation of polyplexes with pDNA as well as siRNA was examined by quenching of the ethidium bromide fluorescence. Briefly, pDNA (15 μg mL^{-1}) or siRNA (1 μM) in a total volume of 100 μL HBG buffer were incubated with ethidium bromide (0.4 μg mL^{-1}) for 10 min at room temperature. Subsequently, polyplexes with different amounts of polymer (various N/P ratios) were prepared in black 96-well plates (Nunc Thermo Fisher). The samples were incubated at room temperature for 15 min. The fluorescence of the samples was measured at an excitation wavelength of 525 nm and an emission wavelength of 605 nm using a microplate reader (TECAN Infinite M200 Pro, Crailsheim, Germany). A sample containing only pDNA and ethidium bromide was used to calibrate the device to 100% fluorescence against a background of 0.4 μg mL^{-1} of ethidium bromide in

HBG solution. The percentage of dye displaced upon polyplex formation was calculated using eqn (1):

$$\mathrm{RFU}[\%] = \frac{F_{\mathrm{sample}} - F_0}{F_{\mathrm{pDNA}} - F_0} \times 100 \quad (1)$$

Here, RFU is the relative fluorescence and F_{sample}, F_0, and F_{pDNA} are the fluorescence intensities of a given sample, the ethidium bromide in HBG alone, and the ethidium bromide intercalated into pDNA alone.

Heparin dissociation assay

To investigate the release of pDNA from polyplexes, the heparin dissociation assay was performed. Polyplexes with an N/P ratio of 30 were prepared as described above in a total volume of 100 μL HBG buffer containing ethidium bromide (0.4 μg mL^{-1}). After incubation in the dark at room temperature for 15 min, the polyplexes were transferred into a black 96-well plate, and heparin of indicated concentrations was added. The solution was mixed and incubated for further 30 min at 37 °C in the dark. The fluorescence of ethidium bromide was measured at Ex 525 nm/Em 605 nm with a Tecan microplate reader. The percentage of intercalated ethidium bromide was calculated as described before.

Dynamic and electrophoretic light scattering

Dynamic light scattering (DLS) was performed on a Zetasizer Nano ZS (Malvern Instruments, Herrenberg) with a He–Ne laser operating at a wavelength of λ = 633 nm. All measurements (30 runs, triplicate) were carried out at 25 °C after an equilibration time of 120 s. The counts were detected at an angle of 173°. The mean particle size was approximated as the effective (*z*-average) diameter and the width of the distribution as the polydispersity index of the particles (PDI) obtained by the cumulants method assuming a spherical shape. Electrophoretic light scattering (ELS) was used to measure the zeta potential (ζ). The measurement was performed on a Zetasizer Nano ZS (Malvern Instruments, Herrenberg, Germany) by applying laser Doppler velocimetry. For each measurement, 20 runs were carried out using the slow-field reversal and the fast-field reversal mode at 150 V. Each experiment was performed in triplicate a 25 °C. The zeta potential was calculated from the electrophoretic mobility (μ) according to the Henry equation. Henry coefficient f(ka) was calculated according to Oshima.

Determination of the cytotoxicity

Cytotoxicity studies were performed with the mouse fibroblast cell line L929 (CCL-1, ATCC), as recommended by ISO10993-5. The cells were routinely cultured in Dulbecco's modified eagle's medium (DMEM, Lonza, Basel) supplemented with 10% fetal calf serum (FCS), 100 U mL^{-1} penicillin and 100 μg mL^{-1} streptomycin at 37 °C in a humidified 5% (v/v) CO_2 atmosphere.

In detail, cells were seeded at 10^4 cells per well in a 96-well plate and incubated for 24 h, whereas no cells were seeded in the outer wells. Subsequently, the testing substances (polymers) at indicated concentrations (from 0.25 μg mL^{-1} to 1 mg mL^{-1}) were added to the cells and the plates were incubated for further 24 h. Control cells were incubated with fresh culture medium. Subsequently, the medium was replaced by a mixture of fresh culture medium and Alamar-Blue solution (Life technologies, Darmstadt, Germany), prepared according to the manufacturer's instructions. After a further incubation of 4 h at 37 °C, the fluorescence was measured at Ex 570/Em 610 nm, with untreated cells on the same well plate serving as negative controls. The negative control was standardized as 0% of metabolism inhibition and referred as 100% viability. Cell viability below 70% was considered indicative of cytotoxicity. Data are expressed as mean ± SD of three determinations.

Hemolysis assay

The interaction of polymers with cellular membranes was investigated by analyzing the release of hemoglobin from erythrocytes. Blood from sheep, collected in heparinized tubes, was provided by the Institute of Laboratory Animal Science and Animal Welfare, Friedrich-Schiller University Jena. The blood was centrifuged at 4500 × *g* for 5 min, and the pellet was washed three times with cold 1.5 mM phosphate buffered saline (PBS, pH 7.4). After dilution with PBS in a ratio of 1 : 7, aliquots of erythrocyte suspension were mixed 1 : 1 with the polymer solution and incubated in a water bath at 37 °C for 60 min. After centrifugation at 2400 × *g* for 5 min, the hemoglobin release into the supernatant was determined spectrophotometrically using a microplate reader (TECAN Infinite M200 Pro, Crailsheim, Germany) at a wavelength of 544 nm. Complete hemolysis (100%) was achieved using 1% Triton X-100 serving as positive control. Pure PBS was used as negative control (0% hemolysis). The haemolytic activity of the polycations was calculated as follow (2):

$$\%\ \mathrm{Hemolysis} = 100 \times \frac{\left(A_{\mathrm{Sample}} - A_{\mathrm{Negative\ control}}\right)}{A_{\mathrm{Positive\ control}}} \quad (2)$$

A value less than 2% hemolysis rate were classified as non-hemolytic, 2 to 5% as slightly haemolytic and values >5% as hemolytic. Experiments were run in triplicates and were performed with three different batches of donor blood.

Erythrocyte aggregation

Erythrocytes were isolated as described above. The erythrocyte suspension were mixed 1 : 1 with the polymer solutions (100 μL total volume) in a clear flat bottomed 96-well plate. The cells were incubated at 37 °C for 2 h, and the absorbance was measured at 645 nm in a microplate reader. Cells, which were treated with PBS served as negative control and 25 kDa bPEI (50 μg mL^{-1}, Polysciences) was used as positive control. Absorbance values of the test solutions lower than the negative control were regarded as aggregation. Experiments were run in triplicates and were performed with three different batches of donor blood.

Polyplex uptake

HEK-293 cells (CRL-1573, ATCC) were cultured in RPMI 1640 medium (Lonza, Basel) supplemented with 10% FCS, 100 μg mL^{-1} streptomycin, 100 U mL^{-1} penicillin and 2 mM L-glutamine at 37 °C in a humidified 5% CO_2 (v/v) atmosphere.

For uptake studies, cells were seeded at a density of 10^5 cells per mL in 24-well plates and cultured for 24 h. One hour prior to the addition of the polyplexes, the medium was changed to OptiMEM (Life Technologies, Darmstadt, Germany). The polyplexes were prepared as described above and at least 50 μL polyplexes in solution were added to the cells. The plates were incubated for 4 h at 37 °C, 5% CO_2.

For kinetic studies of the polyplex uptake within 4 h, pDNA was labeled with YOYO-1 iodide prior to the polyplex preparation. For labeling of 1 μg pDNA, 0.026 μL of 1 M YOYO-1 solution was mixed with pDNA and incubated for 20 min at 4 °C protected from light. Afterwards, HBG buffer and polymers were added at the indicated N/P ratio and the polyplexes were formed as described previously. The cells were harvested 0.5, 1, 2 and 4 h after polyplex addition and 10% trypan blue was added to quench the outer fluorescence of the cells. For energy-dependent uptake studies, cells were equilibrated in OptiMEM at 4 °C 1 h prior polyplex addition. The plates were incubated at 4 °C for 4 h. To determine the relative uptake of the polyplexes, 10^4 cells were measured by flow cytometry using a Cytomics FC 500 (Beckman Coulter) and the amount of viable cells showing YOYO-1 signal were gated. Dead cells were identified *via* counterstaining with propidium iodide (PI). The experiments were performed at least three times independently.

For inhibition experiments, cells were treated with 100 μM 5-(*N*-ethyl-*N*-isopropyl)amiloride (EIPA) in standard culture media 30 min prior to polyplex addition. Subsequently, **P3** and **lPEI** polyplexes were added to the cells and incubated for further 4 h. Afterwards, the cells were harvested and analyzed as described above *via* flow cytometry or were further prepared for STEM imaging.

Transfection of adherent cells

For transfection of adherent HEK-293 cells, the cells were seeded at a density of 10^5 cells per mL in 24-well plates and incubated for 24 h at 37 °C, 5% CO_2. One hour prior to transfection, the cells were washed with PBS and supplemented with 0.5 mL OptiMEM or fresh serum containing growth medium (RPMI 1640). The polyplexes were prepared as described above, and were added to the cells (50 μL per well). After an incubation time of 4 h at 37 °C, the supernatant was replaced by fresh growth medium and the cells were incubated for further 20 h. For analysis *via* flow cytometry (Cytomics FC 500, Beckman Coulter), cells were harvested by trypsinization. For determination of the viability during flow cytometry, dead cells were identified *via* counterstaining with propidium iodide. For determination of the transfection efficiency, 10^4 viable cells expressing EGFP were gated. The experiments were performed three times independently. Regarding the Bafilomycin experiments, 175 nM Bafilomycin was added to the cells in OptiMEM and incubated for 20 min, prior to the polyplex addition. The knockdown studies were performed with stable EGFP expressing CHO cells (CCL-61, ATCC, stable transfected with pEGFP-N1) and the corresponding siRNA (against *egfp*, riboxx, Germany). The polyplexes were incubated in OptiMEM for 6 h and measured after 72 h *via* flow cytometry.

Electron microscopy

Scanning transmission electron microscopy with high-angle annular dark-field detection (STEM-HAADF) was carried out using a Technai G^2 system (FEI), with 120 kV or 200 kV acceleration voltage on ultrathin slices of resin-embedded cell samples.

For cell preparation, HEK-293 cells (10^5 cells mL^{-1}) were seeded on 6-well plates and incubated for 4 h at 37 °C with the respective polyplex samples (N/P 30). The cells were harvested, washed with PBS and fixed for 2 h with glutaraldehyde (2% in PBS, prepared from 8% EM grade stock solution) on ice. Subsequent to aldehyde fixation, the cells were washed with PBS prior to the fixation with OsO_4 for 1 h (1% in PBS, prepared from 4% EM grade stock solution, both purchased from EMS, Hatfield). After this, the cells were washed with MilliQ water and staining with uranyl acetate solution was carried out for 1 h and protected from light (1% in solution in MilliQ water prepared from depleted uranyl acetate dihydrate purchased from EMS, Hatfield). Subsequently, the sample was washed with pure water prior to dehydration by an ethanol/water series (50%, 70%, 90%, 2 × 100% dry EtOH, purified with a Solvent Purification System and stored over molecular sieves). Thereafter, the cells were transferred into BEEM capsules (Plano, Wetzlar), in which the cell suspension was immersed in mixtures of Embed 812 (EMS, Hatfield) and ethanol (Embed/EtOH = 1 : 1 v/v for 1 hour, 2 : 1 v/v for 12 h, pure Embed 812 for 4 h). Subsequent to a further exchange of the embedding medium, the resin was allowed to harden at 70 °C for 24 h. From the resin block, ultrathin sections with a thickness of 80 nm were cut with an ultramicrotome (PT-XL PowerTome, RMC, Tucson) using a diamond knife (RMC, Tucson). The ultrathin resin sections were applied on a carbon supported copper grid (400 mesh, Quantifoil, Jena).

Confocal microscopy and structured illumination microscopy

Live cell imaging was performed for uptake studies. In detail, HEK cells (10^5 cells mL^{-1}) were seeded on glass-bottomed dishes (ibidi, Germany, thickness 170 ± 5 μm for high-resolution fluorescence microscopy) and cultivated for 24 h in a humidified atmosphere. One hour prior to the polymer addition, the cells were rinsed with phosphate buffered saline (PBS) and the medium was changed to OptiMEM. The polyplexes were formed with Cy5-labeled **P3** and YOYO-labeled pDNA or Cy3-labeled siRNA, added to the cells and incubated for further 4 h. Subsequently, medium was replaced by fresh culture medium or PBS supplemented with Hoechst 33342 for nucleus staining, LysoTracker Red DND-99 or LysoTracker Green DND-26 (all from Thermo Fisher Scientific) for lysosome staining.

Imaging was performed with LSM880, Elyra PS.1 system (Zeiss, Oberkochen, Germany) applying a 63× 1.4 NA plan apochromat oil objective. For SIM imaging, cells were grown on high precision cover glasses (Marienfeld-Superior, 18 × 18 mm, 170 ± 5 μm certified thickness) at a density of 5×10^4 cells mL^{-1}, fixed with paraformaldehyde (2% in PBS) and embedded in prolong gold antifading reagent (Thermo Fisher Scientific). Regarding the SIM performance, excitation wavelengths of 405 nm

(exc. grating 28.0 μm), 488 nm (exc. grating 34.0 μm), 561 nm (exc. grating 42.0 μm) and 642 nm (exc. grating 42.0 μm resp. 51.0 μm) were used. The following four color channels were used for both microscopy techniques: Nucleus (Hoechst 33342 staining, excitation wavelength 405 nm, BP 420–480 + LP 750, grey), pDNA (YOYO-1 Iodide, excitation wavelength 488 nm, BP 495–550 + LP 750, green), polymer **P3** (Cy-5 labeling, excitation wavelength 642 nm, LP 655, blue) and lysosome (CellLight Lysosomes-RFP BacMam 2.0, excitation wavelength 561 nm, BP 570–620 + LP 750, red). The grating position and axial position of the sample table were controlled by piezo controllers. Images were recorded with a sCMOS camera (pco.edge, Kehlheim, German), cooled to 5 °C. Reconstructions and deconvolution were performed with the commercial ZEN2 software installed on the system (Zeiss, Oberkochen, Germany).

Statistical analysis

The values represent the mean ± SD. For the calculation of the standard derivation of two or more different groups, the two sample *t*-test (student's *t*-test) or the ANOVA was used. Statistical significance was defined as * for *p*-values of <0.05 and # for *p*-values <0.005.

Results and discussion

Polymer synthesis

As chain transfer reactions are more likely to occur during polymerization of 2-methyl-2-oxazoline,[39] 2-ethyl-2-oxazoline was used as monomer for the polymerization of the precursor homopolymer, being able to decrease cytotoxicity of aspired copolymers.[40]

PEtOx was synthesized according to a literature procedure by microwave supported cationic ring-opening polymerization (CROP).[41] The degree of polymerization of 575 was calculated from the tosylate ^{1}H NMR signals of MeOTos before purification. In order to ensure the absence of water, the polymerization solutions were prepared in a glove box under nitrogen atmosphere yielding **PEtOx** with a dispersity *Đ* of 1.3 (SEC: DMAc, 0.21% LiCl, standard: PS, Table 1). This homopolymer served as precursor for the subsequent copolymer synthesis.

PEtOx was hydrolyzed in a microwave synthesizer (Scheme 1a) to yield the copolymer poly(2-ethyl-2-oxazoline-*stat*-ethylene imine) (**P(EtOx-*stat*-EI)**) with an EtOx content of 54% (calc. from ^{1}H NMR).[38]

To introduce primary amines to the polymers, a fraction of the ethyleneimine units was functionalized with *N*-succinimidyl-4-pentenate to introduce alkene functionalities (Scheme 1b).[42] While the synthesis of poly(2-butenyl-2-oxazoline) is possible *via* the polymerization of the respective monomers,[36] these units do not withstand the conditions of the acidic hydrolysis of PEtOx. Three different copolymers of P(EtOx-*stat*-EI-*stat*-ButEnOx) (**preP1** to **preP3**) with varying ratios of secondary amines and 2-(3-butenyl-2-oxazoline)s (1 : 3, 1 : 2, 1 : 1) were synthesized while maintaining a constant EtOx content of 54% (Table 1). The introduction of primary amines was performed by thiol–ene photoaddition. Hence, the copolymers P(EtOx-*stat*-EI-*stat*-AmButOx) (**P1** to **P3**) were synthesized by reaction of the corresponding precursor copolymers (**preP1** to **preP3**) with a protected aminothiol under UV irradiation and subsequent deprotection to yield the primary amine group (Scheme 1c and d).

Characterization by ^{1}H NMR spectroscopy confirms the presence of 2-ethyl-2-oxazoline (EtOx) as well as ethylene imine (EI) units (Fig. 2, **PEtOx** and **P(EtOx-*stat*-EI)**). The integrals of the signals of the EtOx side chain (A, B) as well as the signals of the backbone (C) remain constant during further reactions and are, therefore, used as reference.

The successful functionalization with the activated acid *N*-succinimidyl-4-pentenate is exemplified by the proton signals of the double bond (ButEnOx) that appear at 5.9 ppm (–*H*C═CH_2, H) and 5.1 ppm (–HC═CH_2, I) for the copolymer **preP3**. The first signal is used to calculate the composition of the formed copolymer by comparing the signals of the ethylene imine backbone (between 3.00 to 2.66, NH–CH_2–CH_2, D) and the methyl protons of the EtOx side chain (between 1.22 to 0.97, CH_2–CH_3, A). The successful functionalization of **preP1** to **preP3** with the thiol is shown by the disappearance of the double bond signals after the photoaddition (***boc*P3**). The signals of the newly formed CH_2 groups appear at 2.40 (I′) and 1.70 ppm (H′), respectively. Furthermore, a singlet of the *tert*-butyloxycarbonyl (boc) protecting group is obtained at 1.50 ppm (L). After treatment with

Table 1 Composition and molar masses for **PEtOx**, **P(EtOx-*stat*-EI)**, **preP1** to **preP3** and **P1** to **P3**

		Composition[a]		Amine ratio	NMR[b]	AF4		SEC	
Abbr.	Name	*X* [%]	*Y* [%]	$sec_X : prim_Y$	M_n [g mol^{-1}]	M_n [g mol^{-1}]	*Đ*	M_n [g mol^{-1}]	*Đ*
PEtOx	$PEtOx_{575}$	—	—	—	57 000	57 000	1.2	69 000	1.3
P(EtOx-*stat*-EI)	$P(EtOx_{54\%}$-*stat*-$EI_X)$	46	—	—	42 100	31 300	1.3	48 000	1.3
preP1	$P(EtOx_{54\%}$-*stat*-EI_X-$ButEnOx_Y)$	12	34	—	58 100	25 500	1.4	36 000	2.1
preP2	$P(EtOx_{54\%}$-*stat*-EI_X-$ButEnOx_Y)$	17	29	—	55 800	30 900	1.3	34 500	1.6
preP3	$P(EtOx_{54\%}$-*stat*-EI_X-$ButEnOx_Y)$	23	23	—	53 000	30 400	1.3	36 000	1.6
P1	$P(EtOx_{54\%}$-*stat*-EI_X-$AmButOx_Y)$	12	34	1 : 2.8	73 200	35 300	1.7	30 500	1.6
P2	$P(EtOx_{54\%}$-*stat*-EI_X-$AmButOx_Y)$	17	29	1 : 1.7	68 600	43 700	1.7	39 000	1.6
P3	$P(EtOx_{54\%}$-*stat*-EI_X-$AmButOx_Y)$	23	23	1 : 1	63 100	30 500	1.6	31 500	1.5

[a] Determined by ^{1}H NMR (calculated from the ratio of EtOx, ButEnOx signals and EI backbone). [b] Determined by ^{1}H NMR (calculated from tosylate signals of MeOTos before purification).

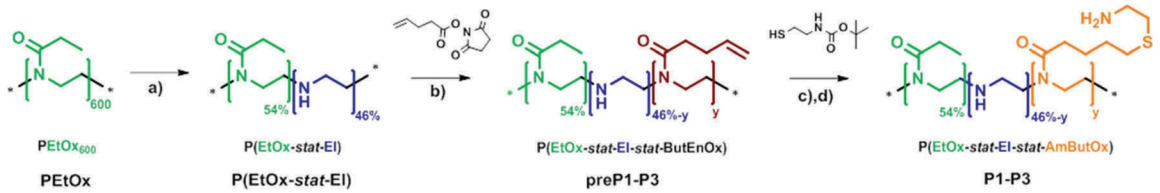

Scheme 1 Schematic representation of the synthesis of cationic copolymers. (a) Partial hydrolysis of poly(2-ethyl-2-oxazoline) in a microwave synthesizer, (b) post-polymerization functionalization with *N*-succinimidyl-4-pentenate, (c) thiol–ene photo-addition of 2-(boc-amino)ethanethiol at 365 nm and (d) deprotection using trifluoroacetic acid.

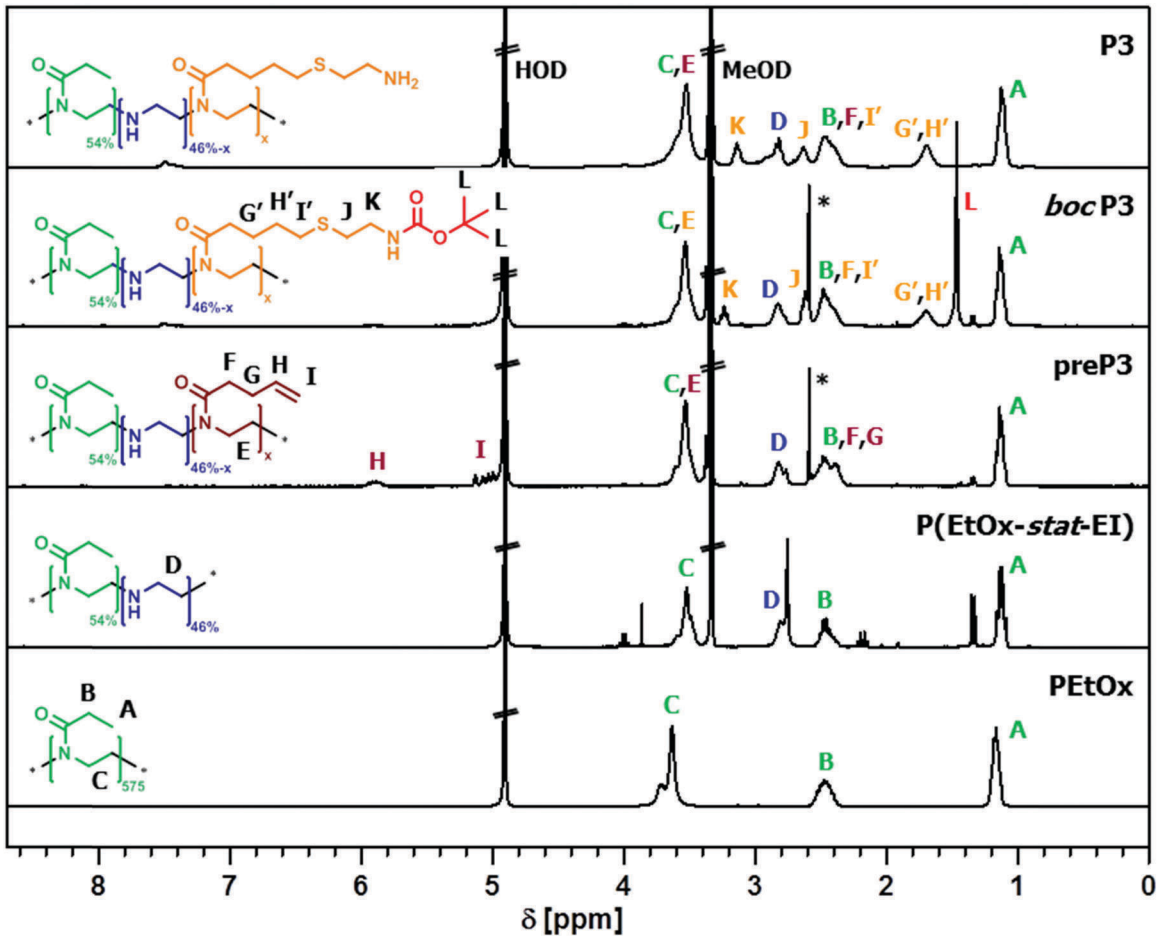

Fig. 2 Comparison of ^{1}H NMR spectra of **PEtOx**, **P(EtOx-*stat*-EI)**, **preP3**, ***boc*P3** and the final product **P3** (* side product *N*-hydroxysuccinimide) (300 MHz, MeOD).

trifluoroacetic acid (TFA) and precipitation into diethyl ether, the signal of the protecting group disappears, indicating the successful deprotection of ***boc*P1** to **bocP3** and, consequently, the synthesis of P(EtOx-*stat*-EI-*stat*-AmButOx) (**P1** to **P3**).

A comparison of the composition and molar masses of the prepared copolymers obtained by asymmetric flow field-flow fractionation (AF4) and size exclusion chromatography (SEC) is shown in Table 1. Although a trend is clearly visible, the obtained values should be handled with care due to the fact that the introduction of double bond containing ButEnOx units as well as the cationic amine units (primary and secondary) could lead to undesired column and membrane interactions and, hence, to a change in the elution behavior. SEC traces, exemplified for the synthesis of **P2**, are depicted in the ESI† (Fig. S1).

To enable *in vitro* imaging, copolymer **P3** was labeled using one equivalent of Cy5–NHS per polymer chain. Successful dye functionalization and purification *via* dialysis (3500 g mol^{-1} cut-off) was verified by size exclusion chromatography (SEC), revealing no trace of unbound dye (ESI,† Fig. S2).

Bio- and hemocompatibility

Biocompatibility represents a critical parameter for PEI based polymers. One option to reduce the known cytotoxicity of PEI[12,13,43]

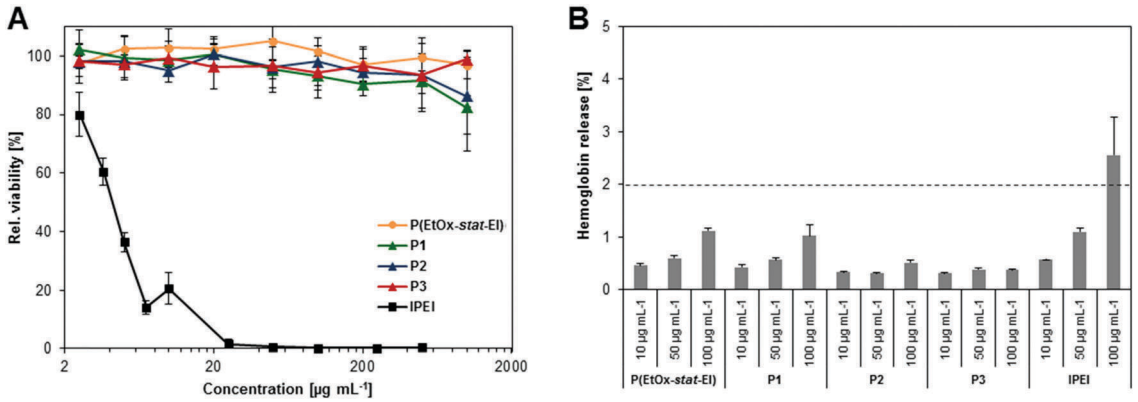

Fig. 3 Determination of bio- and hemocompatibility. (A) Relative viability of L929 cells after 24 h incubation with the polymers at different concentrations according to ISO10993-5. (B) Hemolysis assay of erythrocytes after incubation with polymers at the indicated concentrations. Triton X-100 served as positive control (98.8% hemolysis) and PBS as negative control (0.2%). A value less than 2% hemolysis rate was classified as non-hemolytic, 2 to 5% as slightly hemolytic and values >5% as hemolytic. Values represent the mean ± S.D. (n = 3).

is the introduction of EtOx units.[31] The copolymers introduced here (**P1** to **P3**) possess an oxazoline content of 54%, expected to decrease severe cytotoxic effects. The cytotoxicity of **P1** to **P3** was investigated in comparison to **lPEI** (Fig. 3A), obtained by full hydrolysis of **P(EtOx-*stat*-EI)**. Besides **lPEI**, commercial available linear poly(ethylene imine) (**comlPEI**, 25 kDa, Polyscience) was used as internal control. The results of the following *in vitro* experiments performed with **comlPEI** are summarized in the ESI† (Fig. S18–S20).

As assumed, **lPEI** leads to a significant reduction of cell viability at low concentrations (IC_{50} of 3.6 µg mL^{-1}), which is in accordance to literature data.[3] Despite a high molar mass (>25 kDa), **P(EtOx-*stat*-EI)** as well as **P1** to **P3** showed no cytotoxicity after 24 h using polymer concentrations up to 1 mg mL^{-1} (IC_{50} > 1 mg mL^{-1}, Fig. 3A). This improvement on cell viability is attributed to the introduced EtOx content of 54% within the copolymers and is consistent with literature reports on partially hydrolyzed POx.[32]

The blood compatibility of the copolymers was further investigated by assessment of the hemolytic activity (Fig. 3B) as well as the aggregation of erythrocytes. The treatment of **P(EtOx-*stat*-EI)** and **P1** to **P3** did not show any hemolytic activity in a concentration range from 10 to 50 µg mL^{-1}. A slight hemolysis (~1% hemoglobin release) could be revealed at higher concentrations of **P(EtOx-*stat*-EI)** and **P1** (100 µg mL^{-1}). In contrast, **lPEI** revealed an increased interaction with the cellular membranes of the blood cells resulting in hemoglobin releases above 2% (100 µg mL^{-1}) and, moreover, in a strong agglomeration of erythrocytes (see ESI,† Fig. S3 and S4). The later was not observed with EtOx containing copolymers (**P(EtOx-*stat*-EI)**, **P1** to **P3**) indicating a good hemo- and biocompatibility.

Characterization of the polyplexes

Despite the beneficial impact of EtOx on the biocompatibility of the polymers, their impact on the polyplex formation was investigated. For this purpose, the ethidium bromide quenching assay (EBA) was used to investigate the condensation of plasmid DNA (pDNA) by **P1** to **P3** as well as **P(EtOx-*stat*-EI)**, at different nitrogen (polymer) to phosphate (DNA) ratios (N/P). Ethidium bromide is excluded from its binding sites within the oligonucleotides because of the electrostatic and hydrophobic interactions between polymer and the nucleic acid, leading to a reduction in fluorescence that can be correlated to the affinity of the complexation.[44,45] All copolymers (**P1** to **P3**) revealed decreasing fluorescence intensities below 40% relative fluorescence units (RFU, Fig. 4A). Stable polyplexes indicated by a plateau were reached at higher N/P ratios 5 to 40, whereby no significant differences between **P1**, **P2**, **P3** and **lPEI** were observed. In contrast, the precursors **PEtOx** (data not shown) and **P(EtOx-*stat*-EI)** did not form appropriate polyplexes. It can be assumed that the EtOx units prevent a strong binding of the DNA to the secondary amines of the PEI backbone. This reduced complexation affinity is compensated by the introduction of the more flexible side chains consisting of AmButOx (primary amines) within **P1** to **P3**, which apparently are essential for the polyplex formation. Interestingly, the combination of EI and AmButOx seems to be beneficial, since a comparable copolymer **P(MeOx-*stat*-AmButOx)** without ethylene imine units revealed reduced pDNA complexation around 60% RFU in a previous study.[17] A synergistic effect between both, primary amines in the side chain and secondary amines in the backbone, leads to an improved binding of DNA despite an EtOx content of 54%. The following studies of **P1** to **P3** were performed with polyplexes formed at N/P 30 as this guarantees stable polyplex formation.

To analyze the stability and the dissociation properties of the formed polyplexes, the heparin dissociation assay was performed.[46–48] Heparin, a sulfated glycosaminoglycan, has an anionic character and competes with the nucleic acid of the polyplex. With increasing amount of heparin, the pDNA dissociates from the polymer and the polyplex dissolves. As indicated in Fig. 4B, polyplexes formed with partially hydrolyzed PEtOx (**P(EtOx-*stat*-EI)**) as well as **P2** and **P3** polymers revealed a reversible binding, achieving 80% dissociation at 5 U mL^{-1} heparin. A higher heparin concentration (20 U mL^{-1}) was required for **P1** reaching 80% dissociation. One reason for

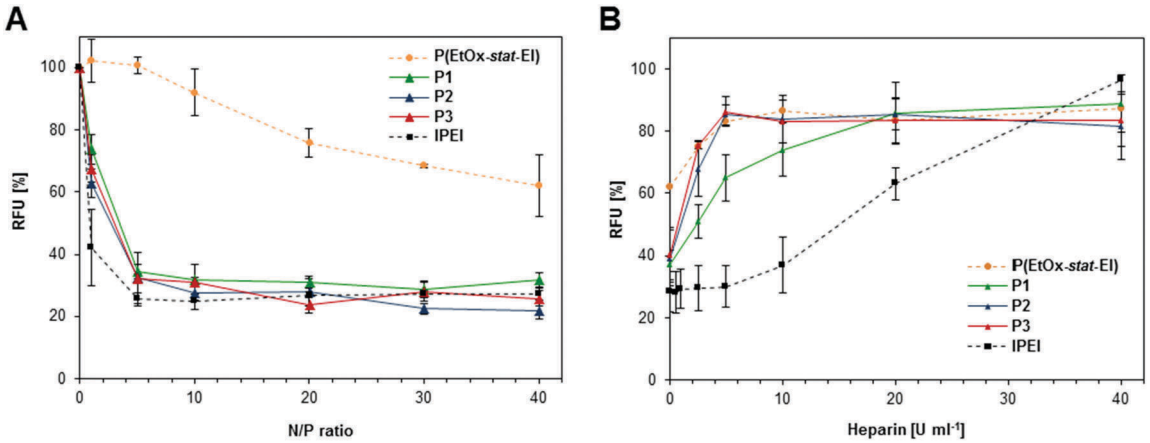

Fig. 4 Polyplex formation and stability with pDNA using the polymers **P(EtOx-*stat*-EI)**, **P1**, **P2**, **P3** as well as **lPEI**, which was used as positive control. (A) Complexation affinity (ethidium bromide quenching assay) of all polymers at the indicated N/P ratios. (B) Dissociation assay of polyplexes formed at N/P 30 using heparin. Values represent the mean ± S.D. (n = 3).

this might be the higher amount of AmButOx, responsible for an enhanced binding to the genetic material. However, a full release from the copolymers **P1** to **P3** could not be achieved using heparin. Therefore, another polyanion, namely poly(methacrylic acid) (PMAA, DP = 200), was successfully used as competitor (Fig. S5, ESI†). **lPEI** required an increased amount of heparin (40 U mL^{-1}) as compared to the copolymers. These results confirm the weakening of the electrostatic interactions caused by the presence of EtOx units, which are beneficial for a fast release of the genetic material.

As polyplexes are usually internalized into cells *via* endocytic pathways, the size as well as the charge of the complexes is of crucial importance. For efficient delivery, critical sizes of polymeric nanocarriers up to 200 nm are recommended.[33,49] As depicted in Table 2, the polyplexes formed with **P1** to **P3** at N/P 30 exhibit a favorable size of approximately 150 nm with a positive net charge, as determined by dynamic and electrophoretic light scattering. **P(EtOx-*stat*-EI)** formed complexes with a z-average of 242 ± 73.4 nm and high polydispersity (0.46) supporting the inefficient polyplex formation as observed by EBA.[50] Polyplexes formed with **lPEI** revealed a smaller complex size of 80 nm with a positive net charge comparable to previous studies.[46] These results support our assumption that the EtOx units impede the compact packaging of the genetic material into small polyplexes. This can be compensated by the presence of AmButOx units resulting in polyplex sizes between **lPEI** and loosely bound **P(EtOx-*stat*-EI)** polyplexes. Therefore, the tailored combination of EtOx and AmButOx units within the copolymer structure can be used to design polyplexes with required properties.

Table 2 Size and surface charge (zeta potential) of pDNA complexes at N/P 30 measured *via* dynamic light as well as electrophoretic light scattering

Polymeric system	z-Average [d, nm]	PDI	Zeta potential [mV]
P(EtOx-*stat*-PEI)	242 ± 73.4	0.46	20 ± 0.44
P1	158 ± 1.0	0.23	27 ± 0.25
P2	143 ± 1.4	0.21	23 ± 0.11
P3	154 ± 1.4	0.23	23 ± 0.12
lPEI	80 ± 2.3	0.17	33 ± 4.23

Transfection efficiency

Based on the previous results, the polymers **P1** to **P3** appear to be promising candidates as non-viral gene delivery agents and were, therefore, analyzed regarding their transfection efficiency (TE) using human embryonic kidney (HEK) cells and pDNA containing a enhanced green fluorescence protein reporter gene (*egfp*). The TE was determined by flow cytometry analyzing all viable cells (PI staining) which successfully express EGFP (see ESI,† Fig. S6 and S7). To investigate the interaction with serum proteins, a side effect of cationic polymers, the cells were transfected in serum reduced media (OptiMEM) and in serum containing media (RPMI1640 supplemented with 10% FCS) (Fig. 5). The use of serum offers test conditions more comparable to an *in vivo* situation and represents a known challenge for the performance of the polymers due to the inhibitory effect of serum proteins on the cellular uptake process.[51,52]

It should be noted that higher N/P ratios were required for the copolymers as all nitrogen atoms were taken into account for the N/P calculations. This includes also the amide functionalities of EtOx and AmButOx although they are not capable to interact with the pDNA. **P1**-based polyplexes were less efficient as indicated by a TE below 50%. High TEs over 60% were achieved in serum reduced conditions for **P2** and **P3** polyplexes at N/P 30 to 50. Comparable TEs were obtained for **lPEI** at N/P20. Compared to the transfection in OptiMEM, the EGFP transfection level of **P1** to **P3** at N/P 50 in serum containing media did not change considerably. Due to the cytotoxic effect of **lPEI** and the influence of serum proteins the cell viability as well as the TE decreased rapidly with increasing N/P ratios.

The combination of high cell viability (no cyto-/hemotoxicity) and formidable transfection performance even in the presence of proteins underlines the potential of **P2** and, in particular, **P3** as preferable gene delivery vectors. Moreover, **P3** also withstands

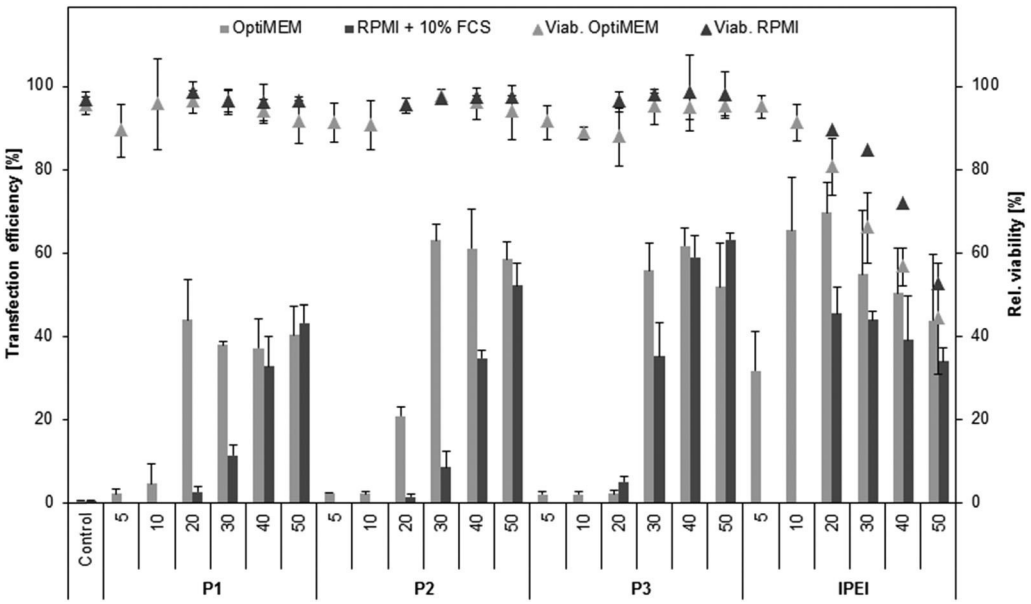

Fig. 5 Transfection efficiency of copolymers **P1** to **P3** and **lPEI** for adherent HEK cells in serum reduced (OptiMEM, light grey) and serum containing media (RPMI + 10% FCS, dark grey) at different N/P ratios after 24 h. Values represent the mean ± S.D. (n = 3).

a comparison to **lPEI** and the literature known 'gold standard for transfection', **comlPEI** (see ESI,† Fig. S18).

Uptake mechanism

For cationic polyplexes, the internalization into cells by endocytosis followed by the endosomal release of the pDNA into the cytosol and the subsequent transport into the nucleus is reported.[53,54] To clarify this process and to understand the excellent transfection performance of the copolymers, the uptake mechanism was investigated. An uptake kinetic using polyplexes formed with YOYO-1 labeled pDNA was performed to detect the internalization within cells by flow cytometry (Fig. 6). All tested polymers exhibited a fast and time-dependent cellular uptake. In detail, almost 90% of measured cells internalized polyplexes after 4 h when medium is changed

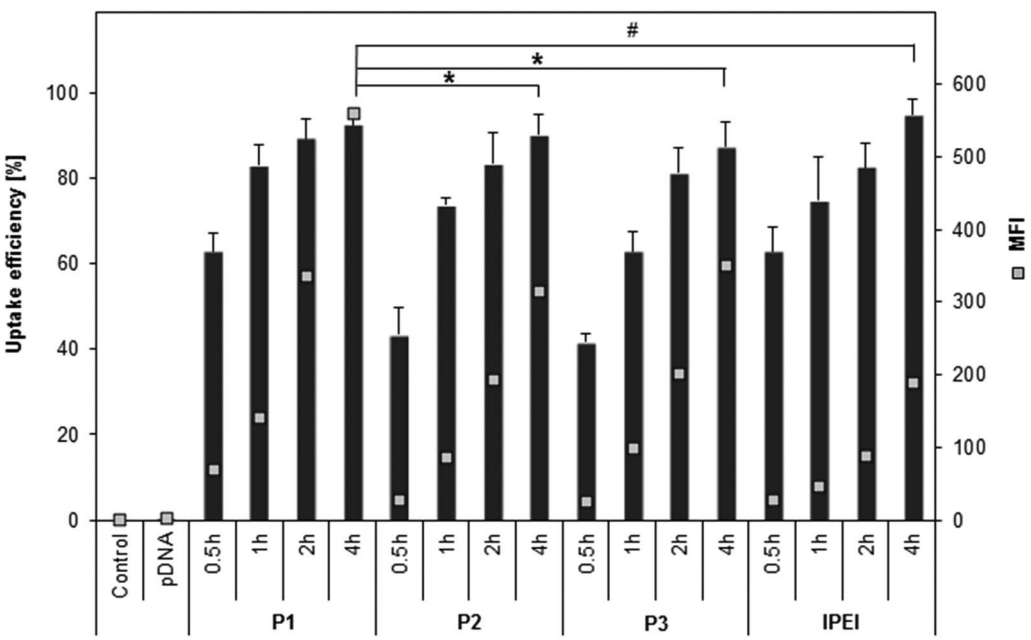

Fig. 6 Uptake study. Polyplexes formed with YOYO-1 labeled pDNA were incubated with HEK cells in OptiMEM for indicated time points using the copolymers **P1** to **P3** and **lPEI** (N/P ratio 30) as control. Statistical analysis (t-test) was used to compare the MFI after 4 h of **P1** with **P3** and **lPEI**, * represents $p < 0.05$ and # $p < 0.005$ of MFI values using student's t-test. Values represent the mean ± S.D. (n = 3).

according to standard transfection protocol. In particular, **P1** as well as **lPEI** showed an enhanced uptake efficiency after 30 min (~60%) compared to **P2** and **P3** (40%). Although most of the cells internalized polyplexes, the quantities (mean fluorescence intensities, MFI) differ significantly after 4 h (Fig. 6). Higher internalized polyplex concentrations were detected in cells using **P2**, **P3** (twofold) and **P1** (threefold) compared to **lPEI**. An explanation might be the introduction of AmButOx to the copolymers for enhanced complexation with the genetic material and cellular uptake, while the EtOx content possessing reduced membrane disruption.

To preclude an uptake by passive membrane diffusion, the uptake of YOYO-1 stained polyplexes was performed at 4 °C and 37 °C, respectively (Fig. S8B, ESI†). Polyplexes of all tested polymers were internalized into cells at 37 °C with approximately 90% efficiency. In contrast, the uptake efficiency was significantly decreased to approximately 10% at 4 °C for all samples. This indicates an energy-dependent uptake (endocytotic process). Furthermore, bafilomycin, a proton pump (H^+-ATPase) inhibitor, was used to prevent endosomal release caused by acidification (Fig. S8A, ESI†). The inhibition of an endosomal escape prevents the release of pDNA into the cytoplasm, the transfer into the nucleus and the EGFP expression. As expected, the TE significantly decreased after treatment with bafilomycin for all tested polymers to <5%. This indicates the involvement of the endosomal uptake and release as critical steps during the transfection mechanism, as it is reported for PEI.[43,55]

High resolution microscopy of polyplex–cell interactions

Deeper insights into the uptake mechanism and the fate of polyplexes within the cells were obtained with microscopic studies including confocal microscopy, structured illumination microscopy (SIM) and high-angular annular dark-field scanning transmission electron microscopy (HAADF-STEM).

Confocal microscopy as well as SIM studies were performed with HEK cells and polyplexes based on YOYO-1 labeled pDNA and Cy5-labeled **P3** representing the polymer with the overall highest transfection efficiency compared to **lPEI**. Fluorescence imaging of cells, in particular SIM images, revealed a co-localization of pDNA-bound **P3** polyplexes (blue) within the lysosomes/late endosomes (red, RFP labeling, Fig. 7 and Fig. S9 and S10, ESI†). The detection of the YOYO-signal within the cytoplasm that was not co-localized with lysosomal structures reveals that pDNA is released from the polyplex itself. Considering the low concentration of heparin required to destabilize the polyplex, an efficient release of pDNA into the cytoplasm can be assumed. As SIM provides a resolution of approx. 100 nm, a more detailed insight into the polyplex behavior within the lysosomes/late endosomes was obtained compared to conventional confocal imaging. A non-centrically localization of **P3** polyplexes

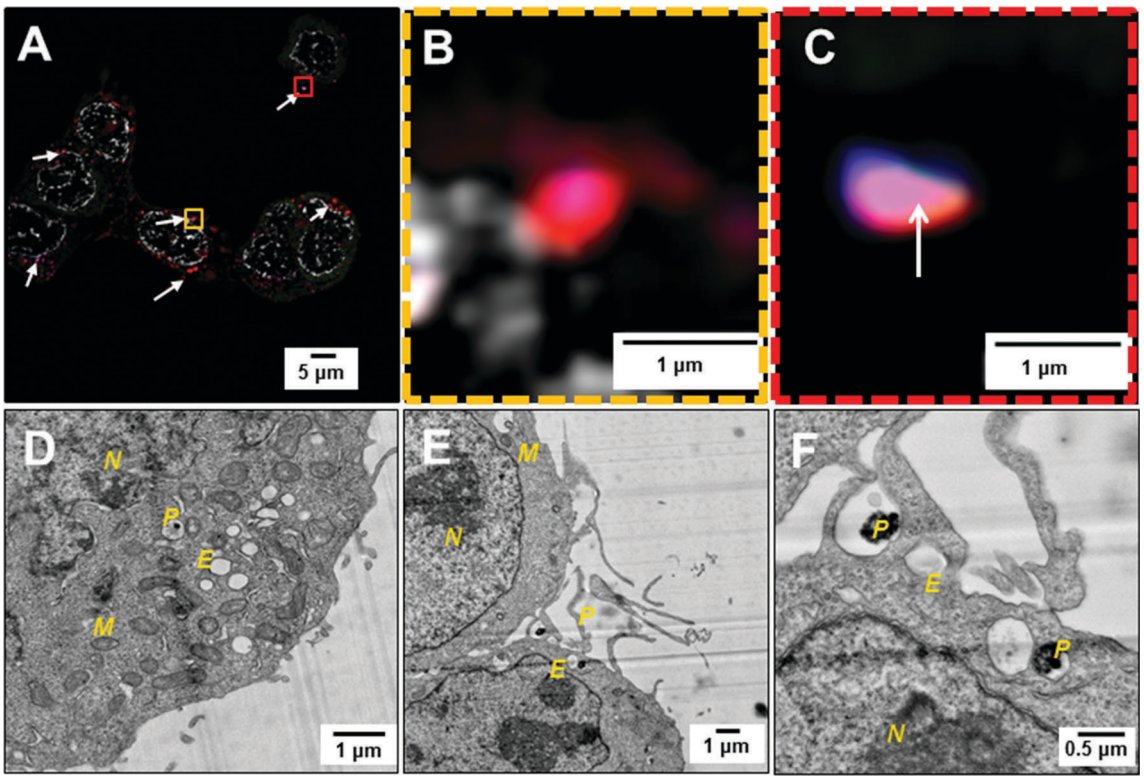

Fig. 7 High resolution imaging. (A) Structured illumination image of **P3**-based polyplexes within cells (deconvolved data). White arrows indicate co-localization of **P3**-pDNA polyplexes within lysosomes. (B and C) Magnified view of the yellow and red, dash-lined frame in (A): **P3**-Cy5 polyplex within the endosome. 63× Oil Obj. 1.4 NA. Grey: Hoechst 33342. Red: lysosomal membrane (RFP). Green: plasmid DNA labeling (YOYO-1). Blue: polymer labeling (Cy-5). (D–F) HAADF-STEM images of **P3**-based polyplexes taken up by HEK cells. The following letters correspond to cell organelles: N = cell nucleus, M = mitochondria, E = endosomal compartment, P = polyplex.

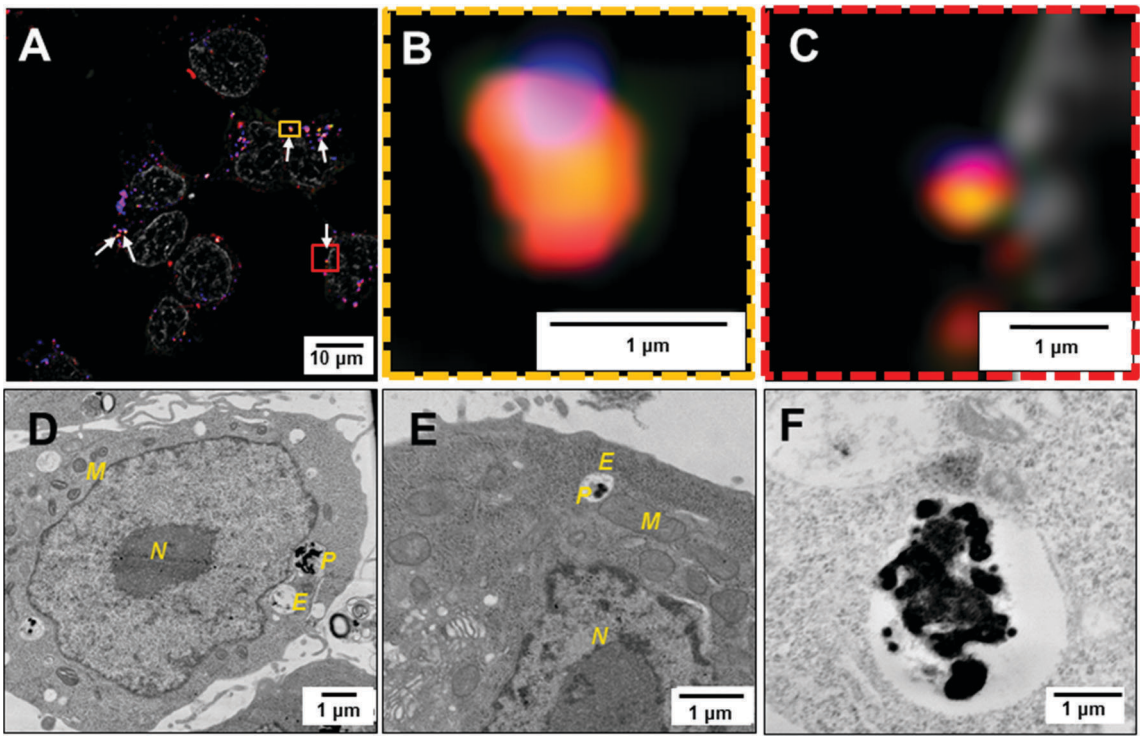

Fig. 8 High resolution imaging. (A) Structured illumination image of **lPEI**-based polyplexes within HEK cell, white arrows indicates full co-localization (deconvolved data). (B and C) Magnified zoom of yellow and red, dash-lined frame in (A): **lPEI-Cy5** polyplex within the endosome. 63× oil obj. 1.4 NA. Grey: Hoechst 33342. Red: lysosomal membrane (RFP). Green: plasmid DNA labeling (YOYO-1). Blue: polymer labeling (Cy-5). (D–F) HAADF-STEM images of **lPEI**-based polyplex taken up by HEK-293 cell. The following letters correspond to cellular structures: N = cell nucleus, M = mitochondria, E = endosomal compartment, P = polyplex.

(Cy5 and YOYO-1 signal) within the endosome (red) was observed, being in close vicinity to the endosomal membrane (Fig. 7A and zoom-in Fig. 7B and C, single channel splitting: Fig. S11, ESI†). This could be attributed to a strong interaction between the polyplex and the cytoplasmic membrane at the time of the cellular uptake or a strong interaction of the polyplex with the endosomal membrane caused by acidification. However, also **lPEI** polyplexes (Cy5 and YOYO-1 signal) were localized in close vicinity to the endosomal membrane (Fig. 8A and zoom-in Fig. 8B and C, single channel splitting: Fig. S12, ESI†). Interestingly, a higher number of larger endosomes bearing polyplex signals with an apparent larger spatial dimension was found for **lPEI** in contrast to **P3**. To study the interaction of both polymers with the endosomal membrane in more detail, STEM on embedded sections was carried out to confirm this assumption. STEM provides a resolution in the low nanometer range, elucidating the subcellular ultrastructural context, and particularly, highlighting membrane structures. EM images revealed an uptake of single **P3** polyplexes into vesicles with sizes of 200 to 500 nm ($n > 10$ vesicles of different sections were analyzed, Fig. S13, ESI†). Although, the polyplexes themselves provide only poor electron contrast, their structures were highlighted efficiently within the cellular environment (Fig. 7D–F) in the sample by sample staining. This can be explained by the strong affinity of the amines of the polymer and phosphates of the DNA to the heavy metal stains (OsO_4 and uranylacetate, respectively). The close vicinity between **P3** polyplex and the endosomal membrane was confirmed. We attribute this observation to a preceding active cell membrane-driven uptake event, initiated by strong interaction of a single polyplex with the membrane. We observed an uptake event involved by membrane ruffles and lamellipodia-like structures (Fig. 7E and F), supporting our previous findings concerning an energy-dependent uptake, such as by macropinocytosis. We therefore investigated cells after incubation with **P3** polyplexes in the presence of the inhibitor, 5-(*N*-ethyl-*N*-isopropyl)amiloride (EIPA, 100 µM). Our experiments support the assumption, since only 25% of the cells internalized **P3** polyplexes after 4 h (see ESI,† Fig. S14). Performing STEM imaging, we observed no **P3** polyplexes within the cytoplasm (see ESI,† Fig. S15A and B). This underlines an uptake mechanism *via* macropinocytosis.

STEM images of **lPEI** polyplexes revealed larger endosomes with sizes of 500 to 1500 nm ($n > 10$ vesicles of different sections were analyzed, Fig. S16, ESI†) bearing more than a single polyplex as well as increased cellular membrane rupture (Fig. 8D–F). The presence of multiple polyplexes within large endosomes explains the large spatial dimension of the polyplex signals as being found in SIM images (Fig. 8F). STEM images of cells, which were incubated with **lPEI** polyplexes in the presence of a macropinocytosis inhibitor (EIPA), revealed indeed a cellular internalization (see ESI,† Fig. S15C and D). However, the uptake efficiency was apparently lower compared to the

standard uptake protocol (~65% YOYO-positive cells after 4 h) and hints towards alternative uptake mechanisms in addition to macropinocytosis. It was already demonstrated that **lPEI** possesses a high membrane activity (see erythrocyte aggregation, Fig. S3 and S4, ESI†), which is in association with polymer aggregation in serum containing media[5] and could lead to enhanced uptake of multiple polyplexes within single endosomes. Aggregated polyplexes could be also responsible for a reduced uptake because of a size-limited uptake mechanism, *e.g.* endocytosis. The presence of EtOx subunits within **P3** shields the formed polyplexes from aggregation caused by protein interaction prior to uptake. This might be a reason for a more efficient cellular uptake and the high transfection efficiency of the respective copolymer. Based on this data, the efficient endosomal release of single **P3** polyplexes is impressive compared to agglomerated **lPEI** polyplexes. Due to the high buffer capacity of **lPEI**, an enhanced protonation of amines followed by the swelling of the endosomes might occur, as it is hypothesized for the "proton sponge" effect.[6,51,53,54,56] In case of **P3**, the full protonation of the primary/secondary amines could lead to a destabilization of the membrane indicating a membrane rupture and the subsequent release of the cargo into the cytosol. A previous study of Zuhorn and co-workers describes a similar process for PEI polyplexes supporting these findings.[52] Additionally, the authors showed that the release did not come along with a complete rupture of the endosome. As the polymers **P1** to **P3** possess a content of 12 to 23% secondary amines and a content of primary amines of 34 to 23%, they do not show such a severe swelling of endosomal compartments like **lPEI** polyplexes. Nevertheless, it can be assumed that a protonation of the primary amines in the side chain within the endosomal compartments forces the interaction of the polymers with the endosomal membrane leading to an efficient endosomal release. These results indicate that not only the buffer capacity and the swelling of endosomal compartments but also the interaction of the polymer with the endosomal membrane facilitate the escape from the endosome, which is in accordance to literature data and visualized in detail.[51,52]

siRNA delivery

To further investigate the potential of the modified PEI copolymers, the delivery efficiency for siRNA was determined. Although DNA and siDNA represent genetic material they differ in certain characteristics. Most importantly, siRNA is smaller (<30 base pairs (bp) compared to 4700 bp pDNA) and more rigid. From a biological point of view, pDNA has to be transferred across the nuclear barrier to the cell nuclei, whereas siRNA has to be released from the polyplex in the cytoplasm to form the RNA-induced silencing complex (RISC).[57]

The copolymers **P1** to **P3** were further investigated regarding the influence of primary and secondary amines for siRNA delivery. High binding affinity to siRNA (<40%) of all tested polymers was observed by EBA (Fig. 9A). Positively charged polyplexes with a size of <200 nm were formed, whereas **lPEI** polyplexes exhibited a compact size of around 83 nm (Table 3). This trend was also observed for the pDNA based polyplexes (see Table 2).

A GFP-expressing CHO cell line was used to estimate the knockdown efficiency (Fig. 9B). Interestingly, **P1** showed superior knockdown efficiency for siRNA (244 ± 50.3 MFI), compared to **P3** (317 ± 19.3 MFI), which was identified as best performer for pDNA transfection. Both, **P1** and **P2**, led to a significant reduction of around 40% of the fluorescence intensity of EGFP-expressing cells. In contrast, **P3** showed only 10 to 20% reduction of MFI. Interestingly, **lPEI** as well as branched PEI

Table 3 Size and surface charge (zeta potential) of the siRNA complexes at N/P 30 measured *via* dynamic light as well as electrophoretic light scattering in water-based HBG buffer

Polymeric system	*z*-Average [d, nm]	PDI	Zeta potential [mV]
P1	102 ± 1.2	0.15	21 ± 1.2
P2	124 ± 1.5	0.13	25 ± 1.0
P3[a]	149 ± 12.6	0.49	22 ± 0.1
lPEI	83 ± 2.3	0.23	33 ± 1.6

[a] Intensity weighted size distribution revealed a mean peak of 257 nm (68%).

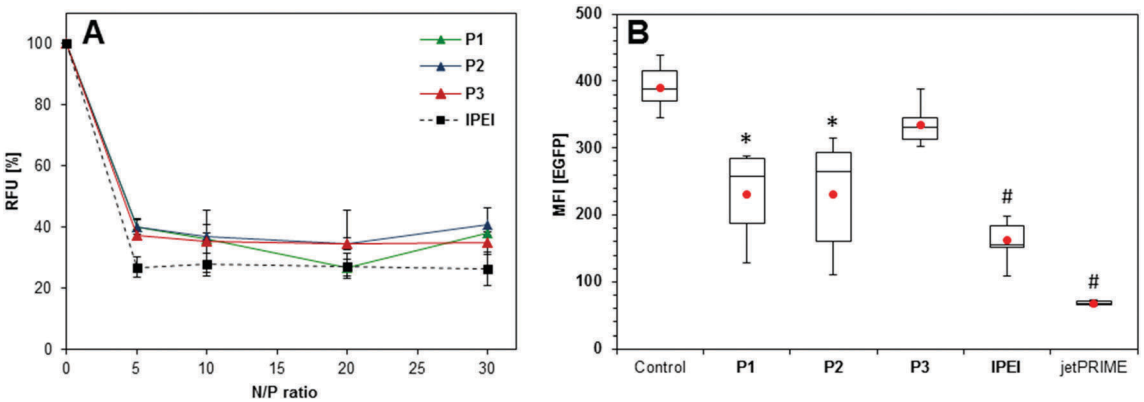

Fig. 9 Investigations of the siRNA delivery. (A) Binding affinity of siRNA to **P1** to **P3** and **lPEI** at different N/P ratios measured by the fluorescence quenching of ethidium bromide. The fluorescence of pure siRNA represents 100% RFU. (B) siRNA knockdown mediated by **P1** to **P3**, **lPEI** and jetPRIME polyplexes at N/P 30 after 72 h. Stable EGFP-expressing CHO cells were transfected with polyplexes formed using siRNA able to knock down *egfp*. Statistical analysis (*t*-test) was used to compare the mean fluorescence intensity (MFI) of the control with **P1** to **P3** and **lPEI**, * represents $p < 0.05$ and # $p < 0.005$. The values represent the mean ± S.D. ($n \geq 3$).

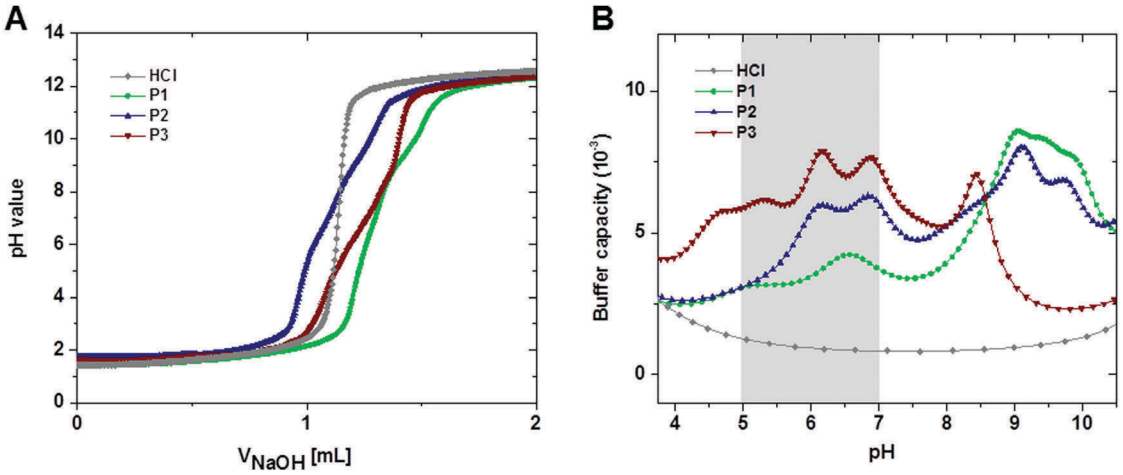

Fig. 10 (A) Acid–base titration curves of an acidified solution of the cationic copolymers **P1** to **P3** (~5 mg mL^{-1}) dissolved in 4 mL hydrogen chloride (HCl, 0.06 M) and neutralized with sodium hydroxide (0.1 M). For comparison, 0.06 M HCl was titrated accordingly. Precipitation of **lPEI** at pH 7 prevents the interpretation of the respective titration curve. (B) The buffer capacities of the cationic copolymers **P1** to **P3** were calculated from A utilizing the relation $\beta = dn(OH^-)/dpH$ and presented as a function of the pH value. For comparison, the buffer capacity of HCl is included.

(**bPEI**) revealed high knockdown potentials of around 60% (Fig. 9B). **ComlPEI** was less efficient and exhibited comparable efficiencies to the copolymers **P1** and **P2** (Fig. S20, ESI†). However, the highest knockdown (>80%, ~68 ± 3.9 MFI) was achieved with the positive control jetPRIME (cationic, polymeric transfection reagent, Polyplus). The fluorescence intensities were not reduced when using scrambled siRNA (negative control, see ESI,† Fig. S17). The polymers **P1** and **P2** revealed adequate knockdown levels, but are not as effective as commercially available siRNA transfection agents. Nevertheless, the promising performance and high biocompatibility of these 3rd generation PEIs could be developed in future studies by optimizing the polymeric design and composition as a higher AmOx content shows improved performance.

To understand the different performances of the copolymers depending on the genetic material, the endosomal release has to be considered. For successful delivery of siRNA a fast and efficient release from the endosome into the cytosol is beneficial, whereas the transfection efficiency of pDNA is increased, when it is transported to the perinuclear region inside endosomal compartments.[58]

From the titration of the polymers **P1** to **P3** (Fig. 10A) the buffer capacities of the respective copolymers were calculated ($\beta = dn(OH^-)/dpH$) and expressed as a function of the pH value (Fig. 10B). The copolymers show considerable higher buffer capacities with increasing EI content for pH values between 5 and 7 (endosomal release environment). As **P3** revealed the

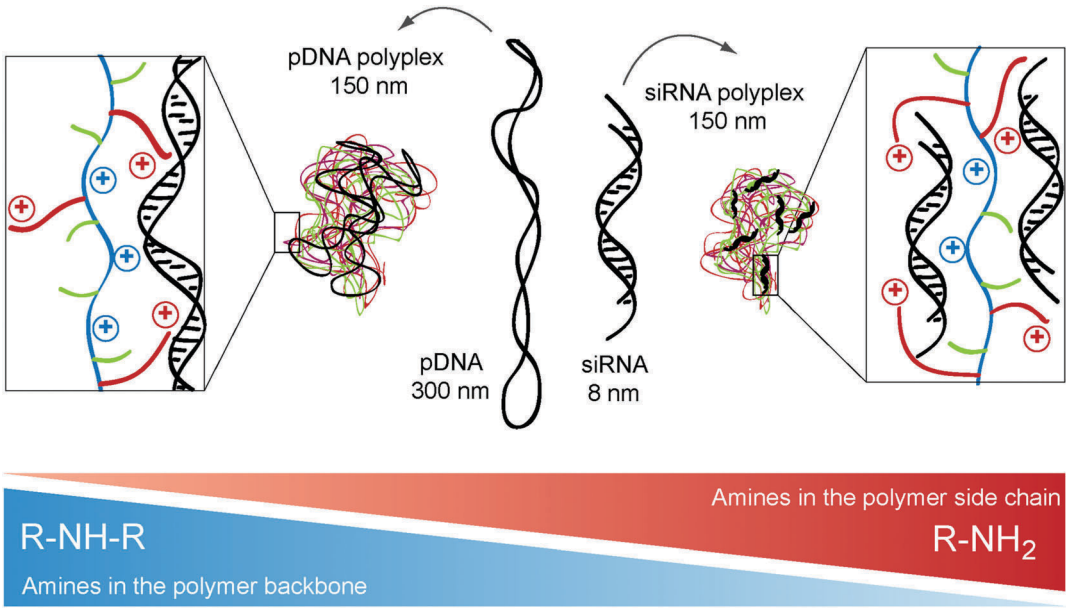

Fig. 11 Schematic representation of the polyplex formation illustrating the interaction of 3rd generation poly(ethylene imine) with pDNA or siRNA.

highest buffer capacity at acidic conditions, this could be an explanation for the diminished performance for siRNA delivery due to a delayed endosomal escape. In contrast, **P1** showed the highest degree of protonation at endosomal pH values facilitating a faster endosomal release into the cytosol by interaction of the charged amines with the endosomal membrane. It should be kept in mind, that **P1** and **P2** revealed also a high buffer capacity at a pH value around 9, in contrast to **P3**, which could be a hint for different performances.

Moreover, it could be assumed that the different physicochemical parameters of the genetic material (size, topology) play a crucial role for the interaction with the 3rd generation PEIs (Fig. 11). siRNA is small and stiff preferentially interacting with the primary amines in the polymer side chain. In contrast to that, the large pDNA requires the interaction with the primary amines (flexible side chains) as well as the secondary amines (backbone). This enabled an tremendous enhancement of pDNA delivery compared to literature reported polymer systems, *e.g.* P(EtOx-*stat*-MeOx).[17]

Conclusion

The introduced 3rd generation PEI copolymers has shown to present several advantages in contrast to 1st (PEI) and 2nd (single PEI modifications) generation approaches in terms of efficient polymeric gene delivery. Starting from high molar mass PEtOx, partially hydrolyzed **P(EtOx-*stat*-EI)** copolymers were synthesized. Subsequently, different amounts of the ethylene imine subunits were functionalized, introducing alkene groups which, in turn, could be used to attach primary amine groups in the side chains using thiol–ene chemistry. While the EtOx content of these polymers remained constant, the ratio between primary and secondary amine groups was varied to obtain a series of copolymers. It should be highlighted that no adverse effects on the cell viability was observed for polymer concentrations up to 1 mg mL^{-1} in contrast to **lPEI** (IC_{50} = 3.6 μg mL^{-1}). Remarkably, these 3rd generation PEIs were, in contrast to the 2nd generation **P(EtOx-*stat*-EI)**, able to form well-defined complexes with various genetic materials, in detail pDNA and siRNA. Besides a fast uptake, the delivery of pDNA revealed comparable transfection efficiencies to **lPEI**. In serum containing media, the performance of copolymer-based polyplexes could even exceed the efficiency of **lPEI**. Furthermore, the copolymers (in particular **P1** and **P2**) revealed siRNA delivery capability as well. Nevertheless, an optimization of this approach should be further pursued in future studies. Noteworthy, a different ratio of primary to secondary amines is required to form appropriate polyplexes with siRNA emphasizing the multivalence and potential of the presented polymeric system.

Using live cell confocal microscopy, super-resolution microscopy as well as transmission electron microscopy of ultrathin sections of embedded cell samples, the transfection mechanism was elucidated in more detail. In contrast to **lPEI**, where endosomes contained multiple polyplexes in swollen endosomes, copolymer based polyplexes present themselves individually within the endosomal compartments. This was attributed to a lower protein interaction of **PEtOx** containing vectors, preventing agglomeration in serum containing media prior to uptake as well as to a diminished membrane interaction. This feature also leads to a release process based on membrane interactions of the described polyplexes in contrast to the ''proton sponge'' effect hypothesized for PEI. The 3rd generation PEI outperforms PEI of former generations (1st and 2nd) concerning an overall concept in terms of toxicity as well as transfection efficiency for a wide range of genetic materials. Thus, it represents a promising alternative for more complex transfection approaches including hard-to-transfect cells or *in vivo* studies.

Acknowledgements

The authors would like to thank Dr. Michael Wagner for AF4 measurements and Carolin Fritzsche for support of the cyto- and hemocompatibility assays. This project was funded by the German Federal Ministry of Education & Research (BMBF, #031A518B Vectura, #13N13416 smart-dye-livery), the Thüringer Ministerium für Wirtschaft, Wissenschaft, und Digitale Gesellschaft (TMWWDG, ProExzellenzI, NanoConSens; ProExzellenzII, NanoPolar). The funding of the collaborative research center ChemBioSys (SFB 1127) by the Deutsche Forschungsgemeinschaft (DFG) is highly acknowledged. MR and AT are grateful for the financial support in the frameworks of ''Carl-Zeiss-Strukturmaßnahme'' and the Carl-Zeiss Stiftung. MH gratefully acknowledges the DFG (GZ: HA 7725/1-1) for funding. The LSM880 ELYRA PS.1 was further funded with a grant from the DFG. The transmission electron microscope was obtained with a grant from the European Funds for Regional Developments (EFRE) and the DFG.

References

1 U. Laechelt and E. Wagner, *Chem. Rev.*, 2015, **115**, 11043–11078.
2 A. C. Rinkenauer, S. Schubert, A. Traeger and U. S. Schubert, *J. Mater. Chem. B*, 2015, **3**, 7477–7493.
3 U. Lungwitz, M. Breunig, T. Blunk and A. Göpferich, *Eur. J. Pharm. Biopharm.*, 2005, **60**, 247–266.
4 M. A. Mintzer and E. E. Simanek, *Chem. Rev.*, 2009, **109**, 259–302.
5 M. Neu, D. Fischer and T. Kissel, *J. Gene Med.*, 2005, **7**, 992–1009.
6 O. Boussif, F. Lezoualc'h, M. A. Zanta, M. D. Mergny, D. Scherman, B. Demeneix and J. P. Behr, *Proc. Natl. Acad. Sci. U. S. A.*, 1995, **92**, 7297–7301.
7 W. T. Godbey, M. A. Barry, P. Saggau, K. K. Wu and A. G. Mikos, *J. Biomed. Mater. Res.*, 2000, **51**, 321–328.
8 S. De Smedt, J. Demeester and W. Hennink, *Pharm. Res.*, 2000, **17**, 113–126.
9 I. Y. Perevyazko, M. Bauer, G. M. Pavlov, S. Hoeppener, S. Schubert, D. Fischer and U. S. Schubert, *Langmuir*, 2012, **28**, 16167–16176.
10 M. Jager, S. Schubert, S. Ochrimenko, D. Fischer and U. S. Schubert, *Chem. Soc. Rev.*, 2012, **41**, 4755–4767.

11 P. Chollet, M. C. Favrot, A. Hurbin and J.-L. Coll, *J. Gene Med.*, 2002, **4**, 84–91.
12 J. H. Jeong, S. H. Song, D. W. Lim, H. Lee and T. G. Park, *J. Controlled Release*, 2001, **73**, 391–399.
13 Y. Yue, F. Jin, R. Deng, J. Cai, Z. Dai, M. C. M. Lin, H.-F. Kung, M. A. Mattebjerg, T. L. Andresen and C. Wu, *J. Controlled Release*, 2011, **152**, 143–151.
14 M. Thomas, Q. Ge, J. J. Lu, J. Chen and A. Klibanov, *Pharm. Res.*, 2005, **22**, 373–380.
15 W. Y. Seow, K. Liang, M. Kurisawa and C. A. E. Hauser, *Biomacromolecules*, 2013, **14**, 2340–2346.
16 C. Englert, M. Hartlieb, P. Bellstedt, K. Kempe, C. Yang, S. K. Chu, X. Ke, J. M. García, R. J. Ono, M. Fevre, R. J. Wojtecki, U. S. Schubert, Y. Y. Yang and J. L. Hedrick, *Macromolecules*, 2015, **48**, 7420–7427.
17 A. C. Rinkenauer, L. Tauhardt, F. Wendler, K. Kempe, M. Gottschaldt, A. Traeger and U. S. Schubert, *Macromol. Biosci.*, 2015, **15**, 414–425.
18 S. Taranejoo, J. Liu, P. Verma and K. Hourigan, *J. Appl. Polym. Sci.*, 2015, 132.
19 S. Ochrimenko, A. Vollrath, L. Tauhardt, K. Kempe, S. Schubert, U. S. Schubert and D. Fischer, *Carbohydr. Polym.*, 2014, **113**, 597–606.
20 M. Noga, D. Edinger, E. Wagner, G. Winter and A. Besheer, *J. Biomater. Sci., Polym. Ed.*, 2014, **25**, 855–871.
21 M. Ogris, S. Brunner, S. Schuller, R. Kircheis and E. Wagner, *Gene Ther.*, 1999, **6**, 595–605.
22 H. Petersen, P. M. Fechner, D. Fischer and T. Kissel, *Macromolecules*, 2002, **35**, 6867–6874.
23 K. Knop, R. Hoogenboom, D. Fischer and U. S. Schubert, *Angew. Chem., Int. Ed.*, 2010, **49**, 6288–6308.
24 J. Liu, X. Jiang, L. Xu, X. Wang, W. E. Hennink and R. Zhuo, *Bioconjugate Chem.*, 2010, **21**, 1827–1835.
25 N. Zhao, S. Roesler and T. Kissel, *Int. J. Pharm.*, 2011, **411**, 197–205.
26 G. Zhang, J. Liu, Q. Yang, R. Zhuo and X. Jiang, *Bioconjugate Chem.*, 2012, **23**, 1290–1299.
27 Y. Yamazaki, M. Nango, M. Matsuura, Y. Hasegawa, M. Hasegawa and N. Oku, *Gene Ther.*, 2000, **7**, 1148–1155.
28 A. Sato, S. Kawakami, M. Yamada, F. Yamashita and M. Hashida, *J. Drug Targeting*, 2001, **9**, 201–207.
29 X. Wang, D. Niu, C. Hu and P. Li, *Curr. Pharm. Des.*, 2015, **21**, 6140–6156.
30 A. T. Press, A. Traeger, C. Pietsch, A. Mosig, M. Wagner, M. G. Clemens, N. Jbeily, N. Koch, M. Gottschaldt, N. Bézière, V. Ermolayev, V. Ntziachristos, J. Popp, M. M. Kessels, B. Qualmann, U. S. Schubert and M. Bauer, *Nat. Commun.*, 2014, **5**, 5565–5577.
31 H. P. C. Van Kuringen, J. Lenoir, E. Adriaens, J. Bender, B. G. De Geest and R. Hoogenboom, *Macromol. Biosci.*, 2012, **12**, 1114–1123.
32 R. Shah, Z. Kronekova, A. Zahoranová, L. Roller, N. Saha, P. Saha and J. Kronek, *J. Mater. Sci.: Mater. Med.*, 2015, **26**, 1–12.
33 R. Luxenhofer, G. Sahay, A. Schulz, D. Alakhova, T. K. Bronich, R. Jordan and A. V. Kabanov, *J. Controlled Release*, 2011, **153**, 73–82.
34 S.-D. Li and L. Huang, *J. Controlled Release*, 2010, **145**, 178–181.
35 A. C. Rinkenauer, A. Schallon, U. Günther, M. Wagner, E. Betthausen, U. S. Schubert and F. H. Schacher, *ACS Nano*, 2013, **7**, 9621–9631.
36 A. Gress, A. Völkel and H. Schlaad, *Macromolecules*, 2007, **40**, 7928–7933.
37 A. Krieg, C. Pietsch, A. Baumgaertel, M. D. Hager, C. R. Becer and U. S. Schubert, *Polym. Chem.*, 2010, **1**, 1669–1676.
38 H. M. L. Lambermont-Thijs, F. S. van der Woerdt, A. Baumgaertel, L. Bonami, F. E. Du Prez, U. S. Schubert and R. Hoogenboom, *Macromolecules*, 2010, **43**, 927–933.
39 M. Litt, A. Levy and J. Herz, *J. Macromol. Sci., Chem. A*, 1975, **9**, 703–727.
40 M. Bauer, S. Schroeder, L. Tauhardt, K. Kempe, U. S. Schubert and D. Fischer, *J. Polym. Sci., Part A: Polym. Chem.*, 2013, **51**, 1816–1821.
41 M. Bauer, C. Lautenschlaeger, K. Kempe, L. Tauhardt, U. S. Schubert and D. Fischer, *Macromol. Biosci.*, 2012, **12**, 986–998.
42 C. Englert, L. Tauhardt, M. Hartlieb, K. Kempe, M. Gottschaldt and U. S. Schubert, *Biomacromolecules*, 2014, **15**, 1124–1131.
43 T. Bieber, W. Meissner, S. Kostin, A. Niemann and H. P. Elsasser, *J. Controlled Release*, 2002, **82**, 441–454.
44 J. B. Lepecq and C. Paoletti, *J. Mol. Biol.*, 1967, **27**, 87–106.
45 A. J. Geall and I. S. Blagbrough, *J. Pharm. Biomed. Anal.*, 2000, **22**, 849–859.
46 A. Kwok and S. L. Hart, *Nanomedicine*, 2011, **7**, 210–219.
47 M. Ruponen, S. Ylä-Herttuala and A. Urtti, *Biochim. Biophys. Acta*, 1999, **1415**, 331–341.
48 S. Sundaram, S. Viriyayuthakorn and C. M. Roth, *Biomacromolecules*, 2005, **6**, 2961–2968.
49 J. Rejman, V. Oberle, I. S. Zuhorn and D. Hoekstra, *Biochem. J.*, 2004, **377**, 159–169.
50 R. V. Benjaminsen, M. A. Mattebjerg, J. R. Henriksen, S. M. Moghimi and T. L. Andresen, *Mol. Ther.*, 2013, **21**, 149–157.
51 M. Wagner, A. C. Rinkenauer, A. Schallon and U. S. Schubert, *RSC Adv.*, 2013, **3**, 12774–12785.
52 Z. U. Rehman, D. Hoekstra and I. S. Zuhorn, *ACS Nano*, 2013, **7**, 3767–3777.
53 A. M. Funhoff, C. F. van Nostrum, G. A. Koning, N. M. E. Schuurmans-Nieuwenbroek, D. J. A. Crommelin and W. E. Hennink, *Biomacromolecules*, 2004, **5**, 32–39.
54 A. Akinc, M. Thomas, A. M. Klibanov and R. Langer, *J. Gene Med.*, 2005, **7**, 657–663.
55 J. Rejman, A. Bragonzi and M. Conese, *Mol. Ther.*, 2005, **12**, 468–474.
56 J. P. Behr, *Acc. Chem. Res.*, 2012, **45**, 980–984.
57 A. T. Da Poian, F. A. Carneiro and F. Stauffer, *Braz. J. Med. Biol. Res.*, 2005, **38**, 813–823.
58 C. Scholz and E. Wagner, *J. Controlled Release*, 2012, **161**, 554–565.

Electronic Supplementary Material (ESI) for Journal of Materials Chemistry B.

SUPPORTING INFORMATION:

3rd Generation Poly(ethylene imine)s for Gene Delivery

Tanja Bus,[a,b,†] Christoph Englert,[a,b,†] Martin Reifarth,[a,b,c,d] Philipp Borchers,[a,b]
Matthias Hartlieb,[a,b,#] Antje Vollrath,[a,b] Stephanie Hoeppener,[a,b]
Anja Traeger,[a,b,] Ulrich S. Schubert[a,b,]**

[a] *Laboratory of Organic and Macromolecular Chemistry (IOMC), Friedrich Schiller University Jena, Humboldtstrasse 10, 07743 Jena, Germany*

[b] *Jena Center for Soft Matter (JCSM), Friedrich Schiller University Jena, Philosophenweg 7, 07743 Jena, Germany*

[c] *Institute of Physical Chemistry and Abbe Center of Photonics, Friedrich Schiller University Jena, Helmholtzweg 4, 07743 Jena, Germany*

[d] *Leibniz Institute of Photonic Technology, Albert-Einstein-Strasse 9, 07745 Jena, Germany*

[†] *The authors contributed equally to this work*

[#] *Current address: Department of Chemistry, University of Warwick, Gibbet Hill Road, Coventry, CV4 7AL, UK.*

Email: ulrich.schubert@uni-jena.de, anja.traeger@uni-jena.de

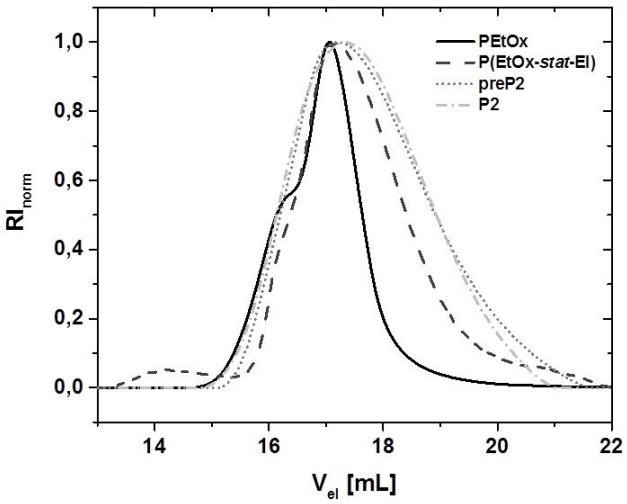

Figure S1. Size exclusion chromatography traces of the starting homopolymer **PEtOx** and the copolymers **P(EtOx-*stat*-EI)**, **preP2** and **P2** (*N*,*N*-dimethylacetamide, 0.21% LiCl, calibration: polystyrene).

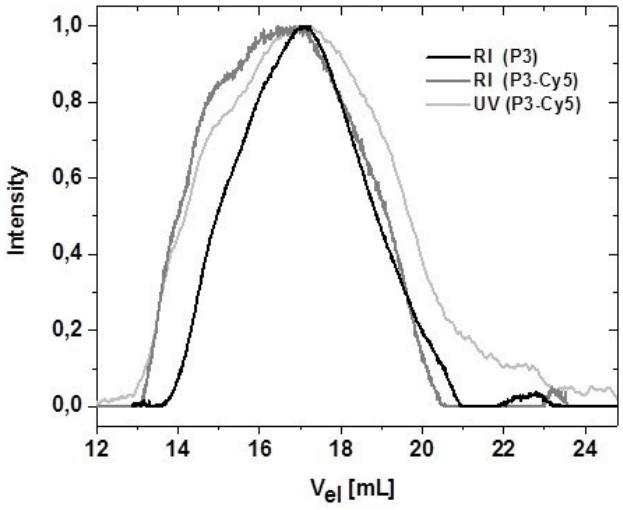

Figure S2. Size exclusion chromatography elugrams of the labeled copolymer **P3** (**P3-Cy5**) in comparison to the unlabeled starting material (**P3**) (*N*,*N*-dimethylacetamide, 0.21% LiCl, calibration: polystyrene).

Hemocompatibility of PEI-based polyplexes

The erythrocyte aggregation of the PEI copolymers was performed in parallel with high molar mass lPEI polymers as positive controls. **lPEI** show membrane-perturbing activity at high concentrations (100 µg mL^{-1}) leading to the aggregation of erythrocytes as indicated in the photospectrometrically measurement and by light microscopy. This effect was not seen with the copolymers **P1** to **P3**.

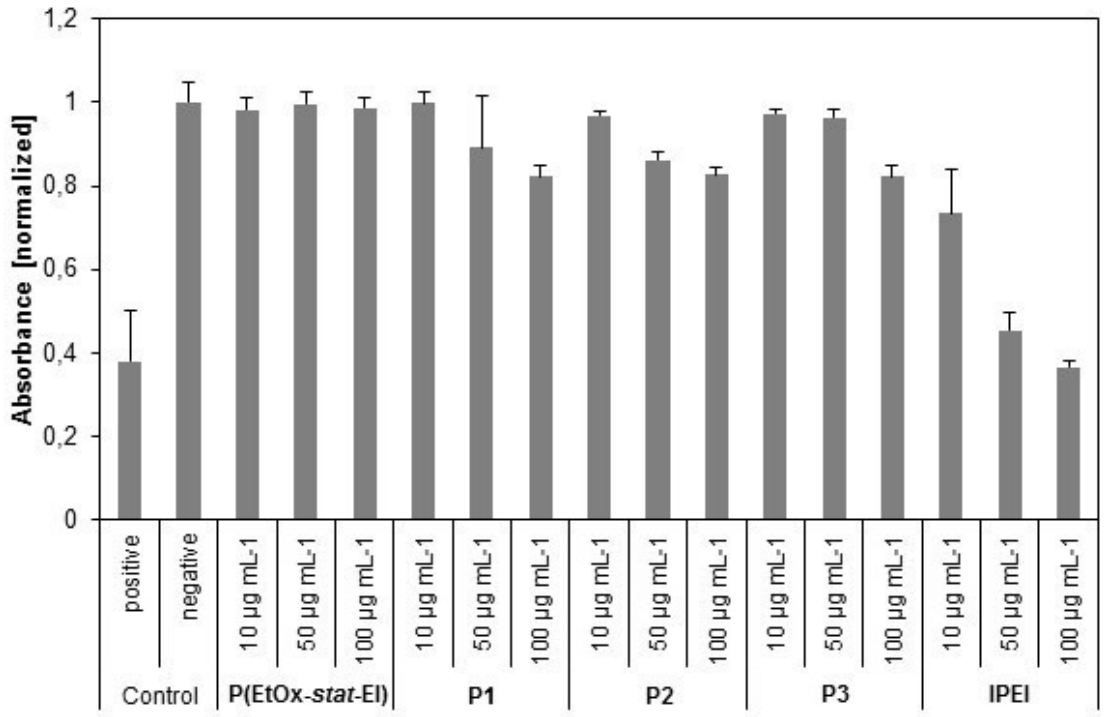

Figure S3. Erythrocyte aggregation of the tested polymers at indicated concentrations. bPEI (25 kDa) served as positive control resulting in high aggregation formation and PBS as negative control. Values represent the mean ± S.D. (n=3).

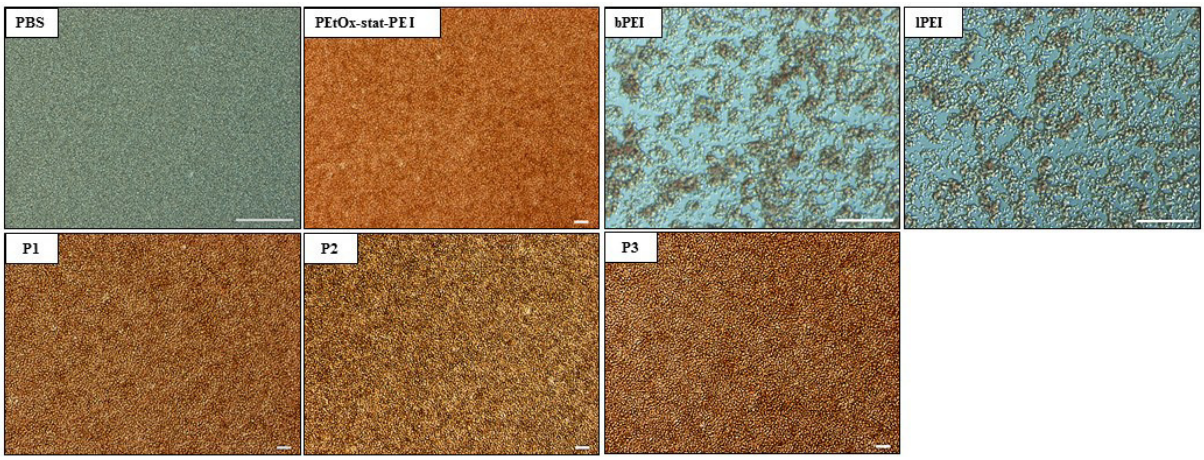

Figure S4. Light microscopy of erythrocyte aggregation of the polymers **P1** to **P3**, **PEtOx** and both **lPEI** polymers. PBS served as negative control, while bPEI (25kDa) was served as positive control. Scale bar = 50 µm.

Interaction of polymers with genetic material

The polyplex dissociation assay was performed aside from heparin with poly(methacrylic acid) (PMAA) (DP = 200) as competing factor. To keep equal conditions, same PMAA concentrations as for heparin were used during the measurement.

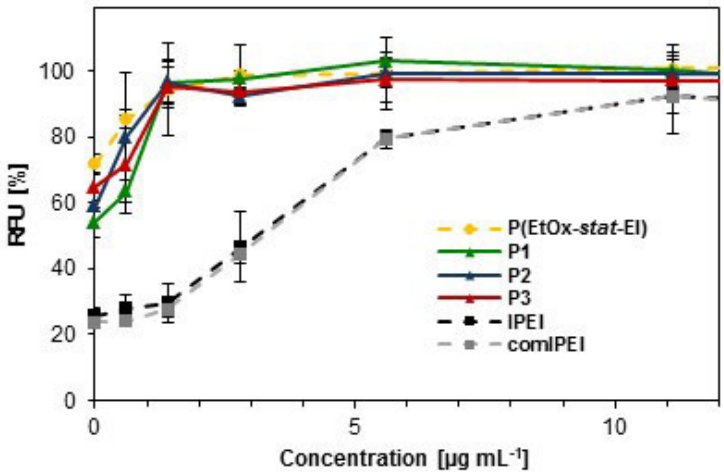

Figure S5. Dissociation assay of polyplexes formed with pDNA at N/P 30 and with increasing PMAA concentrations, which correlates to heparin concentrations.

Analysis of polyplex uptake and transfection of cells

The uptake and transfection studies were performed with HEK cells and pDNA encoding the EGFP (enhanced green fluorescence protein) or with YOYO-labeled pDNA. Transfection efficiency was determined by measuring the amount of viable cells (PI stained) expressing EGFP after 24 h *via* flow cytometry, whereas non-transfected cells served as negative control. To determine the amount of EGFP expressing cells, the histogramm of control cells was used and the percentage of cells within the gated area was defined as transfection efficiency in percentage.

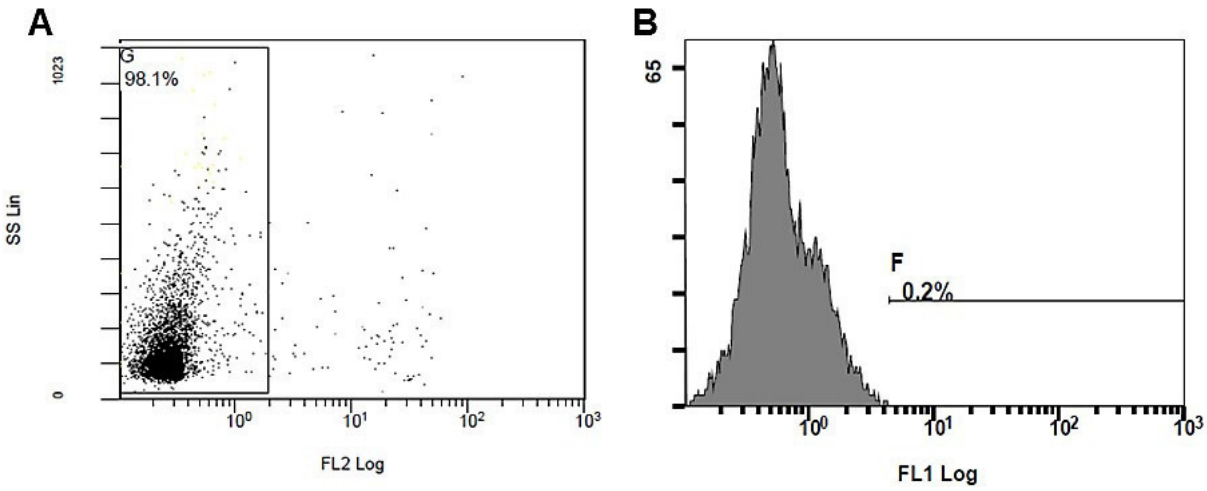

Figure S6. Flow cytometry measurements. A) Dot-plot of PI stained HEK cells for determining cell viability. FL2 Log represents red fluorescence of PI stained cells. All cells within the specified area G represent all measured viable cells. B) Histogramm of non-transfected cells served as control. FL1 Log represents green fluorescence by EGFP expression.

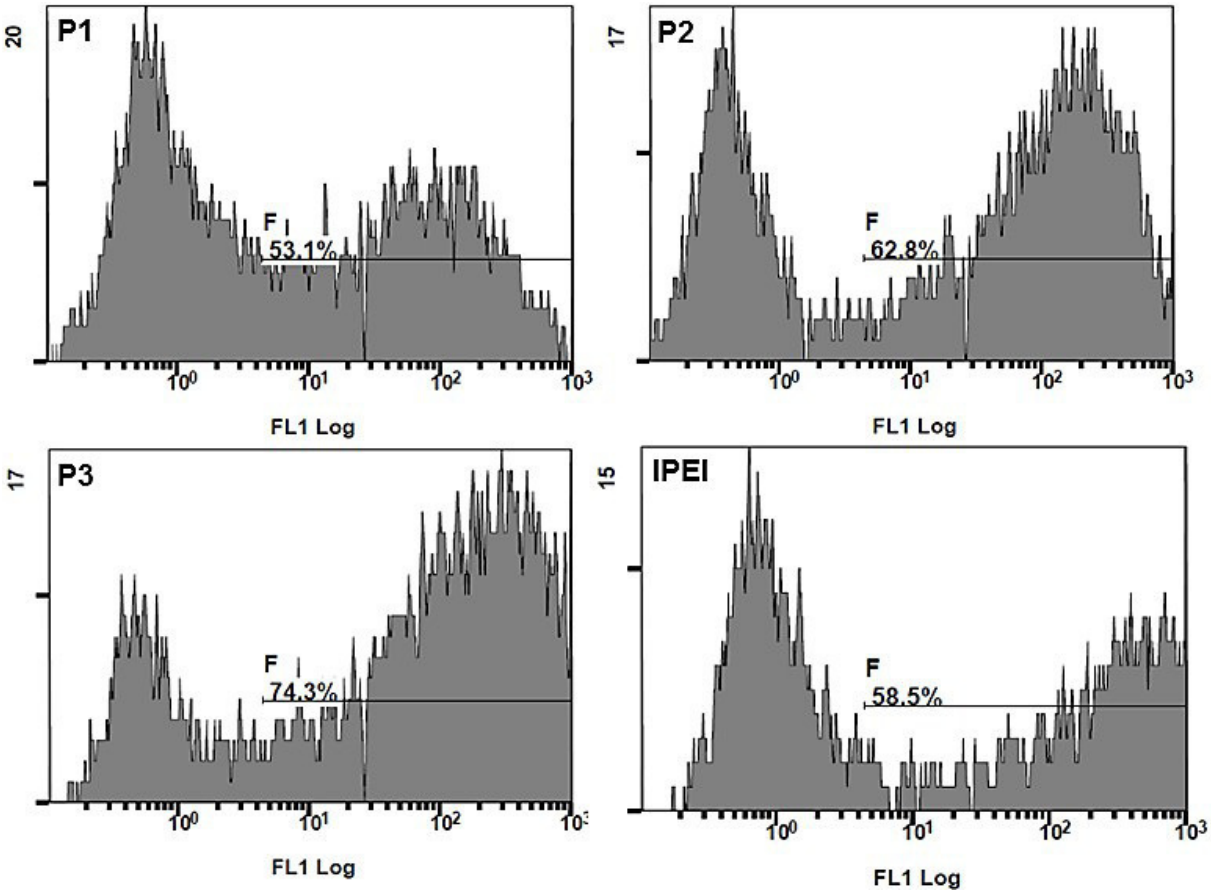

Figure S7. Histograms of flow cytometry measurements determining positive EGFP-expressing HEK cells after 24 h post-transfection with **P1** to **P3** and lPEI (N/P 30). Only viable HEK cells (PI staining) were gated. FL1 Log represents green fluorescence by EGFP expression.

To investigate the uptake mechanism in detail, cells were treated at different conditions with bafilomycin (proton pump inhibitor) or at 4 °C and 37 °C.

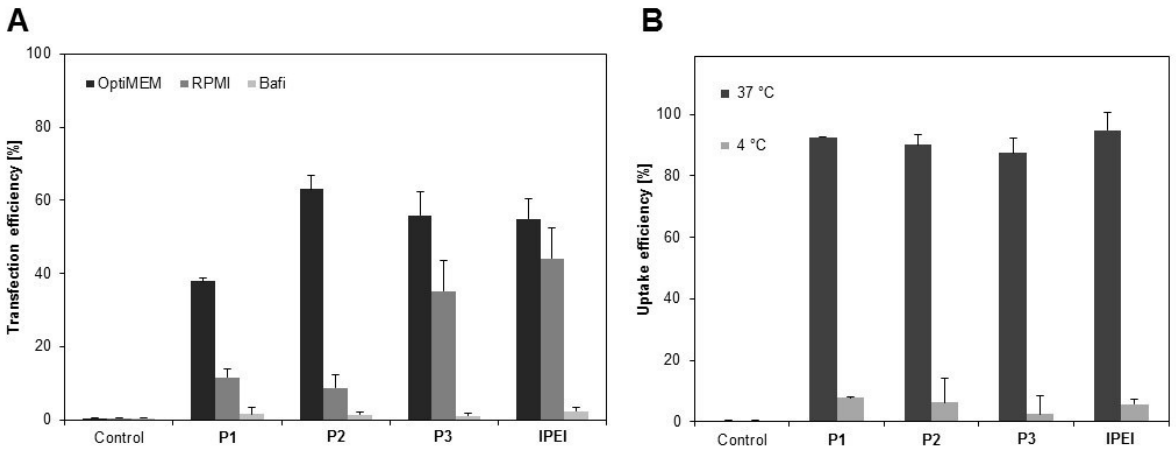

Figure S8. A) Uptake study: amount of cells taken up YOYO-1 labeled pDNA after 4 h at different temperatures (4 °C and 37 °C) using the copolymers **P1** to **P3** and **lPEI** (N/P ratio 30) as controls. Values represent the mean (n = 3). B) Comparison of the transfection efficiency of **P1** to **P3** and **lPEI** for adherent HEK cells in serum reduced (OptiMEM) and serum containing media (RPMI + 10% FCS) as well as after bafilomycin treatment at N/P 30. Values represent the mean (n = 3).

Live cell imaging

Confocal as well as structured illumination microscopy were used to investigate the uptake process of polyplexes in more detail and for visualization purposes. Therefore, non-treated control HEK cells as well as **P3** polyplexes added to HEK cells in serum reduced media were analyzed.

Control: pDNA transfection

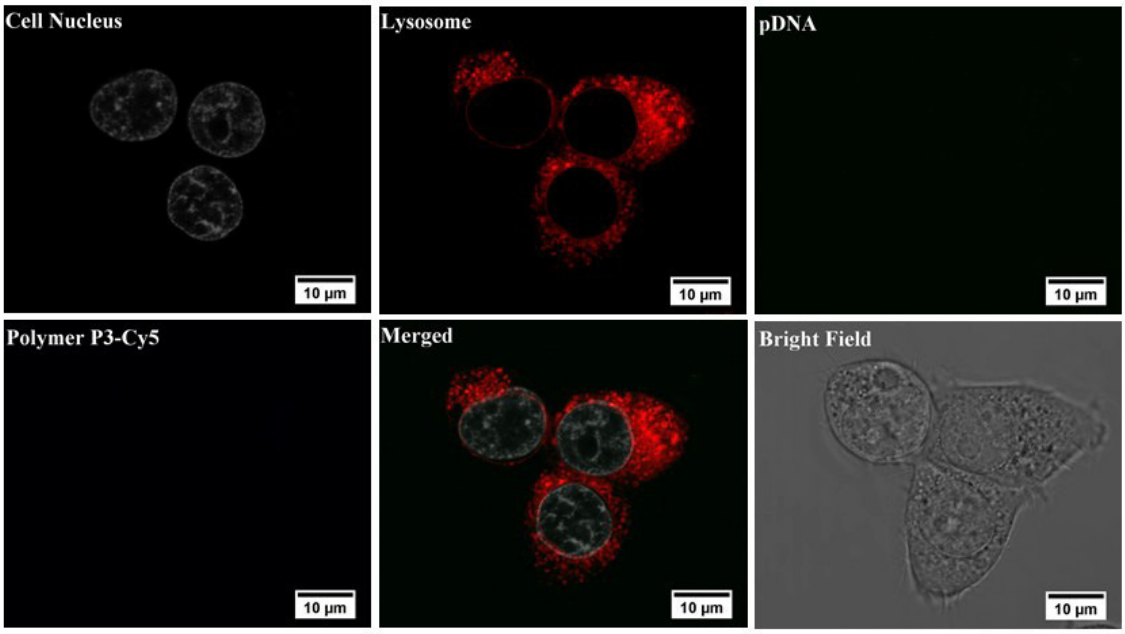

Figure S9. Uptake studies: HEK cells in serum reduced media without polyplexes served as negative controls. The cells were analyzed after 4 h *via* confocal laser scanning microscopy. The cell nucleus was stained with Hoechst 33342, the lysosomes with LysoTracker Red.

P3-Cy5: pDNA transfection

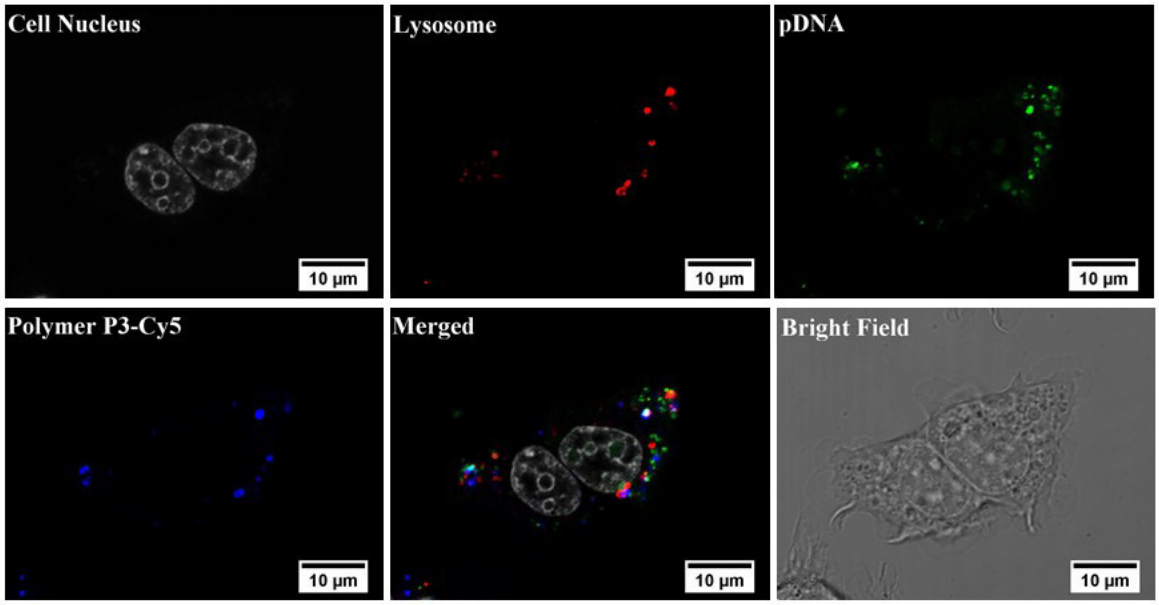

Figure S10. Uptake studies: Pure YOYO-labeled pDNA was added to HEK cells in serum reduced media. The cells were analyzed after 4 h *via* confocal laser scanning microscopy. The cell nucleus was stained with Hoechst 33342, the lysosomes with LysoTracker Red.

Structured illumination microscopy (SIM)

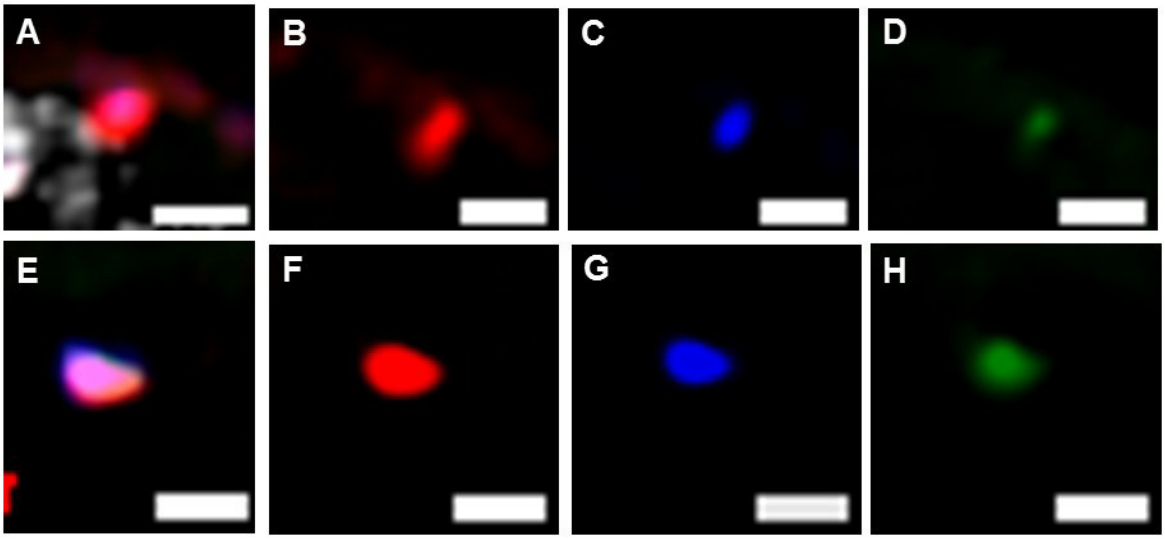

Figure S11. Magnified SIM images of endosome bearing polyplexes formed with **P3** in the presence of DNA (SIM data, deconvolved, acquired with 63x Oil Obj. 1.4 NA). Red; Lysosomal membrane (RFP). Green: pDNA labeling (YOYO-1). Blue: Polymer labeling (Cy5). A and E: Merged channels. B-D, F-H: split channels. Scale bars = 1 µm,

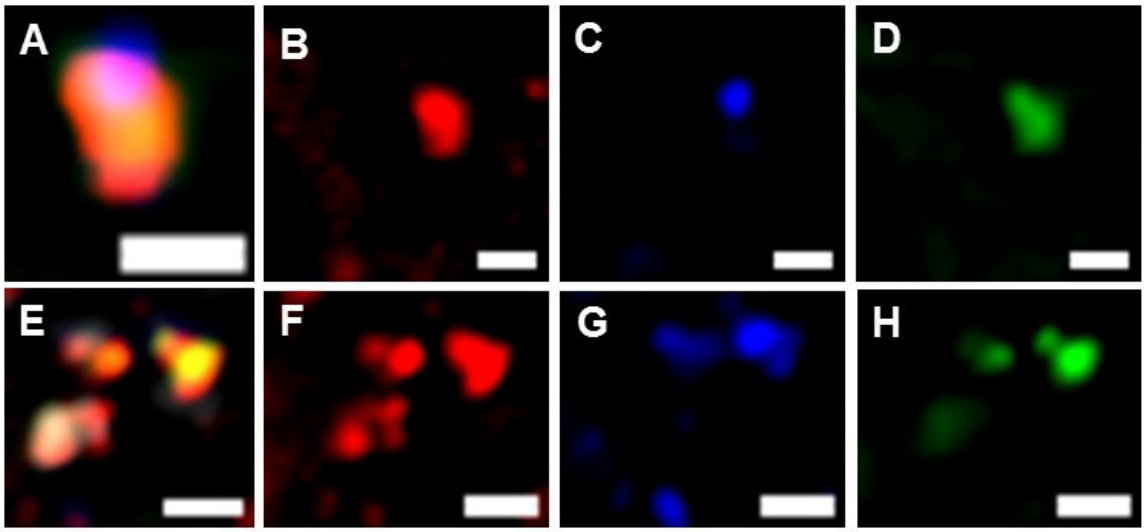

Figure S12. Magnified SIM images of endosome bearing polyplexes formed with **lPEI** in the presence of DNA (SIM data, deconvolved, acquired with 63x Oil Obj. 1.4 NA). Red; Lysosomal membrane (RFP). Green: pDNA labeling (YOYO-1). Blue: Polymer labeling (Cy5). A and E: Merged channels. B-D, F-H: split channels. Scale bars = 1 µm,

Scanning transmission electron microscopy (STEM)

To obtain deeper insights into the uptake mechanism and the fate of polyplexes inside the cell as well as the endosomal environment, scanning transmission electron microscopy (STEM) were performed. The images display a section (thickness of the resin slice: 80 nm) through the cell and sizes are determined by a two-dimensional section through the cell. This can only conditionally make a statement of the actual size of the three-dimensional vesicle. More than 5 sections (and ~ 10 vesicles) of different cells were analyzed to evaluate our findings.

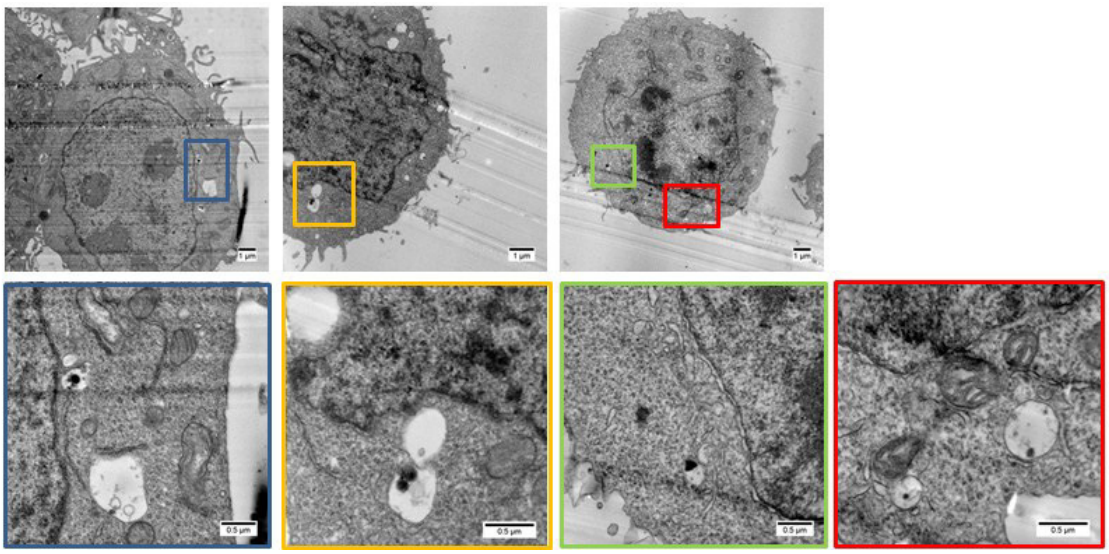

Figure S13. STEM images of polyplex uptake in HEK cells at standard conditions. Polyplexes were formed with **P3** and pDNA. Cells were harvested after 4 h.

Macropinocytosis inhibitor

For inhibition experiments, cells were treated with 100 µM 5-(*N*-ethyl-*N*-isopropyl)amiloride (EIPA) in standard culture media 30 min prior to polyplex addition. Subsequently, **P3** and lPEI polyplexes were added to the cells and incubated for further 4 h. Afterwards, the cells were harvested and analyzed as described above *via* flow cytometry or were further prepared for STEM imaging.

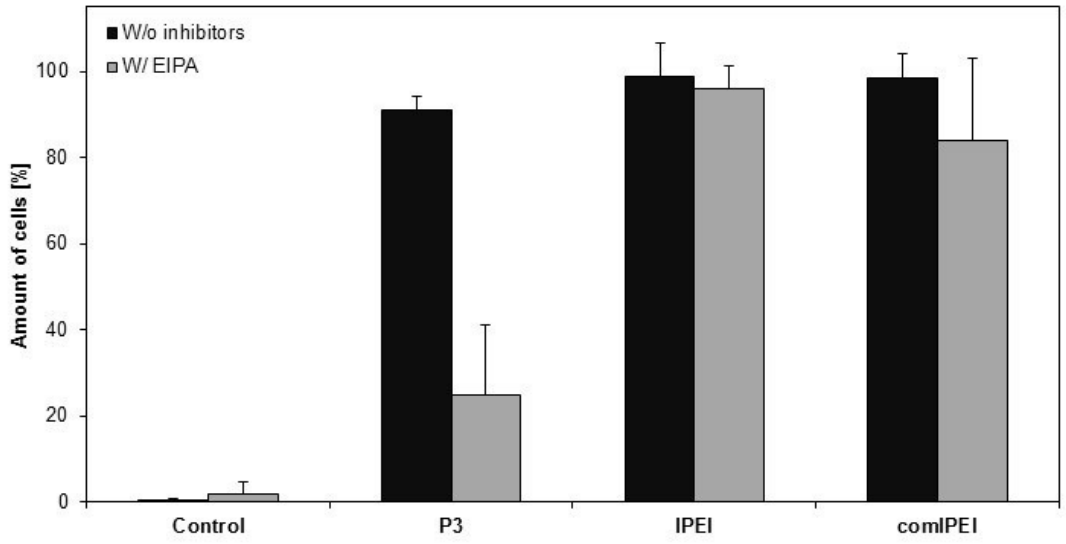

Figure S14. Polyplex uptake (YOYO-labeled pDNA) in HEK cells after treatment with EIPA (macropinocytosis inhibitor).

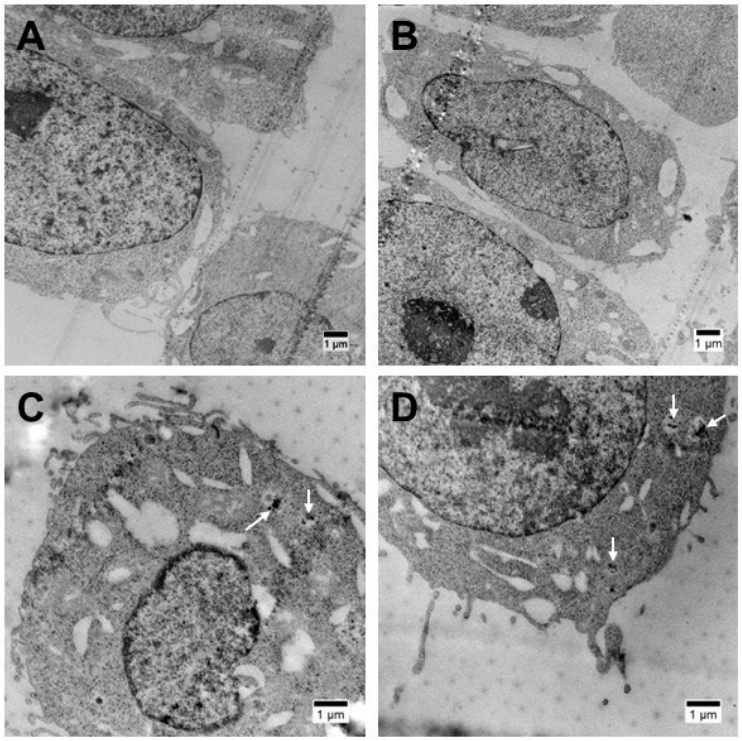

Figure S15. STEM images of polyplex uptake in HEK cells after treatment with EIPA (macropinocytosis inhibitor). A-B) Uptake of **P3** polyplexes. C-D) Uptake of **lPEI** polyplexes. White arrows indicate vesicles with polyplexes.

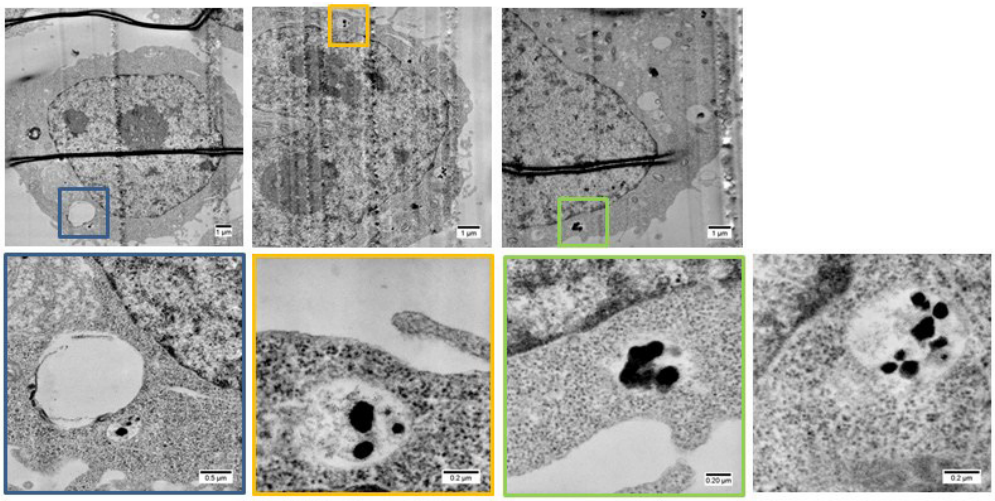

Figure S16. STEM images polyplex uptake in HEK cells at standard conditions. Polyplexes were formed with **lPEI** and pDNA. Cells were harvested after 4 h.

siRNA delivery

A stable GFP-expressing CHO cell line was transfected with the polymers **P1** to **P3** as well as PEI using scrambled siRNA as negative control. The knockdown of EGFP was analyzed *via* flow cytometry by measuring the MFI of all viable cells (PI staining).

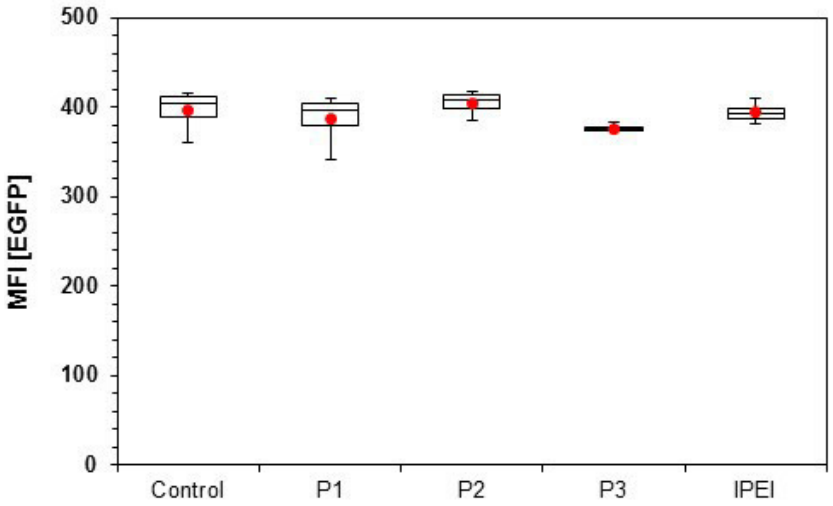

Figure S17. siRNA transfection efficiency mediated by **P1** to **P3** as well as PEI polyplexes at N/P 30 after 72 h. Stable EGFP-expressing CHO cells were transfected with scrambled siRNA served as negative control. The values represent the mean ± S.D., $n \geq 3$.

Comparison of lPEI and commercial lPEI25k (comlPEI, Sigma Aldrich)

The cytotoxicity tests of the PEI copolymers were performed in parallel with high molar mass lPEI polymers as positive controls. Fully hydrolyzed PEtOx, thus lPEI as well as the commercially available lPEI (25 kDa, **comlPEI**) obtained from Polysciences were used. The synthesized lPEI shows a higher cytotoxicity (IC_{50} at ~ 4 µg mL^{-1}), whereas the commercial PEI reaches 50% cell viability at 25 µg mL^{-1}. The reduced cytotoxicity could be attributed to residual, N-acyl groups from polymerization, which is also stated by the supplier.[39] Furthermore, the hemolysis and the erythrocyte aggregation assay were performed with both PEIs. Both polymers show membrane-perturbing activity at high concentrations (100 µg mL^{-1}) leading to hemoglobin release and the aggregation of erythrocytes. This effect was not seen with the copolymers **P1** to **P3**.

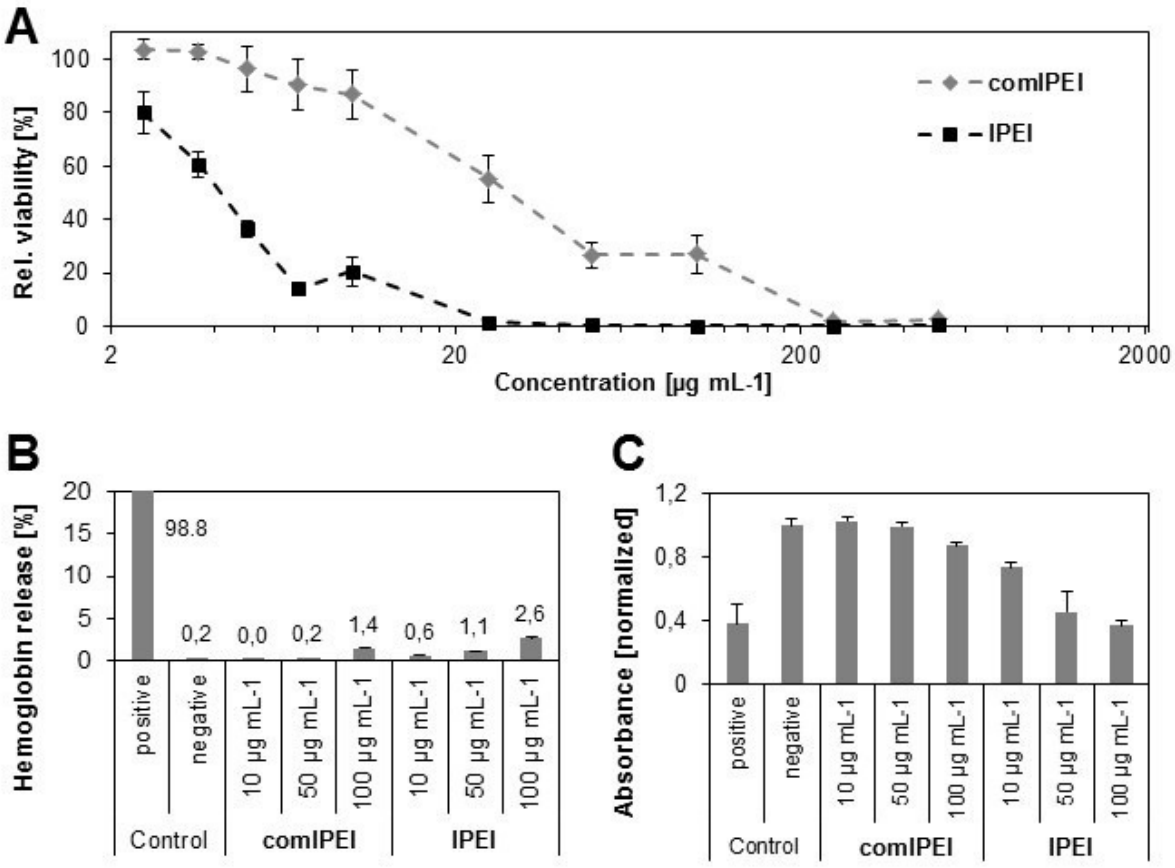

Figure S18. Comparison of **lPEI** and commercially available PEI (**comlPEI**, Polysciences). A) Cytotoxicity assay treating L929 cells with the synthesized **lPEI** as well as **comlPEI** at indicated concentrations. B) Hemolysis assay of erythrocytes after incubation with polymers at indicated concentrations. Triton X-100 served as positive control (100% hemolysis) and PBS as negative control. C) Erythrocyte aggregation of the tested polymers at indicated concentrations. bPEI (25 kDa) served as negative control resulting in high aggregation formation and PBS as negative control. Values represent the mean ± S.D. (n=3).

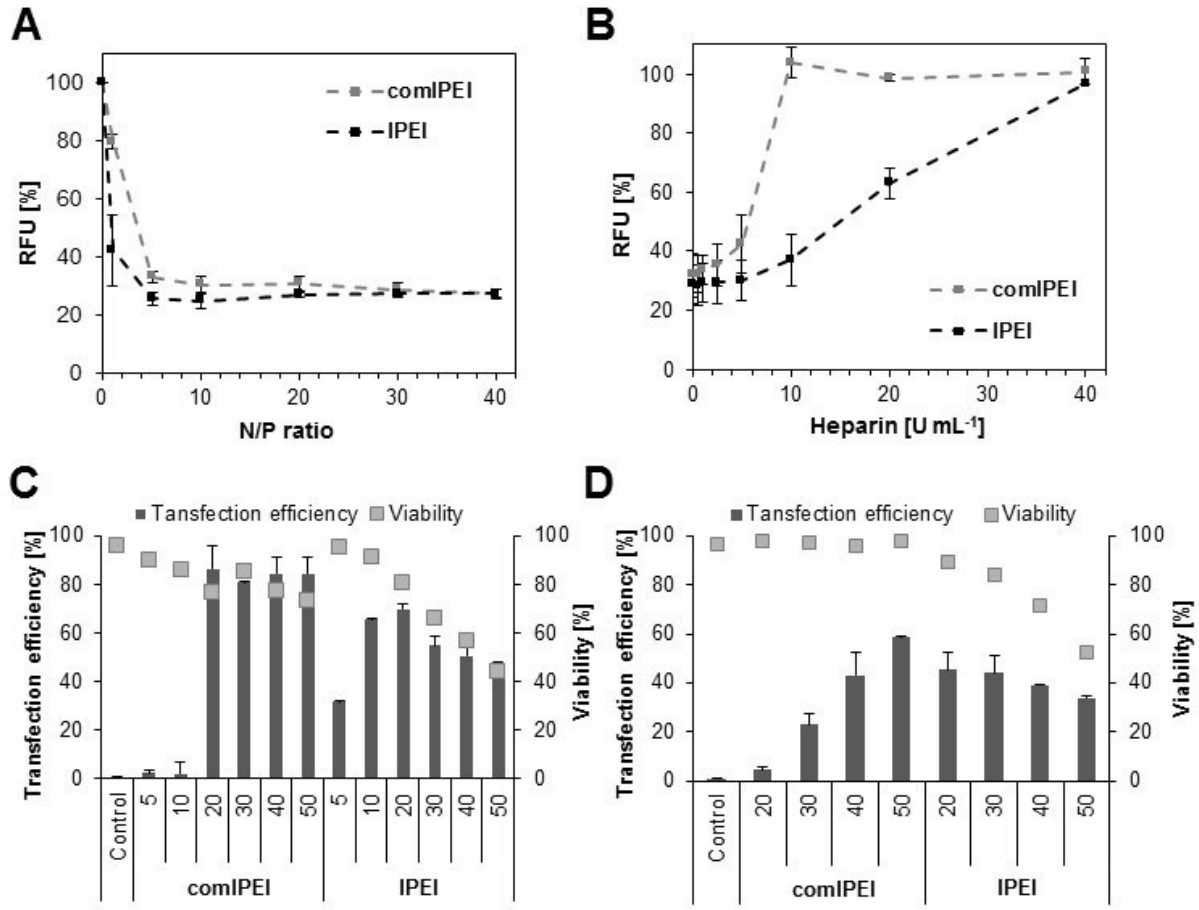

Figure S19. Comparison of **lPEI** and commercially available PEI (**comlPEI**, Polysciences). A) Complexation affinity (EBA) of mentioned polymers using pDNA at the indicated N/P ratios. B) Dissociation assay with heparin of polyplexes formed with pDNA at N/P 30. C-D) Transfection efficiency of both PEI polymers for adherent HEK cells in serum reduced (C) as well as serum containing (D) media at different N/P ratios after 24 h. Values represent the mean ± S.D. (n=3).

Besides the synthesized lPEI, comlPEI was used as control for the ethidium bromide quenching assay (Figure S18A). Both polymers show a high complexation affinity with pDNA, while a faster polyplex formation of lPEI could be detected at N/P 5. Regarding the heparin dissociation assay, comlPEI achieved a full decomplexation of genetic material at a heparin concentration of 10 U mL^{-1} (Figure S19B). For the complete release of pDNA (100% RFU) from lPEI polyplexes, 40 U mL^{-1} heparin was required. The uptake and transfection studies were

performed with HEK cells and pDNA encoding the EGFP (enhanced green fluorescence protein). Transfection efficiency was determined by measuring the amount of cells expressing EGFP after 24 h *via* flow cytometry. ComlPEI shows high TE > 80% at N/P ratios of 20 to 50 in serum reduced media, which is comparable to other studies. It has to be mentioned that with increasing N/P ratio, i.e. the polyplex concentration, the cell viability is reduced. This effect could be prevented using serum containing media for transfection, whereas a significant reduction of up to 70% (at N/P 20) of TE is occured.

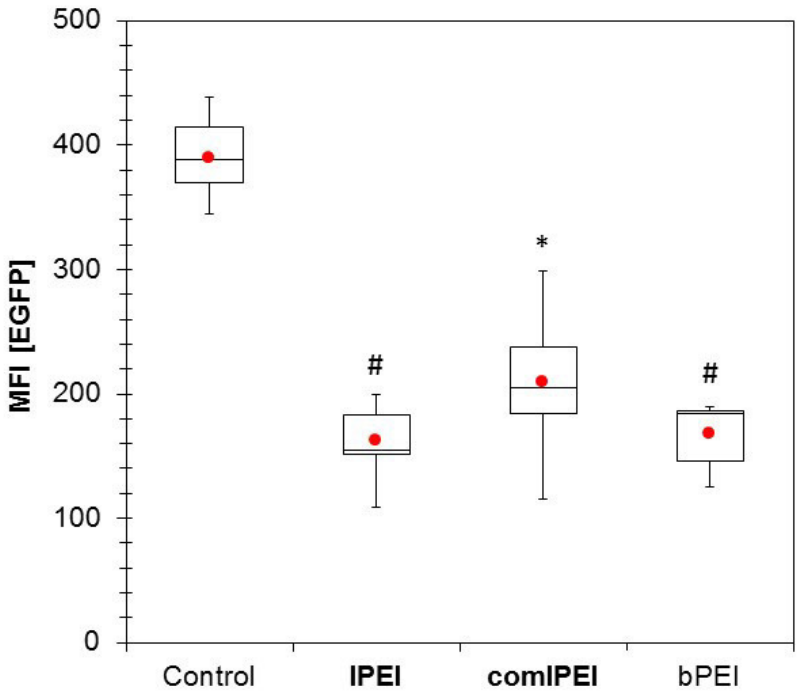

Figure S20. siRNA transfection efficiency mediated by PEI polyplexes at N/P 30 after 72 h. Stable EGFP-expressing CHO cells were transfected with polyplexes formed using siRNA able to knock down *egfp*. Statistical analysis (t-test) was used to compare the MFI of the control with PEI, * represents $p < 0.05$ and # $p < 0.005$. The values represent the mean ± S.D., n ≥

PUBLICATION 6

Crossing the blood-brain barrier: Glutathione-conjugated poly(ethylene imine) for gene delivery

C. Englert,‡ A-K. Trützschler,‡ M. Raasch, T. Bus, P. Borchers,
A. S. Mosig, A. Traeger, U. S. Schubert

J. Control. Release **2016**, *241*, 1-14

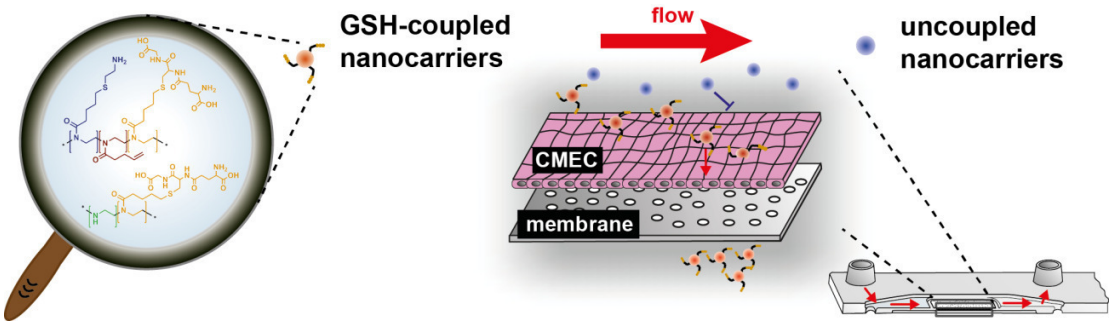

‡ Authors contributed equally.

Journal of Controlled Release 241 (2016) 1–14

Contents lists available at ScienceDirect

Journal of Controlled Release

journal homepage: www.elsevier.com/locate/jconrel

Crossing the blood-brain barrier: Glutathione-conjugated poly(ethylene imine) for gene delivery

Christoph Englert [a,b,1], Anne-Kristin Trützschler [a,b,1], Martin Raasch [c,d], Tanja Bus [a,b], Philipp Borchers [a,b], Alexander S. Mosig [b,c,d,*], Anja Traeger [a,b,**], Ulrich S. Schubert [a,b,***]

[a] Laboratory of Organic and Macromolecular Chemistry (IOMC), Friedrich Schiller University Jena, Humboldtstrasse 10, 07743 Jena, Germany
[b] Jena Center for Soft Matter (JCSM), Friedrich Schiller University Jena, Philosophenweg 7, 07743 Jena, Germany
[c] Institute of Biochemistry II, Jena University Hospital, Nonnenplan 2-4, 07743 Jena, Germany
[d] Center for Sepsis Control and Care, Jena University Hospital, Erlanger Allee 101, 07747 Jena, Germany

ARTICLE INFO

Article history:
Received 29 June 2016
Received in revised form 24 August 2016
Accepted 28 August 2016
Available online 30 August 2016

Keywords:
Poly(ethylene imine)
Blood-brain barrier
Microfluidic biochip
L-Glutathione
Non-viral gene delivery

ABSTRACT

The targeted drug delivery to the central nervous system represents one of the major challenges in pharmaceutical formulations since it is strictly limited through the highly selective blood-brain barrier (BBB). L-Glutathione (GSH), a tripeptide and well-known antioxidant, has been studied in the last years as potential candidate to facilitate the receptor-mediated transcytosis of nanocarriers. We thus tested whether GSH decoration of a positively charged polymer, poly(ethylene imine), with this vector enables the transport of genetic material and, simultaneously, the passage through the BBB. In this study, we report the synthesis of GSH conjugated cationic poly(ethylene imine)s *via* ecologically desirable thiol-ene photo-addition. The copolymers, containing 80% primary or secondary amine groups, respectively, were investigated concerning their bio- and hemocompatibility as well as their ability to cross a hCMEC/D3 endothelial cell layer mimicking the BBB within microfluidically perfused biochips. We demonstrate that BBB passage depends on the used amino-groups and on the GSH ratio. Thereby the copolymer containing secondary amines showed an enhanced performance. We thus conclude that GSH-coupling represents a feasible and promising approach for the functionalization of nanocarriers intended to cross the BBB for the delivery of drugs to the central nervous system.

1. Introduction

Discovered by Paul Ehrlich in 1885 and named by Max Lewandowsky in 1900, the blood-brain barrier (BBB) is known as one of the most challenging obstacles concerning the delivery of drugs and therapeutic nucleic acids [1,2]. Within the BBB, specialized endothelial cells of the cerebral vasculature (cerebral microvascular endothelial cell, CMEC) form an endothelial layer that strictly regulates the passage of small molecules. The tightness of the BBB is furthermore regulated by astrocytes and pericytes that are in direct contact with the CMECs [3]. The BBB passage of molecules depends on several parameters, including the molecular size, lipid solubility, hydrophilicity, and the degree of dissociation. The passage of macromolecules as well as of 98% of small molecules (<400 g mol^{-1}) is prevented under physiological conditions [4]. Besides the passive transport, which comprises the diffusion of small molecules [5], the active transport of amino acids and macromolecules such as transferrin is described to be mediated by carrier proteins or transcytosis [6]. While the transport of different amino acids is well-investigated [7], the transport of L-glutathione (GSH), a tripeptide which is known as antioxidant that lowers the oxidative stress level within the brain, is currently under investigation [8–10].

In order to circumvent the BBB, several methods including the invasive direct injection into the central nervous system (CNS) and the non-invasive nasal delivery of nanoparticular and liposomal carriers as well as of covalently targeted small molecules have been investigated [11,12]. However, nasal delivery possesses the difficulty to adjust the therapeutic delivery due to individually varying absorption profiles, limited volume and long term side effects [11].

Introducing targeting molecules to nanocarriers is the key to benefit from the active transporting systems and to enable also the passage of larger drugs. Non-viral receptor- and adsorptive-initiated transcytosis, as well as carrier-mediated transport can be used for an active transcellular vector-based drug delivery. By using larger biomolecules like antibodies and peptides [13,14], additional surface modifications like PEGylation and polysorbate 80 ("Tween 80" or polyoxyethylene(20)

* Correspondence to: A.S. Mosig, Center for Sepsis Control and Care, Jena University Hospital, Erlanger Allee 101, 07747 Jena, Germany.
** Correspondence to: A. Traeger, Jena Center for Soft Matter (JCSM), Friedrich Schiller University Jena, Philosophenweg 7, 07743 Jena, Germany.
*** Correspondence to: U.S. Schubert, Laboratory of Organic and Macromolecular Chemistry (IOMC), Friedrich Schiller University Jena, Humboldtstrasse 10, 07743 Jena, Germany.
E-mail addresses: alexander.mosig@med.uni-jena.de (A.S. Mosig), anja.traeger@uni-jena.de (A. Traeger), ulrich.schubert@uni-jena.de (U.S. Schubert).
[1] The authors contributed equally to this work.

http://dx.doi.org/10.1016/j.jconrel.2016.08.039
0168-3659/

sorbitan monooleate) [15] or small molecule conjugation (such as GSH), BBB passage could be revealed successfully [16–19]. The latter has been successfully used to modify nanoparticles for drug delivery resulting in an enhanced passaging ability of the BBB [20,21]. Recently, Grover et al. combined two known techniques to create a novel nanoparticle system (PEGylation and GSH coating), while Gaillard *et al.* showed the improvement of the BBB passage using liposomal carrier systems [20,21]. The 2-BBB company has already started with two clinical trials regarding liposomal based PEGylated and GSH decorated particles bearing doxorubicin and methylprednisolone [22]. At the end of 2014 positive results from phase 1 were announced showing a BBB passage and anti-tumor properties. This reveals that the decoration with GSH seems to be a promising targeting approach also for other carrier systems. While the choice of targeting molecules influences the transcytosis efficiency, the nanocarrier material should be adopted to the transported drug. Therefore, synthetic as well as natural polymers (*e.g.* polysaccharides, proteins) have been used for the transport of drugs and genetic material [23]. Among others, polybutylacrylate (polysorbate 80) [24] and PLA/PGA or PLGA (TAT [25] or polysorbate 80 [26]) have been successfully established in *in vivo* tests for the encapsulation of hydrophobic drugs. In order to enable nucleic acid delivery to the central nervous system (as novel treatment option of neuronal-related diseases), there is an urgent need for appropriate binding nanocarriers. Cationic polymers, in particular poly(ethylene imine) (PEI), represent a class of suitable candidates for the complexation of genetic material by electrostatic interactions [27]. Due to its superior buffering ability enabling endosomal escape, PEI is known as the gold standard of polymeric carriers for gene delivery *in vitro* [28]. However, its potential is accompanied with high cytotoxicity and non-biodegradability [29]. The functionalization of the linear PEI backbone [30] and the addition of side chains, creating copolymers, represent a powerful strategy to overcome these limitations and have been extensively studied attaching various carbohydrates [31–33] or polymers like poly(ethylene glycol) [34].

However, these *in vitro* studies were based on standard cell culture techniques under static culture conditions. Shear forces as observed *in vivo* and their impact on endothelial cells [35] as first cells to come in contact with administered drugs have not been addressed. Microfluidics can serve as a tool to reduce this transferability gap. Recently, we reported a microfluidically supported biochip model of the BBB with the proof-of-concept of the modulation of the BBB permeability by inflammatory cytokines [36]. To mimic the cerebral endothelial cell layer of the BBB, hCMEC/D3 cell layers have been used that specifically express cerebral endothelial marker proteins including cell adhesion and tight junction proteins as well as CNS related transporter proteins. *In vitro* the cell line forms a tight endothelial cell layer that shows similarities with the BBB even in the absence of astrocytes or pericytes [37–39]. Thus HCEMC/D3 cells were already used in various BBB models [40,41] for mechanistically studies on leukocyte transmigration [42], nanoparticle uptake and transcytosis [43,44].

In this study, we describe for the first time a nanocarrier design that combines vector as well as charge optimized properties for crossing the BBB and that enables complexation of nucleic acids. We focused on the installation of GSH moieties on the backbone of high molar mass linear PEI. A post-polymerization functionalization process was applied to obtain double bond functionalities and defined quantities of cationic ethylene imine units. Since reduced GSH provides a free thiol end group, thiol-ene photo-addition was used to modify the PEI backbone avoiding potentially hazardous metal catalysts. Comparable amounts of primary amine groups in the polymer side chain were installed in a second approach on the PEI backbone for an enhanced polyplex stability. The copolymers were characterized concerning their polyplex formation, toxicity, hemocompatibility and their potential to deliver nucleic acids across the BBB. We want to demonstrate that polyplexes, formed by GSH-modified PEI-based polymers and plasmid DNA, are able to cross an endothelial cell model of the BBB under physiological shear stress of 4 dyn cm^{-2}.

2. Results and discussion

To conjugate GSH to a cationic polymer backbone (using a poly(ethylene imine)-derivative), the thiol-ene photo-addition reaction was utilized. It can be performed under mild conditions (no thermal energy, no toxic metal catalysts) without generating harmful side products. The solubility properties of GSH limits the click reaction to water. To investigate the influence of different amine functionalities on the balance between stable polyplex formation and BBB passage, materials either containing solely secondary amines or bearing additional primary amines were synthesized.

2.1. Polymer synthesis

The homopolymer poly(2-ethyl-2-oxazoline) (PEtOx) was synthesized according to literature procedure [9]. For this purpose, the cationic ring-opening polymerization (CROP) of the monomer 2-ethyl-2-oxazoline was performed in a microwave reactor. The precursor revealed a degree of polymerization of 575 (calculated from the tosylate ^{1}H-NMR signal integrals of MeOTos before purification) and a dispersity of 1.3 (SEC: DMAc, 0.21% LiCl, calibration: polystyrene). PEtOx was further treated with half-concentrated hydrochloric acid and heated to reflux overnight [45]. The resulting linear poly(ethylene imine) (**P1**) exhibited a degree of hydrolysis of > 95% (calculated from ^{1}H-NMR). **P1** served as the main polymer for the installation of all functionalities including the GSH moieties. To investigate the influence of different cationic charges on the biocompatibility and the DNA binding affinity, primary as well as secondary amine functionalities were introduced to the polymer backbone besides the GSH functionalities [46]. This versatile approach required two different synthesis pathways (see Scheme 1).

The first one comprises of the partial functionalization of linear poly(ethylene imine) (**P1**) with *N*-succinimidyl-4-pentenate to introduce double bond functionalities yielding the P(EI-*stat*-ButEnOx) copolymer (**P2**) (see Scheme 1a, strategy I) [47]. Since the homopolymer poly(2-butenyl-2-oxazoline) (which can be synthesized by a CROP of the respective monomers) does not withstand the conditions of acidic or basic hydrolysis, the mentioned post-polymerization modification strategy was applied. Preliminary studies of copolymers consisting of varying contents of ethylene imine (EI) and 2-butenyl-2-oxazoline units (ButEnOx) resulted in a critical amount of EI units required for the formation of stable polyplexes [47]. Therefore, a ButEnOx content of 27% was installed onto the backbone of **P1**, resulting in an EI content of 78% (**2**) (see Table 1). The introduction of GSH (reduced state, for the schematic representation of the structure see Scheme 1) was performed by a thiol-ene photoaddition while maintaining a constant EI content of 78% (Scheme 1c). Since GSH shows only limited solubility properties, the click reaction was performed in water utilizing the photoinitiator Irgacure® 2959. The full conversion resulted in the copolymer P($EI_{73\%}$-*stat*-$GluButOx_{27\%}$) (**3**).

In a second approach primary amine moieties were installed on the polymer backbone to investigate their influence on the interaction with DNA. While primary amine groups are known to promote superior complexation of nucleic acids [48,49], secondary amines reveal an enhanced buffer capacity resulting in a fast endosomal release [50]. The previously mentioned modification strategy was used (Scheme 1a, strategy II) to synthesize a fully functionalized poly(2-butenyl-2-oxazoline) (**P4**). Subsequently, the protected aminothiol was added to **P4** under UV irradiation (Scheme 1b) to yield the copolymer P(*boc*$AmButOx_{82\%}$-*stat*-$ButEnOx_{18\%}$) (**P5**) (Table 1). In a second photo-addition step, reduced GSH was introduced to the backbone of **P5** analog to the previously described first synthesis route (Scheme 1c, strategy II). Under these conditions, the conversion of the double bonds was incomplete (56% of the origin double bond functionalities remained), even after an additional functionalization step. Almost certainly, the content of flexible side chains containing sterically demanding protection groups hinders the full modification. Furthermore, the introduction of a defined amount

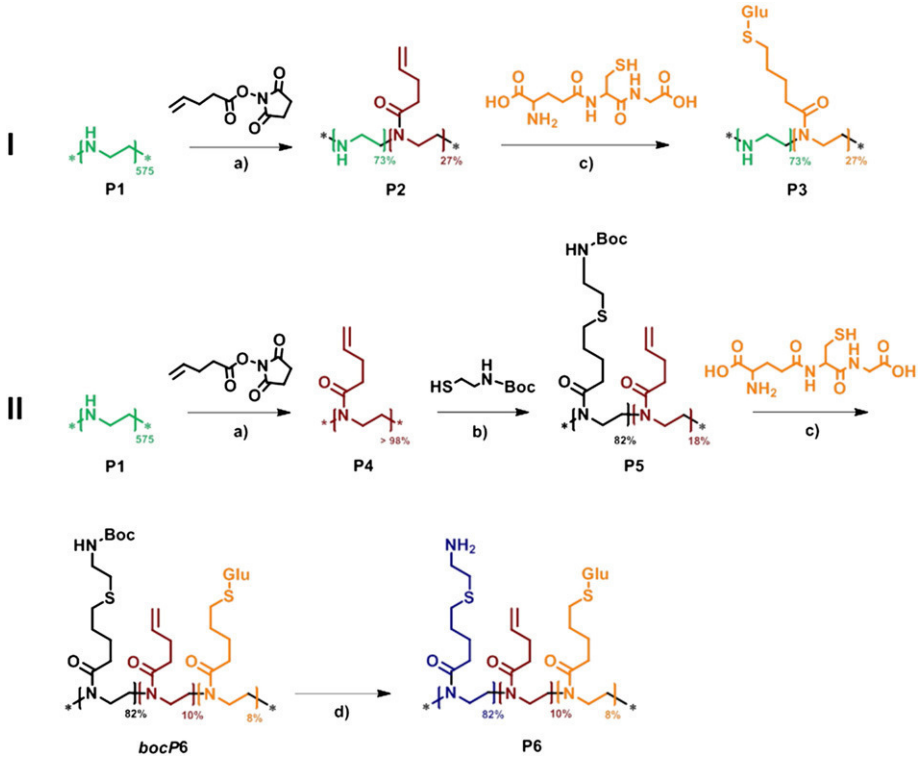

Scheme 1. Schematic representation of the synthesis of I) P(EI-*stat*-GluButOx) (**P3**) and II) P(AmButOx-*stat*-ButEnOx-*stat*-GluButOx) (**P6**), respectively. a) Functionalization of linear poly(ethylene imine) (**P1**). b) Thiol-ene photo-addition of *tert*-butyl-(2-mercaptoethyl)carbamate to the copolymer backbone. c) Thiol-ene photo-addition of L-glutathione to the copolymer backbone. d) Deprotection of primary amine side chains.

of bulky GSH (~8%) could result in an additional hindrance, which limits the degree of functionalization. The deprotection of ***boc*P6** (Scheme 1d) resulted in the final polymer P(AmButOx$_{82\%}$-*stat*-ButEnOx$_{10\%}$-*stat*-GluButOx$_{8\%}$) (**P6**). Focusing on the amount of amine groups within the copolymers, a comparison of **P3** and **P6** concerning this point is part of further investigations.

Characterization by ^{1}H-NMR spectroscopy (Fig. 1) confirmed the almost complete hydrolysis of PEtOx revealing one main signal for the backbone of **P1** between 3.70 and 3.20 ppm (NR—C*H*$_2$—C*H*$_2$, A). In addition, 5% remaining 2-ethyl-2-oxazoline units can be found. The appearance of the double bond signals for **P2** at 5.81 ppm (*CH*$_2$═C*H*—, E) and 4.95 ppm (*CH*$_2$═CH—, F) confirm the successful functionalization with *N*-succinimidyl-4-pentenate. The former signal is compared to the unaffected ethylene imine backbone to determine the composition of the formed copolymer **P2** (degree of functionalization: 27%). The disappearance of the double bond signals after the thiol-ene photoaddition confirmed the complete functionalization with GSH. Besides the additional protons observed after the click reaction (E′ and F′), the signals of GSH can be assigned to the respective protons (see Fig. 1). The very specific GSH signal for the CH group of the cysteine unit appears at 4.54 ppm (NR—*CH*—CH$_2$—S, H).

The complete functionalization of **P1** resulted in polymer **P4**, indicated by the disappearance of the signals assigned to the ethylene imine backbone (between 3.70 and 3.20 ppm) (see Fig. 2). Instead, the signals assigned to the double bonds at 5.8 ppm (*CH*$_2$═C*H*—, D) and 4.96 ppm (*CH*$_2$═CH—, E) as well as to the backbone (3.45–3.53, NR—*CH*$_2$—*CH*$_2$, A) could be observed. The successful attachment of side chains bearing primary amine groups and GSH moieties is shown by the CH$_2$ signals nearby the amine group around 2.8 ppm (NH$_2$—*CH*$_2$—*CH*$_2$), the signal of the *boc*-protecting group which disappears after deprotection (1.4 ppm, *CH*$_3$ boc) and the specific GSH protons of **P6**.

The composition of the prepared polymers (and respective intermediates) is depicted in Table 1. Asymmetric flow field-flow fractionation (AF4) was utilized to determine the molar masses of the starting polymer **P1** and the final products **P3** and **P6**. Since the intermediates reveal different solubility behaviors, another characterization method had to be chosen. Therefore, size exclusion chromatography (SEC) was used to determine the molar masses of **P2**, **P4**, **P5** and ***boc*P6**. However, in both cases the presence of cationic amine units (primary or secondary) and/or double bond functionalities resulted in undesired column and membrane interactions and, therefore, a change in the elution behavior (increased dispersities) [51,52]. Although the obtained values indicate lower molar masses compared to the calculated values, a trend is visible.

To confirm the successful photo-addition of GSH and the formation of a single (polymeric) species (**P3**, **P6**), diffusion-ordered NMR spectroscopy (DOSY NMR) was performed. GSH clearly revealed a higher diffusion coefficient compared to the polymeric species. The decreasing values for the GSH decorated **P2** indicate an increase of the hydrodynamic radius of **P3** in solution (Fig. 3A). This can be explained by the bulky GSH moiety. Comparable results are obtained for **P6** (Fig. 3B).

2.2. Bio- and hemocompatibility

Biocompatibility represents a critical parameter for potential non-viral vectors in biomedical applications. *In vitro* studies were performed using the precursor **P2** and the final GSH-conjugated polymers **P3** and **P6** in comparison to the linear PEI (**P1**) to evaluate their bio- and hemocompatibility (Fig. 4A and Supporting information Fig. S1). **P4** and **P5** were excluded due to their insolubility in aqueous media. **P1** exhibited a high cytotoxicity at low polymer concentrations (IC_{50} of ~4 μg mL^{-1}) because of its high molar mass and cationic charge density (leading to membrane damages followed by the possible initiation of apoptosis [53,54]). Interestingly, the attachment of 27% GSH resulted in a strong reduction of the cytotoxicity. **P3** revealed an IC_{50} value of

Table 1
Composition and molar masses for (*co*-)polymers **P1** to **P6**.

		Composition[a]			NMR[b]	AF4		SEC[c,d]	
		X	Y	Z	Mn	Mn	Đ	Mn	Đ
Abr.	Name	[%]	[%]	[%]	[gmol^{-1}]	[gmol^{-1}]		[gmol^{-1}]	
P1	$LPEI_x$	>98	0	0	24,800	9900	1.4	n.d.	n.d.
P2	P(EI_x–*stat*–$ButEnOx_y$)	73	27	0	37,500	n.d.	n.d.	31,400[c]	1.2
P3	P(EI_x–*stat*–$GluButOx_z$)	73	0	27	85,200	21,000	2.0	n.d.	n.d.
P4	$PButEnOx_y$	0	>98	0	71,900	n.d.	n.d.	44,000[c]	1.5
P5	P(*boc*$AmButOx_x$–*stat*–$ButEnOx_y$)	82	18	0	155,300	n.d.	n.d.	23,400[d]	1.9
***boc*P6**	P(*boc*$AmButOx_x$–*stat*–$ButEnOx_y$–*stat*–$GluButOx_z$)	82	10	8	169,500	n.d.	n.d.	38,400[d]	1.7
P6	P($AmButOx_x$–*stat*–$ButEnOx_y$–*stat*–$GluButOx_z$)	82	10	8	122,300	63,300	1.8	n.d.	n.d.

[a] Determined by ^{1}H NMR (calculated from the ratio of x, y and z signals)

[b] Determined by ^{1}H NMR (calculated from tosylate signals of MeOTos before purification)

[c] SEC 1: $CHCl_3$/*i*PrOH/NEt_3 94:2:4, polystyrene calibration

[d] SEC 2: DMAc, 0.21% LiCl, polystyrene calibration

n.d. – not determined. All polymers soluble in aqueous media and /or insoluble in organic solvents were measured at AF4 – MALS system.

~270 μg mL^{-1} and even polymer concentrations up to 150 μg mL^{-1} revealed nearly no cytotoxic effects (relative viability ≥ 85%). The precursor **P2** also exhibited a lower cytotoxicity compared to **P1** (see Supporting information Fig. S1A). The replacement of the ethylene imine units by flexible primary amine containing side chains for **P6** led to an increased cytotoxicity (IC_{50} value of ~44 μg mL^{-1}) compared to **P3**. Furthermore, the incomplete thiol-ene photoaddition resulted in a lower content of GSH and, likewise, unmodified double bond functionalities, which could both influence the biocompatibility. However,

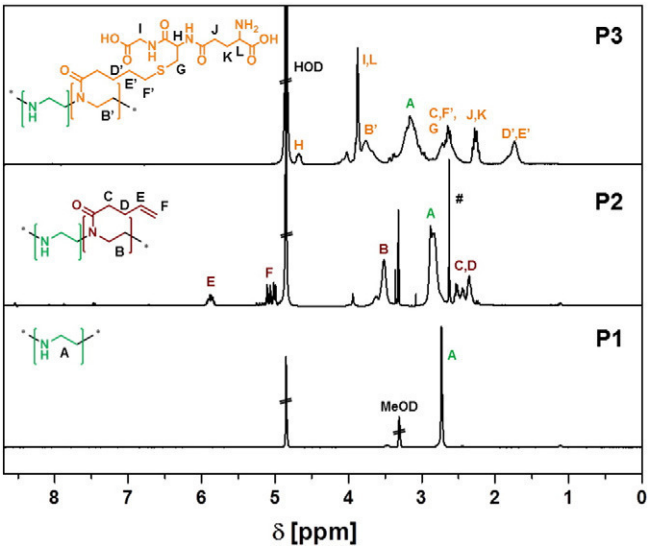

Fig. 1. Comparison of ^{1}H-NMR spectra of **P1** to **P3** (# side product *N*-hydroxysuccinimide) (400 MHz, D_2O/MeOD).

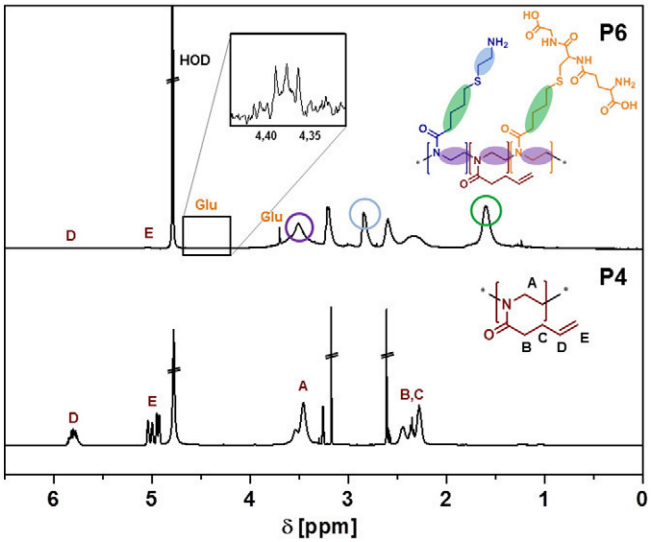

Fig. 2. Comparison of ^{1}H-NMR spectra of **P4** and **P6** (400 MHz, D_2O/MeOD and D_2O).

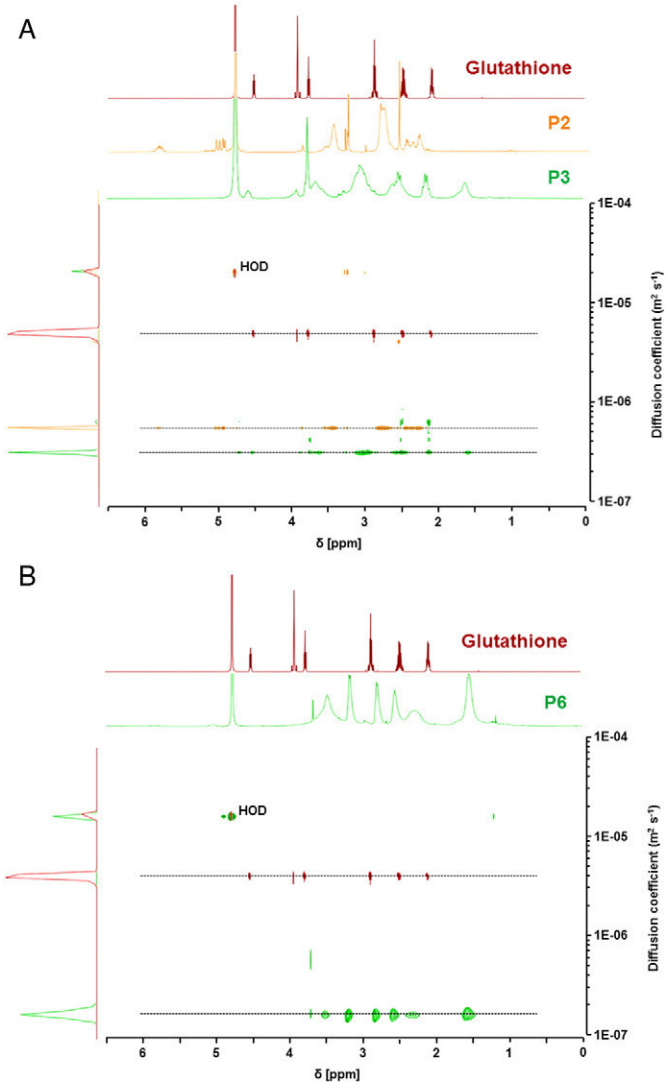

Fig. 3. Diffusion ordered NMR spectra of: A) **P2**, **P3** and L-glutathione and B) **P6** and L-glutathione (400 MHz, D_2O).

polymer concentrations of **P3** and **P6** from 2 to 5 μg mL^{-1} were used for the preparation of polyplexes, which are in an acceptable range beyond the cytotoxicity-inducing concentrations. The cytotoxicity test was not only performed with L292 cells according to the ISO protocol 10993-5 but the assay was also performed with HEK as well as hCMEC/3D cells for a detailed determination of the causal relation of toxicity and related interactions (see Supporting information Fig. S2 A). In static culture the hCMEC revealed a different performance during cytotoxicity tests and showed only 10% relative viability for **P1** at a concentration of 2 μg mL^{-1} and also a decreased viability for **P6** whereas **P3** revealed no cytotoxic effects up to 500 μg mL^{-1}. While the IC_{50} values of **P1** and **P6** decreased up to a 2-fold higher concentration, **P3** showed no cytotoxic effect at all independent of the used cell line (Fig. S2B).

To investigate the blood compatibility of **P2**, **P3** and **P6**, the hemolytic activity as well as the aggregation of erythrocytes was assessed (Fig. 4B, Supporting information Figs. S3 and S4). All investigated copolymers did not show any hemolytic activity in a concentration range from 10 to 100 μg mL^{-1}. **P1** as well as **P2** (SI Fig. S1B) revealed a slightly hemolytic activity at higher concentrations (50 to 100 μg mL^{-1}) indicated by a hemoglobin releases of 2% as well as strong agglomeration of erythrocytes (see Supporting information, Fig. S3). While no agglomeration for **P3** was observed, indicating a good hemocompatibility, **P6** showed distinct interactions with cellular membranes of erythrocytes leading to aggregation. Obviously, the type of amines within the polymer side chain represents a crucial factor for the interaction with cells, in particular with the plasma membrane, and is therefore linked to the biocompatibility properties. This fact was also assumed by Dekie et al. concluding this from glutamic acid derivatives [55]. However, Fischer et al. mentioned that these effects have to be mentioned relative to the polymer class and can also be influenced by factors like charge density (number of amines and three dimensional arrangements) [54].

As reported earlier, primary amines revealed an increased affinity to cellular membranes compared to secondary amines, indicated by a higher toxicity [56]. Tripathi et al. demonstrated the successful reduction of the cytotoxicity by pyridoxyl derivatization of primary amines of branched PEI [57]. This behavior supports the findings observed for **P3** and **P6**.

2.3. Characterization of the polyplexes

An efficient delivery of nucleic acids, like plasmid DNA, into cells depends on several parameters. They comprise of the compact condensation of the genetic material, the masking of negative charges, the prevention of degradation and the efficient dissociation from the vector after transfer into the cellular cytoplasm or nucleus. PEI derivatives, in particular PEI disulfide linked rabies virus glycoprotein, have been shown to enable the delivery of neurogenic microRNA into the brain [58]. To investigate the binding affinity of **P1**, **P2** (SI Fig. S1C), **P3** as

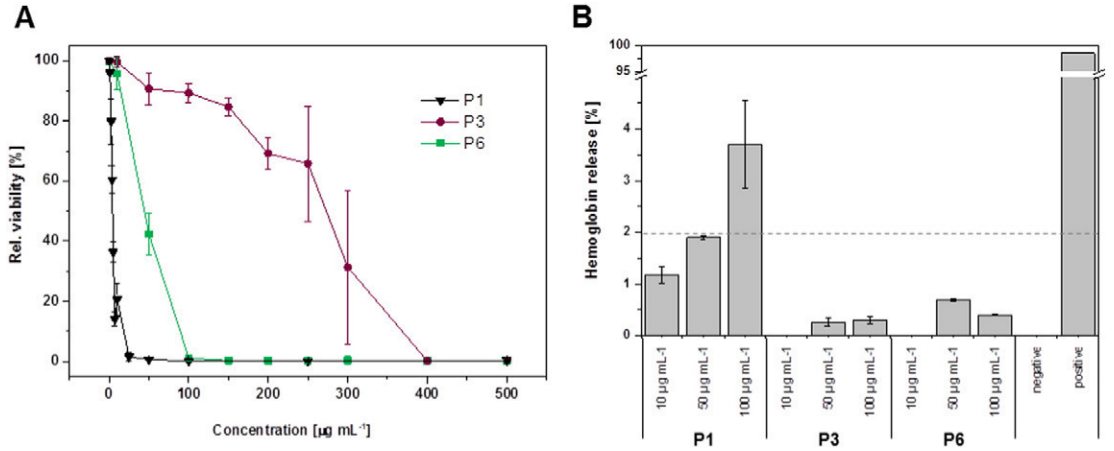

Fig. 4. Bio- & hemocompatibility. A) Relative viability of L929 cells after 24 h incubation with the respective polymers at indicated concentrations. B) Hemolysis assay of erythrocytes after incubation with polymers at indicated concentrations. Triton X-100 was used as positive and PBS as negative control. A value < 2% hemolysis is classified as non-hemolytic, 2–5% as slightly hemolytic and values > 5% as hemolytic. Values represent the mean ± S.D. (n = 3).

well as **P6** with plasmid DNA as model system, the ethidium bromide quenching assay (EBA) was utilized. Polyplexes were formed at different nitrogen (polymer) to phosphate (DNA) ratios (N/P). Due to the electrostatic and hydrophobic interactions between the polymer and the pDNA, ethidium bromide is excluded from its binding sites within the oligonucleotides resulting in a reduction of fluorescence intensity [59,60].

All polymers revealed a decreasing fluorescence intensity with increasing N/P ratios that resulted in a plateau, indicating stable polyplex formation (Fig. 5A and Supporting information Fig. S1D). While the positive control **P1** exhibited a fast polyplex formation starting at N/P 5, **P2**, **P3** and **P6** revealed a stable polyplex formation at higher N/Ps from 20 to 40 reaching 60%, 45% and 30% relative fluorescence units (RFU), respectively. A possible explanation for the slightly lower binding affinity could be the ethylene imine units which are shielded by the bulky GSH moieties as well as a lower zeta potential of **P3** (4.06 mV) compared to **P6** (28.4 mV) (see Table S5). For **P6**, primary amine groups are attached through flexible side chains, which are easier accessible for the pDNA. Additionally primary amines are known to promote pDNA compensation [61].

The heparin dissociation assay was used to analyze the stability and the dissociation behavior of the formed polyplexes [62,63]. Heparin is a natural polyanion with one of the highest density of negative charges and can effectively bind to the positive charged polymers **P3** and **P6**. It competes with the pDNA within the polyplex and forces the release of the nucleic acid. The free nucleic acid is able to rebind free ethidium bromide (added in the same concentration as for the EBA) causing an increase of the fluorescence intensity (Fig. 5B). In the case of the **P3** and **P6** polyplexes, the pDNA was released very fast at low heparin concentrations. While **P3** revealed a reversible binding, reaching 90% dissociation at 10 U mL^{-1} heparin, **P6** showed full dissociation (~100% RFU at 10 U mL^{-1}). In contrast, **P1** required higher concentrations of heparin (40 U mL^{-1}) for almost full release (~95% RFU), which underlines the stability of **P1**/pDNA polyplexes and is in accordance to literature data [46].

An efficient delivery, comprising of the internalization of polyplexes into cells *via* endocytic pathways, requires defined sizes and charges of the complexes. Therefore, critical sizes of polymeric carriers up to 200 nm are recommended [64]. As shown in Table 2, the formed polyplexes of **P3** and **P6** revealed z-averages of 282 nm and 117 nm at a N/P ratio of 20, respectively, which are calculated from the correlation function. Since the intensity of the particle scattering is proportional to the sixth power of its diameter (Rayleigh approximation), larger particles or agglomerates of free polymer chains result in comparatively more light scattering and higher intensity than smaller ones. Therefore, the intensity-weighted diameters (z-averages) determined by dynamic light scattering are supplemented by the number-weighted sizes revealing a calculated number percentage over 95. Although the calculated sizes can only be seen as informative basis, they are in good agreement with the favorable size of polyplexes. The zeta potential changes during the synthesis from well-known positive charged **P1** (28.4 mV) to the GSH bearing conjugate **P3** (−6.9 mV). In this case, a potential explanation could be that the positive charge of the former PEI backbone is complexing the DNA meanwhile the GSH carboxylic acid moieties are present at the outside of the polyplex resulting in a negative value of −6.9 mV while the precursor **P2** showed comparable size and zeta potential as **P1**. The results of **P2** can be found in the Supporting information, Table S6. The change in charge cannot be observed in the case of **P6**. Here, the lower content of GSH and the side chains with more flexible primary amines reduce the effect of the GSH functionalities.

Table 2
Size and zeta potential measured in 20 mM 4-(2-hydroxethyl) piperazine-1-ethanesulfonic acid (HEPES) and 5% (w/v) glucose, pH 7.2 of pDNA complexes of **P1**, **P3** and **P6** at N/P 20 measured by dynamic light scattering.

Polymeric system	z-Average [d/nm]	PDI	Number-weighted size [d/nm]	Zeta potential [mV]
P1	132 ± 28	0.24	61 ± 18	28.4 ± 2.7
P3	282 ± 5	0.38	109 ± 18	−6.9 ± 0.1
P6	117 ± 1	0.31	61 ± 16	33.2 ± 1.5

2.4. Uptake efficiency

To investigate the potential of the different polymers to deliver nucleic acids, cellular uptake studies were performed with adherent human embryonic kidney (HEK) cells as well as hCMEC/3D in OptiMEM and EndoGro media (see Supporting information, Figs. S7 and S8). For this purpose, YOYO-1 labeled pDNA was used for the polyplex formation at N/P 20 to detect the time-depended cellular internalization by flow cytometry. A fast polyplex uptake in HEK cells was revealed for **P6** polyplexes exhibiting ~50% internalization after 15 min, >80% internalization after 1 h, and a nearly complete uptake of polyplexes after 2 to 4 h similar to **P1**. Taking the aggregation data of **P6** into account, the strong interaction with the cellular membrane, led to enhanced uptake efficiency. In contrast, **P3** polyplexes exhibited only poor uptake efficiencies with <10% of HEK cells positive for internalized **P3** polyplexes (Fig. 6A). These results were also confirmed by life cell imaging after 1 h (Fig. 6B). Interestingly, the precursor of **P3** without GSH, **P2**, exhibited

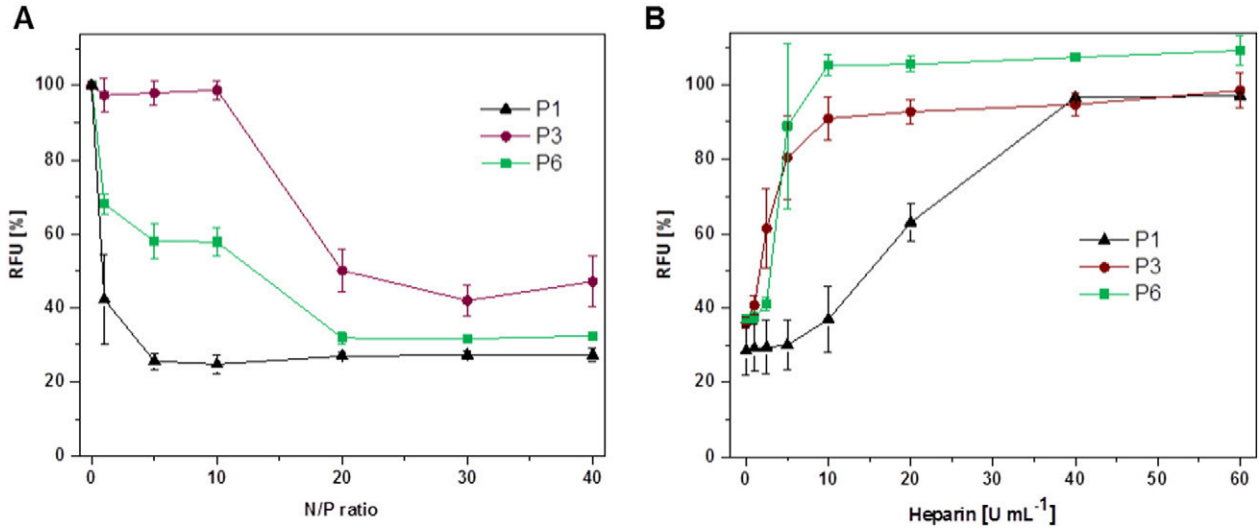

Fig. 5. Polyplex formation and stability with pDNA using the polymers **P1**, **P3** and **P6**. A) Complexation affinity (ethidium bromide quenching assay) of respective polymers at indicated N/P ratios. B) Dissociation assay of polyplexes formed at N/P 40 using heparin (0 to 60 U mL^{-1}). Values represent the mean ± S.D. (n = 3).

an enhanced polyplex uptake comparable to **P6** (see Supporting information, Fig. S1E). Compared to HEK cell experiments the uptake of **P6** decreased in hCMEC/3D cells independently from the culture media used to 20 to 40%. In contrast, the results of **P1** and **P3** uptake did not changed significantly.

Taking the MFI of uptaken pDNA into account, comparable results were also obtained for the transfection efficiencies of the polymers **P1**, **P3** and **P6 in HEK cells**. A transfection efficiency of over 60% of HEK cells was achieved for **P1**, whereas reduced transfection efficiencies were found for **P3** and **P6** of around 30% and 5%, respectively (see Supporting information, Fig. S9).

2.5. Blood-brain barrier passaging performance within the biochip approach

The GSH modified polyplexes were subsequently investigated towards their ability to cross the endothelial layer of the BBB. HCMEC/D3 cells resembling the cerebral endothelial cell layer of the BBB were cultured on a suspended membrane within MOTiF biochips that were recently shown to enable an improved culture of endothelial cells under physiological perfusion conditions [65]. Here, the membrane serves as a cell substrate that is perfused from the apical side of the endothelial cell layer. The cells were grown until full confluence to form a densely packed layer (see Supporting information, Fig. S10). Additionally, immunofluorescence staining for characteristic adherens and tight junction proteins was performed to confirm the integrity of the microvascular endothelial layer before perfusion (see Fig. 7, first row). HCMEC exhibit prominent staining of VE-Cadherin, a key component of adherens endothelial junction and mediator of Claudin-5 expression [66]. Claudin-5 is the main claudin-class protein expressed in BBB endothelial cells and a key regulator of its permeability [67]. Another VE-Cadherin regulated protein is β-Catenin, which plays an important role in maintenance of the BBB integrity and related signaling [68,69]. In addition, we investigated the distribution of occludin, another protein important for tight junction formation and for regulating paracellular permeability [70]. Occludin is associated with cytoplasmic scaffolding and regulatory protein ZO-1 [3]. Claudin-5, β-Catenin, ZO-1 and occludin were found all expressed and localized to intercellular junctions formed by hCMEC. Perfusion with precursor polymer **P1** resulted in a significant loss of endothelial junctional markers (see Fig. 7). Arrowheads indicate a reduced staining of the proteins at the intercellular contacts. This observation is in accordance to the results obtained for the biocompatibility of **P1** on L929 cells (see Fig. 4A) as well as on hCMEC (see Supporting information S2). In flow experiments hCMEC seem to be rendered more susceptible to PEI uptake since already a concentration of 0.1 μg mL^{-1} revealed a strong impact on the cell viability (see Fig. 4A). In 2006 Mennesson et al. already showed that an increase in the polyplex-cell membrane interaction and binding capabilities under flow conditions is altered by shear and sedimentation velocity forces [71]. As demonstrated in hemocompatibility tests, **P1** leads to erythrocyte aggregation and, therefore, to strong membrane interactions. We speculate that in the presence of flow this interaction could

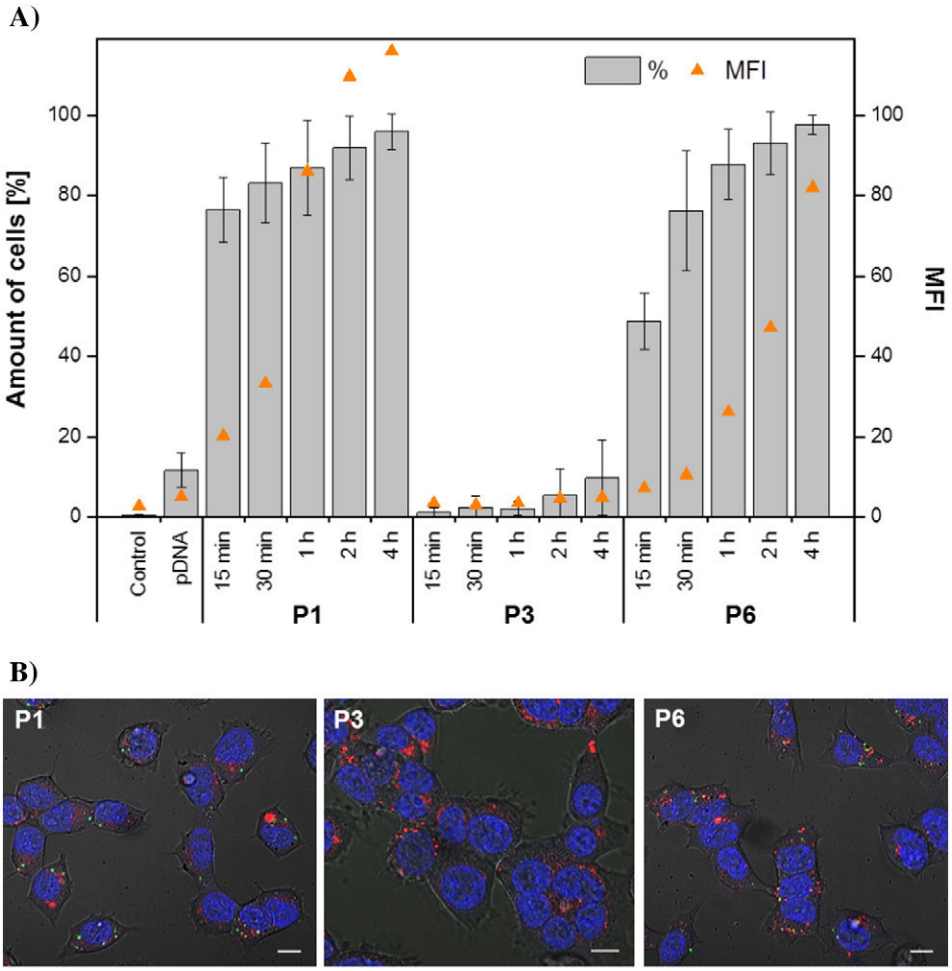

Fig. 6. Cellular uptake study of **P1**, **P3** and **P6** polyplexes (N/P 20) using YOYO-1 labeled pDNA. A) HEK cells were treated with polyplexes for 15 min to 4 h and uptake was analyzed *via* flow cytometry (MFI – mean fluorescence intensity). Values represents the mean ± S.D. (n = 3). B) Confocal microscopy of HEK cells, which were incubated for 1 h with polyplexes (green). Cell nuclei were stained with Hoechst (blue), lysosomes with LysoTracker Red (red). Scale bar = 10 μm.

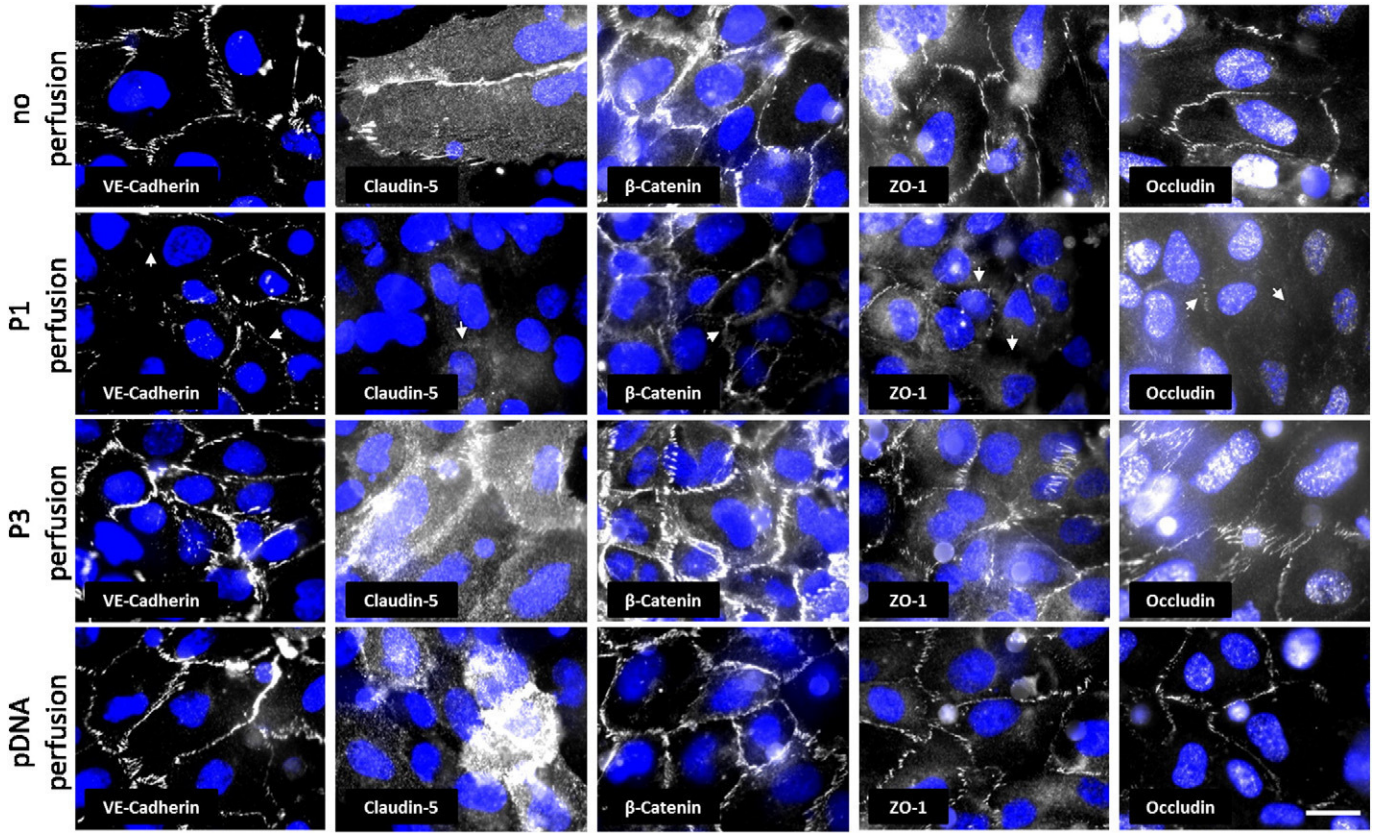

Fig. 7. Expression of BBB relevant junctional marker proteins before and after polyplex perfusion. pDNA served as control group. Arrowheads show breakdown or diminished expression of adherens (VE-Cadherin) and tight junction components evoked by polyplex **P1**. Nuclei are stained in blue (scale bar 20 nm, n = 3).

be promoted which results in a disruption of tight junctions and increased cytotoxicity. In contrast, perfusion with polyplex **P3** as well as free pDNA, serving as control, revealed no impact on adherens or tight junction formation (see Fig. 7). We thus conclude that under flow conditions the tightness of the hCMEC layers is not impaired by the polyplexes, except for polyplex **P1**.

The biochip design allows the quantification of nanoparticles taken up by the endothelial layer through fluorescence measurements as well as the exact determination of the total amount of polyplexes that crossed the endothelial barrier. The imperviousness of the model system, in particular for the endothelial cell layer, was proven for YOYO-1 labeled pDNA without nanocarrier (see Supporting information, Fig. S11). In order to demonstrate the need of glutathione moieties for a successful passage, the precursor **P2** was investigated for comparison reasons. For the polyplex **P6**, we observed the highest uptake into the endothelial cell layer that was associated with a polyplex aggregation (Fig. 8A; see also Supporting information Fig. S3), which was also observed in kinetic studies using HEK cells. In contrast, polyplexes **P1** and **P2** show a lower enrichment at the endothelial layer. **P3** exhibited the weakest enrichment within the endothelial layer compared to other polymers. An image analysis of the quantitative uptake revealed that the internalization of the polyplex **P6** within the endothelial barrier was significantly higher compared to the internalization of the polyplexes **P1** and **P2**, respectively (Fig. 8B). Interestingly, the highest difference in the endothelial uptake of all polyplexes tested was observed for **P3,** even with a significant difference regarding the GSH free precursor **P2** (see Fig. S12).

To further elucidate the trans-endothelial transport of the different polyplexes, we measured its enrichment in the lower chamber underneath the endothelial barrier of the biochip (Fig. 8C). GSH was reported to facilitate a crossing of the nanocarriers through the BBB [21]. We thus tested whether pDNA bound to **P3** could be delivered through the endothelial barrier more efficiently than polyplexes **P1**, **P2** or **P6** (high uptake efficiency and strong interaction with endothelial layer). After 30 min of perfusion we observed a significant increase of polyplex **P1** translocation through the endothelial that remained at this level up to 60 min of perfusion. A viability test revealed that **P1** was toxic already at low concentrations (Fig. 4A). A similar effect was further confirmed by immunofluorescence staining of several endothelial adherens and tight junction proteins involved in maintenance of barrier integrity. Accordingly, **P1** induced a leakage of hCMEC/D3 cell layers under flow conditions. The difference in our observations under flow conditions compared to static culture conditions, where the final concentration of 0.5 μg mL^{-1} was still in an acceptable range, can likely be explained by a significantly increased total amount of polyplexes presented to the cells within the similar incubation time compared to the static cell culture. This could be an explanation to the unexpected polyplex passage after 30 min. In contrast, we observed a continuously increasing transport of the polyplex **P3** through the endothelial layer reaching a maximum at 60 min. Indeed, a significantly difference is observed compared to the non-passaging precursor polyplex **P2** without glutathione modification. Taking the results of the uptake studies into account, a highly "active" polymer like **P6** within HEK cells can perform in a different way compared to microvascular endothelial cell interactions. It is not beneficial for a passage through the BBB due to its strong interaction with any kind of cells, independent of proper uptake or not. These results indicate that *in vivo* **P6** would probably adhere to and might be partly internalized by endothelial blood vessel cells, followed by cargo release instead of passing the cell layer. Importantly, the pure pDNA, the precursor polyplex using **P2** without GSH and **P6** containing only 8%

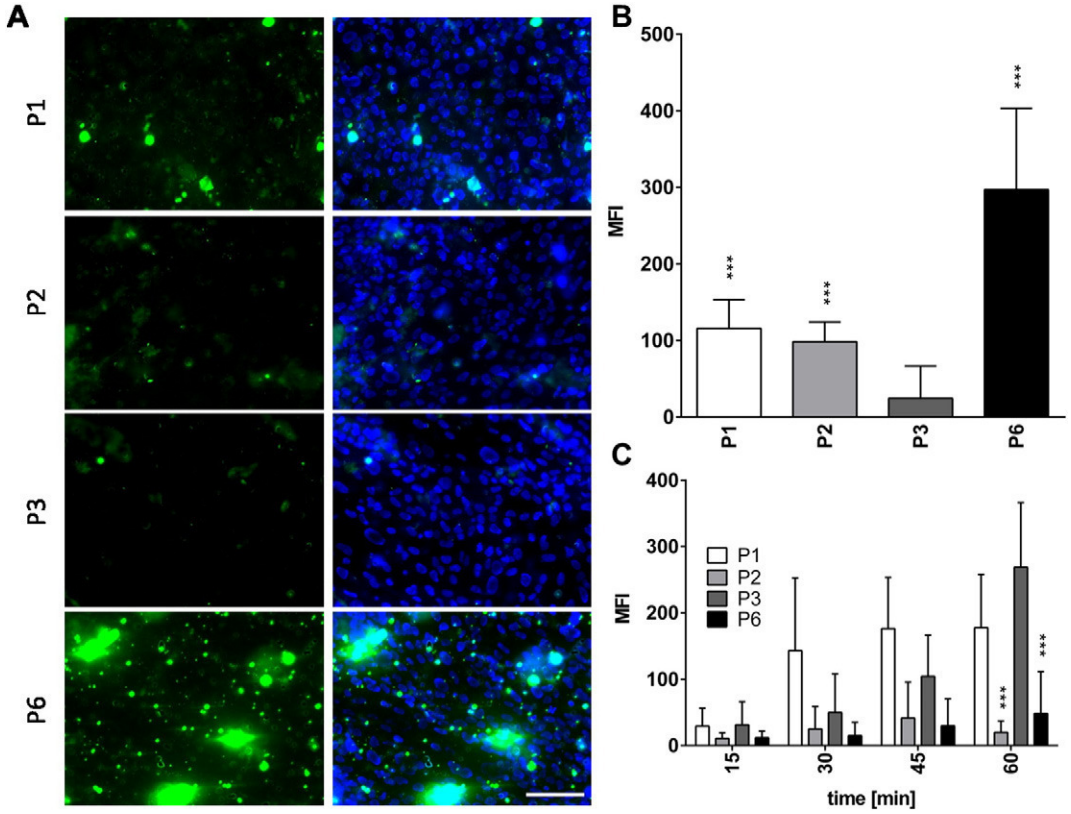

Fig. 8. Performance of the GSH-conjugated polyplexes **P1**, **P2**, **P3** and **P6** in a microfluidically supported biochip assay mimicking permeability of the BBB. A) Microscopic images display polyplex uptake (green) with the hCMEC/D3 cells (nuclei stained with DAPI (blue)) under a physiologic shear stress of 4 dyn cm^{-2}. B) Quantificational analysis of polyplexes at the cellular barrier. C) Passage of polyplexes **P1**, **P2**, **P3** and **P6** through BBB-like hCMEC/D3 cell layer over time. * significances *vs.* **P3**; ***$p < 0.001$; $n = 3$; scale bar 100 nm.

coupled GSH were virtually prevented from crossing the endothelial layer. Only **P3** showed no interaction neither with HEK cells nor endothelia cells, but was able to pass the BBB and, therefore, was identified as a promising candidate as BBB nanocarrier. These results further indicate the strong influence of the polymer design/composition for a BBB carrier balancing the GSH content, DNA binding potential and cellular interactions.

3. Conclusion

In this study, the synthesis of L-glutathione (GSH) bearing cationic polymers is described. To enable the transport of genetic material, ~80% amine functionalities of different nature (primary amines in side chains and secondary amine groups in polymer backbones) were installed within a poly(ethylene imine) derivative. A post-polymerization modification technique followed by a thiol-ene photo-addition in water was used to attach the GSH moieties. The cationic polymers investigated in this study exhibited cytotoxic side effects. The insertion of different types of amines in combination with GSH improved the cell viability compared to poly(ethylene imine). While the presence of primary amines in **P6** still revealed adverse effects on the cell viability combined with a strong interaction with cellular membranes, **P3** exhibited a superior cell viability as well as a good hemocompatibility. Despite the functionalization with negatively charged GSH, the copolymers were able to bind and release plasmid DNA. These features supported the potential application as attractive gene delivery agents for the passage of the BBB.

Studies with biochip embedded cerebral microvascular endothelial cell layers perfused under physiological shear stress conditions revealed a significantly enhanced passage of the BBB for the GSH modified candidate containing secondary amine functionalities. Interestingly, the primary amines led to strong interactions with cells combined with remarkable high uptake efficiency independent of the utilized cell types. However, this functionalization likely mediates an intracellular incorporation within the BBB and, thus, renders the nanocarriers (**P6**) unsuitable to efficiently cross the endothelial layer of the BBB. While **P1** showed an unexpected cell layer passaging effect which is probably due to a reduced tightness of the cell layer, the nanocarrier precursor (**P2**) as well as the uncomplexed plasmid DNA nanocarriers revealed significantly reduced ability to cross the endothelial BBB compared to GSH-coupled nanocarriers with higher GSH amounts (**P3**). The GSH-coupling of nanocarriers thus represents a promising approach to efficiently cross the BBB while avoiding cellular toxicity as shown in this first proof-of-concept study *in vitro*. However, follow-up studies are required to further characterize trans-endothelial transport across the BBB. To proof the feasibility of GSH-coupled nanocarriers as novel therapeutic option for drug-delivery to the CNS also more complex *in vivo* models will be investigated in the future.

4. Experimental part

4.1. Materials

Unless otherwise stated, the chemicals were used without further purification. Trifluoroacetic acid, ethanol, methanol, Irgacure® 2959, *tert*-butyl-(2-mercaptoethyl)carbamate and reduced L-glutathione were purchased from Sigma Aldrich. The following chemicals were ordered from the suppliers in brackets: 2-Ethylen-2-oxazoline (Acros Organics), 4-dimethylaminopyridine (Merck Millipore), 2,2-dimethoxy-1,2-diphenylethan-1-one (TCI America), hydrochloric acid (VWR Chemicals). *N*-succinimidyl-4-pentenate was synthesized according to literature procedures [72]. AlamarBlue, YOYO-1 iodide, Hoechst 33342 trihydrochloride (10 mg mL^{-1} solution) as well as LysoTracker Red

DND-99 were obtained from Life Technologies (Thermo Fisher, Germany). If not stated otherwise, cell culture media and supplements (L-glutamine, antibiotics) were obtained from Lonza (Basel, Switzerland) and Biochrom (Merck Millipore, Germany), respectively. All other chemicals were purchased from standard suppliers and used without further purification.

4.2. General methods and instrumentation

An Initiator Sixty single-mode microwave synthesizer from Biotage, equipped with a noninvasive IR sensor (accuracy: 2%), was used for polymerization under microwave irradiation.

Proton (^{1}H) nuclear magnetic resonance (NMR) spectra were recorded in deuterated water or methanol, at room temperature using a Bruker Advance I (300 MHz) or a Bruker Advance III HD (400 MHz) spectrometer; chemical shifts (δ) are expressed in parts per million relative to TMS. Size exclusion chromatography (SEC) was measured on a Agilent 1200 series system equipped with a PSS degasser, a G1310A pump, a G1362A refractive index detector and a PSS GRAM guard column running with dimethylacetamide (DmAc) with 0.21% of lithium chloride. For further measurements a Shimadzu system using a SCL-10A VP controller equipped with a DGU-14A degasser, a LC-10AD VP pump, a RID-10A refractive index detector and a PSS SDV guard and linear S column running with chloroform/*iso*-propanol/triethylamine (94:2:4) was utilized. The Techlab oven used for both systems was set to 40 °C and the molar masses were calculated using polystyrene (PS) standards. Asymmetric flow field-flow fractionation (AF4) was performed on an AF2000 MT system (Postnova Analytics, Landberg, Germany) coupled to an UV (PN3211, 260 nm), RI (PN3150), MALS (PN3070, 633 nm) detector. The eluent is delivered by two different pumps (tip and focus-flow) and the sample is injected by an autosampler (PN5300) into the channel. The channel has a trapezoidal geometry and an overall area of 31.6 cm^2. The nominal height of the spacer was 500 μm and a regenerated cellulose membrane with a molar mass cut-off of 10,000 g mol^{-1} (M_n) was used as the accumulation wall. All experiments were carried out at 25 °C and the eluent was 20 mM NaCl in 25 mM sodium acetate buffer at pH 3.5. The detector flow rate was set to 0.5 mL min^{-1} for all samples and 50 μL (10 mg mL^{-1}) were injected with an injection flow rate of 0.2 mL min^{-1} for 7 min. For all samples the cross-flow was set to 2 mL min^{-1}. After the focusing period and a transition time of 1 min, the cross flow was kept constant for 1 min and was then decreased under a power function gradient 0.40 to zero within 15 min. Afterwards the cross-flow was kept constant at zero for 20 min to ensure complete elution. For the calculation of the molar mass a Zimm plot was used. The refractive index increment (d*n*/d*c*) of all samples was measured by manual injection of a known concentration directly into the channel without any focusing or cross-flow. The d*n*/d*c* was calculated as the average of at least three injections from the area under the RI curve. The cytotoxicity studies as well as ethidium bromide and heparin assays were performed using a microplate reader (Tecan Infinite M200 Pro, Crailsheim, Germany). For the uptake studies of HEK-293 and hCMEC/D3 cells a flow cytometer, Cytomics FC 500 (Beckman Coulter, Krefeld, Germany) and a confocal laser scanning microscope LSM880 (Carl Zeiss, Jena, Germany) were used (see below).

4.3. Synthesis of linear poly(ethylene imine) (**P1**)

The polymerization of the monomer 2-ethyl-2-oxazoline using the initiator methyl tosylate was performed in a microwave synthesizer according to literature procedures [9]. The resulting poly(2-ethyl-2-oxazoline) (**PEtOx**, DP = 575, 5.0 g) was further hydrolyzed in 6 M hydrochloric acid (HCl) at 100 °C for 16 h under heating to reflux [73]. The excess of HCl and formed propionic acid was removed under reduced pressure. After dissolving in water, the solution was neutralized by the addition of 3 M sodium hydroxide (pH > 8). The precipitated linear poly(ethylene imine) was filtered off and, subsequently, redissolved in 15 mL *N*,*N*-dimethylformamide to remove the formed salt. After repeated precipitation in 400 mL ice-cold diethyl ether, the obtained product was dried under reduced pressure at 85 °C for three days. ^{1}H-NMR was used to determine the degree of hydrolysis of the resulting polymer **1** (yield: 1.85 g, 85%).

PEtOx: DP = 575. ^{1}H-NMR (300 MHz, D_2O): δ 3.70–3.20 (—NR—CH_2—CH_2), 2.41–2.08 (CH_2—CH_3), 1.09–0.79 (CH_2—CH_3) ppm.
P1: EtOx:EI [%] = 5:95. ^{1}H-NMR (300 MHz, MeOD): δ 3.58–3.41 (NR—CH_2—CH_2), 2.91–2.61 (NH—CH_2—CH_2), 2.56–2.36 (CH_2—CH_3), 1.18–1.06 (CH_2—CH_3) ppm. AF4: M_n = 9900 g mol^{-1}, Đ = 1.4.

4.4. Synthesis of P(EI-stat-ButEnOx) (**P2**, **P4**)

Double bond functionalities were installed on the backbone of **P1** by a post-polymerization modification process. For this purpose, **P1** (for **P2**: 751 mg, for **P4**: 765 mg) and the catalyst 4-*N*,*N*-dimethylaminopyridine (DMAP, for **P2**: 120 mg, 0.98 mmol, for **P4**: 360 mg, 2.95 mmol) were dissolved in pyridine (V = 5 mL) at 80 °C. In a second vial, *N*-succinimidyl-4-pentenate (for **P2**: 707 mg, for **P4**: 4.012 g) was dissolved in pyridine (V = 5 mL) and heated to 80 °C. The two solutions were combined to a 5 wt% mixture (5 mL pyridine were added) of **P1**. The reaction mixture was stirred for 21 h at 80 °C. The polymer solution was precipitated in 500 mL ice-cold diethyl ether. The filtered product was washed with 50 mL diethyl ether and dried under reduced pressure to constant weight (yield: **P2**: 0.83 g, 73%, **P4**: 1.29 g, 58%).

P2: EI:ButEnOx [%] = 73:27. ^{1}H-NMR (400 MHz, D_2O): δ 2.28–2.46 (m, CH_2 ButEnOx), 2.63–2.85 (m, NH—CH_2—CH_2), 3.35–3.62 (m, NR—CH_2—CH_2), 4.9–5.0 (dd, CH_2═CH—), 5.76–5.86 (m, CH_2═CH—) ppm. SEC ($CHCl_3$/*i*PrOH/NEt_3): M_n = 31,400 g mol^{-1}, Đ = 1.20.
P4: EI:ButEnOx [%] = 0:100. ^{1}H-NMR (400 MHz, D_2O): δ 2.27–2.44 (m, CH_2 ButEnOx), 3.45–3.53 (m, NR—CH_2—CH_2), 4.92–5.04 (dd, CH_2═CH), 5.76–5.84 (m, CH_2═CH) ppm. SEC ($CHCl_3$/*i*PrOH/NEt_3): M_n = 44,000 g mol^{-1}, Đ = 1.53.

4.5. Synthesis of P(EI-stat-GluButOx) via thiol-ene photo-addition (**P3**)

In a microwave vial, P($EI_{73\%}$-*stat*-ButEnO$x_{27\%}$) (**P2**: 740 mg) and a 1.2-fold excess per double bond of reduced L-glutathione (1.11 g, 3.6 mmol) were dissolved in 15 mL Milli-Q water (5 wt% of **P2**). The radical photoinitiator Irgacure® 2959 (100 mg, 0.45 mmol) was added and the reaction mixture was degassed with argon for 30 min. The clear solution was stirred in a UV-chamber (λ = 365 nm) for 17 h and, subsequently, dialyzed against water using Spectra/Por 1 dialysis membrane (6000 to 8000 g mol^{-1} cut-off). The product **P3** was lyophilized and obtained as a yellowish powder (yield: 770 mg, 44%).

P3: EI:GluButOx [%] = 73:27. ^{1}H-NMR (400 MHz, D_2O): δ 1.60–1.71 (m, CH_2—CH_2—S—), 2.12 (q, NCH—CH_2—CH_2—C═O), 2.45–2.64 (m, NCH—CH_2—CH_2—C═O, CH_2 ButOx), 2.87–3.30 (m, CH_2—S—CH_2—CH_2, NH—CH_2—CH_2), 3.63–3.95 (m, NR—CH_2—CH_2, NR—CH_2—COOH, NH_2—CH), 4.54 (m, NR—CH—CH_2—S) ppm. AF4: M_n = 21,000 g mol^{-1}, Đ = 2.0.

4.6. Synthesis of P(bocAmButOx-stat-ButEnOx) via thiol-ene photo-addition (**P5**)

In a similar procedure, PButEnOx (**P4**, 1.13 g) and 2-(*boc*-amino)ethanethiol (1.19 g, 6.7 mmol) were dissolved in 15 mL methanol (7.5 wt% of **P4**). 2,2-Dimethoxy-2-phenylacetophenone (DMPA, 88 mg, 0.40 mmol) was added as photoinitiator and the reaction

mixture was degassed with argon for 30 min. Subsequently, the solution was stirred in a UV-chamber (λ = 365 nm) for 17 h. Precipitation in 400 mL ice-cold diethyl ether, washing with 50 mL of diethyl ether and drying under reduced pressure for three days resulted in a yellowish powder **P5** (yield: 1.94 g, 80%).

P5: *boc*AmButOx:ButEnOx [%] = 82:18. ^{1}H-NMR (300 MHz, MeOD): δ 1.42 (s, *CH*$_3$ boc), 1.65 (s, *CH*$_2$—S—CH$_2$—CH$_2$—NR), 2.37–2.63 (m, m, *CH*$_2$ ButEnOx, S—CH$_2$—*CH*$_2$—NR), 3.50 (m, NR—*CH*$_2$—*CH*$_2$, S—*CH*$_2$—CH$_2$—NR), 4.96–5.09 (dd, *CH*$_2$═CH), 5.84 (m, CH$_2$═*CH*) ppm. SEC (DMAc, 0.21% LiCl): M_n = 23,400 g mol^{-1}, Đ = 1.86.

4.7. Synthesis of P(bocAmButOx-stat-ButEnOx-stat-GluButOx) via thiol-ene photo-addition (boc**P6**)

The conjugation of reduced L-glutathione (GSH) to the copolymer **P5** was performed similar to the conjugation to **P3**. For this purpose, **P5** (1.01 g) was dissolved in 17 mL ethanol (6 wt% of **P5**). The photoinitiator Irgacure® 2959 (321 mg, 1.4 mol) and a 1.2-fold excess per double bond of GSH (252 mg, 0.82 mmol) was added, the reaction mixture was degassed with argon for 30 min and stirred in a UV-chamber (λ = 365 nm) for 48 h. An aliquot of 50 μL was taken and characterized *via* ^{1}H-NMR. Due to still incomplete photo-addition, additional GSH (150 mg, 0.49 mmol) was added to the reaction mixture and irradiated for further 48 h. The copolymer was purified by dialysis against ethanol using Spectra/Por 1 dialysis membrane (6000 to 8000 g mol^{-1} cut-off) and dried under reduced pressure for four days (yield: 735 mg, 67%).

***boc*P6**: *boc*AmButOx:ButEnOx:GluButOx [%] = 82:10:8. ^{1}H-NMR (300 MHz, MeOD): δ 1.32–1.48 (s, *CH*$_3$ boc), 1.67 (m, *CH*$_2$—S—CH$_2$—CH$_2$—NR), 2.20 (m, NCH—*CH*$_2$—CH$_2$—C═O), 2.17–2.60 (m, NCH—*CH*$_2$—CH$_2$—C═O, CH$_2$ ButOx), 3.08–3.91 (m, *CH*$_2$—S—CH$_2$—CH$_2$, NR—*CH*$_2$—*CH*$_2$, NR—*CH*$_2$—COOH, NH$_2$—*CH*), 4.58 (m, NR—*CH*—CH$_2$—S), 5.02 (*CH*$_2$═CH), 5.34 (CH$_2$═*CH*) ppm. SEC (DMAc, 0.21% LiCl): M_n = 38,400 g mol^{-1}, Đ = 1.74.

4.8. Synthesis of P(AmButOx-stat-ButEnOx-stat-GluButOx) via deprotection (**P6**)

The protected copolymer ***boc*P6** (615 mg) was dissolved in dichloromethane (24 mL) and trifluoroacetic acid (40 mL) was added. The reaction mixture was stirred for 20 h at room temperature and, subsequently, precipitated in 300 mL ice-cold diethyl ether. The residue was filtered off, washed with 30 mL diethyl ether, re-dissolved in methanol and shaken overnight with Amberlyst® A21 (free base) (~0.5 mg). After filtration, the solvent was removed and the copolymer **P6** lyophilized.

P6: AmButOx:ButEnOx:GluButOx [%] = 82:10:8. ^{1}H-NMR (400 MHz, D$_2$O): δ 1.60 (*CH*$_2$—S—CH$_2$—CH$_2$—NR), 2.05 (NCH—*CH*$_2$—CH$_2$—C═O), 2.32–3.73 (NCH—*CH*$_2$—CH$_2$—C═O, CH$_2$ ButOx, *CH*$_2$—S—CH$_2$—CH$_2$, NR—*CH*$_2$—*CH*$_2$, NR—*CH*$_2$—COOH, NH$_2$—*CH*$_2$—C*H*$_2$), 4.38 (NR—*CH*—CH$_2$—S), 5.06 (*CH*$_2$═CH), 5.84 (CH$_2$═*CH*) ppm. AF4: M_n = 63,300 g mol^{-1}, Đ = 1.82.

4.9. Determination of the cytotoxicity

Cytotoxicity studies were performed with the mouse fibroblast cell line L929 (CCL-1, ATCC), as recommended by ISO10993-5 as well as with HEK-293 and hCMECs/D3 cells. The cells were routinely cultured in Dulbecco's modified eagle's medium (DMEM, Lonza) supplemented with 10% fetal calf serum (FCS), 100 U mL^{-1} penicillin and 100 μg mL^{-1} streptomycin at 37 °C in a humidified 5% (v/v) CO_2 atmosphere. In detail, cells were seeded at 10^4 cells per well in a 96-well plate and incubated for 24 h, whereas no cells were seeded in the outer wells. Afterwards, the substances to be tested (polymers) at indicated concentrations (from 10 μg mL^{-1} to 500 μg mL^{-1}) were added to the cells and the plates were incubated for further 24 h. Control cells were incubated with fresh culture medium. Subsequently, the medium was replaced by a mixture of fresh culture medium and Alamar-Blue solution, prepared according to the manufacturer's instructions. After an additional incubation of 4 h at 37 °C, the fluorescence was measured at Ex 570/Em 610 nm, with untreated cells on the same well plate serving as negative controls. The negative control was standardized as 0% of metabolism inhibition and referred as 100% viability. Cell viability below 70% was considered indicative of cytotoxicity. Data are expressed as mean ± S.D. of three determinations.

4.10. Hemolysis assay

The interaction of polymers with cellular membranes was examined by analyzing the release of hemoglobin from erythrocytes. Blood from sheep, collected in heparinized tubes, were provided by the Institute of Laboratory Animal Science and Animal Welfare, Friedrich Schiller University Jena. The blood was centrifuged at 4500 × *g* for 5 min, and the pellet was washed three times with cold 1.5 mM phosphate buffered saline (PBS, pH 7.4). After dilution with PBS in a ratio of 1:7, aliquots of erythrocyte suspension were mixed 1:1 with the polymer solution and incubated in a water bath at 37 °C for 60 min. After centrifugation at 2400 × *g* for 5 min, the hemoglobin release into the supernatant was determined spectrophotometrically using a microplate reader at 544 nm wavelength. Complete hemolysis (100%) was achieved using 1% Triton X-100 serving as positive control. Pure PBS was used as negative control (0% hemolysis). The hemolytic activity of the polycations was calculated as follow (Eq. (1)):

$$\%\text{Hemolysis} = 100 * \frac{(A_{Sample} - A_{Negative\ \ control})}{A_{Positive\ \ control}} \quad (1)$$

A value < 2% hemolysis rate was considered as non-hemolytic, 2 to 5% as slightly hemolytic and values > 5% as hemolytic. Experiments were run in triplicates and were performed with three different batches of donor blood.

4.11. Erythrocyte aggregation

The erythrocyte suspension was mixed 1:1 with the polymer solutions (100 μL total volume) in a clear flat bottomed 96-well plate. The cells were incubated at 37 °C for 2 h, and the absorbance was measured at 645 nm in a microplate reader. Cells, which were treated with PBS served as negative control and 25 kDa bPEI (50 μg mL^{-1}, Polyscience) was used as positive control. Absorbance values of the test solutions lower than the negative control were regarded as aggregation. Experiments were run in triplicates and were performed with three different charges of donor blood from sheep.

4.12. Polyplex preparation

Polyplexes of pDNA and polymers were prepared by mixing stock solutions of 15 μg mL^{-1} pDNA and different amounts of polymers (1 mg mL^{-1}) to obtain various N/P ratios (nitrogen of polymer to phosphate of pDNA) in HBG buffer (20 mM 4-(2-hydroxethyl) piperazine-1-ethanesulfonic acid (HEPES) and 5% (w/v) glucose, pH 7.2). The solutions were vortexed for 10 s at maximal speed and incubated at room temperature for 20 min to ensure complex formation.

4.13. Ethidium bromide quenching assay

The formation of polyplexes with pDNA was examined by quenching of the ethidium bromide fluorescence as described previously [56]. Briefly, 15 μg mL^{-1} pDNA in a total volume of 100 μL HBG buffer

(HEPES buffered glucose) were incubated with ethidium bromide (0.4 μg mL^{-1}) for 10 min at room temperature. Afterwards, polyplexes with increasing amounts of indicated polymers (regarding N/P ratio) were prepared in black 96-well plates (Nunc Thermo Fisher). The samples were incubated at room temperature for 15 min before fluorescence measurements. The fluorescence of the samples was measured at an excitation wavelength of 525 nm and an emission wavelength of 605 nm using a microplate reader. A sample solely containing pDNA and EtBr was used to calibrate the device to 100% fluorescence against a background of 0.4 μg mL^{-1} of EtBr in HBG solution. The percentage of dye displaced upon polyplex formation was calculated using Eq. (2):

$$\mathrm{RFU}\,[\%] = \frac{F_{sample} - F_0}{F_{pDNA} - F_0} * 100 \quad (2)$$

RFU is defined as the relative fluorescence and F_{sample}, F_0, and F_{pDNA} are the fluorescence intensities of a given sample, the ethidium bromide in HBG alone, and the ethidium bromide intercalated into pDNA alone.

4.14. Heparin dissociation assay

To investigate the release of pDNA from the polyplexes, the heparin dissociation assay was performed. Polyplexes with a N/P ratio of 40 were prepared as described above in a total volume of 100 μL HBG buffer containing ethidium bromide (0.4 μg mL^{-1}). After incubation in the dark at room temperature for 15 min, the polyplexes were transferred into a black 96-well plate, and heparin of indicated concentrations was added. The solution was mixed and incubated for further 30 min at 37 °C in the dark. The fluorescence of ethidium bromide was measured at Ex 525 nm/Em 605 nm with a Tecan microplate reader. The percentage of intercalated ethidium bromide was calculated as described before.

4.15. Dynamic and electrophoretic light scattering

Dynamic light scattering (DLS) was performed on a Zetasizer Nano ZS (Malvern Instruments, Herrenberg) with a He-Ne laser operating at a wavelength of $\lambda = 633$ nm. All measurements (30 runs, triplicate) were carried out at 25 °C after an equilibration time of 120 s. The counts were detected at an angle of 173°. The mean particle size was approximated as the effective (z-average) diameter and the width of the distribution as the polydispersity index of the particles (PDI) obtained by the cumulants method assuming a spherical shape. Electrophoretic light scattering (ELS) was used to measure the zeta potential (ζ). The measurement was performed on a Zetasizer Nano ZS (Malvern Instruments, Herrenberg, Germany) by applying laser Doppler velocimetry. For each measurement, 20 runs were carried out using the slow-field reversal and the fast-field reversal mode at 150 V. Each experiment was performed in triplicate a 25 °C. The zeta potential was calculated from the electrophoretic mobility (μ) according to the Henry Equation. Henry coefficient f(ka) was calculated according to Oshima.

4.16. Polyplex uptake

HEK-293 cells (CRL-1573, ATCC) were cultured in RPMI 1640 medium supplemented with 10% FCS, 100 μg mL^{-1} streptomycin, 100 IU mL^{-1} penicillin and 2 mM L-glutamine at 37 °C in a humidified 5% (v/v) CO_2 atmosphere. For uptake studies, cells were seeded at a density of 10^5 cells per mL in 24-well plates and cultured for 24 h. One hour prior to the addition of the polyplexes, the medium was changed to OptiMEM (Thermo Fisher, Germany). For the uptake kinetic study within 4 h, pDNA was labeled with YOYO-1 iodide prior to the polyplex preparation. For labeling of 1 μg pDNA, 0.026 μL of 1 M YOYO-1 solution was mixed with pDNA and incubated for 20 min at 4 °C protected from light. Afterwards, HBG buffer and the polymers were added at the indicated N/P ratio and the polyplexes were formed as described previously. The cells were harvested 15 min, 30 min, 1 h, 2 h and 4 h after polyplex addition and 10% trypan blue was added to quench the outer fluorescence of the cells. To determine the relative uptake of the polyplexes, 10,000 cells were measured by flow cytometry using a Cytomics FC 500 (Beckman Coulter) and the amount of viable cells showing YOYO-1 signal were gated. Dead cells were identified *via* counterstaining with propidium iodide. The experiments were performed at least three times independently. The uptake studies of hCMECs were performed in OptiMEM and EndoGro media, respectively. For live cell imaging HEK cells (10^5 cells mL^{-1}) were seeded in glass-bottomed, 4-chamber dishes (CELLVIEW, Greiner Bio-One, Germany) and cultured for 24 h. One hour prior to polymer addition, the cells were rinsed with phosphate buffered saline (PBS) and the media were changed to OptiMEM. Polyplexes were prepared at N/P 20 as described above and incubated for further 1 h. Afterwards, the media were replaced with fresh culture media supplemented with LysoTracker Red DND-99 and Hoechst 33342 for lysosome and nucleus staining, respectively. The living cells were imaged with a LSM880 using the following excitation wavelengths/laser lines 405 nm (for Hoechst), 488 nm (for YOYO-1) and 561 nm (for LysoTracker Red).

4.17. Transfection of adherent cells

For transfection of adherent HEK-293 cells, the cells were seeded at a density of 10^5 cells mL^{-1} in 24-well plates and incubated for 24 h at 37 °C, 5% (v/v) CO_2. One hour prior to transfection, the cells were washed with PBS and supplemented with serum-reduced media (OptiMEM). Polyplexes were prepared as described above, and were added to the cells (50 μL per well). After an incubation time of 4 h at 37 °C, the supernatant was replaced by fresh growth medium and the cells were further incubated for 20 h. For analysis *via* flow cytometry (Cytomics FC 500, Beckman Coulter), the cells were harvested by trypsinization and 10^4 cells were analyzed. For determination of the viability during flow cytometry, dead cells were identified *via* counterstaining with propidium iodide. For determination of the transfection efficiency, viable cells expressing EGFP were gated. The experiments were performed independently three times.

4.18. Immunofluorescence microscopy.

Cells were fixed with ice cold methanol for 10 min at −20 °C, permeabilized with 0.1% Saponin and blocking was done with 3% normal donkey serum. Antibody staining was performed using mouse-anti-human VE-Cadherin, mouse-anti-human β-Catenin (both BD Biosciences, Heidelberg, Germany), mouse-anti-human Claudin-5, rabbit-anti-human ZO-1 and rabbit-anti-human Occludin (all Life Technologies, Karlsruhe, Germany) overnight. Secondary antibodies donkey-anti-rabbit Cy3 (Dianova, Hamburg, Germany) and donkey-anti-mouse AlexaFluor647 (Life Technologies) as well as DAPI (Life Technologies) were applied for 1 h at room temperature. Samples were embedded in fluorescence mounting medium (Dako, Hamburg, Germany) and imaged on an Axio Observer.Z1 fluorescence microscope (Carl Zeiss AG, Jena, Germany). Image analysis was performed using ImageJ2 software (Fiji).

4.19. Dynamic cell culture assay

MOTiF biochips were made by injection moulding of polystyrene and manufactured by microfluidic Chip Shop (Jena, Germany) as described previously [65]. Chip geometry and embedded structures are shown in Supporting information, Fig. S10. The human cerebral microvascular endothelial cell line hCMEC/D3 (BIOZOL, Eching, Germany) was cultured in EndoGRO-MV Basal Medium supplemented with 5% (v/v) FCS, 0.2% (v/v) EndoGRO-LS supplement, 5 ng/mL recombinant human epidermal growth factor, 10 mM L-glutamine, 1 μg mL^{-1} hydrocortisone-hemisuccinate, 0.75 U mL^{-1} heparin-sulfate, 50 μg mL^{-1}

ascorbic acid (all additives were obtained from Merck-Millipore, Darmstadt, Germany), and 100 U mL^{-1} penicillin and 100 μg mL^{-1} streptomycin at 37 °C in a humidified 5% (v/v) CO_2 atmosphere. The membrane within the biochip was coated with 150 μg mL^{-1} collagen A (Biochrom, Berlin, Germany) for at least 1 h prior to cell seeding. hCMEC/D3 were seeded at a density of 0.75×10^5 cm^{-2} in the upper channel to grow on top of the membrane. Cells were cultured until fully confluent after four to five days. Afterwards, biochips were connected to an Ismatec peristaltic pump (Cole Parmer, Wertheim, Germany) *via* gas permeable silicon tubing (Cole Parmer and microfluidic Chip Shop) at 37 °C in a humidified 5% (v/v) CO_2 atmosphere and accustomed to flow conditions with a flow rate of 175 μL min^{-1} (corresponding shear stress of 2 dyn cm^2) for 30 min. Meanwhile polyplex formation at a N/P ratio of 20 was performed in hCMEC/D3 cell culture medium as stated above with additionally applying YOYO-1 as reporter dye. As corresponding controls polyplex solutions without dye were used. Subsequently shear stress was increased to 4 dyn cm^2 and polyplex solutions were applied for 1 h. For sampling 30 μL from the lower channel system were taken whereas the first 15 μL were discarded to ensure sampling from under the membrane and not just from the microchannels. Samples were taken every 15 min. Afterwards, cells were washed gently by flushing the upper and lower microchannels three times with PBS. Nuclei were stained with Hoechst 33342. Membranes and supernatants were analyzed using an Axio Observer.Z1 fluorescence microscope (Carl Zeiss AG, Jena, Germany) applying a filter with 470 nm excitation and 525 nm emission wave lengths. At least three images per sample were taken. Fluorescence images were analyzed with the ImageJ2 software whereas controls were subtracted for quantification.

4.20. Statistical analysis

The values represent the mean ± S.D. Direct comparison of two different groups was done with two-tailed, non-paired student's test. For multiple comparisons analysis by two-way ANOVA was performed using Turkey's multiple testing as post-test. Statistical significant was defined with p-values of <0.05.

Acknowledgment

The authors would like to thank Carolin Fritzsche for the support with the bio assays and Gabriele Sentis and Dr. Peter Bellstedt for nuclear magnetic resonance measurements. We gratefully acknowledge Dr. Johannes C. Brendel for helpful discussions. The funding of the collaborative research center ChemBioSys (SFB 1127) by the Deutsche Forschungsgemeinschaft (DFG), the Carl Zeiss Foundation (scholarship for AT), the German Federal Ministry of Education and Research (BMBF # 031A518B Vectura) and the German Federal Institute of Risk Assessment (grant number 1329-533) are highly acknowledged. The LSM880 ELYRA PS.1 was further founded with a grant from the DFG.

Appendix A. Supplementary data

Supplementary figures and tables S1–S12. This material is available free of charge *via* the Internet at http://pubs.acs.org. Supplementary data associated with this article can be found in the online version, at http://dx.doi.org/10.1016/j.jconrel.2016.08.039.

References

[1] P. Ehrlich, Das Sauerstoffbedürfnis des Organismus, eine farbenanalytische Studie, Hirschwald, Berlin, 1885.
[2] M. Lewandowsky, Zur Lehre von der Cerebrospinalflüssigkeit, Z. Klin. Med. 40 (1900) 480–494.
[3] N.J. Abbott, A.A.K. Patabendige, D.E.M. Dolman, S.R. Yusof, D.J. Begley, Structure and function of the blood–brain barrier, Neurobiol. Dis. 37 (2010) 13–25, http://dx.doi.org/10.1016/j.nbd.2009.07.030.
[4] V.A. Levin, Relationship of octanol/water partition coefficient and molecular weight to rat brain capillary permeability, J. Med. Chem. 23 (1980) 682–684, http://dx.doi.org/10.1021/jm00180a022.
[5] X. Liu, M. Tu, R.S. Kelly, C. Chen, B.J. Smith, Development of a computional approach to predict blood-brain barrier permeability, Drug Metab. Dispos. 32 (2004) 132–139, http://dx.doi.org/10.1124/dmd.32.1.132.
[6] C.C. Visser, L.H. Voorwinden, D.J.A. Crommelin, M. Danhof, A.G. de Boer, Characterization and modulation of the transferrin receptor on brain capillary endothelial cells, Pharm. Res. 21 (2004) 761–769, http://dx.doi.org/10.1023/B:PHAM.0000026425.69874.8e.
[7] B.V. Zlokovic, The blood-brain barrier in health and chronic neurodegenerative disorders, Neuron 57 (2008) 178–201, http://dx.doi.org/10.1016/j.neuron.2008.01.003.
[8] R. Kannan, R. Chakrabarti, D. Tang, K.J. Kim, N. Kaplowitz, GSH transport in human cerebrovascular endothelial cells and human astrocytes: evidence for luminal localization of Na+-dependent GSH transport in HCEC1, Brain Res. 852 (2000) 374–382, http://dx.doi.org/10.1016/S0006-8993(99)02184-8.
[9] M. Bauer, C. Lautenschlaeger, K. Kempe, L. Tauhardt, U.S. Schubert, D. Fischer, Poly(2-ethyl-2-oxazoline) as alternative for the stealth polymer poly(ethylene glycol): comparison of in vitro cytotoxicity and hemocompatibility, Macromol. Biosci. 12 (2012) 986–998, http://dx.doi.org/10.1002/mabi.201200017.
[10] R. Kannan, J.F. Kuhlenkamp, E. Jeandidier, H. Trinh, M. Ookhtens, N. Kaplowitz, Evidence for carrier-mediated transport of glutathione across the blood-brain barrier in the rat, J. Clin. Invest. 85 (1990) 2009–2013, http://dx.doi.org/10.1172/JCI114666.
[11] C.M. Berlin, D.G. May-McCarver, D.A. Notterman, R.M. Ward, D.N. Weismann, G.S. Wilson, J.T. Wilson, Alternative routes of drug administration—advantages and disadvantages, Pediatrics 100 (1997) 143–152, http://dx.doi.org/10.1542/peds.100.1.143.
[12] A. Mistry, S. Stolnik, L. Illum, Nanoparticles for direct nose-to-brain delivery of drugs, Int. J. Pharm. 379 (2009) 146–157, http://dx.doi.org/10.1016/j.ijpharm.2009.06.019.
[13] X. Wen, K. Wang, Z. Zhao, Y. Zhang, T. Sun, F. Zhang, J. Wu, Y. Fu, Y. Du, L. Zhang, Y. Sun, Y. Liu, K. Ma, H. Liu, Y. Song, Brain-targeted delivery of trans-activating transcriptor-conjugated magnetic PLGA/lipid nanoparticles, PLoS One 9 (2014) e106652, http://dx.doi.org/10.1371/journal.pone.0106652.
[14] B. Oller-Salvia, M. Sanchez-Navarro, E. Giralt, M. Teixido, Blood-brain barrier shuttle peptides: an emerging paradigm for brain delivery, Chem. Soc. Rev. (2016), http://dx.doi.org/10.1039/C6CS00076B.
[15] J. Kreuter, Nanoparticulate systems for brain delivery of drugs, Adv. Drug Deliv. Rev. 47 (2001) 65–81, http://dx.doi.org/10.1016/S0169-409X(00)00122-8.
[16] L. Nobs, F. Buchegger, R. Gurny, E. Allémann, Surface modification of poly(lactic acid) nanoparticles by covalent attachment of thiol groups by means of three methods, Int. J. Pharm. 250 (2003) 327–337, http://dx.doi.org/10.1016/S0378-5173(02)00542-2.
[17] K. Kafedjiiski, M. Werle, F. Föger, A. Bernkop-Schnürch, Synthesis and in vitro characterization of a novel poly(acrylic acid)-glutathione conjugate, J. Drug. Deliv. Sci. Tech. 15 (2005) 411–417, http://dx.doi.org/10.1016/S1773-2247(05)50081-9.
[18] S.S. More, R. Vince, Design, synthesis and biological evaluation of glutathione peptidomimetics as components of anti-parkinson prodrugs, J. Med. Chem. 51 (2008) 4581–4588, http://dx.doi.org/10.1021/jm800239v.
[19] N. Raval, T. Mistry, N. Acharya, S. Acharya, Development of glutathione-conjugated asiatic acid-loaded bovine serum albumin nanoparticles for brain-targeted drug delivery, J. Pharm. Pharmacol. 67 (2015) 1503–1511, http://dx.doi.org/10.1111/jphp.12460.
[20] A. Grover, A. Hirani, V. Sutariya, Blood-barin barrier permeation of glutathione-coated nanoparticle, J. Pharm. Pharm. Sci 1 (2014), http://dx.doi.org/10.15226/2374-6866/1/1/00103.
[21] P.J. Gaillard, C.C.M. Appeldoorn, J. Rip, R. Dorland, S.M.A. van der Pol, G. Kooij, H.E. de Vries, A. Reijerkerk, Enhanced brain delivery of liposomal methylprednisolone improved therapeutic efficacy in a model of neuroinflammation, J. Control. Release 164 (2012) 364–369, http://dx.doi.org/10.1016/j.jconrel.2012.06.022.
[22] P.J. Gaillard, C.C.M. Appeldoorn, R. Dorland, J. van Kregten, F. Manca, D.J. Vugts, B. Windhorst, G.A.M.S. van Dongen, H.E. de Vries, D. Maussang, O. van Tellingen, Pharmacokinetics, brain delivery, and efficacy in brain tumor-bearing mice of glutathione pegylated liposomal doxorubicin (2B3-101), PLoS One 9 (2014) e82331, http://dx.doi.org/10.1371/journal.pone.0082331.
[23] T. Patel, J. Zhou, J.M. Piepmeier, W.M. Saltzman, Polymeric nanoparticles for drug delivery to the central nervous system, Adv. Drug Deliv. Rev. 64 (2012) 701–705, http://dx.doi.org/10.1016/j.addr.2011.12.006.
[24] J. Kreuter, R.N. Alyautdin, D.A. Kharkevich, A.A. Ivanov, Passage of peptides through the blood-brain barrier with colloidal polymer particles (nanoparticles), Brain Res. 674 (1995) 171–174, http://dx.doi.org/10.1016/0006-8993(95)00023-J.
[25] K.S. Rao, M.K. Reddy, J.L. Horning, V. Labhasetwar, TAT-conjugated nanoparticles for the CNS delivery of anti-HIV drugs, Biomaterials 29 (2008) 4429–4438, http://dx.doi.org/10.1016/j.biomaterials.2008.08.004.
[26] S.A. Kulkarni, S.-S. Feng, Effects of surface modification on delivery efficiency of biodegradable nanoparticles across the blood–brain barrier, Nanomedicine 6 (2011) 377–394, http://dx.doi.org/10.2217/nnm.10.131.
[27] J. Wang, Z. Lu, M.G. Wientjes, J.L.-S. Au, Delivery of siRNA therapeutics: barriers and carriers, AAPS J. 12 (2010) 492–503, http://dx.doi.org/10.1208/s12248-010-9210-4.
[28] M.A. Mintzer, E.E. Simanek, Nonviral vectors for gene delivery, Chem. Rev. 109 (2009) 259–302, http://dx.doi.org/10.1021/cr800409e.
[29] J.H. Jeong, S.H. Song, D.W. Lim, H. Lee, T.G. Park, DNA transfection using linear poly(ethylenimine) prepared by controlled acid hydrolysis of poly(2-ethyl-2-oxazoline), J. Control. Release 73 (2001) 391–399, http://dx.doi.org/10.1016/S0168-3659(01)00310-8.
[30] C. Englert, M. Hartlieb, P. Bellstedt, K. Kempe, C. Yang, S.K. Chu, X. Ke, J.M. García, R.J. Ono, M. Fevre, R.J. Wojtecki, U.S. Schubert, Y.Y. Yang, J.L. Hedrick, Enhancing the biocompatibility and biodegradability of linear poly(ethylene imine) through con-

trolled oxidation, Macromolecules 48 (2015) 7420–7427, http://dx.doi.org/10.1021/acs.macromol.5b01940.
[31] K. Kunath, A. von Harpe, D. Fischer, T. Kissel, Galactose-PEI–DNA complexes for targeted gene delivery: degree of substitution affects complex size and transfection efficiency, J. Control. Release 88 (2003) 159–172, http://dx.doi.org/10.1016/S0168-3659(02)00458-3.
[32] W. Cheng, C. Yang, J.L. Hedrick, D.F. Williams, Y.Y. Yang, P.G. Ashton-Rickardt, Delivery of a granzyme B inhibitor gene using carbamate-mannose modified PEI protects against cytotoxic lymphocyte killing, Biomaterials 34 (2013) 3697–3705, http://dx.doi.org/10.1016/j.biomaterials.2013.01.090.
[33] C. Englert, M. Fevre, R.J. Wojtecki, W. Cheng, Q. Xu, C. Yang, X. Ke, M. Hartlieb, K. Kempe, J.M. García, R.J. Ono, U.S. Schubert, Y.Y. Yang, J.L. Hedrick, Facile carbohydrate-mimetic modifications of poly(ethylene imine) carriers for gene delivery applications, Polym. Chem. (2016), http://dx.doi.org/10.1039/c6py00940a (in press).
[34] M. Ogris, S. Brunner, S. Schüller, R. Kircheis, E. Wagner, PEGylated DNA/transferrin-PEI complexes: reduced interaction with blood components, extended circulation in blood and potential for systemic gene delivery, Gene Ther. 6 (1999) 595–605.
[35] B.J. Ballermann, A. Dardik, E. Eng, A. Liu, Shear stress and the endothelium, Kidney Int. 54 (1998) 100–108, http://dx.doi.org/10.1046/j.1523-1755.1998.06720.x.
[36] M. Raasch, K. Rennert, T. Jahn, C. Gärtner, G. Schönfelder, O. Huber, A. Seiler, A. Mosig, An integrative microfluicically supported in vitro model of an endothelial barrier combined with cortical spheroids simulates effects of neuroinflammation in neocortex development, Biomicrofluidics 10 (2016), http://dx.doi.org/10.1063/1.4955184 (in press).
[37] B.B. Weksler, E.A. Subileau, N. Perrière, P. Charneau, K. Holloway, M. Leveque, H. Tricoire-Leignel, A. Nicotra, S. Bourdoulous, P. Turowski, D.K. Male, F. Roux, J. Greenwood, I.A. Romero, P.O. Couraud, Blood-brain barrier-specific properties of a human adult brain endothelial cell line, FASEB J. 19 (2005) 1872–1874, http://dx.doi.org/10.1096/fj.04-3458fje.
[38] B. Weksler, I.A. Romero, P.-O. Couraud, The hCMEC/D3 cell line as a model of the human blood brain barrier, Fluids Barriers CNS 10 (2013) 1–10, http://dx.doi.org/10.1186/2045-8118-10-16.
[39] B. Poller, H. Gutmann, S. Krähenbühl, B. Weksler, I. Romero, P.-O. Couraud, G. Tuffin, J. Drewe, J. Huwyler, The human brain endothelial cell line hCMEC/D3 as a human blood-brain barrier model for drug transport studies, J. Neurochem. 107 (2008) 1358–1368, http://dx.doi.org/10.1111/j.1471-4159.2008.05730.x.
[40] L. Cucullo, P.-O. Couraud, B. Weksler, I.-A. Romero, M. Hossain, E. Rapp, D. Janigro, Immortalized human brain endothelial cells and flow-based vascular modeling: a marriage of convenience for rational neurovascular studies, J. Cereb. Blood Flow Metab. 28 (2008) 312–328, http://dx.doi.org/10.1038/sj.jcbfm.9600525.
[41] L.M. Griep, F. Wolbers, B. de Wagenaar, P.M. ter Braak, B.B. Weksler, I.A. Romero, P.O. Couraud, I. Vermes, A.D. van der Meer, A. van den Berg, BBB on chip: microfluidic platform to mechanically and biochemically modulate blood-brain barrier function, Biomed. Microdevices 15 (2013) 145–150, http://dx.doi.org/10.1007/s10544-012-9699-7.
[42] B.P. Daniels, L. Cruz-Orengo, T.J. Pasieka, P.-O. Couraud, I.A. Romero, B. Weksler, J.A. Cooper, T.L. Doering, R.S. Klein, Immortalized human cerebral microvascular endothelial cells maintain the properties of primary cells in an in vitro model of immune migration across the blood brain barrier, J. Neurosci. Methods 212 (2013) 173–179, http://dx.doi.org/10.1016/j.jneumeth.2012.10.001.
[43] D. Ye, M.N. Raghnaill, M. Bramini, E. Mahon, C. Aberg, A. Salvati, K.A. Dawson, Nanoparticle accumulation and transcytosis in brain endothelial cell layers, Nanoscale 5 (2013) 11153–11165, http://dx.doi.org/10.1039/C3NR02905K.
[44] D. Ye, K.A. Dawson, I. Lynch, A TEM protocol for quality assurance of in vitro cellular barrier models and its application to the assessment of nanoparticle transport mechanisms across barriers, Analyst 140 (2015) 83–97, http://dx.doi.org/10.1039/C4AN01276C.
[45] H.M.L. Lambermont-Thijs, F.S. van der Woerdt, A. Baumgaertel, L. Bonami, F.E.D. Prez, U.S. Schubert, R. Hoogenboom, Linear poly(ethylene imine)s by acidic hydrolysis of poly(2-oxazoline)s: kinetic screening, thermal properties, and temperature-induced solubility transitions, Macromolecules 43 (2010) 927–933, http://dx.doi.org/10.1021/ma9020455.
[46] T. Bus, C. Englert, M. Reifarth, P. Borchers, M. Hartlieb, A. Vollrath, S. Hoeppener, A. Traeger, U.S. Schubert, 3rd Generation Poly(ethylene imine)s for Gene Delivery, 2016 (submitted).
[47] C. Englert, L. Tauhardt, M. Hartlieb, K. Kempe, M. Gottschaldt, U.S. Schubert, Linear poly(ethylene imine)-based hydrogels for effective binding and release of DNA, Biomacromolecules 15 (2014) 1124–1131, http://dx.doi.org/10.1021/bm4017572.
[48] M. Neu, D. Fischer, T. Kissel, Recent advances in rational gene transfer vector design based on poly(ethylene imine) and its derivatives, J. Gene Med. 7 (2005) 992–1009, http://dx.doi.org/10.1002/jgm.773.
[49] S.K. Samal, M. Dash, S. Van Vlierberghe, D.L. Kaplan, E. Chiellini, C. van Blitterswijk, L. Moroni, P. Dubruel, Cationic polymers and their therapeutic potential, Chem. Soc. Rev. 41 (2012) 7147–7194, http://dx.doi.org/10.1039/C2CS35094G.
[50] J.C. Sunshine, D.Y. Peng, J.J. Green, Uptake and transfection with polymeric nanoparticles are dependent on polymer end-group structure, but largely independent of nanoparticle physical and chemical properties, Mol. Pharm. 9 (2012) 3375–3383, http://dx.doi.org/10.1021/mp3004176.
[51] B. Wittgren, A. Welinder, B. Porsch, Molar mass characterization of cationic methyl methacrylate–ethyl acrylate copolymers using size-exclusion chromatography with online multi-angle light scattering and refractometric detection, J. Chromatogr. A 1002 (2003) 101–109, http://dx.doi.org/10.1016/S0021-9673(03)00729-5.
[52] R. Roemling, K. Tokunaga, H. Monyama, Analysis of cationic polymers by size exclusion chromatography (SEC), LC-GC Europe (2008) 47–48.
[53] S.M. Moghimi, P. Symonds, J.C. Murray, A.C. Hunter, G. Debska, A. Szewczyk, A two-stage poly(ethylenimine)-mediated cytotoxicity: implications for gene transfer/therapy, Mol. Ther. 11 (2005) 990–995, http://dx.doi.org/10.1016/j.ymthe.2005.02.010.
[54] D. Fischer, Y. Li, B. Ahlemeyer, J. Krieglstein, T. Kissel, In vitro cytotoxicity testing of polycations: influence of polymer structure on cell viability and hemolysis, Biomaterials 24 (2003) 1121–1131, http://dx.doi.org/10.1016/S0142-9612(02)00445-3.
[55] L. Dekie, V. Toncheva, P. Dubruel, E.H. Schacht, L. Barrett, L.W. Seymour, Poly-L-glutamic acid derivatives as vectors for gene therapy, J. Control. Release 65 (2000) 187–202, http://dx.doi.org/10.1016/S0168-3659(99)00235-7.
[56] A.C. Rinkenauer, L. Tauhardt, F. Wendler, K. Kempe, M. Gottschaldt, A. Traeger, U.S. Schubert, A cationic poly(2-oxazoline) with high in vitro transfection efficiency identified by a library approach, Macromol. Biosci. 15 (2015) 414–425, http://dx.doi.org/10.1002/mabi.201400334.
[57] S.K. Tripathi, N. Gupta, M. Mahato, K.C. Gupta, P. Kumar, Selective blocking of primary amines in branched polyethylenimine with biocompatible ligand alleviates cytotoxicity and augments gene delivery efficacy in mammalian cells, Colloids Surf. B 115 (2014) 79–85, http://dx.doi.org/10.1016/j.colsurfb.2013.11.024.
[58] D.W. Hwang, S. Son, J. Jang, H. Youn, S. Lee, D. Lee, Y.-S. Lee, J.M. Jeong, W.J. Kim, D.S. Lee, A brain-targeted rabies virus glycoprotein-disulfide linked PEI nanocarrier for delivery of neurogenic microRNA, Biomaterials 32 (2011) 4968–4975, http://dx.doi.org/10.1016/j.biomaterials.2011.03.047.
[59] J.B. Lepecq, C. Paoletti, Federation of european biochemical societies 3rd meeting: a fluorescent complex between ethidium bromide and nucleic acids, J. Mol. Biol. 27 (1967) 87–106, http://dx.doi.org/10.1016/0022-2836(67)90353-1.
[60] A.J. Geall, I.S. Blagbrough, Rapid and sensitive ethidium bromide fluorescence quenching assay of polyamine conjugate–DNA interactions for the analysis of lipoplex formation in gene therapy, J. Pharm. Biomed. Anal. 22 (2000) 849–859, http://dx.doi.org/10.1016/S0731-7085(00)00250-8.
[61] A.C. Rinkenauer, S. Schubert, A. Traeger, U.S. Schubert, The influence of polymer architecture on in vitro pDNA transfection, J. Mater. Chem. B 3 (2015) 7477–7493, http://dx.doi.org/10.1039/C5TB00782H.
[62] S. Sundaram, S. Viriyayuthakorn, C.M. Roth, Oligonucleotide structure influences the interactions between cationic polymers and oligonucleotides, Biomacromolecules 6 (2005) 2961–2968, http://dx.doi.org/10.1021/bm0502314.
[63] A. Kwok, S.L. Hart, Comparative structural and functional studies of nanoparticle formulations for DNA and siRNA delivery, Nanomed. Nanotechnol. 7 (2011) 210–219, http://dx.doi.org/10.1016/j.nano.2010.07.005.
[64] R. Luxenhofer, G. Sahay, A. Schulz, D. Alakhova, T.K. Bronich, R. Jordan, A.V. Kabanov, Structure-property relationship in cytotoxicity and cell uptake of poly(2-oxazoline) amphiphiles, J. Control. Release 153 (2011) 73–82, http://dx.doi.org/10.1016/j.jconrel.2011.04.010.
[65] R. Martin, R. Knut, J. Tobias, P. Sven, H. Thomas, H. Otmar, S. Ingo, B. Holger, L. Stefan, F. Harald, M. Alexander, Microfluidically supported biochip design for culture of endothelial cell layers with improved perfusion conditions, Biofacrication 7 (2015) 015013, http://dx.doi.org/10.1088/1758-5090/7/1/015013.
[66] J. Gavard, J.S. Gutkind, VE-cadherin and claudin-5: it takes two to tango, Nat. Cell Biol. 10 (2008) 883–885, http://dx.doi.org/10.1038/ncb0808-883.
[67] W. Jia, R. Lu, T.A. Martin, W.G. Jiang, The role of claudin-5 in blood-brain barrier (BBB) and brain metastases (review), Mol. Med. Rep. 9 (2014) 779–785, http://dx.doi.org/10.3892/mmr.2013.1875.
[68] E. Dejana, F. Orsenigo, M.G. Lampugnani, The role of adherens junctions and VE-cadherin in the control of vascular permeability, J. Cell Sci. 121 (2008) 2115–2122, http://dx.doi.org/10.1242/jcs.017897.
[69] S. Liebner, M. Corada, T. Bangsow, J. Babbage, A. Taddei, C.J. Czupalla, M. Reis, A. Felici, H. Wolburg, M. Fruttiger, M.M. Taketo, H. von Melchner, K.H. Plate, H. Gerhardt, E. Dejana, Wnt/β-catenin signaling controls development of the blood–brain barrier, J. Cell Biol. 183 (2008) 409–417, http://dx.doi.org/10.1083/jcb.200806024.
[70] T. Hirase, J.M. Staddon, M. Saitou, Y. Ando-Akatsuka, M. Itoh, M. Furuse, K. Fujimoto, S. Tsukita, L.L. Rubin, Occludin as a possible determinant of tight junction permeability in endothelial cells, J. Cell Sci. 110 (1997) 1603–1613 (doi:).
[71] E. Mennesson, P. Erbacher, M. Kuzak, C. Kieda, P. Midoux, C. Pichon, DNA/cationic polymer complex attachment on a human vascular endothelial cell monolayer exposed to a steady laminar flow, J. Control. Release 114 (2006) 389–397, http://dx.doi.org/10.1016/j.jconrel.2006.06.006.
[72] A. Gress, A. Völkel, H. Schlaad, Thio-click modification of poly[2-(3-butenyl)-2-oxazoline], Macromolecules 40 (2007) 7928–7933, http://dx.doi.org/10.1021/ma071357r.
[73] J.C. Fernandes, X. Qiu, F.M. Winnik, M. Benderdour, X. Zhang, K. Dai, Q. Shi, Linear polyethylenimine produced by partial acid hydrolysis of poly(2-ethyl-2-oxazoline) for DNA and siRNA delivery in vitro, Int. J. Nanomedicine 8 (2013) 4091–4102, http://dx.doi.org/10.2147/IJN.S47413.

PUBLICATION 7

D-Fructose-decorated poly(ethylene imine) for human breast cancer cell targeting

C. Englert,‡ M. Pröhl,‡ J. A. Czaplewska, C. Fritzsche, E. Preußger, U. S. Schubert, A. Traeger, M. Gottschaldt

Macromol. Biosci. **2017**, *17*, 1600502

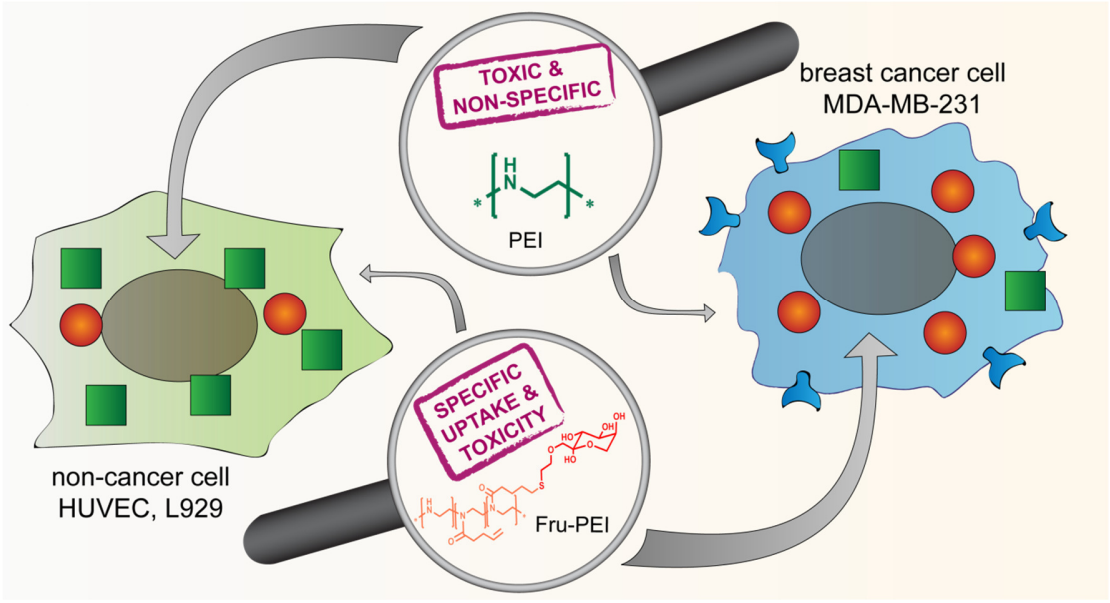

‡ Authors contributed equally.

D-Fructose-Decorated Poly(ethylene imine) for Human Breast Cancer Cell Targeting

Christoph Englert, Michael Pröhl, Justyna A. Czaplewska, Carolin Fritzsche, Elisabeth Preußger, Ulrich S. Schubert, Anja Traeger, Michael Gottschaldt*

The high affinity of GLUT5 transporter for D-fructose in breast cancer cells has been discussed intensely. In this contribution, high molar mass linear poly(ethylene imine) (LPEI) is functionalized with D-fructose moieties to combine the selectivity for the GLUT5 transporter with the delivery potential of PEI for genetic material. The four-step synthesis of a thiol-group bearing D-fructose enables the decoration of a cationic polymer backbone with D-fructose via thiol-ene photoaddition. The functionalization of LPEI is confirmed by 2D NMR techniques, elemental analysis, and size exclusion chromatography. Importantly, a D-fructose decoration of 16% renders the polymers water-soluble and eliminates the cytotoxicity of PEI in noncancer L929 cells, accompanied by a reduced unspecific cellular uptake of the genetic material. In contrast, the cytotoxicity as well as the cell specific uptake is increased for triple negative MDA-MB-231 breast cancer cells. Therefore, the introduction of D-fructose shows superior potential for cell targeting, which can be assumed to be GLUT5 dependent.

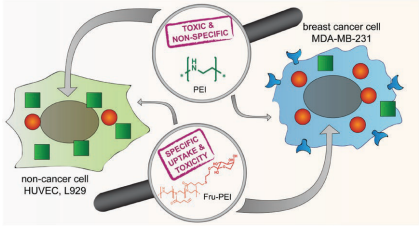

1. Introduction

With around 1.65 million new cases of cancer and around 590 thousand deaths resulted from cancer in 2015 in the United States, human breast cancer represents the second leading death cause after heart diseases. Among them, 230 thousand new cases derive from breast cancer from which around 41 thousand ended deadly.[1] It is described as a highly heterogeneous type of cancer with manifold grades and types.[2] The number of specific targets is high, in which 60%–80% of all cases are hormone receptors of the human epidermal growth factor receptor (HER) family that can be targeted by endocrine therapy.[3] By lacking progesterone and estrogene receptor overexpression as well as amplification of HER2 genes at the same time, a tumor type with a shorter median time from relapse to death was identified in 1987 and is nowadays treated with Trastuzumab, a monoclonal antibody.[4] Triple-negative tumors are described by the lack of hormone receptor expression as well as HER2 receptors, an aggressive type with insufficient therapy options and poor prognosis, which represents roughly 15% of all breast cancer tumors.[3] Besides the treatment with the monoclonal antibody Bevacizumab, that blocks angiogenesis by inhibiting vascular endothelial growth factor A, there are more than 50 clinical trials ongoing, which address various targets such as the epidermal growth factor,[5] Src tyrosine kinase,[6] and heat shock protein 90 to develop strategies against this aggressive kind of breast cancer.[7]

Another target, which is controversially discussed in the present literature, is the GLUT5 transporter, a highly affine D-fructose transporter.[8] While Gowrishankar

C. Englert, M. Pröhl, Dr. J. A. Czaplewska, C. Fritzsche, E. Preußger, Prof. U. S. Schubert, Dr. A. Traeger, Dr. M. Gottschaldt
Laboratory of Organic and Macromolecular Chemistry (IOMC)
Friedrich Schiller University Jena
Humboldtstrasse 10, 07743 Jena, Germany
E-mail: michael.gottschaldt@uni-jena.de
C. Englert, M. Pröhl, Dr. J. A. Czaplewska, C. Fritzsche, E. Preußger, Prof. U. S. Schubert, Dr. A. Traeger, Dr. M. Gottschaldt
Jena Center for Soft Matter (JCSM)
Friedrich Schiller University Jena
Philosophenweg 7, 07743 Jena, Germany

et al. declined the overexpression of GLUT5 in all breast cancer tissues,[9] Nualart and co-workers claimed GLUT5 as overexpressed in 85% of 33 tested breast cancer cell lines,[10] also confirmed for estrogen-receptor positive MCF-7 and triple-negative MDA-MB-231 breast cancer cell lines.[11] Nevertheless, that implies a possible enhanced selectivity of anticancer agents by the attachment of D-fructose and its derivatives. Previous studies revealed that modifications at C1- and C6-position of the sugar are tolerated by the GLUT5 transporter.[12] For this reason, D-fructose was successfully attached to dyes,[13] metal complexes,[14] polymers,[15] and nanoparticles[16] and tested with various breast cancer cell lines, revealing an increased uptake for the D-fructose conjugated compounds and structures.

Nowadays, one opportunity of cancer treatment is the manipulation of the pathways in tumors on the level of the cellular genetic information, e.g., by the introduction of genetic material. This promising anticancer approach has gained increasing interest over the last decade and various potential carriers have been investigated.[15] Since viral vectors possess considerable cytotoxicities and immunological concerns, nonviral vectors like cationic cell penetrating peptides,[17] antibodies[18] and lipid-based carriers[19] have been intensively investigated. Cationic polymers, e.g., poly(ethylene imine) (PEI), represent another class of suitable candidates to complex genetic material by electrostatic interactions.[20] Due to its superior buffering ability leading to endosomal escape ("proton sponge effect"), PEI is known as the gold standard of polymeric carriers for gene delivery.[21] However, its full potential is restricted through its high cytotoxicity and non-biodegradability.[22] One useful strategy to overcome these limitations is the modification of the PEI backbone[23] and/or the introduction of side chains. The latter approach has been extensively studied, e.g., by functionalization of PEI with various carbohydrates[24] or stealth polymers, like poly(ethylene glycol).[25]

Herein, we focused on the installation of D-fructose moieties at side chains of high molar mass linear PEI to combine the selectivity for the GLUT5 transporter and the delivery potential of genetic material. To remain a defined quantity of cationic ethylene imine units, a post-polymerization functionalization using *N*-succinimidyl-4-pentenate was chosen. This enables the synthesis of glycopolymer structures[26] by the reaction with thiol sugars utilizing the metal-free thiol-ene photoaddition. The designed copolymer and respective precursors were investigated concerning their bio- and hemocompatibility, their affinity for binding and release of genetic material (exemplified for plasmid DNA) and their specific cellular uptake (MDA-MB231 breast cancer vs. noncancer L929 and primary human umbilical vein endothelial cells, HUVEC).

2. Experimental Section

2.1. Materials

2-Ethyl-2-oxazoline (EtOx) and methyl tosylate were obtained from Acros Organics, distilled (over barium oxide (BaO) in the case of EtOx), and stored under argon atmosphere. Pyridine, methanol, dichloromethane, 4-*N*,*N*-dimethylamino-pyridine (DMAP), 2,2-dimethoxy-2-phenylacetophenone (DMPA) and rhodamine B isothiocyanate were obtained from Sigma-Aldrich (Steinhausen, Germany) and are of analytical grade and are used without further purification. Acetonitrile was purified on a MBraun solvent purification system (MB SPS-800). *N*-Succinimidyl-4-pentenate was prepared according to literature procedures.[27] Ethidium bromide solution (1%, 10 mg mL^{-1}) was purchased from Carl Roth (Karlsruhe, Germany). AlamarBlue, YOYO-1 iodide, Hoechst 33342 trihydrochloride, heparin and **Cy5** dye were obtained from Thermo Fisher (Germany). Plasmid pEGFP-N1 (4.7 kb, Clontech, USA encoding green fluorescent protein (EGFP) was isolated with the Giga Plasmid Kit provided by Qiagen (Hilden, Germany). If not stated otherwise, cell culture materials, cell culture media and solutions were obtained from Biochrom (Berlin, Germany).

2.2. General Methods and Instrumentation

The polymerizations as well as the hydrolysis of poly(2-ethyl-2-oxazoline) were performed under microwave irradiation in an Initiator Sixty single-mode microwave synthesizer from Biotage, equipped with a noninvasive IR sensor (accuracy 2%). Chromatographic separations were performed using normal phase (NP) silica RediSep Cartridges by Teledyne Isco. The reaction progress was monitored by thin-layer chromatography (TLC) using glass plates precoated with silica gel 60 (Merck).

Proton (^{1}H) nuclear magnetic resonance (NMR) spectra were recorded at room temperature using spectrometers from Bruker (300, 600 MHz). ^{13}C NMR was recorded at 100 MHz. Chemical shifts (δ) are expressed in parts per million relative to tetramethylsilane (TMS).

Size exclusion chromatographic (SEC) investigations were performed on an Agilent Technologies 1200 Series gel permeation chromatography system equipped with a G1329A auto sampler, a G131A isocratic pump, a G1362A refractive index detector, and both a PSS Gram 30 and a PSS Gram 1000 column placed in series. As eluent a 0.21% LiCl solution in *N*,*N*-dimethylacetamide (DMAc) was used at 1 mL min^{-1} flow rate and a column oven temperature of 40 °C. Molar masses were calculated using poly(styrene) standards. High-resolution electron spray ionization mass spectrometry (HR-ESI-MS) was measured with a Bruker MicroQTof and elemental analysis were measured with a Leco CHN-932.

2.2.1. Synthesis of 1-(2-(Benzyloxy)ethyl)-2,3:4,5-di-O-isopropylidene-β-D-fructopyranoside (*2*)

6.5 g (25 mmol) of 2,3:4,5-di-*O*-isopropylidene-β-D-fructopyranoside **1** was dissolved in 150 mL of dry THF, 4 g NaH (166.7 mmol) were added and the mixture stirred for 20 min under nitrogen. Subsequently, benzyl 2-bromoethyl ether (10 g, 43.6 mmol) was added dropwise and reaction was conducted for 7 d (controlled during this time with TLC). After no starting material had remained (TLC,

Macromol. Biosci. **2017**, DOI: 10.1002/mabi.201600502

SiO_2, EtOAc/cyclohexane, v/v, 1:2), 50 mL of methanol were slowly added and the reaction mixture was evaporated. The crude product was dissolved in 200 mL of ethyl acetate and washed twice with each 200 mL of saturated $NaHCO_3$ solution and once with 200 mL of water. The organic phase was dried with Na_2SO_4 and the solvent was removed. The product **2** was purified by column chromatography (SiO_2, EtOAc/cyclohexane, v/v, 1:2) and collected as light yellow oil. Yield: 8.69 g (70%).

^{1}H-NMR (300 MHz, $CDCl_3$, δ): 7.39–7.24 (m, 5H, Bn), 4.62–4.58 (dd, J = 7.92 Hz, 2.61 Hz, 1H, H-4), 4.56 (s, 2H, Bn-CH_2), 4.44 (d, J = 2.6 Hz, 1H, H-3), 3.92 (dd, J = 7.9 Hz, 1.1 Hz, 1H, H-5), 3.81 (dd, J = 13 Hz, J = 1.85 Hz, 1H, H-6), 3.77–3.68 (m, 3H, H-1, H-1′, H-6′), 3.67–3.58 (m, 4H, CH_2), 1.54, 1.47, 1.43, 1.35 (4s, 12H, CH_3); ^{13}C-NMR ($CDCl_3$, 75 MHz, δ): 138.26 (Bn-C_q), 128.33, 127.66, 127.56 (Bn), 108.90 (isopropylidene-C_q), 108.54 (isopropylidene-C_q), 102.72 (C2), 73.23 (Bn-CH_2), 72.47 (CH_2), 71.38 (C1), 71.03 (C5), 70.22 (C4), 69.99 (C3), 69.37 (CH_2), 61.01 (C6), 26.56, 25.87, 25.29, 24.03 (CH_3). MS (ESI) m/z: $[M+Na]^+$ calcd for $C_{21}H_{30}O_7Na$, 417.19; found, 417.18; $[M+K]^+$ calcd for $C_{21}H_{30}O_7K$, 433.16; found, 433.16. Anal. calcd. for $C_{21}H_{30}O_7$: C 63.94, H 7.67; found: C 63.90, H 7.69.

2.2.2. Synthesis of 1-(2-(Hydroxyl)ethyl)-2,3:4,5-di-O-isopropylidene-β-D-fructopyranoside (3)

8.38 g (21.2 mmol) of **2** were dissolved in 300 mL of methanol and 0.23 g of palladium on charcoal (3 wt%) were added to the reaction mixture. The reaction flask was evacuated and refilled with hydrogen several times. After stirring for 48 h, the catalyst was filtered off and the solvent was evaporated to obtain the product as colorless oil. Yield: 6.03 g (95%).

^{1}H-NMR (300 MHz, $CDCl_3$, δ): 4.62–4.56 (dd, J = 8.0 Hz, 2.5 Hz, 1H, H-4), 4.35 (d, J = 2.5 Hz, 1H, H-3), 4.26–4.21 (dd, J = 8.0 Hz, 1.1 Hz, 1H, H-5), 3.90 (dd, J = 13.0 Hz, J = 1.8 Hz, 1H, H-6), 3.80–3.56 (m, 5H, H-6, H-1, H-1′, CH_2), 2.18 (s, 1H, OH), 1.53, 1.49, 1.41, 1.34 (4s, 12H, CH_3); ^{13}C-NMR ($CDCl_3$, 75 MHz, δ): 108.98 (C_q), 108.44 (C_q), 102.59 (C2), 73.26 (CH_2), 72.20 (C1), 70.76 (C5), 70.69 (C3), 70.14 (C4), 61.49 (CH_2), 60.97 (C6), 26.44, 25.70, 25.18, 23.89 (CH_3). MS (ESI) m/z: $[M+Na]^+$ calcd for $C_{14}H_{24}O_7Na$, 327.14; found, 327.14; $[M+K]^+$ calcd for $C_{14}H_{24}O_7K$, 343.12; found, 343.12; $[2M+Na]^+$ calcd for $C_{28}H_{48}O_{14}Na$, 631.29; found, 631.29. Anal. calcd. for $C_{14}H_{24}O_7$: C 55.25, H 7.95; found: C 55.24, H 8.14.

2.2.3. Synthesis of 1-(2-(Methanesulfonyl)ethyl)-2,3:4,5-di-O-isopropylidene-β-D-fructopyranoside (4)

5 g (16.4 mmol) of **3** were dissolved in 30 mL of CH_2Cl_2 and 6.825 mL (49.24 mmol) of Et_3N and 20 mg 4-DMAP (0.16 mmol) were added. The reaction mixture was cooled to 0 °C and 3 mL (38.8 mmol) of mesyl chloride were added dropwise to the solution.[28] The reaction mixture was left to slowly warm to room temperature and stirred for 2 h. After no starting material had remained (TLC, SiO_2, EtOAc/cyclohexane, v/v, 2:1), 50 mL CH_2Cl_2 were added and the mixture was washed thrice with each 200 mL of water and twice with each 200 mL of saturated, aqueous $NaHCO_3$ solution. The organic layer was dried over Na_2SO_4 and the solvent was removed. The crude product was dissolved in 10 mL of ethyl acetate, filtered over silica gel and collected as yellowish oil.

Yield: 5.78 g (92%). ^{1}H-NMR ($CDCl_3$, 300 MHz, δ): 4.63–4.58 (dd, J = 7.9 Hz, 2.6 Hz, 1H, H-4), 4.40–4.33 (m, 3H, H-3, CH_2), 4.26–4.21 (dd, J = 7.9 Hz, 0.9 Hz, 1H, H-5), 3.94–3.64 (m, 6H, H-1, H-1′, H-6, H-6′, CH_2), 3.05 (s, 3H, SCH_3), 1.54, 1.47, 1.42, 1.34 (4s, 12H, CH_3); ^{13}C-NMR ($CDCl_3$, 75 MHz, δ): 108.95 (C_q), 108.68 (C_q), 102.38 (C2), 72.84 (CH_2), 70.91 (C5), 70.11 (C4, C3), 69.70 (C1), 68.61 (CH_2), 61.06 (C6), 37.34 (SCH_3), 29.33 (CH_2), 26.52, 25.88, 25.33, 24.00 (CH_3). MS (ESI) m/z: $[M+Na]^+$ calcd for $C_{15}H_{26}O_9SNa$, 405.12; found, 405.12. Anal. calcd. for $C_{15}H_{26}O_9S$: C 47.11, H 6.85, S 8.38; found: C 47.22, H 6.96, S 8.25.

2.2.4. Synthesis of 1-O-(2-Mercapto-ethyl)-2,3:4,5-di-O-isopropylidene-β-D-fructopyranoside (5)

1.311 g (3.43 mmol) of **4** was dissolved in 15 mL 2-butanone, 0.78 g (10.25 mmol) thiourea was added, and the mixture was heated to 95 °C under reflux for 7 h.[29] After no starting material had remained (TLC, SiO_2, EtOAc/cyclohexane, v/v, 2:1), the solvent was evaporated, 15 mL CH_2Cl_2, 15 mL H_2O and 0.874 g $K_2S_2O_5$ (3.93 mmol) were added and the mixture was heated to reflux for 12 h. The organic layer was washed thrice with each 200 mL of water, dried with anhydrous Na_2SO_4, filtered, and evaporated to effort after column chromatography (SiO_2, EtOAc/cyclohexane, v/v, 1:1) the pure product.

Yield: 0.842 g (76.7%). ^{1}H-NMR (600 MHz, $CDCl_3$, δ): 4.61 (dd, J = 7.92 Hz, 2.58 Hz, 1H, H-4), 4.39 (d, J = 2.58 Hz, 1H, H-3), 4.23 (dd, J = 7.92 Hz, 1.32 Hz, 1H, H-5), 3.90 (dd, J = 12.99 Hz, ^3J = 1.83 Hz, 1H, H-6) 3.74–3.70 (m, 2H, H-6′, H-1), 3.65–3.56 (m, 3H, H-1′, CH_2), 2.71–2.68 (m, 2H, CH_2), 1.59 (t, J = 8.25 Hz, 1H, SH), 1.53–1.34 (4s, 12H, CH_3); ^{13}C-NMR (150 MHz, $CDCl_3$, δ): 109.07 (C_q), 108.71 (C_q), 102.64 (C2), 73.62 (CH_2),72.36 (C1), 71.11 (C5), 70.30 (C4), 70.23 (C3), 61.16 (C6), 26.69, 26.02, 25.52, 24.27 (CH_3), 24.14 (CH_2). HRMS (ESI) m/z: $[M+Na]^+$ calcd for $C_{14}H_{24}O_6SNa$, 343.1186; found, 343.1200. Anal. calcd. for $C_{14}H_{24}O_6S$: C 52.48, H 7.55, S 10.01; found: C 52.77, H 7.64, S 10.39.

2.2.5. Synthesis of Linear Poly(ethylene imine) (P1)

Poly(2-ethyl-2-oxazoline) (**PEtOx**) used as starting material in this study was synthesized according to literature procedures.[30] The monomer 2-ethyl-2-oxazoline (3.965 g) and the initiator methyl tosylate (12.42 mg, 0.067 mmol) were dissolved in dry acetonitrile (6.0 mL) under inert conditions in a glovebox. After stirring for a few minutes the microwave vial was heated in a microwave synthesizer for 128 min at 140 °C. The polymerization mixture was diluted with 5 mL dichloromethane and precipitated in 250 mL ice-cold diethyl ether. Subsequently, the precipitate was filtered off and lyophilized (yield: 3.720 g, 94%).

Accordingly, **PEtOx** (degree of polymerization (DP) = 575, 2.7 g) was treated with an excess of 6 M aqueous hydrochloric acid (250 mL) at 100 °C for 16 h under reflux.[31] The excess of hydrochloric acid and the resulting propionic acid were removed under reduced pressure. The residue was dissolved in water followed by the addition of 3 M NaOH to reach pH = 8. Precipitation occurred and the precipitated, hydrolyzed linear poly(ethylene imine) was filtered off. The residue was redissolved in 10 mL of *N*,*N*-dimethylformamide and precipitated two times into 300 mL ice-cold diethyl ether. The obtained product was dried in vacuo at 85 °C. The degree of hydrolysis of the resulting linear poly(ethylene imine) **P1** was determined by ^{1}H NMR spectroscopy (yield: 1.0 g, 85%).

PEtOx: DP = 575. ^{1}H NMR (300 MHz, D_2O, δ): 3.70–3.20 (−NR−CH_2−CH_2), 2.41–2.08 (CH_2−CH_3), 1.09–0.79 (CH_2−CH_3). SEC (DMAc, LiCl): M_n = 69 000 g mol^{-1}, $Đ$ = 1.3.

P1: EtOx:EI [%] = 2:98. ^{1}H NMR (300 MHz, MeOD, δ): 3.58–3.41 (NR−CH_2−CH_2), 2.91–2.61 (NH−CH_2−CH_2), 2.56–2.36 (CH_2−CH_3), 1.18–1.06 (CH_2−CH_3).

2.2.6. Synthesis of P(EI-stat-ButEnOx) (**P2**)

P1 (500 mg) and the catalyst 4-*N*,*N*-dimethylamino-pyridine (DMAP, 50 mg, 0.41 mmol) were dissolved in pyridine (5 mL) at 80 °C. A defined quantity of *N*-succinimidyl-4-pentenate (465 mg) was dissolved in pyridine (5 mL) and heated up to 80 °C. The two solutions were combined and 2 mL pyridine added to obtain a 3 wt% mixture of **P1** and stirred for 16 h at 80 °C. Afterward, the mixture was filtered and precipitated into 300 mL ice-cold diethyl ether (Et_2O). The precipitated copolymer was filtered off and washed with 30 mL of diethyl ether. The purified product **P2** was dried under reduced pressure (yield: 860 mg, 89%).

EI:ButEnOx [%] = 73:27. ^{1}H NMR (600 MHz, DMSO-d_6, δ): 5.89–5.74 (HC=CH_2), 5.06–4.91 (HC=CH_2), 3.58–3.20 (NR−CH−CH_2), 2.80–2.45 (NH−CH_2−CH_2), 2.44–2.34 (CH_2−CH_2−C_2H_3), 2.27–2.16 (CH_2−CH_2−C_2H_3). SEC (DMAc, LiCl, polystyrene): M_n = 8000 g mol^{-1}, $Đ$ = 1.3. Anal. calcd. for $C_{1927}H_{3811}N_{575}O_{155}$: C 61.69, H 10.24, N 21.47; found: C 60.90, H 10.43, N 22.91.

2.2.7. Synthesis of P(EI-stat-ButEnOx-stat-isoFruButOx) via Thiol-Ene Photoaddition (***iso*P3**)

P2 (558 mg) was dissolved in 5 mL methanol. In a second vial, the photoinitiator DMPA (6.5 mg, 0.025 mmol) and a 1.2-fold excess per double bond of **5** (840 mg) were dissolved in methanol (5 mL). The combined solution (5 wt% of **P2**) was deoxygenated with argon for 20 min and stirred in a UV chamber (λ = 365 nm) for 18 h. Subsequently, the copolymer was precipitated two times in 300 mL ice-cold diethyl ether. After filtration, the copolymer was dried under reduced pressure at 40 °C (yield: 980 mg, 70%).

EI:ButEnOx:*iso*FruButOx [%] = 73:11:16. ^{1}H NMR (600 MHz, DMSO-d_6, δ): 5.90–5.74 (HC=CH_2), 5.07–4.88 (HC=CH_2), 4.57 (H-4), 4.27 (H-3), 4.22 (H-5), 3.73 (H-6), 3.66 (−CH_2), 3.55 (H-6, −CH_2), 3.48 (H-1), 3.43 (H-1), 3.40–3.12 (NR−CH_2−CH_2), 2.78–2.46 (NH−CH_2−CH_2), 2.42–2.16 (CH_2−CH_2−C_2H_3), 1.53 (CH_2−CH_2−CH_2−CH_2), 1.47–1.26 (isopropylidene). SEC (DMAc, LiCl): M_n = 11 600 g mol^{-1}, $Đ$ = 1.9. Anal. calcd. for $C_{3123}H_{5835}N_{575}O_{707}S_{92}$: C 57.09, H 8.95, N 12.26, S 4.49; found: C 57.39, H 9.23, N 13.35, S 4.18.

2.2.8. Synthesis of P(EI-stat-ButEnOx-stat-FruButOx) via Deprotection (**P3**)

The cleavage of the isopropylidene groups was performed under acidic conditions.[32] The copolymer ***iso*P3** (685 mg) was dissolved in a THF/H_2O mixture (22.5/22.5 mL) and acidified with 2 M hydrochloric acid (6.75 mL). The solution was heated to 40 °C for 12 h. Subsequently, the mixture was neutralized with 1.2 g $NaHCO_3$ and THF as well as formed acetone were evaporated under reduced pressure. Purification of the deprotected D-fructose conjugate was performed by dialysis against water using a Spectra/Por 3 dialysis membrane (3500 g mol^{-1} cutoff). Finally, the product was lyophilized and obtained as a yellowish powder (yield: 324 mg, 53%). EI:ButEnOx:FruButOx [%] = 73:11:16. SEC (DMAc, LiCl): M_n = 9800 g mol^{-1}, $Đ$ = 1.2. Anal. calcd. for $C_{2571}H_{5099}N_{575}O_{707}S_{92}$: C 52.94, H 8.81, N 13.81, S 5.06; found: C 53.60, H 9.13, N 14.91, S 4.66.

2.3. Polymer Labeling with Cy5 (P1-Cy5)

P1 (40 mg) and triethylamine (360 µL) were dissolved in methanol (10 mL). After addition of the cyanine-5-NHS-ester (1 mg) the reaction was stirred at room temperature overnight. The labeled polymer was precipitated in 250 mL ice-cold diethyl ether, filtered, and redissolved in methanol (15 mL). Further purification was performed by dialysis against a mixture of water/methanol using a Spectra/Por 3 dialysis membrane (3500 g mol^{-1} cutoff). Finally, the product was dried under reduced pressure (yield: 15 mg, 37%; labeling efficiency: 2.0% of dye).

2.4. Copolymer Labeling with Rhodamine (P2-Rho, P3-Rho)

The copolymer (**P2**: 35 mg, **P3**: 40 mg) and triethylamine (200 µL) were dissolved in DMF (4 mL). After addition of Rhodamine B isothiocyanate (0.7 mg) the reaction was stirred at room temperature for 18 h. Purification was performed by dialysis against water using a Spectra/Por 3 dialysis membrane (3500 g mol^{-1} and subsequently 6–8000 g mol^{-1} cutoff). Finally, the product was lyophilized and obtained as a reddish powder. The calculated labeling efficiency (via UV–vis spectroscopy) for conjugation was 1.4% of dye for the **P2-Rho** (yield: 23 mg, 66%) and 30.4% of dye for the labeled **P3** (yield: 26 mg, 65%). To achieve comparable fluorescence intensities, the labeled **P3** was mixed with the unlabeled **P3** (1:19) to obtain **P3-Rho** (new label efficiency: 1.5% of dye).

2.5. Polyplex Preparation

Polyplexes of plasmid desoxyribonucleic acid (pDNA) and selected polymers were prepared by mixing stock solutions of 15 µg mL^{-1} pDNA and the respective polymers (1 mg mL^{-1}) in different amounts to obtain various N/P ratios (nitrogen of polymer to phosphate of pDNA) in HBG (HEPES buffered glucose) buffer (20×10^{-3} M 4-(2-hydroxethyl) piperazine-1-ethanesulfonic acid and 5% (w/v) glucose, pH 7.2). The solutions were vortexed for 10 s at maximal speed and incubated at room temperature for 20 min to ensure a complex formation.

2.6. Determination of Cytotoxicity

Cytotoxicity studies were performed with the mouse fibroblast cell line L929 (CCL-1, ATCC), as recommended by ISO10993-5. Furthermore, the breast cancer cell line MDA-MB-231 and the HUVEC cells were used. The cells were routinely cultured in Dulbecco's modified eagle's medium (Lonza, Basel) supplemented with 10% fetal calf serum (FCS), 100 U mL^{-1} penicillin, and 100 µg mL^{-1} streptomycin at 37 °C in a humidified 5% (v/v) CO_2 atmosphere. HUVEC cells were cultured in M199 Medium (Lonza, Basel) supplemented with 17.5% FCS, 680×10^{-6} M L-glutamin, 25 µg mL^{-1}

Macromol. Biosci. **2017**, DOI: 10.1002/mabi.201600502

heparin, 7.5 g mL^{-1} endothelial mitogenic, Vitamin C (5 μg mL^{-1}), human serum and 100 U mL^{-1} penicillin, and 100 μg mL^{-1} streptomycin at 37 °C in a humidified 5% (v/v) CO_2 atmosphere. In detail, cells were seeded at 1×10^4 cells per well in a 96-well plate and incubated for 24 h, whereas no cells were seeded in the outer wells. Subsequently, **P1**, **P2**, and **P3** were added to the cells in fresh media at indicated concentrations and the plates were incubated for 24 h. Control cells were incubated only with fresh culture medium. Subsequently, media was replaced by a mixture of fresh culture medium and AlamarBlue solution, prepared according to the manufacturer's instructions. After a further incubation of 4 h at 37 °C, the fluorescence was measured at E_x 570/E_m 610 nm, with untreated cells on the same well plate serving as negative controls. The negative control was set as 0% of metabolism inhibition and referred as 100% viability. Cell viability below 70% was considered indicative of cytotoxicity. Data are expressed as mean ± standard deviation (SD) of three independent determinations of six data points each.

2.7. Hemocompatibility and Erythrocyte Aggregation

The interaction of polymers with cellular membranes was investigated by analyzing the release of hemoglobin from erythrocytes. Blood from sheep, collected in heparinized tubes, was provided by the Institute of Laboratory Animal Science and Animal Welfare, Friedrich Schiller University Jena. The blood was centrifuged at 4500 × *g* for 5 min, and the pellet was washed three times with cold 1.5×10^{-3} M phosphate buffered saline (PBS, pH 7.4). After dilution of erythrocytes with PBS in a ratio of 1:7, aliquots of erythrocyte suspension were mixed 1:1 with the indicated polymer solution up to 100 μg mL^{-1} and incubated in a water bath at 37 °C for 60 min. After centrifugation at 2400 × *g* for 5 min, the hemoglobin release into the supernatant was determined spectrophotometrically at a wavelength of 544 nm using a microplate reader (TECAN Infinite M200 Pro, Crailsheim, Germany). Complete hemolysis (100%) was achieved using 1% Triton X-100 serving as positive control. Pure PBS was used as negative control (0% hemolysis). The hemolytic activity of the polycations was calculated using Equation (1)

$$\%\,\text{Hemolysis} = 100 \times \frac{(A_{\text{Sample}} - A_{\text{Negative control}})}{(A_{\text{Positive control}} - A_{\text{Negative control}})} \quad (1)$$

A value less than 2% hemolysis rate was classified as non-hemolytic, 2%–5% as slightly hemolytic and >5% as hemolytic. Experiments were run in triplicates and were performed with three different batches of donor blood.

To study the influence of aggregation, erythrocytes were isolated as described above. The erythrocyte suspensions were mixed 1:1 with the polymer solutions (100 μL total volume) in a clear flat bottomed 96-well plate. The cells were incubated at 37 °C for 2 h, and the absorbance was measured at 645 nm in a microplate reader. Cells, which were treated with PBS, served as negative control and 25 kDa branched PEI (BPEI) (50 μg mL^{-1}, Sigma-Aldrich) was used as positive control. Absorbance values of the test solutions lower than the negative control were regarded as aggregation. Experiments were run in triplicates and were performed with three different batches of donor blood.

2.8. Ethidium Bromide Quenching Assay (EBA)

The formation of polyplexes with pDNA was examined by quenching of the ethidium bromide fluorescence. Briefly, 15 μg mL^{-1} pDNA in a total volume of 100 μL HBG buffer were incubated with ethidium bromide (0.4 μg mL^{-1}) for 10 min at room temperature. Subsequently, polyplexes with different amounts of polymer (various N/P ratios) were prepared in black 96-well plates (Nunc Thermo Fisher). The samples were incubated at room temperature for 15 min before fluorescence measurements. The fluorescence of the samples was measured at an excitation wavelength of 525 nm and an emission wavelength of 605 nm using a Tecan Genios Pro fluorescence plate reader (Tecan, Crailsheim, Germany). A sample containing only pDNA and ethidium bromide was used to calibrate the device to 100% fluorescence against a background of 0.4 μg mL^{-1} of ethidium bromide in HBG solution. The percentage of dye displaced upon polyplex formation was calculated using Equation (2)

$$\text{RFU}\,[\%] = \frac{F_{\text{sample}}}{F_{\text{pDNA}}} \times 100 \quad (2)$$

Here, RFU is the relative fluorescence and F_{sample} and F_{pDNA} are the fluorescence intensities of a given sample and the ethidium bromide intercalated into pDNA alone.

2.9. Heparin Dissociation Assay

To investigate the release of pDNA from polyplexes, the heparin dissociation assay was performed. Polyplexes with an N/P ratio of 30 were prepared as described above in a total volume of 100 μL HBG buffer containing ethidium bromide (0.4 μg mL^{-1}). After incubation in the dark at room temperature for 15 min, the polyplexes were transferred into a black 96-well plate, and heparin solutions of indicated concentrations were added. The solutions were mixed and incubated for further 30 min at 37 °C in the dark. The fluorescence of ethidium bromide was measured at E_x 525 nm/E_m 605 nm with a Tecan microplate reader. The percentage of intercalated ethidium bromide was calculated as described above.

2.10. Dynamic and Electrophoretic Light Scattering (ELS)

Dynamic light scattering was performed on a Zetasizer Nano ZS (Malvern Insturments, Herrenberg) with an He-Ne laser operating at a wavelength of $\lambda = 633$ nm. All measurements (30 runs, triplicate) were carried out at 25 °C after an equilibration time of 120 s. The counts were detected at an angle of 173°. The mean particle size was approximated as the effective (*z*-average) diameter and the width of the distribution as the polydispersity index of the particles (PDI) obtained by the cumulants method assuming a spherical shape. ELS was used to measure the zeta potential (ζ). The measurement was performed on a Zetasizer Nano ZS (Malvern Instruments, Herrenberg, Germany) by applying laser Doppler velocimetry. For each measurement, 20 runs were carried out using the slow-field reversal and the fast-field reversal mode at 150 V. Each experiment was performed in triplicate at 25 °C. The zeta potential was calculated

from the electrophoretic mobility (μ) according to the Henry's equation. Henry coefficient f(ka) was calculated according to Oshima.

2.11. Uptake Studies

For uptake studies, cells were cultured as described above. Subsequently, cells were seeded at a density of 10^5 (HUVEC, 3×10^5) cells per mL in 24-well plates and cultured for 24 h. One hour prior to the addition of the polyplexes, the medium was changed to OptiMEM (Life Technologies, Darmstadt, Germany). The polyplexes were prepared as described above and at least 50 µL polyplex solution of N/P 50 were added to the cells cultured with 500 µL media. The plates were incubated for 1 h at 37 °C under 5% CO_2 atmosphere.

For flow cytometry studies the pDNA (pEGFP-N1) was labeled with YOYO-1 iodide prior to the polyplex preparation. For labeling of 1 µg pDNA, 0.026 µL of 1 M YOYO-1 solution was mixed with pDNA and incubated for 20 min at 4 °C protected from light. Afterward, HBG buffer and polymers were added at the indicated N/P ratio and the polyplexes were formed as described previously. The cells were washed and harvested after 1 h and 10% trypan blue was added to quench the outer fluorescence of the cells. To determine the relative uptake of the polyplexes, 10 000 cells were measured by flow cytometry using a Cytomics FC 500 (Beckman Coulter) and the amount of viable cells showing YOYO-1 signal (FL1) were gated. Dead cells were identified via counterstaining with propidium iodide. The experiments were performed at least three times independently.

Live cell imaging was performed for uptake studies. In detail, cells (10^5 cells mL^{-1}) were seeded on glass-bottomed dishes (Greiner, Germany) and cultivated for 24 h in a humidified atmosphere. One hour prior to the polymer addition, the cells were rinsed with PBS and the medium was changed to OptiMEM. The polyplexes were formed with **P1-Cy5**, or **P2-Rho**, and **P3-Rho**, added to the cells, and incubated for one additional hour. Subsequently, the medium was replaced by fresh culture medium or PBS supplemented with Hoechst 33342 for nucleus staining. Imaging was performed with LSM880, Elyra PS.1 system (Zeiss, Oberkochen, Germany) applying a 63× 1.4 NA plan apochromat oil objective.

2.12. Transfection Studies

For transfection studies HUVEC cells were seeded at a density of 2×10^5 cells mL^{-1} in 24-well plates 1 d before transfection. One hour prior to transfection, cells were rinsed with PBS and supplemented with 1 mL of OptiMEM (Life Technologies). Polyplexes (50 µL) were added to the cells and the plates were incubated for 4 h in the incubator. Afterward, the supernatant was replaced by 1 mL of fresh growth medium and the cells were further incubated for 20 h. For analysis, adherent cells were harvested by trypsinization. The relative expression of EGFP fluorescence of 10^4 cells was quantified via flow cytometry using a Cytomics FC 500 (Beckman Coulter). For determination of the transfection efficiency viable cells expressing EGFP were gated.

3. Results and Discussion

To conjugate a D-fructose derivative to a cationic polymer backbone, the thiol-ene photoaddition was utilized as the method of choice since it can be performed under mild conditions (low temperature, no toxic metal catalysts) in high yields.[33] Previous studies revealed that overexpressed D-fructose receptors of various breast cancer cell lines tolerate only defined positions of the introduced functional groups.[12] Several modifications at the C1 position of fructopyranose have been reported to be tolerated by GLUT5.[13,14,34] Since 1-deoxy-1-mercapto-fructopyranose did not react with the respective copolymers by thiol-ene photoaddition, an ethyl spacer had to be installed at the C1 position between the D-fructose moiety and the thiol group.

3.1. Synthesis of Thio-Functionalized D-Fructose

The D-fructose derivative bearing a thiol-group was obtained in a four-step synthesis from commercially available 2,3:4,5-di-*O*-isopropylidene-β-D-fructopyranoside (1). First, a benzyl ether group was introduced by the conversion of **1** with benzyl-2-bromoethyl ether (Scheme 1) resulting in 1-(2-(benzyloxy)ethyl)-2,3:4,5-di-*O*-isopropylidene-β-D-fructopyranoside (2). In a second step, the benzyl group of **2** was cleaved under standard conditions with H_2/palladium on activated charcoal to obtain **3** in high yield (95%). The OH-group was transformed into a leaving group by mesylation with mesyl chloride under argon atmosphere analog to a literature procedure.[28] In a substitution reaction, the thiol functionality was introduced stepwise by transformation to the isothioronium salt and, subsequently, hydrolysis to yield the product 1-*O*-(2-mercaptoethyl)-2,3:4,5-di-*O*-isopropylidene-β-D-fructopyranoside (**5**).

Characterization of the synthesis pathway by ^{1}H NMR spectroscopy for the compounds **1**–**5** is illustrated in Figure 1. The successful introduction of the "benzyl ethyl" substituent (**1**–**2**) can be followed by the proton signals in the aromatic region (7.24–7.39 ppm), the benzylic CH_2 signal (4.56 ppm), and the disappearance of the OH-quadruplet (2.09 ppm). After cleavage of the benzyl group (**3**), the disappearance of the aromatic and the benzylic CH_2 signals is observed. The successful substitution with mesyl chloride is characterized by the appearance of a sharp singlet at 3.02 ppm (**4**). The disappearance of the mesyl singlet and the appearance of a quadruplet (1.58 ppm) confirm the successful introduction of the thiol group (**5**). For the subsequent polymer modification, the protected thio-fructose **5** was used.

3.2. Synthesis of a D-Fructose Bearing Cationic Copolymer

The homopolymer poly(2-ethyl-2-oxazoline) (**PEtOx**) was synthesized according to a literature procedure by

Macromol. Biosci. **2017**, DOI: 10.1002/mabi.201600502

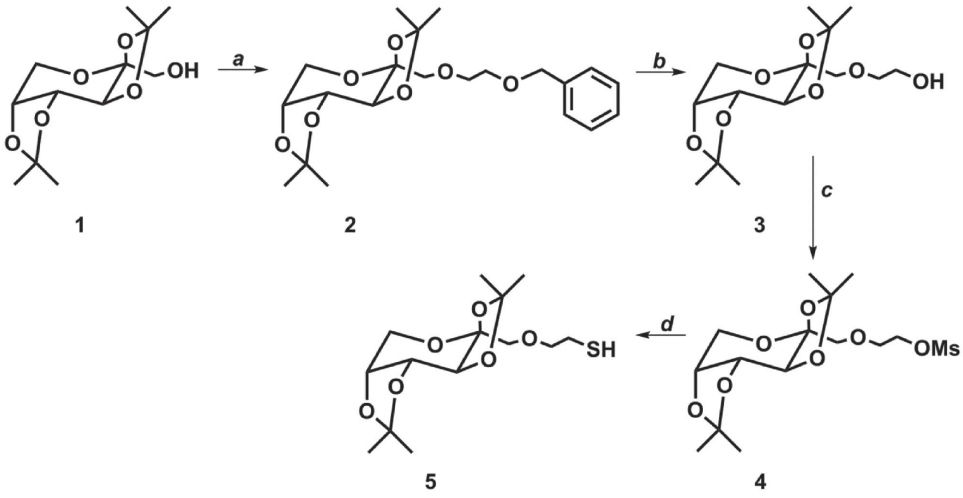

Scheme 1. Schematic representation of the four-step synthesis of 1-*O*-(2-mercapto-ethyl)-2,3:4,5-di-*O*-isopropylidene-*β*-D-fructopyranoside: a) benzyl-2-bromoethyl ether, NaH, THF, rt; b) H_2/Pd, CH_3OH, rt; c) mesyl chloride, Et_3N, 4-DMAP, CH_2Cl_2, 0 °C; d) (1) thiourea, butanone, 95 °C, (2) $K_2S_2O_5$, CH_2Cl_2/H_2O, 50 °C.

microwave supported cationic ring-opening polymerization.[30] Before purification, the NMR signals of tosylate protons of the initiator MeOTos were used to calculate the degree of polymerization (575). This high molar mass homopolymer was used as starting material for the subsequent synthesis of linear poly(ethylene imine) (**P1**). For this purpose, **PEtOx** was hydrolyzed in half concentrated hydrochloric acid (see Scheme 2).[35]

The formed ethylene imine units were functionalized with *N*-succinimidyl-4-pentenate to introduce double bonds to the polymer.[36] The resulting copolymer P(EI-*stat*-ButEnOx) (**P2**) revealed an ethylene imine content

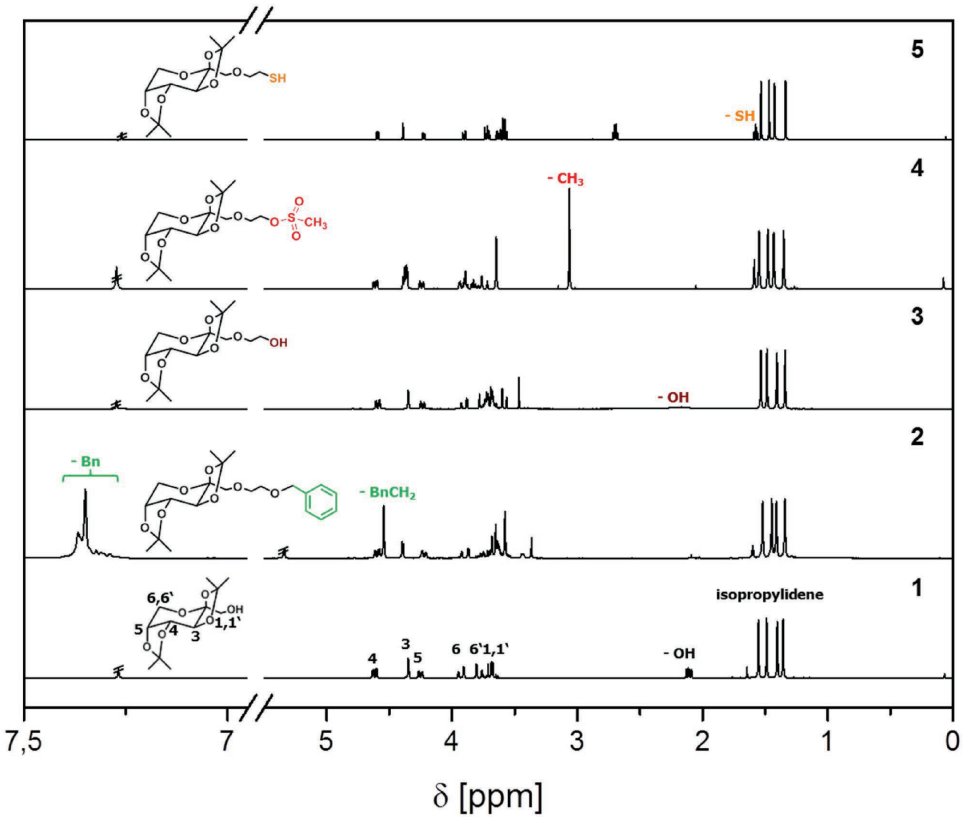

Figure 1. ^{1}H NMR of D-fructose derivatives **1–5** (300 and 600 MHz $CDCl_3/CD_2Cl_2$).

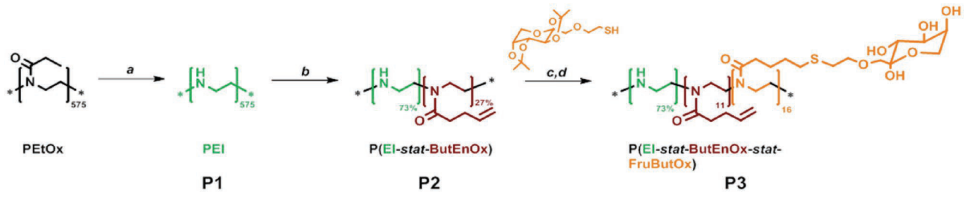

Scheme 2. Schematic representation of the synthesis of P(EI-*stat*-ButEnOx-*stat*-FruButOx): a) 6 M HCl, 100 °C under reflux; b) pyridine, 4-*N*,*N*-dimethylamino-pyridine, N-succinimidyl-4-pentenate, 80 °C; c) D-fructose derivative (**5**), methanol, 2,2-dimethoxy-2-phenylacetophenone, room temperature, UV = 365 nm; d) THF/H_2O, 2 M HCl, 40 °C.

of 73% (referring to the repeating units) to enable an effective binding of genetic material (Table 1). The introduction of the functionalized D-fructose was performed by thiol-ene photoaddition which represents a mild and metal-free reaction type. For this purpose, the corresponding precursor **P2** was converted with the protected thio-fructose **5** under UV irradiation at room temperature to yield the copolymer P(EI-*stat*-ButEnOx-*stat*-*iso*FruButOx) (***iso*P3**). Surprisingly, a full conversion of the double bonds was not possible even after stepwise photoaddition using an excess of protected thio-fructose. Steric hindrance by the bulky side chains (including the isopropylidene protecting groups) could be one possible explanation. However, a high functionalization with carbohydrates rather hinders a stable polyplex formation.[24a] Subsequent deprotection of the isopropylidene groups resulted in P(EI-*stat*-ButEnOx-*stat*-FruButOx) (**P3**) revealing 16% of repeating units functionalized with D-fructose. Interestingly, this content of D-fructose modification rendered the final polymer **P3** water soluble.

Characterization by ^{1}H NMR confirms the presence of 2-butenyl-2-oxazoline (ButEnOx) and ethylene imine (EI) units in **P2** (Figure 2), proven by the appearance of proton signals of the double bond at 5.9 ppm (–HC=CH_2, A) and 5.0 ppm (–HC=CH_2, B). To calculate the composition of the obtained copolymer, the integral of the signals of the double bond (5.9 ppm) was compared to the integral of the ethylene imine backbone (2.9–2.5 ppm). Since the ethylene imine units are not used for further modification, their content remains constant, representing 73% of repeating units of the copolymer. The successful functionalization of **P2** with **5** is shown by the appearance of D-fructose related signals between 4.6 and 3.4 ppm after photoaddition (***iso*P3**, Figure 2). Furthermore, four singlets of the isopropylidene groups appear between 1.5 and 1.1 ppm. After treatment with hydrochloric acid, neutralization, and dialysis against water (cutoff: 3500 g mol^{-1}) the signals of the protecting groups disappeared, indicating the successful deprotection of ***iso*P3** and, consequently, the formation of P(EI-*stat*-ButEnOx-*stat*-FruButOx) (**P3**). The isopropylidene cleavage results in the formation of a hemiketal structure and, therefore, in an equilibrium of pyranoses, furanoses, and an open-chained form, which can be distinguished via 2D NMR spectroscopy according to literature.[34] Since the ring proton signals of D-fructose are covered in the ^{1}H NMR spectra by the signals of the polymer backbone (Figure 2, **P3**), heteronuclear single quantum coherence (HSQC) NMR spectroscopy was used to prove their presence beneath the signals of the copolymer backbone as well as the successful formation of deprotected D-fructose moieties at the polymer (Figure 3).

The successful photoaddition, resulting in a single (polymeric) species (**P3**) and, hence, the absence of degradation, was further confirmed utilizing diffusion-ordered

Table 1. Composition and molar masses for **PEtOx** and **P1**–**P3**.

Abbreviation	Name	NMR[a]	SEC[b]		Sugar content[c]
		M_n (theo) [g mol^{-1}]	M_n [g mol^{-1}]	$Đ$	[mol%]
PEtOx	$PEtOx_{575}$	57 000	69 000	1.3	–
P1	$LPEI_{575}$	24 800	–	–	–
P2	P($EI_{73\%}$-*stat*-$ButEnOx_{27\%}$)	37 500	8000	1.3	–
***iso*P3**	P($EI_{73\%}$-*stat*-$ButEnOx_{11\%}$-*stat*-*iso*-$FruButOx_{16\%}$)	67 000	11 600	1.9	11
P3	P($EI_{73\%}$-*stat*-$ButEnOx_{11\%}$-*stat*-$FruButOx_{16\%}$)	59 600	9800	1.2	12

[a]Determined by ^{1}H NMR (calculated from tosylate signals of MeOTos before purification; [b]SEC: DMAc, 0.21% LiCl, polystyrene calibration; [c]Determined by elemental analysis.

Macromol. Biosci. **2017**, DOI: 10.1002/mabi.201600502

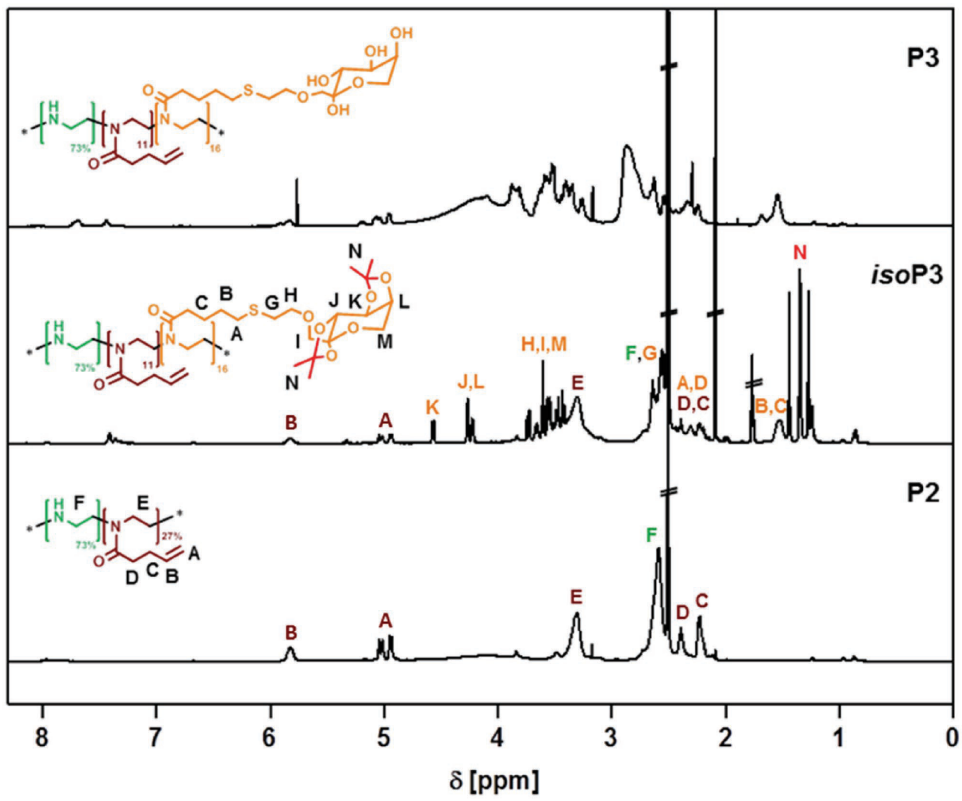

Figure 2. Comparison of ^{1}H NMR spectra of the precursor copolymer **P2**, the protected D-fructose copolymer ***iso*P3** and the final product **P3** (600 MHz, DMSO-d_6).

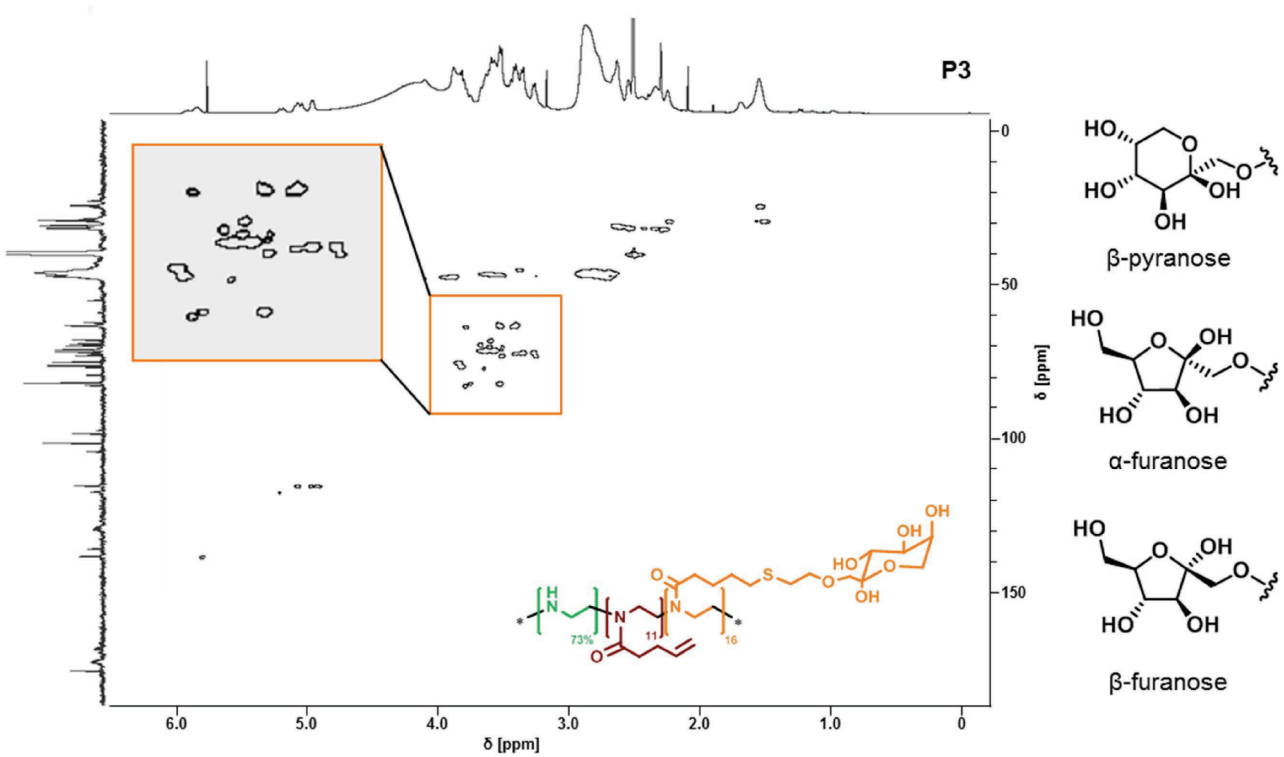

Figure 3. HSQC NMR of the copolymer **P3** (DMSO-d_6, 600 MHz).

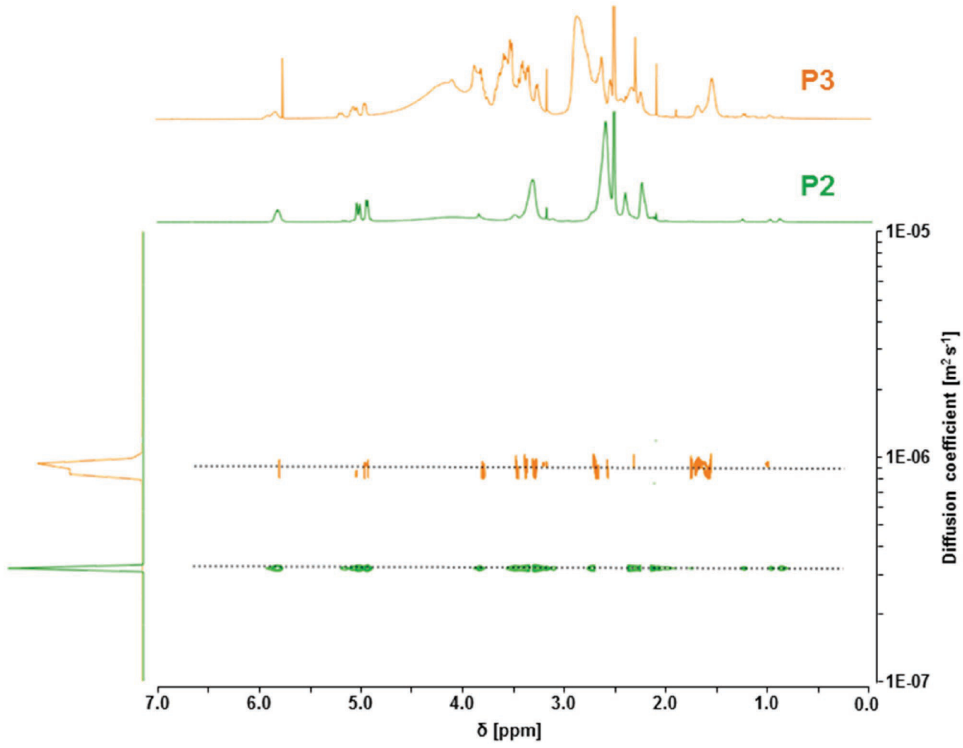

Figure 4. DOSY NMR of the precursor **P2** (green) and the final copolymer **P3** (orange) (DMSO-d_6, 600 MHz, 25 °C).

NMR spectroscopy (DOSY NMR) (Figure 4). The diffusion coefficient of **P3** is larger than for the precursor copolymer **P2**, indicating a decrease of the hydrodynamic radius of the polymer in solution.

A comparison of the composition and molar masses of the prepared copolymers obtained by size exclusion chromatography (SEC) is depicted in Table 1. The cationic polymers **P1**–**P3** show undesired interactions with the column and a change in the elution behavior. Furthermore, an SEC calibration for cationic polymers is not available, which complicates the determination of meaningful accurate molar masses with this technique. For this reason, a meaningful determination of molar masses of the copolymers by size exclusion measurements was not possible. However, for the modified poly(ethylene imine)s a trend is clearly visible. After the photoaddition of the protected thio-fructose the signal of ***iso*P3** is observed at lower elution volumes indicating an increased hydrodynamic volume. Deprotection results in a slight shift to higher elution volumes, and, therefore, to lower molar masses.

To enable a more detailed insight into the uptake in noncancer (L929) and triple negative breast cancer cells (MDA-MB-231) via microscopy, the precursor **P2** and the final copolymer **P3** were labeled using one equivalent of Rhodamine B isothiocyanate per polymer chain. For comparison with the nontargeted standard polymer, **Cy5**-labeled **P1** was used.

3.3. Bio- and Hemocompatibility

Recently, cationic polymers such as PEI have been used extensively as nonviral vectors to deliver genetic material into mammalian cells. The cytotoxicity of the polymers represents a major drawback for potential applications. Former studies revealed increased biocompatibility of linear PEI (LPEI) compared to branched PEI.[37] Furthermore, cytotoxicity strongly depends on the molar mass and the cationic charge density.[22a] This study aimed to investigate the impact of functionalization with D-fructose (**P3**) in noncancerous fibroblast cell line L929, routinely used for toxicity screenings, in HUVEC cell line and in breast cancer cell line MDA-MB-231 compared to linear PEI (**P1**) and the precursor polymer **P2**.

P1 exhibits a concentration-dependent cytotoxicity in the cell lines observed using the AlamarBlue assay (Figure 5). Increased concentrations result in reduced cell viability, as reported before for LPEI of the respective molecular mass.[38] Treatment with 5 μg mL^{-1} decreases the cell viability to 15.8% in L929 cells, 2.8% in HUVEC and 1% in MDA-MB-231 cells, respectively. **P2** causes a dramatically reduced viability of breast cancer cells MDA-MB-231 (IC_{50} < 10 μg mL^{-1}). In contrast, **P2** shows an increased biocompatibility in HUVEC cells (IC_{50} = 205 μg mL^{-1}) and over the entire concentration range in L929 cells (IC_{50} > 500 μg mL^{-1}). The D-fructose-conjugated polymer **P3** displays even improved biological properties. No significant reduction of the viability in mouse fibroblast

Macromol. Biosci. **2017**, DOI: 10.1002/mabi.201600502

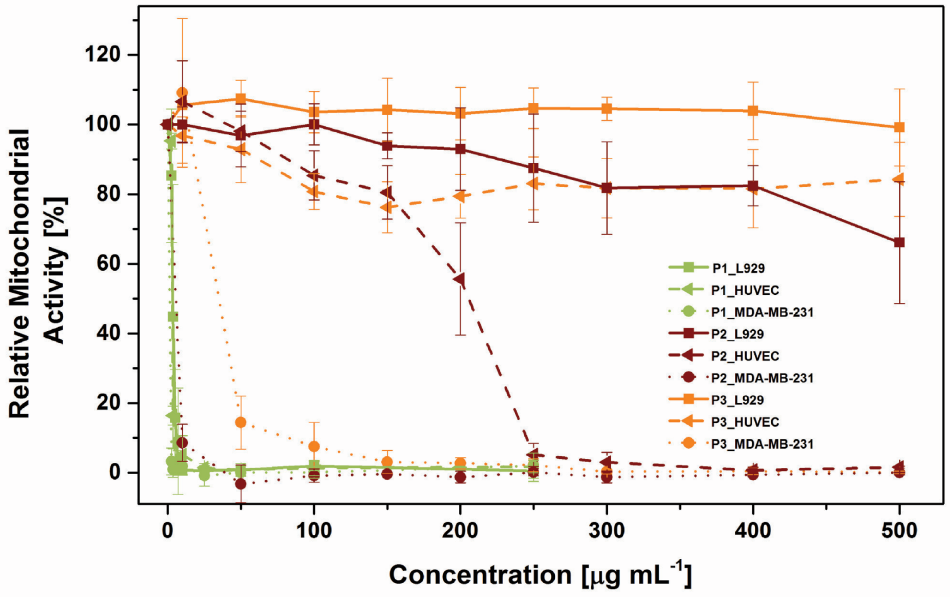

Figure 5. Cell-type-dependent cytotoxicity assay of **P1–P3** using AlamarBlue. Nontreated cells served as 100% relative viability. Cells were treated 24 h with the indicated concentrations of the polymers.

L929 cells and in the primary human endothelial HUVEC cells was observed after 24 h treatment with **P3** for all tested concentrations (IC_{50} > 500 μg mL^{-1}). The cytotoxicity of **P3** (IC_{50} = 35 μg mL^{-1}) toward breast cancer cells is concentration dependent, comparable to **P2**. As a consequence, D-fructose-conjugated polymer **P3** combines strongly enhanced biocompatibility for the noncancer cell line L929 as well as primary human cells HUVEC on the one hand and selective toxicity for breast cancer cell line MDA-MB-231.

Red blood cells (RBC) aggregates are naturally formed by plasma proteins, which is a reversible process.[39] In the presence of various polymers irreversible erythrocyte aggregation can occur due to membrane interactions forming bridges between the polymers and the erythrocytes, which increases the blood viscosity and can be dangerous for vital organs.[40] The erythrocyte aggregation caused by polymers **P1**, **P2**, and **P3** was studied using BPEI as positive control (Figure 6A). None of the investigated polymers revealed a membrane perturbing activity up to 100 μg mL^{-1} and therefore no formation of erythrocyte aggregation was observable. The disruption of the RBC membrane and the detection of hemoglobin, another known side effect of cationic polymers, were measured for all investigated polymers (Figure 6B). As a general trend, it was found that cell release of hemoglobin of **P3** was lower when compared to **P1** or **P2** for all measured concentrations (100 μg mL^{-1}, 2.4%). **P1** and **P2** caused only slight hemolysis (2%–5%) up to 100 μg mL^{-1}. However, **P3** reveals a very high hemocompatibility regarding irreversible RBC aggregation and hemolytic potential. Therefore, it offers outstanding properties for advanced uptake studies.

3.4. Characterization of Polyplexes

To investigate the binding of the D-fructose-bearing copolymers with genetic material, pDNA was utilized for model studies. The efficient delivery of nucleic acids into cells comes along with several requirements. Among others, this comprises the condensation of genetic material in a compact mode as well as the dissociation from the vector after it has been transferred into the cellular cytoplasm or nucleus.[38]

To investigate the condensation of pDNA with **P1**, **P2**, and **P3**, the EBA was used. For this purpose, the oligonucleotides were preincubated with ethidium bromide (EB) resulting in a fluorescent DNA-EB complex. Subsequently, increasing amounts of polymers were added to form polyplexes at different nitrogen (polymer) to phosphate (DNA) ratios (N/P). It should be noted that the N/P calculations are based on all nitrogens (N) of the polymer, also the ones showing no activity for complex formation (amides in the backbone of, e.g., ButEnOx). The electrostatic and hydrophobic interactions between the polymers and the nucleic acid lead to the displacement of EB and, hence, to a reduction of the fluorescence intensity that correlates with the affinity for complexation.[41] The modified polymers (**P2** and **P3**) as well as linear poly(ethylene imine) (**P1**) revealed decreasing fluorescence intensity of ethidium bromide showing an interaction with the DNA (Figure 7A). For **P1**, a stable polyplex formation is observed for N/P ratios between 10 and 40 (≈25% RFU). The polymers **P2** and **P3** revealed a decreased fluorescence intensity plateau between N/P 15 and 40 (57% RFU at N/P 40). The smaller content of ethylene imine

Macromol. Biosci. **2017**, DOI: 10.1002/mabi.201600502

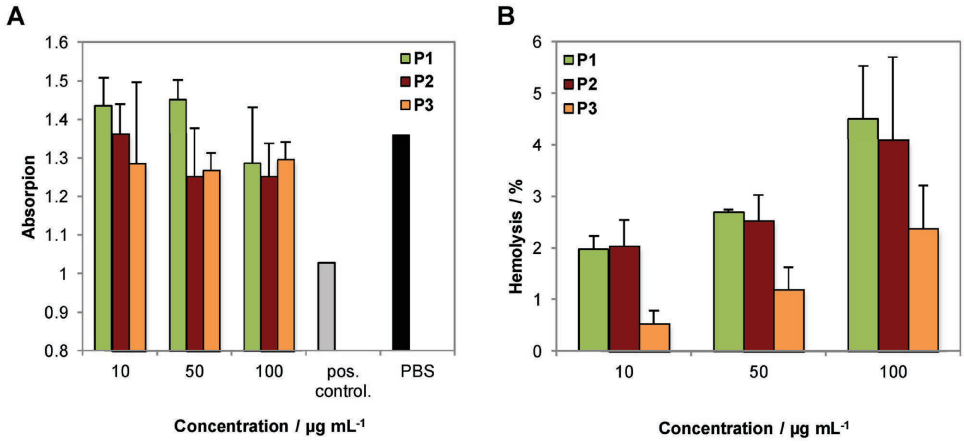

Figure 6. A) Erythrocyte aggregation assay of polymers at indicated concentrations. BPEI served as positive control and PBS as negative control. B) Hemolysis assay of erythrocytes after incubation with polymers at indicated concentrations. Triton X-100 served as positive control (100% hemolysis) and PBS as negative control (1.99%). A value less than 2% hemolysis rate is classified as nonhemolytic, 2%–5% as slightly hemolytic and >5% as hemolytic. Values represent the mean ± SD ($n = 3$).

units (73%) combined with steric challenging side chains (ButEnOx) that hinders a tight attachment to the DNA might be reasons for the higher fluorescence level. However, polymers **P2** and **P3** were able to form polyplexes by complexation with pDNA, as this RFU was also reported for other transfection polymers.[42]

The heparin dissociation assay was used to analyze the formed polyplexes concerning DNA release. Heparin is a sulfated glycosaminoglycan with multiple negative charges in the polymer chain, which competes with the nucleic acid of the polyplex. Increasing amounts of heparin displace the pDNA of the polyplexes. Ethidium bromide is added (in the same concentration as for the EBA) and intercalates into the free pDNA again. As the result, an increase of fluorescence intensity can be observed (Figure 7B). For **P2** and **P3**, the pDNA was released rapidly to nearly 100% (10 U mL^{-1} heparin) whereas **P1** required increased amounts of anionic competitor (40 U mL^{-1} heparin) for a full dissociation, indicating a less pronounced releasing profile. This correlates well with the data determined by the EBA (Figure 7A).

The size of the polyplexes is of crucial importance since they are usually internalized into cells via endocytic pathways. In literature, critical sizes of polymeric nanocarriers up to a maximum of 200 nm are recommended for efficient delivery.[43] As depicted in Table 2, all polyplexes

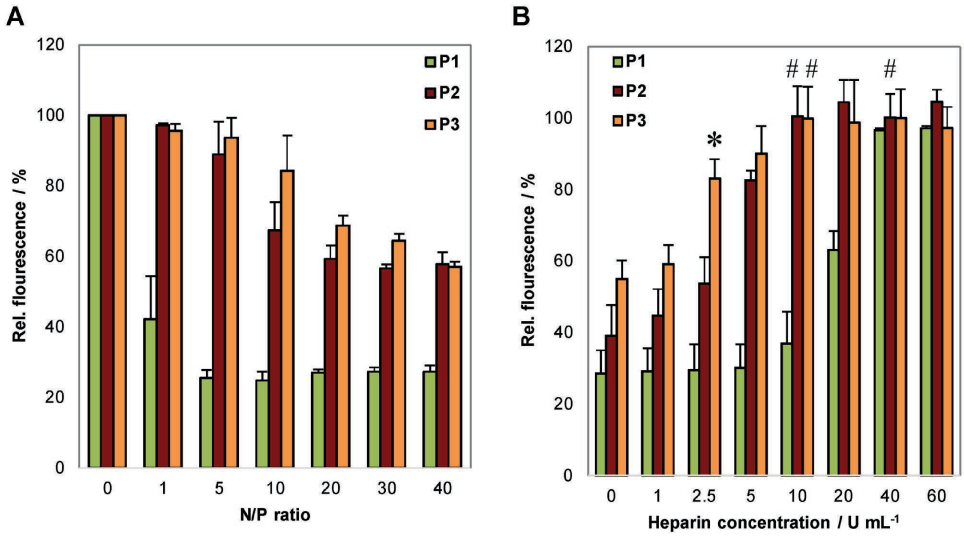

Figure 7. Polyplex formation and stability with plasmid DNA using the polymers **P1**, **P2**, and **P3**. A) Affinity of complexation of respective polymers at indicated N/P ratios (ethidium bromide quenching assay). B) Dissociation assay of polyplexes formed at N/P 20 using heparin (0–60 U mL^{-1}). Values represent the mean ± SD ($n = 3$); * represents a significant ($p < 0.01$) difference between **P2** and **P3**; # indicates no significant difference ($p < 0.05$) to 100% relative fluorescence.

Macromol. Biosci. **2017**, DOI: 10.1002/mabi.201600502

Table 2. Size and zeta potential of pDNA polyplexes of **P1–P3** at N/P 20 in HBG buffer measured by dynamic and electrophoretic light scattering.

Polymeric system	*z*-Average [d nm^{-1}]	PDI	Number-weighted size [d nm^{-1}]	Zeta potential [mV]
P1	217 ± 8	0.47	71 ± 13	24.0 ± 0.4
P2	264 ± 11	0.35	109 ± 33	24.3 ± 1.1
P3	165 ± 1	0.26	83 ± 29	17.6 ± 0.4

are in the nanometer scale with a positive zeta potential; the polyplexes formed of **P1**, **P2**, and **P3** revealed favorable sizes smaller than 200 nm. The slightly increased sizes of the polyplexes formed with the modified polymers **P2** and **P3** can be explained by the introduction of polymeric side chains with bulky groups not interacting with the genetic material. These results show the complexation of large pDNA molecules (300–400 nm pure pDNA) into compact polyplex structures, a central prerequesite for gene delivery.

3.5. Cell-Type-Dependent Uptake Efficiency

Beside complexation and protection of the genetic material, one major challenge is the cellular uptake of the polyplexes. For nontargeted cationic polyplexes, internalization into cells by endocytosis, followed by the endosomal release of the pDNA into the cytosol, is reported.[44] The functionalization of cationic polymers with targeting units such as D-fructose can change the interaction with cells depending on the interaction with cell type specific receptors. This interaction as well as usually fast and specific internalization of polyplexes can be visualized and quantified by microscopy as well as flow cytometry, respectively. For this purpose, pDNA was preincubated with YOYO-1, a DNA specific dye with high fluorescence intensity once intercalated with no displacement during polyplex formation. The cellular uptake into noncancerous L929 as well as HUVEC and breast cancer MDA-MB-231 cells after 1 h (a time point at which no cytotoxicity had been observed) at different concentrations measured by flow cytometry is depicted in Figure 8. **P1** showed a strong uptake in all tested cell types indicating no cell specificity. At N/P 10, **P2** and **P3** revealed no uptake in all three cell lines. **P2** polyplexes at N/P 20 can be detected in MDA-MB-231 and HUVEC cells, higher N/P values induce pDNA uptake in all tested cells. **P3** polyplexes were only detectable in MDA-MB-231 cells at N/P value 20. At N/P 50 the amount of pDNA is even increased compared to **P1** in MDA-MB-231 cells. In contrast to this, the uptake of genetic material into the control cells is reduced. These results indicate a positive influence of D-fructose units toward cell specific uptake of polyplexes into breast cancer cells. Noncancerous L929 and HUVEC cells efficiently take up polyplexes formed with **P1** and **P2**, but less efficient with **P3**. In contrast, D-fructose targeted **P3** enables the uptake of pDNA polyplexes at N/P ratio of 50 into MDA-MB-231 cells in a concentration-dependent manner.

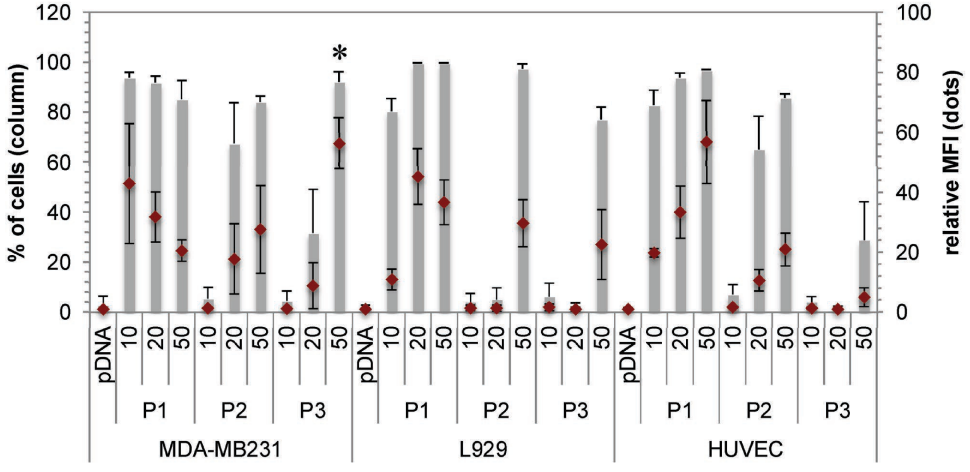

Figure 8. Uptake study. Polyplexes formed with YOYO-1 labeled pDNA were incubated with L929, HUVEC, and MDA-MB-231 cells in OptiMEM for 1 h with the polyplexes of the copolymers **P1–P3** at indicated N/P ratios. The amount of cells (%), which have taken up pDNA polyplexes relative, as well as the mean fluorescence intensity (MFI) of all viable cells compared to pDNA control without polymers were depicted. Values represent the mean ± SD ($n \geq 3$); * represents statistical significant difference in MFI to **P3** N/P 50 of L929 and HUVEC, ANOVA, p-value < 0.01.

To support these findings and to rule out that polyplexes sticking to the cell membrane influence the data from flow cytometry, the uptake of polyplexes with labeled polymers was visualized by live cell confocal laser scanning microscopy (CLSM) (Figure 9). To further investigate cell morphologies, also transmitted light and nuclei staining (Hoechst 33342, blue) was plotted. It can be clearly observed that all cells have taken up polyplexes/polymers, which supports the results of the flow cytometry. Furthermore, some aggregates can be detected in case of **P2** in all cell lines, but to a higher extent in MDA-MB-231. **P3** is also taken up by all investigated cell lines, but the intensity is considerably higher in MDA-MB-231 cells, further supporting the results obtained by flow cytometry.

3.6. Transfection Efficiency

To investigate, whether an increased cell-specific uptake of genetic material results in enhanced transfection efficiency, the delivery and expression of a protein coded on a plasmid DNA was tested (Figure 10). Interestingly, 20%–30% of cells were expressing EGFP if **P1** polyplexes were used, but over 40% were reached in the case of **P2** polyplexes (as it can be found in literature)[45] and only 1% for **P3** polyplexes. Even an increase in the N/P value did not result in an increased transfection efficiency of **P3**. The same trend **P2** > **P1** > **P3** could be observed, if the amount of EGFP is considered (mean fluorescence intensity, MFI). This indicates that **P3** has to be further optimized not just only to deliver genetic material but also to transfect the targeted cells.

Transfection efficiency is the result of some more events than just successful uptake. Besides the uptake, the endosomal release of the polyplexes usually mediated by the proton sponge effect represents another important parameter. In our case, the latter step might be hindered by the amount of coupled fructose residues. Even if the transfection investigations for **P3** failed, the described modification of cationic polymers can be used to further develop the concept of D-fructose conjugated cationic polymers. Potential approaches for future research to increase the transfection efficiencies are the synthesis of different polymer compositions varying the ethylene imine/sugar ratio and, additionally, the introduction of amino functionalities to the side chains (analog to Ref.[38]).

4. Conclusions

A novel thiol-functionalized D-fructose derivative **5** was synthesized starting from commercially available protected D-fructose **1** in a four-step synthesis. Thiol-ene photoaddition of **5** to double bond containing copolymer P(EI-*stat*-ButEnOx) **P2** resulted in the isopropylidene bearing D-fructose conjugated polymer **iso-P3**. Deprotection under acidic conditions led to water soluble polymer

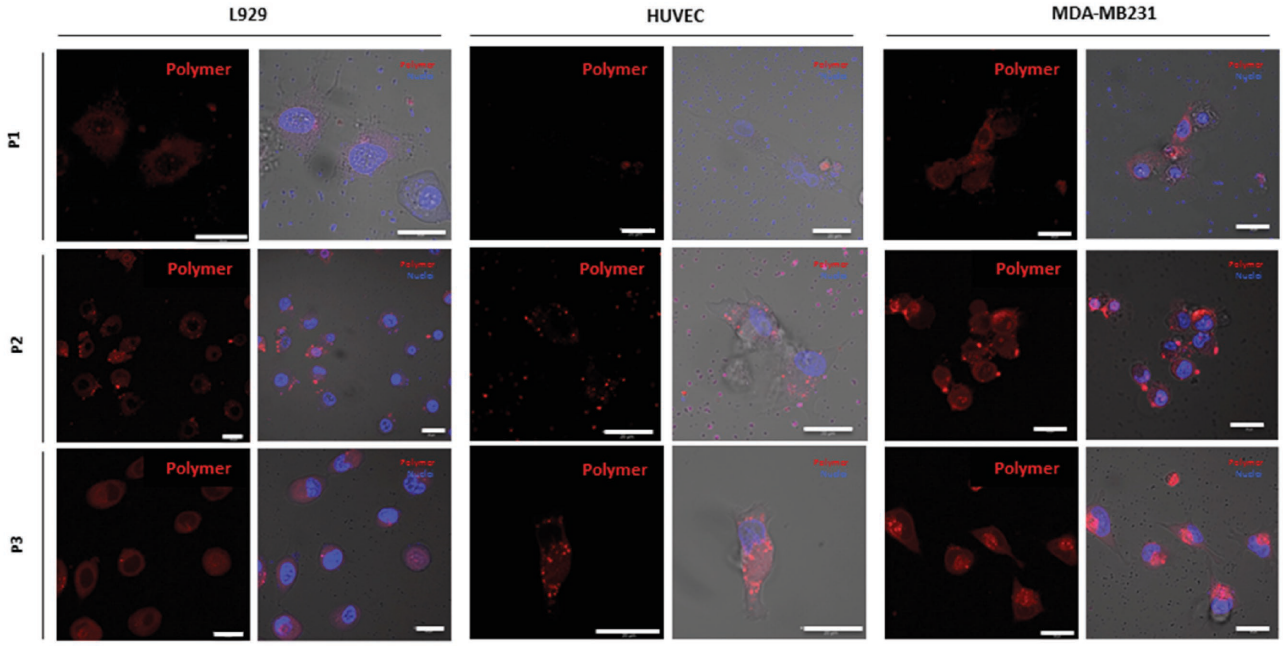

Figure 9. Live cell uptake studies. Polyplexes formed at N/P 50 with labeled polymers (red) **P1-Cy5**, **P2-Rho**, and **P3-Rho** were added to L929, HUVEC, and MDA-MB-231 cells. The cells were analyzed after 1 h via confocal laser scanning microscopy (CLSM) using the same laser settings for each cell line. The cell nucleus was stained with Hoechst 33342 (blue). Scale bar: 20 µm.

Macromol. Biosci. **2017**, DOI: 10.1002/mabi.201600502

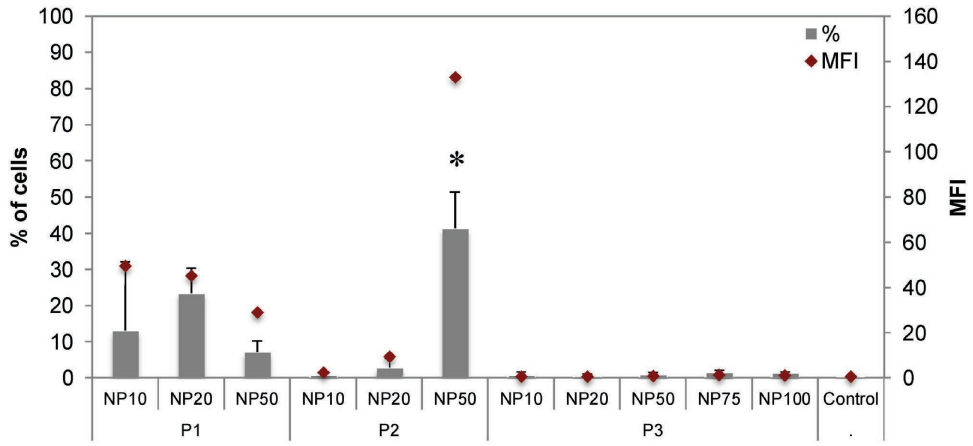

Figure 10. Transfection efficiency measured by the expression of EGFP. Polyplexes formed at N/P 50 with indicated polymers **P1–P3** at increasing N/P values. The amount (%) and the mean fluorescence intensity (MFI) of viable cells expressing EGFP were plotted. * indicates significant difference ($p < 0.05$) to amount of EGFP positive cells observed with **P1**.

P3. To evaluate GLUT5 targeting of D-fructose conjugated polymer **P3** in comparison to sugar-free polymers **P1** and **P2** cytotoxicity, uptake and transfection studies were performed. Cytotoxicity assays of **P3** revealed almost no toxicity against fibroblast cells (L929) as well as human primary HUVEC cells in the tested concentration range (up to 500 μg mL^{-1}), but a very pronounced cytotoxicity for breast cancer cells (MDA-MB-231). Furthermore, no irreversible RBC aggregation and a low hemolytic potential was observed for **P3**. Condensation experiments with pDNA exhibited stable polyplexes of **P3** at an N/P ratio > 15. When treated with anionic competitor heparin (10 U mL^{-1}), polyplexes of **P3** offered a rapid release of pDNA to nearly 100%. Additionally, the polymers were labeled with dyes to obtain **P1-Cy5**, **P2-Rho**, and **P3-Rho**. After the formation of labeled polyplexes, the cell-type-dependent uptake via flow cytometry and live cell CLSM was investigated. At N/P 50, MFI for **P3** was low in L929 or HUVEC and high for MDA-MB-231 cell line, whereas **P1** and **P2** revealed a reverse trend. Results of live cell imaging are in accordance with the results from flow cytometry, indicating cell-type-dependent interaction of D-fructose conjugated polymer **P3**. These findings might be attributed to D-fructose conjugation and therefore to GLUT5 mediated transport into cells.

The determination of the transfection efficiencies revealed unexpected low EGFP expressions, in particular for **P3**. The modification of LPEI only represents one example to install D-fructose on a cationic polymer. To achieve appropriate transfection efficiencies it is necessary to investigate the influence of different polymer compositions comprising varying ethylene imine and D-fructose contents. Further approaches comprise the introduction of different cationic functionalities in the side chains of various polymer classes.

Acknowledgements: C.E. and M.P. contributed equally to this work. The authors would like to thank Matthias Hartlieb for synthesis of poly(2-ethyl-2-oxazoline). This project was funded by the Thüringer Ministerium für Wirtschaft, Wissenschaft, und Digitale Gesellschaft (TMWWDG, ProExzellenzII, NanoPolar). The funding of the collaborative research center ChemBioSys (SFB 1127) by the Deutsche Forschungsgemeinschaft (DFG) is highly acknowledged. A.T. is grateful for the financial support from Carl Zeiss Stiftung and M.G. is grateful for the funding by the DFG (GO 1100/4-1). The LSM880 ELYRA PS.1 was further funded with a grant from the DFG. The authors also would like to thank Alexander S. Mosig for providing HUVEC cells. Primary cell donors were informed about the aim of the study and gave written informed consent. The study and experimental protocols used therein were approved by the ethics committee of the Jena University Hospital (assigned study number 3939-12/13).

Received: November 29, 2016; Revised: February 3, 2017; Published online: ; DOI: 10.1002/mabi.201600502

Keywords: cell-type specific uptake; D-fructose, poly(ethylene imine); nonviral gene delivery; triple-negative MDA-MB-231 breast cancer

[1] R. L. Siegel, K. D. Miller, A. Jemal, *Ca-Cancer J. Clin.* **2015**, *65*, 5.
[2] B. Weigelt, J. S. Reis-Filho, *Nat. Rev. Clin. Oncol.* **2009**, *6*, 718.
[3] R. Chacon, M. Costanzo, *Breast Cancer Res.* **2010**, *12*, S3.
[4] a) J. S. Ross, J. A. Fletcher, K. J. Bloom, G. P. Linette, J. Stec, W. F. Symmans, L. Pusztai, G. N. Hortobagyi, *Mol. Cell. Proteomics* **2004**, *3*, 379; b) F. Tomao, A. Papa, E. Zaccarelli, L. Rossi, D. Caruso, M. Minozzi, P. Vici, L. Frati, S. Tomao, *OncoTargets Ther.* **2015**, *8*, 177.
[5] D. Gholam, A. Chebib, D. Hauteville, M. P. Bralet, C. Jasmin, *Anticancer Drugs* **2007**, *18*, 835.
[6] R. S. Finn, J. Dering, C. Ginther, C. A. Wilson, P. Glaspy, N. Tchekmedyian, D. J. Slamon, *Breast Cancer Res. Treat.* **2007**, *105*, 319.

[7] E. Caldas-Lopes, L. Cerchietti, J. H. Ahn, C. C. Clement, A. I. Robles, A. Rodina, K. Moulick, T. Taldone, A. Gozman, Y. Guo, N. Wu, E. de Stanchina, J. White, S. S. Gross, Y. Ma, L. Varticovski, A. Melnick, G. Chiosis, *Proc. Natl. Acad. Sci. USA* **2009**, *106*, 8368.
[8] K. Miyamoto, S. Tatsumi, A. Morimoto, H. Minami, H. Yamamoto, K. Sone, Y. Taketani, Y. Nakabou, T. Oka, E. Takeda, *Biochem. J.* **1994**, *303*, 877.
[9] G. Gowrishankar, S. Zitzmann-Kolbe, A. Junutula, R. Reeves, J. Levi, A. Srinivasan, K. Bruus-Jensen, J. Cyr, L. Dinkelborg, S. S. Gambhir , *PLoS One* **2011**, *6*, e26902.
[10] A. Godoy, V. Ulloa, F. Rodríguez, K. Reinicke, A. J. Yañez, M. L. García, R. A. Medina, M. Carrasco, S. Barberis, T. Castro, F. Martínez, X. Koch, J. C. Vera, M. T. Poblete, C. D. Figueroa, B. Peruzzo, F. Pérez, F. Nualart, *J. Cell. Physiol.* **2006**, *207*, 614.
[11] K. K. Chan, J. Y. W. Chan, K. K. W. Chung, K.-P. Fung, *J. Cell. Biochem.* **2004**, *93*, 1134.
[12] a) A. Tatibouët, J. Yang, C. Morin, G. D. Holman, *Bioorg. Med. Chem.* **2000**, *8*, 1825; b) J. Yang, J. Dowden, A. Tatibouët, Y. Hatanaka, G. D. Holman, *Biochem. J.* **2002**, *367*, 533.
[13] J. Levi, Z. Cheng, O. Gheysens, M. Patel, C. T. Chan, Y. Wang, M. Namavari, S. S. Gambhir, *Bioconjugate Chem.* **2007**, *18*, 628.
[14] a) K. K.-W. Lo, W. H.-T. Law, J. C.-Y. Chan, H.-W. Liu, K. Y. Zhang, *Metallomics* **2013**, *5*, 808; b) K. Y. Zhang, K. K.-S. Tso, M.-W. Louie, H.-W. Liu, K. K.-W. Lo, *Organometallics* **2013**, *32*, 5098; c) M. Pröhl, T. Bus, J. A. Czaplewska, A. Traeger, M. Deicke, H. Weiss, W. Weigand, U. S. Schubert, M. Gottschaldt, *Eur. J. Inorg. Chem.* **2016**, *2016*, 5197.
[15] a) C. von der Ehe, A. Rinkenauer, C. Weber, D. Szamosvari, M. Gottschaldt, U. S. Schubert, *Macromol. Biosci.* **2016**, *16*, 508; b) A. Abdolmaleki, S. Mallakpour, M. Rostami, *High Perform. Polym.* **2015**, *27*, 903; c) S. Ganda, Y. Jiang, D. S. Thomas, J. Eliezar, M. H. Stenzel, *Macromolecules* **2016**, *49*, 4136; d) A. Dag, M. Callari, H. Lu, M. H. Stenzel, *Polym. Chem.* **2016**, *7*, 1031; e) J. Zhao, H. Lu, P. Xiao, M. H. Stenzel, *ACS Appl. Mater. Interfaces* **2016**, *8*, 16622; f) J. Zhao, H. Lai, H. Lu, C. Barner-Kowollik, M. H. Stenzel, P. Xiao, *Biomacromolecules* **2016**, *17*, 2946.
[16] J. Zhao, K. Babiuch, H. Lu, A. Dag, M. Gottschaldt, M. H. Stenzel, *Chem. Commun.* **2014**, *50*, 15928.
[17] N. Unnamalai, B. G. Kang, W. S. Lee, *FEBS Lett.* **2004**, *566*, 307.
[18] E. Song, P. Zhu, S.-K. Lee, D. Chowdhury, S. Kussman, D. M. Dykxhoorn, Y. Feng, D. Palliser, D. B. Weiner, P. Shankar, W. A. Marasco, J. Lieberman, *Nat. Biotechnol.* **2005**, *23*, 709.
[19] J. Halder, A. A. Kamat, C. N. Landen, L. Y. Han, S. K. Lutgendorf, Y. G. Lin, W. M. Merritt, N. B. Jennings, A. Chavez-Reyes, R. L. Coleman, D. M. Gershenson, R. Schmandt, S. W. Cole, G. Lopez-Berestein, A. K. Sood, *Clin. Cancer Res.* **2006**, *12*, 4916.
[20] J. Wang, Z. Lu, M. G. Wientjes, J. L.-S. Au, *AAPS J.* **2010**, *12*, 492.
[21] O. Boussif, F. Lezoualch, M. A. Zanta, M. D. Mergny, D. Scherman, B. Demeneix, J.-P. Behr, *Proc. Natl. Acad. Sci. USA* **1995**, *92*, 7297.
[22] a) J. H. Jeong, S. H. Song, D. W. Lim, H. Lee, T. G. Park, *J. Controlled Release* **2001**, *73*, 391; b) Y. Yue, F. Jin, R. Deng, J. Cai, Z. Dai, M. C. M. Lin, H.-F. Kung, M. A. Mattebjerg, T. L. Andresen, C. Wu, *J. Controlled Release* **2011**, *152*, 143.
[23] C. Englert, M. Hartlieb, P. Bellstedt, K. Kempe, C. Yang, S. K. Chu, X. Ke, J. M. García, R. J. Ono, M. Fevre, R. J. Wojtecki, U. S. Schubert, Y. Y. Yang, J. L. Hedrick, *Macromolecules* **2015**, *48*, 7420.
[24] a) K. Kunath, A. von Harpe, D. Fischer, T. Kissel, *J. Controlled Release* **2003**, *88*, 159; b) D. Appelhans, H. Komber, M. A. Quadir, S. Richter, S. Schwarz, J. van der Vlist, A. Aigner, M. Müller, K. Loos, J. Seidel, K.-F. Arndt, R. Haag, B. Voit, *Biomacromolecules* **2009**, *10*, 1114; c) W. Cheng, C. Yang, J. L. Hedrick, D. F. Williams, Y. Y. Yang, P. G. Ashton-Rickardt, *Biomaterials* **2013**, *34*, 3697; d) C. Englert, M. Fevre, R. J. Wojtecki, W. Cheng, Q. Xu, C. Yang, X. Ke, M. Hartlieb, K. Kempe, J. M. García, R. J. Ono, U. S. Schubert, Y. Y. Yang, J. L. Hedrick, *Polym. Chem.* **2016**, *7*, 5862.
[25] M. Ogris, S. Brunner, S. Schuller, R. Kircheis, E. Wagner, *Gene Ther.* **1999**, *6*, 595.
[26] S. Slavin, J. Burns, D. M. Haddleton, C. R. Becer, *Eur. Polym. J.* **2011**, *47*, 435.
[27] A. Gress, A. Völkel, H. Schlaad, *Macromolecules* **2007**, *40*, 7928.
[28] G. Adiwidjaja, J.-S. Brunck, K. Polchow, J. Voss, *Carbohydr. Res.* **2000**, *325*, 237.
[29] B. D. Johnston, B. M. Pinto, *J. Org. Chem.* **2000**, *65*, 4607.
[30] M. Bauer, C. Lautenschlaeger, K. Kempe, L. Tauhardt, U. S. Schubert, D. Fischer, *Macromol. Biosci.* **2012**, *12*, 986.
[31] J. C. Fernandes, X. Qiu, F. M. Winnik, M. Benderdour, X. Zhang, K. Dai, Q. Shi, *Int. J. Nanomed.* **2013**, *8*, 4091.
[32] T. J. Dickerson, N. Yamamoto, D. I. Ruiz, K. D. Janda, *J. Am. Chem. Soc.* **2004**, *126*, 11446.
[33] H. C. Kolb, M. G. Finn, K. B. Sharpless, *Angew. Chem., Int. Ed. Engl.* **2001**, *40*, 2004.
[34] C. von der Ehe, A. Rinkenauer, C. Weber, D. Szamosvari, M. Gottschaldt, U. S. Schubert, *Macromol. Biosci.* **2016**, *16*, 508.
[35] H. M. L. Lambermont-Thijs, F. S. van der Woerdt, A. Baumgaertel, L. Bonami, F. E. Du Prez, U. S. Schubert, R. Hoogenboom, *Macromolecules* **2010**, *43*, 927.
[36] C. Englert, L. Tauhardt, M. Hartlieb, K. Kempe, M. Gottschaldt, U. S. Schubert, *Biomacromolecules* **2014**, *15*, 1124.
[37] S. Ferrari, A. Pettenazzo, N. Garbati, F. Zacchello, J. P. Behr, M. Scarpa, *Biochim. Biophys. Acta, Gene Struct. Expression* **1999**, *1447*, 219.
[38] T. Bus, C. Englert, M. Reifarth, P. Borchers, M. Hartlieb, A. Vollrath, S. Hoeppener, A. Traeger, U. S. Schubert, *J. Mater. Chem. B* **2017**, *5*, 1258.
[39] M. I. Ul-Haq, B. F. L. Lai, R. Chapanian, J. N. Kizhakkedathu, *Biomaterials* **2012**, *33*, 9135.
[40] M. Jawanda, B. F. L. Lai, J. N. Kizhakkedathu, K. Ishihara, R. Narain, *Polym. Chem.* **2013**, *4*, 3140.
[41] a) J. B. Lepecq, C. Paoletti, *J. Mol. Biol.* **1967**, *27*, 87; b) A. J. Geall, I. S. Blagbrough, *J. Pharm. Biomed. Anal.* **2000**, *22*, 849.
[42] A. C. Rinkenauer, L. Tauhardt, F. Wendler, K. Kempe, M. Gottschaldt, A. Traeger, U. S. Schubert, *Macromol. Biosci.* **2015**, *15*, 414.
[43] a) R. Luxenhofer, G. Sahay, A. Schulz, D. Alakhova, T. K. Bronich, R. Jordan, A. V. Kabanov, *J. Controlled Release* **2011**, *153*, 73; b) J. Rejman, V. Oberle, I. S. Zuhorn, D. Hoekstra, *Biochem. J.* **2004**, *377*, 159.
[44] a) A. C. Rinkenauer, S. Schubert, A. Traeger, U. S. Schubert, *J. Mater. Chem. B* **2015**, *3*, 7477; b) U. Lächelt, E. Wagner, *Chem. Rev.* **2015**, *115*, 11043.
[45] C. Englert, A.-K. Trützschler, M. Raasch, T. Bus, P. Borchers, A. S. Mosig, A. Traeger, U. S. Schubert, *J. Controlled Release* **2016**, *241*, 1.

PUBLICATION 8

Matrix supported poly(2-oxazoline)-based hydrogels for DNA catch and release

M. Hartlieb, D. Pretzel, C. Englert, M. Hentschel,
K. Kempe, M. Gottschaldt, U. S. Schubert

Biomacromolecules **2014**, *15*, 1970-1978

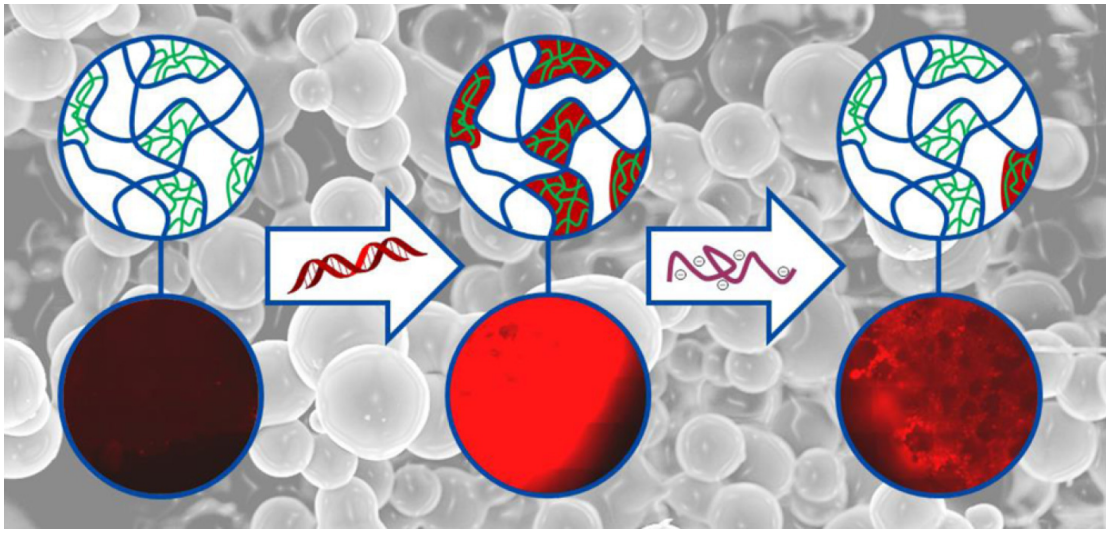

Article

pubs.acs.org/Biomac

Matrix Supported Poly(2-oxazoline)-Based Hydrogels for DNA Catch and Release

Matthias Hartlieb,[†,‡] David Pretzel,[†,‡] Christoph Englert,[†,‡] Martin Hentschel,[§] Kristian Kempe,[†,‡,∥] Michael Gottschaldt,[†,‡] and Ulrich S. Schubert*[,†,‡]

[†]Laboratory of Organic and Macromolecular Chemistry (IOMC), Friedrich Schiller University Jena, Humboldtstrasse 10, 07743 Jena, Germany

[‡]Jena Center for Soft Matter (JCSM), Friedrich Schiller University Jena, Philosophenweg 7, 07743 Jena, Germany

[§]Analytik Jena AG, Konrad-Zuse-Straße 1, 07745 Jena, Germany

Supporting Information

ABSTRACT: We describe the synthesis of matrix supported hydrogel structures based on amine containing poly(2-oxazoline)s and their use to bind and release genetic material for potential applications in diagnostics or pathogen detection. Amine containing poly(2-oxazoline)s were synthesized by copolymerization of 2-ethyl-2-oxazoline with a monomer bearing a *tert*-butyl oxycarbonyl (Boc) protected amine group in the 2-position and subsequent deprotection. The statistical copolymers were used to generate hydrogels and matrix supported hydrogels by cross-linking of a certain fraction of the amine groups with epichlorhydrin. Supported structures were prepared by soaking porous polyethylene (PE) or polypropylene (PP) filter materials in a copolymer/epichlorhydrin solution, which was cross-linked upon heating. Scanning electron microscopy (SEM) of the composites revealed a bead like structure of the gel phase, which could be attributed to a lower critical solution temperature (LCST) behavior of the initial polymer prior to gelation. The dependency of the LCST behavior on the content of amine groups was investigated. Swelling values and the ratio of hydrogel per composite was determined using water sorption analysis. Subsequently, the ability of the systems to absorb and release labeled DNA was tested. Uptake and stimulated release, triggered by changes in pH, temperature, and heparin concentration, were investigated using fluorescence microscopy. Polymerase chain reaction (PCR) proved the successful recovery of the DNA, demonstrating the potential of the presented system for a broad range of molecular biological applications.

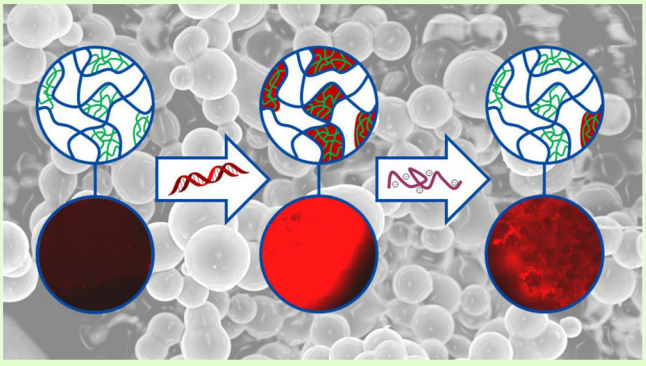

INTRODUCTION

The isolation of nucleic acids from biological samples, such as cells, tissues, and viruses, is of significant importance for DNA-based applications in modern clinical diagnostics,[1] genetic analysis,[2] drug discovery,[3] and pathogen detection.[4] To guarantee a successful and specific detection of DNA sequences in downstream processes, purification of the genetic material is the main requirement. An optimal DNA extraction system comprises the fast and efficient isolation of DNA ideally directly from complex biological samples, the avoidance of toxic reagents and inhibitory substances, and a cost-effective fabrication enabling disposable devices.[5,6] However, the low amount of DNA in cell/tissue extracts and its structural and chemical similarity to other cell components (size, negative charge, molecular mass, and hydrophobicity)[7] results in poor selectivity and considerable coelution.[8]

A broad diversity of DNA purification and extraction techniques have been developed in the past decades, and up to now, no universal purification method exists.[9] Well established approaches are based on, e.g., phenol−chloroform extraction or CsCl/ethidium bromide density gradient centrifugation. These extraction techniques, performed in liquid phases, are time-consuming and associated with the use of toxic, hazardous reagents.[10,11] Solid phase extraction (SPE) techniques using mostly glass fiber, silicon dioxide, diatomaceous earth, nitrocellulose, polyamide, or anion exchange resins as solid phases have become the most common method to prepare DNA samples for genetic analysis and other biomedical techniques.[12−17]

In consideration of the fact that the potential of common SPE is fairly exhausted, future developments need to involve new materials. A highly promising alternative approach is the catch and release of DNA molecules within a three-dimensional hydrogel matrix. Hydrogels possess a high water content, resulting in a mobility of guest molecules by diffusion,[18] are

Received: November 10, 2013
Published: February 26, 2014

dx.doi.org/10.1021/bm500236y | *Biomacromolecules* 2014, 15, 1970−1978

tunable in pore size[19] and chemical functionality,[20] and most importantly, they provide a large surface area for binding of targeted molecules. To make use of these systems for DNA purification processes, hydrogels can be endowed with, e.g., cationic functionalities, which enables electrostatic interactions with the negatively charged DNA. The advantage of this approach over SPE is the avoidance of chaotropic salt solutions and alcohols, which can contaminate the samples and, e.g., inhibit polymerase chain reactions (PCR).[21] In addition, hydrogels exhibit an inherent wettability enabling the efficient interaction with the DNA containing solution in contrast to the often relatively hydrophobic solid surfaces. Elution from the hydrogel can be performed either specifically, using a competitive ligand, or nonspecifically, by changing the pH, ionic strength, or polarity of the solvent depending on the matrix used and the chemical characteristics of the biomolecules.

Poly(2-oxazoline)s (POx) represent a highly promising platform for the synthesis of functional materials. The living cationic ring-opening polymerization (CROP) of 2-oxazolines, which was discovered in 1966,[22−25] enables the design of well-defined (co)polymers with tailored molar mass and functionalities.[26] The polymer properties are mainly determined by the choice of the monomer and can be further fine-tuned by the introduction of functional groups that are able to be modified in postpolymerization reactions.[27,28] The first examples of POx-based hydrogels were reported in 1989 by Saegusa and co-workers. The authors copolymerized conventional monomers with bis-functional oxazolines.[29] In the following years, their method of choice was the partial hydrolysis of POx and the subsequent esterification of the resulting poly(ethylene imine) units. Using this approach, it was possible to introduce several functionalities and to cross-link the polymers via secondary interactions[30−32] or covalent bonds.[33−35] More than one decade later, other groups continued studying POx-based networks and reported different approaches for the network synthesis, e.g., by the preparation of methacrylate functionalized POx macromonomers and their use as cross-linker in radical polymerizations.[36−39] The first example of amine bearing POx and their general ability to form hydrogels was reported by Cesana et al. in 2006.[40] In more detail, we recently studied the kinetics of a 2-oxazoline monomer with a protected amine functionality and were able to produce polymers and networks with defined compositions. Furthermore, we could show that these systems are able to reversibly bind genetic material from solution.[18] However, before these systems can be used in the above-mentioned applications, two problems have to be solved: (i) the lack of mechanical stability of the hydrogels (in particular relevant for common extraction protocols requiring centrifugation steps that cause considerable shear forces) and (ii) the dependence of the release process on high concentrations of heparin, which would interfere with subsequently performed PCR. To overcome the former issue, the use of a supportive inert polymer-based matrix in which the hydrogel component is localized represents a promising approach. While the (amine-containing) hydrogel network is meant to bind and release DNA, the second network introduces additional stability and protects it from mechanical degradation. The latter issue can be overcome by a change in the release stimuli, using temperature and pH changes or by a reduction of the initial heparin concentration.

In this contribution, we report on the fabrication of composite materials composed of a polyethylene (PE) or polypropylene (PP) matrix and amine containing POx hydrogels. To gain insights into the phase conditions during formation of the POx hydrogels, the LCST behavior of the precursor polymer in dependence of the amine content was studied. The microstructure of the produced hydrogels was investigated via SEM, and the ability of the substrates to absorb water from the gas phase was determined using TGA. The potential of the material for binding and release of DNA in dependence of the heparin concentration was studied using fluorescence microscopy.

EXPERIMENTAL SECTION

Materials and Instrumentation. All chemicals and solvents were purchased from Sigma-Aldrich, Merck, Fluka, and Acros. 2-Ethyl-2-oxazoline (EtOx) and methyl tosylate (MeTos) were distilled to dryness prior to use.

2-(4-((*tert*-Butoxycarbonyl)amino)butyl)-2-oxazoline (BocOx) was synthesized as described in our previous work.[41] Filter substrates consisting of PE (90 μm pore size) or PP (120 μm pore size) were purchased from Porex technologies GmbH and perforated to pills with a diameter of 7 mm and a thickness of 1.6 mm. Cy5 labeled DNA was provided by Analytik Jena.

The Initiator Sixty single-mode microwave synthesizer from Biotage, equipped with a noninvasive IR sensor (accuracy 2%), was used for polymerizations under microwave irradiation. Microwave vials were heated overnight to 110 °C and allowed to cool to room temperature under argon atmosphere before usage. All polymerizations were carried out under temperature control. Size-exclusion chromatography (SEC) of protected polymers was performed on a Shimadzu system equipped with a SCL-10A system controller, a LC-10AD pump, a RID-10A refractive index detector, and a PSS SDV column with chloroform/triethylamine (NEt_3)/2-propanol (94:4:2) as eluent. The column oven was set to 50 °C. SEC of the deprotected statistical copolymers was performed on a Shimadzu system with a LC-10AD pump, a RID-10A refractive index detector, a system controller SCL-10A, a degasser DGU-14A, and a CTO-10A column oven using *N*,*N*-dimethylacetamide with 2.1 g/L LiCl as the eluent and the column oven set to 50 °C. Poly(styrene) (PS) samples were used as calibration standards for both solvent systems. Proton NMR spectroscopy (^{1}H NMR) measurements were performed at room temperature on a Bruker AC 300 and 400 MHz spectrometer, using $CDCl_3$ or MeOD as solvents. The chemical shifts are given in ppm relative to the signal from the residual nondeuterated solvent. Fourier transform infrared (FTIR) spectroscopy was performed on an Affinity-1 FT-IR from Shimadzu, using the reflection technique. Gas chromatography (GC) was performed on a GC-2010 from Shimadzu. Acetonitrile was used as an internal standard to determine the monomer conversion. Scanning electron microscopy (SEM) was measured using a field emission scanning electron microscope Gemini 1530 type LEO from Carl Zeiss AG, Germany. Investigated samples were freeze-dried matrix supported hydrogels. Cloud points were determined in a Crystal 16 from Avantium Technologies connected to a chiller (Julabo FP 40) at a wavelength of 500 nm.

Copolymerization of EtOx and BocOx (P(EtOx-stat-BocOx)) (1−5). In a microwave vial, EtOx (181.7 μL, 1.8 mmol), MeTos (90.8 μL, 0.600 mmol), and acetonitrile (11.5 mL) were mixed under inert conditions. After heating in the microwave at 140 °C for 16 min, EtOx (2543 μL, 25.2 mmol) and BocOx (749 μL, 3 mmol) were added under argon stream and the mixture was heated again in the microwave synthesizer (140 °C, 11 min). The solution was diluted with dichloromethane (100 mL) and extracted with saturated aqueous solution of sodium bicarbonate (3 × 100 mL) and water (3 × 100 mL). Subsequently, the solution was concentrated and the polymer was precipitated in 400 mL ice-cold diethyl ether. The white precipitate was filtered and dried in high vacuum (2.77 g, 78%).

^{1}H NMR ($CDCl_3$, 300 MHz): δ = 4.99 (s, 0.2 H, NH), 3.45 (s, 4 H, backbone), 3.11 (s, 0.3 H, CH_2−CH_2−NH (BocOx)), 2.40 (s, 1.9 H, CH_2 (EtOx)), 1.92 (s, 0.3 H, CH_2−CH_2−CO (BocOx)), 1.64 (s, 0.3

Scheme 1. Schematic Representation of the Polymer and Hydrogel Synthesis

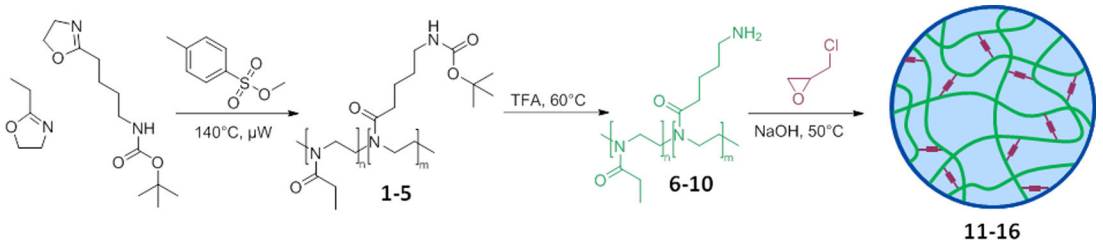

H, $CH_2-CH_2-CH_2$ (BocOx)), 1.53 (s, 0.3 H, CH_2-CH_2-CH2 (BocOx)), 1.42 (s, CH_3 (BocOx)), 1.21 (s, 1.3 H, CH_3 (EtOx)) ppm.

SEC (**9**) (eluent: $CHCl_3$/2-propanol/NEt_3, PS-standard): M_n = 5300 g/mol, M_w = 5700 g/mol, PDI = 1.08.

Deprotection of P(EtOx-stat-BocOx) (P(EtOx-stat-AmOx) (6–10). Exemplarily, P(EtOx-*stat*-BocOx) (1, 2 g) was dissolved in trifluoroacetic acid (TFA) (5 mL) and heated at 60 °C for 1 h. After stirring for 24 h at room temperature, the mixture was diluted with 10 mL of methanol and precipitated in 400 mL of cold diethyl ether. The yellowish precipitate was redissolved in methanol (200 mL) and stirred with Amberlyst A21 for 24 h. Subsequently, the solution was concentrated and the polymer was precipitated in cold diethyl ether (400 mL), filtered, dried in high vacuum, and obtained as a yellowish powder (1.58 g, 87%).

^{1}H NMR (MeOD, 400 MHz): δ = 3.52 (s, 4 H, backbone), 2.96 (0.23 H, s, $CH_2-CH_2-NH_2$), 2.42 (2 H, s, CH_2 (EtOx) + CH_2-CH_2-CO (AmOx)), 1.69 (0.41 H, s, $CH_2-CH_2-CH_2-CH_2$ (AmOx)), 1.11 (2,8 H, s, CH_3 (EtOx)) ppm.

SEC (**18**) (eluent: DMAc/LiCl, PS-standard): M_n = 8,100 g/mol, M_w = 10,200 g/mol, PDI = 1.26.

Investigation of the Cloud Point Behavior of P(EtOx-stat-PAmOx). To determine the temperature responsive solubility changes of P(EtOx-*stat*-AmOx), the polymer was dissolved in distilled water at different concentrations ranging from 0.4 to 100 mg/mL. The solutions were heated from 2 to 100 °C under stirring with a heating rate of 1 °C/min. The turbidity of the solution was recorded as a function of the temperature. The cloud point was defined as the temperature where the solution reaches 50% of transmission. Three heating cycles were performed, and the average value was used. For one measurement point, four samples of identical concentrations were investigated in parallel.

Synthesis of Matrix Supported (11–16) and Nonsupported Hydrogels (17–19). In a typical experiment, the filter substrates were swollen in a 1 mL solution of **9** (200 mg, 0.034 mmol, 0.51 mmol based on amine groups) and epichlorhydrin (6.66 μL, 0.085 mmol) in 5 wt % sodium hydroxide (NaOH) solution. After 10 min, the mixture was heated to 50 °C for 1 h. The filter substrates were separated from the residual gel, washed in water (3 × 100 mL, 1 day), and freeze-dried.

Water Uptake Measurements. The swelling of the matrix supported hydrogels was investigated using a TGA Q5000 SA thermogravimetric analyzer from TA Instruments Eschborn, Germany. For data evaluation the "Universal Analysis Software" was used. Substrates were dried in the machine at 60 °C and 0% relative humidity until weight constancy was reached. Water uptake was performed at room temperature and 90% relative humidity. The measurement was stopped when the samples were saturated with water.

The weight fraction of hydrogel in the composite materials was determined using eq 1.

$$m_{HG}(\text{wt\%}) = \frac{Q_{ges} - Q_F}{Q_{HG} - Q_F} \times 100\% \quad (1)$$

where Q_{ges} = swelling value of the composite, Q_{HG} = swelling value of the hydrogel, and Q_F = swelling value of the host matrix.

DNA Binding and Release of Composite Materials. DNA absorption of matrix supported hydrogels was measured using labeled DNA (Cy5) and a fluorescence microscope (Cell Observer Z1, Carl Zeiss, Jena, Germany) equipped with a mercury arc UV lamp and the appropriate filter combinations for excitation and detection of emission. Images of a series (11 × 11 pictures per well) were captured with a 10× objective using identical instrument settings (e.g., UV lamp power, integration time, and camera gain), and spots of the 96-well plate were addressed using an automated XY table.

The matrix supported gels were swollen in HBG-buffer (HEPES buffered glucose, pH 7) for 30 min and, subsequently, in a DNA solution (500 μL, 10 μg/mL) for 30 min. After washing with buffer solution for another 30 min, the fluorescence of the substrates was detected. The release was accomplished applying a 2 mL of a 6 mg/mL heparin solution in water for 30 min. Surface adherent water was removed before each measurement. Fluorescence pictures were taken from the buffer-swollen material after DNA binding and washing and after the release took place.

Stimuli Responsive Release. The temperature, pH, and heparin concentration dependency of the release process was investigated by measuring the fluorescence of the supernatant of the matrix supported hydrogel after treatment with the respective condition for 1 h. Samples were swollen in a solution of Cy5-labled DNA (200 mL, 10 ng/mL). Subsequently, the solution was removed and the gel was washed using 200 μL of water. Again, the water was removed and replaced with either water, buffer (pH = 4), or heparin solution of varying concentration. After 1 h, the supernatant was analyzed using the Tecan M200 Pro fluorescence microplate reader (Crailsheim, Germany) at the following wavelengths: Ex 649 nm/Em 670 nm.

DNA Extraction and Real-Time PCR Assay. The gDNA extraction of a laboratory isolated strain of *Escherichia coli* K12 was performed with a magnetic particle based system for fully automated isolation and purification of nucleic acids (AJ InnuPure C16). The real-time PCR assay was realized in a AJ TOptical Real-time Thermocycler and was carried out in a 20 μL of reaction mixture with the follow compositions: DNA extract (5 μL), 0.025 units Taq DNA polymerase (AJ innuTaq Hot-A DNA polymerase), 4 mM magnesium chloride, 1.0 mM of deoxy-nucleotriphosphate, 2.5 mM buffer, 1× EvaGreen Fluorescent DNA Stain, and 0.5 μM of each primer. For amplification, an initial denaturation for 2 min at 95 °C was followed by 45 cycles of 95 °C for 30 s, 57 °C for 30 s, and 72 °C for 30 s. In this study, a DNA fragment of *E. coli* LacZ was used as positive control and without DNA as negative control. The PCR products were analyzed by agarose gel electrophoresis using 2.0% agarose gel containing ethidium bromide, and the gels were viewed on a UV transilluminator (AJ Biometra UVsolo TS). Additional information about the primers can be found in the Supporting Information.

RESULTS AND DISCUSSION

Polymer and Hydrogel Synthesis. The synthesis of amine containing poly(2-oxazoline)s (POx)s was carried out, as described previously (Scheme 1).[41] 2-Ethyl-2-oxazoline (EtOx) was copolymerized with 2-(4-((*tert*-butoxycarbonyl)amino)-butyl)-2-oxazoline (BocOx), a 2-oxazoline monomer bearing a Boc-protected amine group in the side chain. To ensure that the initiator, namely methyl tosylate (MeTos), does not attack the Boc-protected amine group of the comonomer, an

macroinitiator containing three repeating units EtOx was synthesized in the first step. The increased sterically hindrance of the oxazolinium species is expected to diminish the reaction with the functional group. The respective primary amine containing copolymers (P(EtOx-*stat*-AmOx)) were obtained after deprotection of the amine group using TFA (Table 1).

Table 1. Selected Analytical Data of the Amine Containing POx

sample no.	polymer	Mn (SEC) [g/mol]	PDI	yield [%]	AmOx [%]
6	P($EtOx_{43}$-*stat*-$PAmOx_5$)	8100	1.26	95	10
7	P($EtOx_{39}$-*stat*-$PAmOx_7$)	8200	1.24	90	15
8	P($EtOx_{32}$-*stat*-$PAmOx_9$)	8700	1.25	93	22
9	P($EtOx_{38}$-*stat*-$PAmOx_{15}$)	9500	1.23	89	27
10	P($EtOx_{32}$-*stat*-$PAmOx_{16}$)	9400	1.24	96	33

The gelation reaction was performed using epichlorhydrin (ECH) as cross-linker. Under the basic conditions applied (pH 14), ECH undergoes a ring-opening reaction with the amine groups of the copolymers. The resulting OH group and the chlorine group of ECH can reform an epoxide moiety by the elimination of hydrochloric acid. This functionality can undergo a second reaction to covalently cross-link the polymers.

Matrix Supported Hydrogels. For the fabrication of matrix supported hydrogels, polymer **9** was selected as it demonstrated good DNA binding capabilities.[41] A host network (PE or PP based porous filter substrate) was swollen in an aqueous solution of polymer (**9**), cross-linker (ECH), and sodium hydroxide for 30 min. The linker concentration was chosen to react with 33% (**11**, **14**), 66% (**12**, **15**), and 100% (**13**, **16**) of the available amine groups. Gelation occurred after 1 h at 50 °C. Subsequently, the filter substrates were separated from the supernatant gel and cleaned from surface adherent gel particles using a spatula. The composite material and the residual gels (**17**–**19**) were purified by washing with distilled water (3 × 5 mL per substrate, 24 h) and freeze-drying (Figure 1). Six different matrix supported gels were prepared comprising two host materials (PP and PE) with the three different degrees of cross-linking. The stoichiometry was calculated in assumption that every amine group reacted once with ECH resulting in a secondary amine. However, the real case is a mix of unreacted, secondary, and tertiary amines within the network.

A first evidence for the successful incorporation of the POx gel within the host matrix could be obtained by the investigation of the water uptake from the gas phase. This measurement was carried out using a special TGA setup where the sample weight can be determined in dependency of the relative humidity and temperature of the surrounding atmosphere. To exclude swelling prior to the measurement, the samples were annealed at 60 °C and 0% humidity for 2 h. After weight constancy was reached, the measurement was started by an increase of the relative humidity to 90% at room temperature. As depicted in Figure 2, the weight of the substrate increases upon this environmental change. The measurement was stopped when no further change of the sample weight could be detected.

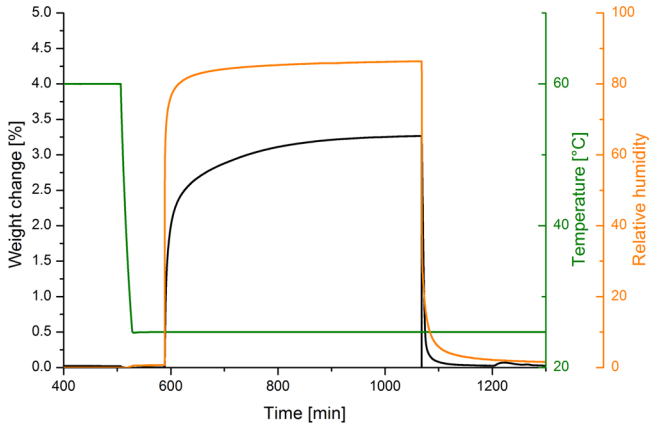

Figure 2. Water uptake measurement of composite **11**.

The composition of hydrogels and matrix supported gels as well as the results of the water uptake studies are summarized in Table 2. The pure POx gels show a good swelling behavior from humid air and absorb up to 66% of their own weight of water. A trend is clearly visible; the higher the degree of cross-linking of the network, the lower the swelling value of the gel.

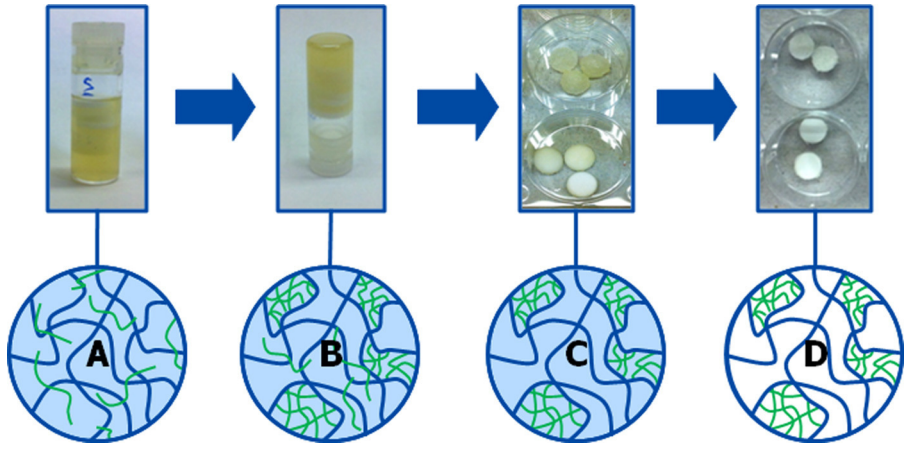

Figure 1. Synthesis of matrix supported gels from POx (green) within a host structure (blue): (A) Host material swollen in polymer solution, (B) gelated polymer within the pores of the host, (C) matrix supported gel separated from residual gel, and (D) isolated as well as freeze-dried product.

dx.doi.org/10.1021/bm500236y | *Biomacromolecules* 2014, 15, 1970–1978

Table 2. Overview of the Synthesized Composite Materials and Hydrogels[a]

	11	12	13	14	15	16	17	18	19	PP	PE
substrate	PP	PP	PP	PE	PE	PE					
ratio ECH/amine (%)	33.0	66.0	100.0	33.0	66.0	100.0	33.0	66.0	100.0		
swelling value (%)	3.3	4.5	3.3	2.2	3.0	1.9	66.5	61.5	53.0	0.0	0.2
gel component (wt %)	5.0	7.3	6.2	3.0	4.6	3.2	100.0	100.0	100.0	0.0	0.0

[a]Polymer **9** was used for the gelation of the hydrophilic component.

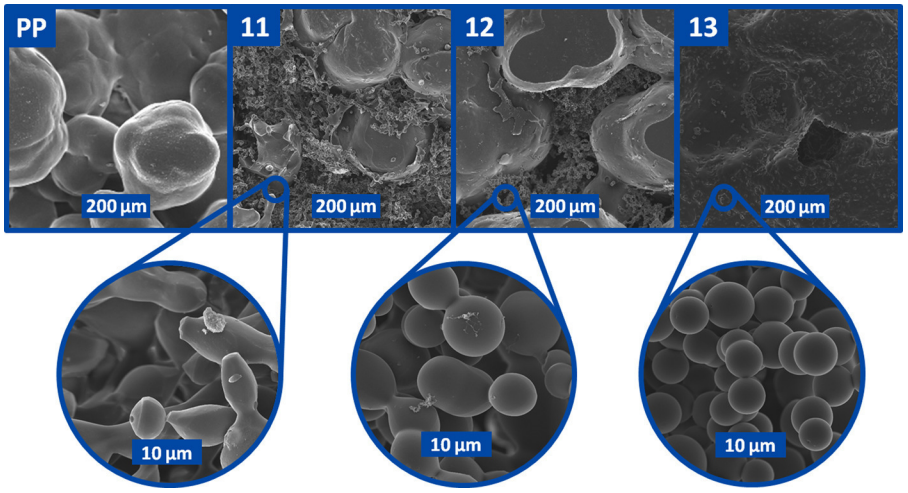

Figure 3. SEM pictures of PP-based composites. The magnified images show the appearance of hydrogel beads with a diameter of 5 to 10 μm.

In contrast, the material based on the PE and PP host substrates only show minimal water uptake of 1.9 to 4.5%. In combination with the water uptake of the bare substrates (0.0% for PP and 0.2% for PE), this clearly indicates the presence of a second, hydrophilic component within the host matrix.

It was possible to calculate the mass of the entrapped gel from the swelling value of the composite and the water uptake of the single components. The fact that the PP-based materials contains more hydrogel is attributed to the pore size of the material which is larger than the one of PE (PP = 120 μm, PE = 90 μm). Therefore, the swelling in the polymer solution prior to gelation is more efficient and results in a higher weight fraction.

A further proof of the proposed structure of the matrix supported gels could be obtained by SEM investigations (Figure 3). The large pore structure of the host material is visible in the first picture (PP). The images of the composites clearly show the existence of a second component within the host matrix consisting of a network of hydrogel beads. The bead size is similar for all different cross-linking degrees. Only the shape becomes more regular with increasing amount of linker. SEM pictures of the PE-based supported hydrogels can be found in the Supporting Information (Figure S2).

LCST of the Copolymers. The appearance of gel particles instead of a homogeneous network was unexpected. To understand this effect, the behavior of the polymer during the process of gelation (aqueous solution of sodium hydroxide (pH 14), 50 °C) was investigated in more detail. Poly(2-ethyl-2-oxazoline) (PEtOx) based systems are known to exhibit lower critical solution temperature (LCST) behaviors in aqueous solution, i.e., EtOx-containing copolymers show a coil-to-globular transition at elevated temperatures.[42] If the polymers reported here reveal a cloud point behavior where the homogeneous solution separates into two phases with different polymer concentrations, gelation of only one phase would lead to gel particles as observed. This phase transition can be investigated measuring the transmission of the solution in dependence of the applied temperatures because the turbidity of the solution increases by the light scattering of one phase.[43]

As depicted in Figure 4, all polymers exhibited cloud points in the investigated concentration range in aqueous solution

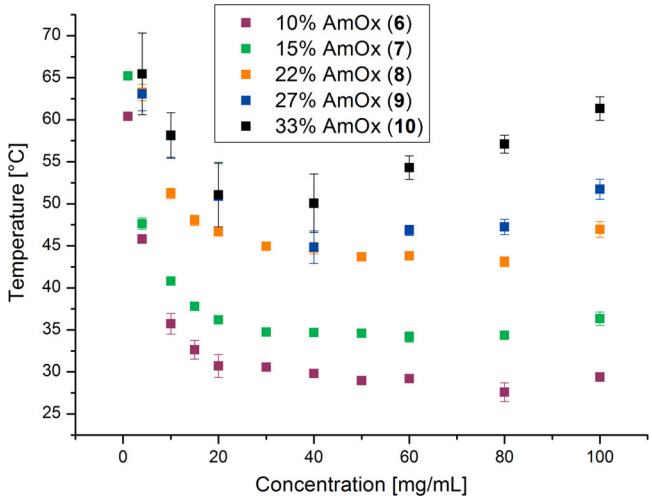

Figure 4. Concentration dependent evaluation of the cloud points of P(EtOx-*stat*-AmOx) at pH 14.

(pH 14). Furthermore, an influence of the polymer composition on the cloud point temperature was observed. An increased AmOx content resulted in increased cloud point temperature, with values between 25 and 65 °C. However, PEtOx itself exhibits a LCST behavior but only at higher molar masses and higher temperatures (61−69 °C for PEtOx with M_n of 20,000 g/mol^{-1}).[42] Therefore, the AmOx monomer seems

dx.doi.org/10.1021/bm500236y | *Biomacromolecules* 2014, 15, 1970−1978

to have a significant effect on the thermal properties of these systems. The incorporation of 10 mol % AmOx causes a decrease of the cloud point temperature to almost as low as room temperature. A further increase of the AmOx amount should lead to a faster response and, therefore, to an even lower cloud point temperature. However, a contrary behavior was observed. This could be attributed to two competing trends. The polymer side chain exhibits two different domains: the hydrophobic alkyl chain and the hydrophilic amine group, which is not protonated at the pH values studied. While the hydrophobic domain induces the phase transition, the amine group promotes the water solubility. A stronger increase of the influence of the amine in comparison to the hydrophobic behavior of the alkyl chain could explain a rising cloud point with increasing amounts of comonomer, as observed. A different explanation could be the chaotropic influence of the high OH^- concentration resulting in a lowering of the cloud point of the PEtOx part.

All investigated polymers exhibit LCSTs between 40 and 80 mg/mL under the conditions of the gelation reaction. Therefore, the polymer solution is phase separated before the gelation occurs. The cross-linking then proceeds in the phase with the high polymer concentration, forming small gel beads as visible in the SEM pictures.

This behavior is favorable for the foreseen application in several aspects. First of all, a bead-like structure provides a large surface to volume ratio, which is beneficial for the purpose of DNA capture and release because the diffusion control of the process is decreased. Moreover, the porous structure of the host material is not completely filled by the gel. This increases the ability of a sample solution to pass through the filter matrix in a given time without the need of intense force which is also beneficial for the targeted application where a sample solution should be pumped through the filter matrix on a short time scale.

DNA Binding and Release. To investigate the ability of the synthesized composites to absorb and release genetic material, Cy5 (Abs, 649 nm; Em, 670 nm) labeled DNA was used. The location and concentration of this DNA derivative can be measured directly by spectroscopic and microscopic techniques tracking the fluorescence of the attached dye. In a general procedure, the matrix supported gels were swollen in HBG-buffer (HEPES buffered glucose, pH 7, 2 mL) for 30 min. Afterward, the samples were transferred into a DNA solution for 30 min. The prior swelling limits the penetration of the gel by DNA to passive diffusion. Subsequently, the gels were cleaned from adhered liquid and washed in buffer solution for another 30 min to exclude the detection of DNA which is not bound (Figure 5).

The samples were investigated using fluorescence microscopy. The results of the measurements for the PP-based composites are depicted in Figure 6 (uptake and release studies of all other supported hydrogels can be found in the Supporting Information, Figure S3).

Figure 5. Schematic representation of the DNA uptake and release by the composite materials. (A) Uptake of fluorescently labeled DNA by the hydrogel component and (B) release of DNA by the addition of heparin.

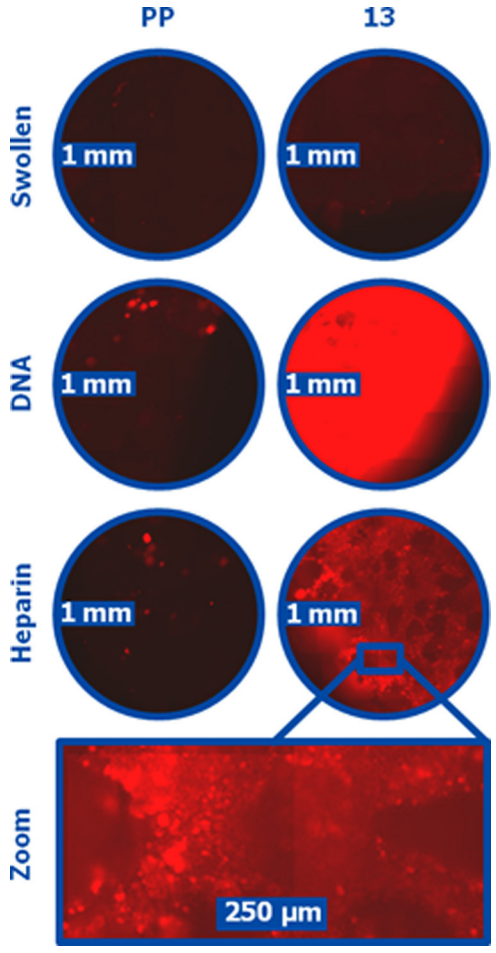

Figure 6. DNA uptake and release of PP-based composite **13**.

The first row shows fluorescence images of the samples which were swollen in buffer solution. The slightly increased intensity of the red color in comparison to the initial PP material resembles the autofluorescence of the hydrogel which is bound to the substrate. After the addition of DNA and a washing step, a bright fluorescence of the composite is visible while the bare PP matrix shows online some bright spots which are attributed to the encapsulation of DNA solution droplets within the pores of the material. Treatment of the filters with heparin solution (6 mg/mL) for 30 min caused a fraction of the bound DNA to be released again as depicted in the last row. Heparin is a polyanion able to replace genetic material in electrostatic complexes. In the enlargement of the picture, the microstructure of the hydrogel beads is clearly visible and provides a further proof that the POx hydrogel is responsible for the binding of DNA because only the beads light up under the fluorescence microscope.

While the release using heparin is an efficient method to regain the bound DNA, it has also drawbacks. The most prominent one is that heparin acts as an inhibitor in a PCR. Therefore, other stimuli for the release of DNA from the gels were tested. The most obvious trigger for this purpose is a change of the temperature. To investigate this influence, the DNA loaded substrates (**13**) were placed in water (500 μL) and heated to a specific temperature between 30 and 90 °C.

dx.doi.org/10.1021/bm500236y | *Biomacromolecules* 2014, 15, 1970−1978

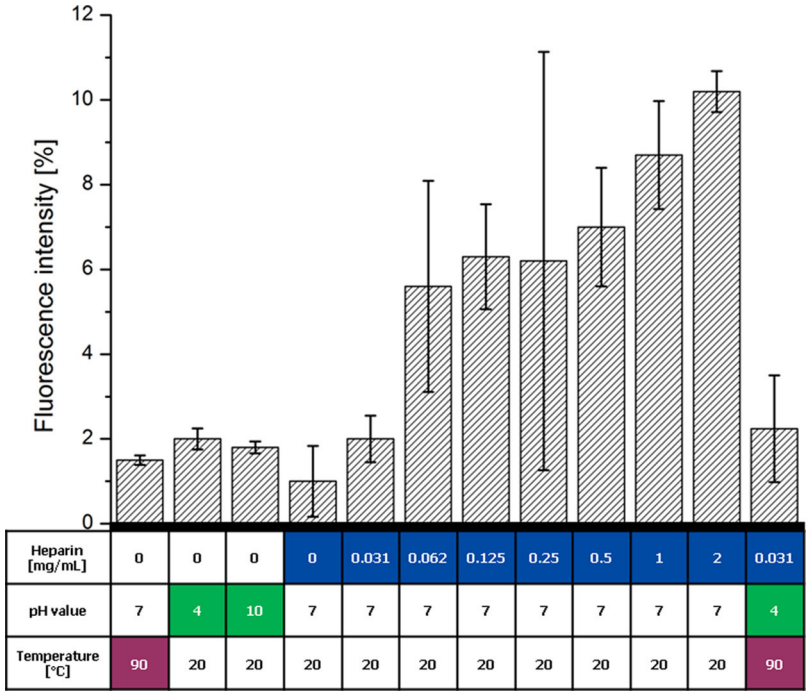

Figure 7. Release studies of the composites varying the temperature, pH value, and heparin concentration.

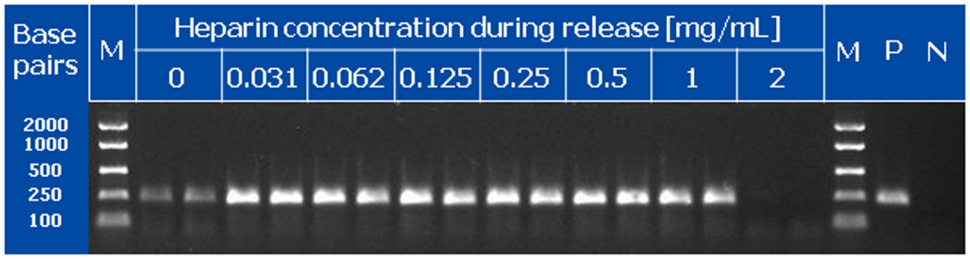

Figure 8. Agarose gel of the heparin released DNA samples after PCR and electrophoresis (M = DNA ladder standard, P = positive control, N = negative control).

After 1 h, the supernatant was transferred into a well plate and the fluorescence was measured using a plate reader. The data were related to reference samples which were treated with the same temperature program but without the presence of a composite. Unfortunately, no release could be detected up to a temperature of 80 °C. At 90 °C, about 1.5% of the labeled DNA was detected in the supernatant (Figure 7). Also a change of pH to lower or higher values did not lead to a sufficient release.

Another possibility to minimize the heparin concentration in the final DNA solution is the variation of the initial heparin amount added to the composite. The DNA is set free from the gel by a replacement with heparin, which blocks the cationic binding site of the network. Because of its higher charge density, heparin has a higher affinity to the gel than the genetic material. If the concentration of heparin is low enough for a complete absorption into the gel but high enough for a partially replacement of DNA, the resulting sample solution would be suitable for a PCR. An increase of the heparin concentration resulted, as expected, in a higher DNA release, although this enhancement is not linearly increasing with the concentration of polyanion. Also, a combination of the three triggers did not result in an increased release of DNA.

PCR Results. To prove the suitability of the presented system for the aimed application, DNA fragments released by heparin were amplified in a real-time PCR process. For this purpose, the three different samples, which were released for each concentration, were pooled and an aliquot was subsequently subjected to PCR. The amplification curves are depicted in the Supporting Information (Figure S4). Additionally, the resulting PCR products were analyzed using conventional agarose gel electrophoresis (Figure 8). The size of the sample products and the positive control matches with the theoretical value of the gene aimed at (LacZ; approximately 228 base pairs). Exclusively, the DNA sample, which was released using 2 mg/mL heparin, was not amplified in the PCR. This is most probably attributed to the inhibitory effect of the higher heparin content. It seems reasonable that in all other cases the heparin concentration is sufficiently low (0.031 to 1 mg/mL) that the majority of the heparin added to the DNA loaded hydrogel is entrapped within the polymer network and hence does not interfere with the subsequent PCR. This assumption is supported by the fact that already very low heparin concentrations around 0.02 mg/mL inhibit the amplification of genetic material in the reported protocol (Supporting Information, Figure S5). For a heparin concentration of 2 mg/mL, the gel sample is saturated with anionic material and hence

dx.doi.org/10.1021/bm500236y | *Biomacromolecules* 2014, 15, 1970−1978

further excess of heparin cannot be hold back. Therefore, no PCR product could be obtained. Having in mind that the DNA release using 1 mg/mL is almost as high as with 2 mg/mL (Figure 7), this effect is negligible for the PCR application presented here.

CONCLUSION AND OUTLOOK

In summary, we demonstrated the successful combination of functional POx hydrogels and polymeric filter substrates. The presence of a gel component within the host material could be proven by an increased water uptake and scanning electron microscopy studies. Furthermore, the amount of incorporated gel could be determined indirectly by the swelling values.

The cloud point behavior of the precursor polymer was investigated to gain insights of the state of dissolution during the hydrogel synthesis. All polymers showed LCST behavior in dependency of the amount of amine containing comonomer in aqueous solution (pH 14). The phase separation of the polymer solution at the conditions of the gelation resulted in the formation of hydrogels with bead-like microstructure as detected by SEM.

It was shown that the composites are able to absorb DNA from solution and that the release was accomplished via a replacement of the genetic material by heparin. Furthermore, the influence of the heparin concentration was examined. PCR studies demonstrated that recovered DNA, which was released with heparin concentrations up to 1 mg/mL, was still intact and could be amplified. Moreover, temperature and pH value were investigated as stimuli for the release of DNA from the hydrogels. However, both resulted in low amounts of free DNA.

Because the release of genetic material from all the hydrogels synthesized so far is rather restricted, further studies will focus on different release stimuli, as well as systems which are able to immobilize DNA on surfaces without the absorption into a three-dimensional substrate. Using this approach, it could be possible to perform a PCR directly on the surface to accumulate DNA copies in the surrounding solution without any need for a DNA release.

ASSOCIATED CONTENT

Supporting Information

PCR primer information, SEM pictures, as well as DNA catch and release studies of all produced composite materials. PCR amplification curves, PCR inhibiting properties of heparin. This material is available free of charge via the Internet at http://pubs.acs.org.

AUTHOR INFORMATION

Corresponding Author

*E-mail: Ulrich.Schubert@uni-jena.de.

Present Address

[‖]For K.K.: Department of Chemical and Biomolecular Engineering, The University of Melbourne, Victoria 3010, Australia.

Notes

The authors declare no competing financial interest.

ACKNOWLEDGMENTS

We thank the Bundesministerium für Bildung und Forschung (Germany) for funding (project: BASIS, 03WKCB01C). Kristian Kempe acknowledges the Alexander von Humboldt Foundation. Grateful thanks to Steffi Stumpf for SEM investigations, Jürgen Vitz for TGA analysis, and Christine Weber for helpful discussions.

ABBREVIATIONS USED

Boc, *tert*-butyl oxycarbonyl; BocOx, 2-(4-((*tert*-butoxycarbonyl)amino)butyl)-2-oxazoline; CROP, cationic ring-opening polymerization; EtOx, ethyl-2-oxazoline; FTIR, Fourier transform infrared; GC, gas chromatography; ^{1}H NMR, proton NMR spectroscopy; LCST, lower critical solution temperature; MeTos, methyl tosylate; NaOH, sodium hydroxide; NEt_3, triethylamine; PCR, polymerase chain reactions; PE, polyethylene; PP, polypropylene; POx, poly(2-oxazoline)s; PS, poly(styrene); SEC, size-exclusion chromatography; SEM, scanning electron microscopy; SPE, solid phase extraction

REFERENCES

(1) Peeters, J.; Van der Spek, P. *Cell Biochem. Biophys.* **2005**, *43*, 149−166.
(2) Gingeras, T. R.; Kwoh, D. Y.; Davis, G. R. *Nucleic Acids Res.* **1987**, *15*, 5373−5390.
(3) Anderton, J. M.; Tokarz, R.; Thill, C. D.; Kuhlow, C. J.; Brooks, C. S.; Akins, D. R.; Katona, L. I.; Benach, J. L. *Infect. Immun.* **2004**, *72*, 2035−2044.
(4) Wong, C. W.; Albert, T. J.; Vega, V. B.; Norton, J. E.; Cutler, D. J.; Richmond, T. A.; Stanton, L. W.; Liu, E. T.; Miller, L. D. *Genome Res.* **2004**, *14*, 398−405.
(5) Reedy, C. R.; Price, C. W.; Sniegowski, J.; Ferrance, J. P.; Begley, M.; Landers, J. P. *Lab Chip* **2011**, *11*, 1603−1611.
(6) Boom, R.; Sol, C. J. A.; Salimans, M. M. M.; Jansen, C. L.; Wertheimvandillen, P. M. E.; Vandernoordaa, J. *J. Clin. Microbiol.* **1990**, *28*, 495−503.
(7) Stadler, J.; Lemmens, R.; Nyhammar, T. *J. Gene Med.* **2004**, *6*, 54−S66.
(8) Diogo, M. M.; Queiroz, J. A.; Prazeres, D. M. F. *J. Chromatogr., A* **2005**, *1069*, 3−22.
(9) Ghanem, A.; Healey, R.; Adly, F. G. *Anal. Chim. Acta* **2013**, *760*, 1−15.
(10) Buckingham, L.; Flaws, M. L., *Molecular Diagnostics: Fundamentals, Methods, and Clinical Applications*; F. A. Davis: Philadelphia, PA, 2007.
(11) Sambrook, J.; Russel, D., *Molecular Cloning: A Laboratory Manual*; Cold Spring Harbor Laboratory Press: New York, 2001; Vol. 3.
(12) *Pierce Strong Ion Exchange Spin Columns*; Thermo Scientific: Hudson, NH, 2007.
(13) *QIAGEN Genomic DNA Handbook*; QIAGEN: Valencia, CA, 2001.
(14) Gjerse, D. T.; Hoang, L.; Hornby, D., *RNA Purification and Analysis: Sample Preparation, Extraction, Chromatography*; Wiley-VCH: Weinheim, Germany, 2009.
(15) Esser, K.-H.; Marx, W. H.; Lisowsky, T. *BioTechniques* **2005**, *39*, 270−271.
(16) Chen, C. W.; Thomas, C. A., Jr *Anal. Biochem.* **1980**, *101*, 339−341.
(17) Carter, M. J.; Milton, l. D. *Nucleic Acids Res.* **1993**, *21*, 1044.
(18) Wiesbrock, F.; Hoogenboom, R.; Leenen, M. A. M.; Meier, M. A. R.; Schubert, U. S. *Macromolecules* **2005**, *38*, 5025−5034.
(19) Koschella, A.; Hartlieb, M.; Heinze, T. *Carbohydr. Polym.* **2011**, *86*, 154−161.
(20) Hoogenboom, R.; Fijten, M. W. M.; Thijs, H. M. L.; van Lankvelt, B. M.; Schubert, U. S. *Des. Monomers Polym.* **2005**, *8*, 659−671.
(21) Nakagawa, T.; Tanaka, T.; Niwa, D.; Osaka, T.; Takeyama, H.; Matsunaga, T. *J. Biotechnol.* **2005**, *116*, 105−111.
(22) Tomalia, D. A.; Sheetz, D. P. *J. Polym. Sci., Part A: Polym. Chem.* **1966**, *4*, 2253−2265.

(23) Seeliger, W.; Aufderhaar, E.; Diepers, W.; Feinauer, R.; Nehring, R.; Thier, W.; Hellmann, H. *Angew. Chem.* **1966**, *78*, 913−927.
(24) Kagiya, T.; Narisawa, S.; Maeda, T.; Fukui, K. *J. Polym. Sci., Part B: Polym. Lett.* **1966**, *4*, 441−445.
(25) Bassiri, T. G.; Levy, A.; Litt, M. *J. Polym. Sci., Part B: Polym. Lett.* **1967**, *5*, 871−879.
(26) Adams, N.; Schubert, U. S. *Adv. Drug Delivery Rev.* **2007**, *59*, 1504−1520.
(27) Guillerm, B.; Monge, S.; Lapinte, V.; Robin, J.-J. *Macromol. Rapid Commun.* **2012**, *33*, 6000−6016.
(28) Kempe, K.; Hoogenboom, R.; Jaeger, M.; Schubert, U. S. *Macromolecules* **2011**, *44*, 6424−6432.
(29) Chujo, Y.; Sada, K.; Matsumoto, K.; Saegusa, T. *Polym. Bull.* **1989**, *21*, 353−356.
(30) Chujo, Y.; Sada, K.; Seagusa, T. *Macromolecules* **1993**, *26*, 6315−6315.
(31) Chujo, Y.; Sada, K.; Saegusa, T. *Macromolecules* **1993**, *26*, 6320−6323.
(32) Chujo, Y.; Sada, K.; Saegusa, T. *Polym. J.* **1993**, *25*, 599−608.
(33) Chujo, Y.; Yoshifuji, Y.; Sada, K.; Saegusa, T. *Macromolecules* **1989**, *22*, 1074−1077.
(34) Chujo, Y.; Sada, K.; Saegusa, T. *Macromolecules* **1990**, *23*, 2636−2641.
(35) Chujo, Y.; Sada, K.; Naka, A.; Nomura, R.; Saegusa, T. *Macromolecules* **1993**, *26*, 883−887.
(36) Christova, D.; Velichkova, R.; Goethals, E. J.; Du Prez, F. E. *Polymer* **2002**, *43*, 4585−4590.
(37) Christova, D.; Velichkova, R.; Loos, W.; Goethals, E. J.; Prez, F. D. *Polymer* **2003**, *44*, 2255−2261.
(38) Rueda, J. C.; Komber, H.; Cedrón, J. C.; Voit, B.; Shevtsova, G. *Macromol. Chem. Phys.* **2003**, *204*, 947−953.
(39) Rueda, J.; Suica, R.; Komber, H.; Voit, B. *Macromol. Chem. Phys.* **2003**, *204*, 954−960.
(40) Cesana, S.; Auernheimer, J.; Jordan, R.; Kessler, H.; Nuyken, O. *Macromol. Chem. Phys.* **2006**, *207*, 183−192.
(41) Hartlieb, M.; Pretzel, D.; Kempe, K.; Fritzsche, C.; Paulus, R. M.; Gottschaldt, M.; Schubert, U. S. *Soft Matter* **2013**, *9*, 4693−4704.
(42) Weber, C.; Hoogenboom, R.; Schubert, U. S. *Prog. Polym. Sci.* **2012**, *37*, 686−714.
(43) Weber, C.; Becer, C. R.; Hoogenboom, R.; Schubert, U. S. *Macromolecules* **2009**, *42*, 2965−2971.

Supporting Information

Matrix supported poly(2-oxazoline)-based hydrogels for DNA catch and release

Matthias Hartlieb[a,b], David Pretzel[a,b], Christoph Englert[a,b], Martin Hentschel[c], Kristian Kempe[a,b,†], Michael Gottschaldt[a,b], Ulrich S. Schubert[a,b,]*

[a] Laboratory of Organic and Macromolecular Chemistry (IOMC), Friedrich Schiller University Jena, Humboldtstrasse 10, 07743, Jena, Germany

[b] Jena Center for Soft Matter (JCSM), Friedrich Schiller University Jena, Philosophenweg 7, 07743, Jena, Germany

[c] Analytik Jena AG, Konrad-Zuse-Straße 1, 07745 Jena, Germany

† Current address: Department of Chemical and Biomolecular Engineering, The University of Melbourne, Victoria 3010, Australia

S1. Primers for qPCR amplification of *Escherichia coli K12*

Target	Sequence	Product size [bp]	Label
LacZ	5'-CTG GCG TAA TAG CGA AGA AG-3' (20)	228	biotin
LacZ	5'-GGA TTG ACC GTA ATG GGA TAG (21)	228	Cy5

S2. SEM pictures of PP and PE substrates and supported hydrogels.

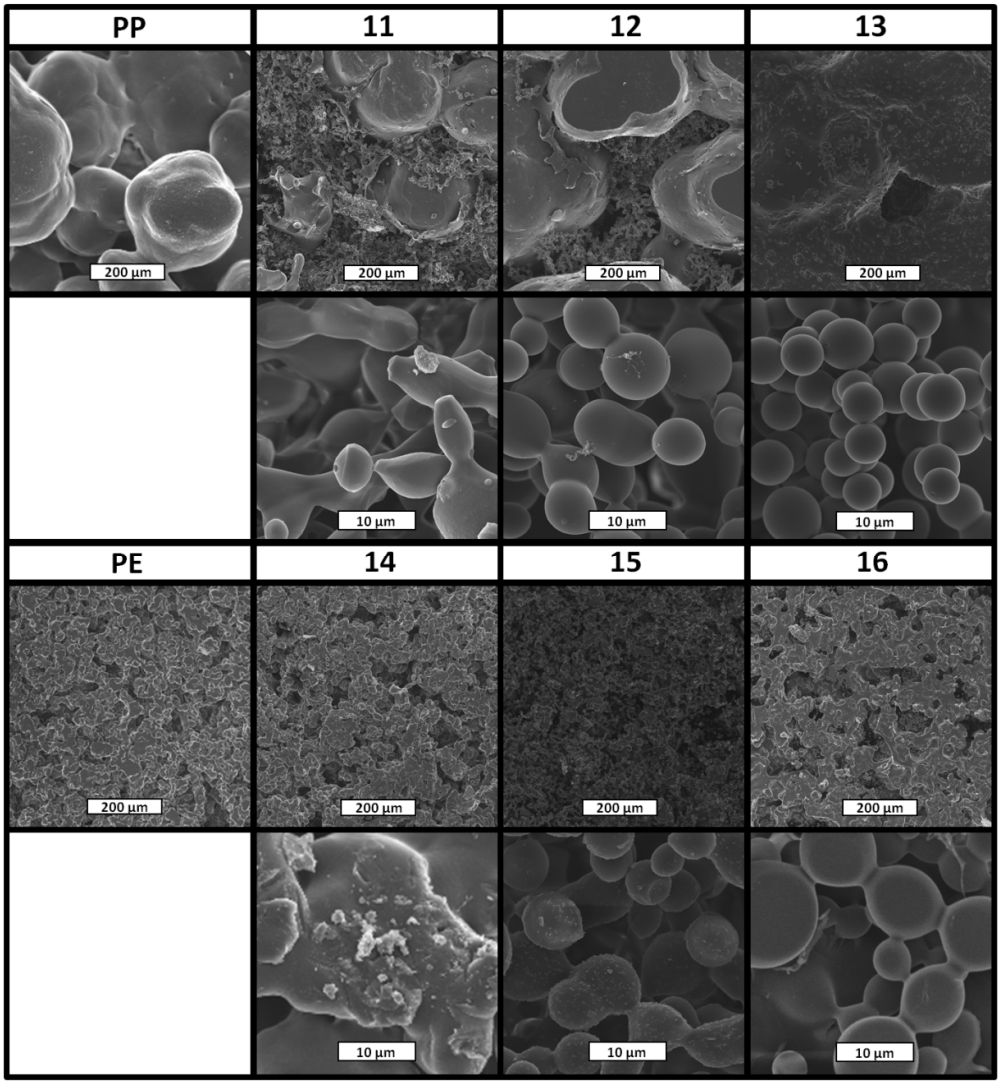

S3. DNA catch and release of all produced supported hydrogels.

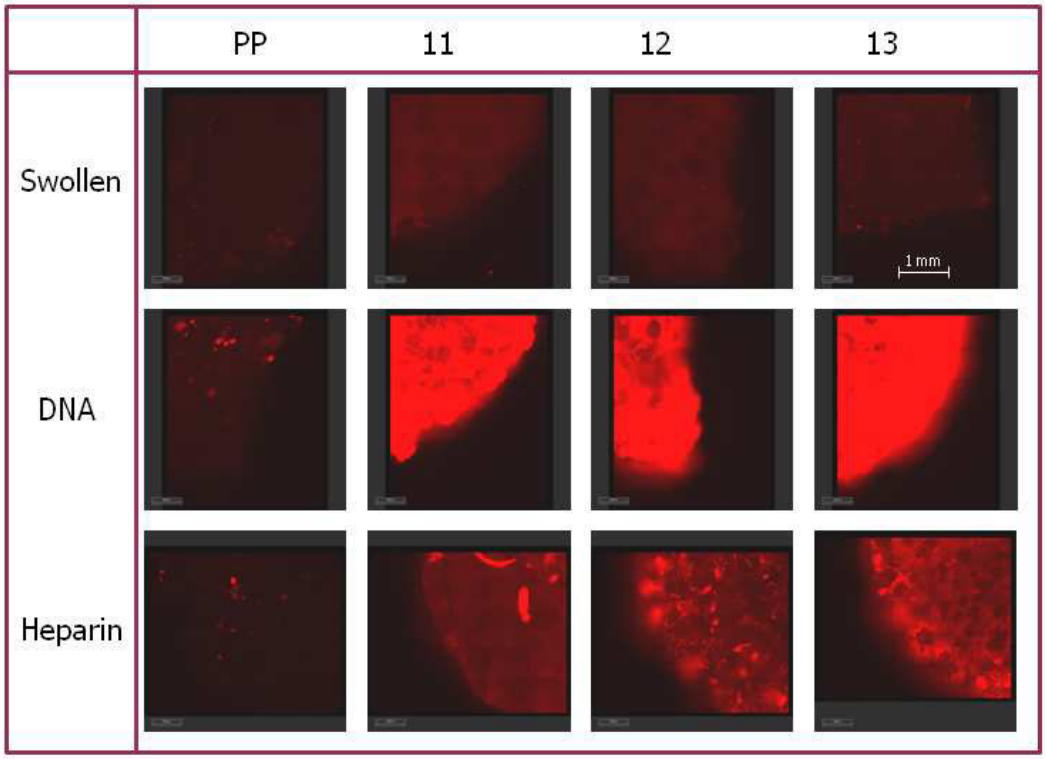

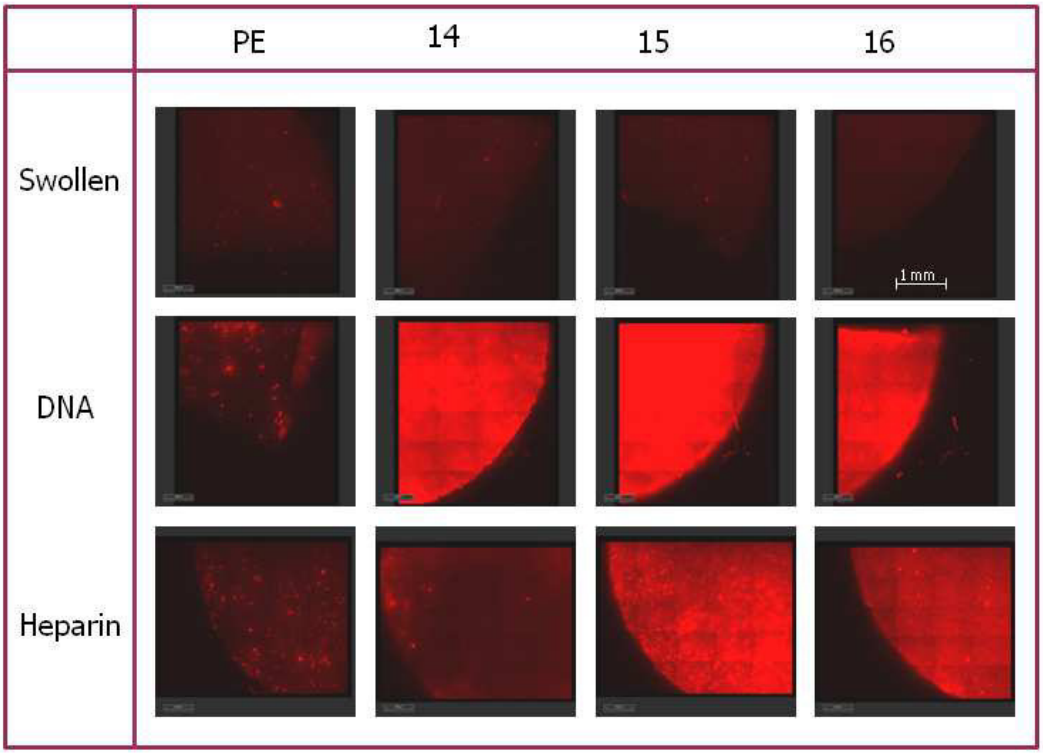

S4. PCR amplification curves.

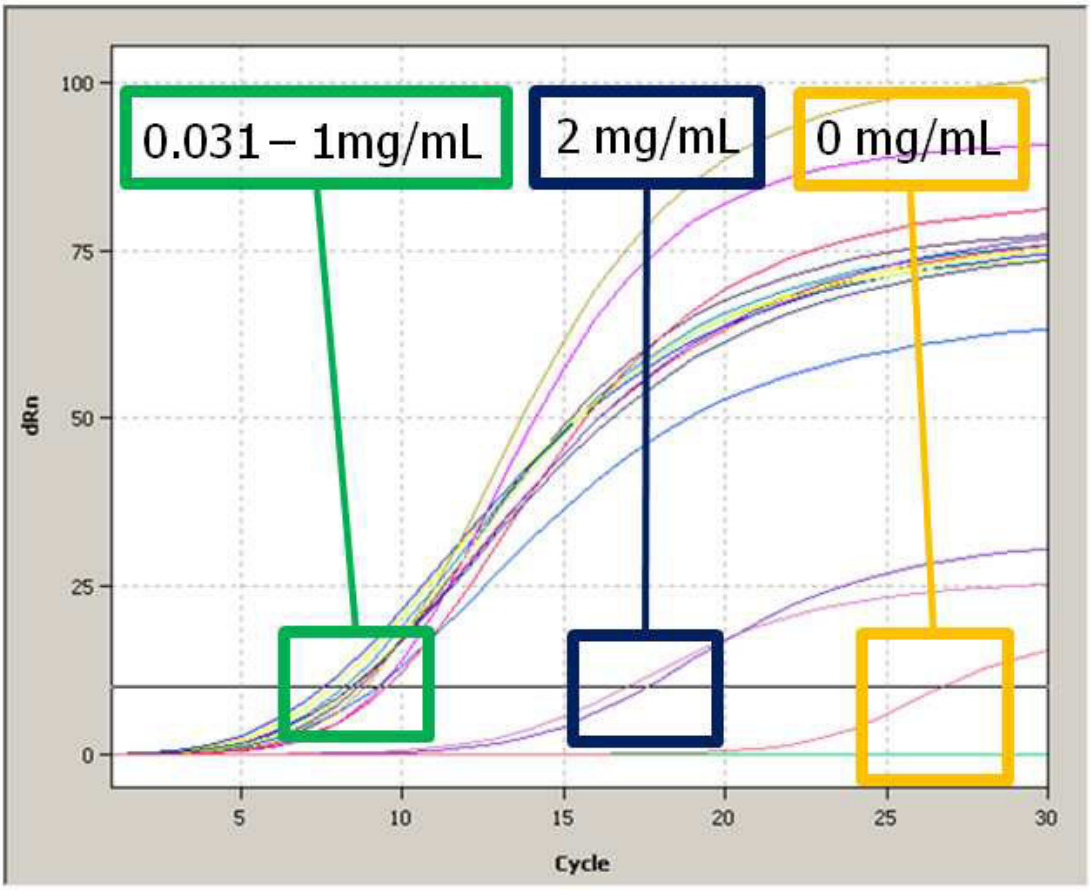

S5. PCR inhibiting properties of herparin for the evaluated system.

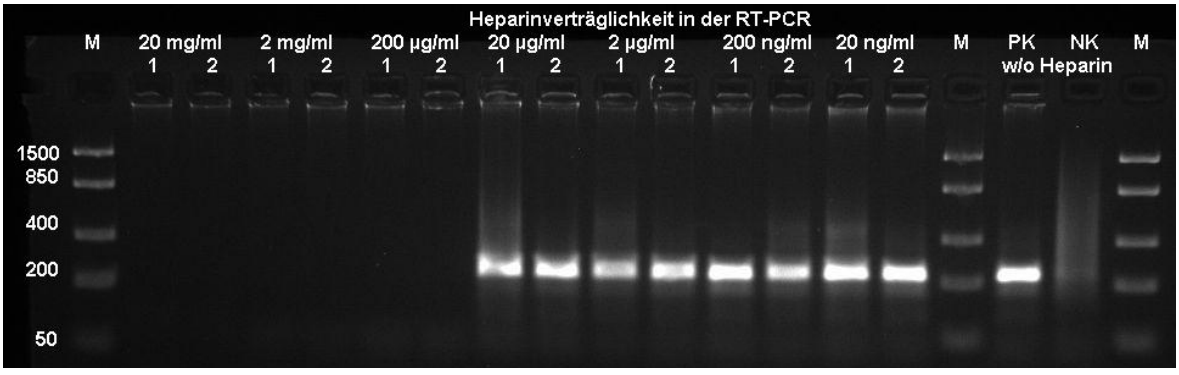

Heparin concentrations down to 20 µg/mL disturb the PCR process.

PUBLICATION 9

Lab in a tube: Purification, amplification and detection of DNA using poly(2-oxazoline) multilayers

M. N. Leiske,‡ M. Hartlieb,‡ C. Paulenz, D. Pretzel, M. Hentschel, C. Englert, M. Gottschaldt, U. S. Schubert

Adv. Funct. Mater. **2015**, *25*, 2458-2466

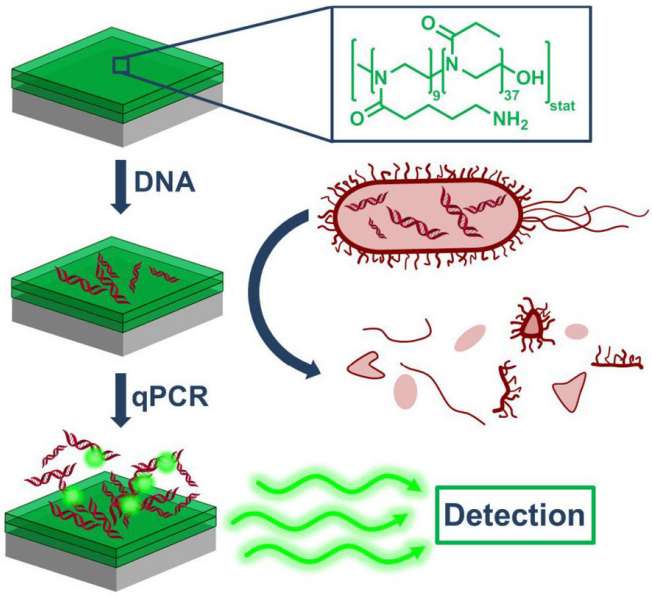

‡ Authors contributed equally.

ADVANCED FUNCTIONAL MATERIALS
www.afm-journal.de

Lab in a Tube: Purification, Amplification, and Detection of DNA Using Poly(2-oxazoline) Multilayers

*Meike N. Leiske, Matthias Hartlieb, Christian Paulenz, David Pretzel, Martin Hentschel, Christoph Englert, Michael Gottschaldt, and Ulrich S. Schubert**

Fast and easy purification and amplification of DNA are prerequisites for the development of point-of-care diagnostics. For this reason covalent coatings of amine containing poly(2-oxazoline)s (POx) on glass and poly(propylene) surfaces are prepared, to reversibly bind genetic material directly from biological samples. The polymer is deposited in a layer-by-layer process, whereas initial immobilization of macromolecules on the surface is accomplished by the use of an epoxy functionalized siloxane monolayer. Alternating treatment with polymer and cross-linker leads to the construction of amine containing POx multilayers on the substrates. Successful deposition is investigated by confocal laser scanning microscopy (using labeled polymers), contact angle measurements, as well as reflectometric interference spectroscopy. The interaction of these layer systems with DNA regarding binding and temperature dependent release is studied using labeled genetic material. Finally, polymerase chain reaction (PCR) vessels are coated with POx layers on the inside, and used for quantitative real-time PCR (qPCR) experiments. It is possible to bind genetic material directly from cell lysates to perform qPCR assays from surface adsorbed DNA within the same tube including amplification, as well as detection. The presented system displays an easy to use device for a point of care diagnostic.

1. Introduction

A reliable and time saving point-of-care diagnostic is one of the most important targets in bioanalytical science.[1] The optimal method would comprise an analysis of sample material directly on the spot, however, operating with the same accuracy as laboratory tests.[2] Moreover, cost efficiency is a major requirement in this context, rendering the design of new bioanalytical devices a highly challenging task.[3] The detection of diseases based on bacterial, fungal, or viral infections can be accomplished by the investigation of the pathogens nucleic acid profiles,[4] providing the opportunity of a fast determination and a targeted medication.[5] The recognition of the genetic material can be accomplished via specialized DNA assays,[6] e.g., based on microchip systems.[7] However, this presents only the last step in bioanalytics. The isolation of nucleic acids from whole tissue and cell samples and, in particular, the separation from proteins is still a prerequisite for downstream analytical processes. The general steps of nucleic acid purification include 1) tissue and/or cell lysis, 2) inactivation of cellular nucleases, and 3) separation of the desired nucleic acids from the cell debris.[8] To separate proteins from genetic material, phenol-chloroform extraction and density gradient centrifugation displayed the method of choice for many years.[8a,9] Besides the use of toxic substances,[9] these liquid phase based methods had the drawback of very time consuming and laborious working steps.[10] An enormous improvement was achieved in 1989, when the first solid phase extraction (SPE) system for DNA purification was described by McCormick et al.[8b] It has the advantage to separate nucleic acids from proteins more effectively, and without the generation of toxic by-products. Since its introduction, the SPE system evolved to the most common and easily adaptable purification method for genetic material.[11] Still, there are remaining disadvantages, such as the labor-intensive multiple washing procedures, the limited loading capacity of the silica matrix, as well as limitations in the extraction efficiency.[8a]

To overcome these restrictions, a challenging alternative approach is the binding of DNA within polymer matrices. Such scaffolds can be considered as a potential alternative for DNA immobilization, based on the fact that they have the potential of low cost production at large scales and mostly exhibit a biocompatible character.[12] Furthermore, they can be functionalized easily,[13] e.g., with positively charged groups, able to interact with the negatively charged phosphate backbone of polynucleotides.[14]

M. N. Leiske, M. Hartlieb, Dr. D. Pretzel, C. Englert, Dr. M. Gottschaldt, Prof. U. S. Schubert
Laboratory of Organic and Macromolecular Chemistry (IOMC)
Friedrich Schiller University Jena
Humboldtstr. 10, 07743 Jena, Germany
E-mail: ulrich.schubert@uni-jena.de
M. N. Leiske, M. Hartlieb, Dr. D. Pretzel, C. Englert, Dr. M. Gottschaldt, Prof. U. S. Schubert
Jena Center for Soft Matter (JCSM)
Friedrich Schiller University Jena
Philosophenweg 7, 07743 Jena, Germany
C. Paulenz, M. Hentschel
Analytik Jena AG
Konrad-Zuse-Str. 1, 07745 Jena, Germany
C. Paulenz
Institute of Pharmacy
Friedrich-Schiller-University
Philosophenweg 14, 07743 Jena, Germany

DOI: 10.1002/adfm.201404510

However, these polymers are mostly water soluble and, therefore, an assignment in biological, water based systems is not possible, since a separation from solution is difficult. For this reason, polymer-based hydrogels offer a great opportunity for a reversible DNA binding and release.[15] Because of their high water content and the resulting permeability of the 3D matrix, as well as the adjustable functionalities and a high surface to volume ratio, hydrogels represent attractive candidates for DNA immobilization. The suitability of poly(2-oxazoline) (POx) based hydrogels[16] and networks composed of POx–poly(ethylenimine) copolymers[17] was already investigated. The amine content and, therefore, the affinity to DNA are adjustable in both systems, resulting in a tunable DNA binding behavior. The combination of charged moieties with hydrophilic monomers such as 2-ethyl-2-oxazoline (EtOx) results in water swellable networks able to interact with genetic material. Furthermore, a release can be induced by the addition of heparin which replaces the DNA, generating eluates compatible with subsequent polymerase chain reaction (PCR) based DNA amplification.[16] However, the diffusion of genetic material within the gel is the limiting factor preventing fast purification procedures. Additionally, also non- or low-charged residues from cell lysis could be entrapped within the pores of the gel and, hence, interfere with downstream processes.

Surface bound polymer coatings are a potential way to overcome the drawbacks discussed above and combine the advantages of hydrogels with diffusion independent, surface mediated processes. The covalent immobilization of POx on glass substrates was already demonstrated in the context of low-fouling coatings;[18] however, to the best of our knowledge, no investigations regarding their bioanalytical potential are reported. A major requirement for DNA purification systems is their compatibility with subsequent PCR processes which are indispensable for a later detection. The PCR was invented by Mullis in 1983 and enveloped to one of the most important methods in bioanalytical science.[19] Via PCR, a few copies of a specific sequence of genetic material can be amplified by the naturally thermostable enzyme polymerase,[20] using specifically, synthesized oligonucleotides (primers) for the gene-of-interest.[19] The process itself consists of three steps:[21] 1) The denaturation (melting), 2) the primer annealing to the specific gene sequences, and 3) the elongation at a polymerase-specific temperature. Without PCR, DNA detection would be impossible due the low amounts of genetic material in biological samples.[22] However, the PCR process is limited by the purity of the bioanalytical samples, as well as by the template DNA amount.[23] Cellular components, remaining from cell lysis or other impurities, can interfere with the process and lead to nonexponential amplification or even a complete inhibition of the process. Therefore, pure polynucleotide solutions with a high concentration are preferable.

In this contribution we describe the synthesis of POx based surface coatings, containing a defined amount of amine groups for DNA binding and release. The polymers are covalently immobilized in a layer-by-layer (LbL) approach, generating films of defined thicknesses, and DNA binding/release profiles. The coating procedure is established on glass and, subsequently, transferred to poly(propylene) (PP), being one of the most common and important materials in bioanalytics. After investigation of the DNA interaction on plain substrates, PCR tubes are coated on the inside, creating a system able to separate DNA from impurities and, moreover, amplify and detect specific sequences by quantitative real-time PCR (qPCR). Exploiting the temperature dependent DNA binding behavior of POx multilayers it is possible to extract and detect DNA directly from cell lysate rendering this "lab in a tube" system a highly versatile and likewise easy to use tool for pathogen detection.

2. Results and Discussion

2.1. Polymerization and Fluorescent Labeling

The synthesis of amine containing POx was reported previously by our group.[15] Briefly, a 2-oxazoline bearing a Boc protected amine group (BocOx) was used in a copolymerization with EtOx to yield a statistical copolymer having 24% of functional comonomer incorporated (P($EtOx_{35}$-*stat*-$BocOx_{11}$, **1**). Deprotection using trifluoroacetic acid (TFA) was applied to obtain amine containing POx (P($EtOx_{37}$-*stat*-$AmOx_9$, **2**) with a molar mass (M_n) of 4600 and a narrow size distribution. Recalculation of the composition by NMR measurements after deprotection resulted in a final AmOx content of 20% (**Table 1**). Since this polymer should be used as a surface coating material, labeling was conducted using fluorescent dyes (fluorescein-5-*N*-hydroxysuccinimide ester for polymer **3** or rhodamine B *iso*-thiocyanate for polymer **4**) which are able to react with amine groups to enable a later detection of deposits. The coupling reaction was performed using one equivalent of dye per polymer chain, leaving a sufficient amount of free amine groups for surface attachment and DNA interaction. The success of the dye functionalization was verified by size-exclusion chromatography (SEC) measurements, comparing the signal from the refractive index (RI)

Table 1. Selected characteristics of the synthesized polymers.

Polymer	Compound	Dye	M_n [gM^{-1}]	$Đ$	Degree of func. [%]	Absorption maximum [nm]	Emission maximum [nm]
1	P($EtOx_{35}$-*stat*-$BocOx_{11}$)	–	4600[a)]	1.30	–	–	–
2	P($EtOx_{37}$-*stat*-$AmOx_9$)	–	9300[b)]	1.13	–	–	–
3	P($EtOx_{37}$-*stat*-$AmOx_8$-*stat*-$FAmOx_1$)	Fluorescein	11 000[b)]	1.16	78	485	530
4	P($EtOx_{37}$-*stat*-$AmOx_8$-*stat*-$RAmOx_1$)	Rhodamine B	12 000[b)]	1.19	5	555	590

[a)]SEC measurements in chloroform; [b)]SEC measurements in DMAc.

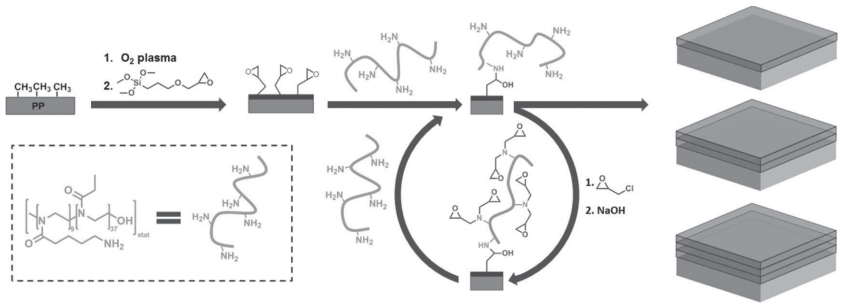

Scheme 1. Schematic representation of the deposition of P(EtOx$_{37}$-*stat*-AmOx$_9$) on substrates by LbL immobilization.

detector with the UV–vis signals. Purification (precipitation, and in the case of polymer **4** preparative size exclusion chromatography) was conducted until no trace of unbound dye was detected in the SEC traces. Overlapping RI and UV–vis traces prove a homogeneous functionalization of the polymeric material (Figure S1, Supporting Information). The efficiency of the labeling reaction was quantified by NMR spectroscopy (Table 1).

2.2. Surface Functionalization

The covalent attachment of amine functionalized POx to (activated) glass substrates was already reported by our group.[24] The method comprises the cleaning and activation by plasma and the subsequent deposition of a siloxane monolayer using 3-glycidyloxypropyl trimethoxysilane (GOPTMS). The epoxide groups of the siloxane layer react readily with the amine groups of the POx material to form a polymeric monolayer on the surface. While glass is a substrate frequently used for functionalization by silanization, also PP was utilized as a support material in this study since it is cheap, flexible, and relatively inert regarding biological processes. For this reason, the surface chemistry described before was transferred to PP. An overview over the performed coating procedures is depicted in **Scheme 1**.

To generate oxygen based functionalities on the highly inert substrate, O_2-plasma was applied. The oxidative conditions lead to the formation of OH groups and other oxygen based functionalities on the surface.[25] These functional groups can be used to attach a siloxane monolayer of GOPTMS. The present epoxide groups were subsequently quenched by the reaction with the amine groups of polymers **2**, **3**, or **4**. The success of the reaction could be verified by contact angle (CA) measurements determining the surface energy, as well as by fluorescence using confocal laser scanning microscopy (CLSM).

To optimize the amount and homogeneity of the deposited POx, the O_2-plasma treatment time, as well as the GOPTMS incubation temperature was altered since coating experiments with conditions described for glass resulted in heterogeneous coated surfaces. Additionally, the incubation time of the polymer was varied between 1, 2, and 24 h. The success of coating experiments was analyzed via CA and CLSM measurements (**Figure 1**). The CA measurements revealed that the hydrophobic character of untreated PP (CA = 88°) decreases after activation with O_2 plasma (CA = 36°), most probably due to the formation of hydroxyl groups. These oxygen functionalities react with GOPTMS to form a monolayer on the surface (CA = 25). After coating with polymer **4**, the hydrophilicity increases (CA < 20°) as a result of the covalently bound macromolecules. According to the CA results, there are no differences in the coating efficiencies for varying incubation times. CLSM measurements at λ_{ex} = 543 nm (λ_{em}: 560–615 nm) were performed for all coated slides, as well as for the blank substrates measuring an increase of fluorescence after coating with fluorescently labeled POx (**4**). The fluorescence intensity does not change significantly by varying either coating conditions or POx incubation time; however, the film homogeneity does, which is indicated by the standard deviation of the signal. An O_2 plasma treatment of 30 min and 1 h GOPTMS incubation at

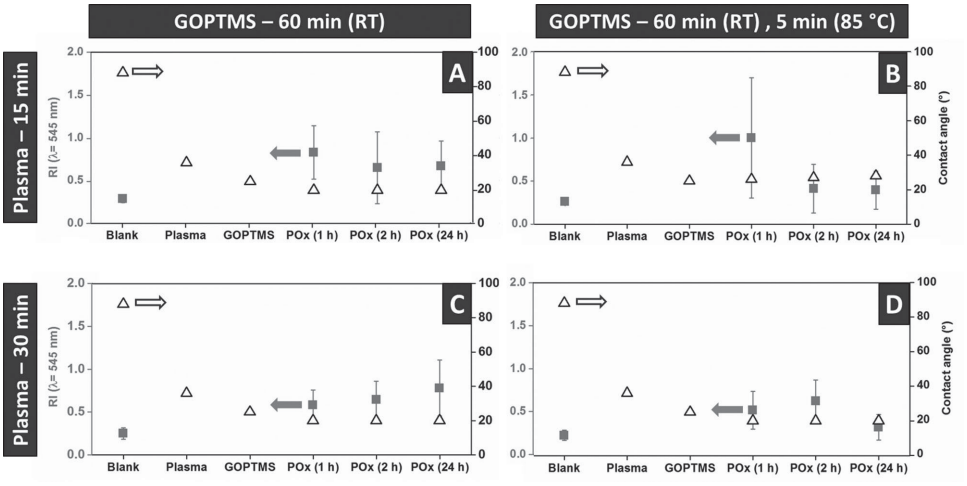

Figure 1. Optimization of the coating conditions for POx (**3**) on PP. The plasma incubation time was investigated using A,B) 15 min or C,D) 30 min of treatment. GOPTMS incubation was performed for A,C) 60 min at RT, or B,D) with an additional heat treatment for 5 min at 85 °C. POx coating was performed for 1, 2, or 24 h at 50 °C. Success and homogeneity of the coating procedure was verified by CA and CLSM.

Table 2. Analytical data of the multilayer POx coatings.

Coating step	CA [°]	POx amount by TGA [wt%]	Layer thickness (on glass) [nm]
Blank	100	–	0.0
O_2 plasma	80	–	0.6
GOPTMS	48	–	0.8
1st POx layer	<20	0.7	3.5
ECH	57	n. d.	n. d.
2nd POx layer	<20	1.3	28.4
ECH	72	n.d.	n.d.
3rd POx layer	<20	1.8	109.4

room temperature (RT) were chosen as the best activation and functionalization conditions because of a high mean fluorescence in combination with the most homogenous distribution of polymer on the surface within a reasonable time (Figure 1C).

2.3. LbL Assembly

The aim of this work is the production of POx coatings having a defined thickness to tailor the strength of interaction with the genetic material. To this end, an LbL deposition method was conducted to produce multilayers of amine containing POx on PP. The general procedure is shown in Scheme 1, starting with the already described deposition of a POx coating on a GOPTMS monolayer. Subsequently, the remaining amine groups were activated by the use of an excess of epichlorohydrin (ECH). The epoxide groups of this cross-linker molecule react with primary and secondary amines present in the first POx layer resulting in tertiary amine groups. In a second step, alkaline conditions are applied, leading to a reformation of an epoxide ring, based on the elimination of hydrochloric acid. The generated epoxide groups can be used to attach a second layer of POx as described before. This cycle can be repeated to immobilize a defined amount of POx layers on the substrate. Within this study films composed of up to three layers were produced. A first indication of a successful layer deposition was generated by CA measurements (**Table 2**). The blank PP substrate produced high CA values due to the hydrophobicity of the material.

Plasma activation, as well as GOPTMS deposition reduces the CA significantly, indicating an effective functionalization. Upon the attachment of POx, the CA decreases below 20° which displays the minimum measurable CA. The activation using ECH cross-linker yields CA values above 50° which is decreased again below 20° upon the addition of another POx layer. This behavior of surface energy changes is in perfect agreement with the successful deposition of POx in an LbL approach.

To gain further insights into the system, thermogravimetric analysis (TGA) experiments were conducted. Pure PP substrates, as well as POx (**2**) were subjected to thermal combustion. The weight loss as a function of temperature was recorded revealing different decomposition temperatures (Figure S2, Supporting Information).

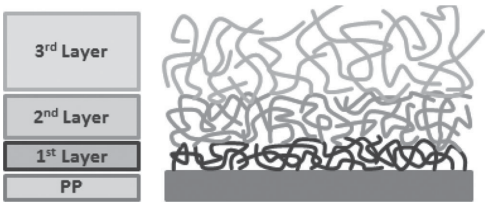

Figure 2. Schematically representation of water-swollen POx multilayers.

Using this information it is possible to calculate the amount of deposited POx on PP from the TGA measurements of the coated samples (Table 2). The relatively linear mass increase per POx layer indicates a homogeneous LbL deposition.

Further analysis of the POx coating was conducted using reflectometric interference spectroscopy (RIFS) measurements. The method determines the thickness of layers on glass substrates having a reflective Ta_2O_5 layer on the opposite site of the coating by measuring the peak shift of light reflected by the polymer layers.[26] For this purpose, glass slides were coated applying the conditions used for PP and analyzed accordingly (Table S1, Supporting Information). During the measurements, a water flow was channeled over the POx surface continuously to generate information about the swollen layers. The exponential increase of the layer thickness is, at first sight, inconsistent with the information obtained from TGA. A varying cross-linking density of individual layers could be an explanation for this discrepancy. The first layer is attached to the substrate via the reaction with epoxide groups directly on the surface, generating a flat film of polymer chains. With every additional layer the mobility of the epoxide binding sites increases generating more loosely bound and mobile POx layers able to incorporate more water into the polymeric matrix, describing the transition from a surface coating to an immobilized hydrogel (**Figure 2**).

As a final proof of the LbL deposition, fluorescence analyses were performed using polymer **3**. All investigated PP slides were coated with three POx layers; however, fluorescently labeled POx was only used in the first, second, or third coating step, respectively. For the other two layers, polymer **2** was used. In this way samples with one fluorescently labeled POx layer and two unlabeled layers are obtained. Every coating step was investigated using CLSM measurements (**Figure 3**). The pictures illustrate the control over the layer deposition by the applied method. A significant increase in fluorescence upon coating with polymer **3** shows the successful immobilization of the material (e.g., A1). The fluorescence signal remains relatively constant upon the addition of further layers (e.g., A2 and A4) proving the existence of LbL structures on the surfaces.

2.4. DNA Binding and Release

The ability of the presented POx films to adsorb genetic material in a reversible manner is a prerequisite for the aimed application. First tests were conducted using the RIFS method (BIAffinity) as described before, however, using DNA solutions instead of pure water to swell the POx layers. Differences at the peak minimum (500 nm) enable information about the layer

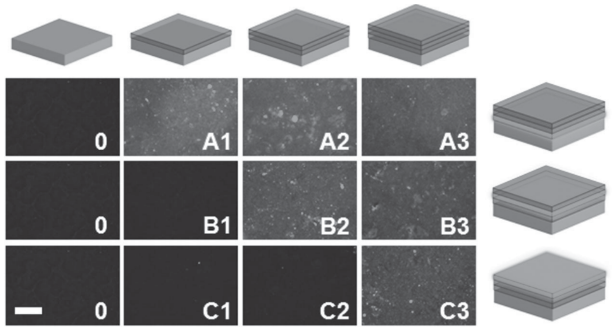

Figure 3. CLSM pictures of fluorescently labeled POx multilayers. Polymer **3** was used for the A) first, B) second, or C) third polymer layer. Pictures were captured of blank PP (0), and after the first (1), second (2), as well as third (3) coating step at a wavelength between 505 and 530 nm. Scale bar: 200 µm.

thickness which, in the end, allows a conclusion about the relative amount of bound DNA (**Figure 4**).

Slides containing a POx monolayer do not show a significant swelling upon addition of DNA while the thickness of coatings with two as well as three polymer layers increases. This trend correlates well with the increase of the hydrogel character per deposited layer. A weaker interconnection between the polymer chains of a film leads to a higher DNA adsorption due to the incorporation of DNA molecules within the layer and an increased interaction between amine groups and the DNA backbone. However, the presence of DNA as a polyanion could also lead to an alteration of the swelling behavior without a distinct binding.

To track the fate of the genetic material in the presence of POx multilayers directly by CLSM investigations, Cy5-labeled DNA strands were used. These measurements allow a quantification of the amount of bound DNA on the substrate assuming that the fluorescence emission increases proportional to the amount of immobilized genetic material. Cy5-labeled DNA lacZ segments were synthesized via PCR using Cy5-labeled primers. After amplification, the PCR products were purified and analyzed via gel electrophoresis. The DNA amount was determined using UV–vis spectroscopy (ScanDrop250).

The time required to establish an equilibrium between bound and unbound DNA is crucial for a later application since

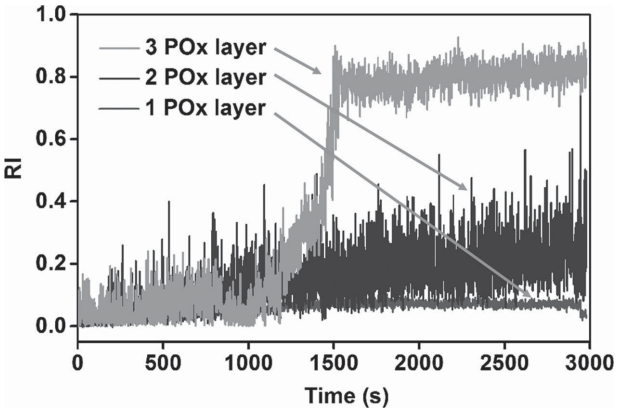

Figure 4. RIFS measurements using a DNA solution of 100 ng µL^{-1} to swell POx multilayers.

it determines the velocity of the first step of, e.g., pathogen detection. To this end, the immobilization of labeled DNA on POx multilayers was investigated (**Figure 5**A). PP chips with a defined surface (78 mm^2) were covered with a water droplet (15 µL) containing 1.5 µg of DNA for a defined time. To exclude an unspecific interaction, the chips were subsequently washed with water at RT.

The CLSM measurements show an increase of fluorescence emission that is proportional to the incubation time of Cy5-labeled DNA strands. Chips containing one POx layer do not show a pronounced uptake behavior which is assumedly a result of the diminished swelling of this monolayer preventing an efficient uptake of the oppositely charged species. In contrast, PP chips with two POx layers reveal an increase in fluorescence up to 5 min incubation time. PP chips with three POx layers show a constant increase in emission up to 2 h. Those results indicate a correlation between the amount of polymer layers and the total DNA adsorption. It is assumable that the hydrogel-like character of chips coated with three layers of POx results in an increasing impact of diffusion processes on the DNA adsorption which is not pronounced for the two-layered systems.

As the polymer associated DNA will be used for surface mediated PCR experiments, the ability of a controllable DNA release behavior is likewise important. Since the genetic material must be available for the polymerase to be amplified, a quantitative release is preferable.

For these experiments, chips loaded for 1 h with the above described procedure were subjected to a temperature dependent washing process (Figure 5B). DNA release studies were not performed for chips containing one polymer layer, due to the fact that the long incubation times necessary for binding makes them unfavorable for further studies. All samples were investigated regarding Cy5 fluorescence before and after the release was accomplished resulting in a percentage amount of released genetic material. The measurements show a release of around 40% of the initially bound DNA at a temperature of 65 °C or above representing ideal conditions for PCR experiments, since the temperature in the amplification cycles varies between 57 and 95 °C. Since no significant improvement regarding DNA binding and release is achieved by the deposition of three instead of two POx layers, further experiments were conducted using a POx double layer.

2.5. PCR Experiments

One major advantage of the presented method is the possibility of coating PP substrates enabling a larger variety in the design of analytical systems. Up to now, only 2D PP slides were used for polymer immobilization. For detection applications, however, it would be favorable to apply POx layers on the inside of PCR reaction vessels. For this reason, PP-tubes (RoboStrip PP white 8-well strips low profile) were coated using the already described procedure. The success of the coating was verified using CLSM measurements of layers deposited using polymer **3** (Figure S3, Supporting Information). However, for qPCR experiments, unlabeled polymers (**2**) were used to avoid interference with fluorescence based detection process. To demonstrate the

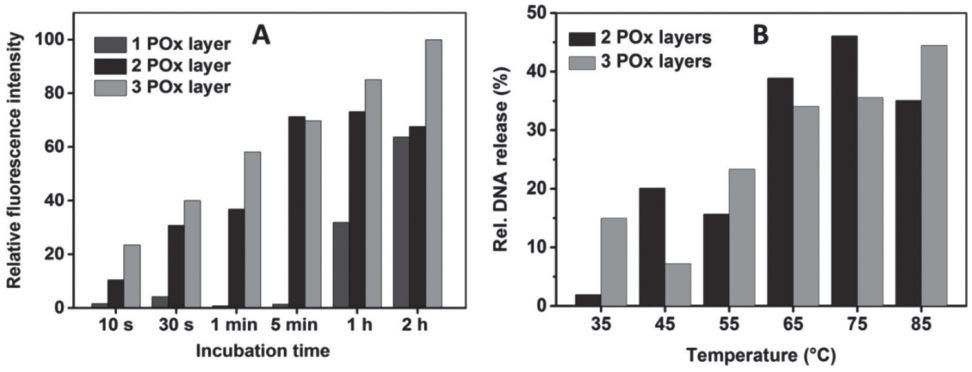

Figure 5. Adsorption and release of Cy5 labeled DNA by POx multilayers. A) Time dependent uptake of labeled genetic material determined by mean fluorescence of POx multilayers after treatment. B) Temperature dependent release of POx multilayers loaded with DNA for 1 h displayed as percentage of the initially bound DNA amount.

convenience of the "lab in a tube"-approach, qPCR assays were performed using coated PCR tubes.

In first experiments, DNA from *Escherichia coli* BL21 (*E. coli*) was extracted with innuPREP DNA Mini Kit (AJ Innuscreen GmbH, Berlin), bound within POx coatings for 1 h at RT, and washed thoroughly. The DNA loaded tubes were filled with 10 µL of qPCR master mix and subjected to qPCR. The assay detects specific gene sequences, like the LacZ-Gene as *E. coli* specific target, by the use of specific primer sequences which only bind to the desired gene. A schematic representation of the whole process is displayed in **Scheme 2**.

The cycle threshold (c_t) value of the qPCR assay shows at which cycle the DNA has reached a defined concentration providing an indication about the efficiency of the process and the amount of available template. After amplification, a positive result is reported by the melting peak of the PCR product, as detected by the use of intercalating dyes. In the case of LacZ, the melting curve of the product should exhibit a peak around 87.5 °C. This melting-point is equivalent to the expected product of 224 base pairs (GenBank sequence accession number: AM946981.2). The results of the detection of extracted *E. coli* samples are shown in **Table 3** and the amplification curves as well as melting points are depicted in Figure S4, Supporting Information. Uncoated tubes with additional template served as a positive control, whereas, a PCR experiment without sample DNA was used as a negative control.

The qPCR result of surface bound DNA is positive for the specific *E. coli*-target and the amplicon shows the same characteristic melting point as the positive control. Also the assay is able to detect *E. coli* DNA in the presence of a background of Herring testes DNA, proving the working principle in the presence of undesired genetic material.

However, for an easy and cost-effective sample analysis it is necessary to bind DNA directly from a cell lysate instead of using already purified genetic material. Consequently, the presence of other (charged) cellular components has to be tolerated. Therefore, an *E. coli* suspension (1.36×10^9 cfu mL^{-1}) was incubated for 10 min at 95 °C to lyse the cells by heat induction. Each 50 µL of this cell lysate were filled in POx modified tubes and incubated for 1 h. To investigate the influence of temperature to the binding behavior during the incubation, the tubes were incubated at 25, 35, 45, 55, and 65 °C (incubation performed on BioShake iQ with adapter for 96×0.2 mL tubes) and the supernatant solution was removed at the specific temperature. Every incubation temperature step was tested positive for *E. coli* DNA with a melting point around 87.3 °C with no detectable melting point on negative control (**Figure 6**).

As shown in the box-plot the c_t values of the qPCR decrease with increasing temperature which indicates a faster amplification process. Generally, the c_t value is dependent on the amount of accessible template (a higher initial DNA concentrations leads to lower values) and the presence of inhibitors

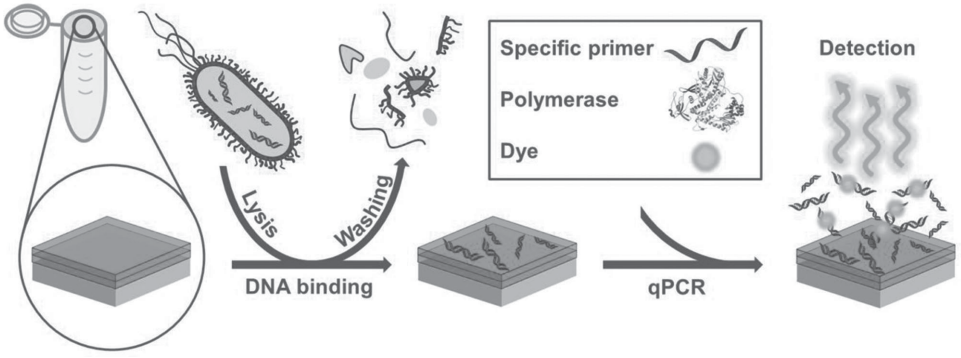

Scheme 2. Working principle of the "lab in a tube" approach. Cells are lysed by heat treatment and genetic material is adsorbed in POx surface coatings. After addition of a specific primer and a PCR master mix, amplification and detection is accomplished in a qPCR process.

Table 3. Results of *E. coli* detection from extracted DNA using the LacZ-gene as target. The amount of bound DNA within the POx coatings could not be determined.

Template	Sample	Amount of DNA [ng]	Melting point [°C]	Mean c_t value	Sample count
E. coli	Positive control	0.6	87.3	16.4	3
	Negative control	0	–	–	3
	Surface bound	n. d.	87.5	20.5	4
E. coli + Herring testes	Positive control	1	87.5	13.7	3
	Negative control	0	–	–	4
	Surface bound	n. d.	87.2	20	4

which increase the c_t value by lowering the efficiency of the reaction. Since the amount of bound DNA is not increasing at higher temperatures (Figure 5B) the latter reason is presumably responsible for the faster amplification. A further indication is given by a narrowing of the value distribution at higher temperatures.

To explain this behavior, the complex composition of the cell lysate can be accounted. While DNA has a high density of negative charge, also other former cell components have potentially negative charges and can interact with the POx layers. The presence of these compounds leads to a disturbance or inhibition of the PCR process, resulting in high c_t values. However, the binding affinity of negatively charged material decreases with increasing temperature, as already demonstrated by temperature dependent release studies (Figure 5B). It is likely that these compounds are released from the POx layers at lower temperatures than the DNA with its multiple negative charges. At 65 °C, the majority of contaminants are present unbound in solution and can be washed away while a considerable amount of genetic material is still adsorbed to the polymer layers, accessible for a subsequent amplification. The performed experiments demonstrate the suitability of POx modified surfaces for a qPCR detection of DNA. Due to the compatibility of the modified PP surface with the qPCR process a combination of sample purification and detection in a single tube or cavity is possible.

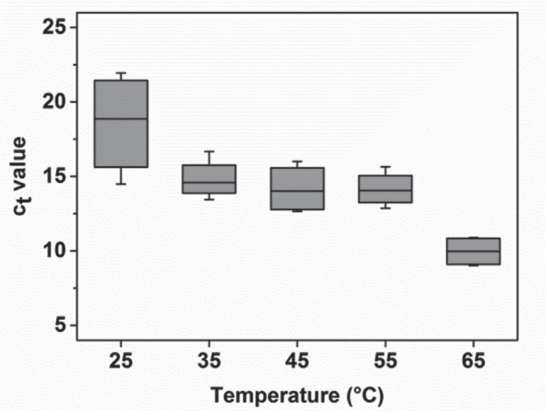

Figure 6. Box-plot of qPCR experiments, performed in POx coated reaction vessels. The tubes were loaded with genetic material from cell lysates at different temperatures and the c_t value of the amplification was recorded.

3. Conclusion

We demonstrated the production of a poly(2-oxazoline) (POx)-based separation and detection system for pathogen analysis without prior purification steps. Covalent amine containing POx multilayers was deposited on PP substrates in a layer-by-layer process. The affinity of DNA to the surface coatings was studied in detail and the binding and release was found to be temperature dependent. PCR tubes, coated with POx were used to bind and purify DNA directly from cell lysates and the amplification of genetic material can be accomplished directly from the adsorbed DNA templates. Moreover, detection can be performed using a qPCR assay. The presented system displays an easy and elegant way to collect sample DNA from biological materials, as well as to perform purification, amplification, and detection within just one coated PCR tube. The method is likewise effective and easy-to-use while requiring only low amounts of functional polymer coating. The straight forward preparation of the layer system and the cost efficiency of the support material should enable for large scale production and automation of detection processes. For this reason, this "lab-in-a-tube" displays a promising tool for bioanalytics. Further studies have to show how reliable the method is concerning varying samples sources, primers and in which concentration ranges a successful detection is possible.

4. Experimental Section

Material and Instrumentation: All chemicals were purchased from Sigma-Aldrich and Merck. 2-Ethyl-2-oxazoline (EtOx) and methyl tosylate (MeTos) were distilled to dryness under argon atmosphere prior to usage. PCR ingredients as well as polypropylene (PP) substrates were provided by Analytik Jena. PP slides (1 × 3 cm) were used for optimization of the coating procedure and verification of the LbL deposition (CA and CLSM measurements). Round PP-chips with a diameter of 0.5 cm were utilized for TGA investigations as well as DNA binding and release studies. For PCR experiments, PCR-tubes (RoboStrip PP white 8–well strips low profile) were coated on the inside. 2-(4-((*tert*-Butoxycarbonyl)amino)butyl)-2-oxazoline (BocOx) was synthesized according to a published procedure.[15]

The polymerization was performed under microwave irradiation, using an Initiator Sixty single-mode microwave synthesizer from Biotage, equipped with a noninvasive IR sensor (accuracy: 2%). Microwave vials were heated overnight to 100 °C under vacuum and allowed to cool to RT under argon before usage. Polymerizations were performed under temperature control.

SEC of the protected statistic copolymers was performed on a Shimadzu system equipped with a SCL-10A system controller, a

LC-10AD pump, a RID-10A RI detector, and a PSS SDV column with chloroform-triethylamine (TEA)-2-propanol (94:4:2) as eluent. The column oven was set to 50 °C.

SEC measurements of the deprotected statistic copolymers and the fluorescently labeled macromolecules were accomplished an a Shimadzu system equipped with a LC-10AD pump, a RID-10A RI detector, a degasser DGU-14A, and a CTO-10A column oven utilizing *N,N*-dimethylacetamide with 2.1 g L^{-1} LiCl as eluent. The column oven was set to 50 °C. Poly(styrene) (PS) samples were used as calibration standards for both solvent systems.

Proton NMR spectroscopy (^{1}H-NMR) measurements were performed at RT on a Bruker AC 300 MHz spectrometer, using $CDCl_3$ or D_2O as solvents. The chemical shifts are given in ppm relative to the signal from the residual nondeuterated solvent.

Absorption and emission spectra of the fluorescently labeled POxs were recorded using the Tecan M200 Pro fluorescence microplate reader (Crailsheim, Germany) at wavelengths from $\lambda = 350$ to 800 nm.

Fluorescence images were obtained using a confocal laser-scanning microscope (CLSM 510 Meta, Zeiss, Jena, Germany), equipped with a 10× objective. Fluorescein-labeled polymers were excited with the 488 nm line of the argon laser. The emitted fluorescence was collected using a 505–530 nm band-pass filter. Scans for the rhodamine-labeled polymers were accomplished using the 543 nm line of the He/Ne laser. The fluorescent emission was recorded with a 560–615 nm band-pass filter. To excite the Cy5-labeled DNA, the He/Ne 633 nm laser was used. Fluorescence was recorded using a 650 nm long-pass filter. To allow a comparison, all images were captured under identical conditions and instrument settings (laser power, pinhole diameter and detector gain). Quantitative image analysis was performed on grayscale converted images using the ImageJ software.

The hydrophilicity of the substrate surfaces was determined using a CA measuring system (OCA 30, Dataphysics, Germany) with droplets of distilled water having a volume of about 10 µL. The measurements were performed in triplicates on different positions of the surface area of the substrates at RT.

TGA was performed under a nitrogen atmosphere on a Netzsch TG 209 F1 Iris in the range from RT to 800 °C with a heating rate of 10 K min^{-1}. The amount of surface bound POx was calculated at a temperature of 280 °C comparing uncoated and coated samples.

The RIFS (BIAffinity) the swelling and DNA binding measurements were accomplished in a new set up, the parallel flow device (Analytik Jena AG), using a flow rate for polymer swelling of 20 µL min^{-1} and for the gDNA binding a flow rate of 5 µL min^{-1} at RT. During DNA binding experiments 100 µL of a gDNA *E. coli* BL21 solution (100 ng μL^{-1}) was injected and channeled in Channel 1 over the coated chip surface and in Channel 2 over the coated chip surface parallel with pure water. The residual DNA content was determined by UV–vis spectroscopy (ScanDrop250).

*Synthesis of P(EtOx$_{35}$-stat-BocOx$_{11}$) (**1**)*: In a microwave vial EtOx (35.3 µL, 0.35×10^{-3} M), MeTos (17.7 µL, 0.12×10^{-3} M), and acetonitrile (2.6 mL) were mixed under inert conditions. After heating in the microwave synthesizer at 140 °C for 19 min EtOx (530 µL, 5.95×10^{-3} M) and BocOx (350 µL, 0.70×10^{-3} M) were added under inert conditions and the reaction mixture was heated to 140 °C for another 13 min. The solution was diluted in CH_2Cl_2 (10 mL) and precipitated in cold diethyl ether (300 mL). The white solid was filtered off and dried in high vacuum to obtain the product as a white powder (810 mg, 88%). ^{1}H NMR ($CDCl_3$, 300 MHz): $\delta = 4.99$ (s, 0.2 H, NH), 3.45 (s, 4 H, backbone), 3.11 (s, 0.3 H, CH_2-CH_2-NH (BocOx)), 2.40 (s, 1.9 H, CH_2 (EtOx)), 1.92 (s, 0.3 H, CH_2-CH_2-CO (BocOx)), 1.64 (s, 0.3 H, CH_2-CH_2-CH_2 (BocOx)), 1.53 (s, 0.3 H, CH_2-CH_2-CH_2 (BocOx)), 1.42 (s, CH_3 (BocOx)), 1.21 (s, 1.3 H, CH_3 (EtOx)) ppm. SEC (eluent: $CHCl_3$-i-propanol-TEA, PS-standard): $M_n = 4600$ g M^{-1}, $M_w = 6000$ g M^{-1}, $Đ = 1.30$.

*Synthesis of P(EtOx$_{37}$-stat-AmOx$_9$) (**2**)*: TFA (10 mL) was added to solid P(EtOx$_{37}$-*stat*-BocOx$_{11}$) (810 mg), heated to 60 °C, and stirred for 1 h. Subsequently, the solution was cooled to RT, stirred for another 12 h, and was diluted by the addition of 10 mL methanol (MeOH) followed by precipitation in cold diethyl ether (500 mL). The white solid was filtered and redissolved in MeOH (50 mL). Amberlyst A21 free base was added and the mixture was stirred at RT for 24 h. The solid phase was filtered off and the solvent was evaporated under reduced pressure. The product was obtained as a slightly yellow powder (450 mg, 60%). ^{1}H-NMR (D_2O, 300 MHz): $\delta = 3.48$ (s, 4 H, backbone), 2.98 (0.23 H, s, CH_2-CH_2-NH_2), 2.23 (2 H, s, CH_2 (EtOx) + CH_2-CH_2-CO (AmOx)), 1.53 (0.41 H, s, CH_2-CH_2-CH_2-CH_2 (AmOx)) 1.11 (2.8 H, s, CH_3 (EtOx)) ppm. SEC (eluent: DMAc-LiCl, PS-standard): $M_n = 9300$ g M^{-1}, $M_w = 12\,000$ g M^{-1}, $Đ = 1.13$.

*Fluorescent labeling of P(EtOx$_{37}$-stat-AmOx$_9$) (**2**) with fluorescein-5-N-hydroxysuccinimide ester (Fluorescein-NHS-ester) (**3**)*: P(EtOx$_{37}$-*stat*-AmOx$_9$) (**2**, 1.35 g, 0.24×10^{-3} M) was dissolved in dimethylformamide (DMF, 50 mL) followed by the addition of the fluorescein-NHS-ester (112 mg, 0.24×10^{-3} M) and TEA (2.5 mL, 18×10^{-3} M). The reaction mixture was stirred at RT for 3 h. Subsequently, the solvent was evaporated and the crude product was redissolved in MeOH (10 mL). The polymer was precipitated in cold diethyl ether (800 mL), filtered and redissolved in MeOH (50 mL). The solvent was evaporated and the product was obtained as yellow powder (1.17 g, 80%). ^{1}H-NMR (D_2O, 300 MHz): $\delta = 6.60$–6.78 (m, 4.7 H, dye), 3.48 (s, 4 H, backbone), 2.98 (0.23 H, s, CH_2-CH_2-NH_2), 2.23 (2 H, s, CH_2 (EtOx) + CH_2-CH_2-CO (AmOx)), 1.53 (0.41 H, s, CH_2-CH_2-CH_2-CH_2 (AmOx)) 1.11 (2.8 H, s, CH_3 (EtOx)) ppm. SEC (eluent: DMAc-LiCl, PS-standard): $M_n = 11\,000$ g M^{-1}, $M_w = 13\,000$ g M^{-1}, $Đ = 1.16$

*Fluorescent Labeling of P(EtOx$_{37}$-stat-AmOx$_9$) (**2**) with Rhodamine B iso-thiocyanate (**4**)*: P(EtOx$_{37}$-*stat*-AmOx$_9$) (**2**, 300 mg, 0.05×10^{-3} M) was dissolved in DMF (20 mL). After addition of rhodamine B *iso*-thiocyanate (26.1 mg, 0.05×10^{-3} M), the reaction was stirred at RT for 48 h. Subsequently, the solvent was evaporated and the crude product was redissolved in MeOH (10 mL). The polymer was precipitated in cold diethyl ether (800 mL), filtered and redissolved in MeOH (50 mL). After evaporation of the solvent, the crude product was purified via preparative size exclusion chromatography (SEC) using bio beads SX-1 and DMF used as eluent. The product was obtained as a pink powder (280 mg, 86%). ^{1}H-NMR (D_2O, 300 MHz): $\delta = 6.70$–6.88 (m, 0.3 H, aromatic peaks), 3.48 (s, 133.2 H, backbone), 1.56 (s, 37.7 H, CH_2 (AmOx)), 1.11 (s, 111.0 H, CH_3 (EtOx)) ppm. SEC (eluent: DMAc-LiCl, PS-standard): $M_n = 12\,000$ g M^{-1}, $M_w = 14\,000$ g M^{-1}, $Đ = 1.19$.

Surface Coating: PP slides (3 × 1 cm), PP Chips (diameter = 0.5 cm), and PCR tubes were washed in a water/ethanol (EtOH) mixture (1:1) for 24 h. The dried material was treated with O_2 plasma for 30 min. Subsequently, the slides were incubated in an excess of GOPTMS molten on the substrates at RT for 1 h and cleaned by washing with DMF repeatedly.

The epoxide functionalized PP was coated in a layer-by-layer (LbL) approach. First, the substrates were incubated in a POx solution (10 wt%, DMF) at 50 °C for 1 h and washed with DMF to create the first polymer. Subsequently, the material was incubated in an ECH solution (1 wt%, DMF) at 50 °C for 1 h and washed with DMF as well as water. Afterwards, the slides were incubated in an aqueous sodium hydroxide solution (5 wt%) at 50 °C for 1 h and washed with water and DMF. This cycle was repeated, until the desired amount of POx layers were deposited on the glass slides. The same procedure was used for BIAffinity glass slides (10 mm × 10 mm; thickness: 1.1 mm; single-sided coated with Ta_2O_5).

DNA Binding and Release: DNA binding and release experiments were performed using Cy5-labeled lacZ amplificates that were synthesized by standardized PCR experiments from lacZ transfected *E. coli* BL21 using Cy5-labeled primers (SI). All experiments were conducted using PP chips coated with one, two, or three POx layers. In each case the first polymer layer was fluorescein labeled (polymer **3**). DNA solution (15 µL) containing 100 ng μL^{-1} Cy5 labeled lacZ DNA was added to the POx coated PP chips and incubated at RT for different times (10, 30 s, 2, 5 min, 1, 2 h). Afterwards, the chips were washed with water (5 × 500 µL) and dried using compressed air. Subsequently, the mean fluorescence was determined by LSM measurements ($\lambda_{ex} = 633$ nm, $\lambda_{em} \geq 650$ nm).

For release, the PP chips were loaded with DNA as described above for 1 h and, subsequently, incubated in water for 1 h at different temperatures. After separation from the solution and drying using compressed air, the mean fluorescence was determined via CLSM

Table 4. Used primer sequences.

Label	Target	Sequence	Nucleotides	Guanin and Cytosin content [%]	T_m [°C]
SekuLZF	LacZ	5′-cgcagcctgaatggc-gaatg-3′	20	60	61.4
SekuLZR	LacZ	5′-gtgagcgagtaacaaccc-gtcg-3′	22	59.1	64.0

(λ_{ex} = 633 nm, $\lambda_{em} \geq$ 650 nm) before and after treatment and the relative DNA release was determined by comparison of the two values.

PCR Experiments: The qPCR assay was designed to detect DNA of *E. coli* in a POx coated and uncoated cavities. Therefore, every qPCR experiment had a minimum three PP POx modified tubes with qPCR master mix and no template as negative control and 1 µL of DNA extract out of 10^7 cfu mL^{-1} *E. coli* as positive control. The qPCR master mix contains: 3×10^{-3} M of $MgCl_2$, 1 × Hot Start Buffer w/o $MgCl_2$ pH 8.5, 0.1×10^{-3} M dNTPs each, 0.025 U μL^{-1} InnuTaq HOT-A DNA polymerase (provided by AJ Innuscreen GmbH, Berlin), one EvaGreen (Jena BioScience GmbH, Jena), 1×10^{-6} M Primer (**Table 4**) each (Eurofins Genomics, Ebersberg), 3% dimethyl sulfoxide (DMSO) (Carl Roth GmbH + Co. KG, Karlsruhe). The qPCR protocol was optimized for sensitivity and specificity up to $<10^1$ cfu (data not shown). For amplification an initial denaturation for 2 min at 95 °C was followed by 10 cycles 95 °C for 5 s, 72 °C for 15 s and 30 cycles 95 °C for 5 s, 67 °C for 5 s, 72 °C for 10 s with one final amplification of 2 min at 72 °C. The qPCR products were analyzed by melting curve measurements with a temperature range from 60 to 95 °C. The whole qPCR was performed using a TOptical Gradient Thermocycler (Biometra GmbH, Göttingen)

Supporting Information

Supporting Information is available from the Wiley Online Library or from the author.

Acknowledgements

M.N.L. and M.H. contributed equally to this work. The authors gratefully acknowledge the Bundesministerium für Bildung und Forschung (Germany) for funding (project: BASIS, 03WKCB01C). We thank to Renzo Paulus for TGA measurements and Dr. Stephanie Höppener for helpful discussions.

Received: December 19, 2014
Published online: March 16, 2015

[1] a) A. Moody, *Clin. Microbiol. Rev.* **2002**, *15*, 66; b) B. C. Ross, L. Marino, F. Oppedisano, R. Edwards, R. M. Robins-Browne, P. D. Johnson, *J. Clin. Microbiol.* **1997**, *35*, 1696; c) A. J. Herring, N. F. Inglis, C. K. Ojeh, D. R. Snodgrass, J. D. Menzies, *J. Clin. Microbiol.* **1982**, *16*, 473.
[2] M. Bally, M. Graule, F. Parra, G. Larson, F. Hook, *Biointerphases* **2013**, *8*, 4.
[3] P. L. Kole, G. Venkatesh, J. Kotecha, R. Sheshala, *Biomed. Chromatogr.* **2011**, *25*, 199.
[4] a) K. Zro, S. Azelmat, Y. Bendouro, J. H. Kuhn, E. El Fahime, M. M. Ennaji, *J. Virol. Methods* **2014**, *204*, 38; b) N. C. Engleberg, B. I. Eisenstein, *Annu. Rev. Med.* **1992**, *43*, 147.
[5] A. T. Press, A. Traeger, C. Pietsch, A. Mosig, M. Wagner, M. G. Clemens, N. Jbeily, N. Koch, M. Gottschaldt, N. Bézière, V. Ermolayev, V. Ntziachristos, J. Popp, M. M. Kessels, B. Qualmann, U. S. Schubert, M. Bauer, *Nat. Commun.* **2014**, *5*, 5565
[6] A. Sassolas, B. D. Leca-Bouvier, L. J. Blum, *Chem. Rev.* **2007**, *108*, 109.
[7] L. Schwenkbier, S. König, S. Wagner, S. Pollok, J. Weber, M. Hentschel, J. Popp, S. Werres, K. Weber, *Microchim. Acta* **2014**, *181*, 1669.
[8] a) C. W. Price, D. C. Leslie, J. P. Landers, *Lab Chip* **2009**, *9*, 2484; b) R. M. McCormick, *Anal. Biochem.* **1989**, *181*, 66.
[9] A. Paterson, C. Brubaker, J. Wendel, *Plant Mol. Biol. Rep.* **1993**, *11*, 122.
[10] P. Chomczynski, N. Sacchi, *Anal. Biochem.* **1987**, *162*, 156.
[11] J. M. Bienvenue, N. Duncalf, D. Marchiarullo, J. P. Ferrance, J. P. Landers, *J. Forensic Sci.* **2006**, *51*, 266.
[12] a) C. R. Reedy, C. W. Price, J. Sniegowski, J. P. Ferrance, M. Begley, J. P. Landers, *Lab Chip* **2011**, *11*, 1603; b) J. Lunt, *Polym. Degrad. Stab.* **1998**, *59*, 145.
[13] J. M. Pollino, M. Weck, *Chem. Soc. Rev.* **2005**, *34*, 193.
[14] L. Zhai, R. L. Pilston, K. L. Zaiger, K. K. Stokes, R. D. McCullough, *Macromolecules* **2002**, *36*, 61.
[15] M. Hartlieb, D. Pretzel, K. Kempe, C. Fritzsche, R. M. Paulus, M. Gottschaldt, U. S. Schubert, *Soft Matter* **2013**, *9*, 4693.
[16] M. Hartlieb, D. Pretzel, C. Englert, M. Hentschel, K. Kempe, M. Gottschaldt, U. S. Schubert, *Biomacromolecules* **2014**, *15*, 1970.
[17] C. Englert, L. Tauhardt, M. Hartlieb, K. Kempe, M. Gottschaldt, U. S. Schubert, *Biomacromolecules* **2014**, *15*, 1124.
[18] L. Tauhardt, K. Kempe, M. Gottschaldt, U. S. Schubert, *Chem. Soc. Rev.* **2013**, *42*, 7998.
[19] K. B. Mullis, H. A. Erlich, N. Arnheim, G. T. Horn, R. K. Saiki, S. J. Scharf, *US Patent No.* US4683195 A, **1987**.
[20] a) M. A. Innis, K. B. Myambo, D. H. Gelfand, M. A. Brow, *Proc. Natl. Acad. Sci. USA* **1988**, *85*, 9436; b) R. Saiki, D. Gelfand, S. Stoffel, S. Scharf, R. Higuchi, G. Horn, K. Mullis, H. Erlich, *Science* **1988**, *239*, 487; c) A. M. Wang, M. V. Doyle, D. F. Mark, *Proc. Natl. Acad. Sci. USA* **1989**, *86*, 9717.
[21] B. I. Eisenstein, *N. Engl. J. Med.* **1990**, *322*, 178.
[22] N. Wellinghausen, C. Frost, R. Marre, *Appl. Environ. Microbiol.* **2001**, *67*, 3985.
[23] J. Ning, J. Liebich, M. Kästner, J. Zhou, A. Schäffer, P. Burauel, *Appl. Microbiol. Biotechnol.* **2009**, *82*, 983.
[24] L. Tauhardt, M. Frant, D. Pretzel, M. Hartlieb, C. Bucher, G. Hildebrand, B. Schroter, C. Weber, K. Kempe, M. Gottschaldt, K. Liefeith, U. S. Schubert, *J. Mater. Chem. B* **2014**, *2*, 4883.
[25] K. T. Lee, J. M. Goddard, J. H. Hotchkiss, *Packag. Technol. Sci.* **2009**, *22*, 139.
[26] O. Birkert, G. Gauglitz, *Anal. Bioanal. Chem.* **2002**, *372*, 141.

ADVANCED FUNCTIONAL MATERIALS

Supporting Information

for *Adv. Funct. Mater.,* DOI: 10.1002/adfm.201404510

Lab in a Tube: Purification, Amplification, and Detection of DNA Using Poly(2-oxazoline) Multilayers

*Meike N. Leiske, Matthias Hartlieb, Christian Paulenz, David Pretzel, Martin Hentschel, Christoph Englert, Michael Gottschaldt, and Ulrich S. Schubert**

Supporting Information

Lab in a tube: Purification, amplification and detection of DNA using poly(2-oxazoline) multilayers

*Meike N. Leiske,[‡] Matthias Hartlieb,[‡] Christian Paulenz, David Pretzel, Martin Hentschel, C. Englert, Michael Gottschaldt, Ulrich S. Schubert**

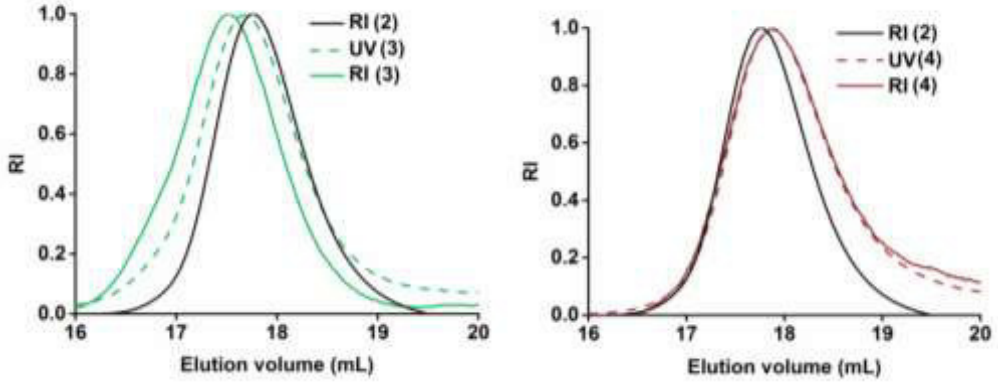

Figure S1: SEC elugrams of labeled polymers (**3** and **4**) in comparison to the unlabeled staring material (**2**).

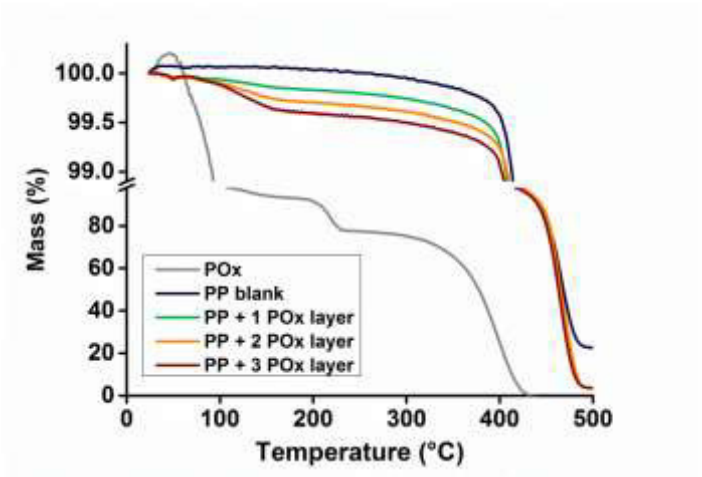

Figure S2: TGA graphs of uncoated PP, pure POx, as well as substrates coated with one, two or three layers of POx.

Table S1: CA values for POx deposition on biaffinity glass. * CA values below 20 ° cannot be measured and are, therefore, specified as < 20 °.

Coating step	CA (°)

Blank	59
O_2 plasma	< 20*
GOPTMS	43
1st POx layer	< 20*
ECH-XL	43
2nd POx layer	< 20*
ECH-XL	44
3rd POx-layer	< 20*

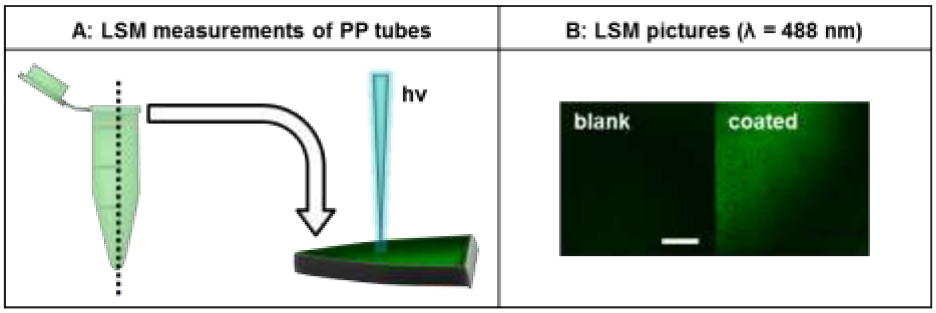

Figure S3: CLSM measurements (λ_{ex} = 488 nm, λ_{em}: 505 to 530 nm) of coated PCR Tubes. A) Scheme of the bisection of PP PCR tubes and measurement on the inner wall; B) comparison of emission between blank value and POx coated tube (scale bar: 200 µm).

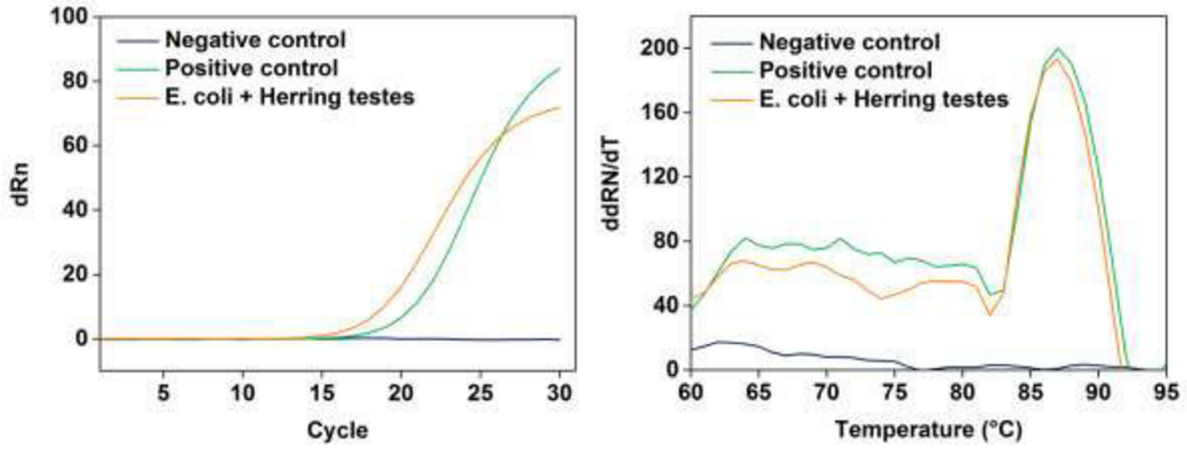

Figure S4: Amplification curves and melting points of qPCR assays using *E. Coli* + Herring testes.

PCR of DNA from lacZ transfected Escherichia coli BL21

Target	Sequence	Product size (base pairs)	Label
LacZ	5'-Cy5-GGA TTG ACC GTA ATG GGA TAG-3'	228	Cy5
LacZ	5'-biotin-CTG GCG TAA TAG CGA AGA GG-3'	228	Biotin

DNA was isolated using the innuPREP DNA/RNA Mini Kit, according to the manufacturer's instructions (Analytik Jena AG). An *E. coli* BL21 pellet was re-suspended in 100 µL TE-buffer to induce cell lysis. Subsequently, 450 µL lysis buffer RL were added and the mixture was incubated at room temperature for 3 min. The mixture was centrifuged at 14,000 rpm for 1 min to separate the lysed from the unlysed parts. A spin filter D was placed on a receiver tube, the supernatant was added and centrifuged at 12,000 rpm for 2 min. 500 µL HS washing solution was added and the mixture was centrifuged for at 12,000 rpm for 1 min. Afterwards, 700 µL lysis buffer were added and the combined solution was centrifuged at 12,000 rpm for 1 min. The filtrate was discarded and the spin filter D containing the extract was added to another receiver tube and centrifuged at 14,000 rpm for another 2 min. Subsequently, a spin filter D was added to an elution tube and, after addition of 100 µL elution buffer, it was incubated at room temperature for 1 min. The mixture was centrifuged at 8,000 rpm for 1 min to obtain the DNA extract into the elution tube. Finally, the DNA concentration was determined *via* UV/VIS spectroscopy (ScanDrop®250) ($\lambda_{1, ex}$ = 260 nm, $\lambda_{2, ex}$ = 280 nm).

The PCR assay was carried out in a 50 µL reaction mixture containing the following compounds: DNA extract (0.5 µL of ~10 ng μL^{-1}), 1.00 units Taq DNA polymerase (AJ innuTaq DNA polymerase), 0.25 mM desoxy-nucleotriphosphates (dNTPs), 0.5 µM of each primer. The PCR was started with an initial denaturation for 3 min at 95 °C followed by 45 cycles with 95 °C for 30 s (denaturation), 57 °C for 30 s (annealing) and 72 °C for 30 s (amplification). At the end of the repeated PCR cycles, the mixture was heated to 72 °C for another 5 min to ensure the completion of the amplificates elongation. The purity of the crude PCR product was controlled by gel electrophoresis, which was performed using a 2% agarose gel containing GelRed (1:25,000). The gels were run for 30 min at 100 V with TAE-buffer, which consists of Tris acetate (2 mol L^{-1}) and EDTA

(0.05 mol L^{-1}), dissolved in deionized water and has a pH value of 8.2 to 8.4 at RT. The gels were imaged on a UV transilluminator (AJ Biometra UVsolo TS).

All PCR and qPCR products were purified using the innuPREP PCRpure Kit, according to the manufacturer's instructions (Analytik Jena). 500 µL binding buffer were added to a spin filter positioned on an elution tube and then spin coated at 12,000 rpm for 2 min. Subsequently, the spin filter was placed into a receiver tube, 10 µL of elution buffer were added and incubated at RT for 1 min, before spin coating at 8,000 rpm for 1 min. Finally, the DNA concentration was determined *via* UV/VIS spectroscopy (ScanDrop®250) ($\lambda_{1,\,ex}$ = 260 nm, $\lambda_{2,\,ex}$ = 280 nm). Since the generated PCR products contained both, biotin- and Cy5-labeled DNA, the biotin-labeled DNA amplificates could be used for the horseradish peroxidase assay and the Cy5-labeled DNA sequences for DNA binding and release determinations based on the DNA derived fluorescence emission intensity.

PUBLICATION 10

Core cross-linked nanogels based on the self-assembly of double hydrophilic poly(2-oxazoline) block copolymers

M. Hartlieb, D. Pretzel, M. Wagner, S. Höppener, P. Bellstedt, M. Görlach, C. Englert, K. Kempe, U. S. Schubert

J. Mater. Chem. B, **2015**, *3*, 1748-1759

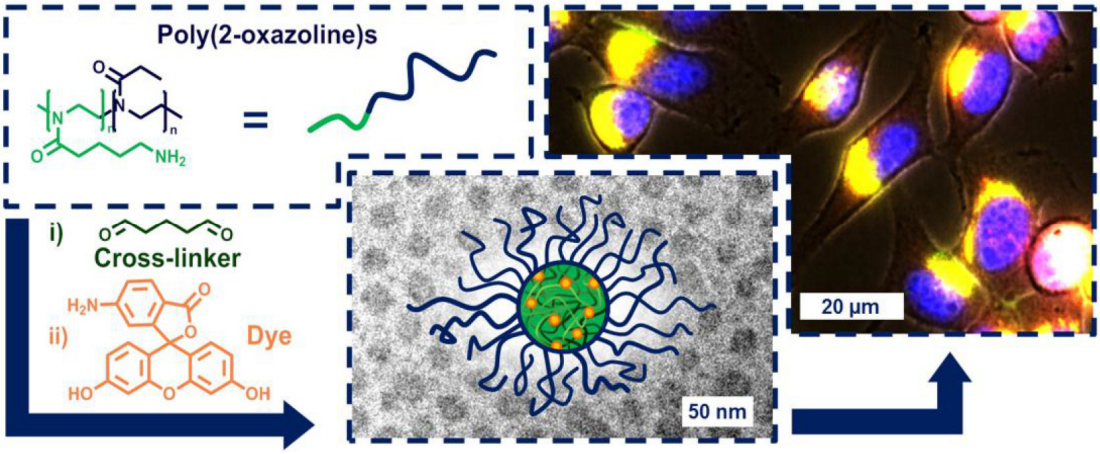

Volume 3 | Number 9 | 7 March 2015 | Pages 1733–2014

Journal of Materials Chemistry B

Materials for biology and medicine

www.rsc.org/MaterialsB

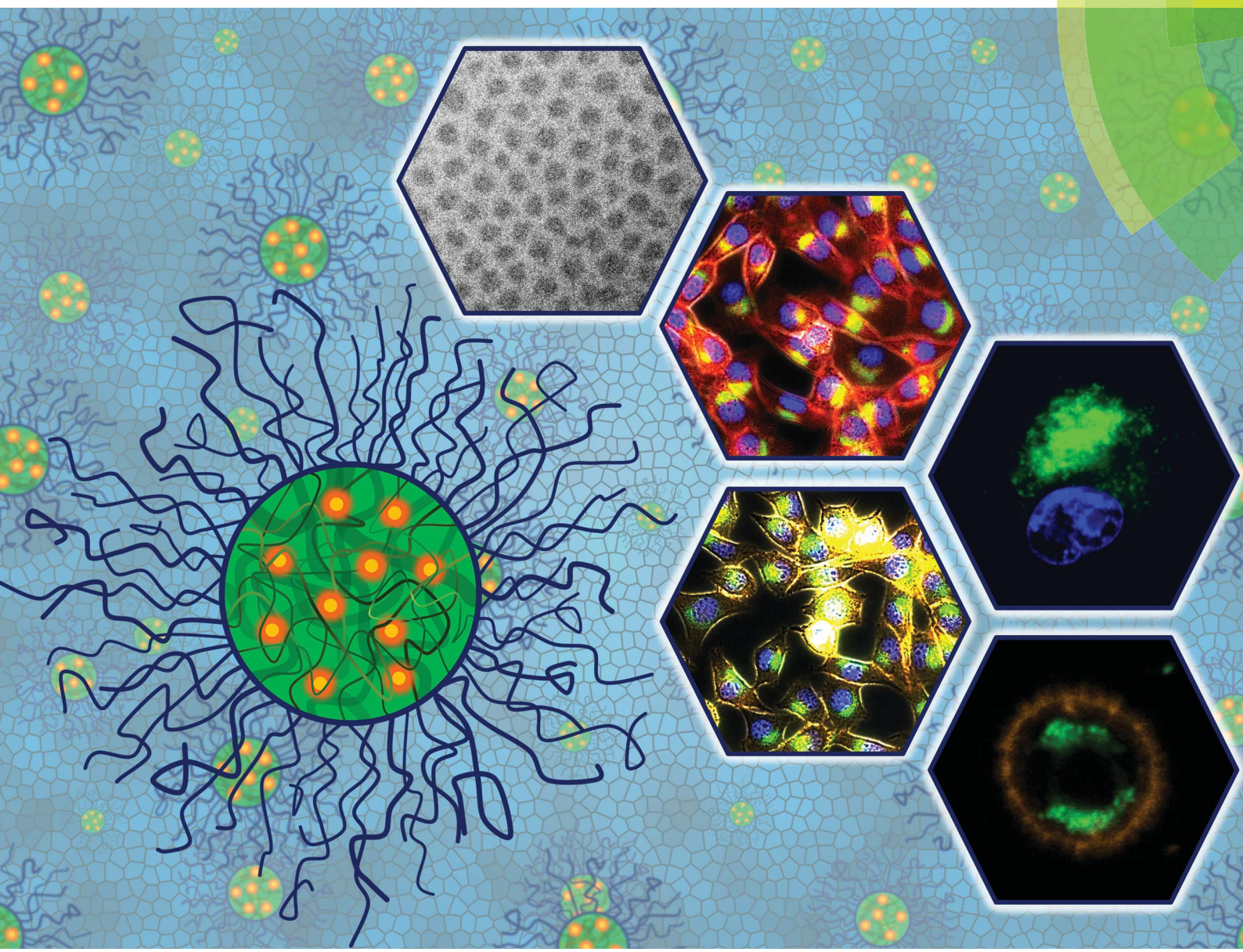

ISSN 2050-750X

ROYAL SOCIETY OF CHEMISTRY

PAPER

Ulrich S. Schubert *et al.*

Core cross-linked nanogels based on the self-assembly of double hydrophilic poly(2-oxazoline) block copolymers

Journal of Materials Chemistry B

PAPER

View Article Online
View Journal | View Issue

Cite this: J. Mater. Chem. B, 2015, 3, 1748

Core cross-linked nanogels based on the self-assembly of double hydrophilic poly(2-oxazoline) block copolymers†

Matthias Hartlieb,[ab] David Pretzel,[ab] Michael Wagner,[ab] Stephanie Hoeppener,[ab] Peter Bellstedt,[c] Matthias Görlach,[c] Christoph Englert,[ab] Kristian Kempe‡[ab] and Ulrich S. Schubert*[ab]

Received 15th December 2014
Accepted 13th January 2015

DOI: 10.1039/c4tb02069c

www.rsc.org/MaterialsB

The synthesis of poly(2-oxazoline)-based block copolymers consisting of a cationic and a hydrophilic segment is described. The self-assembly of these macromolecules in organic solvents results in the formation of micelles and vesicles, respectively, depending on the solvent used. To transfer the systems into water, cross-linking using glutaraldehyde was applied, followed by the consumption of excessive aldehyde functions by either diethylamine or 6-aminofluorescein (6AF). The cross-linked assemblies were analyzed regarding their size and shape by electron microscopy and light scattering methods, as well as for their chemical composition by solid state NMR spectroscopy. 6AF associated samples were examined with respect to their absorption and fluorescence behavior in aqueous environment, revealing an alkaline microenvironment within the presented nanostructures. The toxicity of the systems against mouse fibroblast cell line L929 was examined by the XTT assay and was found to be insignificant for concentrations of up to 2.5 mg mL^{-1}. Flow cytometry and fluorescence microscopy analysis revealed an efficient concentration and time dependent cellular uptake of the nanogels.

Introduction

The term nanomedicine refers to the use of nanoscopic objects in medical applications like drug delivery and has received considerable attention in recent years.[1,2] The utilization of drug carriers, such as liposomes, polymeric micelles, vesicles, nanoparticles, and dendrimers offers numerous advantages. Besides potential control over pharmacokinetics and toxicity, the solubilization and protection of the drug is of paramount interest. In particular, polymeric micelles are frequently studied for the administration of hydrophobic compounds.[3] Such micelles are formed *via* the aqueous self-assembly of block copolymers consisting of hydrophilic and hydrophobic segments.[4] While the hydrophilic shell reduces non-specific interactions with tissue and blood components, the hydrophobic core contains and protects the therapeutic and/or diagnostic molecule. The critical micelle concentration (CMC) of polymeric micelles is rather low (10^{-6} to 10^{-7} mol L^{-1}) as compared to surfactant based nanocarriers (10^{-3} to 10^{-4} mol L^{-1}).[5] However, even above their CMC a component exchange or a disassembly is possible. As a consequence, Lammers and co-workers have recently proposed that cross-linking of such systems and covalent attachment of the cargo are paramount prerequisites for their successful application.[6] Nanogels are covalently cross-linked structures in the nanometer size range and combine beneficial properties of hydrogels (*e.g.* tissue-like structure, biocompatibility, and stimuli responsiveness)[1] with the solubility properties of nano-assemblies, such as nanoparticles or micelles. There are several ways for the production of these structures such as the use of inverse emulsions[7] or *via* polymerization induced phase separation, respectively.[8] One particularly elegant way is the cross-linking of self-assembled structures.

In this context, type and properties of the polymeric material serving as precursor for nanogels are highly important. Besides a well-controlled polymerization process as a prerequisite to yield highly defined block copolymers, the biocompatibility and functionality of the resulting polymers is of outstanding interest.

[a]Laboratory of Organic and Macromolecular Chemistry (IOMC), Friedrich Schiller University Jena, Humboldtstrasse 10, 07743, Jena, Germany. E-mail: ulrich.schubert@uni-jena.de

[b]Jena Center for Soft Matter (JCSM), Friedrich Schiller University Jena, Philosophenweg 7, 07743, Jena, Germany

[c]Biomolecular NMR Spectroscopy, Leibniz Institute for Age Research – Fritz Lipmann Institute, Beutenbergstr. 11, 07745 Jena, Germany

† Electronic supplementary information (ESI) available: Materials and instrumentation; NMR and SEC plots of polymers (Fig. S1 and S2); cloud-points of P(EtOx-*b*-AmOx) (Fig. S3); AF4 data of polymers (Table S1); DLS plots for nanostructures in organic solvent (Fig. S4) and water (Fig. S5); AF4 plots of cross-linked structures (Fig. S6); NMR of assembled structures (Fig. S7); solid state NMR of 6AF (Fig. S8); epifluorescence pictures of cells for FC analysis (Fig. S9); co-localization studies of micelles using epifluorescence (Fig. S10) and CLSM (Fig. S11). See DOI: 10.1039/c4tb02069c

‡ Current address: Department of Chemistry, University of Warwick, Gibbet Hill Road, Coventry, CV4 7AL, UK.

Poly(2-oxazoline)s (POx) represent a promising class of materials for biomedical applications. Such as poly(ethylene glycol) (PEG), poly(2-methyl oxazoline) (PMeOx) and poly(2-ethyl-2-oxazoline) (PEtOx) are highly soluble in water and organic solvents, biocomaptible[9,10] and exhibit stealth properties.[11,12]

The cationic ring-opening polymerization (CROP) of 2-oxazolines provides access to multifunctional polymers with a wide range of possible structural variations, using different functional initiators, terminating agents and functional monomers.[13] This versatility, in combination with the possibility to combine different monomers in distinct architectures, including statistical, gradient or block copolymers, renders the CROP of 2-oxazolines a powerful toolbox to produce functional polymers for biological applications.[14]

POx-based micellar structures were investigated thoroughly over the past decades.[15–21] This includes also studies on the incorporation of anti-cancer drugs.[22–24] However, up to date only a limited number of reports are available on the synthesis and potential of cross-linked POx aggregates. The type of cross-linking reaction is of central interest for designing drug delivery systems with sufficient stability and the ability to release their cargo on demand.[25] Covalently cross-linked POx micelles, stabilized by thiol-yne chemistry,[26,27] epoxide-amine cross-linking,[28] UV mediated cross-linking[29,30] as well as electron beam irradiation[31,32] have been described. To the best of our knowledge only one reversible system using a disulfide bond linker, is reported so far.[33]

Herein, we describe the synthesis of double hydrophilic POx-based block copolymers including a neutral (PEtOx) as well as a cationic (PAmOx) block and their self-assembly in organic solvents. The polymerization of 2-oxazolines carrying a protected amine group was first introduced by Cesana *et al.*[34] and is continuously developed.[35] The self-assembly of the polymers in organic solvents is investigated and the structures are cross-linked by Schiff-base chemistry and covalently loaded with 6-amino fluorescein as a model compound. This connection is known to be reversible[36] enabling a later disassembly. The nanogels were characterized intensively and their interaction with cells was investigated. They exhibit low toxicity and an endosomal localization.

Results and discussion

Polymer synthesis

In this study we describe the synthesis of block copoly(2-oxazoline)s and their self-assembly into nano-scaled objects. The block copolymer P(EtOx-*b*-AmOx) consists of a hydrophilic (EtOx) and a hydrophilic/cationic segment (AmOx). While PEtOx is known to be biocompatible[37,38] and soluble in a wide range of solvents, including water, the second block is (after deprotection) cationically charged due to the primary amine groups in the side chain and, therefore, lacks solubility in organic solvents.

The synthesis of P(EtOx-*b*-AmOx) is depicted in Scheme 1. The polymerization of EtOx, which constitutes the first block, was initiated by methyl tosylate (MeOTos) at 140 °C under microwave irradiation (see ref. 39 for optimized polymerization conditions). After close to full conversion ($\ln([M]_0/[M]_t) = 4$) of the first monomer, the living polymer was chain extended with 2-(4-((*tert*-butoxycarbonyl)amino)butyl)-2-oxazoline (BocOx), the Boc-protected precursor of the cationic AmOx segment, which was deprotected after termination of the polymerization using trifluoroacetic acid (TFA) and Amberlyst A21 solid phase catalyst to remove trifluoroacetate salts. By changing initiator-to-monomer ratios and polymerization times, block copolymers of

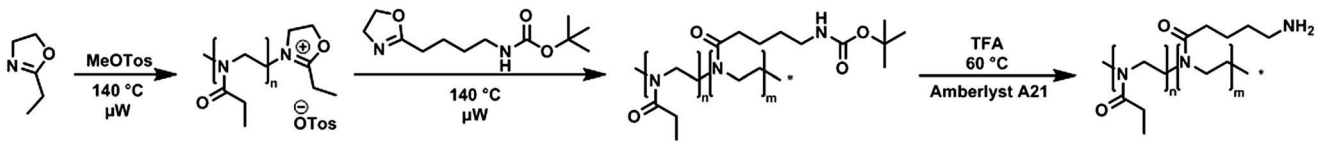

Scheme 1 Schematic representation of the synthesis of amphiphilic block copolymers (P(EtOx-*b*-AmOx)).

Table 1 Analytical data and composition of the prepared block copolymers

		NMR	SEC ($CHCl_3$)		SEC (DMAc)		AF4		
Sample	Composition	M_n [g mol^{-1}]	M_n [g mol^{-1}]	$Đ$	M_n [g mol^{-1}]	$Đ$	M_n [g mol^{-1}]	$Đ$	Co-monomer [%]
1	P($EtOx_{104}$)	10 300	9900	1.11	20 600	1.17			0
2	P($EtOx_{112}$-*b*-$BocOx_6$)	12 600	7700	1.18					5
3	P($EtOx_{92}$-*b*-$BocOx_{10}$)	11 600	7400	1.16					10
4	P($EtOx_{85}$-*b*-$BocOx_{15}$)	12 100	8900	1.20					15
5	P($EtOx_{84}$-*b*-$BocOx_{20}$)	13 200	8900	1.17					20
6	P($EtOx_{70}$-*b*-$BocOx_{22}$)	12 300	7600	1.18					22
7	P($EtOx_{113}$-*b*-$AmOx_5$)	12 000			14 500	1.34	11 700	1.10	5
8	P($EtOx_{92}$-*b*-$AmOx_{10}$)	10 600			16 800	1.23	9200	1.14	10
9	P($EtOx_{72}$-*b*-$AmOx_{18}$)	9700			16 100	1.22	13 300	1.10	18
10	P($EtOx_{82}$-*b*-$AmOx_{23}$)	11 400			18 100	1.23	13 600	1.09	22
11	P($EtOx_{64}$-*b*-$AmOx_{26}$)	10 100			15 600	1.30	12 500	1.26	29

different compositions were prepared, as summarized in Table 1. To investigate the length of the polymer chains, ^{1}H NMR investigations were conducted directly after polymerization and the integral of the initiator tosylate peaks was compared to the integral of the polymer backbone revealing total degree of polymerization (DP) values of around 100 for all macromolecules. The block ratios were calculated from the ^{1}H NMR spectra before and after deprotection, respectively (ESI: Fig. S1 and S2†). The difference in the calculated values can be explained by the overlap of solvent peaks with the EtOx–CH_3-group for polymers **2** to **6**, limiting the accuracy of the determination. After deprotection, these solvent peaks disappear and, thus, we refer in the following to the values obtained from the deprotected polymers. Size exclusion chromatography (SEC) measurements of protected polymers indicated M_n values around 10 000 g mol^{-1}. Low dispersity ($Đ$) values prove a narrow molar mass distribution of the synthesized block copolymers. After deprotection, SEC measurements of the block copolymers were performed in *N*,*N*-dimethyl acetamide (DMAc), a non-selective solvent for both blocks, showing an increase in M_n and $Đ$. However, due to the lack of cationic SEC standards a precise determination of M_n and $Đ$ is hardly possible. The comparison of the SEC derived M_n and $Đ$ values of the PEtOx homopolymer (which increases when changing the solvent to DMAc) indicated a similar size and uniformity of the protected and the deprotected polymers.

As a consequence, to gain further information about the size distribution of the cationic P(EtOx-*b*-AmOx) copolymers, asymmetric flow field-flow fractionation (AF4) investigations were performed. The measurements were carried out at a low pH value (3.5) to ensure a neutral or cationic charge of the membrane resulting in an electrostatic repulsion of the cationic samples to reduce adsorption phenomena. The obtained size values fit well with the expected values based on the monomer-to-initiator ratio and the M_n values derived from the ^{1}H NMR experiments. Since the determination of the molar masses was carried out using a multi-angle laser light scattering detector (MALLS) to obtain absolute molar mass values, the AF4 results are more reliable than the data derived from SEC measurements without available cationic calibration standards. Again, small $Đ$ values indicate narrow size distributions of the block copolymers. Nevertheless, the molar masses obtained by AF4 might be slightly overestimated as most probably some low molar mass fractions are washed out through the membrane (nominal cut-off 10 000 g mol^{-1}). This is supported by a recovery rate of around 75 to 85% (ESI: Table S1†).

Self-assembly, cross-linking and labeling of block copolymers

Since the LCST behavior of the polymers in aqueous solution could not be utilized for a self-assembly (ESI Fig. S3†) of P(EtOx-*b*-AmOx), the low solubility of the cationic block in organic solvents was exploited. First, the self-assembling behavior of P(EtOx-*b*-AmOx) (**7**–**11**) was screened in three organic solvents (MeOH, *i*PrOH and $CHCl_3$) using dynamic light scattering (ESI: Fig. S4†). The results of these measurements are summarized in Table 2. As expected, pure PEtOx showed no aggregation in these solvents. All block copolymers however formed structures in the range between 4 and 112 nm depending on the solvent and the composition. Surprisingly, the ratio between the two blocks did not influence the size of the aggregates as much as the polarity of the solvents used. All samples assembled in $CHCl_3$ formed structures with radii between 4 and 17 nm.

In *i*PrOH, size distributions between 68 and 105 nm were detected, and MeOH led to structures with even larger radii (77 to 113 nm). In dependence on the solvent and block ratio, most of the samples show rather high polydispersity indices, which can be traced back to the formation of a small fraction of aggregates. Therefore, only samples with low PDI values indicating narrow size distributions are selected for further experiments.

To transfer these structures into aqueous solution, the core of the agglomerates has to be cross-linked, as both polymer blocks are readily water soluble. For this purpose, two samples, exhibiting the most uniform size distribution in organic solvents were chosen (labeled with [a] in Table 2) and cross-linked with glutaraldehyde (GA) (Scheme 2). As a *bis*-aldehyde, GA is able to form imine bonds with the amine groups present in the core and, consequently, lock the structure of the assemblies. However, a direct transfer of the micelles into water yielded only hydrogels, which indicated that even though GA was added in stoichiometric amounts, a sufficient number of free amine and aldehyde groups remained to cross-link the colloidal structures among each other. As demonstrated by Lecommandoux and co-workers, the amount of cross-linked amine groups for such reactions is only about 35%, when aiming for a full conversion.[40] To overcome this drawback, low molar mass amines have to be added in large excess after the cross-linking step to consume the residual aldehydes. This strategy, in turn, does not only enable the stabilization of the self-assembled structure, but also allows the simultaneous incorporation of drug molecules or fluorescence labels into the system. Here, diethylamine

Table 2 DLS screening of the self-assembling behavior of the block copolymers in organic solvents (5 mg mL^{-1}; size indication in radius; number plot; no size value is specified, if the number weighted plot shows only the polymer precursor)

	0% AmOx (**1**)		5% AmOx (**7**)		10% AmOx (**8**)		18% AmOx (**9**)		22% AmOx (**10**)		29% AmOx (**11**)	
Solvent	R_h [nm]	PDI	R_h [nm]	PDI	R_h [nm]	PDI	R_h [nm]	PDI	R_h [nm]	PDI	R_h [nm]	PDI
MeOH	—	—	—	—	—	—	113	0.334	83	0.646	77	0.335
*i*PrOH	—	—	71	0.550	105	0.714	99	0.561	92	0.509	68[a]	0.111
$CHCl_3$	—	—	4	0.360	8	0.217	16	0.256	13	0.376	17[a]	0.048

[a] Samples selected for further cross-linking.

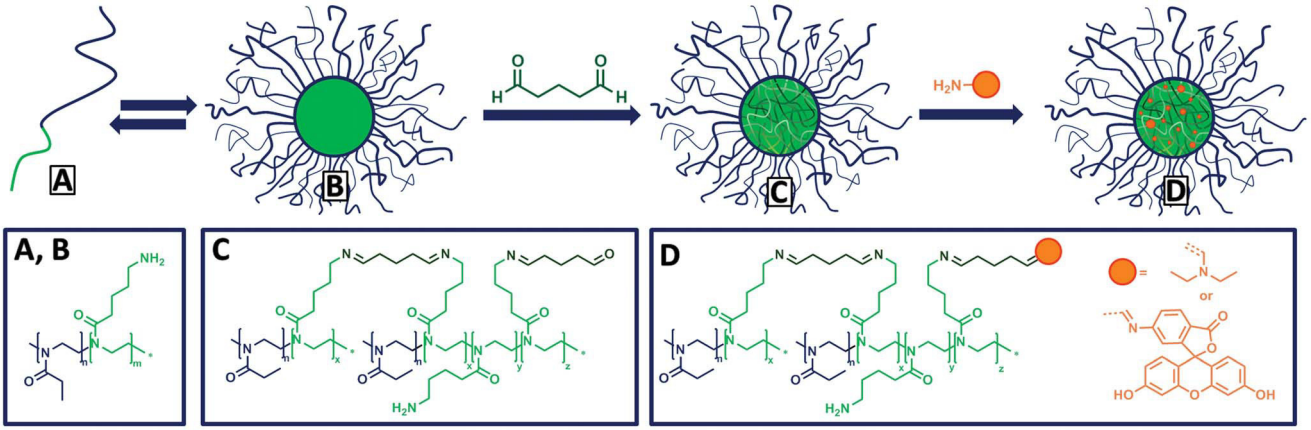

Scheme 2 Schematic representation of the self-assembly of P(EtOx-*b*-AmOx) followed by cross-linking and quenching/loading.

(DEA) and 6-amino fluorescein (6AF), respectively, were used as model substances to quench the cross-linking process. After this treatment the assembled structures could be transferred into aqueous solution, successfully.

Characterization of self-assembled structures by light scattering and electron microscopy

To purify the systems from unbound amine or cross-linker molecules, the crude products were precipitated in diethyl ether and dialyzed in a water–methanol mixture (4 : 1), where methanol acted as a solubility mediator for 6AF, which is barely soluble in water. A first indication of successfully cross-linked structures was provided by DLS experiments, which indicated distributions in the same size range as observed in organic solvents (Table 3, ESI: Fig. S5†). The PDI values of the locked systems increased slightly, which suggests an agglomeration caused by unconsumed aldehyde groups in the core.

However, the values are still in a good range for synthetic nano-sized objects. The zeta potential of all cross-linked assemblies was found to be positive, indicating the presence of free amine groups in the colloid.

A further investigation of size and uniformity was conducted using asymmetric flow field-flow fractionation measurements. Utilizing this technique it is possible to separate the samples by the diffusion coefficient and to determine the hydrodynamic radius (R_h, by online DLS measurements) and the radius of gyration (R_g, by multi-angle laser light scattering (MALLS) measurements). The data depicted in Table 3 (Graphs in ESI: Fig. S6†) are similar to the values obtained by DLS measurements. For samples originating from *i*PrOH the obtained AF4-DLS values are significantly smaller than the collected sizes from the DLS measurements, which can be attributed to the AF4 separation technique. While DLS investigations provide a radius comprising also small fractions of aggregates, after separation by AF4 single colloidal structures are examined. An additional information provided by this analysis is an indication of the particle shape by the comparison of both, hydrodynamic radius and radius of gyration, expressed in the ratio ρ ($\rho = R_g/R_h$). For particles assembled in $CHCl_3$, the R_g value could not be determined since they were too small for detection *via* the MALLS detector (limit around 15 nm).[41] This indicates a R_g below 15 nm and, hence, a ρ ratio less than 0.8, which is characteristic for hard spheres and, therefore, indicated a compact structure like a micellar architecture of the assembled particles.[42] Larger ratios (around 1) as obtained for *i*PrOH derived structures are usually attributed to less dense and soft structures, which might indicate vesicles.[42] A possible explanation for this trend is a swelling of the selective block induced by the different polarity of the solvents used. While the amine group has a potentially cationic charge, the side chain and the backbone of the block can be readily solubilized by organic solvents resulting in a gel-like core instead of a complete collapse of the AmOx segment. Upon increase of polarity of the applied solvent, swelling should concommittantly increase, resulting in a higher steric demand of the selective block, while

Table 3 Characterization data for cross-linked nanostructures (DLS: 5 mg mL^{-1}, size indication in radius). Polymer **11** served as precursor for all assemblies. The content of fluorescein was determined by the absorbance at 470 nm

Sample	Solvent for self-assembly	Capping agent	DLS in solvent		DLS in water			AF4			Content of capping agent (wt%)
			Size, R_h [nm]	PDI	Size, R_h [nm]	PDI	ζ [mV]	R_g	R_h	ρ	
12	$CHCl_3$	DEA	17	0.048	17	0.093	+7	—	19	<0.8	N. d.
13		6AF			15	0.199	+17	—	20.0	<0.8	29
14	*i*PrOH	DEA	68	0.111	59	0.246	+17	41	37	1.11	N. d.
15		6AF			50	0.179	+23	40	40.0	1.00	29

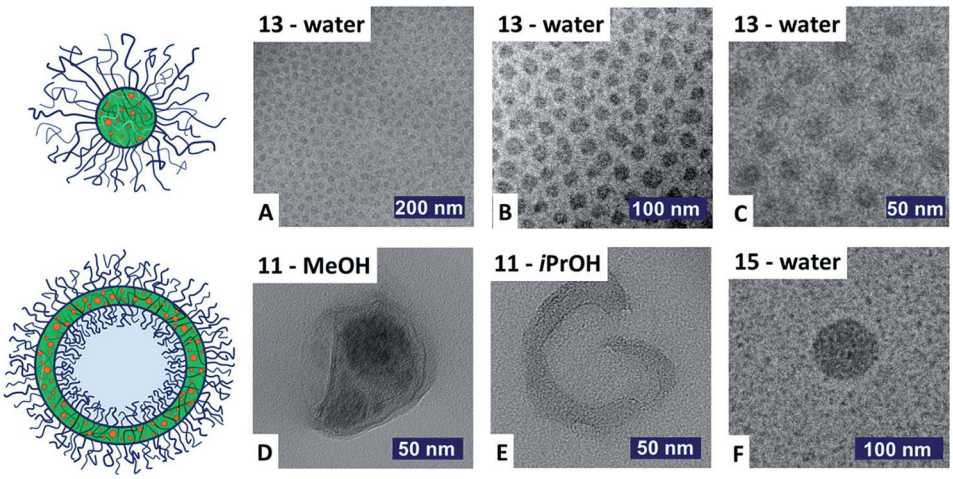

Fig. 1 TEM images of the dried structures assembled in methanol (D) and *i*PrOH (E), and cryoTEM images of self-assembled as well as cross-linked structures (A–C and F).

the hydrophilic PEtOx block reveals a similar solubilization in all solvents used. Thus, the transition from a micellar to a vesicular structure might be attributed to the change in the ratio between the volume of the two segments.[43] Considering the block architectures of P(EtOx-*b*-AmOx) and the fact that a fully stretched polymer chain is with roughly 32 nm length (calculated from the bond length; C–C = 154 pm, C–N = 135 pm under consideration of the bond angles) shorter than the radius of the assemblies, support a vesicular morphology of these samples.

To further investigate the proposed structures, (cryo) transmission electron microscopy (cryoTEM) measurements were performed. Samples in aqueous media (Fig. 1A–C and F) as well as non-cross-linked polymers in organic solvents were investigated (Fig. 1D and E). The non-cross-linked systems could be examined only in the dried state as vitrification of the solutions was not successful. However, structures found in samples derived from MeOH and *i*PrOH (Fig. 1D and E) might originate from the collapse of a vesicle shell, supporting the assumption of a vesicular architecture. The cryoTEM picture of the cross-linked equivalent (Fig. 1F) does not show a hollow sphere which could be attributed to hydrophilicity of the nanogel. The swelling of the structure in water reduces the contrast of the picture compared to TEM investigations in organic solvents. Based on the combined investigations the larger nanostructures will henceforth be referred to as vesicles. Nevertheless, we are aware, that this interpretation of AF4 and TEM data has to be treated with caution and that the hypothesis of a vesicular nanostructure is not fully proven.

Determination of 6AF loading and release

For samples which were loaded with 6AF, the amount of covalently bound dye was determined using its absorption and fluorescence properties. The absorption and emission spectra of 6AF-containing samples were measured in water at a pH value of 7 in order to compare the data to pure 6AF, which was measured in the presence of a 100-fold excess of GA to ensure a quantitative conversion to the imine form (Fig. 2). While 6AF shows the typical absorption and emission spectra of the lacton derivative at a pH value of 7 (low absorption, maximum at 440 nm), both, micelles as well as vesicles absorb and emit similar to the ring-opened di-anionic carboxy isomer state of the dye (Fig. 2A). This behavior seems best explained by the high density of amine groups in the core of the assemblies leading to a locally increased pH value, which, in turn, causes the formation of the di-anionic species characterized by a strong absorption at 490 nm.[44] A closer look at the photochemical behavior of the nano-assemblies shows that even at a pH value of 4 still a significant amount of 6AF emits indicating a alkaline microenvironment within the core of the nanostructures.

To determine the amount of loaded dye, samples were investigated in aqueous NaOH solution (0.1 mol L^{-1}) to ensure the quantitative presence of the carboxy-form of fluorescein in the 6AF calibration. For a better comparison with the bound dye, a 100-fold excess of GA was added to the free 6AF generating the imine derivative *in situ* as described before. Both, absorption as well as fluorescence spectra showed equal maxima and shape for the samples as well as calibration. The amount of incorporated 6AF was found to be 29 wt% of dye per total mass for the micelles, as well as for the vesicles. This is equivalent to 12 6AF molecules per polymer chain, which complies with the conversion of amine groups by GA in similar systems (~35%).[40] An equal loading for both nano-architectures was expected as the chemical composition of both systems should be identical, while only the shape varies.

Liquid and solid state (ss) NMR spectroscopy

While light scattering and electron microscopy experiments shed light on size and shape of the assemblies, they do not provide insights into their chemical composition. Liquid and solid state NMR spectroscopy were employed for a more detailed characterization. Both, micelles and vesicles yield non-turbid solutions in solvents such as water or chloroform. In the liquid state ^{1}H NMR spectra of non-cross-linked polymers in

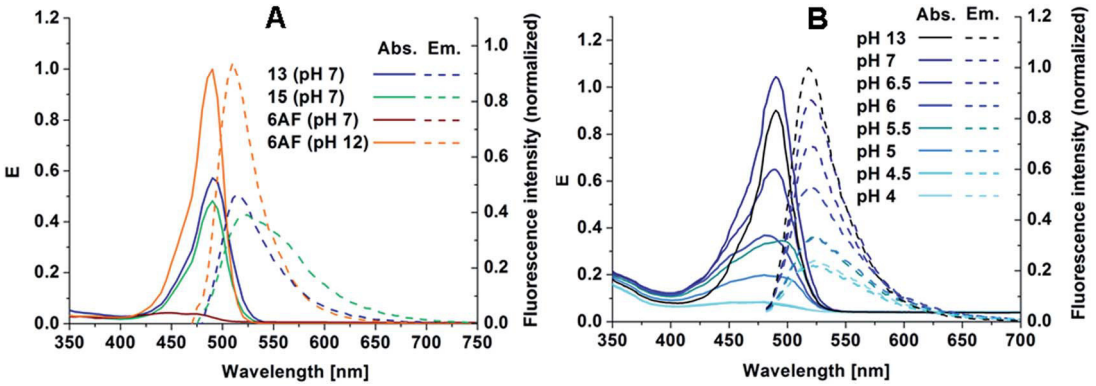

Fig. 2 (A) Absorption and fluorescence spectra of 6AF (pH dependent) and dye quenched nanostructures; (B) pH dependent absorbance and fluorescence of compound **15** (0.05 mg mL^{-1}).

$CHCl_3$ (ESI: Fig. S7†) solely signals of the PEtOx block are visible, probably as they represent highly mobile groups once in contact with the solvent. In contrast, cross-linking of the core is likely to physically link the mobility of individual core components to the overall rotational correlation time of the vesicle/micelle, thereby increasing the relaxation rate of the core components significantly and, hence, leading to an absence of signals attributable to the AmOx side chain, GA and DEA or 6AF, respectively.

To qualitatively assess the cross-linked system, natural abundance CP MAS solid state ^{13}C NMR spectroscopy was employed (Fig. 3). We assigned the prominent signals to the carbonyl functions (A), the backbone (D), and to the side groups (F) and (H), respectively of the abundant PEtOx units. Furthermore, the resonance (E) detectable at ~30 ppm represents two methylene groups of the AmOx side chain. The presence of the AmOx part is also supported by a resonance at 60 ppm (C). The shoulder at 20 ppm (G) is attributed to the outer methylene groups of the AmOx spacer and the GA methylenes. The GA gives in addition rise to a broad resonance at ~160 ppm (B) assigned to its C=N bond. It should also be noted that the GA groups are the least abundant ones in the cross-linked system. Taken together, these tentative assignments are compatible with the relative abundance, and hence, the observed relative intensities of the respective chemical groups. However, a bona fide quantitative assessment *via* integration of signals of the individual chemical groups, as typically performed in liquid state NMR, is not reliable due to the non-uniform efficiency of the cross-polarization transfer (CP) step in the ssNMR experiment and the significant line broadening observed which, in turn, preclude to identify individual groups. In addition, the comparably low intensities of the broad signals (B) and (C), suggest an under-representation of the core, which might be due to a conformational heterogeneity with concomitant line broadening in the cross-linked region. Likewise, signals for the 6AF are of an intensity lower than expected from the quantitative fluorescence analysis (Table 3). To assign resonances arising from the 6AF moiety, we compared commercial microcrystalline 6AF with amorphous and with KOH treated, ring-opened 6AF (ESI: Fig. S8†). From this comparison, we concluded that the signals detectable at 155 ppm, at 120 to 100 ppm and a shifted signal at 75 ppm arise from 6AF. Notably, already the conversion of microcrystalline into amorphous 6AF, produced by dissolving in MeOH, flash-freezing and lyophilisation, caused a severe line broadening in the ssNMR spectra of some of the 6AF resonances and other lines become virtually indetectable. This clearly indicates that a certain degree of conformational heterogeneity ('amorphousness') of the 6AF moiety causes severe line-broadening or in-detectability of some groups in the ssNMR spectra. In summary, we interpret the low intensity signal pattern of the 6AF moiety as resulting from differences in the CP transfer efficiency, severe line broadening and the mainly ring-open form (see Fluorescence experiments) and a residual proportion of amorphous 6AF, the latter giving rise to the signals at 155, 100 to 120 and 80 ppm, respectively.

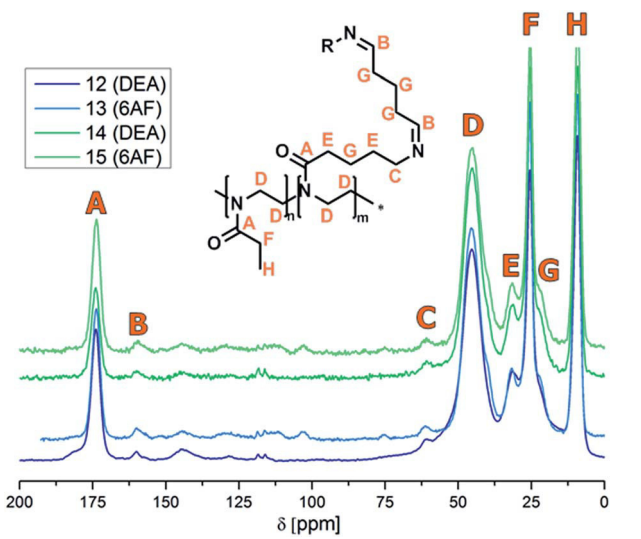

Fig. 3 Solid state ^{13}C NMR spectra of cross-linked micelles (samples **12** and **13**) and vesicles (samples **14** and **15**).

Biocompatibility of self-assembled structures

The evaluation of the biocompatibility is one of the first steps to assess the applicability of the micellar/vesicular structures presented herein for potential biomedical applications. Hence,

adverse effects on the cellular metabolism upon incubation with 6AF labeled micelles (sample **13**) and vesicles (sample **15**) were evaluated using the established L929 cell line, which is characterized and documented by its sensitivity towards cytotoxic agents.[45]

The *in vitro* cytotoxicity experiments were performed *via* a XTT assay according to the German standard institution guideline DIN ISO 10993-5 as a reference for biomaterial testing. After 24 h of incubation with different micelle/vesicle concentrations (0.005, 0.05, 0.5, 2.5 and 5 mg mL^{-1}) the metabolic activity of the treated cells was found to be at the level of the untreated controls, with the exception that only the highest concentration of micelles (5 mg mL^{-1}) led to a significant reduction of cell viability (50%). Interestingly, the vesicular structures did not show any cytotoxic potential even at the highest concentration (Fig. 4 top). One possible explanation for this behavior could be related to the size of the vesicles. The larger diameter of the structures in comparison to micelles leads to a smaller surface/volume ratio. Furthermore, related to the vesicular architecture, half of the surface faces the inside of the nano-assembly. However, the micelle concentrations which did not show an overt toxicity effect were more than adequate for potential applications.

Microscopic assessment of the proportion of live and dead cells confirmed the findings from the XTT assay – the membrane integrity of viable cells was proven by the exclusion of red fluorescent propidium iodide (PI) from cell nuclei indicating their excellent viability (Fig. 4 bottom panel; B3). In addition, the microscopic investigations provided first hints for a cellular internalization of the fluorescein containing micelles (Fig. 4, B5).

In the case of the highest micelle concentration, images revealed a disintegration of the cell membrane (PI positive cell nuclei) accompanied by a reduced intracellular localization of micelles, which might be caused by a diffusion of the micelles through the leaky membrane out of the dead cells (Fig. 4, A3 and A4). These results confirm the low cytotoxicity generally observed for PEtOx-based materials with different molar masses and PEtOx-containing block copolymers, which were evaluated before.[9]

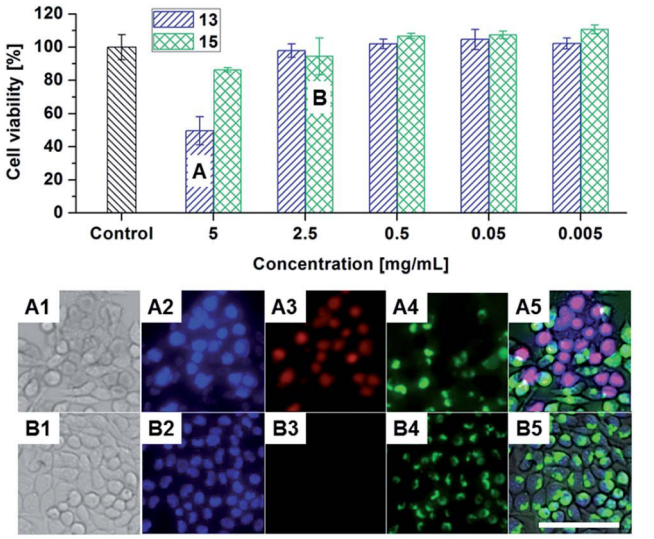

Fig. 4 (Top) Cell viability of L929 mouse fibroblasts after incubation with micelles (**13**)/vesicles (**15**) up to 5 mg mL^{-1} for 24 hours. (Bottom) Representative bright field and fluorescence microscopy images of Hoechst 33342/PI stained L929 mouse fibroblast cells cultured for 24 h in the presence of sample **13** (A1–A5; 5 mg mL^{-1}) and sample **15** (B1–B5; 0.5 mg mL^{-1}). Blue fluorescent Hoechst dye labels nuclei of all cells present (A2 and B2), while red fluorescent PI signals (A3 and B3) indicate nuclei of dead cells. Green fluorescence originates from the dye containing nanostructures (A4 and B4). Additionally, image superimpositions for all four channels are displayed (A5 and B5). Scale bar: 100 μm.

Flow cytometric (FC) investigations on time and concentration dependent uptake

The time and concentration dependent uptake of the fluorescein containing micelles/vesicles was quantified by FC measurements. For this purpose, cells were incubated either with different concentrations (0.05, 0.1, 0.25, and 0.5 mg mL^{-1}) of the materials for 24 h at 37 °C or with one concentration (0.5 mg mL^{-1}) for different time scales (0.5, 1, 3, 12, and, 24 h; 37 °C). Following the incubation, the excess of micelle/vesicle material was removed by washing with PBS. Subsequently, the cells were trypsinized and subjected to FC analysis.

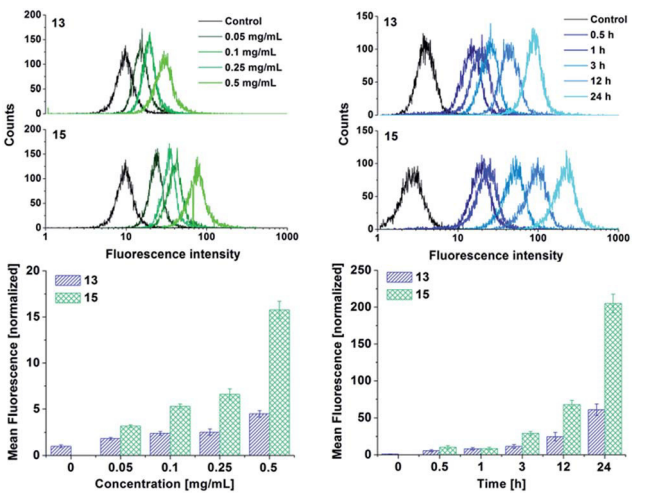

Fig. 5 Flow cytometry investigation on the time and concentration dependent uptake of 6AF containing micelles/vesicles by L929 mouse fibroblasts at 37 °C. For time dependent uptake cells were incubated between 0.5 and 24 h with micelles (**13**)/vesicles (**15**) with a concentration of 0.5 mg mL^{-1}, whereas the concentration dependent uptake was investigated over an incubation time of 24 h using micelle/vesicle concentrations in the range between 0.05 and 0.5 mg mL^{-1}. Cells incubated only with culture medium served as control. For histogram plots the fluorescence intensity on the *x*-axis is plotted against the number of events on the *y*-axis. A shift of the histogram toward the right side demonstrates an increasing amount of dye containing micelles/vesicles associated to the cells. The bar charts depict the results for the corresponding normalized mean fluorescence intensities, obtained from flow cytometry of the analyzed cell populations. The data are expressed as mean ± SD of triplicates.

The fluorescence intensity distributions (histogram plots in Fig. 5) clearly display a concentration-dependent right-shift to higher fluorescence intensity for both, the micellar and vesicular structures indicating a concentration-dependent uptake.

Interestingly, the increase in fluorescence intensity was more pronounced for the vesicle samples, suggesting an increased cellular accumulation/association as compared to micelles.

This becomes evident in quantitative terms when the mean fluorescence intensities (MFI) of the cell populations are evaluated as depicted in the bar charts (Fig. 5). An up to three-fold uptake of the vesicles was obtained as compared to micelles with the same concentration. These results were also confirmed by fluorescence microscopic observations of the treated cell populations (ESI: Fig. S9†). Interestingly, the proportion of "positive cells" having associated micelles or vesicles did not only increase at higher material concentrations but was also higher for vesicular compared to micellar samples, *e.g.* at 0.05 mg mL^{-1} 83 to 13% and at 0.5 mg mL^{-1} 98 to 88% (data not shown).

For the time-dependent uptake trends similar to the concentration-dependent internalization were observed. The cellular accumulation of material proceeds over time for both the micelles and vesicles without reaching a plateau after 24 h. Additionally, the cellular uptake of the vesicular formulation exceeds the internalization rate of the micelles by a factor of 3 and, again, supports the interpretation of a higher cellular internalization of the vesicles. It should be noted that the initially conducted fluorescence measurements of the micelle and vesicle suspensions at equivalent concentrations (weight/volume) demonstrated that both show similar fluorescence values (Fig. 3). Therefore, the observed increase in cell associated fluorescence can clearly be attributed to an enhanced vesicle uptake.

The different cellular internalization efficiencies could be caused by the cellular uptake mechanism. It is known that very large particles enter cells by phagocytosis, whereas, in the case of nanoparticles, most internalization occurs *via* various endocytotic pathways, which can be different with regard to the nature of the surface and the structural properties of nanoparticles (*e.g.* clathrin or caveolin dependent pathways).[46] Depending on the particular pathway and also its energy dependent or independent nature, different internalization rates are achieved[47] – this could also impact the uptake efficiency of the presented micelles and vesicles. To elucidate these phenomena further investigations are required, *e.g.* by assessing or blocking certain uptake pathways using specific inhibitors.

Internalization and co-localization with cellular compartments

The cellular internalization and intracellular localization of micelles and vesicles in L929 cells was further elucidated by epifluorescence and confocal laser scanning microscopy (CLSM) investigations. For this purpose, the cells were incubated for 24 h with 0.5 mg mL^{-1} of the respective substance at 37 °C and, in order to assign the localization of the fluorescent micelles/vesicles to cellular compartments, the living adherent or suspended cells were stained with specific dyes for the cell plasma membrane (Cell Mask Orange), the nuclei (Hoechst 33342 or SytoRed59) or the acidic late endosomes and lysosomes (LysoTracker), respectively.

A representative distribution of fluorescent vesicles in the context of cellular structures in adherent cells is presented in Fig. 6. The epifluorescence images suggest an intracellular localization of the vesicles, since no green fluorescent signal (from the 6AF labeled structures) is detectable at the outer cell membrane, which would be the case when vesicles are adsorbed to, but not transported through the membrane (Fig. 6: A2, A3 and A5). Additionally, no vesicles were observed within the nuclear compartment: They were rather associated with distinct outer nuclear membrane regions (Fig. 6: A5).

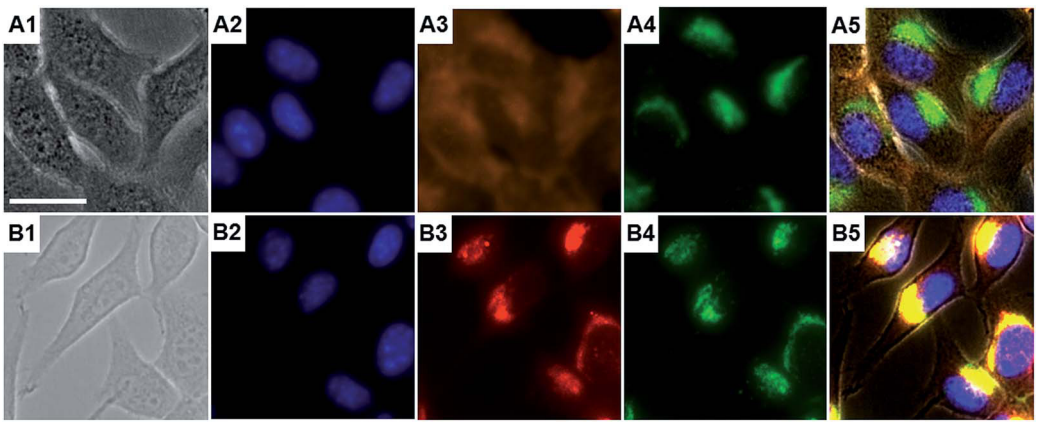

Fig. 6 Representative bright field (A1 and B1) and epifluorescence images of adherent L929 cells after 24 h incubation at 37 °C with vesicles (**15**) at a concentration of 0.1 mg mL^{-1}. Cell nuclei (A2 and B2), cell membranes (A3) or late endosomes/lysosomes (B3) were specifically stained and their fluorescence signal was captured in addition to the fluorescence signal originating from the internalized 6AF labeled vesicles (A4 and B4). Co-localization was examined by superimposing all four channels (A5 and B5). Identical results were obtained for micelles (ESI: Fig. S10†). Scale bar: 20 μm.

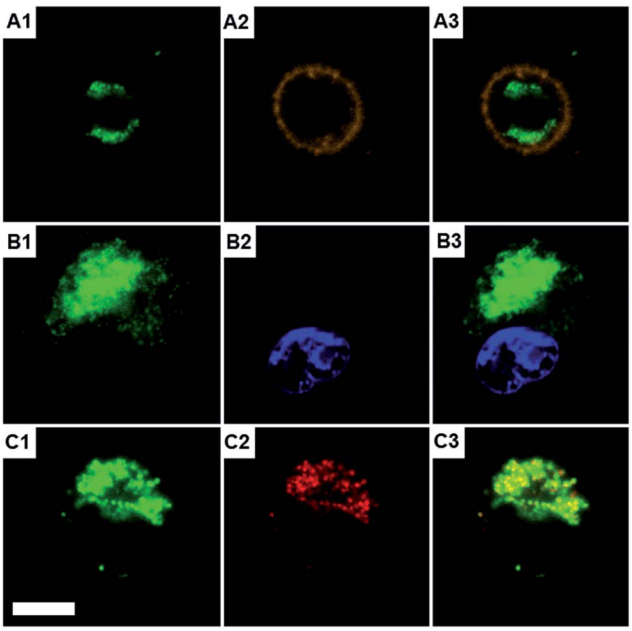

Fig. 7 Representative CLSM images of detached L929 cells after 24 h incubation at 37 °C with vesicles (**15**) at a concentration of 0.1 mg mL^{-1}. Cell membranes (A2), cell nuclei (B2), or late endosomes/lysosomes (C2) were specifically stained and correlated with the fluorescence signal of 6AF labeled vesicles (A1, B1, and C1). Superimposition of both channels (A3, B3 and C3) proves an intracellular (A3) but extranuclear (B3) localization of the vesicles and their apparent co-localization with endosomal structures (C3). Identical results were obtained for micelles (ESI: Fig. S11†). Scale bar: 10 μm.

Hypothesizing that internalization of the vesicles/micelles proceeds *via* endocytotic pathways, an appearance of the internalized structures in the late endosomes or lysosomes was very likely. Indeed, co-localization of stained acidic endosomes and fluorescent vesicles was observed (Fig. 6: B2, B3 and B5). CLSM investigations on cells treated as mentioned above but additionally detached after incubation and subjected to microscopic analysis with precise optical *z*-sectioning through the cell body confirmed an extra-nuclear presence and the complete internalization of the vesicles into the lysosomal compartment (Fig. 7: A1 to C3).

Identical results for internalization and lysosomal localization were obtained for the micellar forms suggesting similar endocytotic uptake and distribution mechanisms for both, vesicles and micelles. It should be noted that only intact nanostructures can be detected by fluorescence in an intracellular environment since the emission intensity of the free dye is strongly diminished at neutral and acidic pH values (Fig. 2). Therefore, the co-localization studies clearly suggest an endosomal location and, hence, a internalization by endocytosis can be assumed. For further studies this behavior could be beneficial because the low pH value within these cellular compartments should lead to a disassembly of the nanostructures and might result in a release of the cargo. With the presented loading, however, no pH dependent release can be investigated due to the low solubility of the dye at neutral and acidic pH values.

Conclusion

In this contribution we describe the synthesis of block copolymers with a neutral hydrophilic (EtOx) and a cationic hydrophilic (AmOx) segment as well as the self-assembling behaviour of the system into micelles and vesicles in organic solvents.

Glutaraldehyde mediated cross-linking resulted in the formation of nanogels, which were covalently loaded with 6-amino fluorescein. A detailed characterization of these nanostructures led to the conclusion that formation of either micellar or vesicular structures, respectively, is significantly dependent upon the nature of the solvent used for assembly. The presented nanogels exhibit a good biocompatibility for concentrations of up to 5 mg mL^{-1} and reveal a concentration and time dependent uptake by cells, presumably by endocytosis, as investigated by co-localization studies.

Further studies will focus on the immobilization of drugs like cytostatica and the investigation of the release of these compounds. Moreover, a variation of the zeta potential by changing the degree of cross-linking will be studied in order to control the interaction with cells and the rate of the uptake.

Experimental section

Information about materials and instrumentation can be found in the ESI.†

Block copolymers of 2-ethyl-2-oxazoline (EtOx) and 2-(4-((*tert*-butoxycarbonyl)amino)butyl)-2-oxazoline (BocOx) (P(EtOx-*b*-BocOx)), (2–6)

In a microwave vial, EtOx (606 μL, 6 mmol), MeOTos (12.1 μL, 0.08 mmol) and acetonitrile (2.9 mL) were mixed under inert conditions. After heating in the microwave synthesizer at 140 °C for 28 min, a solution of BocOx (500 μL, 2 mmol) in acetonitrile (1.5 mL) was added through a syringe and the mixture was heated again in the microwave synthesizer (140 °C, 22 min). The solution was precipitated in cold (−80 °C) diethyl ether. The white precipitate was filtered and dried in high vacuum (994 mg, 92%).

^{1}H NMR ($CDCl_3$, 300 MHz) (**6**): $\delta = 7.67$, (d, 8.1 Hz, 0.018H, tosylate), 7.14 (d, 8.21 Hz, 0.018H, tosylate), 3.46 (s, 4H, backbone), 3.10 (s, 0.5H, CH_2–CH_2–NH (BocOx)), 2.50–2.15 (m, 1.96H, CH_2 (EtOx)/CH_2–CH_2–NHBoc), 1.62 (s, 0.46H, CH_2–CH_2–CH_2 (BocOx)), 1.52 (s, 0.46H, CH_2–CH_2–CH_2 (BocOx)), 1.42 (s, 2.1H, CH_3 (BocOx)), 1.21 (s, 2.1H, CH_3 (EtOx)) ppm.

Size exclusion chromatography (SEC) (**6**) (eluent: $CHCl_3$/*iso*-propanol/NEt_3, PS-standard): $M_n = 7.600$ g mol^{-1}, $M_w = 9.000$ g mol^{-1}, $Đ = 1.18$.

Deprotection of P(EtOx-*b*-BocOx) P(EtOx-*b*-AmOx), (7–11)

Exemplarily, P(EtOx-*b*-BocOx) (**6**, 500 mg) was dissolved in TFA (5 mL) and heated to 60 °C for 1 h. After stirring for 12 h at room temperature, the mixture was diluted with 10 mL methanol and precipitated in 200 mL of cold (−80 °C) diethyl ether. The precipitate was re-dissolved in methanol (100 mL) and stirred with Amberlyst A21 for 48 h. Subsequently, the solvent was

removed, the polymer was dissolved in de-ionized water and freeze dried (−80 °C, 0.003 mbar). The polymer was obtained as white powder (456 mg, 91%).

^{1}H NMR (*N*,*N*-dimethyl formamide (DMF)-D_7, 300 MHz) (**11**): δ = 5.37 (s, 1.7H, NH_2),3.69 (s, 4H, backbone), 3.23 (s, 0.55H, CH_2–CH_2–NH_2), 2.78–2.45 (m, 2.1H, CH_2 (EtOx)/CH_2–CH_2–CO (AmOx)), 2.06–1.72 (m, 1.1H, CH_2–CH_2–CH_2–CH_2 (AmOx)), 1.2 (s, 2.5H, CH_3 (EtOx)) ppm.

SEC (**11**) (eluent: DMAc/LiCl, PS-standard): M_n = 15 600 g mol^{-1}, M_w = 20 300 g mol^{-1}, $Đ$ = 1.30.

Determination of cloud point behavior in aqueous sodium hydroxide solution

To investigate the cloud point behavior, P(EtOx-*b*-AmOx) was dissolved in an aqueous solution of sodium hydroxide (5 wt%) in concentrations varying from 2.5 to 20 mg mL^{-1}. The turbidity was recorded as a function of the temperature, which was modulated between 2 and 98 °C in three cycles (1 °C min^{-1}). The cloud point was determined at 50% transmission. Cloud points were measured in a Crystal 16 from Avantium Technologies connected to a chiller (Julabo FP 40) at a wavelength of 500 nm.

Self-assembly and cross-linking

To create nanostructures, the block copolymer (**11**, 150 mg, 0.015 mmol, 0.39 mmol of amine) was dissolved in the respective solvent (MeOH, *i*PrOH or $CHCl_3$, 5 mg mL^{-1}) and stirred for 3 h. Subsequently, glutaraldehyde (19.5 mg, 0.195 mmol, 0.5 eq. per amine) was added and the solution was stirred for another 3 h. With proceeding reaction time the color of the solution changed from colorless to yellow. To quench the excess aldehyde function, diethylamine or 6-amino fluorescein was added, respectively, and stirred for 12 h. Subsequently, the amount of solvent was reduced under an argon stream and the residual was precipitated in 100 mL cold diethyl ether (−80 °C). To purify the self-assembled structures from residual amine and cross-linker, dialysis in MeOH–water (1 : 4) was applied using a membrane with a molar mass cut off of 3500 g mol^{-1} (Roth Zellutrans). After the extraction was finished, the dialysis medium was changed to pure water and the aqueous solution was freeze dried to yield an orange powder (140 mg). The size distribution of all intermediate steps was examined by dynamic light scattering (DLS) measurements.

Determination of dye loading content by absorbance/fluorescence

The absorbance/fluorescence of nanostructures was investigated under alkaline conditions (1 mol L^{-1} NaOH in water) in diluted solution (0.1, 0.05 and 0.025 mg mL^{-1}). The absorbance was determined at a wavelength of 490 nm and compared to a dilution series of 6AF in the same aqueous NaOH solution. To the 6AF stock solution a 100 fold excess of glutaraldehyde was added to ensure that only the imine species of 6AF is present. Emission was detected at an excitation wavelength of 450 nm. Micellar samples as well as 6AF calibration exhibit an emission maximum at 510 nm. All measurements were carried out in a 96 well-plate format with 200 μL per well and double determination for each measuring point. The read out was accomplished using a Tecan M200 Pro fluorescence micro plate reader (Crailsheim, Germany). DEA loaded nanostructures served as a reference for all measurements.

Cytotoxicity assay

For the cytotoxicity screening, the mouse fibroblast cell line L929 was purchased from a commercial cell bank (Cell line service, Eppelheim, Germany). The cells were routinely cultured as follows: cell culture media Dulbecco's modified eagle's medium (DMEM) was supplemented with 10% fetal calf serum, 100 U mL^{-1} penicillin, and 100 μg mL^{-1} streptomycin (all components from Biochrom, Berlin, Germany) at 37 °C in a humidified atmosphere with 5% (v/v) CO_2. The cytotoxicity was determined using a XTT assay following the ISO/EN 10993 part 5 protocol: cells were seeded in 96-well plates at a density of 1 × 10^4 cells per well and grown as monolayer cultures for 24 h. The cells were subsequently incubated separately with different concentrations of the micelles and vesicles (from 0.005 to 5 mg mL^{-1}) for 24 h. Control cells were incubated with fresh culture medium. After incubation, the cells were washed once with PBS and a mixture of 100 μL fresh medium and 50 μL of a XTT solution, prepared according to the manufacturer's instructions, were added to each well. After 4 h at 37 °C, 100 μL of each solution were transferred to a new micro titer plate and the optical density (OD) was measured photometrically. The control was standardized as 0% of metabolism inhibition and referred as 100% viability. Cell viability below 70% was considered indicative of cytotoxicity. Data are expressed as mean ± SD of six determinations.

Photometrical and microscopical methods

For the photometric absorbance measurements, a TECAN Infinite M200 PRO plate reader (TECAN, Crailsheim, Germany) was used to measure the absorption of samples from the XTT cytotoxicity assay (570 nm with a background correction of the optical density (OD) at 690 nm). Each well containing the sample was measured in four different spots each with 25 flashes per scan.

The evaluation of micelles/vesicles uptake was performed by flow cytometry (FC) measured on a Beckmann Coulter Cytomics FC-500 equipped with Uniphase Argon ion laser, 488 nm, 20 mW output and analyzed with the Cytomics CXP software. For time dependent uptake, cells (L929) were incubated between 30 min and 24 h with micelles (**13**)/vesicles (**15**) at a concentration of 0.5 mg mL^{-1}, whereas the concentration dependent uptake was investigated over an incubation time of 24 h using micelle/vesicle concentrations in the range between 0.05 and 0.5 mg mL^{-1}. Cells incubated with culture medium only served as control. Data are expressed as mean ± SD of three determinations. To visualize the viability of cells after incubation with the micelles/vesicles as well as for the time/concentration dependent kinetic studies on cellular uptake, the blue/red/green fluorescence signal of cells cultured in a 96 well plate and stained with Hoechst 33342 and propidium iodide (PI) was

observed on a Cell Observer Z1 fluorescence microscope (Carl Zeiss, Jena, Germany) equipped with a mercury arc UV lamp and the appropriate filter combinations for excitation and detection of emission. Images of a series were captured with a 40× objective using identical instrument settings (*e.g.* UV lamp power, integration time, camera gain) and cell-spots in the 96 well plate were addressed using an automated XY table.

For CLSM analysis of uptake and co-localization with cell organelle, the nuclei, late endosomes/lysosomes and cell membranes were either stained with SYTO®Red 59, LysoTracker Red or Cell Mask Orange. CLSM images were acquired using a Zeiss LSM 510 META (Carl Zeiss) with excitation wavelengths/emission filters of 633 nm/LP 650 nm for SYTO®Red and 543 nm/BP 585 to 615 nm for LysoTracker Red and Cell Mask Orange respectively.

Images were captured with a Plan-Apochromat 63× objective and in multitrack mode, enabling single excitation and emission of fluorescence dyes. Co-localization was visualized in overlay images of the multiple channels.

Microscopic evaluation of cell viability. In addition to the above described measurement of the metabolic cell activity by the XTT assay, viability of the cells after exposure to the micelles and vesicles was examined microscopically using a propidium iodide (PI)/Hoechst staining assay. After incubation with the test substances, the cells were washed once with PBS, submerged with medium containing PI (10 μg mL^{-1}) and Hoechst 33342 (10 μg mL^{-1}) and incubated for 10 min at 37 °C. During that time, PI enters into the nuclei of dead cells *via* the leaky cell membrane, whereas the dye is kept outside of viable cells. Hoechst dye is capable of fluorescently labeling nuclei of dead and viable cells and was used to tag the entire cell collective. The blue (Hoechst), red (PI), and green (6AF labeled vesicles and micelles) fluorescence signals of cells were captured on a fluorescence microscope.

Fluorescence microscopy for kinetic studies on cellular uptake of micelles (13)/vesicles (15)

For kinetic investigations concerning a concentration dependent uptake, the cells, growing as a semiconfluent cell layer in 6 well plates, were incubated separately with different concentrations (0.05, 0.1, 0.25 and 0.5 mg mL^{-1}) of micelles and vesicles for 24 h at 37 °C under 5% CO_2 atmosphere. Control cells were incubated with fresh culture medium. After incubation, the solutions were aspirated from the wells and any excess materials were removed by washing the cell layer three times with PBS. For flow cytometry, the adherent cells were detached by trypsin treatment and 10.000 cells were analyzed using gates of forward and side scatters to exclude debris and cell aggregates. For microscopic analysis, the adherent cells were additionally stained with Hoechst 33342 (10 μg mL^{-1}) and immediately subjected to fluorescence imaging.

For kinetic investigation concerning a time dependent uptake, cells were treated with 0.5 mg mL^{-1} of micelles or vesicles for 0.5 h, 1 h, 3 h, 12 h and 24 h at 37 °C under 5% CO_2 atmosphere. Subsequent analysis was performed as mentioned above.

Co-localization study

In order to analyze the micelle/vesicle uptake and co-localization with cell organelle, adherent cells were treated with 0.1 mg mL^{-1} of micelles/vesicles for 24 h at 37 °C under 5% CO_2 atmosphere. Subsequently, the nuclei, late endosomes/lysosomes and cell membranes were stained with Hoechst 33342 and LysoTracker Red or Cell Mask Orange according to manufactures instructions (all dyes from Life Technologies, Darmstadt, Germany) and the adherent cell populations were, subsequently, subjected to microscopic investigation immediately using an epifluorescence microscope. In order to prove an effective internalization of the fluorescent micelles (**13**)/vesicles (**15**) and to exclude a false positive fluorescence signal by a simple adsorption on the extracellular leaflet of the cell membrane, CLSM was utilized to perform an optical *z*-sectioning through the cells. For that purpose, adherent cells were enzymatically detached after the above mentioned incubation with the micelles/vesicles. The nuclei, late endosomes/lysosomes and cell membranes were stained with SYTO®Red 59, LysoTracker Red or Cell Mask Orange according to manufactures instructions and, subsequently, fixed with 4% paraformaldehyde dissolved in PBS. Aliquots of the cell suspensions were then transferred onto microscopic slides, decorated with coverslips and subjected to CLSM analysis.

Acknowledgements

Cryo-TEM investigations were performed at the cryo-TEM facilities of the Jena Center for Soft Matter (JCSM). The TEM facilities were funded by a grant of the DFG (German Research Foundation) and the EFRE (European Fund for Regional Development). The Leibniz Institute for Age Research – Fritz Lipmann Institute (FLI) is a member of the Leibniz Society and is financially supported by the State of Thuringia and the Federal Government of Germany.

Notes and references

1 G. Liu and Z. An, *Polym. Chem.*, 2014, **5**, 1559–1565.
2 R. Tong, L. Tang, L. Ma, C. Tu, R. Baumgartner and J. Cheng, *Chem. Soc. Rev.*, 2014, **43**, 6982–7012.
3 H. Wei, R.-X. Zhuo and X.-Z. Zhang, *Prog. Polym. Sci.*, 2013, **38**, 503–535.
4 W. Xu, P. Ling and T. Zhang, *J. Drug Delivery*, 2013, **2013**, 15.
5 H. Ding, X. Wang, S. Zhang and X. Liu, *J. Nanopart. Res.*, 2012, **14**, 1–13.
6 M. Talelli, C. J. F. Rijcken, W. E. Hennink and T. Lammers, *Curr. Opin. Solid State Mater. Sci.*, 2012, **16**, 302–309.
7 S. E. Averick, E. Paredes, A. Irastorza, A. R. Shrivats, A. Srinivasan, D. J. Siegwart, A. J. Magenau, H. Y. Cho, E. Hsu, A. A. Averick, J. Kim, S. Liu, J. O. Hollinger, S. R. Das and K. Matyjaszewski, *Biomacromolecules*, 2012, **13**, 3445–3449.
8 W. Chen, M. Zheng, F. Meng, R. Cheng, C. Deng, J. Feijen and Z. Zhong, *Biomacromolecules*, 2013, **14**, 1214–1222.

9 R. Luxenhofer, G. Sahay, A. Schulz, D. Alakhova, T. K. Bronich, R. Jordan and A. V. Kabanov, *J. Controlled Release*, 2011, **153**, 73–82.
10 M. Bauer, S. Schroeder, L. Tauhardt, K. Kempe, U. S. Schubert and D. Fischer, *J. Polym. Sci., Part A: Polym. Chem.*, 2013, **51**, 1816–1821.
11 M. C. Woodle, C. M. Engbers and S. Zalipsky, *Bioconjugate Chem.*, 1994, **5**, 493–496.
12 S. Zalipsky, C. B. Hansen, J. M. Oaks and T. M. Allen, *J. Pharm. Sci.*, 1996, **85**, 133–137.
13 B. Guillerm, S. Monge, V. Lapinte and J.-J. Robin, *Macromol. Rapid Commun.*, 2012, **33**, 6000–6016.
14 O. Sedlacek, B. D. Monnery, S. K. Filippov, R. Hoogenboom and M. Hruby, *Macromol. Rapid Commun.*, 2012, **33**, 1648–1662.
15 P. Persigehl, R. Jordan and O. Nuyken, *Macromolecules*, 2000, **33**, 6977–6981.
16 R. Hoogenboom, M. M. Leenen, H. Huang, C.-A. Fustin, J.-F. Gohy and U. S. Schubert, *Colloid Polym. Sci.*, 2006, **284**, 1313–1318.
17 U. Mansfeld, S. Hoeppener, K. Kempe, J.-M. Schumers, J.-F. Gohy and U. S. Schubert, *Soft Matter*, 2013, **9**, 5966–5974.
18 R. Takahashi, T. Sato, K. Terao, X.-P. Qiu and F. M. Winnik, *Macromolecules*, 2012, **45**, 6111–6119.
19 R. Obeid, E. Maltseva, A. F. Thünemann, F. Tanaka and F. M. Winnik, *Macromolecules*, 2009, **42**, 2204–2214.
20 T. B. Bonné, K. Lüdtke, R. Jordan and C. M. Papadakis, *Macromol. Chem. Phys.*, 2007, **208**, 1402–1408.
21 R. Ivanova, T. Komenda, T. B. Bonné, K. Lüdtke, K. Mortensen, P. K. Pranzas, R. Jordan and C. M. Papadakis, *Macromol. Chem. Phys.*, 2008, **209**, 2248–2258.
22 R. Luxenhofer, A. Schulz, C. Roques, S. Li, T. K. Bronich, E. V. Batrakova, R. Jordan and A. V. Kabanov, *Biomaterials*, 2010, **31**, 4972–4979.
23 Y. Han, Z. He, A. Schulz, T. K. Bronich, R. Jordan, R. Luxenhofer and A. V. Kabanov, *Mol. Pharm.*, 2012, **9**, 2302–2313.
24 A. Schulz, S. Jaksch, R. Schubel, E. Wegener, Z. Di, Y. Han, A. Meister, J. Kressler, A. V. Kabanov, R. Luxenhofer, C. M. Papadakis and R. Jordan, *ACS Nano*, 2014, **8**, 2686–2696.
25 R. K. O'Reilly, C. J. Hawker and K. L. Wooley, *Chem. Soc. Rev.*, 2006, **35**, 1068–1083.
26 N. t. Brummelhuis and H. Schlaad, *Polym. Chem.*, 2011, **2**, 1180–1184.
27 N. Engelhardt, A. Ernst, A.-L. Kampmann and R. Weberskirch, *Macromol. Chem. Phys.*, 2013, **214**, 2783–2791.
28 C. Legros, A.-L. Wirotius, M.-C. De Pauw-Gillet, K. C. Tam, D. Taton and S. Lecommandoux, *Biomacromolecules*, 2014, **16**, 183–191.
29 H. Huang, R. Hoogenboom, M. A. M. Leenen, P. Guillet, A. M. Jonas, U. S. Schubert and J.-F. Gohy, *J. Am. Chem. Soc.*, 2006, **128**, 3784–3788.
30 Y. Liu, Y. Wang, Y. Wang, J. Lu, V. Piñón and M. Weck, *J. Am. Chem. Soc.*, 2011, **133**, 14260–14263.
31 S. Zschoche, J. C. Rueda, M. Binner, H. Komber, A. Janke, K.-F. Arndt, S. Lehmann and B. Voit, *Macromol. Chem. Phys.*, 2012, **213**, 215–226.
32 S. Zschoche, J. Rueda, V. Boyko, F. Krahl, K.-F. Arndt and B. Voit, *Macromol. Chem. Phys.*, 2010, **211**, 1035–1042.
33 C. Legros, M.-C. De Pauw-Gillet, K. C. Tam, S. Lecommmandoux and D. Taton, *Polym. Chem.*, 2013, **4**, 4801–4808.
34 S. Cesana, J. Auernheimer, R. Jordan, H. Kessler and O. Nuyken, *Macromol. Chem. Phys.*, 2006, **207**, 183–192.
35 M. Hartlieb, D. Pretzel, K. Kempe, C. Fritzsche, R. M. Paulus, M. Gottschaldt and U. S. Schubert, *Soft Matter*, 2013, **9**, 4693–4704.
36 C. Legros, M.-C. De Pauw-Gillet, K. C. Tam, S. Lecommandoux and D. Taton, *Eur. Polym. J.*, 2015, **62**, 322–330.
37 J. Kronek, Z. Kroneková, J. Lustoň, E. Paulovičová, L. Paulovičová and B. Mendrek, *J. Mater. Sci.: Mater. Med.*, 2011, **22**, 1725–1734.
38 J. Kronek, E. Paulovičová, L. Paulovičová, Z. Kroneková and J. Lustoň, *J. Mater. Sci.: Mater. Med.*, 2012, **23**, 1457–1464.
39 F. Wiesbrock, R. Hoogenboom, C. H. Abeln and U. S. Schubert, *Macromol. Rapid Commun.*, 2004, **25**, 1895–1899.
40 J. Rodríguez-Hernández, J. Babin, B. Zappone and S. Lecommandoux, *Biomacromolecules*, 2005, **6**, 2213–2220.
41 M. Wagner, S. Holzschuh, A. Traeger, A. Fahr and U. S. Schubert, *Anal. Chem.*, 2014, **86**, 5201–5210.
42 W. Burchard, in *Branched Polymers II*, ed. J. Roovers, Springer Berlin Heidelberg, 1999, vol. 143, pp. 113–194.
43 J. N. Israelachvili, D. J. Mitchell and B. W. Ninham, *J. Chem. Soc., Faraday Trans. 2*, 1976, **72**, 1525–1568.
44 R. Sjöback, J. Nygren and M. Kubista, *Spectrochim. Acta, Part A*, 1995, **51**, L7–L21.
45 T. Tsuchiya, *J. Biomater. Appl.*, 1994, **9**, 138–157.
46 S. Xiang, H. Tong, Q. Shi, J. C. Fernandes, T. Jin, K. Dai and X. Zhang, *J. Controlled Release*, 2012, **158**, 371–378.
47 S. Lerch, M. Dass, A. Musyanovych, K. Landfester and V. Mailänder, *Eur. J. Pharm. Biopharm.*, 2013, **84**, 265–274.

Electronic Supplementary Material (ESI) for Journal of Materials Chemistry B.

Supporting information

Core cross-linked micelles and vesicles based on the self-assembly of double hydrophilic poly(2-oxazoline) block copolymers

Matthias Hartlieb,[1,2] David Pretzel,[1,2] Michael Wagner,[1,2] Stephanie Hoeppener,[1,2] Peter Bellstedt,[3] Matthias Görlach,[3] Christoph Englert,[1,2] Kristian Kempe,[1,2,†] Ulrich S. Schubert[1,2,*]

1 Laboratory of Organic and Macromolecular Chemistry (IOMC), Friedrich Schiller University Jena, Humboldtstrasse 10, 07743, Jena, Germany

2 Jena Center for Soft Matter (JCSM), Friedrich Schiller University Jena, Philosophenweg 7, 07743, Jena, Germany

3 Biomolecular NMR Spectroscopy, Leibniz Institute for Age Research – Fritz Lipmann Institute, Beutenbergstr. 11, 07745 Jena, Germany

† Current address: Department of Chemistry, University of Warwick, Gibbet Hill Road, Coventry, CV4 7AL, U.K.

* Address correspondence to ulrich.schubert@uni-jena.de

I Materials and instrumentation

Chemicals and solvents were purchased from Sigma-Aldrich, Merck, Fluka, and Acros. 2-Ethyl-2-oxazoline (EtOx) and methyl tosylate (MeOTos) were distilled to dryness prior to use. EtOx was dried using barium oxide before distillation. 2-(4-((*tert*-Butoxycarbonyl)amino)butyl)-2-oxazoline (BocOx) was synthesized as described in a previous publication.[1]

The Initiator Sixty single-mode microwave synthesizer from Biotage, equipped with a non-invasive IR sensor (accuracy: 2%), was used for polymerizations under microwave irradiation.

Microwave vials were heated overnight to 110 °C and allowed to cool to room temperature under argon atmosphere before use. All polymerizations were carried out under temperature control. Size-exclusion chromatography (SEC) of protected polymers was performed on a Shimadzu system equipped with a SCL-10A system controller, a LC-10AD pump, a RID-10A refractive index detector and a PSS SDV column with chloroform/triethylamine (NEt_3)/*iso*-propanol (94:4:2) as eluent. The column oven was set to 50 °C. SEC of the deprotected statistical copolymers was performed on a Shimadzu system with a LC-10AD pump, a RID-10A refractive index detector, a system controller SCL-10A, a degasser DGU-14A, and a CTO-10A column oven using *N,N*-dimethyl acetamide (DMAc) with 2.1 g L^{-1} LiCl as the eluent and the column oven set to 50 °C. Poly(styrene) (PS) samples were used as calibration standards for both solvent systems. Proton NMR spectroscopy (^{1}H NMR) measurements were performed at room temperature on a Bruker AC 300 and 400 MHz spectrometer, using $CDCl_3$ or *N,N* dimethyl formamide (DMF)-D_7 as solvents. The chemical shifts are given in ppm relative to the signal of the residual non-deuterated solvent.

Batch dynamic light scattering (DLS) was performed on a Zetasizer Nano ZS (Malvern Instruments, Herrenberg, Germany). All measurements were performed in folded capillary cells (DTS1071, Malvern Instruments, Herrenberg, Germany). After an equilibration time of 180 s, 3 × 30 s runs were carried out at 25 °C (λ = 633 nm). The counts were detected at an angle of 173°. Each measurement was performed in triplicate. Apparent hydrodynamic radii, R_h, were calculated according to the Stokes–Einstein equation.

Laser Doppler velocimetry was used to measure the electrokinetic potential, also known as zeta potential. The measurements were performed on a Zetasizer Nano ZS (Malvern Instruments, Herrenberg, Germany) in folded capillary cells (DTS1071). For each measurement, 15 runs were

carried out using the fast-field and slow-field reversal mode at 150 V. Each experiment was performed in triplicate at 25 °C. The zeta potential (ζ) was calculated from the electrophoretic mobility (μ) according to the Henry Equation.[2] The Henry coefficient, f(ka), was calculated according to Ohshima.[3]

Cryo-TEM investigations were conducted with a FEI Tecnai G^2 20 at 200 kV acceleration voltage. Specisms were vitrified by a Vitrobot Mark V system on Quantifoil grids (R2/2). The blotting time was 1 s with blotting force offset of 0. The amount of solution was 7 μL. Samples were plunge frozen in liquid ethane and stored under liquid nitrogen until transferred to the Gatan ncryo-holder and brought into the microscope. Images were acquired with a 4k × 4k CCD Eagle camera.

Solid state (ss) NMR spectroscopy

One-dimensional (1D) natural abundance ^{13}C cross polarization magic angle spinning ssNMR spectroscopy was carried out using a Bruker Avance II spectrometer operating at ^{1}H (^{13}C) frequencies of 500 (125) MHz and using a 3.2 mm triple resonance probe. Sample temperature was 293 K at 20 kHz spinning frequency. Cross polarization (CP) contact time was 1.5 ms, and ^{1}H decoupling was performed using 90 kHz decoupling field strength. Final spectra were collected with 295006 scans and a 2 s recycle time, processed (exponential window function; line broadening 20 Hz) and evaluated with Bruker Topspin. Referencing was relative to Adamantan, setting the methine line to 29.46 ppm relative to neat trimethylsilane.[4]

Asymmetric flow field-flow fractionation (AF4)

Asymmetric flow field-flow fractionation (AF4) was performed on an AF2000 MT System (Postnova Analytics, Landsberg, Germany) coupled to an UV (PN3211, 260 nm), RI (PN3150), MALLS (PN3070, 633 nm) and DLS (ZetaSizerNano ZS, 633 nm) detector. The eluent is delivered by two different pumps (tip and focus-flow) and the sample is injected by an auto-sampler (PN5300) into the channel. The channel has a trapezoidal geometry and an overall area of 31.6 cm^2. The nominal height of the spacer was 500 µm and a regenerated cellulose membrane with a molar mass cut-off of 10,000 g mol^{-1} was used as accumulation wall. All experiments were carried out at 25 °C. For molar mass determination of the polymers, the eluent was composed of 25 mM acetate buffer at a pH value of 3.5 and 20 mM NaCl. The detector flow rate was set to 0.5 mL min^{-1} for all samples and 50 µL (5 mg mL^{-1}) were injected with an injection flow rate of 0.2 mL min^{-1} for 7 min. For all samples the cross-flow was set to 1.8 mL min^{-1}. After the focusing period and a transition time of 1 min, the cross flow was kept constant for 3 min and then decreased under a power function gradient (0.4) to 0 within 15 min. Afterwards, the cross-flow was kept constant at zero for at least 20 min to ensure complete elution. For characterization of the colloidal structures, the eluent was 0.025% NovaChem Surfactant 100 detergents mix. The detector flow rate was set to 0.5 mL min^{-1} for all samples and 20 µL (5 mg mL^{-1}) were injected with an injection flow rate of 0.2 mL min^{-1} for 7 min. For all samples the cross-flow was set to 1.0 mL min^{-1}. After the focusing period and a transition time of 1 min, the cross flow was kept constant for 2 min and then decreased under a power function gradient (0.4) to 0 within 18 min. Afterwards, the cross-flow was kept constant at zero for at least 25 min to ensure complete elution. For calculation of the molar mass and the radius of gyration, a Zimm plot was used. All measurements were repeated three times. The refractive

index increment (dn/dc) of all samples was measured by manual injection of a known concentration directly into the channel without any focusing or cross-flow. The dn/dc was calculated as the average of at least three injections from the area under the RI curve (AUC_{RI}).

II Analytics of P(EtOx)-*b*-(BocOx) and P(EtOx)-*b*-(AmOx)

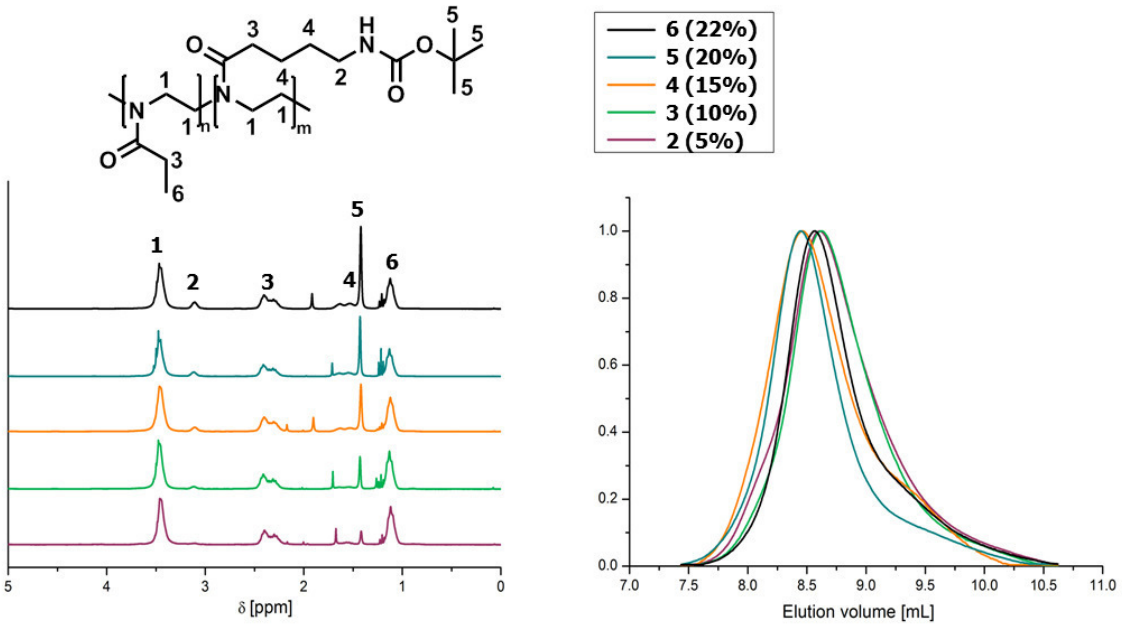

Figure S1. ^{1}H NMR spectra (300 MHz, $CDCl_3$) and size exclusion chromatograms (chloroform/NEt_3/*iso*-propanol) of the protected block copolymers (P(EtOx-*b*-BocOx, **2**-**6**) with BocOx-contents between 5 and 22%.

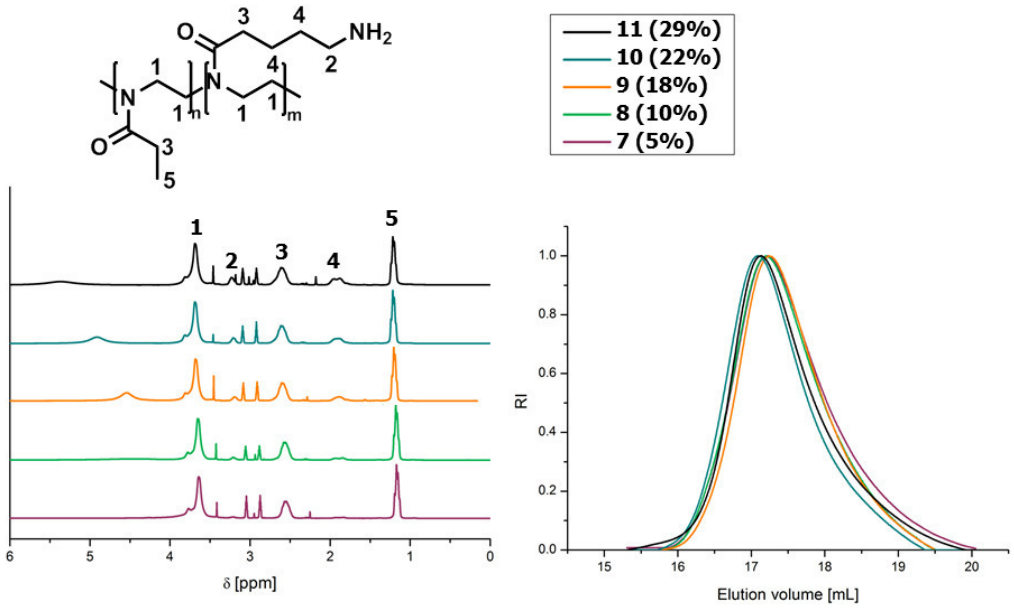

Figure S2. ^{1}H NMR spectra (300 MHz, DMF-D_7) and size exclusion chromatograms (*N,N*-dimethyl acetamide) of the deprotected block copolymers (P(EtOx-*b*-AmOx, **7**-**11**) with AmOx-contents between 5 and 29%.

Table S1. Asymmetric flow field flow fractionation (AF4) data of the deprotected block copolymers.

Sample	dn/dc [mL g^{-1}]	M_n [g mol^{-1}]	Error [g mol^{-1}]	M_w [g mol^{-1}]	Error [g mol^{-1}]	M_z [g mol^{-1}]	Error [g mol^{-1}]	Đ	Error	Rec [%]	Error [%]
7	0.153	11,700	670	12,900	530	14,000	560	1.10	0.024	73.7	0.1
8	0.160	9,200	360	10,500	840	11,300	860	1.14	0.065	74.9	0.9
9	0.153	13,300	340	14,600	270	15,900	260	1.10	0.008	77.6	0.3
10	0.156	13,600	430	14,900	450	16,600	820	1.09	0.003	77.1	0.5
11	0.139	12,500	500	15,700	180	18,100	380	1.26	0.039	75.9	0.9

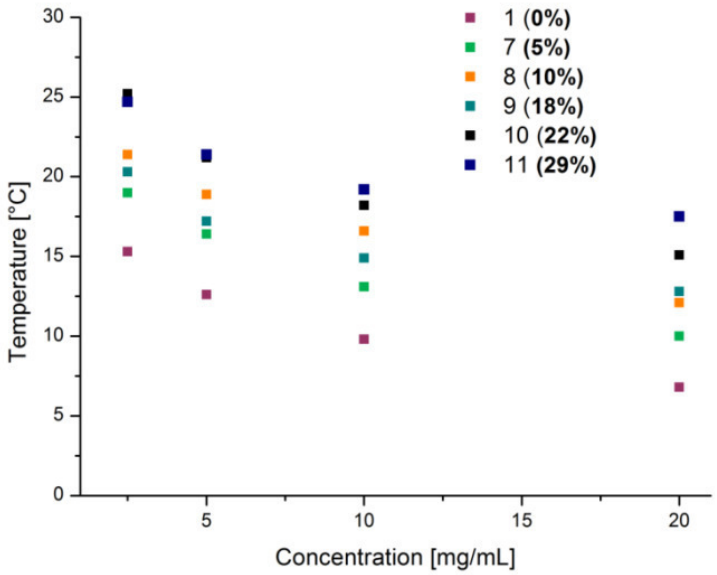

Figure S3. Cloud-points of P(EtOx-*b*-AmOx) in dependency of the concentration.

In a recent publication we described the formation of cationic hydrogels, originating from statistical copolymers P(EtOx-*stat*-AmOx) with comparable compositions, which were formed due to phase separation during the gelation leading to micron-sized hydrogel beads.[5] Such a behavior was observed under strong alkaline conditions (5 wt% aqueous NaOH) at elevated temperatures (50 °C). As a consequence, the prepared P(EtOx-*b*-AmOx) block copolymers were investigated regarding their LCST behavior at the conditions described earlier, revealing a similar phase transition (Figure S3). However, also a PEtOx homopolymer was included into the study and exhibited a lower T_{cp} than any of the copolymers. This prompted us to conclude that PEtOx is the segment which undergoes phase separation upon heating. This can be explained by a chaotropic influence of the high hydroxyl ion concentration in solution.[6, 7] Therefore, the phase separation at these conditions cannot be exploited to create micellar systems with the cationic building block in the core since PEtOx collapses at increasing temperatures.

III Analytics of cross-linked and non-cross-linked self-assembled structures.

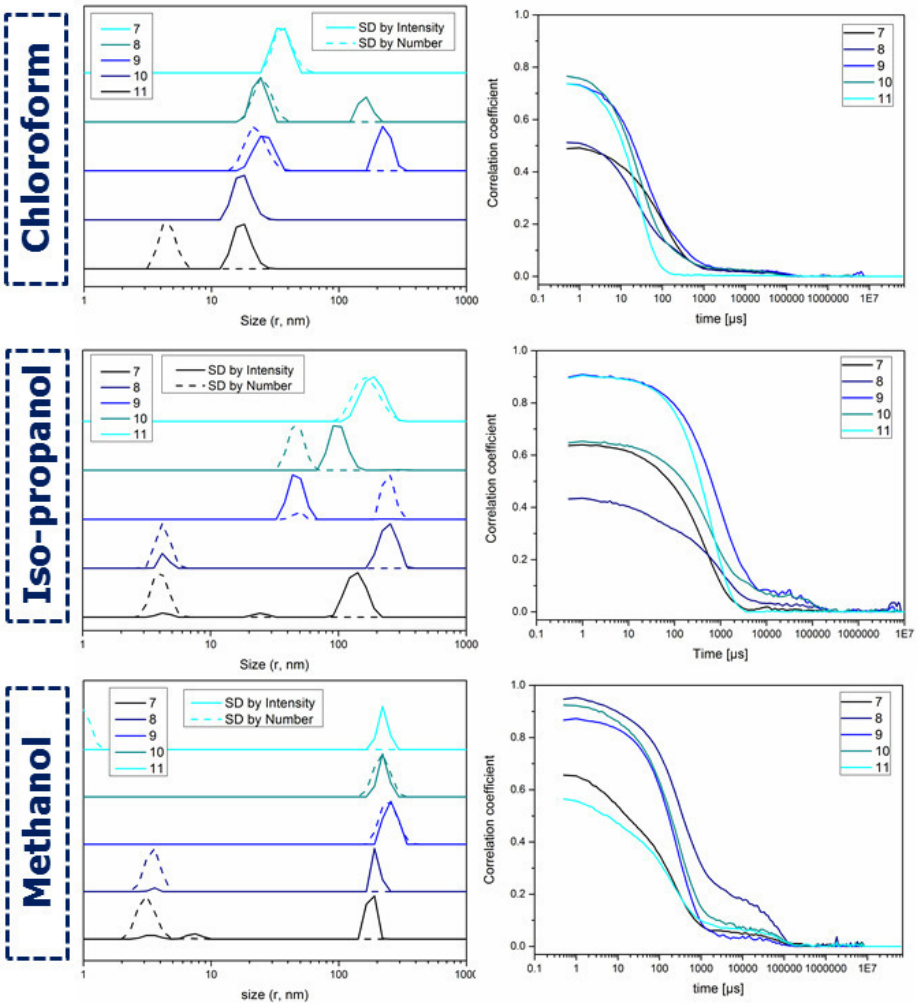

Figure S4. DLS size distributions and correlation functions of P(EtOx-*b*-AmOx) in organic solvents (1 mg mL^{-1}).

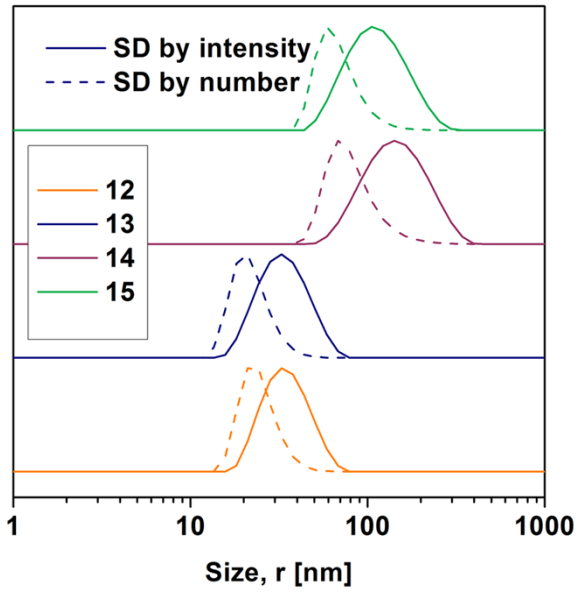

Figure S5. DLS size distributions of cross-linked nanostructures in water.

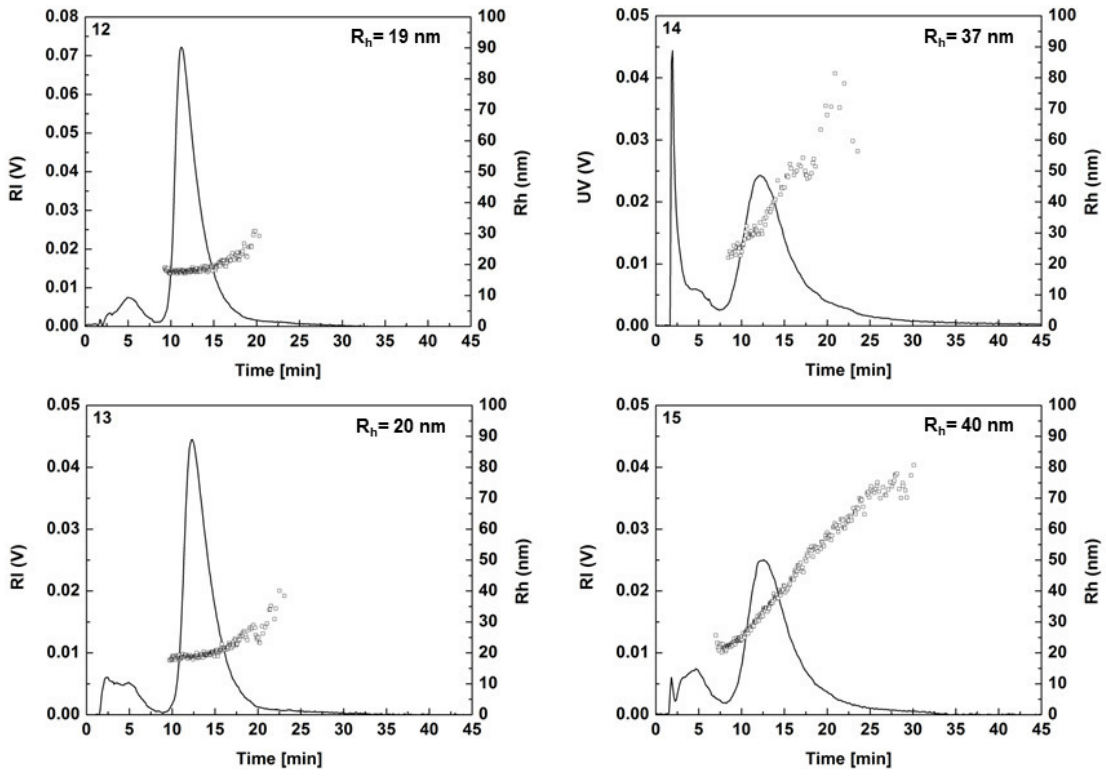

Figure S6. AF4 elugrams of cross-linked nanostructures (in 0.025% NovaChem Surfactant 100 detergents mix).

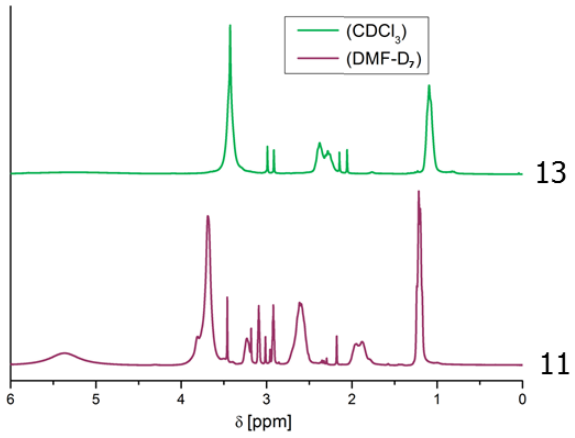

Figure S7. Comparison of the ^{1}H NMR spectra of polymer **11** in $CDCl_3$ (self-assembly) and DMF-D_7 (no assembly).

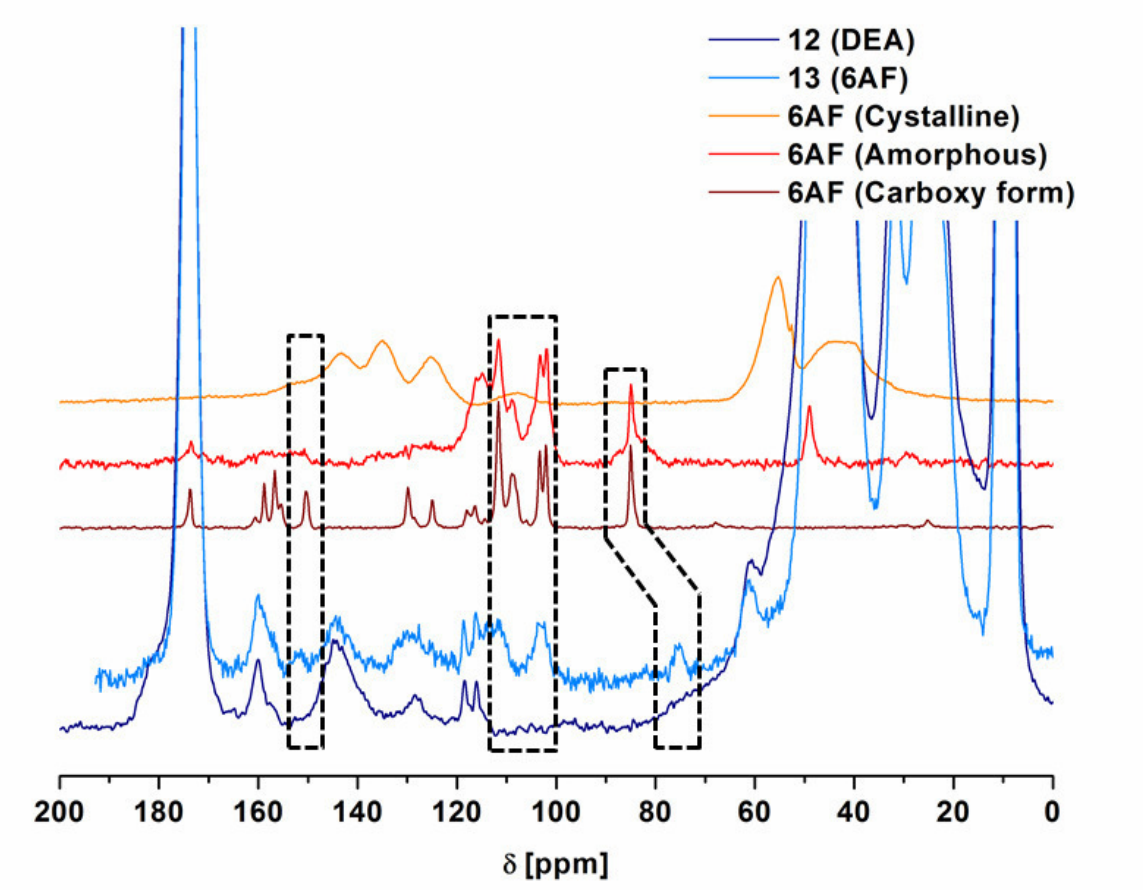

Figure S8. Solid state ^{13}C NMR spectra of different 6AF forms and micelles with (**13**) and without (**12**) 6AF. Commercial, microcrystalline 6AF, amorphous 6AF and KOH-induced ring-opened 6AF were analyzed by natural abundance ^{13}C CP MAS ssNMR. All MAS ssNMR spectra were acquired at 293 K, with 295006 scans, 2 s recycle time and a CP contact time of 1.5 ms. Microcrystalline 6AF was used as commercially supplied, amorphous 6AF was produced by dissolving commercial 6AF in MeOH, flash-freezing in liquid N_2 and subsequent lyophilisation; ring-open 6AF was derived from microcrystalline material by dissolving it in 1 M KOH, subsequent flash-freezing and lyophilisation.

IV Cellular uptake and co-localization studies of nano-assemblies.

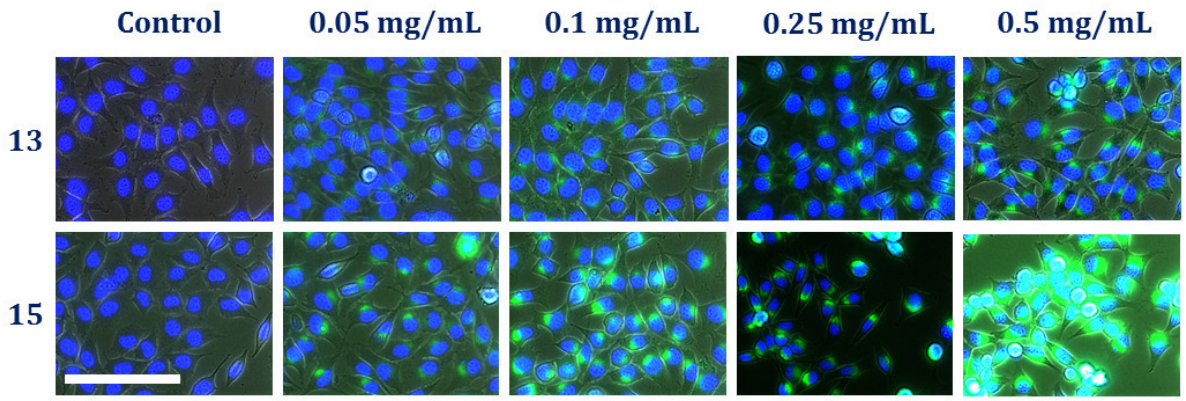

Figure S9. Fluorescence microscopy images on the concentration dependent uptake of dye containing micelles (**13**)/vesicles (**15**) by L929 mouse fibroblasts. Cells were incubated for 24 h using micelle/vesicle concentrations in the range between 0.05 and 0.5 mg mL^{-1}. Cells incubated with culture medium only served as control. The cell nuclei were stained with blue fluorescent Hoechst 33342. Shown are fluorescence images resulting from superimposing the blue and green channels. Increasing green fluorescence emitted by the dye-containing micelles/vesicles indicates a concentration dependent internalization of both structures with an elevated uptake of vesicles *vs.* micelles. Scale bar 50 µm.

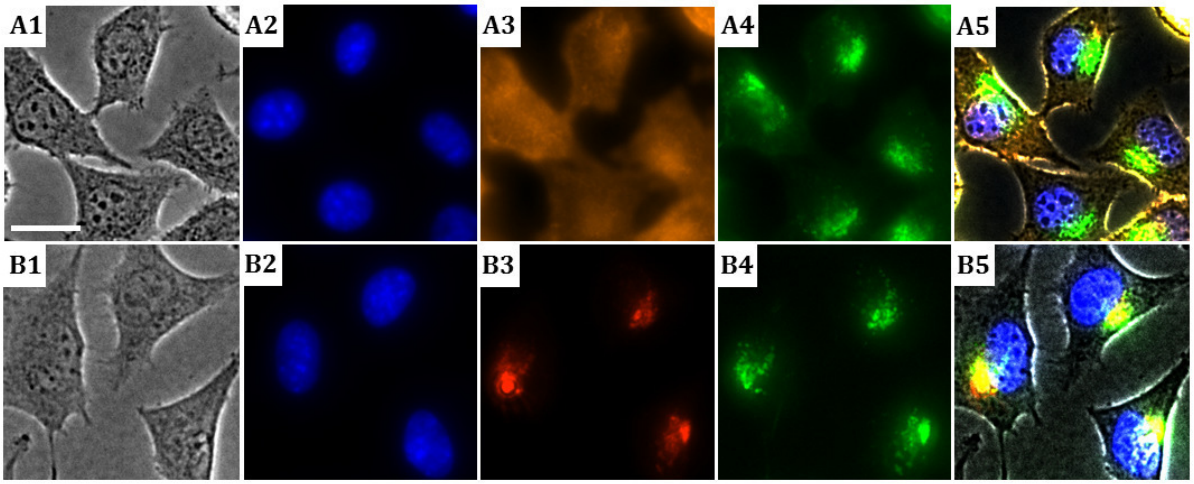

Figure S10. Representative bright field (A1 and B1) and epifluorescence images of adherent L929 cells after 24 h incubation at 37 °C in the presence of micelles (**13**) at a concentration of 0.1 mg mL^{-1}. Cell nuclei (A2 and B2), cell membranes (A3) or late endosomes/lysosomes (B3) were specifically stained and their fluorescence signal was captured in addition to the fluorescence signal originating from the internalized 6AF labeled vesicles (A4 and B4). Superimposition of all four channels (A5 and B5). Scale bar: 20 µm.

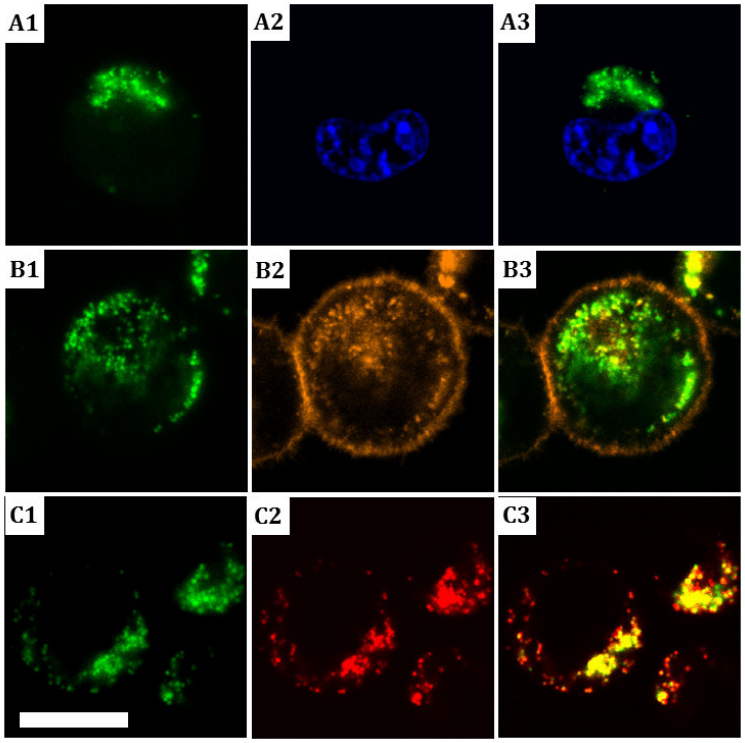

Figure S11. Representative CLSM images of detached L929 cells after 24 h incubation at 37 °C in the presence of micelles (**13**) at a concentration of 0.1 mg mL^{-1}. Cell membranes (A2), cell nuclei (B2), or late endosomes/lysosomes (C2) were specifically stained and correlated with the fluorescence signal of 6AF labeled micelles (A1, B1, and C1). Superimposition of both channels (A3, B3 and C3) proves intracellular (A3) but extra-nuclear (B3) localization of the vesicles and their apparent co-localization with lysosomal structures (C3). Scale bar: 10 µm.

References

1. M. Hartlieb, D. Pretzel, K. Kempe, C. Fritzsche, R. M. Paulus, M. Gottschaldt and U. S. Schubert, *Soft Matter*, 2013, **9**, 4693-4704.
2. A. V. Delgado, F. Gonzalez-Caballero, R. J. Hunter, L. K. Koopal and J. Lyklema, *J. Colloid Interface Sci.*, 2007, **309**, 194-224.
3. H. Ohshima, *Journal of Colloid and Interface Science*, 1994, **168**, 269-271.
4. C. R. Morcombe and K. W. Zilm, *J. Magn. Reson.*, 2003, **162**, 479-486.
5. M. Hartlieb, D. Pretzel, C. Englert, M. Hentschel, K. Kempe, M. Gottschaldt and U. S. Schubert, *Biomacromolecules*, 2014, **15**, 1970-1978.
6. M. M. Bloksma, D. J. Bakker, C. Weber, R. Hoogenboom and U. S. Schubert, *Macromol. Rapid Commun.*, 2010, **31**, 724-728.
7. F. E. Bailey and R. W. Callard, *J. Appl. Polym. Sci.*, 1959, **1**, 56-62.